

PONTIFICIA UNIVERSIDAD CATÓLICA DEL PERÚ

FACULTAD DE CIENCIAS E INGENIERÍA



**TEXTURES AND COMPOSITION OF HYDROTHERMAL TOURMALINE IN THE
CHACALTAYA-KELLHUANI-MILLUNI DISTRICT, LA PAZ, BOLIVIA**

Tesis para obtener el título profesional de Ingeniera Geóloga

AUTORA

ANGELA DANIELA CASTRO MORANTE

ASESOR

Dr. LISARD TORRÓ I ABAT

CO-ASESOR

Dr. MATTHIEU HARLAUX (University of Nevada, Reno)

Lima, agosto de 2023

Informe de Similitud

Yo, Lisard Torr3 i Abat,

docente de la Facultad de Ciencias e Ingenier3a de la Pontificia

Universidad Cat3lica del Per3, asesor de la tesis titulada

Textures and composition of hydrothermal tourmaline in the Chacaltaya-Kellhuani-Milluni district, La Paz, Bolivia,

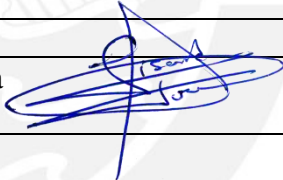
de la autora

Angela Daniela Castro Morante

dejo constancia de lo siguiente:

- El mencionado documento tiene un 3ndice de puntuaci3n de similitud de 15 %. As3 lo consigna el reporte de similitud emitido por el software *Turnitin* el 04/08/2023.
- He revisado con detalle dicho reporte y la Tesis y no se advierten indicios de plagio.
- Las citas a otros autores y sus respectivas referencias cumplen con las pautas acad3micas.

Lugar y fecha: Lima a 4 de agosto de 2023

Apellidos y nombres del asesor:	
DNI: Torr3 i Abat, Lisard	Firma 
ORCID: 0000-0002-3557-8334	

Resumen

Los minerales pertenecientes al supergrupo de la turmalina son muy útiles para registrar las condiciones fisicoquímicas de su cristalización y rastrear los procesos geológicos asociados a la formación de depósitos minerales. Este estudio presenta nuevos resultados sobre la petrografía y geoquímica de turmalina en el distrito Triásico de Chacaltaya-Kellhuani-Milluni (oeste de Bolivia), ubicado en el segmento norte de la Cordillera Real dentro del Cinturón Estannífero de los Andes Centrales. El área de estudio se encuentra alrededor del stock granítico de Chacaltaya, aproximadamente 5 km al sur del granito de Huayna-Potosí. En este distrito, la mineralización hidrotermal está asociada a greisen, brechas y vetas. Se distinguen tres tipos principales de turmalina hidrotermal, de acuerdo a la petrografía: i) Tur-1, que presenta un color naranja y se manifiesta como cristales esqueléticos dispersos o como reemplazamiento pseudomórfico de cristales primarios de feldespato potásico en el granito greisenizado de Chacaltaya, como cristales euhedrales a subhedrales diseminados que a menudo forman agregados radiales en el greisen, y como fragmentos de cristales en brechas cementadas por turmalina; ii) Tur-2, que se presenta como cristales aciculares muy finos de color verde oscuro que componen el cemento de las brechas; y iii) Tur-3, que forma cristales elongados subhedrales de color verde con tonalidades marrones con zonación oscilatoria dentro de las vetas y cristales anhedrales muy finos en el halo de las vetas. Tanto Tur-2 como Tur-3 muestran evidencia textural de co-cristalización con casiterita tanto en brechas hidrotermales como en vetas. Los tres tipos petrográficos pertenecen al grupo de las turmalinas alcalinas y se caracterizan por ser ricas en Fe, en su mayoría cercanas a la composición del chorlo, extendiéndose en parte a los campos composicionales de la foitita y dravita. La superposición composicional de los tres tipos petrográficos de turmalina sugiere un continuo en la evolución del fluido hidrotermal que reflejaría un enfriamiento progresivo del sistema desde Tur-1 a Tur-

3, lo que finalmente habría conducido a la cristalización de casiterita coetáneamente a la cristalización de Tur-2 y Tur-3.

Palabras clave

Yacimientos estanníferos, alteración hidrotermal, Cinturón Estannífero de los Andes Centrales, Bolivia, petrografía, composición geoquímica

Abstract

Minerals of the tourmaline supergroup are useful to decipher the physicochemical conditions of its crystallization and to trace geologic processes associated with the formation of ore deposits. This study presents new results on the petrography and geochemistry of tourmaline from the Triassic Chacaltaya-Kellhuani-Milluni district (western Bolivia), located in the northern segment of the Cordillera Real within the Central Andean tin belt. The study area lies around the Chacaltaya granitic stock about 5 km south of the Huayna-Potosí granite. Here, hydrothermal mineralization is associated with greisen, breccia, and veins. Three main petrographic types of hydrothermal tourmaline are distinguished: i) Tur-1, which is orange in color and occurs as scattered skeletal crystals or pseudomorphic replacement of primary K-feldspar in the greisenized Chacaltaya granite, as disseminated euhedral to subhedral crystals mostly forming radial aggregates in greisen, and as crystal fragments in tourmaline-cemented breccias; ii) Tur-2, which appears as very fine acicular grains with a dark-green color composing the cement of breccias; and iii) Tur-3, which forms elongated green-brownish subhedral, oscillatory-zoned crystals within veins, and anhedral, very fine-grained crystals in the halos of veins. Both Tur-2 and Tur-3 show textural evidence of co-crystallization with cassiterite in both hydrothermal breccias and veins. The three petrographic types of tourmaline belong to the alkali group and are characterized by Fe-rich compositions, in majority close to the schorl endmember, and partly extending into the compositional fields of foitite and dravite.

Overlapping tourmaline compositions suggest a progressive cooling of the ore-forming system from Tur-1 to Tur-3, eventually leading to cassiterite deposition during the crystallization of Tur-2 and Tur-3.

Keywords

Tin deposits, hydrothermal alteration, Central Andean tin belt, Bolivia, petrography,
geochemical composition



Acknowledgments

First of all, I would like to thank my family for all the immense support they have given to me through my career path and the making of this thesis.

I would like to thank to all of my professors, specially to my thesis advisor, Dr. Lisard Torró i Abat, for trusting in me, giving me the opportunity to develop research in an area of my interest, sharing his knowledge, and giving me life lessons in the process. Also, my absolute gratitude goes to Dr. Matthieu Harlaux, my thesis co-advisor, for sharing his knowledge, experience, and support through this process. Additionally, I thank Dr. Jean Vallance for his participation in the expedition to the Central Andean tin belt in 2020 during which the studied samples were collected and Dr. Thierry Sempere for his remarkable collaboration in the polishing of the Geological Setting chapter of this thesis. Furthermore, I would like to thank Dr. Fredrik Sahlström and Dr. Diego Benites for their very valuable corrections for the defense of my thesis.

Finally, I thank my friends from the first semester and the ones from the Geological Engineering Program, who have always given to me their company, unconditional love, and support.

This study was economically supported by the Peruvian PROCENCIA-FONDECYT project 1122-2020 E041-2020-01-01 and the FAI-0009-2021 project granted by the Pontificia Universidad Católica del Perú (PUCP).

Table of contents

1. INTRODUCTION.....	1
1.1. Tourmaline as tracer of geological processes.....	1
1.2. The Central Andean tin belt: a major metalliferous province in the Andean highlands.....	3
1.3. Previous studies on tourmaline in ore deposits from the Central Andean tin belt.....	6
1.4. Conundrum.....	9
1.5. Objectives.....	10
1.6. Hypothesis.....	10
2. GEOLOGICAL SETTING.....	11
2.1. Geology of the Central Andes in Bolivia and southern Peru.....	11
2.2. Regional geology of the Central Andean tin belt.....	21
2.3. Geology of the Chacaltaya-Kellhuani-Milluni district.....	24
3. MATERIALS AND METHODS.....	29
3.1. Sampling and sample preparation.....	29
3.2. Analytical methods.....	29
3.2.1. Optical microscopy.....	29
3.2.2. Electron microprobe (EPMA)	29
4. RESULTS.....	31
4.1. Petrography.....	31
4.1.1. Chacaltaya stock.....	33
4.1.2. Chacaltaya greisen.....	34
4.1.3. Tourmaline breccia (granite cupola)	36
4.1.4. Cassiterite-bearing quartz-tourmaline veins.....	37
4.2. Mineral geochemistry.....	40

4.2.1. White mica.....	40
4.2.2. Tourmaline.....	42
5. DISCUSSION.....	49
5.1. Tourmaline stability in the Chacaltaya granitic stock.....	49
5.2. Tourmaline textures and environment of crystallization.....	52
5.3. Tourmaline chemistry as a tracer of hydrothermal fluid evolution.....	53
6. CONCLUSIONS.....	55
7. REFERENCES.....	57

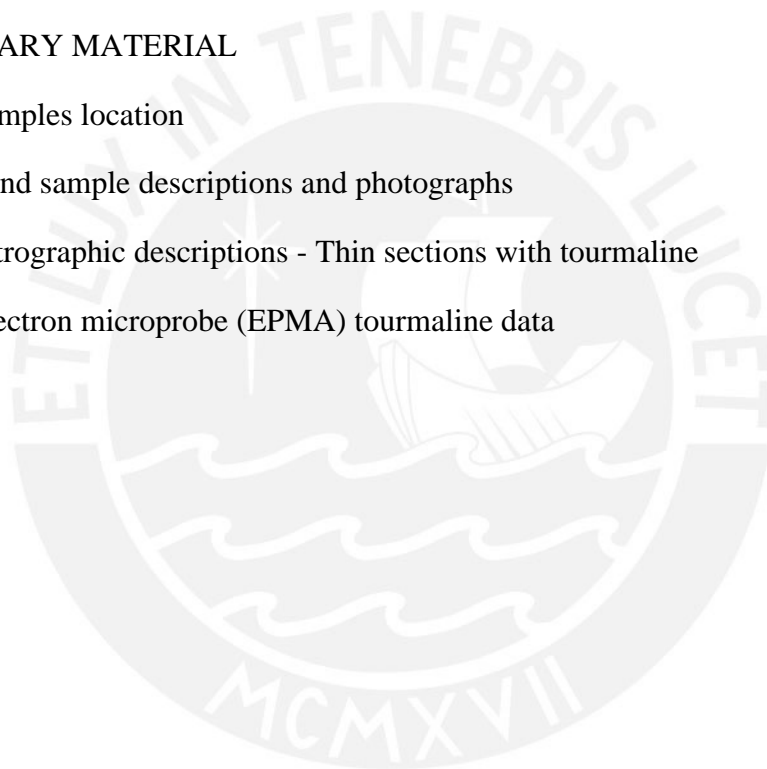
SUPPLEMENTARY MATERIAL

Appendix A: Samples location

Appendix B: Hand sample descriptions and photographs

Appendix C: Petrographic descriptions - Thin sections with tourmaline

Appendix D: Electron microprobe (EPMA) tourmaline data



Index of images

Figure 1. Map of the Central Andes showing the location of the Eastern and Western Cordilleras, the Altiplano, and the Central Andean tin belt.....	12
Figure 2. Tectonic evolution of the present-day western proto-margin of the Amazonian craton.....	18
Figure 3. Late Paleozoic igneous rocks and Late Permian-Triassic granites.....	20
Figure 4. Geological map of the Chacaltaya-Kellhuani-Milluni district and surrounding areas north of the City of La Paz.....	28
Figure 5. Tourmaline in different types of mineralization found in the Chacaltaya-Kellhuani-Milluni district.....	32
Figure 6. Photomicrographs illustrating petrographic features of the least altered samples at the Chacaltaya granitic stock.....	34
Figure 7. Photomicrographs illustrating petrographic features of the greisen in the Chacaltaya stock.....	35
Figure 8. Photomicrographs illustrating petrographic features of the tourmaline breccias.....	37
Figure 9. Photomicrographs illustrating petrographic features of the cassiterite-bearing tourmaline veins.....	39
Figure 10. Compositions of white micas from the greisen in the Chacaltaya stock.....	42
Figure 11. Compositional variation diagrams for the three petrographic types of tourmaline from the Chacaltaya-Kellhuani-Milluni district.....	45
Figure 12. Transmitted light photomicrograph (TL), backscattered electron image (BSE) and X-ray elemental maps for hydrothermal tourmaline (Tur-1) disseminated in a quartz-white mica greisen from Chacaltaya (2020-KELL-23-TS1).....	47
Figure 13. Transmitted light photomicrograph (TL), backscattered electron image (BSE) and X-ray elemental maps showing Discrete internal zoning and oscillatory zoning (specifically in the rim) in hydrothermal tourmaline crystal (Tur-1) surrounded by acicular tourmaline crystal aggregates (Tur-2) in a tourmaline breccia (2020-KELL-24-TS1).....	47
Figure 14. Transmitted light photomicrograph (TL), backscattered electron image (BSE) and X-ray elemental maps showing chemical zoning in hydrothermal tourmaline crystal (Tur-3) from the quartz-cassiterite-tourmaline veins (2020-KELL-01-A-TS1).....	48
Figure 15. Transmitted light photomicrograph (TL), backscattered electron image (BSE) and X-ray elemental maps showing chemical zoning in hydrothermal tourmaline crystal (Tur-3) from the quartz-cassiterite-tourmaline veins (2020-KELL-01-A-TS3).....	48

Index of tables

Table 1. Representative analyses of white micas from the greisen in the Chacaltaya stock, including chemical composition and structural formulae normalized to 11 atoms of O (EPMA data).....41

Table 2. Summary of the compositions for tourmaline group minerals from the Chacaltaya-Kellhuani-Milluni district including chemical composition and structural formula.....44



1. Introduction

1.1. *Tourmaline as tracer of geological processes*

Tourmaline supergroup minerals are, crystallographically, noncentrosymmetric and polar trigonal borosilicates (Hawthorne and Henry 1999) with a space symmetry group R3m (Hawthorne and Dirlam 2011). They show a variety of habits, including stubby, tabular, acicular, and fibrous (Hawthorne and Dirlam 2011). Their general chemical formula (Mills et al. 2009) can be written as:

$X Y_3 Z_6 [T_6 O_{18}] (B O_3)_3 V_3 W$, where:

X = vacancy, Na, K, Ca, Pb²⁺;
Y = Li, Mg, Fe²⁺, Mn²⁺, Cu, Al, V³⁺, Cr³⁺, Fe³⁺, Mn³⁺, Ti⁴⁺;
Z = Mg, Fe²⁺, Al, V³⁺, Cr³⁺, Fe³⁺;
T = Si, B, Al;
B = B;
V = OH, O, and
W = OH, F, O.

According to the IMA (2023), 37 tourmaline species are defined in terms of chemical composition, where the main criterion to differentiate them is the dominance of a specific chemical constituent at a particular crystallographic site. Tourmaline supergroup minerals show a wide spectrum of colors, such as black, brown, orange, blue, different tones of green and yellow, and purple to pink, but can also be colorless, and zoning is common (Hawthorne and Dirlam 2011). Color is determined by field transition element contents, intervalence charge transfer interactions, and color centers. Chromophore cations in tourmaline include Fe²⁺, Fe³⁺, Mn²⁺, Mn³⁺, Ti⁴⁺, Cu²⁺, and V³⁺ (Pezzotta and Laurs 2011).

The wide compositional range possible within the general chemical formula for tourmaline supergroup minerals reflects the flexibility of the structure to adjust

its composition in response to changing temperature and/or pressure conditions during crystallization (Dutrow and Henry 2011). This allows tourmaline to be stable over most conditions found in the crust (van Hinsberg et al. 2011a).

Several features make tourmaline supergroup species useful indicator minerals to trace evolving crystallization conditions and geologic processes. Firstly, they are stable over a wide P-T-X range and can precipitate in a variety of settings (magmatic, sedimentary, metamorphic, and hydrothermal; Dutrow and Henry 2011; van Hinsberg et al. 2011a, b). Tourmaline supergroup minerals may also accommodate a wide spectrum of geochemically contrasting elements in its crystal structure (Marschall and Jiang 2011). In addition, the chemical and isotope information is preserved because intracrystal element diffusion in the tourmaline lattice is negligible up to temperatures of 600 °C (van Hinsberg et al. 2011a). Lastly, tourmalines are chemically and physically robust during sedimentary transport, diagenesis, and metamorphism (Marschall and Jiang 2011).

Tourmaline occurs in various types of hydrothermal deposits such as volcanogenic massive sulfides (VMS), sedimentary-exhalative (SEDEX), iron oxide-copper-gold (IOCG), mesothermal Au, porphyry Cu ± Mo ± Au, granite-related Sn-W and U deposits (Slack and Trumbull 2011). Besides hydrothermal deposits, gemstone tourmaline can be found in pegmatites (most commonly in those of the B-enriched LCT family) or in rare-metal (Ta, Li, Cs) granites (London 2008; Pezzotta and Laurs 2011; Slack and Trumbull 2011). Its widespread occurrence in a variety of mineral deposits makes tourmaline a useful exploration tool (Jiang 1998; Slack and Trumbull 2011; Trumbull et al.

2019; Zheng et al. 2019; Harlaux et al. 2021a; Li et al. 2022). For example, Grzela et al. (2019) and Sciuba et al. (2021) used tourmaline composition to constrain provenance in exploration for orogenic gold deposits since, according to these authors, tourmaline in this deposit type most commonly belongs to the alkali group, has a dravitic composition, and has higher contents of Sr, V, and Ni and low Zn, Cu, Sn, Pb, Li, Be, Ga, Sn, Nb, Ta, U, and Th compared to tourmaline from other deposit types and geological environments. Sciuba et al. (2021) determined that Sr/Sn vs. V/Nb, Sr/Li vs. V/Sn, Sr/Sn vs. V/Be, and Sr/Sn vs. Ni/Nb binary plots discriminate tourmaline from orogenic gold deposits from tourmaline from other mineralization styles. Li et al. (2022) proposed the (Sn + Li) vs. (Ni + V + Zn), (Σ REE + Y + Zr) vs. (Ni + V + Zn) and V vs. Zn plots to discriminate tourmaline crystallized in granitic rocks, IOCG deposits, orogenic gold deposits, and porphyry deposits. These authors concluded that tourmaline from porphyry deposits, including their study case in the Bilihe porphyry Au deposit in Inner Mongolia, China, yields particular signatures that include high Y, Zr, and REE, moderate Ba, Sn, Nb, Ta, and Ni, and low Zn contents.

1.2. The Central Andean tin belt: a major metalliferous province in the Andean highlands

The Central Andean tin belt has an approximate extension of 900 km and reaches a maximum width of 150 km near Potosí in Bolivia. It stretches through Bolivia from SE Peru to NW Argentina (Fig. 1; Ahlfeld 1967; Turneure 1971; Grant et al. 1979). Magmatic-hydrothermal mineralization in the Central Andean tin belt is associated with Triassic and Cenozoic, felsic to intermediate,

plutonic, and subvolcanic stocks, which intruded into metasedimentary and sedimentary rocks, as described in Section 3.2 below.

This metallogenic belt has produced 14% of the historic world tin output until 2021 (Lehmann 2021). Since the 16th century, when the Cerro Rico de Potosí Ag deposit was discovered, hundreds of Sn-W-(Ag) deposits have been mined in the Central Andean tin belt, including some world-class deposits such as Llallagua, Cerro Rico de Potosí, and Oruro in Bolivia and San Rafael in Peru (Mlynarczyk and Williams-Jones 2005). In the first half of the 20th century, when the demand for tin exceeded that for silver (Espinoza 2010), tin mining in Bolivia was dominated by three businessmen, the so-called “Barones del Estaño”, namely Patiño, Hochschild, and Aramayo. By 1952, the government had nationalized the mines (Espinoza 2010). By 1990, COMIBOL (a Bolivian Mining state-owned corporation) became an intermediary for foreign companies to exploit mines (Espinoza 2010). Huanuni and Colquiri are the only mines that still operate under the administration of COMIBOL.

According to the International Tin Association (ITA 2020), tin production in 2019 in the Central Andean tin belt (including Peru, Bolivia, and Argentina) amounted to 37 000 t, and reserves summed up to 469 000 t. Currently, the main tin producer in the Central Andean tin belt is the San Rafael mine, operated by the company MINSUR. According to MINSUR reports, from 1969 to 2019, the San Rafael mine produced about 26 608 700 t ore averaging 3.7% Sn (MINSUR S.A. 2020). In 2019, there was a total production of 20 273 t of Sn, and in 2020 production was 20 648 t of Sn (MINSUR S.A. 2021). MINSUR (2021) reports

estimated reserves (including underground and stockpiles) of 6.1 Mt ore at 2.14% Sn.

In Bolivia, the Llallagua deposit totals a historical production estimated between 0.5 and 1 Mt Sn (Redwood and Rice 1997), which ranks it among the world's largest hard-rock tin deposits. Currently, the largest tin producer in Bolivia is the Huanuni deposit, operated by Empresa Minera Huanuni belonging to COMIBOL. Empresa Minera Huanuni, created in 1987, produced 7 073 t of tin concentrate in 2019 and 5 469 t in 2020 from the Huanuni deposit (ITA 2021). In 2018, the total reserves increased to 7 597 516 t ore for a mine lifetime of 8 years; including resources, the mine lifetime is estimated at 18 years (COMIBOL 2018). At the beginning of May 2021, Huanuni started operating the Lucianita processing plant, which aims to increase the processing capacity up to 3 000 t per day.

Beyond tin, the Central Andean tin belt hosts the world's largest silver deposit, Cerro Rico de Potosí, accounting for at least 86 000 t (2 800 Moz) of Ag production prior to colonial exploitation (Sillitoe et al. 1998; Sillitoe 2004). Cerro Rico de Potosí's cumulative production has exceeded 2 Goz Ag and 100 000 t Sn since 1544 (Rice et al. 2005). In addition to base and precious metals, relatively high contents of In (up to 10 wt.%), a critical raw material according to the European Commission (2020) and the United States Geological Survey (2020), have been described in several ore deposits from Bolivia (Ishihara et al. 2011; Cacho et al. 2019; Torres et al. 2019; Torró et al. 2019a,b) and Argentina (Ishihara et al. 2011; Márquez-Zavalía et al. 2020).

1.3. *Previous studies on tourmaline in ore deposits from the Central Andean tin belt*

Tourmaline is conspicuous in most mineral deposits and associated intrusive rocks along the Central Andean tin belt (Lindgren 1926; Ahlfeld 1967; Kelly and Turneure 1970; Grant et al. 1979; McBride et al. 1983; Lehmann 1985; Sugaki and Kitakaze 1988; Lehmann et al. 1990, 2000; Columba and Cunningham 1993; Dietrich et al. 2000; Heuschmidt et al. 2002; Kontak and Clark 2002; Mlynarczyk and Williams-Jones 2006; Betkowski et al. 2017; Harlaux et al. 2020, 2021a,b; Gemmrich et al. 2021). The ubiquitous presence of tourmaline along the Central Andean tin belt is correlated with a high activity of B (and other volatile elements) in the magmatic-hydrothermal systems (Dietrich et al. 2000; Lehmann et al. 2000; Müller et al. 2001). In the classical study by Kelly and Turneure (1970), tourmaline is described as typical in tin ores related to the altered wall rock bordering cassiterite veins. At Llallagua, these authors described sheeted zones bordered by dark-colored tourmalinized porphyry and breccia dikes replaced by tourmaline, both cut by tin-bearing veins. At Morococala, a large, elongated body of tourmalinized and silicified greywackes concentrates narrow transverse tin-bearing veins (Kelly and Turneure 1970). In the same locality, it was suggested that disseminated cassiterite occurs in the altered wall rock and minor tourmaline accompanies quartz during the early veining stage (Kelly and Turneure 1970). Tourmaline is mostly related to high-temperature hydrothermal alteration and hence concentrates in magmatic-hydrothermal centers associated with granitic cupolas or apophyses (Lehmann 1985; Lehmann et al. 2000).

Detailed petrographic and geochemical studies on tourmaline are available for the San Rafael deposit. The studies of Mlynarczyk and Williams-Jones (2006)

and Harlaux et al. (2020, 2021a) described tourmaline deposited during magmatic and hydrothermal stages in this deposit. Mlynarczyk and Williams-Jones (2006) discriminated three main stages of tourmaline deposition: magmatic and early post-magmatic, early hydrothermal, and syn-ore. According to these authors, the magmatic tourmaline is related to the evolved phase of the plutons and forms small (40–400 μm), yellow (in thin section), euhedral to subhedral prismatic crystals that are disseminated throughout the plutonic rock; in contrast, early post-magmatic tourmaline, which replaced cordierite, can be distinguished by its blue color (in thin section). Early hydrothermal tourmaline is the most abundant in the deposit. It appears as yellow, colorless, and blue (in thin section) fine-grained, short-prismatic to acicular crystals hosted by dyke-like tourmaline–quartz microbreccias – both in the clasts and the matrix –, early veins and their alteration haloes, and as replacement of mafic minerals and feldspar in granitic assemblages. Ore-stage tourmaline crystallized along with abundant cassiterite as open-space infills in veins surrounded by chlorite haloes; within the veins, tourmaline grades inward from massive orange-colorless (in thin section) to green and finally to khaki-green to dark-green acicular crystals. Likewise, Harlaux et al. (2020, 2021a,b) discriminated three generations of tourmaline in the San Rafael deposit corresponding to i) late magmatic tourmaline (Tur 1) forming nodules of brown-orange, anhedral to subhedral millimeter-sized grains (Tur 1a) and millimeter-sized greenish to orange-brownish, euhedral to subeuhedral grains as disseminations in peraluminous granites (Tur 1b); ii) pre-ore hydrothermal tourmaline (Tur 2), which is the volumetrically most abundant and occurs as orange brownish to bluish subhedral sub-millimetric crystals that appear as

phenocryst replacement (Tur 2a), and orange-brown to green and acicular, subeuhedral crystals ranging from 100 μm up to several millimeters in size that infill open space in veins (Tur 2b), and fine-grained randomly orientated brown grains infilling open space in breccias (Tur 2c); and iii) syn-ore hydrothermal tourmaline (Tur 3) forming pale to dark blue (Tur 3a) or green (Tur 3b) microscopic veinlets and overgrowths.

The composition of most of the samples tested by Mlynarczyk and Williams-Jones (2006) and Harlaux et al. (2020) corresponds to dravite $[\text{NaMg}_3\text{Al}_6[\text{Si}_6\text{O}_{18}](\text{BO}_3)_3(\text{OH})_3(\text{OH})]$ –schorl $[\text{NaFe}^{2+}_3\text{Al}_6[\text{Si}_6\text{O}_{18}](\text{BO}_3)_3(\text{OH})_3(\text{OH})]$ solid-solution series, extending toward the alkali-free (Mg-foitite $[\square(\text{Mg}_2\text{Al})\text{Al}_6[\text{Si}_6\text{O}_{18}](\text{BO}_3)_3(\text{OH})_3(\text{OH})]$ and foitite $[\square(\text{Fe}^{2+}_2\text{Al})\text{Al}_6[\text{Si}_6\text{O}_{18}](\text{BO}_3)_3(\text{OH})_3(\text{OH})]$) and “oxy-tourmaline” (oxy-dravite $[\text{Na}(\text{Al}_2\text{Mg})(\text{Al}_5\text{Mg})[\text{Si}_6\text{O}_{18}](\text{BO}_3)_3(\text{OH})_3\text{O}]$ and oxy-schorl $[\text{Na}(\text{Fe}^{2+}_2\text{Al})\text{Al}_6[\text{Si}_6\text{O}_{18}](\text{BO}_3)_3(\text{OH})_3\text{O}]$) end-members. Major element composition of late-magmatic tourmaline (Tur 1 in Harlaux et al. 2020, 2021a,b) is relatively homogeneous (dravitic), and the composition of Tur 2 overlaps those of Tur 1, thus suggesting a continuum in the evolution of physical-chemical conditions during the magmatic-hydrothermal transition. Compositions of Tur 3 are mostly schorl-foitite. The great compositional change between Tur 2 and Tur 3 suggests temperature and salinity decrease.

Trace element analysis of tourmaline from San Rafael performed by Harlaux et al. (2020) showed contrasting composition for Tur 1 and Tur 2, which both yield high Li, K, Mn, Zn, and light REE (LREE) contents, and Tur 3, which yields high Sr and heavy REE (HREE) contents. According to these authors, the progressive decrease of Eu/Eu* ratio (from 20 to 2) (quantified by the ratio

$(\text{Eu}/\text{Eu}^*)_{\text{N}} = \text{Eu}_{\text{N}}/(\text{Sm}_{\text{N}} \times \text{Gd}_{\text{N}})^{0.5}$, where N corresponds to the chondrite normalization), and increasing Sn contents (from 10s to >1,000 ppm) from Tur 1 to Tur 3 reflect the evolution of the magmatic-hydrothermal system from reducing to more oxidizing conditions.

In situ O and B isotope analysis of tourmaline from San Rafael performed by Harlaux et al. (2021a) showed that late-magmatic (Tur 1) and pre-ore hydrothermal (Tur 2) tourmaline have similar $\delta^{18}\text{O}$ (10.6‰ to 14.1‰) and $\delta^{11}\text{B}$ (-11.5‰ to -6.9‰) values while syn-ore hydrothermal tourmaline (Tur 3) has lower $\delta^{18}\text{O}$ (4.9‰ to 10.2‰) and in part higher $\delta^{11}\text{B}$ (-9.9‰ to -5.4‰) values. With these results, the authors interpreted that Tur 1 and Tur 2 formed in an evolving magmatic-hydrothermal system, while Tur 3 recorded a mixing between a Sn-rich magmatic brine and meteoric waters.

1.4. *Conundrum*

Different studies have proven that tourmaline is a useful tracer of geological processes. In the Central Andean tin belt, tourmaline is conspicuous, used to decipher the evolution of magmatic and hydrothermal systems (Mlynarczyk and Williams-Jones 2006; Harlaux et al. 2020, 2021a). Regardless, no detailed study of tourmaline has been conducted in the Chacaltaya-Kellhuani-Milluni district. A study of the petrography and geochemistry of the tourmaline in this district will provide further understanding of the evolving conditions during the crystallization of tourmaline and associated cassiterite mineralization.

1.5. Objectives

General objective:

To constrain evolving conditions of the mineralizing fluids in the Chacaltaya-Kellhuani-Milluni district from textures and major element composition of tourmaline.

Specific objectives:

1. Petrographically determine textures of tourmaline and its paragenetic relationship with ore and other hydrothermal alteration phases;
2. Analyze the major and minor element composition of tourmaline; and
3. Constrain the environment of crystallization and the evolution of hydrothermal fluids connected to tourmaline deposition.

1.6. Hypothesis

In the Chacaltaya-Kellhuani-Milluni district, different petrographic types of tourmaline may occur, each with different geochemical features. Tourmaline petrographic types deposited coevally with cassiterite are expected, providing direct insights into the conditions and processes associated with ore formation. The different petrographic and geochemical features of tourmaline petrographic types can be connected to an evolving hydrothermal system.

2. Geological setting

2.1. *Geology of the Central Andes in Bolivia and southern Peru*

The Andes may be subdivided into three segments: the Northern, Central, and Southern Andes (e.g., Wörner et al. 2018a; Kay and Mpodozis 2020). The Central Andes formed as the result of a long-lived, quasi-continuous east-dipping subduction of the Nazca (and precursor Farallón) plate beneath the western margin of South America since at least the Early Jurassic (Mégard 1984; Ramos 2018; Kay and Mpodozis 2020), and probably since as early as the Late Paleozoic (Mišković et al. 2009). The Central Andes *sensu stricto* (~3° to 33° S), where the study zone is located, comprises three morphotectonic provinces, which from east to west are the Eastern Cordillera (Cordillera Oriental), the Altiplano, and the Western Cordillera (Cordillera Occidental) as shown in Figure 1 (Ahlfeld 1956; Jenks 1956; James 1971a; Suárez-Soruco 2000; Wörner et al. 2018a). In addition, the deformed Sub-Andean Belt morphotectonic unit serves as a tectonic transition between the Eastern Cordillera and the nearly undeformed Amazonian lowlands to the east (e.g., Roeder and Chamberlain 1995; Sempere 1995; Baby et al. 2018). In its central portion, the Andes – and the coast and trench at the same latitudes – bend ~45° in the so-called Bolivian or Central Andean orocline, with the northern branch trending NW-SE and the southern branch trending N-S.

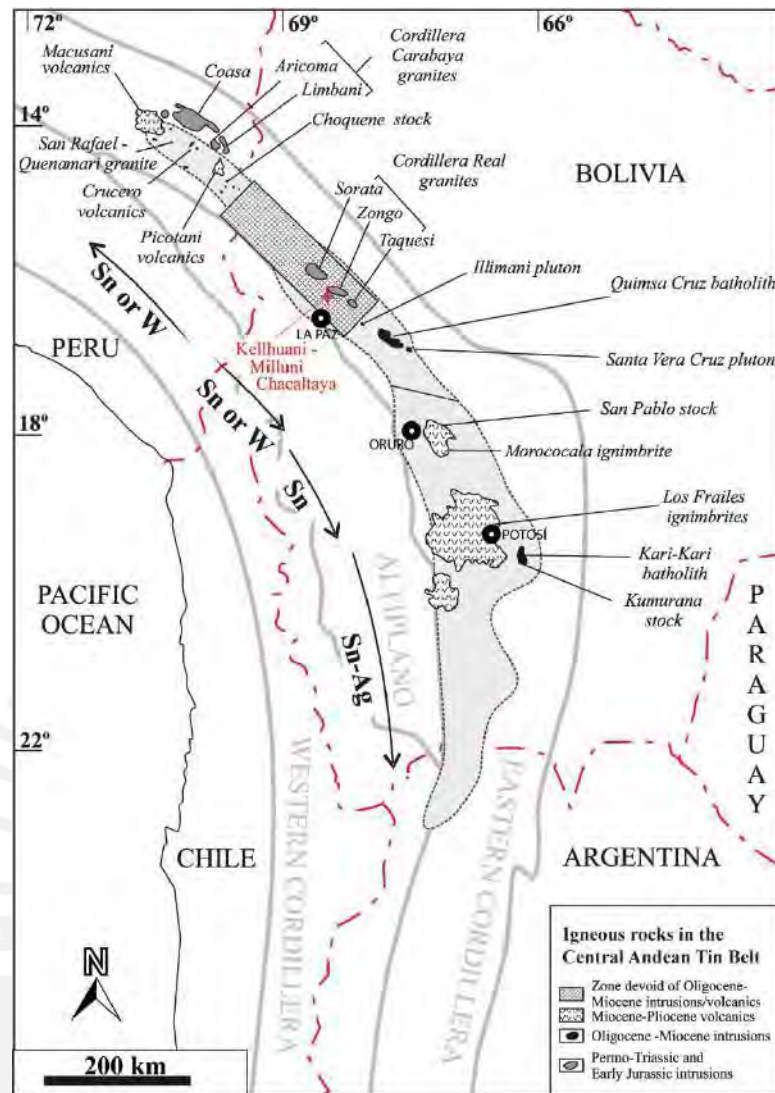


Figure 1. Map of the Central Andes showing the location of the Eastern and Western Cordilleras, the Altiplano, and the Central Andean tin belt (light grey color) as well as the location of the main plutons and volcanic deposits along this metallogenic province. Modified from Mlynarczyk and Williams-Jones (2005).

In the Western Cordillera, subduction-related intermediate and felsic volcanic and plutonic rocks have intruded into and extruded over deformed Mesozoic to Cenozoic sedimentary and volcanic rocks (James 1971a,b; Kono et al. 1989). Sempere and Jacay (2008) defined the Western Cordillera and Altiplano as the ‘magmatic Andes’. These authors argue that in the western Andes, tectonic shortening was local and subordinate to arc-related magmatic mass transfer, from mantle to crust, as the main cause of crustal thickening. This idea contrasts with

those exposed by other authors, who suggest that compressive events have largely modeled the Western Cordillera during the Incaic (Eocene and early Oligocene) and the Pliocene stage of the Quechua orogeny mostly through the reactivation of older structures formed during previous orogenic events (e.g., Mégard 1984; Richter et al. 1975; Carlotto 2013). Geomorphological and isotopic evidence indicates that the Western Cordillera reached its modern elevation by ca. 16 Ma (Saylor and Horton 2014). The crest of the Western Cordillera is dominated by a ~100-km-wide volcanic mountain chain at high altitude. It includes the active Central Volcanic Zone located between the modern volcanically inactive Peruvian and Chilean flat-slab segments to the north and south (Kay and Mpodozis 2020).

At the latitudes of the Central Andes in Bolivia, southern Peru, and northernmost Chile (~15° to 22° S), the Altiplano (which comprises the northern part of the Altiplano-Puna plateau stretching ~15° to 28° S; Kay and Mpodozis 2020) separates the Eastern and Western cordilleras. The Altiplano is an internally drained plateau between 3600 and 4100 m. It comprises a series of intermontane basins covered by Cenozoic volcanic and sedimentary deposits and mostly overlying Paleozoic sedimentary rocks over a Precambrian basement (Richter et al. 1975; Wörner et al. 2018a; Kay and Mpodozis 2020). The Puna-Altiplano plateau has been the locus of the latest Oligocene to modern volcanism, including the formation of large ignimbrite plateaus such as the Los Frailes Volcanic Complex in Bolivia (Schneider 1985; Keller 2010; Kato 2013; Wörner et al. 2018b; de Silva and Kay 2018). Progressively younger ages of plateau ignimbrites to the south have been interpreted as the result of steepening of the subducting Nazca plate following the north-to-south passage of the aseismic Juan Fernández ridge (de Silva and Kay 2018). The Altiplano plateau, with a prominent crustal

thickness of 60-65 km (Beck et al. 1996), underwent major uplift after 10 Ma (Schildgen and Hoke 2018 and references therein). Its structure and origin are still under discussion. Husson and Sempere (2003) proposed that the crustal thickening and uplift of the Altiplano is driven by a lateral flow from adjacent overthickened Eastern and Western cordilleras. Kay and Mpodozis (2020) suggest that asthenospheric mantle rising and melting in a widening mantle wedge favored ductile deformation of a hot crust during compressional shortening in the late Oligocene and Miocene. Additional mechanisms invoked to contribute to the topographic growth of the Altiplano plateau include magmatic additions (de Silva and Kay 2018; Kay and Mpodozis 2020) and delamination of the lower crust and ensued isostatic uplift (Wörner et al. 2018a). Considering this relatively rapid and recent (i.e., after 10 Ma; Schildgen and Hoke 2018) uplift and the fact that sedimentary units younger than ca. 10 Ma are mostly undeformed (Kay and Mpodozis 2020) after 10 Ma tectonic shortening contributed apparently little to the uplift of the Altiplano.

The Eastern Cordillera, which hosts the Central Andean tin belt, exposes diverse strata, including a ~10-km-thick polydeformed and locally metamorphosed Ordovician, Silurian, and Devonian marine sequence discordantly overlain by Jurassic and Cretaceous marine and nonmarine sedimentary rocks (Sempere 1995; Sempere et al. 1997; Suárez-Soruco 2000). Igneous rocks were emplaced in the Eastern Cordillera during several intervals from the Late Mesoproterozoic until the Miocene (Suárez-Soruco 2000; Chew et al. 2007, 2016; Mišković et al. 2009). The Eastern Cordillera is referred by Sempere and Jacay (2008) as the “tectonic Andes”. It has been formed by the inversion and shortening of a Late Permian – Middle Jurassic rift system since the Oligocene (Sempere et al. 1990, 2002, 2008;

Gillis et al. 2006; Ramos 2018). Crustal thickening and uplift were most intense during the late Oligocene and early Miocene, particularly in the Central Andean area, where the crust is the thickest (>70 km; James 1971a; Beck et al. 1996; Sempere et al. 2008; Gibert et al. 2020) and compression continues to the present day. The Cenozoic formation of the Eastern Andes was concomitant with the bending of the orogen and trench along the Bolivian orocline. This bending might have resulted from differential along-strike plate coupling driving to domains with contrasting shortening in the upper plate, the formation of stress belts in the upper-plate interior propagating to the Eastern Cordillera, and the widening of the Central Andes (Sempere et al. 1990; MacFadden et al. 1995; McQuarrie 2002; Arriagada et al. 2008; Maffione et al. 2009; Capitanio et al. 2011; Hu et al. 2021). Recent works that attest to significant post-Miocene to recent uplift in the Eastern Andes include Lease et al. (2013) and Whipple and Gasparini (2014).

Rocks cropping out in the Eastern Cordillera of Peru and Bolivia have recorded 1.1 G.y. of intermittent magmatism. Plutonism developed during several orogenic and post-orogenic/rifting episodes affecting the Western Amazonia continental margin (Chew et al. 2007, 2016; Mišković et al. 2009; Ramos 2018 and references therein). Early to middle Carboniferous continental arc-related magmatism formed an intrusive belt composed of calc-alkaline granodioritic and granitic batholiths along the western margin of Gondwana, which is now exposed throughout the south-central and northern Peruvian segment of the Eastern Cordillera (Mišković et al. 2009). Mišković et al. (2009) interpreted that Middle Pennsylvanian cessation of arc magmatism in the Eastern Cordillera of Peru was connected to a shallow-subduction episode.

Magmatism was initiated in the Late Permian to Late Triassic (250–190 Ma) slightly inboard of the Carboniferous arc (Fig. 3). Plutonism in this stage is characterized by the emplacement of dominantly peraluminous granitic batholiths along the Eastern Cordillera and a southward younging trend from central Peru to NW Bolivia (Mišković et al. 2009). The Triassic (~240 - ~220 Ma) granitic rocks are located in the Cordillera Real of Bolivia (Gillis et al. 2006; Cordani et al. 2019; Iriarte et al. 2021), including those that are genetically connected with the magmatic-hydrothermal Sn-Zn-Pb mineralization at the Chacaltaya-Kellhuani-Milluni district (Lehmann et al. 1990; Gemmrich et al. 2021). The emplacement of these granitic rocks can be interpreted as a major Late Permian to Middle Jurassic magmatism across the central Eastern Cordillera during post-orogenic extensional collapse caused by the dismembering of Pangea (Kontak et al. 1985; Sempere et al. 2002; Mišković et al. 2009). Extensional conditions resulted in the development of a regional-scale rift system across the western margin of Pangea that is recorded in the present-day territories of Colombia, Ecuador, Peru, Bolivia, Argentina, and Chile (Fig. 3; Spikings et al. 2016 and references therein). In the Central Andes, rifting led to diachronic lithospheric thinning propagating from central Peru in the Middle Triassic (ca. 145-140 Ma; Spikings et al. 2016) into Bolivia in the Late Triassic – Middle Jurassic along what was to become the axis of the Eastern Cordillera (Fig. 3; Sempere et al. 2002) and, unlike in the northern Andes, rifting was aborted before oceanic lithosphere formed (Spikings et al. 2016). Noble et al. (1978) and Reitsma (2012) proposed that such rifting occurred in a back-arc basin. However, the conspicuous lack of arc-related rocks in outcrops of this age at the latitudes of present-day Peru and Bolivia may be interpreted as the existence of a continental rift system (Mišković et al. 2009;

Spikings et al. 2016). Mišković et al. (2009) proposed that the shift from arc-related to post-orogenic non-arc magmatism was primarily connected to the early Permian counterclockwise block rotation that would have resulted in a highly oblique subduction of the proto-Pacific Panthalassic ocean beneath the western margin of Gondwana (Fig. 2a, b). This change in plate dynamics would have led to the development of strike-slip tectonics across the upper plate continental margin; concomitantly, the drastic diminution of the orthogonal subduction component and the oceanward continental margin concavity (Fig. 2c) would have resulted in a southward-propagating slab rollback and, ultimately, in the eventual slab detachment as a consequence of slab weakening by thermal diffusion (see also Franzese and Spalletti 2001). Syn-rift depocenters were filled with volcano-sedimentary sequences (Mitu Group in Peru; Lower Serere Group in Bolivia) in which dominantly subaerial siliciclastic sedimentary rocks are intercalated with bimodal peralkaline pyroclastic deposits and alkaline basaltic lava flows (Kontak et al. 1990; Soler and Sempere 1993; Sempere et al. 2002; Mišković et al. 2009; Spikings et al. 2016).

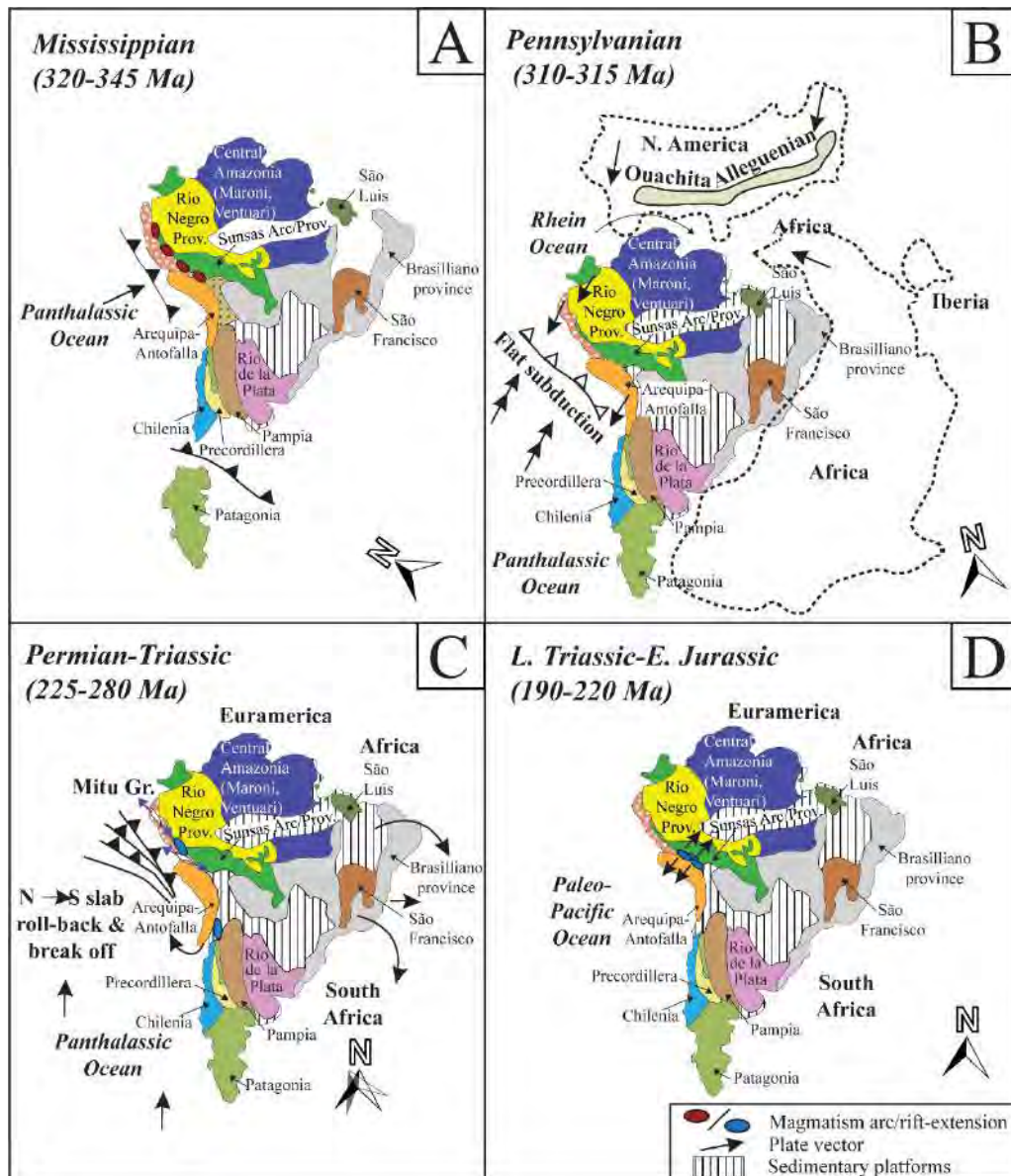


Figure 2. Tectonic evolution of the present-day western proto-margin of the Amazonian craton. In C, dashed areas represent non-Gondwanan domains. Modified from Mišković et al. (2009).

The emplacement of plutonic rocks in the upper crust is interpreted as derived from crustal anatexis induced by high heat flow during crustal thinning and asthenospheric mantle upwelling in a widening mantle wedge, and the profuse production and underplating of mantle-derived basic magmas during the Mitu (or regionally equivalent) rifting (Kontak et al. 1985, 1990; Farrar et al. 1990;

Mišković et al. 2009; Spikings et al. 2016). In addition, their isotopic compositions suggest that these anatectic crustal melts mixed with a juvenile component, namely the cogenetic alkaline and sub-alkaline intra-plate (Mitu) mantle-derived melts (Spikings et al. 2016). The fact that some peraluminous Late Triassic granites (e.g., Zongo–Yani pluton in Bolivia; Limacpampa pluton in Peru) are foliated points to deformation contemporaneous with their emplacement; in addition, for the Zongo-Yani pluton it was determined that its emplacement was synchronous with low-pressure metamorphism and development of schistosity in the intruded Paleozoic shales and quartzites, with a high heat flow and a thermal structure centered on the granite (Bard et al. 1974).

In the Eastern Cordillera, Late Permian-Triassic granite plutons are exposed between 10° S and 17° S (Fig. 3) and crop out more extensively in the Cordillera Real of Bolivia (including the Huato, Illampu, Yani, Huayna Potosí, Zongo, and Taquesi batholiths; Gillis et al. 2006; Cordani et al. 2019) and the contiguous Cordillera de Carabaya in Peru (including the San Gabán, Coasa, Limbani, and Aricama plutons; Kontak et al. 1985, 1990; Mišković et al. 2009). In addition, volumetrically significant Triassic magmatism is recorded in Cordillera de Andahuaylas in southern Peru (Spikings et al. 2016). It is noteworthy that south of 17° S, where the Andean shortening and/or rift inversion is more distributed (Sempere et al. 2002), only NW- to N-oriented alkaline and tholeiitic basaltic dykes of Triassic to Cretaceous ages crop out (Fig. 3; Soler and Sempere 1993; Sempere et al. 2002). Peraluminous Triassic granitoids intruding Paleozoic rocks “reappear” in the northernmost tip of Peru extending to contiguous Ecuador within the Amotape-Tahuín geotectonic domain across the Peruvian Cordillera de la

Costa morphotectonic unit (Fig. 3; Litherland et al. 1994; Ulrich 2005; Sánchez et al. 2006; Bellido et al. 2009; Espinoza et al. 2021; Espinoza 2021).

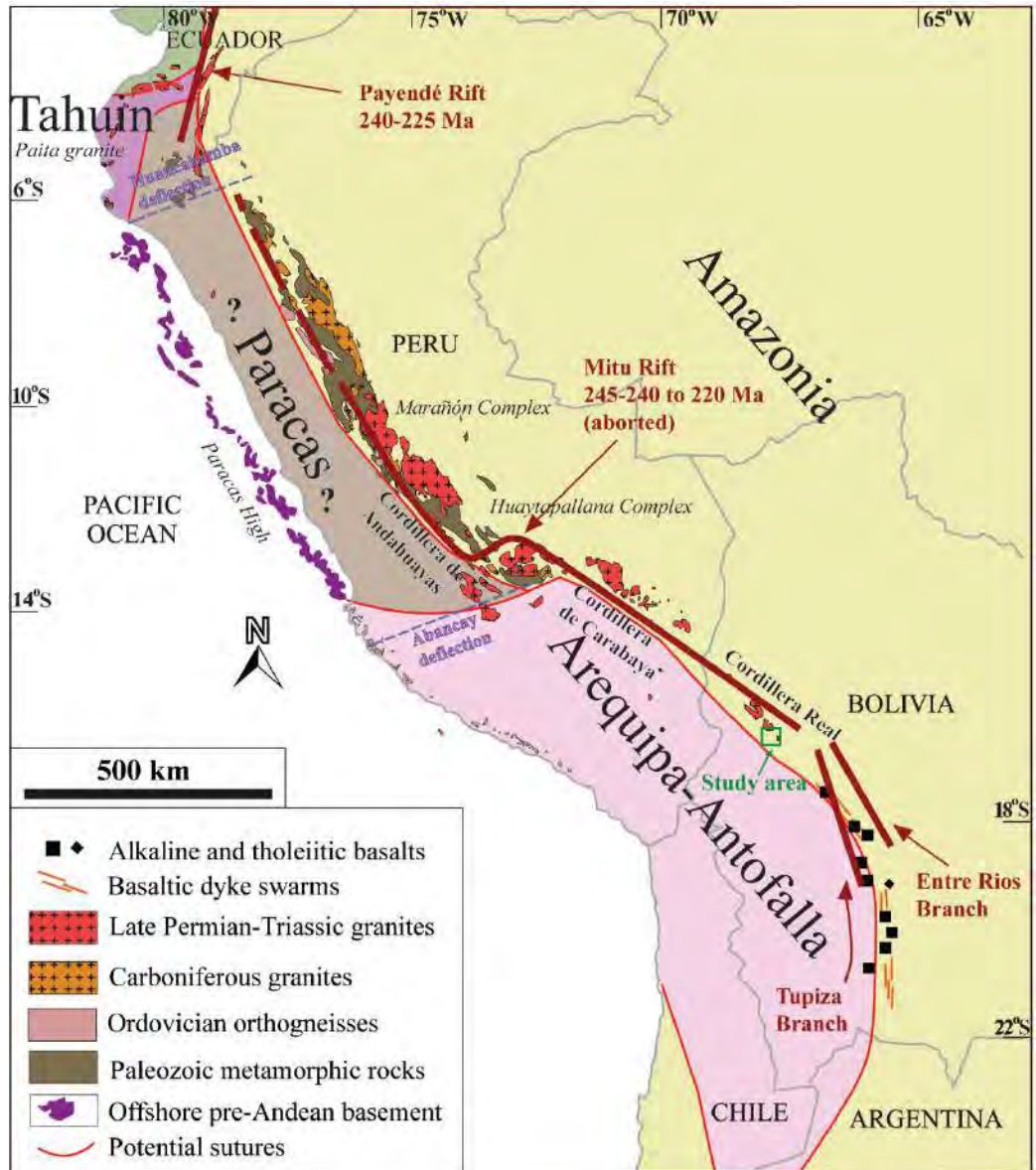


Figure 3. Late Paleozoic igneous rocks and Late Permian-Triassic granites. The outline of the Arequipa terrane is based on Carlier et al. (2005) and Mamani et al. (2008, 2010); other boundaries are based on Ramos (2008, 2009, 2018) and Carlotto et al. (2009). Triassic granitoids/ plutons extracted from Miskovik et al. (2009), Chew et al. (2016), Spikings et al. (2016), and Ramos (2018). Paita granite extracted from Espinoza (2021) and Espinoza et al. (2021). State of the art discussion on the presence of Sialic Paracas basement can be found in Chew et al. (2016).

2.2. *Regional geology of the Central Andean tin belt of Bolivia*

Mineralized belts are distributed roughly parallel to the three Andean morphotectonic units described above. At the latitude of La Paz, Bolivia, these belts include, from west to east, porphyry Cu-Mo±Au deposits (Western Cordillera), high-sulfidation Au and porphyry Au-(Cu) deposits (Altiplano), and porphyry Sn-W-Bi-Sb-Ag-Au deposits and polymetallic deposits (Eastern Cordillera) (Sillitoe 2004; Mlynarczyk and Williams-Jones 2005; Fontboté 2018).

The interaction between the Farallon/Nazca and South American plates governed the petrogenesis of ore-related magmatism and tectonic triggers to ore mineralization (Lehmann 1982, 2004; Lehmann et al. 1990; Sandeman et al. 1995; Sillitoe 2004; Mlynarczyk and Williams-Jones 2005; Fontboté 2018).

The Central Andean tin belt is located along the Eastern Cordillera, stretching over >900 km mostly across Bolivia, with short extensions into northernmost Argentina and SE Peru (Fig. 1). The Central Andean tin belt contains various world-class granite- and porphyry-related tin-bearing systems and is known for its exceptional Sn, Ag, W, and base metal endowment (Ahlfeld 1967; Lehmann et al. 2000; Mlynarczyk and Williams-Jones 2005). Outside the Central Andean tin belt, only a few scattered tin deposits and showings have been found in Argentina (Vil Achay deposit; Lehmann et al. 1990), Chile (Capitana Mine, Arica; Zentilli et al. 2018), and central Peru (i.e., Ayawilca deposit, Pasco; Benites et al. 2022).

The location of the Central Andean tin belt coincides with the central segment of the arcuate mountain range, where the crust and lithosphere are thickest (Mlynarczyk and Williams-Jones 2005). The Bolivian orocline divides the belt into two segments: a southern branch, trending N-S, and a northern branch, trending NW-SE (Ahlfeld 1967; Lehmann 1982, 2004; Lehmann et al. 1990,

2000; Sillitoe 2004; Mlynarczyk and Williams-Jones 2005; Maffione et al. 2009).

In the northern branch, mineralization consists mainly of Sn-W veins and stratabound ores, which are related to batholiths of Triassic and Oligocene age; in the southern branch, mineralization is Miocene and consists mainly of Sn, Sn-W, and Sn-polymetallic veins formed in epithermal and xenothermal environments (Mlynarczyk and Williams-Jones 2005).

Two major periods of Sn-W-polymetallic mineralization have been identified in the Central Andean tin belt: a mid-Triassic to Early Jurassic period, which is mostly restricted to the Cordillera Real of Bolivia, and a latest Oligocene-Miocene period, which comprises most of the ore deposits and affected the entire belt (Turneure 1971; Sillitoe et al. 1975; Gemrich et al. 2021). Both periods of tin ore deposition are connected to S-type, peraluminous granitic magmatism belonging to the reduced, ilmenite-bearing series (Lehmann et al. 1990; Lehmann 2004; Mlynarczyk and Williams-Jones 2005). The granitic melts resulted from partial melting of a 10–15 km-thick succession of carbon- and boron-rich, pelitic strata of early to Middle Paleozoic (Late Cambrian to Silurian) age, with an up to 30% mantle component. Lehmann et al. (2000) analyzed melt inclusions in quartz phenocrysts from the Central Andean tin belt porphyries, as they are considered to represent a pre-eruptive stage of the magmatic system, and determined that the silicate melt was enriched in incompatible lithophile elements (e.g., Rb, Li, Cs, B, As and Sn), which may be attributed to extended fractional crystallization (Sugaki et al. 1981; Lehmann et al. 1990, 2000; Lehmann 2004). Dietrich et al. (2000) and Lehmann et al. (2000) propose that these evolved melts mixed with primitive melts within the underlying magma chambers previous to shallow emplacement. Harlaux et al. (2021b), using geochemical and petrological data from the San

Rafael intrusive complex, also concluded that the ore deposition resulted from an injection of high-temperature mantle-derived mafic melts into a reduced, fractionated magma reservoir, which exsolved the Sn-(Cu)-rich magmatic fluids that later ascended into the granitic cupola and mixed with meteoric waters. High magma boron and carbon contents due to partial melting of the shale sequences would have had a control on magma evolution by providing a low oxidation state (below the pyrite-magnetite-pyrrhotite buffer during the tin ore stage) and depressing the solidus temperature of the fractionated melt, which is necessary for the formation of a tin ore system (Eugster 1986; Lehmann et al. 1990).

Sillitoe and Lehmann (2021) studied the origin of Cu-bearing Sn deposits, including those along the Central Andean tin belt. They concluded that the most important process for their generation is mixing between ascendant oxidized, magnetite-series magmas with reduced, ilmenite-series silicic magmas generated by assimilation-fractional crystallization (AFC) processes in a thickened crust. In back-arc or post-collisional settings, melting of the mantle by decompression generates mafic magmas, whose high temperature may trigger partial melting of metasedimentary crustal rocks leading to the formation of ilmenite-series magmas associated with Sn mineralization. Therefore, these authors propose that oxidized fluids exsolved from such mafic magmas can supply Cu to silicic chambers by adding it to reduced Sn-bearing fluids.

It is widely accepted that metallogenic reiteration in the Triassic and Tertiary mineralization events in the Central Andean tin belt is explained by the convergence of geodynamic factors driving a high heat flow triggering partial melting of thick sequences of pelitic sediments in a thickened arc crust favoring protracted magma residence time and fractional crystallization. The Triassic event

consisted of rift-related granitic magmatism in a back-arc setting (McBride et al. 1983; Kontak et al. 1990; Lehmann et al. 1990; Mišković et al. 2009), while the Tertiary event is interpreted to reflect changes in the mantle melt productivity induced by the south-migrating subduction of the Juan Fernandez Ridge and delamination of the subcontinental lithospheric mantle that triggered the deposition of caldera complexes and ignimbrite deposits (de Silva and Kay 2018). Mamani et al. (2010) interpreted that arc migration developed between 130 Ma to 45 Ma from an offshore position to a position up to 200 km northwards, coinciding with the Andahuaylas-Yauri batholith; since then, the arc has migrated back southeastwards starting at ca. 31–30 Ma. This back-migration was associated with a steepening of the slab, which induced decompression and mantle upwelling, resulting in voluminous high-K mafic magmatism from 30 Ma to 24 Ma (Kontak et al. 1986; Baldellón et al. 1994; Sandeman et al. 1995; Mamani et al. 2010). This mafic magmatism seems to have continued episodically through the Neogene and Quaternary.

2.3. Geology of the Chacaltaya-Kellhuani-Milluni district, Bolivia

The Chacaltaya-Kellhuani-Milluni district is located 20 km north of the city of La Paz, in the northern segment of the Cordillera Real (Fig. 4). The district is situated about 5 km south of the Triassic Huayna-Potosí muscovite-biotite granite batholith that displays transitions to a granodioritic composition (Ahlfeld and Branisa 1960 in Evernden et al. 1977; McBride et al. 1983; Lehmann 1985; Gillis et al. 2006; Cordani et al. 2019; Iriarte et al. 2021).

In the Chacaltaya-Kellhuani-Milluni district, the outcropping stratigraphic succession comprises the 650-m-thick, mid-Silurian Uncía Formation, consisting dominantly of dark shales and siltstones interbedded with thin sandstone beds and the overlying, 700-m-thick, late-Silurian Catavi Formation, consisting of interbedded quartz-arenites and mudstones. In the study area, individual quartzitic beds of the Catavi Formation consist of metasiltstones and metasandstones and may reach 30 m thick (Lehmann 1985). In the central part of the Cerro Chacaltaya massif, the Paleozoic metasedimentary rocks are intruded by a small stock of peraluminous granite porphyry with an exposed surface of 0.5 km² (Lehmann 1985). Despite of pervasive alteration, relicts of a muscovite-chlorite-biotite-quartz-andalusite assemblage can be identified in the Catavi Formation along the contact-metamorphic aureole around the Chacaltaya intrusion. McBride et al. (1983) provide a K/Ar muscovite date of 210 ± 6 Ma for the Chacaltaya porphyry stock. This date overlaps, within the limits of the analytical error, with U-Pb zircon concordia dates of 222.3 ± 2.4 and 220.8 ± 1.9 Ma for two granite samples from the Huayna Potosí pluton provided by Cordani et al. (2019), and with a U-Pb cassiterite date for Kellhuani at 218.3 ± 5.5 Ma determined by Gemmrich et al. (2021).

Three types of mineralization have been described in the Chacaltaya-Kellhuani-Milluni district: greisen, breccia, and veins. Greisen mineralization occurs in most of the exposed Chacaltaya granitic stock (Lehmann 1985). The greisen is characterized by coarse-grained quartz, muscovite, cassiterite, tourmaline, siderite, and fluorite (Lehmann 1985). The hydrothermal alteration halo, composed of a granoblastic assemblage of quartz, chlorite, muscovite/sericite, and siderite, can be observed several kilometers away from the stock and its

dimensions are controlled by a fracture pattern radiating around the stock, which provided permeability for hydrothermal fluids (Lehmann 1985). Tourmaline becomes very abundant towards the Chacaltaya stock.

The breccia mineralization, not described by Lehmann (1985), occurs mainly at the eastern side of the Chacaltaya stock. A few SE-trending breccia bodies have extensions of up to 200 m and very irregular thicknesses of up to 20 m. They consist of heterolithic breccia with angular clasts of host Paleozoic metamorphic rocks and greisen cemented by tourmaline containing cassiterite and minor sulfides crystallized in open spaces.

Discordant vein systems and concordant-stratabound veins and veinlets are widespread across the district. The most important discordant vein system is located at the Milluni mine, where the Veta Rothschild (10/80 °E) occurs over a distance of 1.6 km (Lehmann 1985). In these veins systems, Lehmann (1985) described four successive mineral stages: (1) a tin-tungsten stage with quartz, fluorite, siderite, tourmaline, chlorite, cassiterite, hematite, muscovite, and wolframite; (2) a base-metal stage with quartz, fluorite, siderite, arsenopyrite, pyrrhotite, chalcopyrite, sphalerite, stannite, galena, and pyrite; (3) a stage of pyrrhotite alteration to pyrite-marcasite aggregates; and (4) a supergene alteration stage forming scorodite, covellite, limonite, and native gold.

The strata-bound mineralization is chiefly associated with quartzitic lithologies of the Catavi Formation, whereas the shales are mostly barren. At the regional scale, mineralization is conformable with the strata, whereas at the outcrop scale, they are disconformable, with the mineralization confined to a network of veinlets cutting through the quartzites (Lehmann 1985). The mineralogy consists of quartz, tourmaline, cassiterite and chlorite, and lesser proportions of fluorite, siderite,

hematite, muscovite, albite, and sulfides like chalcopyrite, pyrrhotite, and pyrite (Lehmann 1985).



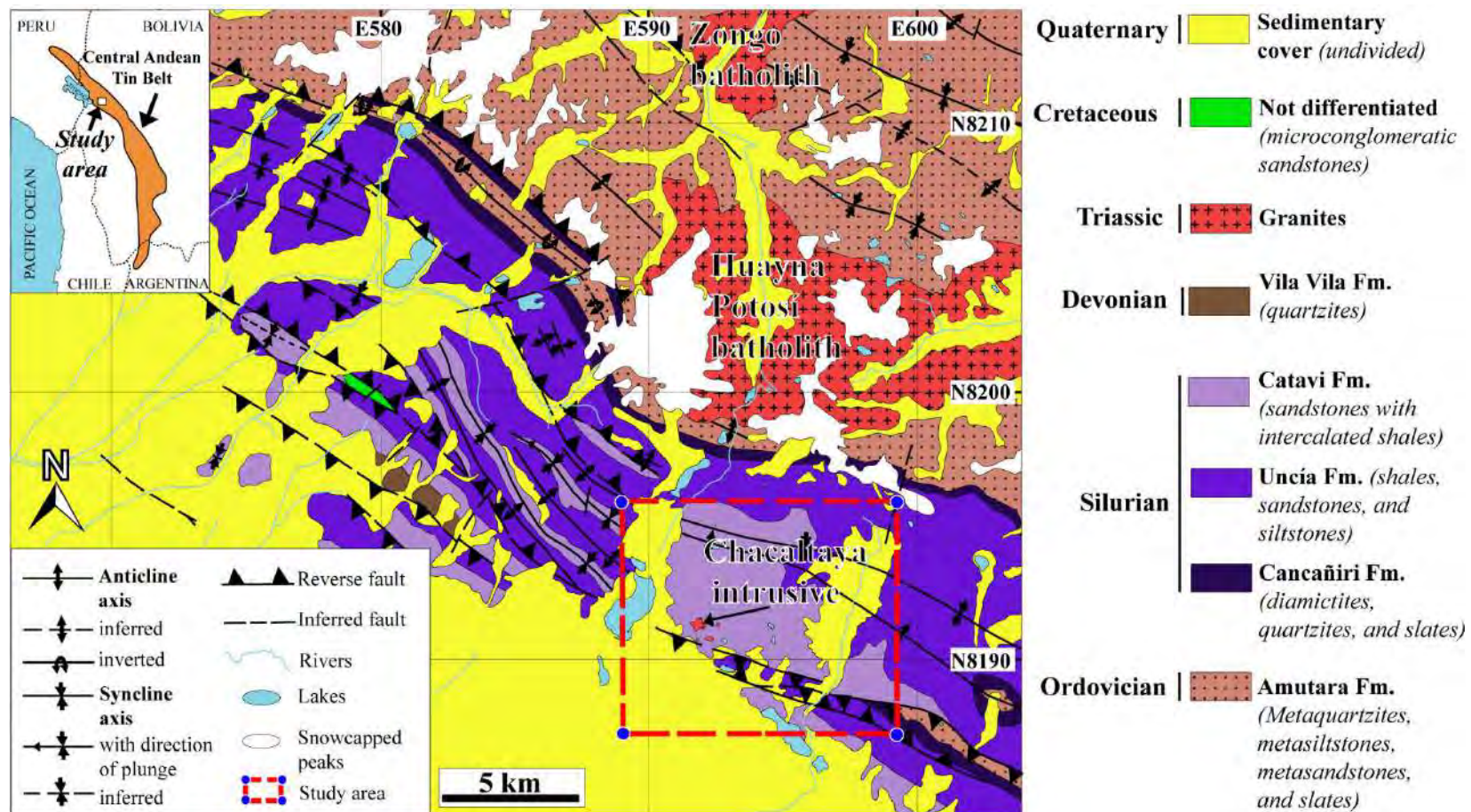


Figure 4. Geological map of the Chacaltaya-Kellhuani-Milluni district and surrounding areas north of the City of La Paz. Modified from Servicio Geológico de Bolivia - Geobol (1995a,b). The inset shows the location of the study area within the Central Andean tin belt. Abbreviations: Fm. = Formation.

3. Materials and methods

3.1. *Sampling and sample preparation*

Fifty-one rock samples were collected in the Chacaltaya (n=15), Kellhuani (n=16), Milluni (n=11), and Kalauyo (n=9) areas. The locations of the samples are provided in Appendix A. Descriptions and photographs of mineralogical and textural features of hand samples are provided in Appendix B.

3.2. *Petrography*

Thirteen polished thin sections were prepared at the *Servei de Làmina Prima* of the University of Barcelona. Thin sections correspond to rock samples from the granite stock (n=2), greisen (n=3), and tourmaline breccia (n=3) at Chacaltaya, and to rock samples from quartz-tourmaline-cassiterite veins (n=5) at Kellhuani and Kalauyo. The thin sections were studied by conventional optical microscopy using both transmitted and reflected light. Petrographic descriptions and photomicrographs of each of the studied thin sections are provided in Appendix C.

3.3. *Electron probe microanalysis (EPMA)*

Major and minor element analyses of tourmaline and white mica were performed at the *Centres Científics i Tecnològics de la Universitat de Barcelona* (CCiTUB) using a JEOL JXA-8230 electron microprobe equipped with wavelength-dispersive spectrometer (WDS) detectors. The accelerating voltage was set to 15 kV, the beam current to 15 nA, and the beam diameter to 5 μm . The analyses were performed using the following natural and synthetic standards and lines: diopside

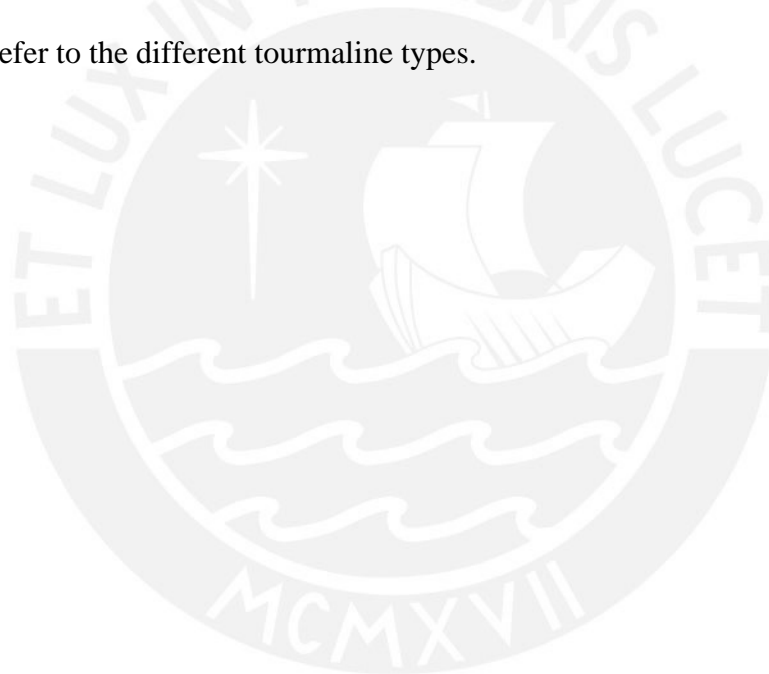
(Si, K α), kyanite (Al, K α), rutile (Ti, K α), Cr₂O₃ (Cr, K α), periclase (Mg, K α), albite (Na, K α), fluorite (F, K α), hematite (Fe, K α), rhodonite (Mn, K α), wollastonite (Ca, K α), orthoclase (K, K α), and AgCl (Cl, K α). The detection limits for each element oxide were 0.09 wt% for SiO₂, 0.06 wt% for Al₂O₃, 0.15 wt% for TiO₂, 0.18 wt% for Cr₂O₃, 0.08 wt% for MgO, 0.08 wt% for Na₂O, 0.08 wt% for FeO, 0.08 wt% for MnO, 0.04 wt% for CaO, 0.02 wt% for K₂O, 0.14 wt% for F, and 0.02 wt% for Cl. White mica compositions were normalized to 11 atoms of O, and Fe_{total} = Fe²⁺. The chemical data of tourmaline were stoichiometrically recalculated using the WinTac software created by Yavuz et al. (2014) by normalizing to 15 cations for the Y + Z + T sites and assuming a stoichiometric 3 atoms for B and 4 atoms for OH + F, based on the general formula XY₃Z₆[T₆ O₁₈][B O₃]₃V₃W (Henry et al. 2011). Chemical compositions are reported in weight percent (wt%) of the oxides, and the structural formulas are expressed in atoms per formula unit (apfu). A full EPMA dataset for tourmaline is provided in Appendix D.

The same instrument operated with an accelerating voltage set to 15 kV and a beam current set to 100 nA, with a focused beam, a step (pixel) size of 20 μ m, and a counting time of 30 ms/pixel was used to obtain elemental (Si, Al, Ti, Cr, Fe, Mg, Mn, Ca, Na, K, F, Cl) X-ray maps. The X-ray maps were processed with software DWImager (Torres-Roldán and Garcia Casco, unpublished) and consist of the X-ray intensity signals of the elements or element ratios (color-coded; expressed in counts/nA per s), voids, polish defects, and mineral phases other than tourmaline were masked out and overlain onto a gray-scale SEM-BSE image which contains the basic textural information of the scanned areas (see Garcia-Casco 2007).

4. Results

4.1. Petrography

This study focuses on tourmaline associated with different types of mineralization found in the Chacaltaya-Kellhuani-Milluni district (Fig. 5). Several petrographic types of tourmaline were established based on detailed textural observations. Since the temporality between the petrographic types of tourmaline could not be always clearly established, we deliberately avoid the use of the term “generation” to refer to the different tourmaline types.



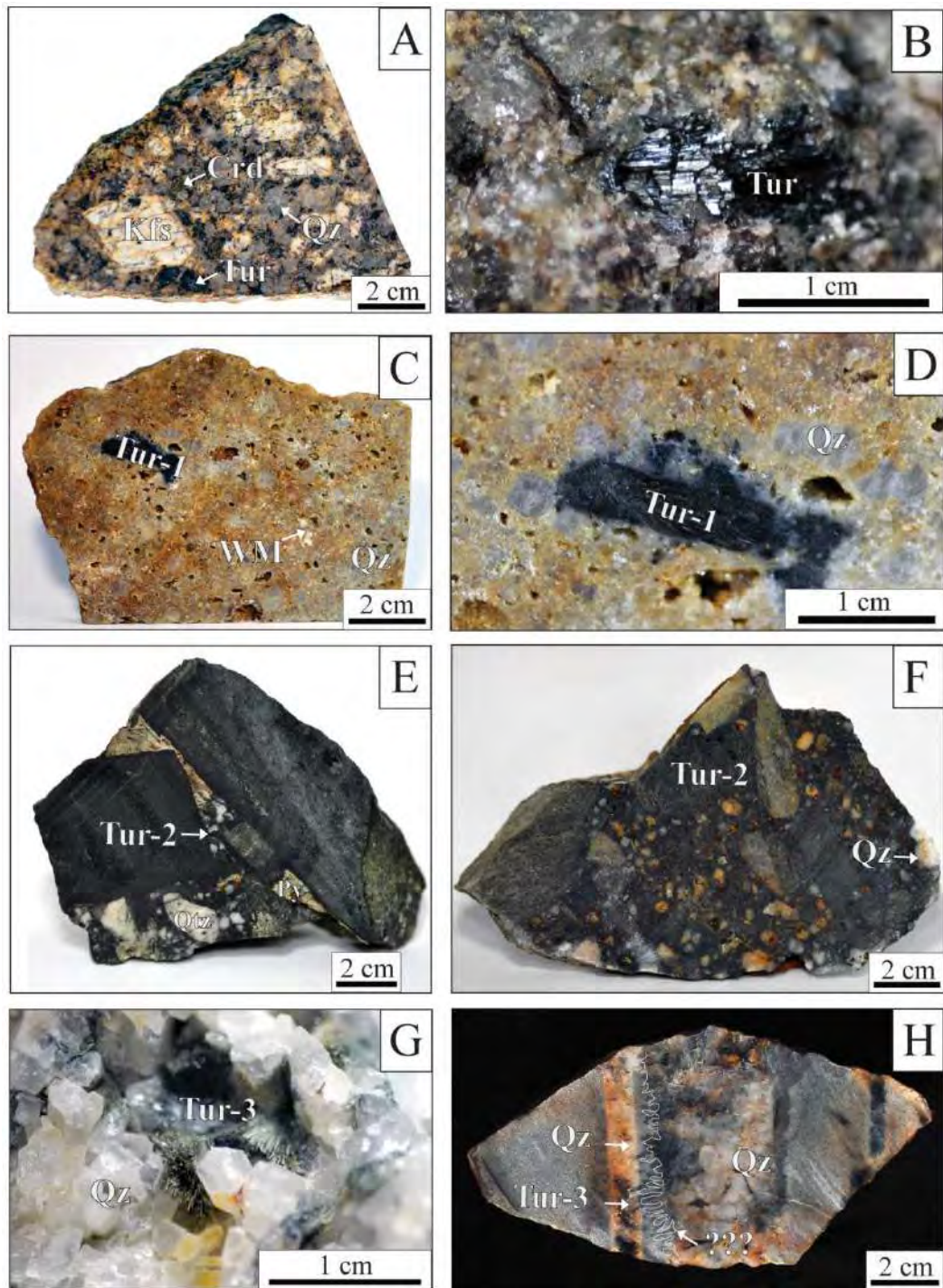


Figure 5. Tourmaline in different types of mineralization found in the Chacaltaya-Kellhuani-Milluni district. (A) Chacaltaya granitic porphyry stock with euhedral to subhedral megacrysts of K-feldspar in a groundmass composed of mm-sized K-feldspar, quartz, and cordierite; hydrothermal tourmaline occurs as a replacement of K-feldspar. (B) Detail of acicular black tourmaline crystals disseminated in greisen. (C) Greisen sample mainly constituted of quartz, tourmaline, and muscovite. (D) Detail of black aggregate of tourmaline pseudomorphically

replacing a K-feldspar phenocryst in greisen. (E-F) Tourmaline breccias composed of angular heterolithic clasts of variable size (0.5-15 cm) cemented by tourmaline; the clasts include greisen and black quartzites (probably derived from the hosting Catavi Formation). Cassiterite and sulfide mineralization form triangular-acute angle textures as it infills space between angular clasts. (G) Aggregates of fine-grained tourmaline needles of dark greenish color overgrown on euhedral quartz in a vein. (H) Quartz-cassiterite-tourmaline vein hosted by quartzites of the Catavi Formation. Euhedral to subhedral translucent quartz crystals up to 2 cm long have comb-like textures indicative of open-space crystallization. The most striking feature in this sample is found along the vein selvage, which contains dark brown, subhedral to euhedral short-prismatic to ovoid crystals of unknown nature. Abbreviations: Crd = cordierite; Kfs = K-feldspar; Qz = quartz; Tur = tourmaline; WM = white mica.

4.1.1. *Chacaltaya stock*

Most of the exposed portion of the Chacaltaya porphyritic stock is hydrothermally altered. The least altered samples are composed of quartz, plagioclase, K-feldspar, and cordierite variably replaced by an assemblage of tourmaline, quartz, and coarse- and fine-grained sericite (Fig. 6).

The groundmass consists of a fine-grained assemblage of quartz, plagioclase and white mica. K-feldspar megacrysts locally show a rim of poikilitic quartz that is aligned along the crystal edges (Fig. 6A). Cordierite crystals are pervasively altered to a sericite – chlorite assemblage (pinitization; Fig. 6B). Plagioclase crystals are also found inside the K-feldspar megacrysts and are partially altered to sericite (Fig. 6C). Subhedral to skeletal, orange tourmaline crystals (Tur-1) with sizes between 0.5 and 6 mm occur disseminated in the Chacaltaya stock, commonly as replacement of K-feldspar phenocrysts (Fig. 6D).

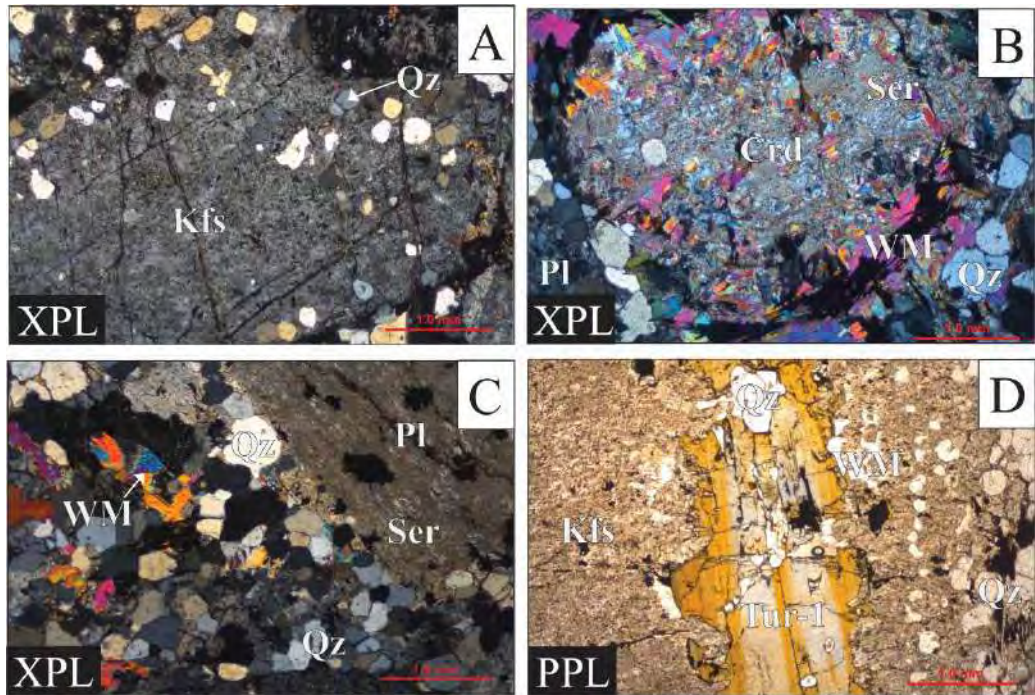


Figure 6. Photomicrographs illustrating petrographic features of the least altered samples at the Chacaltaya granitic stock. (A) K-feldspar megacrysts with poikilitic quartz affected by pervasive alteration. (B) Cordierite altered to white mica and chlorite (pinite). (C) Fine-grained white mica and quartz in the granitic groundmass next to a plagioclase phenocryst pervasively altered to sericite. (D) Subhedral, zoned tourmaline (Tur-1) crystal. Abbreviations: Crd = cordierite; Kfs = K-feldspar; Pl = plagioclase; Qz = quartz; Ser = sericite; Tur = tourmaline; WM = white mica.

4.1.2. *Chacaltaya greisen*

The greisen superimposed on the Chacaltaya stock is composed of an assemblage of quartz, tourmaline, white mica, and local fluorite (Fig. 7). Secondary white mica and quartz are intergrown (Figs. 7A-B). White mica crystals reach 3.5 mm in length. Locally, relict igneous quartz phenocrysts are preserved and surrounded by a fine-grained white mica-quartz assemblage

(Figs. 7A-B). These quartz phenocrysts have irregular shapes and show dissolution engulfment filled by quartz and white mica.

Hydrothermal tourmaline (Tur-1) consists of euhedral to subhedral skeletal crystals of orange color and lengths from 1700 μm to 2 cm, generally forming radial aggregates (Figs. 7C-D). Some crystals present a color zonation along growth faces. Tourmaline is locally altered to and overgrown by a blue mineral with Si- and Al-rich composition, probably dumortierite, as determined by SEM-EDS analysis (Figs. 7C-D).

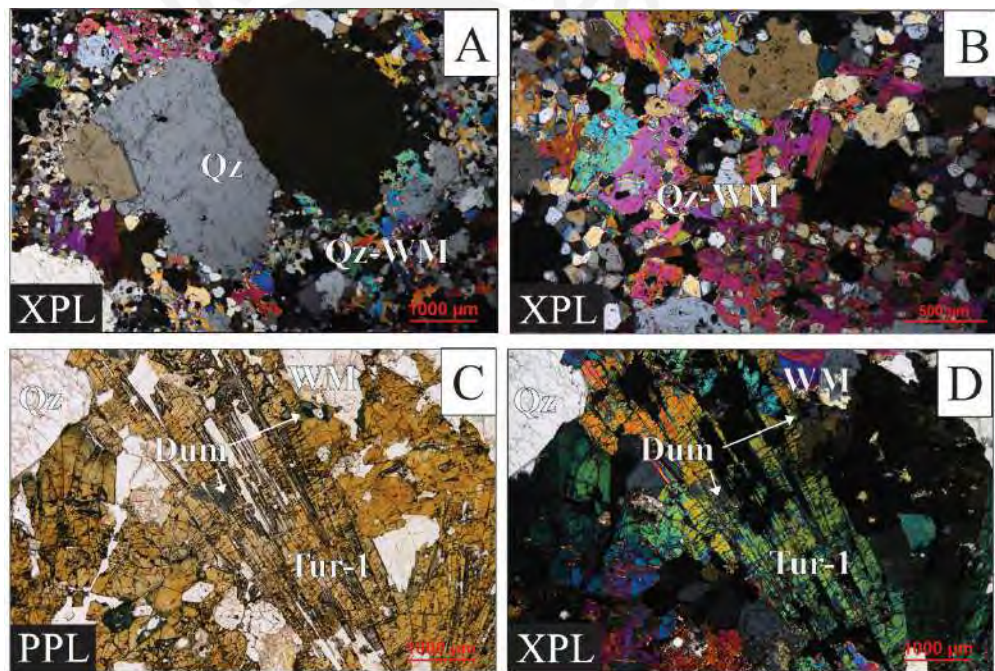


Figure 7. Photomicrographs illustrating petrographic features of the greisen in the Chacaltaya stock. (A) Relict igneous quartz phenocrysts disseminated in a secondary assemblage of white mica and quartz. (B) Fine-grained intergrowth of white mica and quartz. (C) Radial aggregates of tourmaline (Tur-1) crystals. Tourmaline (Tur-1) is altered by a blue mineral with a splintered appearance, probably dumortierite. (D) Same image as in C in crossed polarized light. Abbreviations: Dum = dumortierite; Qz = quartz; Tur = tourmaline; WM = white mica.

4.1.3. *Tourmaline-cemented breccias*

Tourmaline-cemented breccias comprise rock and crystal fragments cemented by an assemblage of tourmaline, quartz, white mica, and metallic mineralization of cassiterite, pyrite, and chalcopyrite. Most clasts correspond to host quartzites and some to greisen, the latter including Tur-1 as described in the previous section. Clasts are angular and their sizes range from a few mm to some tens of cm. They do not show specific orientation but generally exhibit triangular-acute angle interstitial space.

Interstitial space between rock fragments is filled with crystal fragments of quartz and locally, Tur-1, and finely intergrown tourmaline (Tur-2), quartz, cassiterite, and sulfides. Tur-2 composes the cement of breccias (Figs. 8A-B). It is characterized by a fine-grained acicular texture (10-900 μm) and a dark green color. Isolated Tur-1 clasts up to 1 mm in size are cemented or epitaxially overgrown by Tur-2 (Figs. 8A-B, D). Tur-2 is also found as dark green acicular crystals (100-1500 μm) growing perpendicular to former triangular cavities and intergrown with cassiterite, pyrite, and chalcopyrite (Fig. 8C). Goethite occurs as an alteration product of pyrite.

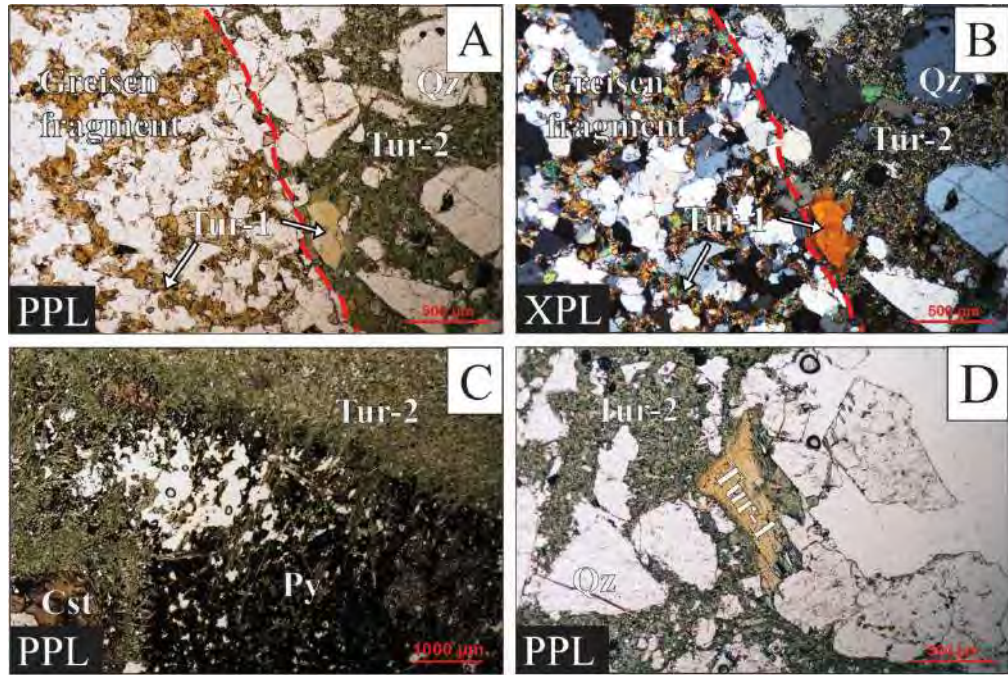


Figure 8. Photomicrographs illustrating petrographic features of the tourmaline-cemented breccias. (A) Very fine-grained dark green acicular tourmaline crystals (Tur-2) cementing quartz angular clasts and a greisen rock fragment (left side) hosting Tur-1 crystals. (B) Same image as in A in crossed polarized light. (C) Open space filling with Tur-2 acicular crystals intergrown with cassiterite and pyrite. (D) Clasts of Tur-1 and quartz disseminated in the Tur-2a matrix. Abbreviations: Cst = cassiterite; Py = pyrite; Qz = quartz; Tur = tourmaline.

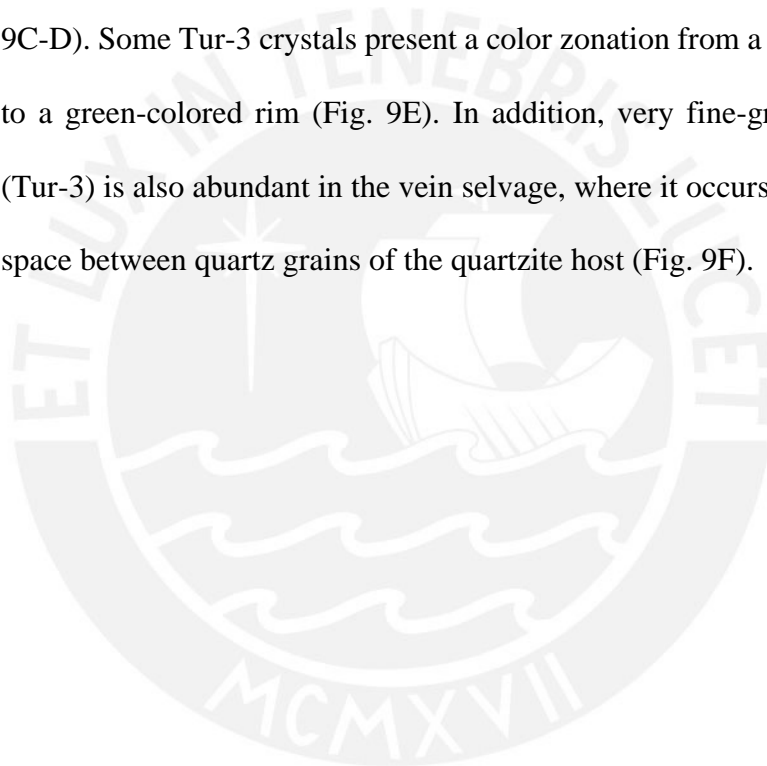
4.1.4. Cassiterite-bearing quartz-tourmaline veins

The studied cassiterite-bearing quartz-tourmaline veins are hosted by quartzites of the Catavi Formation in the Kellhuani and Kalauyo areas. The veins are dominantly composed of quartz, tourmaline (Tur-3), cassiterite, carbonates, and lesser amounts of fluorite and sulfide minerals (Figs. 9A-B).

Quartz composing the vein is distinguished from the quartz in quartzite for its comb-like textures, euhedral to subhedral habits and larger crystal sizes (up to

2 cm in length). Siderite, fluorite and sulfides fill the interstitial spaces between the quartz grains along the central portion of the veins, whereas cassiterite and tourmaline are more abundant towards the rims of the veins where they occur intergrown with comb-textured quartz.

Tur-3 is green-brownish in color. Within the veins, it appears as subhedral elongated to acicular crystals ranging from 30 to 1800 μm in length forming radial aggregates (Figs. 9A-E) and intergrown with cassiterite crystals (Figs. 9C-D). Some Tur-3 crystals present a color zonation from a blue-colored core to a green-colored rim (Fig. 9E). In addition, very fine-grained tourmaline (Tur-3) is also abundant in the vein selvage, where it occurs filling interstitial space between quartz grains of the quartzite host (Fig. 9F).



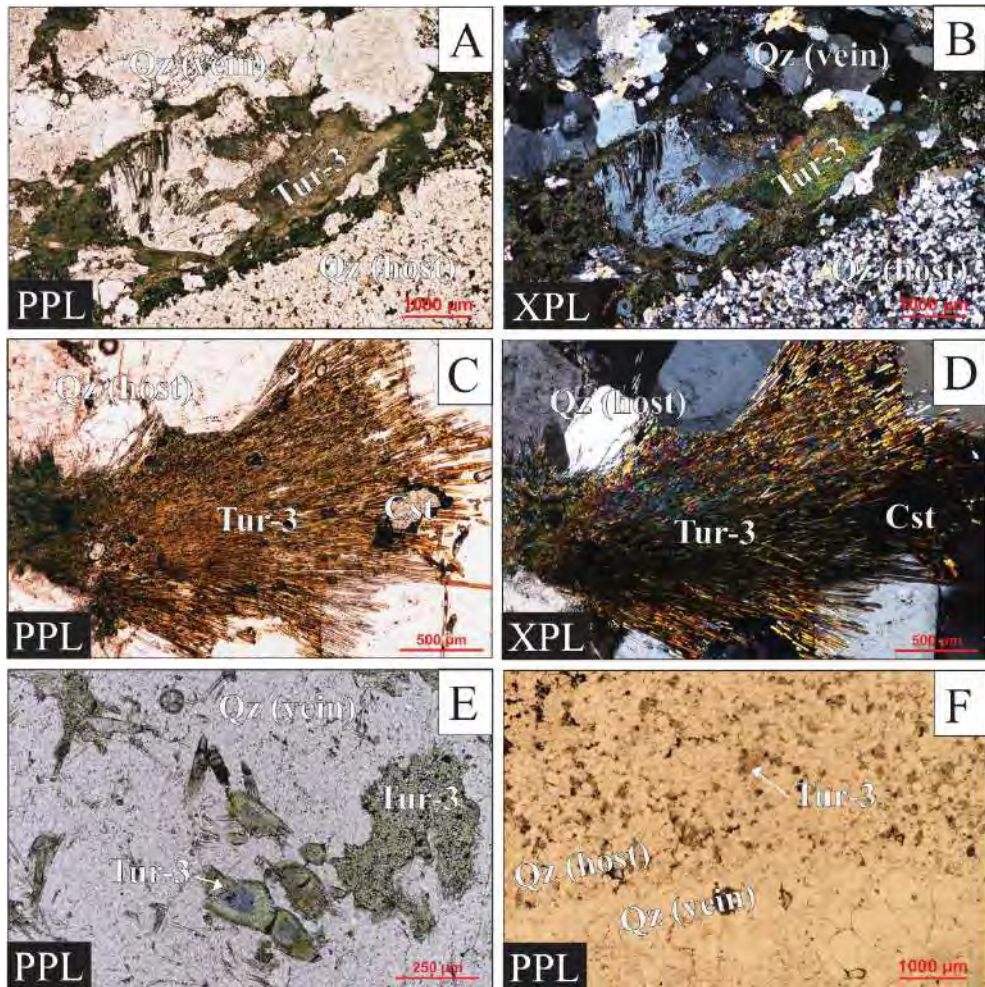


Figure 9. Photomicrographs illustrating petrographic features of the cassiterite-bearing tourmaline veins. (A) Quartz-Tur-3 vein cutting the quartzite host. (B) Same image as in A in crossed polarized light. (C) Radial aggregate of acicular Tur-3 crystals intergrown with cassiterite. (D) Same image as in C in crossed polarized light. (E) Zoned crystals of Tur-3 within vein. (F) Tur-3 in the vein selvage, filling interstitial space between quartz grains in the host quartzite. Abbreviations: Cst = cassiterite; Qz = quartz and Tur = tourmaline.

4.2. Mineral geochemistry

4.2.1. White mica

Representative EMPA analyses of white micas from the greisen in the Chacaltaya stock are shown in Table 1. The analyzed crystals display a continuous, relatively small compositional range between muscovite $[\text{KAl}_2(\text{AlSi}_3\text{O}_{10})(\text{OH})_2]$ and phengite $[\text{KAl}_{1.5}(\text{Mg,Fe})_{0.5}(\text{Al}_{0.5}\text{Si}_{3.5}\text{O}_{10})(\text{OH})_2]$, with muscovite being the predominant composition (Figure 5a). The white micas exhibit a low Tschermak $[\text{Si}(\text{Mg,Fe})\text{Al}_2]$ exchange along the dioctahedral mica series, which relates muscovite to the celadonite $[\text{K}(\text{MgFe}^{3+}\square)(\text{Si}_4\text{O}_{10})(\text{OH})_2]$ end-members (Figs. 5A,C). The Tschermak exchange component approximates to the composition of muscovite/paragonite $[\text{NaAl}_2(\text{AlSi}_3\text{O}_{10})(\text{OH})_2]$.

Table 1. Representative analyses of white micas from the greisen in the Chacaltaya stock, including chemical composition and structural formulae normalized to 11 atoms of O (EPMA data).

Mineral	White mica														Avg	SD	
	Sample	2020-KELL-22-B-TS6							2020-KELL-22-B-TS1								
		B		D			I		A		D		F				
Label	WM-001	WM-002	WM-002	WM-003	WM-004	WM-001	WM-002	WM-001	WM-002	WM-001	WM-002	WM-003	WM-004				
SiO ₂ (wt. %)	45.88	45.34	45.04	45.33	45.36	45.39	45.61	46.03	45.07	45.62	46.01	46.07	44.95	45.58	0.38		
TiO ₂	0.34	0.38	0.37	0.34	0.33	0.31	0.31	0.19	0.29	0.37	0.27	0.20	0.24	0.30	0.05		
Al ₂ O ₃	33.70	33.46	34.18	34.86	35.13	34.29	32.91	34.10	35.35	35.05	32.31	33.97	34.37	33.96	1.04		
FeO (a)	1.75	2.09	1.75	1.72	1.75	1.93	2.65	1.55	1.27	1.55	2.79	1.88	2.02	2.03	0.64		
MnO	<d.l.	<d.l.	<d.l.	<d.l.	<d.l.	<d.l.	<d.l.	<d.l.	<d.l.	<d.l.	<d.l.	<d.l.	<d.l.	<d.l.	-		
MgO	0.90	0.85	0.58	0.64	0.60	0.77	1.01	0.66	0.51	0.61	0.99	0.66	0.53	0.78	0.21		
Na ₂ O	0.67	0.67	0.78	0.76	0.80	0.52	0.71	0.49	0.77	0.81	0.77	0.68	0.77	0.72	0.09		
K ₂ O	9.60	9.71	9.97	10.01	10.02	10.21	9.84	10.09	9.86	10.01	9.91	9.90	9.46	9.82	0.18		
F	0.56	0.83	1.26	1.61	1.27	0.49	1.17	0.63	0.42	1.29	1.50	0.80	1.07	1.19	0.54		
Cl	<d.l.	0.03	<d.l.	<d.l.	0.02	<d.l.	0.02	<d.l.	0.03	<d.l.	<d.l.	<d.l.	0.03	0.03	0.02		
H ₂ O (b)	4.14	3.97	3.78	3.66	3.83	4.18	3.82	4.11	4.21	3.84	3.66	4.04	3.85	3.84	0.26		
Sum	97.54	97.32	97.71	98.94	99.11	98.09	98.04	97.85	97.77	99.15	98.22	98.20	97.29	98.22	0.59		
Total (c)	97.30	96.96	97.18	98.26	98.57	97.88	97.54	97.59	97.59	98.60	97.59	97.86	96.83	97.72	0.51		
Si (a.p.f.u)	3.13	3.11	3.09	3.07	3.06	3.09	3.13	3.13	3.06	3.08	3.15	3.13	3.09	3.11	0.03		
Ti	0.02	0.02	0.02	0.02	0.02	0.02	0.02	0.01	0.01	0.02	0.01	0.01	0.01	0.02	0.00		
Al	2.71	2.71	2.76	2.78	2.80	2.75	2.66	2.73	2.83	2.79	2.61	2.72	2.78	2.73	0.07		
Fe	0.10	0.12	0.10	0.10	0.10	0.11	0.15	0.09	0.07	0.09	0.16	0.11	0.12	0.12	0.04		
Mn	-	-	-	-	-	-	-	-	-	-	-	-	-	-	-		
Mg	0.09	0.09	0.06	0.07	0.06	0.08	0.10	0.07	0.05	0.06	0.10	0.07	0.05	0.08	0.02		
Na	0.09	0.09	0.10	0.10	0.11	0.07	0.09	0.06	0.10	0.11	0.10	0.09	0.10	0.10	0.01		
K	0.83	0.85	0.87	0.87	0.86	0.89	0.86	0.87	0.85	0.86	0.87	0.86	0.83	0.85	0.02		
F	0.12	0.18	0.27	0.35	0.27	0.10	0.25	0.14	0.09	0.28	0.33	0.17	0.23	0.26	0.12		
Cl	-	0.00	-	-	0.00	-	0.00	-	0.00	-	-	-	0.00	0.00	0.00		
OH	1.88	1.82	1.73	1.65	1.73	1.90	1.74	1.86	1.91	1.72	1.67	1.83	1.76	1.74	0.12		
Mg+Fe	0.19	0.21	0.16	0.16	0.16	0.19	0.25	0.15	0.12	0.15	0.26	0.17	0.17	0.19	0.06		
Fe+Mg+Ti+(Si-3)	0.34	0.34	0.27	0.25	0.24	0.29	0.40	0.29	0.20	0.24	0.43	0.31	0.27	0.32	0.08		

(a) Total Fe expressed as FeO.

(b) H₂O wt. % concentration was calculated on the basis of 2 OH p.f.u.

(c) Sum - oxygen equivalent to F and Cl.

a.p.f.u.: atoms per formula unit; <d.l.: below detection limit.



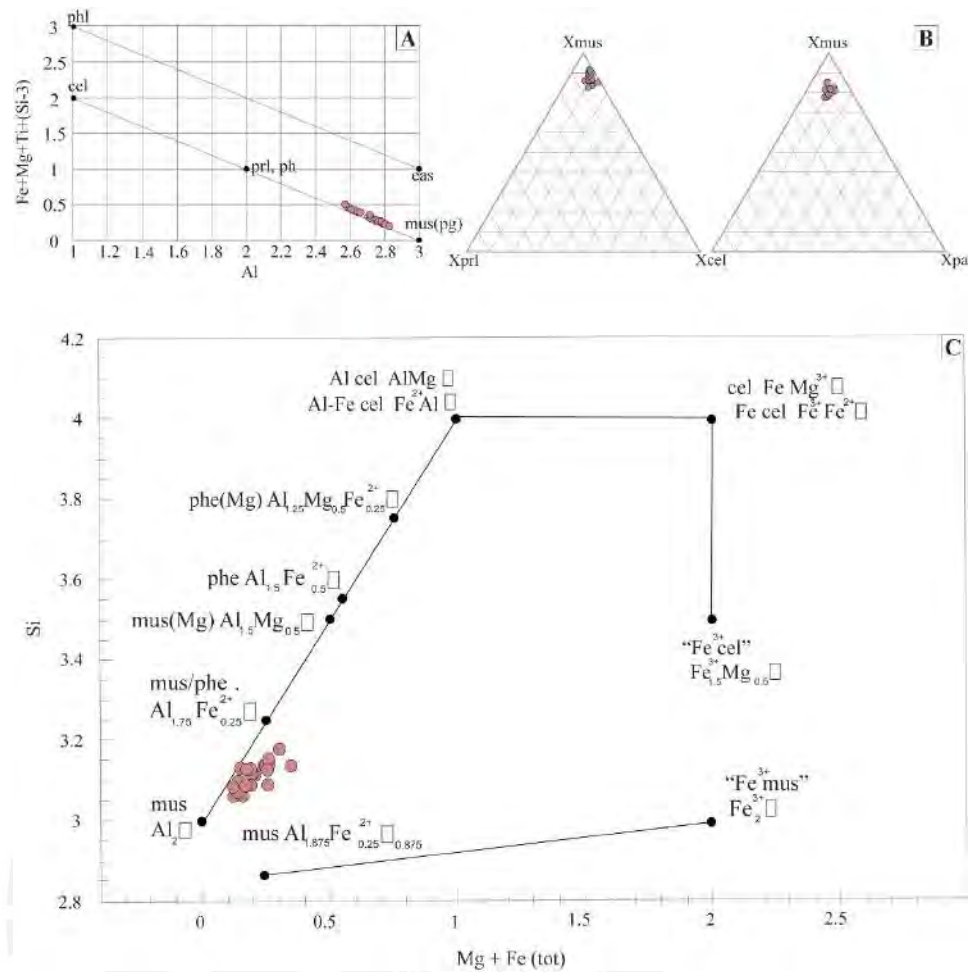


Figure 10. Compositions of white micas from the greisen in the Chacaltaya stock plotted in the Al vs. Fe+Mg+Ti+(Si-3) binary diagram (A), muscovite-pyrophyllite-celadonite-paragonite ternary diagrams (upper right) and in the Si vs. Mg+Fe binary diagram. Abbreviations: cel = celadonite; eas = eastonite; mus = muscovite; pg, pa= paragonite; phe, ph = phengite; phl = phlogopite; prl = pyrophyllite.

4.2.2. Tourmaline

Chemical compositions of the three tourmaline petrographic types from the Chacaltaya-Kellhuani-Milluni district are shown in Figure 6 and Table 2, and the full dataset is reported in Appendix D. Overall, the analyzed tourmaline crystals have variable contents of Fe (0.892-3.302 apfu), Mg (0.085-1.705

apfu), Al (4.678-7.226 apfu), as well as of the minor elements Na (0.207-0.934 apfu), Ca (<d.l.-0.414 apfu), and Ti (<d.l.-0.185 apfu).

The three analyzed tourmaline petrographic types (Tur-1 to Tur-3) belong to the alkali group (Fig. 6E) and have dominantly Fe-rich compositions, close to the schorl $[\text{NaFe}^{2+}_3\text{Al}_6[\text{Si}_6\text{O}_{18}](\text{BO}_3)_3(\text{OH})_3(\text{OH})]$ endmember, partly extending into the compositional fields of foitite $[\square(\text{Fe}^{2+}_2\text{Al})\text{Al}_6[\text{Si}_6\text{O}_{18}](\text{BO}_3)_3(\text{OH})_3(\text{OH})]$ and dravite $[\text{NaMg}_3\text{Al}_6[\text{Si}_6\text{O}_{18}](\text{BO}_3)_3(\text{OH})_3(\text{OH})]$ (Figs. 6A-B). Tur-1 has mostly foititic to schorl compositions, with $\text{Fe}/(\text{Fe} + \text{Mg}) = 0.58$ to 0.94 and $X_{\square}/(X_{\square} + \text{Na} + \text{K}) = 0.19$ to 0.61 . Tur-2 is characterized by mostly schorl to foititic compositions, with $\text{Fe}/(\text{Fe} + \text{Mg}) = 0.54$ to 0.97 and $X_{\square}/(X_{\square} + \text{Na} + \text{K}) = 0.08$ to 0.7 . Similarly, Tur-3 has mostly schorl to foititic compositions overlapping with Tur-1 and Tur-2, with $\text{Fe}/(\text{Fe} + \text{Mg}) = 0.35$ to 0.92 and $X_{\square}/(X_{\square} + \text{Na} + \text{K}) = 0.05$ to 0.72 .

The three petrographic types of tourmaline overlap in composition, and the strongest compositional variations are attributed to two dominant substitution vectors: $\text{Fe}^{2+} \text{Mg}_{-1}^{2+}$ as indicated by the linear trend in the Fe vs. Mg diagram (Fig. 6B) and $(\square\text{Al}^{3+})_{+1}(\text{Na}^+\text{R}^{2+})_{-1}$ as indicated by the linear trend in the Al vs. X_{\square} diagram (Fig. 6C). Variations in the Ca vs. Mg diagram (Fig. 6D) can possibly be related to the coupled heterovalent substitution $(\square\text{Al}^{3+}_2)_{+1}(\text{Ca}^{2+}\text{Mg}^{2+}_2)_{-1}$.

When plotted in the ternary diagram Al-Fe-Mg (Fig. 11F; Henry and Guidotti 1985), the majority of tourmaline data fall into the compositional field of tourmaline associated with Li-poor granitic rocks with some data plotting in the field of tourmaline associated with metasedimentary rocks.

Table 2. Summary of the compositions for tourmaline group minerals from the Chacaltaya-Kellhuani-Milluni district including chemical composition and structural formulas.

Summary of Major and Minor Element Compositions of Tourmaline from the Chacaltaya-Kellhuani-Milluni district determined by EMPA						
	Tur 1		Tur 2		Tur 3	
	Avg	SD	Avg	SD	Avg	SD
SiO ₂ (wt. %)	34.82	0.75	34.48	0.73	35.38	0.67
TiO ₂	0.33	0.19	0.20	0.19	0.21	0.28
Al ₂ O ₃	33.84	1.76	31.23	1.28	30.66	2.59
FeO (a)	12.53	1.54	14.42	1.81	13.99	3.17
MnO	0.01	0.04	0.05	0.22	0.01	0.04
MgO	1.85	0.63	2.23	0.81	3.15	1.35
CaO	0.20	0.13	0.23	0.12	0.62	0.49
Na ₂ O	1.78	0.21	1.91	0.34	1.80	0.37
K ₂ O	0.03	0.01	0.03	0.02	0.04	0.11
F	0.56	0.21	0.42	0.20	0.32	0.23
Cl	<d.l.		<d.l.		<d.l.	
H ₂ O calc.	2.93	0.10	3.01	0.13	3.12	0.16
B ₂ O ₃ calc.	10.22	0.21	10.07	0.15	10.20	0.16
Total	98.87	1.67	98.11	1.40	99.36	1.31
Structural formula calculated on the basis of 15 cations (Y + Z + T)						
Si (apfu)	5.92	0.06	5.95	0.08	6.03	0.07
Al (z)	6.00	0.02	5.99	0.04	5.86	5.86
Al (y)	0.70	0.23	0.31	0.18	0.28	0.22
Ti	0.04	0.02	0.03	0.03	0.03	0.04
Fe	1.79	0.24	2.08	0.27	2.00	0.47
Mn	0.00	0.01	0.01	0.03	0.00	0.01
Mg	0.47	0.16	0.57	0.21	0.80	0.34
Ca	0.04	0.02	0.04	0.02	0.11	0.09
Na	0.59	0.08	0.64	0.11	0.60	0.12
K	0.01	0.00	0.01	0.01	0.01	0.02
X _□	0.37	0.08	0.31	0.12	0.28	0.14
OH	3.33	0.12	3.46	0.14	3.54	0.16
F	0.30	0.12	0.23	0.11	0.17	0.12
Cl	-	-	-	-	-	-
X _□ /(X _□ + Na + K)	0.38	0.38	0.32	0.12	0.31	0.14
Fe/(Fe + Mg)	0.79	0.07	0.78	0.08	0.71	0.12

apfu: atoms per formula unit; <d.l.: below detection limit

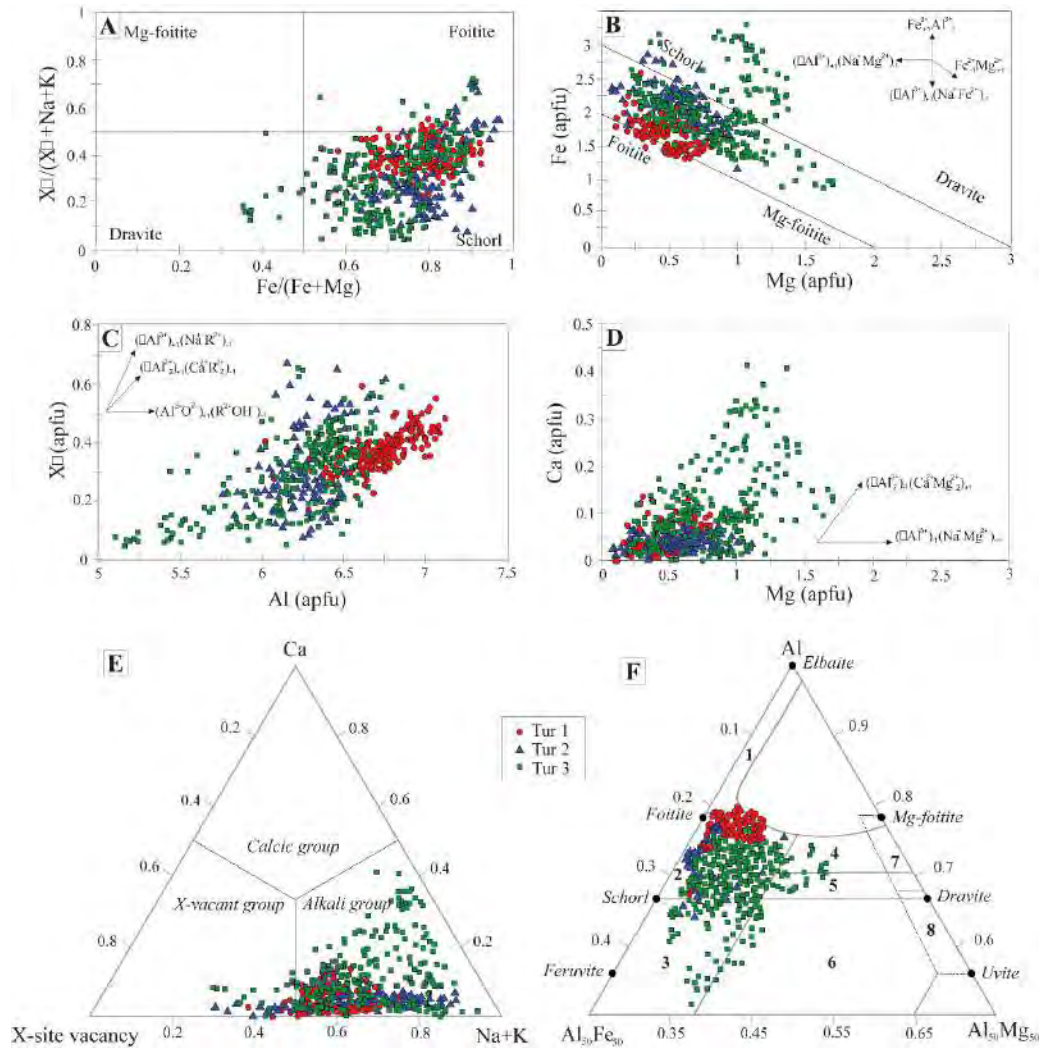


Figure 11. Compositional variation diagrams for the three petrographic types of tourmaline from the Chacaltaya-Kellhuani-Milluni district. (A) Fe/(Fe + Mg) vs. $X_{\square}/(X_{\square} + Na + K)$ diagram. (B) Mg vs. Fe. (C) Al vs. X_{\square} diagram. (D) Mg versus Ca diagram. (E) Ca- X_{\square} -Na + K ternary diagram (X-site occupancy). (F) Al-Fe-Mg ternary diagram (Y- and Z-site occupancy). The fields correspond to the compositional range tourmaline hosted in different rock types (Henry and Guidotti 1985): (1) Li-rich granitoid, pegmatites and aplites; (2) Li-poor granitoids and their associated pegmatites and aplites; (3) Fe³⁺-rich quartz-tourmaline rocks (hydrothermally altered granites); (4) Metapelites and metapsammities coexisting with an Al-saturating phase; (5) Metapelites and metapsammities not coexisting with an Al-saturating phase; (6) Fe³⁺-rich quartz-tourmaline rocks, calc-silicate rocks, and metapelites; (7) Low-Ca meta-ultramafics and Cr-, V-rich metasediments and (8) Metacarbonates and meta-pyroxenites.

X-ray elemental maps for major and minor elements (Al, Fe, Na, Mg, Mn, Ti) in the three petrographic types of tourmaline are shown in Figures 12 to 15. For Tur-1, patchy zoning is evidenced in the map with different areas in the same crystal exhibiting variable Al, Fe, Na, Mg, and Ti contents (Figure 12).

Figure 13 covers an area of the tourmaline breccia in which a clast of Tur-1 is epitaxially overgrown and cemented by Tur-2. The Tur-1 clast is homogeneous in composition. Relative to Tur-1, the surrounding Tur-2 shows higher contents of Mn and lower contents of Na, Mg, Ti, and F.

For Tur-3, zoning at the micron scale is observed for several major and minor elements (Al, Fe, Na, Mg, Mn, Ti, and Ca; Figures 14 and 15). The zoning is convoluted and oscillatory with bands that are Fe- and Ca-rich and Na- and Mg-poorer alternating with bands with the opposite compositional trends.

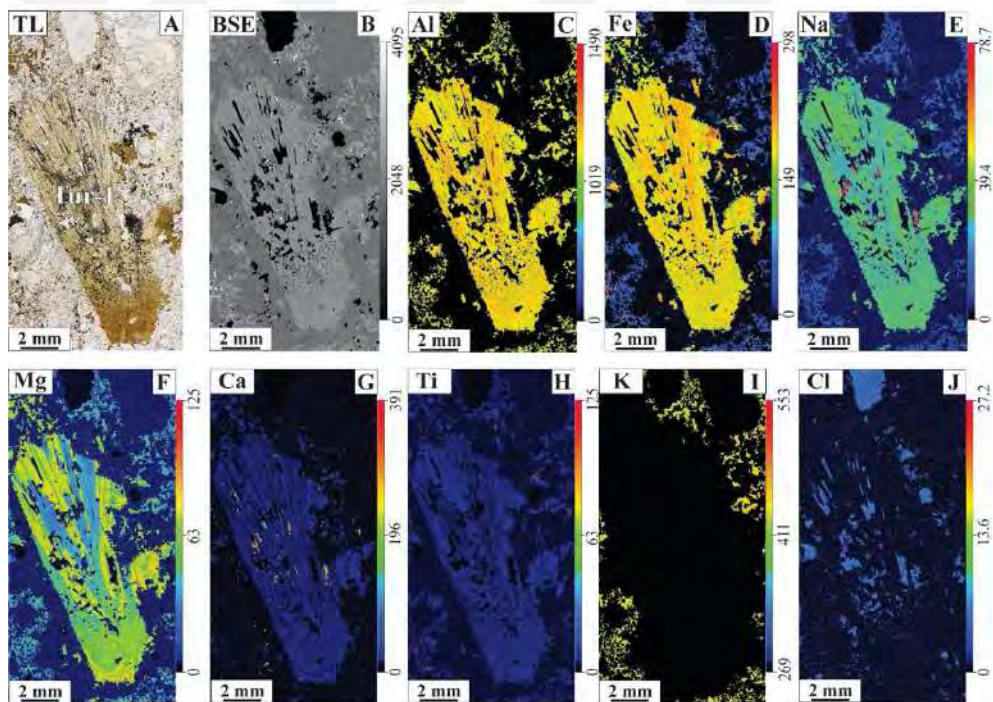


Figure 12. Transmitted light photomicrograph (TL), backscattered electron image (BSE) and corresponding X-ray elemental maps for hydrothermal tourmaline (Tur-1) disseminated in a quartz-white mica greisen from Chacaltaya (2020-KELL-23-TS1). Relative intensities of elements are shown with a color scale.

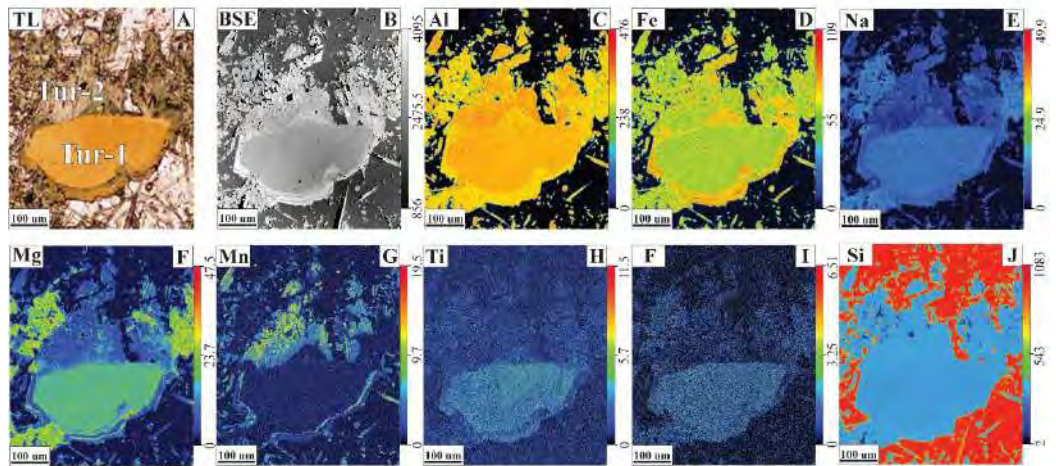


Figure 13. Transmitted light photomicrograph (TL), backscattered electron image (BSE) and corresponding X-ray elemental maps showing Discrete internal zoning and oscillatory zoning (specifically in the rim) in hydrothermal tourmaline crystal (Tur-1) surrounded by acicular tourmaline crystal aggregates (Tur-2) in a tourmaline breccia (2020-KELL-24-TS1). Relative intensities of elements are shown with a color scale.

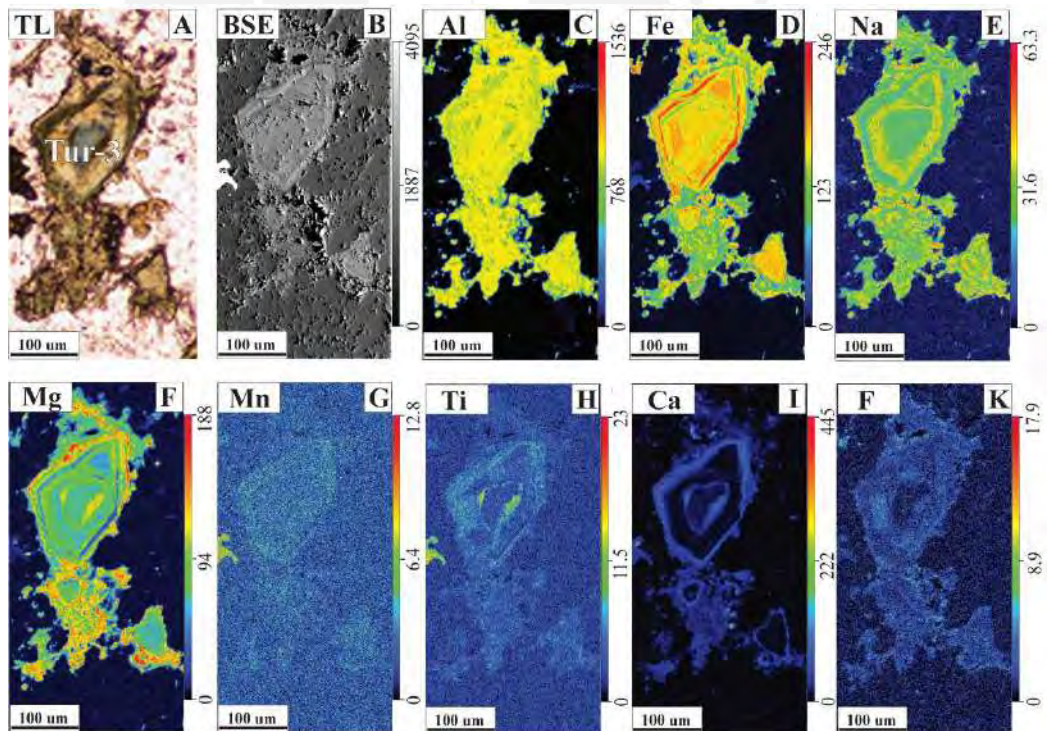


Figure 14. Transmitted light photomicrograph (TL), backscattered electron image (BSE) and corresponding X-ray elemental maps showing chemical zoning in hydrothermal tourmaline crystal (Tur-3) from the quartz-cassiterite-tourmaline veins (2020-KELL-01-A-TS1). Relative intensities of elements are shown with a color scale.

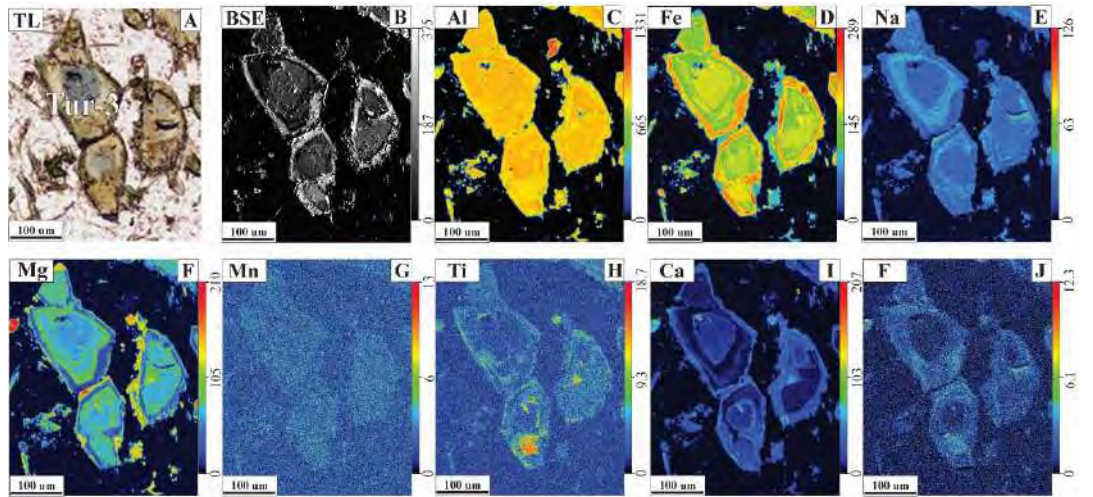
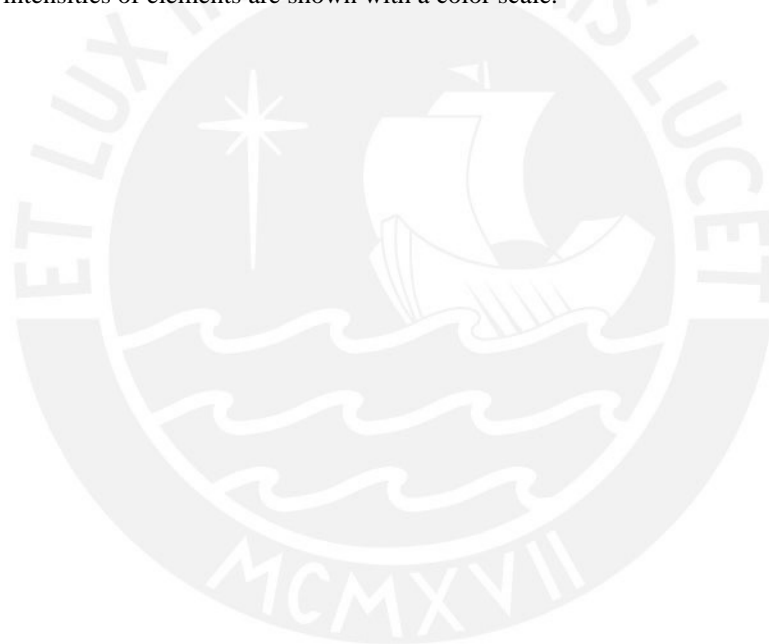


Figure 15. Transmitted light photomicrograph (TL), backscattered electron image (BSE) and corresponding X-ray elemental maps showing chemical zoning in hydrothermal tourmaline crystal (Tur-3) from the quartz-cassiterite-tourmaline veins (2020-KELL-01-A-TS3). Relative intensities of elements are shown with a color scale.



5. Discussion

5.1. *Tourmaline stability in the Chacaltaya granitic stock*

Based on our work and previous studies, we can rule out the presence of magmatic tourmaline in the Chacaltaya district. Even in the least altered samples of the Chacaltaya granite stock, we observe no evidence of magmatic tourmaline intergrown with the granitic groundmass and only hydrothermal tourmaline is found in greisens, breccias, and veins. This contrasts with the nearby Oligocene (ca. 24 Ma) San Rafael Sn(-Cu) deposit in the Cordillera de Carabaya of southeast Peru, where late-magmatic tourmaline has been described as nodules and disseminations in the cordierite-biotite peraluminous granites (Kontak and Clark, 2002; Mlynarczyk and Williams-Jones, 2006; Harlaux et al., 2020). In the Chacaltaya district, the earliest tourmaline generation identified is related to greisenization of the granitic stock (Tur-1) and hence is interpreted to be the product of post-magmatic alteration caused by B-rich hydrothermal fluids.

The Chacaltaya granitic stock belongs to the cordierite-bearing peraluminous granitoid type (CPG of Barbarin 1999). In peraluminous granites, the excess of aluminum following feldspar crystallization is consumed to form various Al-rich mineral phases such as muscovite, cordierite, andalusite, garnet and tourmaline (Clarke 1981). The stability of tourmaline in peraluminous magmas is controlled mainly by (1) the boron content of the protolith and (2) the extent of partial melting and magmatic fractionation (Pesquera et al. 2013). Granitic melts are initially undersaturated with respect to tourmaline but may become saturated when the B₂O₃ content increases while the Fe-Mg content decreases upon crystal fractionation, eventually leading to tourmaline crystallization (Wolf and London 1997). The B₂O₃ content of the silicate melt is constant while tourmaline is in

equilibrium, but low initial Fe-Mg contents in the magma limits the quantity of boron that can be consumed to form tourmaline (Wolf and London 1997).

There is no consensus about the concentration of boron needed to saturate a silicate melt and to start crystallizing tourmaline. Using experimental studies, Pesquera et al. (2013) inferred that the minimum concentration of B to saturate tourmaline in granitic melts is 500-900 ppm. Previous studies determined that the boron contents required for crystallizing tourmaline in granitic melts range from ~0.1 wt.% B₂O₃ at 500°C to ~4–6 wt.% B₂O₃ at 800°C (Benard et al. 1985; Scaillet et al. 1995; Wolf and London 1997; Spicer et al. 2004; London 2011). Boron contents in the least altered samples from the Chacaltaya granite range between 130 and 300 ppm (avg. = 215 ppm B; Lehmann 1979). Using the whole-rock geochemical data of Lehmann (1979), zircon saturation temperatures of ~750 °C are estimated for the Chacaltaya granite stock with the equation of Boehnke et al. (2013). Noteworthy, Iriarte et al. (2021) reported similar zircon saturation temperatures for the Huayna Potosí granites using the same approach. Consequently, the boron concentration of the Chacaltaya granitic melt was too low to initiate the crystallization of tourmaline at temperatures of ~750 °C, which would explain the lack of magmatic tourmaline.

Wolf and London (1997) worked on the influence of peraluminosity on tourmaline stability, quantified by the parameter ASI (alumina saturation index) that is defined as the molar ratio $Al_2O_3/(Na_2O + K_2O + CaO)$. They found that tourmaline becomes unstable in granitic melts with $ASI < 1.2$ at 700-750°C regardless of their boron content, and that more boron and/or higher ASI are required to stabilize tourmaline with increasing F contents. According to lithochemical data from Lehmann (1979), the Chacaltaya granite has ASI values ranging between 1.1 and

1.4 (avg. = 1.3) similar to those of the Huayna Potosí granites (ASI = 1.0-1.5; avg. = 1.3). Therefore, Triassic granites in the Chacaltaya district are moderately to strongly peraluminous and their ASI values encompass those of other “tin granites” from the Central Andean tin belt including the Oligocene San Rafael granitic suite (ASI = 1.1-1.5; Kontak and Clark 2002; Mlynarczyk 2005; Harlaux et al. 2021b) and Oligocene-Miocene tin porphyries of the Cordillera Real of Bolivia (ASI = 0.9-1.2; Avila-Salinas 1990).

Wolf and London (1997) also showed that higher F contents, common in highly evolved granitic magmas, result in higher boron content and/or ASI required to crystallize magmatic tourmaline. The Chacaltaya granitic melt shows high F contents (115-1575 ppm, avg. = 672 ppm; Lehmann, 1979)

Pesquera et al. (2013) described tourmaline as an accessory or absent when micas are dominant since the latter can incorporate significant amounts of B (up to >1000s ppm), thus inhibiting the saturation of tourmaline in the melt. The crystallization of micas (in particular, biotite) may have further depleted the residual magma in B (Wolf and London 1997; Pesquera et al. 2013).

That the Chacaltaya biotite-cordierite granite did not reach tourmaline saturation may be the result of low initial B contents of the granitic melt, high F contents, elevated solidus temperatures, and/or crystallization of micas, all together limiting decomposition reactions of biotite and cordierite and the crystallization of tourmaline.

5.2. *Tourmaline textures and environment of crystallization*

Tourmaline from the Chacaltaya-Kellhuani-Milluni district shows variable textures, including selective replacement of igneous phases in greisenized granites, disseminations in greisen, fine-grained cement in breccias, and acicular grains in cassiterite-bearing veins.

Tourmaline in greisen (Tur-1) with skeletal habit (Figs. 7C-D) is interpreted to be formed by the replacement of original igneous minerals, such as K-feldspar phenocrysts, during the infiltration of B-bearing aqueous fluids and greisenization of the granitic stock, likely at high temperatures ($> 400\text{-}500^{\circ}\text{C}$), according to previous studies on greisen (Halter et al. 1998; Breiter et al. 2017; Launay et al. 2021). The lack of significant optical (Fig. 7C) and compositional (Figs. 12A-J) zoning in Tur-1 suggests a relatively homogeneous composition of the hydrothermal fluids during its crystallization.

Tourmaline in breccias (Tur-2) and cassiterite-bearing tourmaline veins (Tur-3) is mostly fibrous. Fibrous tourmaline usually forms where there is an open fluid-filled space at lower temperatures ($< 400^{\circ}\text{C}$) in hydrothermal systems (Dutrow and Henry 2016; Harlaux et al. 2020). Crystallization of tourmaline as open-space filling at the Chacaltaya district is also supported by the fact that crystals grew perpendicular to the clast borders in triangular and acute-angle spaces in the breccias (Figs. 5E, 8C) and to host rocks in veins, where in the latter tourmaline is intergrown with comb-like, coarse-grained quartz (Fig. 9). The oscillatory and convoluted zoning in Tur-3 grains suggest rapidly-changing conditions during crystallization, as discussed below.

5.3. *Tourmaline chemistry as a tracer of hydrothermal fluid evolution*

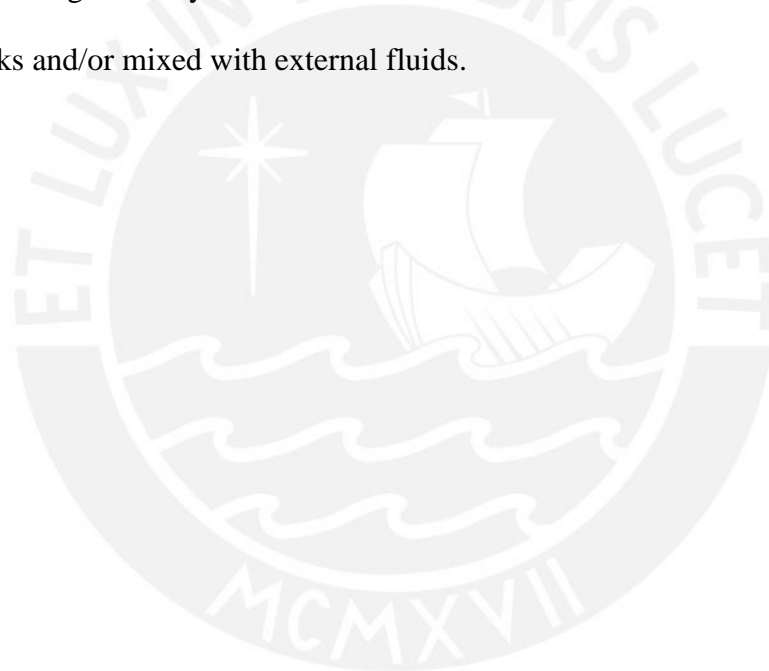
The Fe/(Fe + Mg) value of magmatic tourmaline varies according to the oxygen fugacity in granitic magmas and tends to increase as granitic magmas evolve and become more oxidized (da Costa et al. 2021). On the other hand, experimental work showed a correlation between salinity and the Fe/(Fe + Mg) ratio of tourmaline, so decreasing fluid salinities produce tourmaline with more schorlitic compositions (von Goerne et al., 2011; Orlando et al., 2017). This ratio also varies according to the source of the magmas and the crystallizing phases (London 2011). The fact that Fe/(Fe + Mg) ratios of the different tourmaline petrographic types (Tur-1 to Tur-3) overlap (Fig. 11) would suggest that oxygen fugacity and salinity of mineralizing fluids were relatively steady during the evolution of the magmatic-hydrothermal system.

In spite of their broadly overlapping Fe-Mg compositions, a few Tur-3 analyses show lower Fe/(Fe + Mg) values resulting in a larger range of Fe/(Fe + Mg) ratios in Tur-3 relative to Tur-1 and Tur-2. These variations in Tur-3 are also revealed by the growth and convolute zoning, which are visible in sections perpendicular to the tourmaline c-axis (Fig. 15). The observed compositional zoning in Tur-3 could reflect rapid changes in the hydrothermal system with pulses of relatively more reduced and saline fluids (correlated with lower Fe/(Fe + Mg) in tourmaline) alternating with pulses of more oxidized and diluted fluids.

It is also Tur-3 that shows the largest variations in Ca (Fig. 11D), whereas Na contents are similar amongst the three tourmaline types (Table 2). The Ca and Na contents and the Ca/Na ratio in hydrothermal tourmalines directly correlated to the aqueous fluid composition from which it crystallizes (von Goerne et al. 2011).

Calcium enrichment in a significant number of Tur-3 analyses compared to Tur-1 and Tur-2 would hence point to an increasing $\text{Ca}/(\text{Ca} + \text{Na})$ ratio in the hydrothermal fluids. Such evolution may be explained by a higher degree of fluid-rock interaction in veins relative to greisen and hydraulic breccias (Dutrow and Henry 2016).

Greisen-hosted Tur-1 likely formed at high-temperature ($> 450^\circ\text{C}$) during subsolidus alteration of the Chacaltaya granitic stock, while breccia- (Tur-2) and vein-hosted (Tur-3) tourmaline likely formed at lower temperature ($<400^\circ\text{C}$) due to cooling of the hydrothermal fluids which interacted with the metamorphic host rocks and/or mixed with external fluids.



6. Conclusions

The present study documents the textures and compositional variations of hydrothermal tourmaline in the Chacaltaya-Kellhuani-Milluni district, La Paz, Bolivia. The main conclusions are the following:

1. Three hydrothermal tourmaline types are distinguished based on petrographic observations. Tur-1 occurs as replacement of igneous minerals in the greisenized Chacaltaya granite and as clasts in tourmaline-cemented breccias. Tur-2 composes the cement of breccias and is characterized by a very fine-grained acicular texture. Tur-3 appears as subhedral crystals that form radial aggregates in the cassiterite-bearing quartz veins and as very fine-grained crystals in vein selvages. Tur-2 and Tur-3 co-crystallized with cassiterite in hydrothermal breccias and veins, respectively.
2. The absence of magmatic tourmaline in the Chacaltaya S-type, biotite-cordierite granite is interpreted to result from low initial B contents of the granitic melt, high F contents, elevated solidus temperatures, and/or crystallization of micas, all together limiting decomposition reactions of biotite and cordierite and the crystallization of tourmaline. The generation of B-rich hydrothermal fluids is interpreted to derive from a renewed injection of granitic melts in the crystallizing granitic stock.
3. The three tourmaline petrographic types (Tur-1 to Tur-3) belong to the alkali group and have dominantly Fe-rich compositions close to the schorl endmember, partly extending into the compositional fields of foitite and dravite. Tur-1 has $Fe/(Fe + Mg) = 0.58$ to 0.94 and $X_{\square}/(X_{\square} + Na + K) = 0.19$ to 0.61 . Tur-2 is characterized by $Fe/(Fe + Mg) = 0.54$ to 0.97 and $X_{\square}/(X_{\square} + Na + K) = 0.08$ to 0.70 . Tur-3 has $Fe/(Fe + Mg) = 0.35$ to 0.92 and $X_{\square}/(X_{\square} + Na + K) = 0.05$ to 0.72 . The largely overlapping major element

compositions of the different tourmaline types is interpreted to reflect generally steady chemical conditions of the hydrothermal fluids from which they crystallized.

4. In greisen samples, major element compositions of white mica are homogeneous and range between muscovite and phengite, with muscovite being the predominant component.



7. References

- Ahlfeld F (1956) Handbook of South American Geology: An Explanation of the Geologic Map of South America. *Geol S Am Mem* 65:167-186. <https://doi.org/10.1130/MEM65-p167>
- Ahlfeld F (1967) Metallogenetic epochs and provinces of Bolivia. *Miner Deposita* 2:291-311. <https://doi.org/10.1007/bf00207022>
- Ahlfeld F, Branisa L (1960) *Geología de Bolivia*. Instituto Boliviano del Petróleo, Don Bosco Edit., La Paz
- Arriagada C, Roperch P, Mpodozis C, Cobbold PR (2008) Paleogene building of the Bolivian Orocline: Tectonic restoration of the central Andes in 2-D map view. *Tectonics* 27:1-14. <https://doi.org/10.1029/2008TC002269>
- Avila-Salinas WA (1990) Tin-bearing granites from the Cordillera Real, Bolivia; a petrological and geochemical review. *Plutonism from Antarctica to Alaska. Geol Soc Am S* 241:5-159. <https://doi.org/10.1130/SPE241-p145>
- Baby P, Calderón Y, Hurtado C, Louterbach M, Espurt N, Brusset S, Roddaz M, Brichau S, Eude A, Calves G, Quispe A, Ramirez L, Bandach A, Bolaños R (2018) The Peruvian sub-Andean foreland basin system: Structural overview, geochronologic constraints, and unexplored plays. *Petroleum basins and hydrocarbon potential of the Andes of Peru and Bolivia: AAPG Memoir* 117:87-116. <https://doi.org/10.1306/13622118M1173767>
- Baldellón E, Fornari M, Espinoza F, Soler P (1994) Sucesión estructural de la zona Serranía de las Minas. *XI Congreso Geológico de Bolivia, Memorias*:238–247
- Barbarin B (1999) A review of the relationships between granitoid types, their origins and their geodynamic environments. *Lithos* 46:605-626. [https://doi.org/10.1016/S0024-4937\(98\)00085-1](https://doi.org/10.1016/S0024-4937(98)00085-1)
- Bard JP, Botello R, Martinez C, Subieta T (1974) Relations entre tectonique, métamorphisme et mise en place d'un granite éohercynien à deux micas dans la Cordillère Real de Bolivie (massif de Zongo-Yani). *Série Géologie* 6:3-18
- Beck SL, Zandt G, Myers SC, Wallace TC, Silver PG, Drake LA (1996) Crustal-thickness variations in the central Andes. *Geology* 24:407-410. [https://doi.org/10.1130/0091-7613\(1996\)024<0407:ctvitc>2.3.co;2](https://doi.org/10.1130/0091-7613(1996)024<0407:ctvitc>2.3.co;2)
- Bellido F, Valverde P, Jaimes F, Carlotto V, Díaz-Martínez E (2009) Datación y caracterización geoquímica de los granitoides peraluminicos de los Cerros de Amotape y de los macizos de Illescas y Paita (noroeste de Perú). *Bol Soc Geol Perú* 103:197-213
- Benard F, Moutou P, Pichavant M (1985) Phase-relations of tourmaline leucogranites and the significance of tourmaline in silicic magmas. *J Geol* 93:271-291. <https://doi.org/10.1086/628952>

- Benites D, Torró L, Vallance J, & Laurent O, Quispe C, Rosas S, Uzieda M, Holm-Denoma C, Pianowski L, Camprubí A, Colás V, Fernández-Baca Á, Giraldo L, Chelle-Michou C, Saez J, Kouzmanov K, Fontboté L (2022). Geology, mineralogy, and cassiterite geochronology of the Ayawilca Zn-Pb-Ag-In-Sn-Cu deposit, Pasco, Peru. *Miner Deposita* 57:1-27. <https://doi.org/10.1007/s00126-021-01066-z>
- Betkowski WB, Rakovan J, Harlov DE (2017) Geochemical and textural characterization of phosphate accessory phases in the vein assemblage and metasomatically altered Llallagua tin porphyry. *Miner Petrol* 111:547-568. <https://doi.org/10.1007/s00710-017-0510-6>
- Breiter K, Ďurišová J, Hrstka T, Korbelová Z, Vaňková MH, Galiová MV, Kanický V, Rambousek P, Knésl I, Dobeš P, Dosbaba M (2017) Assessment of 880 magmatic vs. metasomatic processes in rare-metal granites: a case study of the 881 Cínovec/Zinnwald Sn–W–Li deposit, Central Europe. *Lithos* 292:198-217. <https://doi.org/10.1016/j.lithos.2017.08.015>
- Boehnke P, Watson EB, Trail D, Harrison TM, Schmitt AK (2013) Zircon saturation revisited. *Chem Geol* 351:324–334. <https://doi.org/10.1016/j.chemgeo.2013.05.028>
- Cacho A, Melgarejo JC, Camprubí A, Torró L, Castillo-Oliver M, Torres B, Artiaga D, Tauler E, Martínez A, Campeny M, Alfonso P, Arce-Burgoa O (2019) Mineralogy and distribution of critical elements in the Sn–S–Pb–Ag–Zn Huanuni deposit, Bolivia. *Minerals* 9:753. <https://doi.org/10.3390/min9120753>
- Capitanio FA, Faccenna C, Zlotnik S, Stegman DR (2011) Subduction dynamics and the origin of Andean orogeny and the Bolivian orocline. *Nature* 480:83-86. <https://doi.org/10.1038/nature10596>
- Carlier G, Lorand JP, Liégeois JP, Fornari M, Soler P, Carlotto V, Cárdenas J (2005) Potassic-ultrapotassic mafic rocks delineate two lithospheric mantle blocks beneath the southern Peruvian Altiplano. *Geology* 33:601-604. [https://doi.org/10.1016/0012-8252\(82\)90040-X](https://doi.org/10.1016/0012-8252(82)90040-X)
- Carlotto V (2013) Paleogeographic and tectonic controls on the evolution of Cenozoic basins in the Altiplano and Western Cordillera of southern Peru. *Tectonophysics* 589:195-219. <https://doi.org/10.1016/j.tecto.2013.01.002>
- Carlotto V, Quispe J, Acosta H, Rodríguez R, Romero D, Cerpa L, Mamani M, Díaz E, Navarro P, Jaimes F, Velarde K, Lu S, Cueva E (2009) Dominios geotectónicos y metalogénesis del Perú. *Bol Soc Geol Perú* 103:1-89
- Chew DM, Schaltegger U, Košler J, Whitehouse MJ, Gutjahr M, Spikings RA, Miškovíc A (2007) U-Pb geochronologic evidence for the evolution of the Gondwanan margin of the north-central Andes. *Geol Soc Am Bull* 119:697-711. <https://doi.org/10.1130/B26080.1>
- Chew DM, Pedemonte G, Corbett E (2016) Proto-Andean evolution of the Eastern Cordillera of Peru. *Gondwana Res* 35:59-78. <https://doi.org/10.1016/j.gr.2016.03.016>
- Clarke DB (1981) The mineralogy of peraluminous granites: A review. *Can Mineral* 19:3-17

- Columba C, Cunningham CG (1993) Geologic model for the mineral deposits of the La Joya District, Oruro, Bolivia. *Econ Geol* 88:701-708. <https://doi.org/10.2113/gsecongeo.88.3.701>
- COMIBOL (2018) Potencial Mineralógico: Vida Útil de la Mina. Empresa Minera Huanuni. <https://emhuanuni.gob.bo/index.php/institucional/estructura>. Accessed 5 Dec 2021
- Cordani UG, Iriarte AR, Sato K (2019) Geochronological systematics of the Huayna Potosí, Zongo and Taquesi plutons, Cordillera Real of Bolivia, by the K/Ar, Rb/Sr and U/Pb methods. *Braz J Geol* 49: e20190016. <https://doi.org/10.1590/2317-4889201920190016>
- da Costa IR, Antunes IMHR, Récio C (2021) The Mg/(Fe+ Mg) ratio and the Ti and A site contents of tourmaline as promising indicators of granitic magma evolution. *J Iber Geol* 47:307-321. <https://doi.org/10.1007/s41513-020-00158-5>
- de Silva SL, Kay MS (2018) Turning up the heat: high-flux magmatism in the Central Andes. *Elements* 14:245-250. <https://doi.org/10.2138/gselements.14.4.245>
- Dietrich A, Lehmann B, Wallianos A (2000) Bulk rock and melt inclusion geochemistry of Bolivian tin porphyry systems. *Econ Geol* 95:313-326. <https://doi.org/10.2113/gsecongeo.95.2.313>
- Dutrow BL, Henry DJ (2011) Tourmaline: A geologic DVD. *Elements* 7:301-306. <https://doi.org/10.2113/gselements.7.5.301>
- Dutrow BL, Henry DJ (2016) Fibrous tourmaline: A sensitive probe of fluid compositions and petrologic environments. *Can Mineral* 54:311-335. <https://doi.org/10.3749/canmin.1600019>
- Espinoza A (2021) Análisis petromineralógico, geoquímico y estructural de las fases magmática, tardi-magmática y post-magmática del Granito de Paita (Dominio Amotape-Tahuín): ¿Un sistema Greisen en el Norte del Perú?. Tesis de grado. Pontificia Universidad Católica del Perú
- Espinoza A, Stipetich S, Hurtado de Mendoza R, Sáez J, Vallance J (2021) Pegmatitas, apatitas, greisen y anomalías de estaño en el leucogranito triásico de Paita, Piura. *XII Proexplor* 2021:193-197
- Espinoza J (2010) Minería Boliviana: Su realidad. Plural, La Paz
- Eugster HP (1986) Minerals in hot water. *Am Mineralogist* 71:655-673
- European Commission (2020) Study on the EU's list of Critical Raw Materials (final report). Eur Commis. <https://doi.org/10.2873/904613>.
- Evernden JF, Kriz SJ, Cherroni MC (1977) Potassium-argon ages of some Bolivian rocks. *Econ Geol* 72:1042-1061. <https://doi.org/10.2113/gsecongeo.72.6.1042>
- Farrar E, Clark AH, Heinrich SM (1990) The age of the Zongo pluton and the tectonothermal evolution of the Zongo-San Gabán Zone in the Cordillera Real, Bolivia. Extended abstracts, 1st International Symposium on Andean Geodynamics, Grenoble, pp 171-174

- Fontboté L (2018) Ore deposits of the Central Andes. *Elements* 14:257-261. <https://doi.org/10.2138/gselements.14.4.257>
- Franzese JR, Spalletti LA (2001) Late Triassic- Early Jurassic continental extension in southwestern Gondwana: tectonic segmentation and pre-break-up rifting. *J S Am Earth Sci* 14:257-270. [https://doi.org/10.1016/S0895-9811\(01\)00029-3](https://doi.org/10.1016/S0895-9811(01)00029-3)
- García-Casco A (2007) Magmatic paragonite in trondhjemites from the Sierra del Convento mélange, Cuba. *Am Mineral* 92:1232-1237. <https://doi.org/10.2138/am.2007.2598>
- Gemrich L, Torró L, Melgarejo JC, Laurent O, Vallance J, Chelle-Michou C, Sempere T (2021) Trace element composition and U-Pb ages of cassiterite from the Bolivian tin belt. *Miner Deposita* 56:1491-1520. <https://doi.org/10.1007/s00126-020-01030-3>
- Gibert L, Deino A, Valero L, Anaya F, Lería M, Saylor B, Croft DA (2020) Chronology of Miocene terrestrial deposits and fossil vertebrates from Quebrada Honda (Bolivia). *Palaeogeogr Palaeoclimatol* 560:110013. <https://doi.org/10.1016/j.palaeo.2020.110013>
- Gillis RJ, Horton BK, Grove M (2006) Thermochronology, geochronology, and upper crustal structure of the Cordillera Real: Implications for Cenozoic exhumation of the central Andean plateau. *Tectonics* 25:TC6007. <https://doi.org/10.1029/2005TC001887>
- Grant JN, Halls C, Avila Salinas W, Snelling NJ (1979) K-Ar ages of igneous rocks and mineralization in part of the Bolivian tin belt. *Econ Geol* 74:838-851. <https://doi.org/10.2113/gsecongeo.74.4.838>
- Grzela D, Beaudoin G, Bédard É (2019) Tourmaline, scheelite, and magnetite compositions from orogenic gold deposits and glacial sediments of the Val-d'Or district (Québec, Canada): Applications to mineral exploration. *J Geochem Explor* 206:106355. <https://doi.org/10.1016/j.gexplo.2019.106355>
- Halter WE, Williams-Jones AE, and Kontak DJ (1998) Modeling fluid-rock interaction during greisenization at the East Kemptville tin deposit: implications for mineralization. *Chem Geol* 150: 1-17. [https://doi.org/10.1016/S0009-2541\(98\)00050-3](https://doi.org/10.1016/S0009-2541(98)00050-3)
- Harlaux M, Kouzmanov K, Gialli S, Laurent O, Rielli A, Dini A, Chauvet A, Menzies A, Kalinaj A, Fontboté L (2020) Tourmaline as a tracer of late-magmatic to hydrothermal fluid evolution: The world-class San Rafael tin (-copper) deposit, Peru. *Econ Geol* 115:1665-1697. <https://doi.org/10.5382/ECONGEO.4762>
- Harlaux M, Kouzmanov K, Gialli S, Marger K, Bouvier A-S, Baumgartner LP, Rielli A, Dini A, Chauvet A, Kalinaj M, Fontboté L (2021a) Fluid mixing as primary trigger for cassiterite deposition: Evidence from in situ $\delta^{18}\text{O}$ - $\delta^{11}\text{B}$ analysis of tourmaline from the world-class San Rafael tin (-copper) deposit, Peru. *Earth Planet Sc Lett* 563:116889. <https://doi.org/10.1016/j.epsl.2021.116889>
- Harlaux M, Kouzmanov K, Gialli S, Clark AH, Laurent O, Corthay G, Prado E, Dini A, Chauvet A, Ulianov A, Chiaradia M, Menzies A, Villón G, Kalinaj M, Fontboté L (2021b) The upper Oligocene San Rafael intrusive complex (Eastern Cordillera,

- southeast Peru), host of the largest-known high-grade tin deposit. *Lithos* 400-401, 106409. <https://doi.org/10.1016/j.lithos.2021.106409>
- Hawthorne FC, Dirlam DM (2011) Tourmaline the Indicator Mineral: From Atomic Arrangement to Viking Navigation. *Elements* 7:307-312. <https://doi.org/10.2113/gselements.7.5.307>
- Hawthorne FC, Henry DJ (1999) Classification of the minerals of the tourmaline group. *Eur J Mineral* 11:201-216. <https://doi.org/10.1127/ejm/11/2/0201>
- Henry DJ, Guidotti CV (1985) Tourmaline as a petrogenetic indicator mineral: an example from the staurolite-grade metapelites of NW Maine. *Am Mineral* 70:1-15
- Henry DJ, Novak M, Hawthorne FC, Ertl A, Dutrow BL, Uher P, Pezzotta, F (2011) Nomenclature of the tourmaline-supergroup minerals. *Am Mineral* 96:895-913. <https://doi.org/10.2138/am.2011.3636>
- Heuschmidt B, Bellot de la Torre J, Miranda Angles V, Claire Zapata M (2002) Las áreas prospectivas de Bolivia para yacimientos metalíferos. *B Serv Nac Geol Min* 30:154
- Hu J, Liu L, Gurnis M (2021) Southward expanding plate coupling due to variation in sediment subduction as a cause of Andean growth. *Nat Commun* 12:7271. <https://doi.org/10.1038/s41467-021-27518-8>
- Husson L, Sempere T (2003) Thickening the Altiplano crust by gravity-driven crustal channel flow. *Geophys Res Lett* 30:1-4. <https://doi.org/10.1029/2002gl016877>
- IMA (2023) The New IMA List of Minerals. <http://cnmnc.units.it/>. Accessed 24 Jul. 2023
- Iriarte A, Cordani U, Sato K (2021) Geochronology of the Cordillera Real granitoids, the inner magmatic arc of Bolivia. *Andean Geol* 48:403-441. <http://doi.org/10.5027/andgeoV48n3-3326>
- Ishihara S, Murakami H, Márquez-Zavalía MF (2011) Inferred indium resources of the Bolivian tin-polymetallic deposits. *Resour Geol* 61:174-191. <https://doi.org/10.1111/j.1751-3928.2011.00157.x>
- ITA (2020) Global Resources & Reserves. *Int Tin Assoc*
- ITA (2021) Huanuni's Lucianita plant begins operations. *Int Tin Assoc*. Accessed 5 Dec 2021
- James DE (1971a) Andean crustal and upper mantle structure. *J Geophys Res* 76:3246-3271. <https://doi.org/10.1029/JB076i014p03246>
- James DE (1971b) Plate tectonic model for the evolution of the Central Andes. *Geol Soc Am Bull* 82:3325-3346. [https://doi.org/10.1130/7606\(1971\)82\[3325:PTMFTE\]2.0.CO;2](https://doi.org/10.1130/7606(1971)82[3325:PTMFTE]2.0.CO;2)
- Jenks WF (1956) Handbook of South American Geology: An Explanation of the Geologic Map of South America. *Geol Soc Am Mem* 65. <https://doi.org/10.1130/MEM65-pxiii>

- Jiang SY (1998) Stable and radiogenic isotope studies of tourmaline: an overview. *J Geol Soc Czech* 43:75-90
- Kato JJ (2013) Geochemistry of the Neogene Los Frailes Ignimbrite Complex on the Central Andean Altiplano Plateau. B.S. Thesis, Cornell University
- Kay SM, Mpodozis C (2020) The Andes. *Econ Geol* 2:1-15. <https://doi.org/10.1016/b978-0-08-102908-4.00173-9>
- Keller CB (2010) Chemical Constraints on the Origin of the Frailes Volcanic Complex in the Central Andean Altiplano Plateau, Bolivia. B.S. Thesis, Cornell University. <https://doi.org/10.31237/osf.io/y6kv4>
- Kelly WMC, Turneure FS (1970) Mineralogy, paragenesis and geothermometry of the tin and tungsten deposits of the Eastern Andes, Bolivia. *Econ Geol* 65:609-680. <https://doi.org/10.2113/gsecongeo.65.6.609>
- Kono M, Fukao Y, Yamamoto A (1989) Mountain building in the Central Andes. *J Geophys Res* 94:3891–3905. <https://doi.org/10.1029/JB094iB04p03891>
- Kontak DJ, Clark AH (2002) Genesis of the giant, bonanza San Rafael lode tin deposit, Peru: origin and significance of pervasive alteration. *Econ Geol* 97:1741-1777. <https://doi.org/10.2113/gsecongeo.97.8.1741>
- Kontak DJ, Clark AH, Farrar E, Strong DF (1985) The rift associated Permo-Triassic magmatism of the Eastern Cordillera: a precursor to the Andean orogeny. In: Pitcher, WS, Atherton MP, Cobbing J, Beckinsale RD (eds) *Magmatism at a plate edge: The Peruvian Andes*. Blackie, Glasgow, and Halsted Press, New York: 36-44. https://doi.org/10.1007/978-1-4899-5820-4_5
- Kontak DJ, Clark AH, Pearce TH, Strong DF, Baadsgaard H (1986) Petrogenesis of a Neogene shoshonite suite, Cerro Moromoni, Puno, southeastern Peru. *Can Mineral* 24:117-135
- Kontak DJ, Farrar E, Clark AH, Archibald DA (1990) Eocene tectono-thermal rejuvenation of an upper Paleozoic-lower Mesozoic terrane in the Cordillera de Carabaya, Puno, southeastern Peru, revealed by K-Ar and ⁴⁰Ar/³⁹Ar dating. *J S Am Earth Sci* 3:231-246. [https://doi.org/10.1016/0895-9811\(90\)90005-L](https://doi.org/10.1016/0895-9811(90)90005-L)
- Launay G, Sizaret S, Lach P, Melleton J, Gloaguen E, Poujol M (2021) Genetic relationship between greisenization and Sn-W mineralizations in vein and greisen deposits: Insights from the Panasqueira deposit (Portugal). *BSGF-Earth Sciences* 1093. <https://doi.org/10.1051/bsgf/2020046>
- Lehmann B (1979) Schichtgebundene Sn-lagerstätten in der Cordillera Real, Bolivien: 1098 Ph.D. thesis, Berlin, Germany, University of Berlin 154. <https://doi.org/10.23689/idgeo-5270>
- Lehmann B (1982) Metallogeny of tin: magmatic differentiation versus geochemical heritage. *Econ Geol* 77:50-59. <https://doi.org/10.2113/gsecongeo.77.1.50>

- Lehmann B (1985) Formation of the strata-bound Kellhuani tin deposits, Bolivia. *Min Deposita* 20:169-176. <https://doi.org/10.1007/BF00204561>
- Lehmann B (2004) Metallogeny of the Central Andes: Geotectonic framework and geochemical evolution of the porphyry system in Bolivia and Chile during the last 40 million years. In: Khanchuk AI, Gonevchuk GA, Mitrokhin AN, Simanenko LF, Cook NJ, Seltmann R (eds) *Metallogeny of the Pacific Northwest: Tectonics, Magmatism and Metallogeny of Active Continental Margins*. Vladivostok, Russia 118-122
- Lehmann B (2021) Formation of tin ore deposits: A reassessment. *Lithos* 402: 105756. <https://doi.org/10.1016/j.lithos.2020.105756>
- Lehmann B, Mahawat C (1989) Metallogeny of tin in central Thailand: a genetic concept. *Geology* 17:426-429
- Lehmann B, Ishihara S, Michel H, Miller J, Rapela C, Sanchez A, Tistl M, Winkelmann L (1990) The Bolivian tin province and regional tin distribution in the Central Andes: a Reassessment. *Econ Geol* 85:1044-1058. <https://doi.org/10.2113/gsecongeo.85.5.1044>
- Lehmann B, Dietrich A, Heinhorst J, Métrich N, Mosbah M, Palacios C, Schneider H-J, Wallianos A, Webster J, Winkelmann L (2000) Boron in the Bolivian tin belt. *Min Deposita* 35:223-232. <https://doi.org/10.1007/s001260050017>
- Li W, Qiao X, Zhang F, Zhang L (2022) Tourmaline as a potential mineral for exploring porphyry deposits: a case study of the Bilihe gold deposit in Inner Mongolia, China. *Min Deposita* 57:61-82. <https://doi.org/10.1007/s00126-021-01051-6>
- Lindgren W (1926) Replacement in the tin-bearing veins of Caracoles, Bolivia. *Econ Geol* 21: 135-144. <https://doi.org/10.2113/gsecongeo.21.2.135>
- Litherland M, Aspden JA, Jemielita RA (1994) The Metamorphic Belts of Ecuador. *British Geol Surv, Overseas Mem* 11:147
- London D (2008) Pegmatites. *Can Mineral Spec Publ* 10
- London D (2011) Experimental synthesis and stability of tourmaline: A historical overview. *Can Mineral* 49:117-136. <https://doi.org/10.3749/canmin.49.1.117>
- Macfadden BJ, Anaya F, Swisher CC (1995) Neogene paleomagnetism and oroclinal bending of the central Andes of Bolivia. *J Geophys Res* 100:8153-8167. <https://doi.org/10.1029/95JB00149>
- Maffione M, Speranza F, Faccenna C (2009) Bending of the Bolivian orocline and growth of the central Andean plateau: Paleomagnetic and structural constraints from the Eastern Cordillera (22-24°S, NW Argentina). *Tectonics* 28: TC4006. <https://doi.org/10.1029/2008TC002402>
- Mamani M, Tassara A, Wörner G (2008) Composition and structural control of crustal domains in the Central Andes. *Geochem Geophys Geosy* 9:3

- Mamani M, Wörner G, Sempere T (2010) Geochemical variations in igneous rocks of the Central Andean orocline (13°S to 18°S): Tracing crustal thickening and magma generation through time and space. *Geol Soc Am Bull* 122:162-182. <https://doi.org/10.1130/B26538.1>
- Márquez-Zavalía MF, Vymazalová A, Galliski MÁ, Watanabe Y, Murakami H (2020) Indium-bearing paragenesis from the Nueva Esperanza and Restauradora veins, Capillitas mine, Argentina. *J Geosci* 65:97-109. <https://doi.org/10.3190/jgeosci.304>
- Marschall HR, Jiang SY (2011) Tourmaline isotopes: No element left behind. *Elements* 7:313-319. <https://doi.org/10.2113/gselements.7.5.313>
- McBride SL, Robertson RCR, Clark AH, Farrar E (1983) Magmatic and metallogenetic episodes in the northern tin belt, Cordillera Real, Bolivia. *Geol Rdsch* 72:685-713
- McQuarrie N (2002) Initial plate geometry, shortening variations, and evolution of the Bolivian orocline. *Geology* 30:867-870. [https://doi.org/10.1130/0091-7613\(2002\)030<0867:IPGSVA>2.0.CO;2](https://doi.org/10.1130/0091-7613(2002)030<0867:IPGSVA>2.0.CO;2)
- Mégard F (1984) The Andean orogenic period and its major structures in central and northern Peru. *J Geol Soc London* 141:893-900
- Mills SJ, Hatert F, Nickel EH, Ferraris G (2009) The standardisation of mineral group hierarchies: Application to recent nomenclature proposals. *Eur J Mineral* 21:1073-1090. <https://doi.org/10.1127/0935-1221/2009/0021-1994>
- Minsur S.A., 2018, Annual report: December 31, 2018, 57 p., www.minsur.com.
- Minsur S.A., 2020, Annual report: December 31, 2020, 70 p., www.minsur.com.
- Minsur S.A., 2021, Annual report: December 31, 2021, 70 p., www.minsur.com.
- Mišković A, Spikings RA, Chew DM, Kosler J, Ulianov A, Schaltegger U (2009) Tectonomagmatic evolution of Western Amazonia: Geochemical characterization and zircon U-Pb geochronologic constraints from the Peruvian Eastern Cordilleran granitoids. *Geol Soc Am Bull* 121:1298-1324. <https://doi.org/10.1130/B26488.1>
- Mlynarczyk MSJ (2005) Constraints on the genesis of lode-style tin mineralization: Evidence from the San Rafael tin-copper deposit, Peru: Unpublished Ph.D. thesis, Montréal, Canada, McGill University 360
- Mlynarczyk MSJ, Williams-Jones AE (2005) The role of collisional tectonics in the metallogeny of the Central Andean tin belt. *Earth Planet Sci Lett* 240:656-667. <https://doi.org/10.1016/j.epsl.2005.09.047>
- Mlynarczyk MSJ, Williams-Jones AE (2006) Zoned tourmaline associated with cassiterite: Implications for fluid evolution and tin mineralization in the San Rafael Sn-Cu deposit, southeastern Peru. *Can Mineral* 44:347-365. <https://doi.org/10.2113/gscanmin.44.2.347>

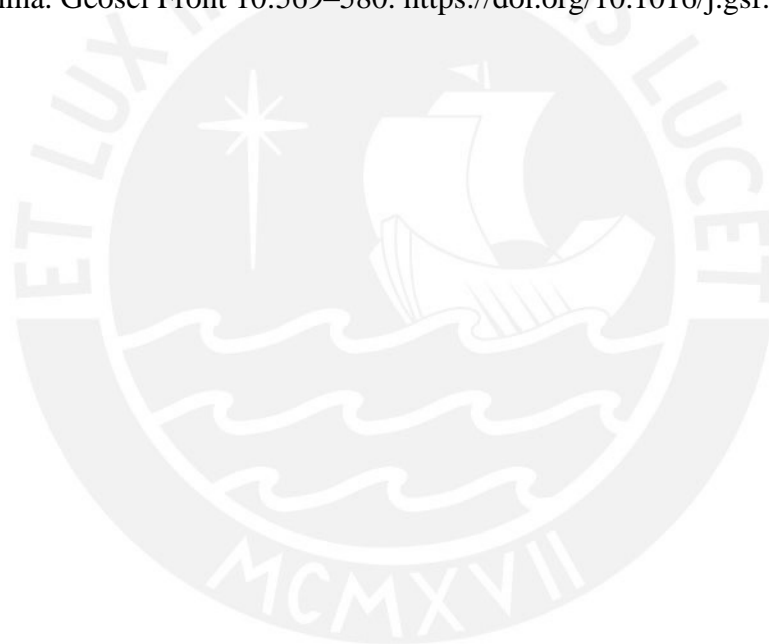
- Müller B, Frischknecht R, Seward T, Heinrich C, Camargo Gallegos W (2001) A fluid inclusion reconnaissance study of the Huanuni tin deposit (Bolivia), using LA-ICP-MS micro-analysis. *Miner Deposita* 36:680–688. <https://doi.org/10.1007/s001260100195>
- Noble DC, Silberman ML, Megard F, Bowman HR (1978) Comendite (peralkaline rhyolites) and basalt in the Mitu Group, Peru: evidence of Permian-Triassic crustal extension in the Central Andes. *U.S. Geol Surv* 6:453-457
- Orlando A, Ruggieri G, Chiarantini L, Montegrossi G, Rimondi V (2017) Experimental investigation of biotite-rich schist reacting with B-bearing fluids at upper crustal conditions and correlated tourmaline formation. *Minerals* 7:155–178. <https://doi.org/10.3390/min7090155>
- Pesquera A, Torres-Ruiz J, García-Casco A, Gil-Crespo PP (2013) Evaluating the controls on tourmaline formation in granitic systems: A case study on peraluminous granites from the central Iberian zone (CIZ), western Spain. *J Petrol* 54:609-634. <https://doi.org/10.1093/petrology/egs080>
- Pezzotta F, Laurs BM (2011) Tourmaline: The kaleidoscopic gemstone. *Elements* 7:333-338. <https://doi.org/10.2113/gselements.7.5.333>
- Ramos VA (2008) The basement of the Central Andes: The Arequipa and related terranes. *Annu Rev Earth Pl Sc* 36:289-324. <https://doi.org/10.1146/annurev.earth.36.031207.124304>
- Ramos VA (2009) Anatomy and global context of the Andes: Main geologic features and the Andean orogenic cycle. In: Kay SM, Ramos VA, Dickinson W (eds) *Backbone of the Americas: Shallow subduction, plateau uplift, and ridge and terrane collision*. *Geol Soc Am Mem* 204:31-65. [https://doi.org/10.1130/2009.1204\(02\)](https://doi.org/10.1130/2009.1204(02))
- Ramos VA (2018) Tectonic evolution of the Central Andes: From terrane accretion to crustal delamination. *AAPG Mem* 117:1-34. <https://doi.org/10.1306/13622115M1172855>
- Redwood SD, Rice CM (1997) Petrogenesis of Miocene basic shoshonitic lavas in the Bolivian Andes and implications for hydrothermal gold, silver and tin deposits. *J S Am Earth Sci* 10:203-221. [https://doi.org/10.1016/S0895-9811\(97\)00024-2](https://doi.org/10.1016/S0895-9811(97)00024-2)
- Reitsma MJ (2012) Reconstructing the Late Paleozoic-Early Mesozoic plutonic and sedimentary record of South-East Peru: orphaned backarcs along the western margin of Gondwana. PhD thesis *Terre & Environment* 111. University of Geneva, Switzerland
- Rice CM, Steele GB, Barfod DN, Boyce AJ, Pringle MS (2005) Duration of magmatic, hydrothermal, and supergene activity at Cerro Rico de Potosí, Bolivia. *Econ Geol* 100:1647-1656. <https://doi.org/10.2113/gsecongeo.100.8.1647>
- Richter D, Ludington S, Soria-Escalante E (1975) Geologic Setting. In: *Geology and Mineral Resources of the Altiplano and Cordillera Occidental, Bolivia*. U.S. Geol Surv Denver:14-24. <https://doi.org/10.3133/b1975>

- Roeder D, Chamberlain RL (1995) Structural geology of Sub-Andean fold and thrust belt in northwestern Bolivia. *Petroleum basins of South America: AAPG Mem* 62:459-479. <https://doi.org/10.1306/M62593>
- Sánchez J, Palacios O, Feininger T, Carlotto V, Quispesivana L (2006) Puesta en evidencia de granitoides Triásicos en los Amotapes-Tahuín: Deflexión de Huancabamba. XIII Congreso Peruano de Geología, Resúmenes Extendidos del Perú 13:312-315
- Sandeman HA, Clark AH, Farrar E (1995) An integrated tectono-magmatic model for the evolution of the southern Peruvian Andes (13°-20°S) since 55 Ma. *Int Geol Rev* 37:1039-1073. <https://doi.org/10.1080/00206819509465439>
- Saylor JE, Horton BK (2014) Nonuniform surface uplift of the Andean plateau revealed by deuterium isotopes in Miocene volcanic glass from southern Peru. *Earth Planet Sc Lett* 387:120-131. <https://doi.org/10.1016/j.epsl.2013.11.015>
- Scaillet B, Pichavant M, Roux J (1995) Experimental crystallization of leucogranite magmas. *J Petrol* 36:663-705. <https://doi.org/10.1093/petrology/36.3.663>
- Schildgen TF, Hoke GD (2018) The Topographic Evolution of the Central Andes. *Elements* 14:231-236. <https://doi.org/10.2138/gselements.14.4.231>
- Schneider A (1985) Eruptive processes, mineralization and isotopic evolution of the Los Frailes KariKari region, Bolivia, PhD Thesis. Imperial College of Science and Technology, University of London
- Sciuba M, Beaudoin G, Makvandi S (2021) Chemical composition of tourmaline in orogenic gold deposits. *Miner Deposita* 56:537-560. <https://doi.org/10.1007/s00126-020-00981-x>
- Sempere T (1995) Phanerozoic evolution of Bolivia and adjacent regions. In: Tankard AJ, Suárez R, Welsink HJ (eds) *Petroleum Basins of South America*. AAPG Mem 62:207-230. <https://doi.org/10.1306/M62593C9>
- Sempere T, Jacay J (2006) Estructura tectónica del sur del Perú (Antearco, Arco, y Altiplano suroccidental). XIII Congreso Peruano de Geología, Extended abstracts 324-327
- Sempere T, Hérail G, Oller J, Bonhomme MG (1990) Late Oligocene-early Miocene major tectonic crisis and related basins in Bolivia. *Geology* 18:946-949. [https://doi.org/10.1130/0091-7613\(1990\)018<0946:LOEMMT>2.3.CO;2](https://doi.org/10.1130/0091-7613(1990)018<0946:LOEMMT>2.3.CO;2)
- Sempere T, Butler RF, Richards DR, Marshall LG, Sharp W, Swisher CC III (1997) Stratigraphy and chronology of Late Cretaceous - Early Paleogene strata in Bolivia and Northwest Argentina. *Geol Soc Am Bull* 109:709-727. [https://doi.org/10.1130/0016-7606\(1997\)109%3C0709:SACOUC%3E2.3.CO;2](https://doi.org/10.1130/0016-7606(1997)109%3C0709:SACOUC%3E2.3.CO;2)
- Sempere T, Carlier G, Soler P, Fornari M, Carlotto V, Jacay J, Arispe O, Néraudeau D, Cárdenas J, Rosas S, Jiménez N (2002) Late Permian-Middle Jurassic lithospheric thinning in Peru and Bolivia, and its bearing on Andean-age tectonics. *Tectonophysics* 345:153-181. [https://doi.org/10.1016/S0040-1951\(01\)00211-6](https://doi.org/10.1016/S0040-1951(01)00211-6)

- Sempere T, Folguera A, Gerbault M (2008) New insights into the Andean evolution: an introduction to contributions from the 6th ISAG symposium (Barcelona, 2005). *Tectonophysics* 459:1-13. <https://doi.org/10.1016/j.tecto.2008.03.011>
- Servicio Geológico de Bolivia - Geobol (1995a) Carta geológica de Bolivia, La Paz (Hoja 5944), scale 1:100000, La Paz
- Servicio Geológico de Bolivia - Geobol (1995b) Carta geológica de Bolivia, Milluni (Hoja 5945), scale 1:100000, La Paz
- Sillitoe RH (2004) Musings on future exploration targets and strategies in the Andes. *Econ Geol Spec Publ* 11:1-14. <https://doi.org/10.5382/sp.11.01>
- Sillitoe RH, Lehmann B (2021) Copper-rich tin deposits. *Miner Deposita* 57:1-11. <https://doi.org/10.1007/s00126-021-01078-9>
- Sillitoe RH, Halls C, Grant JN (1975) Porphyry Tin Deposits in Bolivia. *Econ Geol* 70:913-927. <https://doi.org/10.2113/gsecongeo.70.5.913>
- Sillitoe RH, Steele GB, Thompson JFH, Lang JR (1998) Advanced argillic lithocaps in the Bolivian tin-silver belt. *Miner Deposita* 33:539-546. <https://doi.org/10.1007/s001260050170>
- Slack JF, Trumbull RB (2011) Tourmaline as a recorder of ore-forming processes. *Elements* 7:321-326. <https://doi.org/10.2113/gselements.7.5.321>
- Soler P, Sempere T (1993) Stratigraphie, géochimie et signification paléotectonique des l'Oches volcaniques basiques mésozoïques des Andes boliviennes. *Comptes Rendus de l'Académie des Sciences de Paris* 316:777-784
- Spicer EM, Steven G, Buick IS (2004) The low-pressure partial-melting behaviour of natural boron-bearing metapelites from the Mt. Stafford area, central Australia. *Contrib Mineral Petr* 148:160-179. <https://doi.org/10.1007/s00410-004-0577-z>
- Spikings R, Reitsma MJ, Boekhout F, Mišković A, Ulianov A, Chiaradia M, Gerdes A, Schaltegger U (2016) Characterisation of Triassic rifting in Peru and implications for the early disassembly of western Pangaea. *Gondwana Res* 35:124-143. <https://doi.org/10.1016/j.j.gr.2016.02.008>
- Suárez-Soruco R (2000) Compendio de geología de Bolivia. *Revista técnica de yacimientos petrolíferos fiscales bolivianos* 18:1-166
- Sugaki A, Ueno H, Shimada N, Kitakaze A, Hayashi K, Shima H, Sanjines O, Saavedra M (1981) Geological study on the polymetallic hydrothermal deposits in the Oruro district, Bolivia. *Sci Rep Res Tohoku III* 15:1-52
- Sugaki A, Kitakaze A (1988) Tin-bearing minerals from Bolivian polymetallic deposits and their mineralization stages. *Mining and Geology* 38:419-435

- Torres B, Melgarejo JC, Torró L, Camprubí A, Castillo-Oliver M, Artiaga D, Campeny M, Tauler E, Jiménez-Franco A, Alfonso P, Arce-Burgoa OR (2019) The Poopó polymetallic epithermal deposit, Bolivia: mineralogy, genetic constraints, and distribution of critical elements. *Minerals* 9:472. <https://doi.org/10.3390/min9080472>
- Torró L, Melgarejo JC, Gemmrich L, Mollinedo D, Cazorla M, Martínez A, Pujol-Solà N, Farré-de-Pablo J, Camprubí A, Artiaga D, Torres B, Alfonso P, Arce O (2019a) Spatial and temporal control on the distribution of indium in xenothermal vein-deposits: the Huari Huari district, Potosí, Bolivia. *Minerals* 9:304. <https://doi.org/10.3390/min9050304>
- Torró L, Cazorla M, Melgarejo JC, Camprubí A, Tarrés M, Gemmrich L, Campeny M, Artiaga D, Torres B, Martínez A, Mollinedo D, Alfonso P, Arce-Burgoa OR (2019b) Indium mineralization in the volcanic dome-hosted Ánimas-Chocaya-Siete Suyos polymetallic deposit, Potosí, Bolivia. *Minerals* 9:604. <https://doi.org/10.3390/min9100604>
- Trumbull RB, Garda GM, Xavier RP, Cavalcanti JAD, Codeço MS (2019) Tourmaline in the Passagem de Mariana gold deposit (Brazil) revisited: major-element, trace-element and B-isotope constraints on metallogenesis. *Miner Deposita* 54:395-414. <https://doi.org/10.1007/s00126-018-0819-z>
- Turneure FS (1971) The Bolivian tin-silver province. *Econ Geol* 66:215-225. <https://doi.org/10.2113/gsecongeo.66.2.215>
- Ulrich TD (2005) Summary Report on Ar/Ar Dating for MAP: GAC. Activity PE – 05 Peru. Laboratory Pacific Centre for Isotopic and Geochemical Research Earth & Ocean Sciences, University of British Columbia. Vancouver
- U.S. Geological Survey (2020) Mineral commodity summaries 2020. U.S. Geological Survey 200. <https://doi.org/10.3133/mcs2020>.
- van Hinsberg VJ, Henry DJ, Dutrow BL (2011a) Tourmaline as a petrologic forensic mineral: A unique recorder of its geologic past. *Elements* 7:327-332. <https://doi.org/10.2113/gselements.7.5.327>
- van Hinsberg VJ, Henry DJ, Marschall HR (2011b) Tourmaline: An ideal indicator of its host environment. *Can Mineral* 49:1-16. <https://doi.org/10.3749/canmin.49.1.1>
- von Goerne G, Franz G, van Hinsberg VJ (2011) Experimental determination of Na-Ca distribution between tourmaline and fluid in the system CaO-Na₂O-MgO-Al₂O₃-SiO₂-B₂O₃-H₂O. *Can Mineral* 49:137–152. <https://doi.org/10.3749/canmin.49.1.137>
- Whipple KX, Gasparini NM (2014) Tectonic control of topography, rainfall patterns, and erosion during rapid post-12 Ma uplift of the Bolivian Andes. *Lithosphere* 4:251-268. <https://doi.org/10.1130/L325.1>
- Wolf MB, London D (1997) Boron in granitic magmas: Stability of tourmaline in equilibrium with biotite and cordierite. *Contrib Mineral Petr* 130:12-30. <https://doi.org/10.1007/S004100050346>

- Wörner G, Schildgen TF, Reich M (2018a) The Central Andes: Elements of an Extreme Land. *Elements* 14:225-230. <https://doi.org/10.2138/gselements.14.4.225>
- Wörner G, Mamani M, Blum-Oeste M (2018b) Magmatism in the Central Andes. *Elements* 14:237-244. <https://doi.org/10.2138/gselements.14.4.237>
- Yavuz F, Karakaya N, Yildirim DK, Karakaya MC (2014) A Windows program for calculation and classification of tourmaline-supergroup (IMA-2011). *Comput Geosci* 63: 70-87. <https://doi.org/10.1016/j.cageo.2013.10.012>
- Zentilli M, Salas-Olivares RA, Graves MC (2018) A unique Sn-bearing Bi-Ag-Sb, polymetallic, epithermal district in the Chilean Andes: Capitana Mine, Tignamar, Arica-relation to the Proterozoic-Paleozoic Belén Metamorphic Complex. XV Congreso Geológico Chileno
- Zheng Z, Chen Y, Deng X, Yue S, Chen H, Wang Q (2019) Tourmaline geochemistry and boron isotopic variations as a guide to fluid evolution in the Qiman Tagh W–Sn belt, East Kunlun, China. *Geosci Front* 10:569–580. <https://doi.org/10.1016/j.gsf.2018>





Supplementary material

Appendix A

Samples location



Sample	UTM Coordinates (m)		Elevation (m)	Locality
	East	North		
2020-KELL-001	594265	8189677	4619	Kellhuani
2020-KELL-002	594172	8189693	4619	Kellhuani
2020-KELL-003	594022	8189813		Kellhuani
2020-KELL-004	594460	8189673		Kellhuani
2020-KELL-005	594527	8189751	4736	Kellhuani
2020-KELL-006	594518	8189764	4724	Kellhuani
2020-KELL-007	594537	8189880	4727	Kellhuani
2020-KELL-008	594485	8190668	4812	Kellhuani
2020-KELL-009	594007	8191856	5050	Kellhuani
2020-KELL-010	595612	8189518	4753	Kalauyo
2020-KELL-011	595438	8189378	4740	Kalauyo
2020-KELL-012	595719	8189187	4692	Kalauyo
2020-KELL-013	595915	8188949	4626	Kalauyo
2020-KELL-014	596292	8188450	4380	Kalauyo
2020-KELL-015	596188	8188029	4315	Kalauyo
2020-KELL-016	596211	8188067	4317	Kalauyo
2020-KELL-017	593920	8189459	4474	Kellhuani
2020-KELL-019	591984	8191203	4963	Chacaltaya
2020-KELL-020	591984	8191203	4963	Chacaltaya
2020-KELL-021	591984	8191203	4963	Chacaltaya
2020-KELL-022	591984	8191203	4963	Chacaltaya
2020-KELL-023	591635	8190737	4881	Chacaltaya
2020-KELL-024	591862	8190599	4785	Chacaltaya
2020-KELL-025	591896	8190561	4774	Chacaltaya
2020-KELL-026	591708	8190759	4704	Chacaltaya
2020-KELL-027	591926	8190822	4699	Chacaltaya
2020-KELL-028	591951	8190905	4843	Chacaltaya
2020-KELL-029	591917	8190844	4816	Chacaltaya
2020-KELL-030	591869	8190817	4802	Chacaltaya
2020-KELL-031	591563	8190495	4853	Chacaltaya
2020-KELL-032	591269	8190818	4861	Chacaltaya
2020-KELL-033	590378	8192318	4622	Chacaltaya
2020-KELL-034	591426	8194694	4732	Milluni
2020-KELL-035	591532	8194175	4717	Milluni
2020-KELL-036	591563	8195309	4720	Milluni
2020-KELL-037	591635	8195194	4725	Milluni
2020-KELL-038	591635	8195194	4725	Milluni
2020-KELL-039	591715	8195005	4733	Milluni
2020-KELL-040	591772	8194907	4742	Milluni
2020-KELL-041	591754	8195191	4757	Milluni
2020-KELL-042	591875	8195082	4766	Milluni

2020-KELL-043	591889	8195103	4774	Milluni
2020-KELL-044	591927	8194973	4766	Milluni
2020-KELL-045	592745	8189584	4574	Kellhuani
2020-KELL-046	592887	8189935	4714	Kellhuani
2020-KELL-047	592846	8190129	4765	Kellhuani
2020-KELL-048	592898	8189974	4736	Kellhuani
2020-KELL-049	592895	8189917	4715	Kellhuani
2020-KELL-050	592852	8189786	4679	Kellhuani
2020-KELL-051	597185	8188531	4404	Kalauyo
2020-KELL-052	597131	8188560	4736	Kalauyo



Appendix B

Hand sample descriptions and photographs



2020-KELL-01-A



2020-KELL-01-A



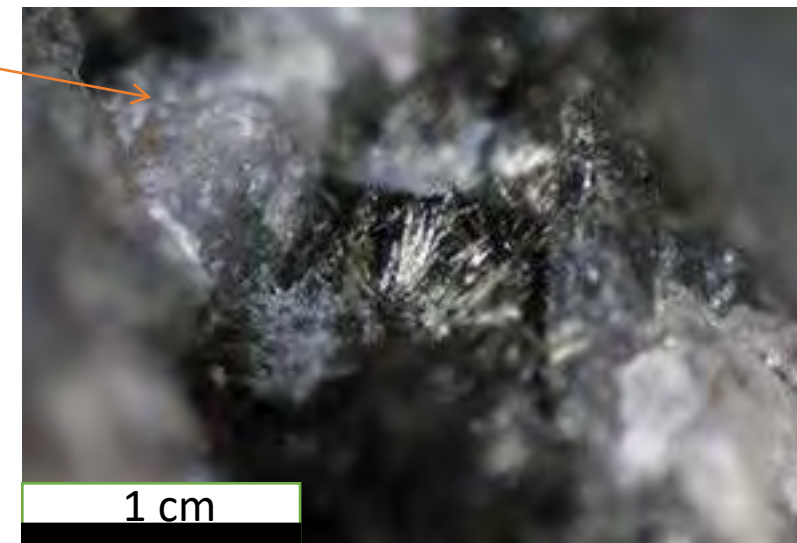
2020-KELL-01-A



Quartz-cassiterite veins hosted by Catavi Fm. quartzites. The main vein is approximately 3.5 cm wide and contains a mineralization of quartz with lesser proportions of cassiterite, sulfides, and carbonates. Euhedral to subhedral translucent quartz crystals up to 2 cm long describe comb textures. Cassiterite, sulfides and carbonates appear mostly occupying interstitial space between comb quartz crystals. Cassiterite crystals are pale brown in color and mm-sized, and occur mostly as scattered subhedral grains towards the central part of the vein. Carbonates are anhedral, dark brown in color (siderite?), and contain scarce sulfide minerals, mostly minute pyrite crystals (<1mm). The most striking texture in this sample is observed in the vein selvage, which contains dark brown, subhedral to euhedral short-prismatic to ovoid crystals (tourmaline?). These short-prismatic brown crystals are mostly oriented perpendicular to the vein contact. In addition, this brown mineral also occurs as mm-wide massive aggregates along of parallel to the vein contacts. Locally, short-prismatic brown crystals describe radial arrangements around semicircular massive brown mineralization.

Other veins in the sample are around 1 cm wide and show similar paragenesis as the vein described above. However, tourmaline mineralization in the selvage of the previously described vein extends into these narrower veins.

2020-KELL-01-B



Vein hosted by Catavi Fm quartzites.

The vein is 2.5 cm wide and is composed of quartz, tourmaline, and sulfides (arsenopyrite?). Two types of quartz have been distinguished: i) milky massive granular quartz, and ii) hyaline, euhedral quartz. Relatively abundant acicular crystals, with lengths up to 3 mm, and very dark green to black color (tourmaline?) appear within vein quartz. These acicular dark crystals appear as individual specimens and forming radial aggregates.

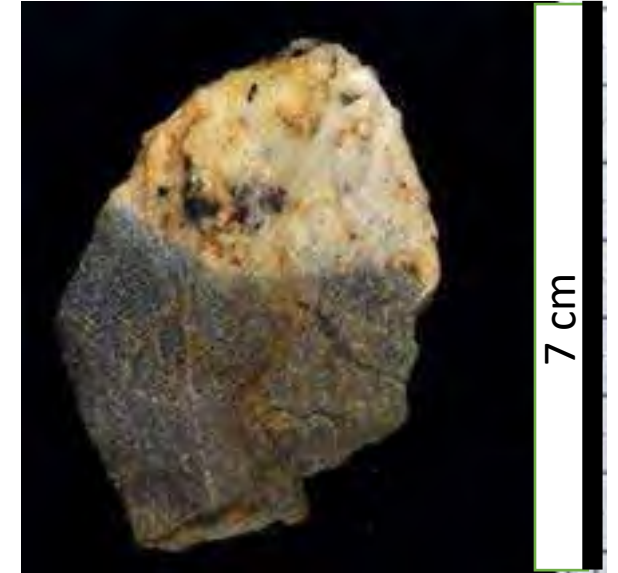
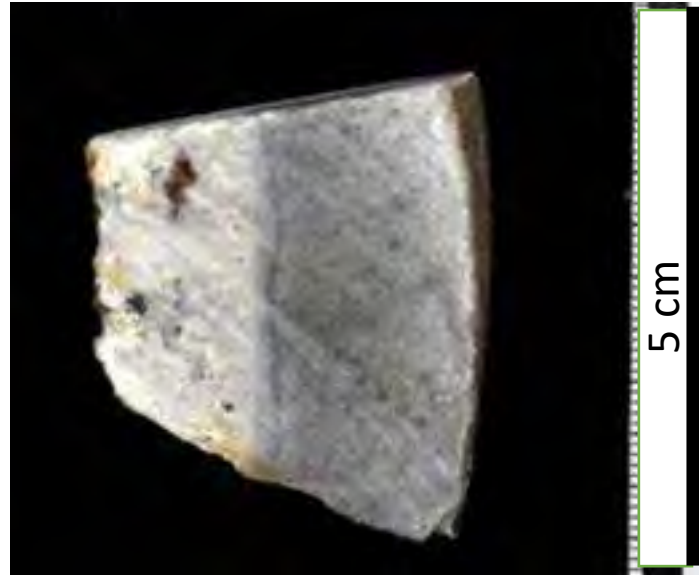
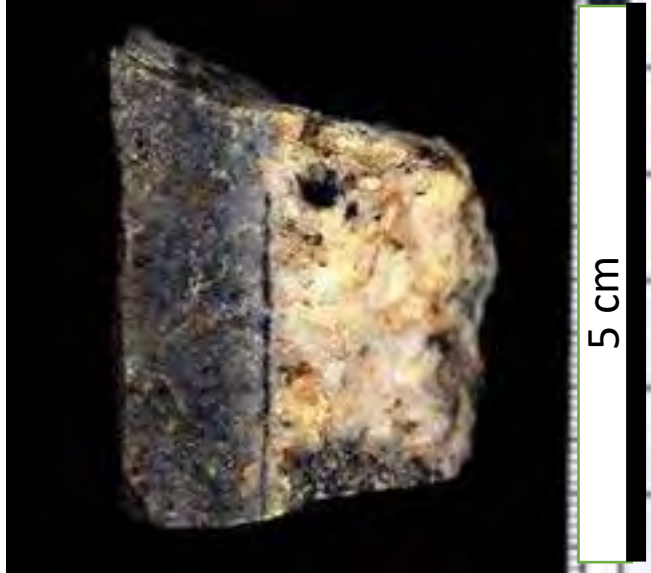
2020-KELL-01-C



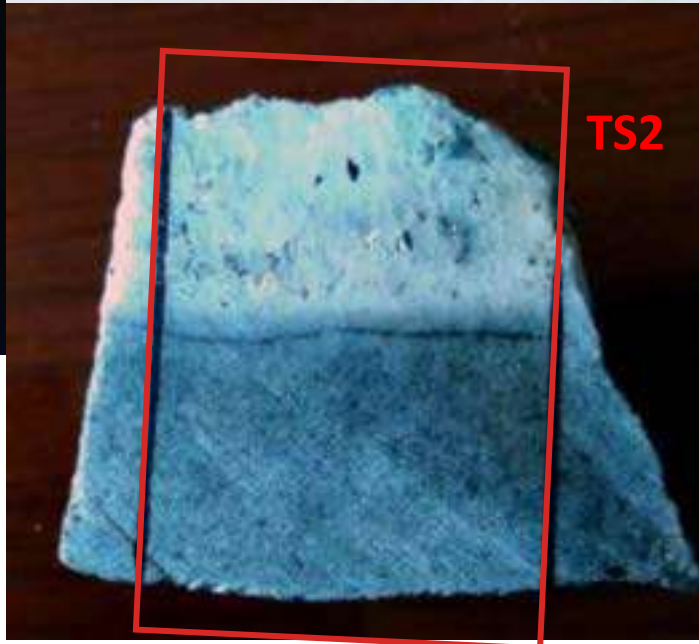
Veins in. Catavi Fm quartzites.

Veins range between 0.5 and 2 cm in width. Vein infill is mostly composed of mm-sized subhedral and euhedral hyaline quartz crystals drawing comb textures. Dark brown carbonates (siderite?) occupy the interstitial space between quartz crystals, mostly along the central part of the vein. Scattered mm-sized subhedral pyrite crystals appear along the contacts between quartz and carbonates. Interstitial to vein quartz there is also a white matt mineral (sericite??). The veins are surrounded by a narrow (< 1mm) black halo (tourmaline?).

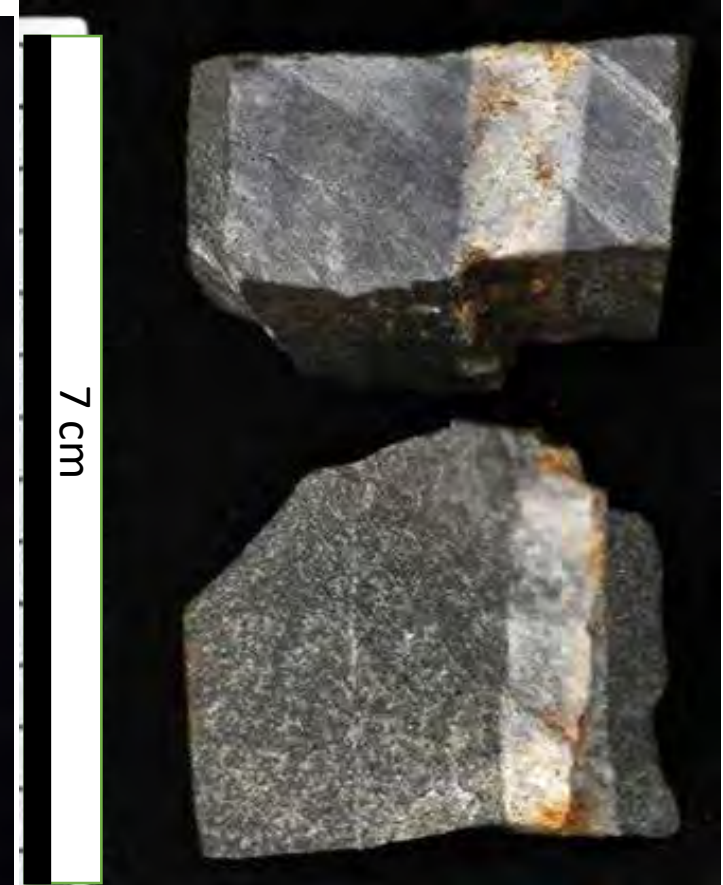
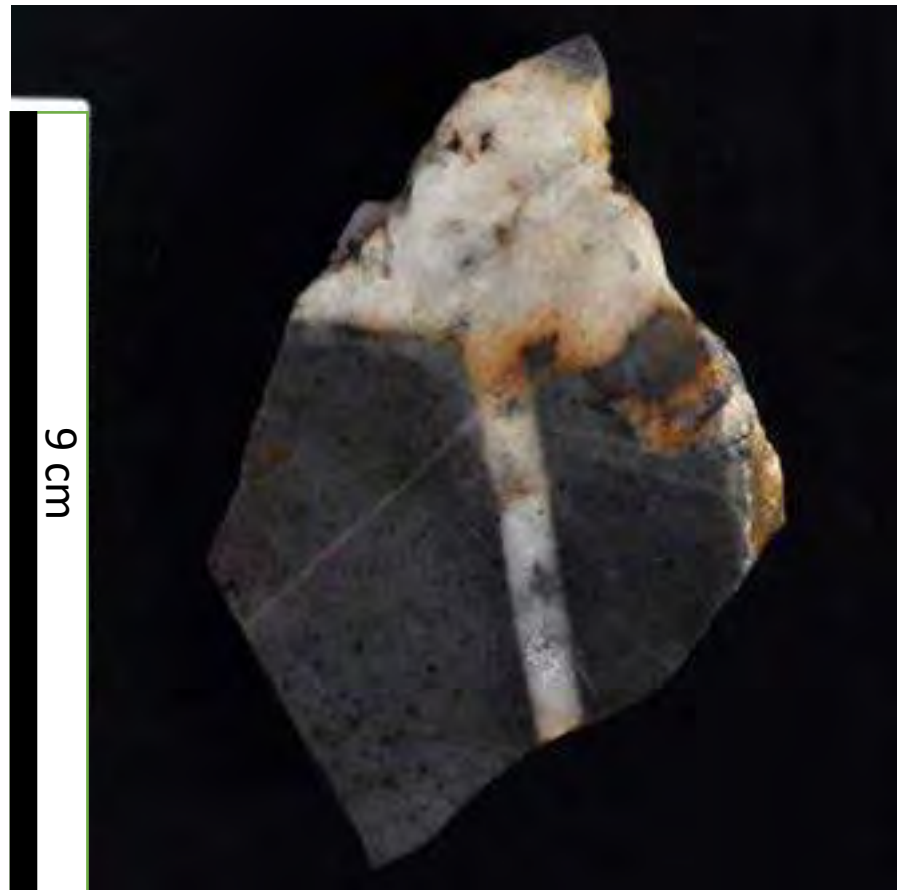
2020-KELL-01-C



2020-KELL-01-C



2020-KELL-02



Veins in Catavi Fm. quartzite.

Vein system including a 7-mm-wide feeder vein and the main vein (up to 4 cm wide), which is oriented perpendicular to the first. Both have milky quartz as the main phase, and lesser proportions of cassiterite and sulfide minerals. The main vein shows euhedral-subhedral quartz crystals up to 2 cm in length. Cassiterite forms mm-sized subhedral-euhedral brown crystals, and sulfide minerals (pyrite, arsenopyrite? sphalerite?) occupy interstitial space between quartz crystals. Pyrite forms mm-sized subhedral crystals. The main vein shows narrow, irregular alteration halos (< 2mm) of massive black cassiterite. Also, the wall rock host some mm-sized black spots (vitreous shine; tourmaline?).

There is a second system on veins which are up to 1 cm wide composed of milky quartz and a black mineral (tourmaline??).

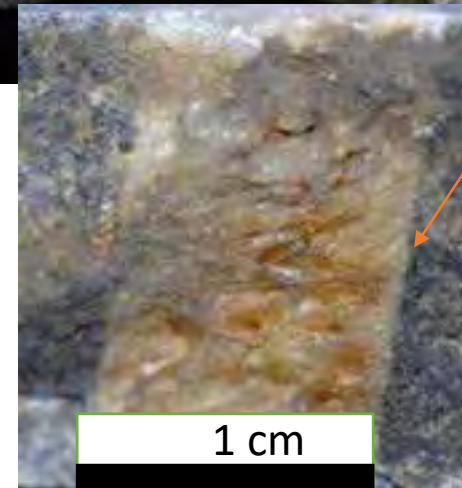
2020-KELL-02



7 cm

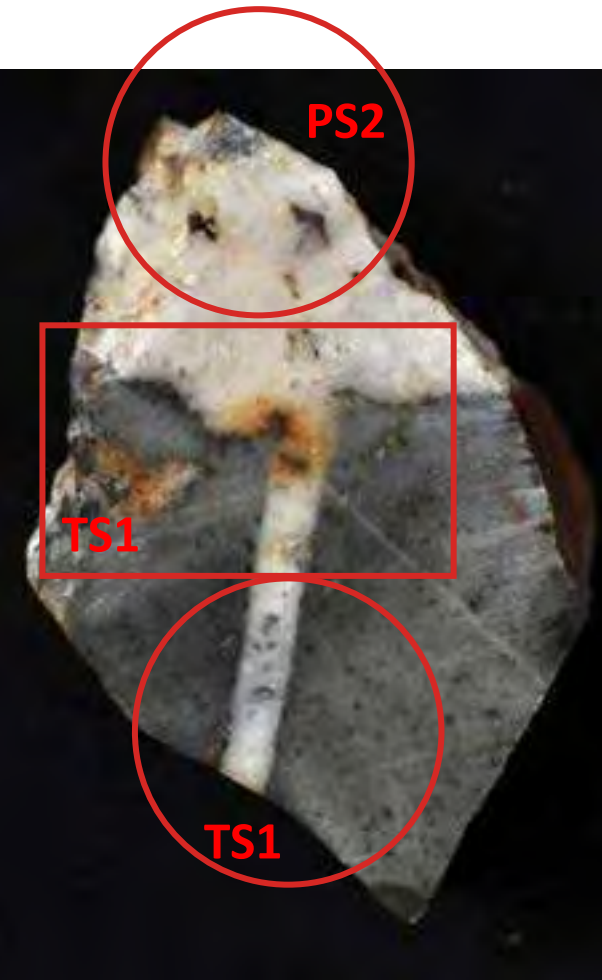


9 cm

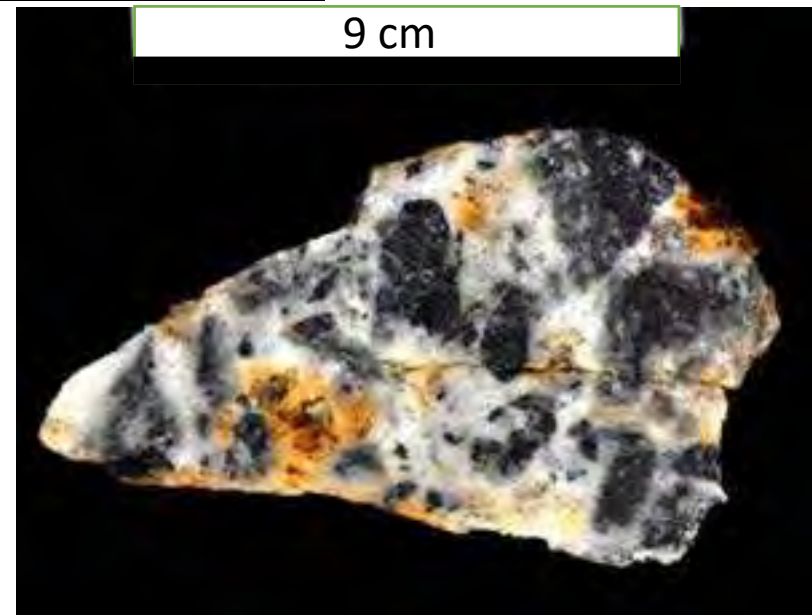
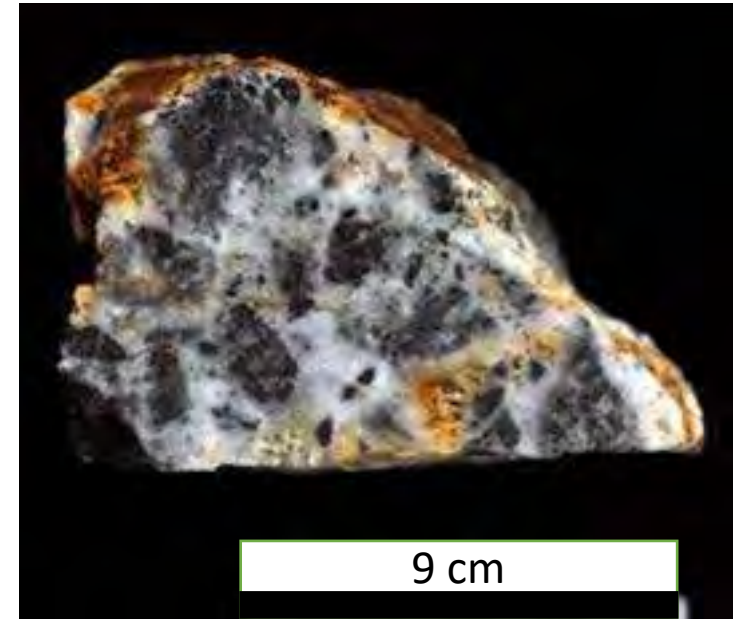
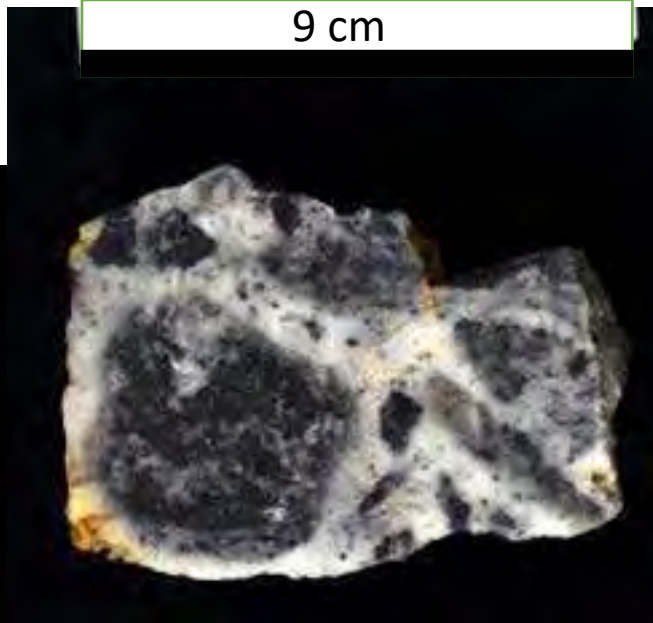
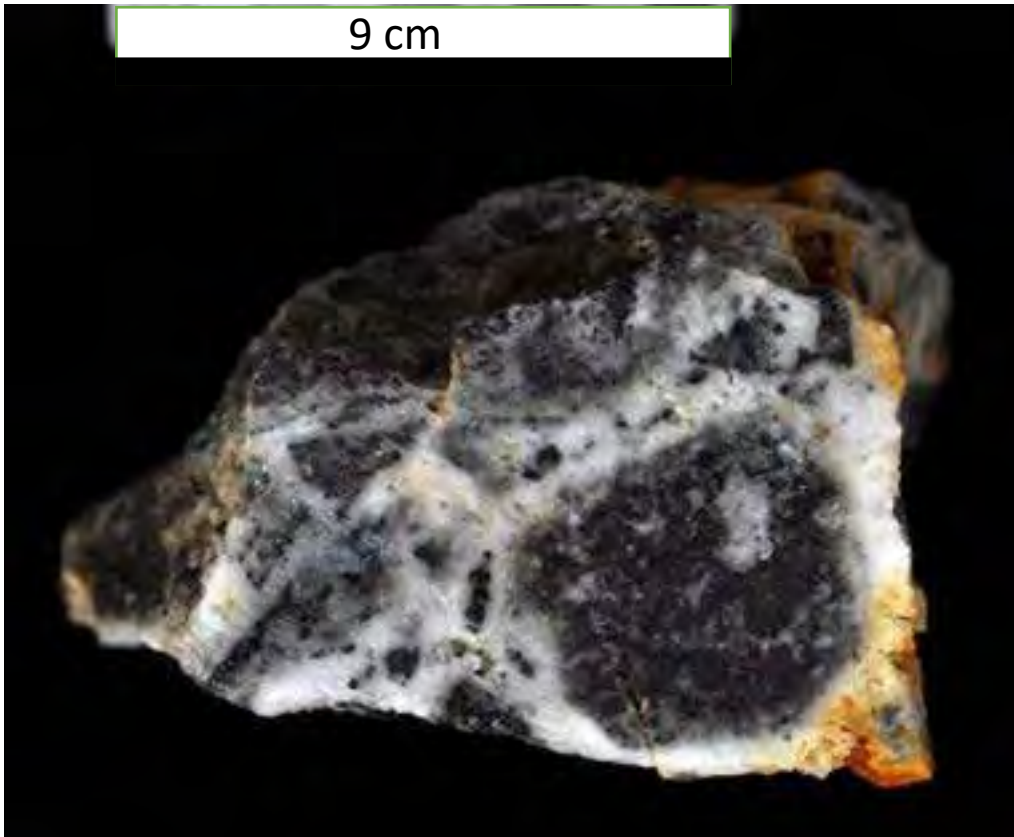


1 cm

2020-KELL-02



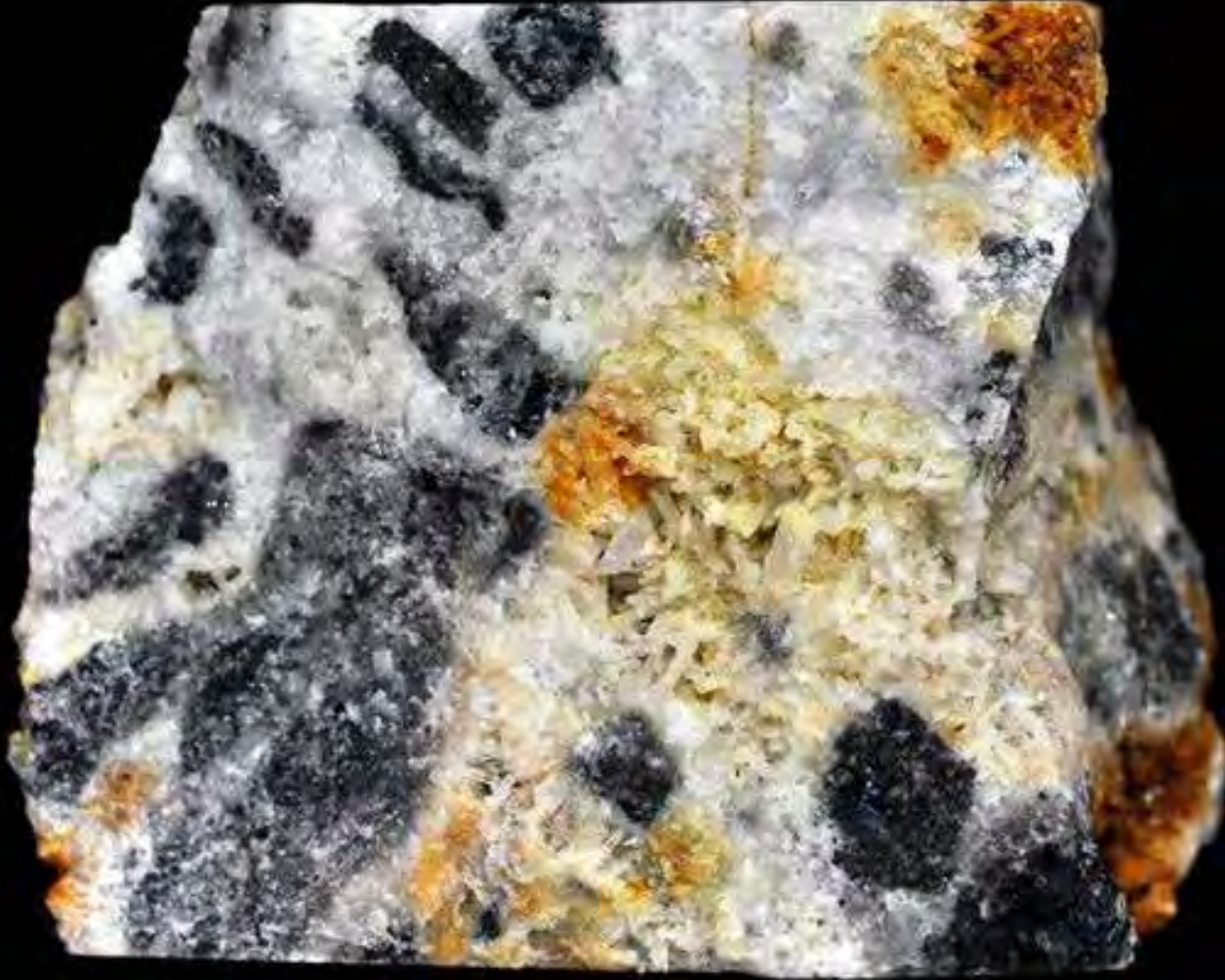
2020-KELL-03



Mineralized breccia. The breccia is composed of sphalerite irregular clasts with curvilinear outlines and sizes up to 8 cm that are veined and cemented by milky quartz. There is also a dissemination of pyrite in both the white cement and the sphalerite clasts. Cavities are filled with elongated euhedral quartz crystals up to 1 cm long.

2020-KELL-03

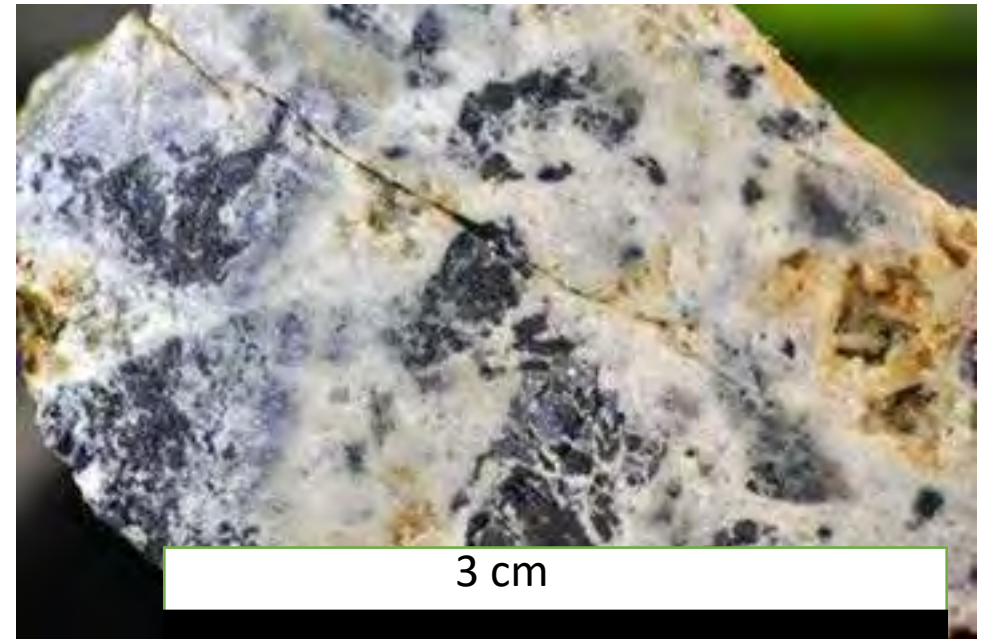
9 cm



3 cm



3 cm

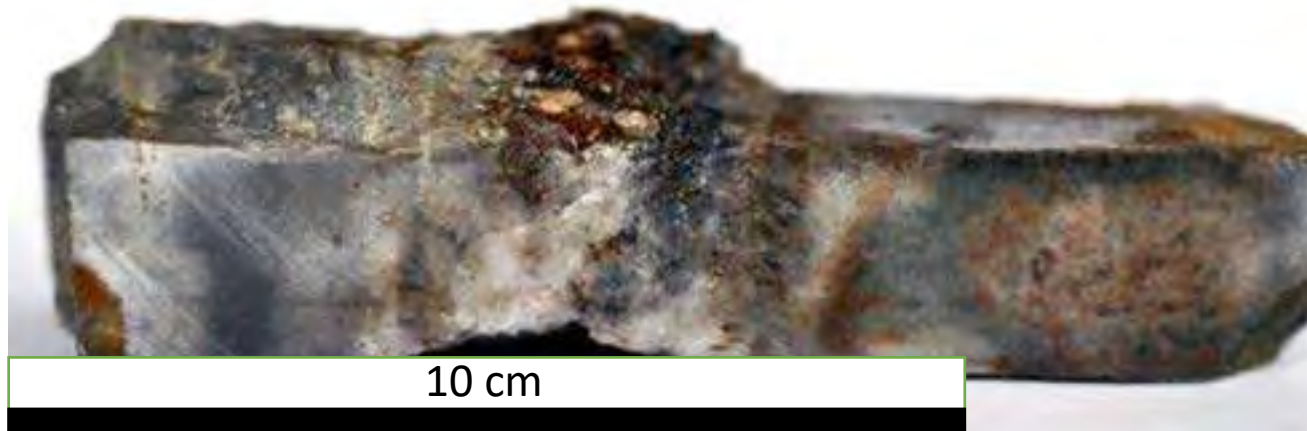


2020-KELL-03



TS1 (not cut)

2020-KELL-04



Veins in Catavi Fm. quartzite. The main vein is approximately 3 cm wide and contains a mineralization of quartz with lesser proportions of cassiterite, carbonates, sulfides, and a purplish mineral (fluorite?). Subhedral quartz crystals up to 1.5 cm long describe comb textures. Cassiterite, sulfides and carbonates appear mostly occupying interstitial space between vein quartz crystals. Carbonates are anhedral, dark brown in color (siderite?) and occur both as filling of interstitial space between quartz crystals chiefly along the central part of the vein and as thin veinlets < 1mm in thickness. Scarce cassiterite crystals, brown in color and mm-sized, occur randomly distributed in vein quartz. The sulfide mineralization is mostly constituted of minute pyrite crystals (<1mm) spatially associated to Fe carbonates in the central area of the vein. The vein is surrounded by a narrow (~3mm) dark halo, which contain acicular dark brown crystals (tourmaline?) oriented perpendicular to the vein contact.

2020-KELL-04



9 cm

9 cm



3 cm

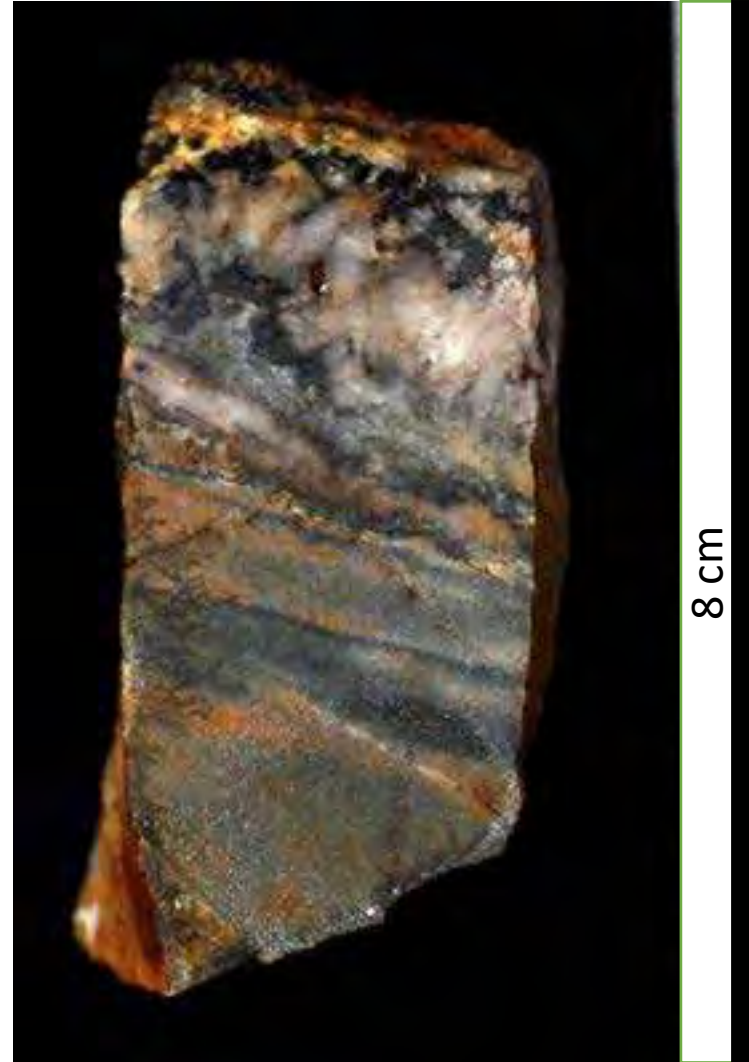
2020-KELL-04



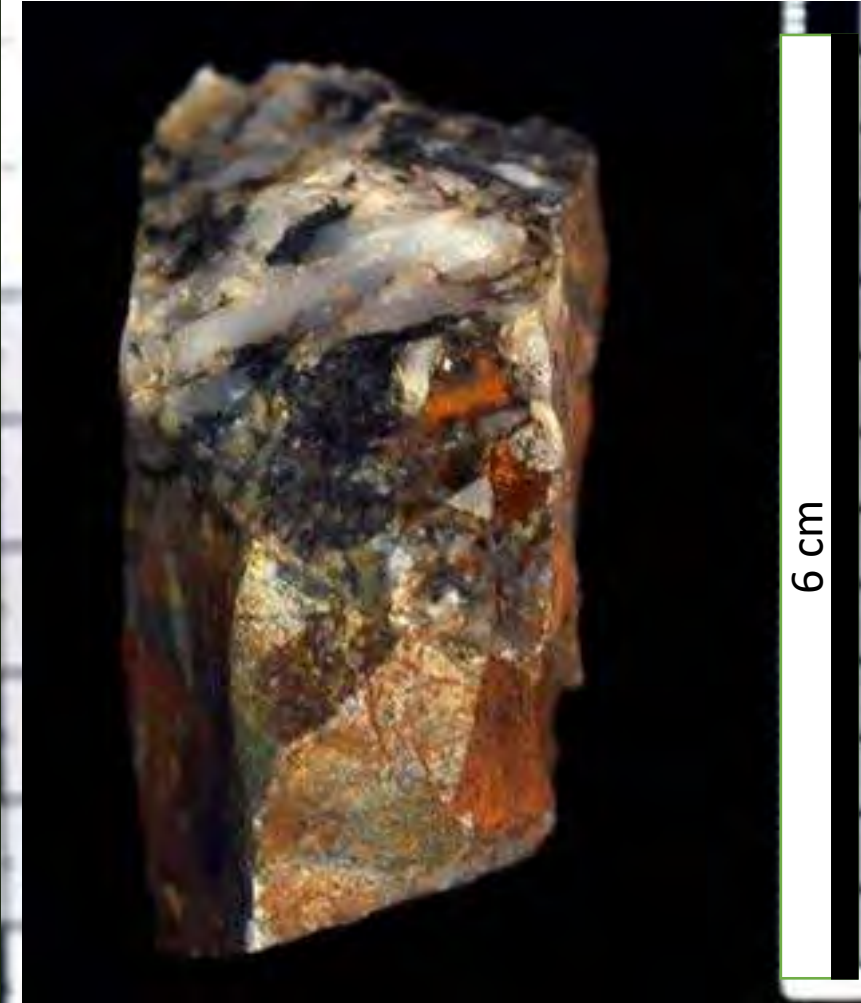
2020-KELL-05



8 cm



8 cm



6 cm

Veins in Catavi Fm. quartzite. The main vein is approximately 3 cm wide and contains mineralization of quartz with lesser proportions of cassiterite, and a black mineral (tourmaline?). The mineral distribution within the vein is complex and include banded and comb textures. The outer sector of the vein is dominated by tanded textures alternating bright (mostly milky quartz) and dark (including dark-green colors: tourmaline? chlorite?) bands. The vein passes inwards to dominant subhedral milky quartz crystals up to 2 cm across coronated by a mineralization of anhedral Fe-rich carbonates (siderite?). A black mineral (tourmaline?) and mm-sized dark-brown cassiterite appear intergrown with comb quartz crystals. Minute pyrite subhedral crystals (<1mm) appear scattered within the vein.

2020-KELL-05



2020-KELL-06

9 cm



Black slate (Catavi Fm.)

9 cm

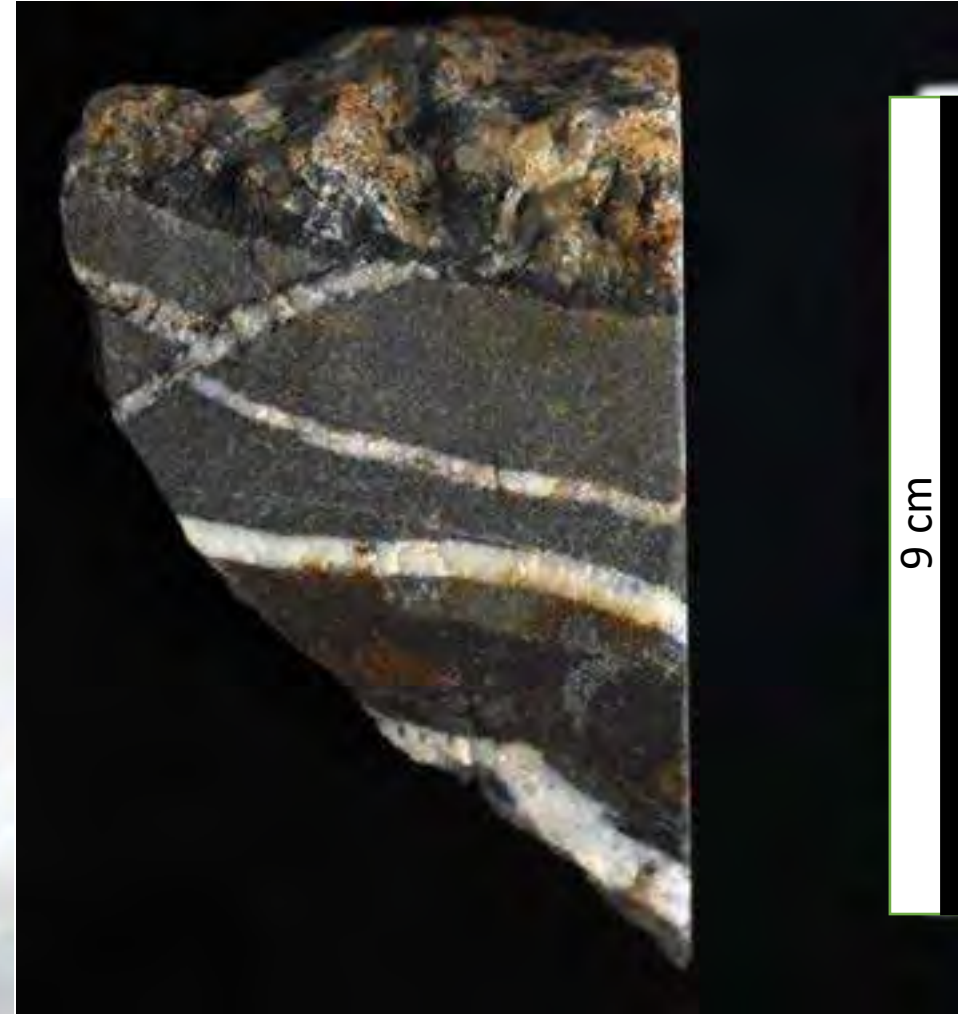


2020-KELL-07



Veins hosted by Catavi Fm. quartzites. Two main vein systems are identified. Veins of the first system are < 0.5 cm wide, composed mostly of massive milky quartz and lesser amounts of reddish-brown cassiterite subhedral cassiterite crystals < 1 mm across, and do not show alteration haloes. Veins of the second vein system are composed of quartz, tourmaline, cassiterite, muscovite, carbonates and fluorite, show dark (tourmaline) alteration haloes, and cut and displace veins of the first system. The thickest vein in the studied sample belong to this second vein system and contains a dark rim of tourmaline crystals overgrown by euhedral to subhedral translucent quartz crystals up to 1 cm long describe comb textures. Comb quartz crystals are coronated by intergrown mm-sized subhedral muscovite crystals and dark brown carbonates (siderite?) towards the core of the vein. Also, by a soft translucent mineral (fluorite?) which form crystals up to 1 cm across.

2020-KELL-07

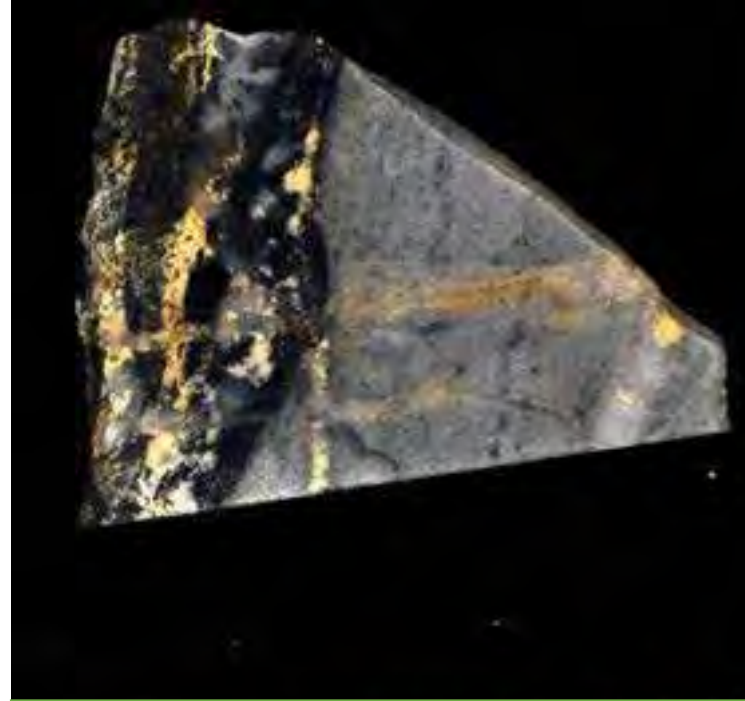


2020-KELL-07

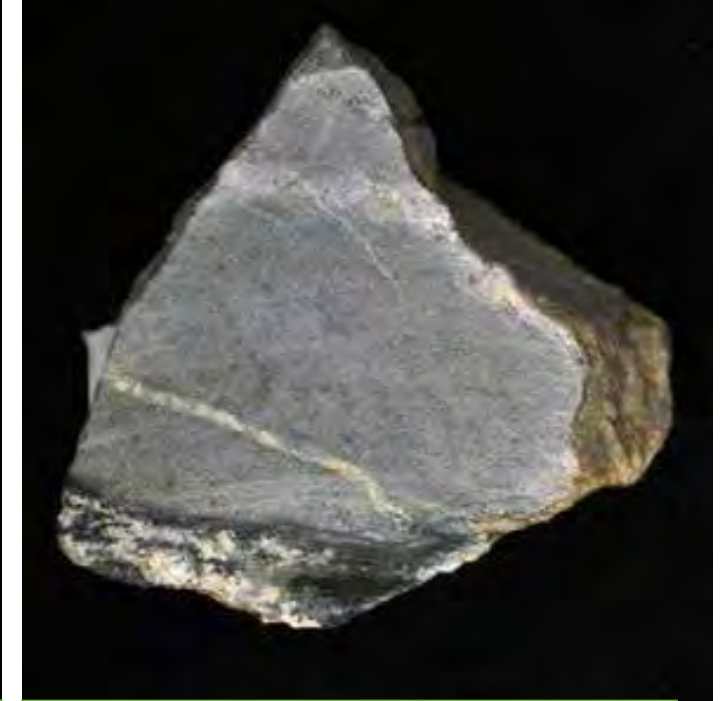


2020-KELL-08

9 cm



8 cm



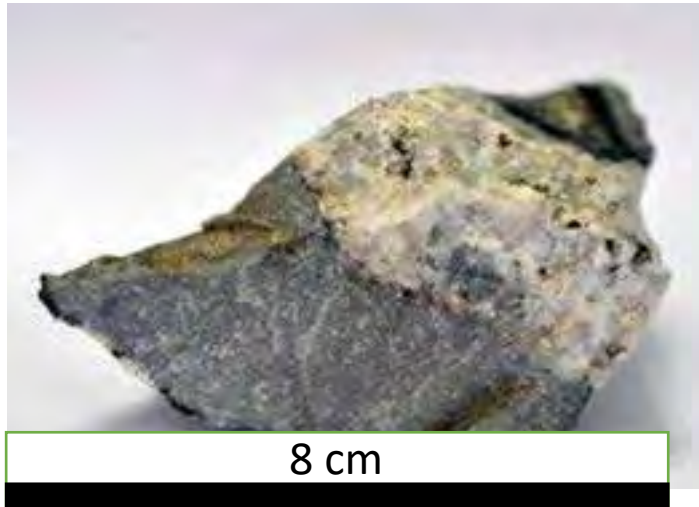
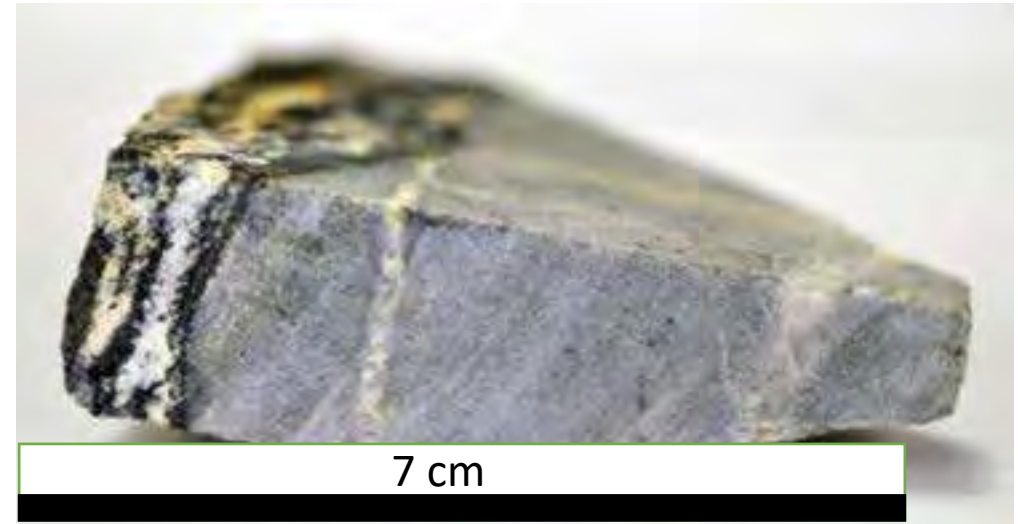
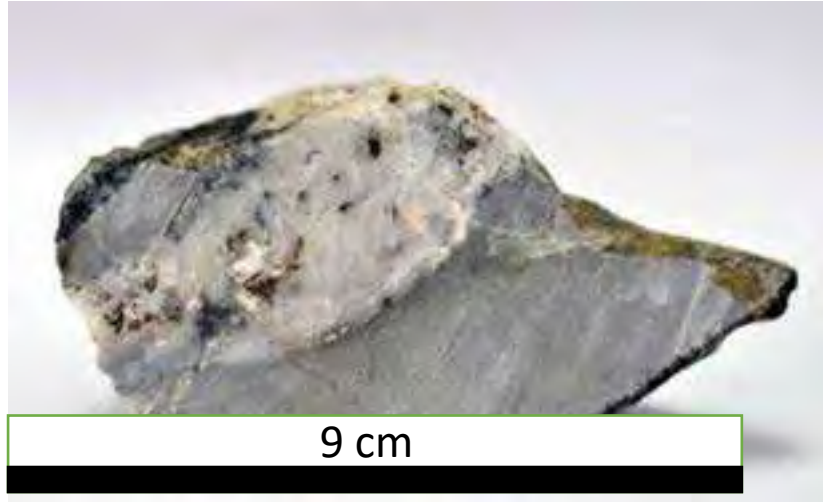
9 cm



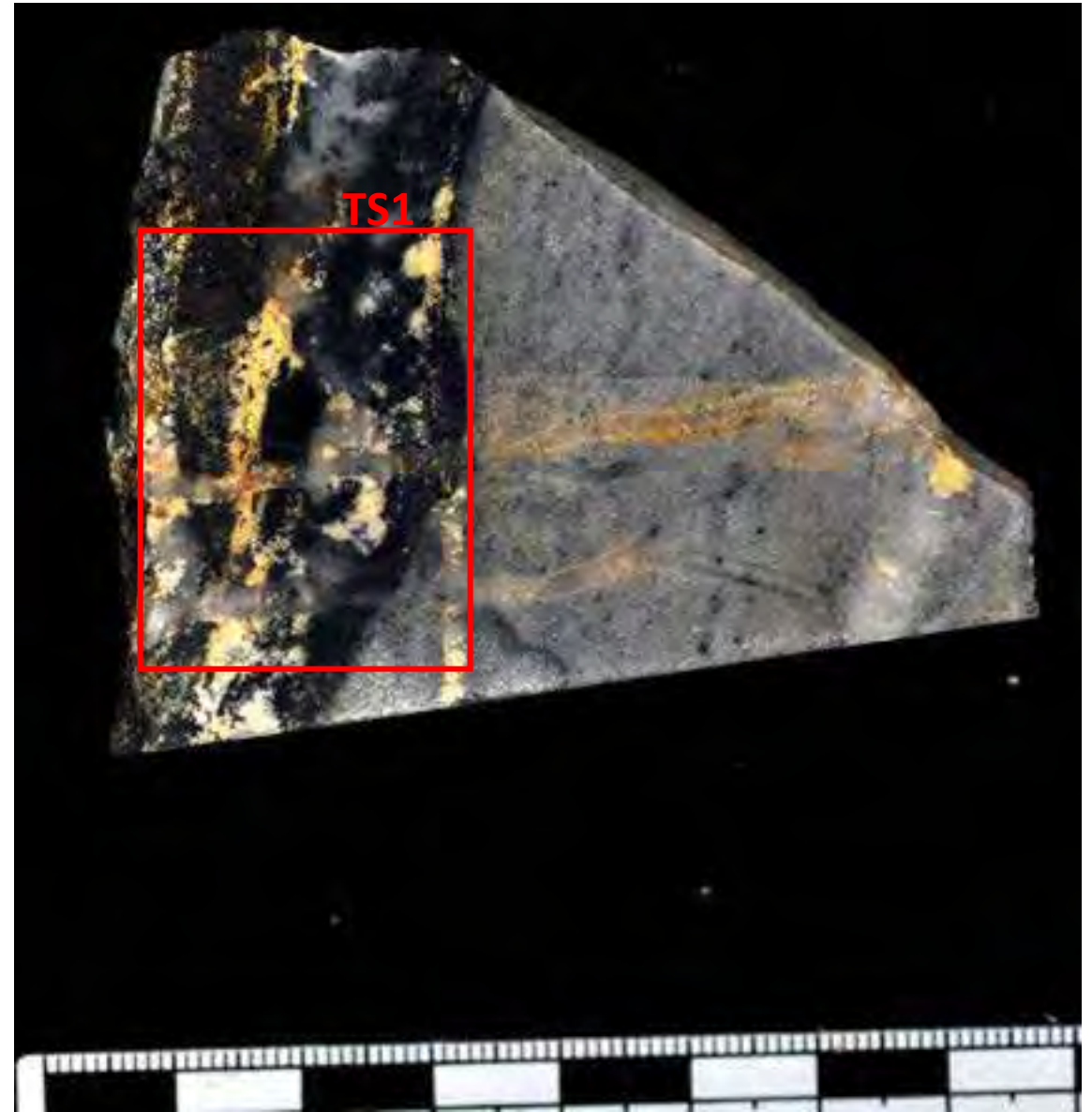
9 cm

Veins hosted by Catavi Fm. quartzites. Two main vein systems are identified. The first vein system comprises veins that are up to 3 cm thick and their mineralogy includes quartz, tourmaline, and cassiterite. Subhedral granular quartz crystals up to 1 cm long. The quartz is surrounded by a stripe of black tourmaline crystals (1 mm wide). Cassiterite subhedral crystals are pale brown in color and mm-sized. This assemblage is altered to a soft, cream-colored, matt lustre mineral (clay) forming massive bands and patches. These veins are cut by veins of the second system, which are <0.5 cm thick and contain a quartz- and carbonate-rich mineralization with minute (< 1 mm) euhedral pyrite crystals. Carbonates are pale yellow in color.

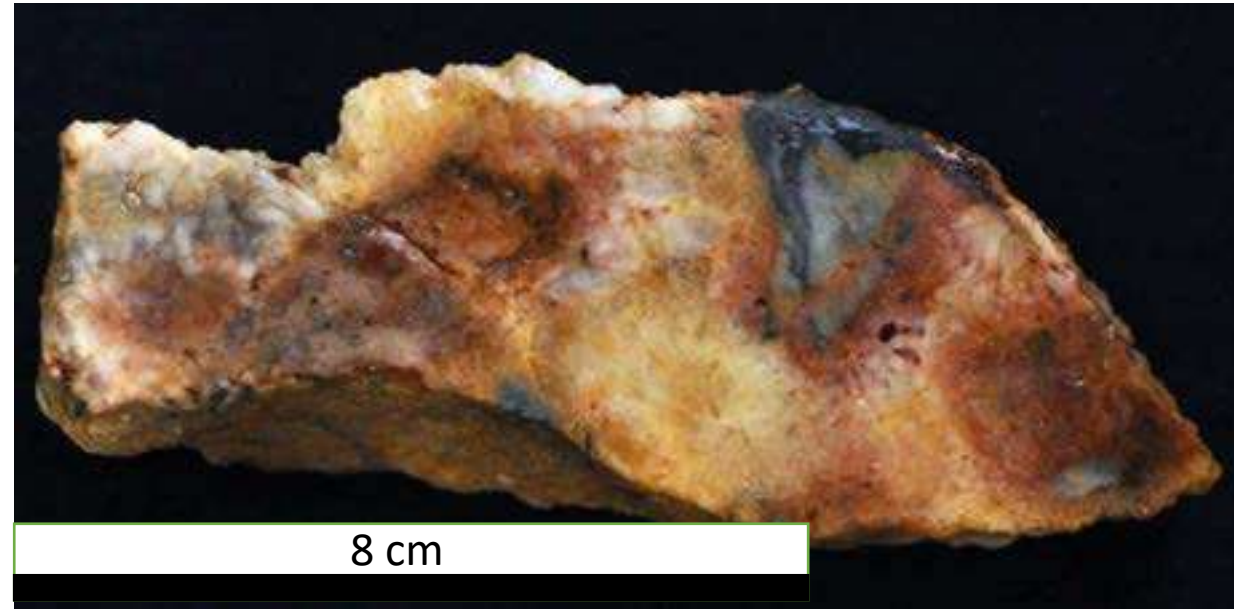
2020-KELL-08



2020-KELL-08



2020-KELL-09-A



Hydrothermal breccia. Angular to sub-angular rock clasts up to 3 cm long, presumably from the hosting Catavi Fm., are cemented by semi-massive milky quartz which grades away from the clasts to euhedral milky quartz crystals up to 1 cm long. Scarce minute subhedral pyrite (<1 mm) and anhedral Fe-rich carbonates are intergrown with quartz crystals.

2020-KELL-09-A



2020-KELL-09-B



9 cm



9 cm

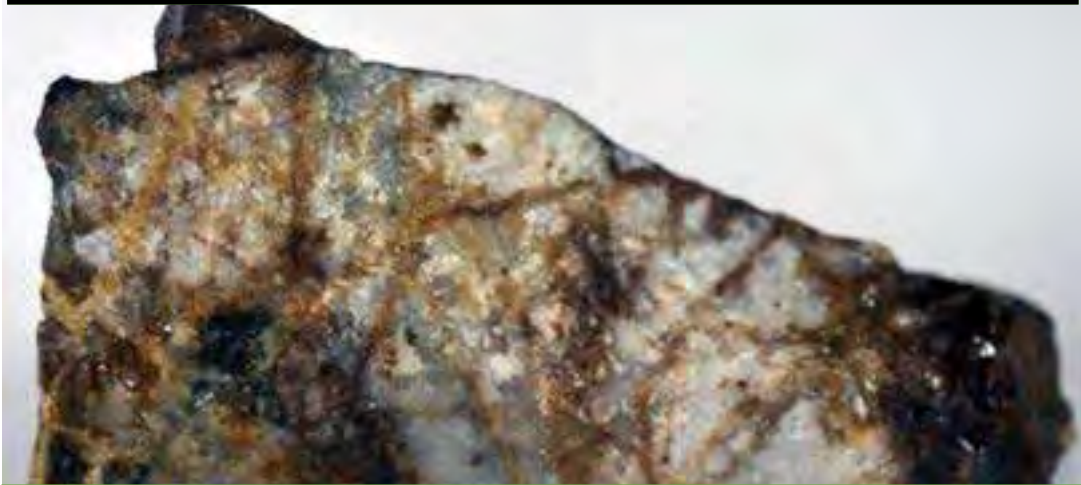
Veins hosted by Catavi Fm. quartzites.

Veins show a complex internal structure which approximate a banded-crustiform arrangement, and are up to 6 cm in thickness. Their mineralogy is dominated by quartz, lesser amounts of Fe-rich carbonates, a black mineral (tourmaline?), and traces of cassiterite and pyrite. From the contact with the host rock to the core of the vein, there is a gradation from tourmaline (?) - massive milky quartz, massive milky quartz, euhedral to subhedral milky quartz crystals up to 2 cm long describing comb textures, and to Fe-rich carbonate. Dark-green tourmaline (?) crystals are subhedral and up to 5 mm in length. In addition to massive infilling in the core of the vein, Fe-rich carbonate also appear forming a network of narrow veintlets (~1mm thick) cutting the aforementioned mineral assemblages. Pyrite forms <1 mm euhedral and subhedral crystals that appear randomly distributed in the massive milky quartz.

2020-KELL-09-B



9 cm



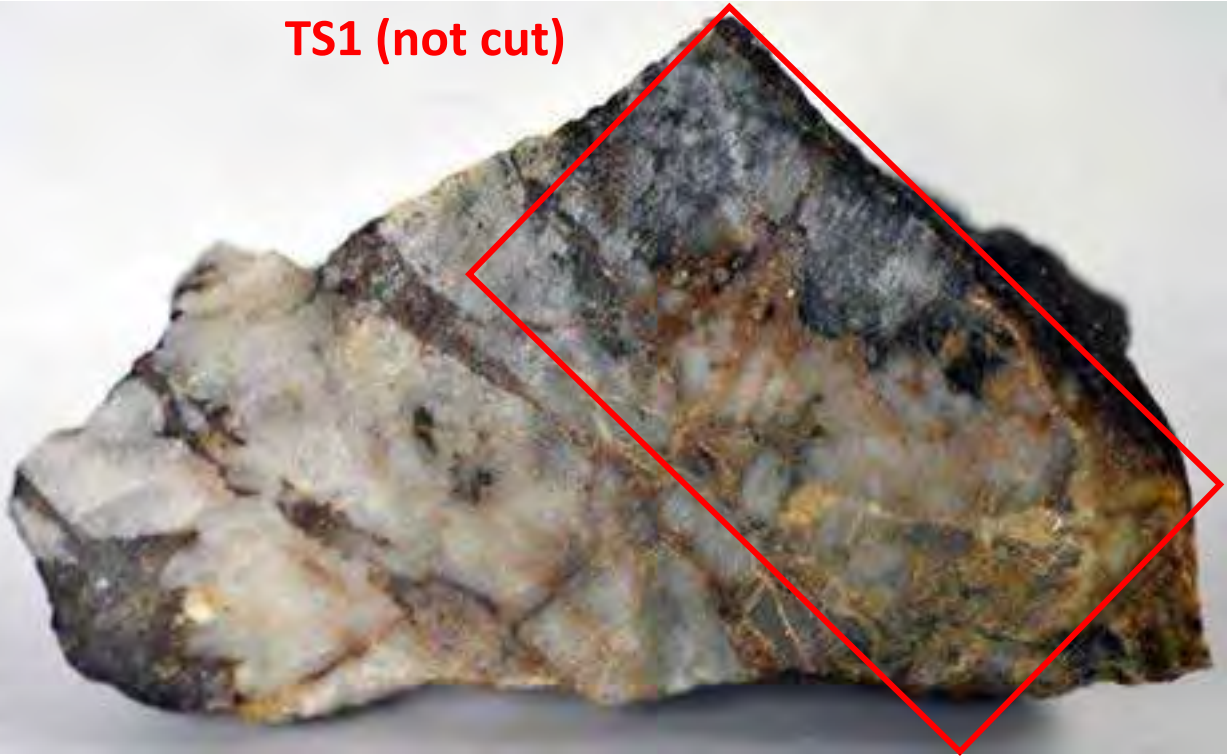
9 cm



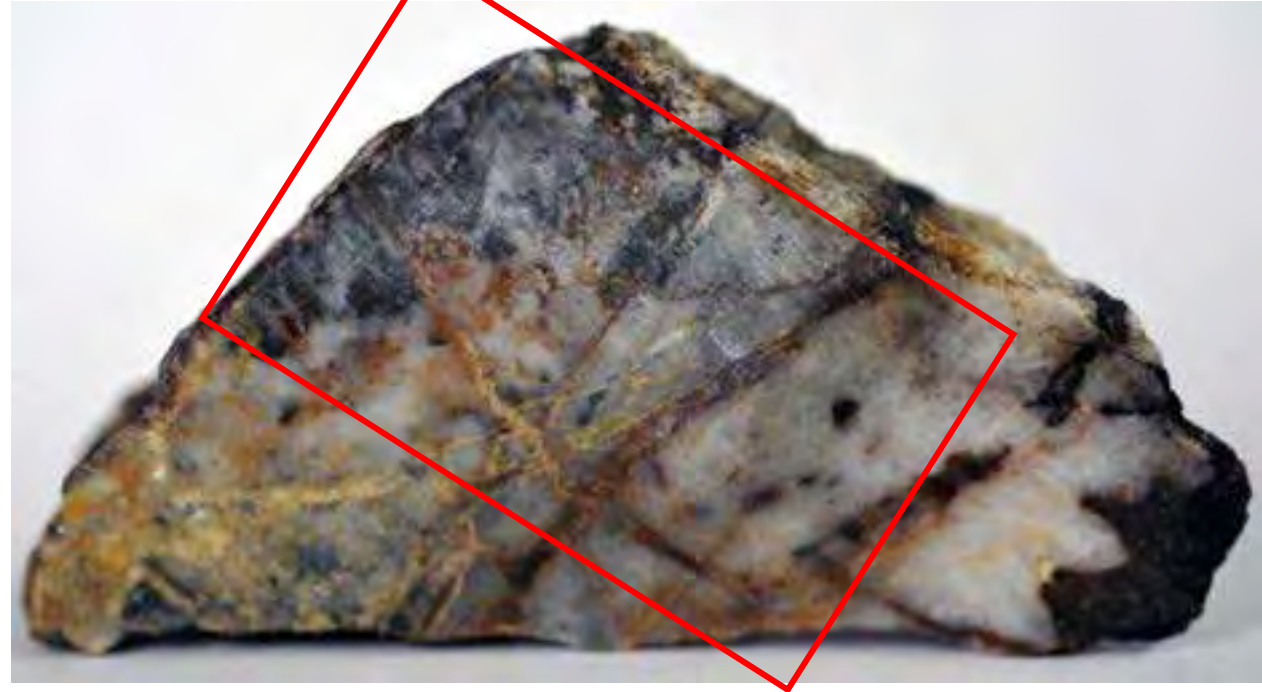
8 cm

2020-KELL-09-B

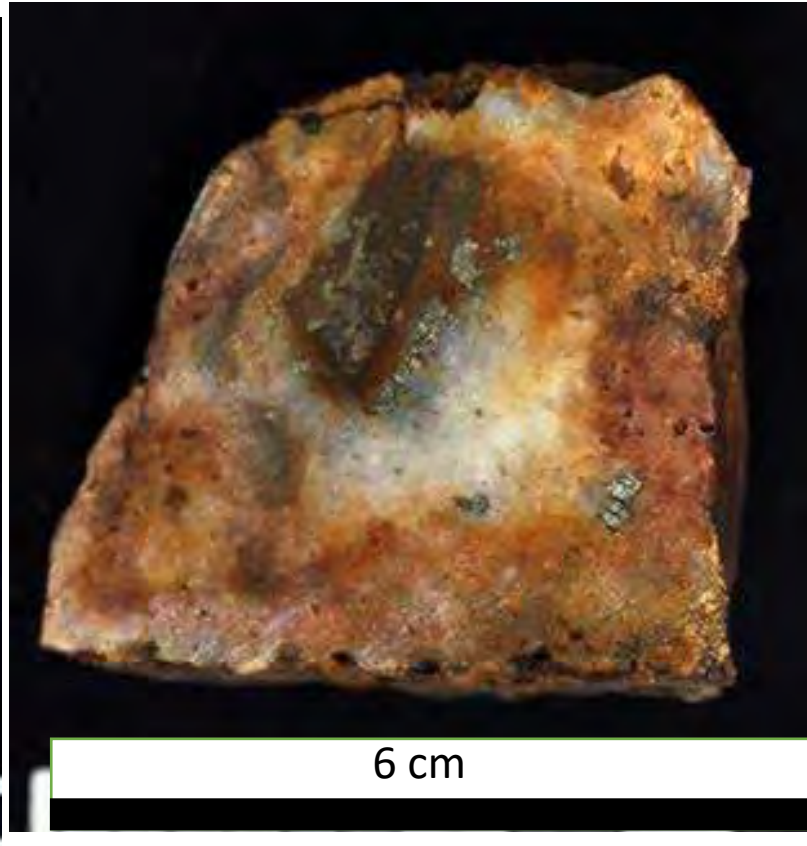
TS1 (not cut)



TS2 (not cut)



2020-KELL-09-C

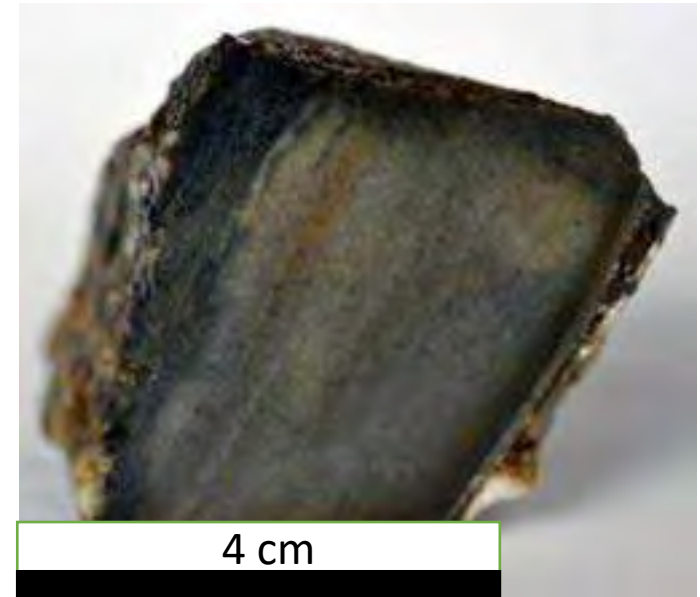
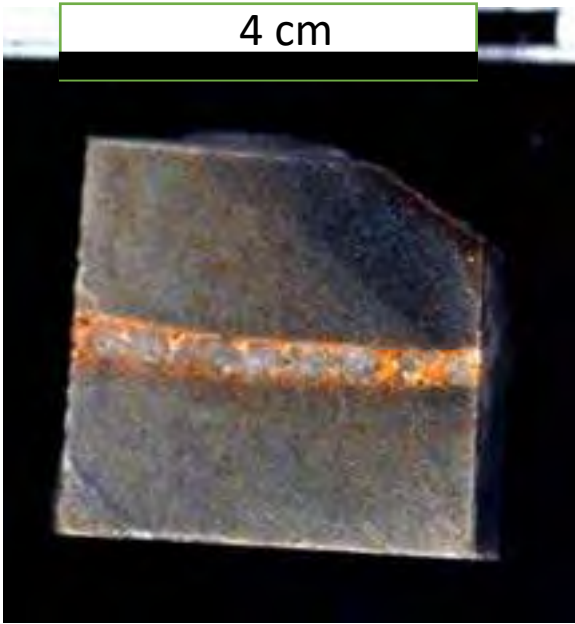
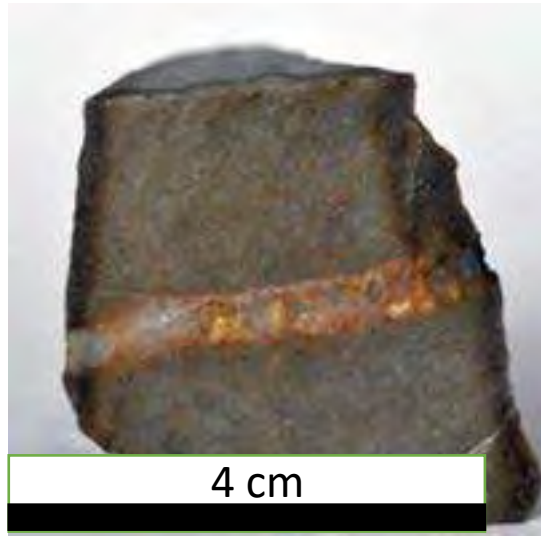


Mineralized breccia. Angular to sub-angular rock clasts (probably derived from hosting Catavi Fm. quartzites) with sizes in the range between 5 mm to 3 cm (long axis) are cemented by concentric layers of milky quartz drawing cocarde textures. Geodes of euhedral milky quartz crystals up to 2 cm in length and overgrowing Fe-rich bladed carbonates are common. Interstitial space between quartz crystals and secondary porosity (dissolution?) are lined with Fe-rich carbonate and euhedral pyrite crystals (<1 mm). Dark brown subhedral cassiterite crystals occupy the interstitial space between quartz crystals.

2020-KELL-09-C



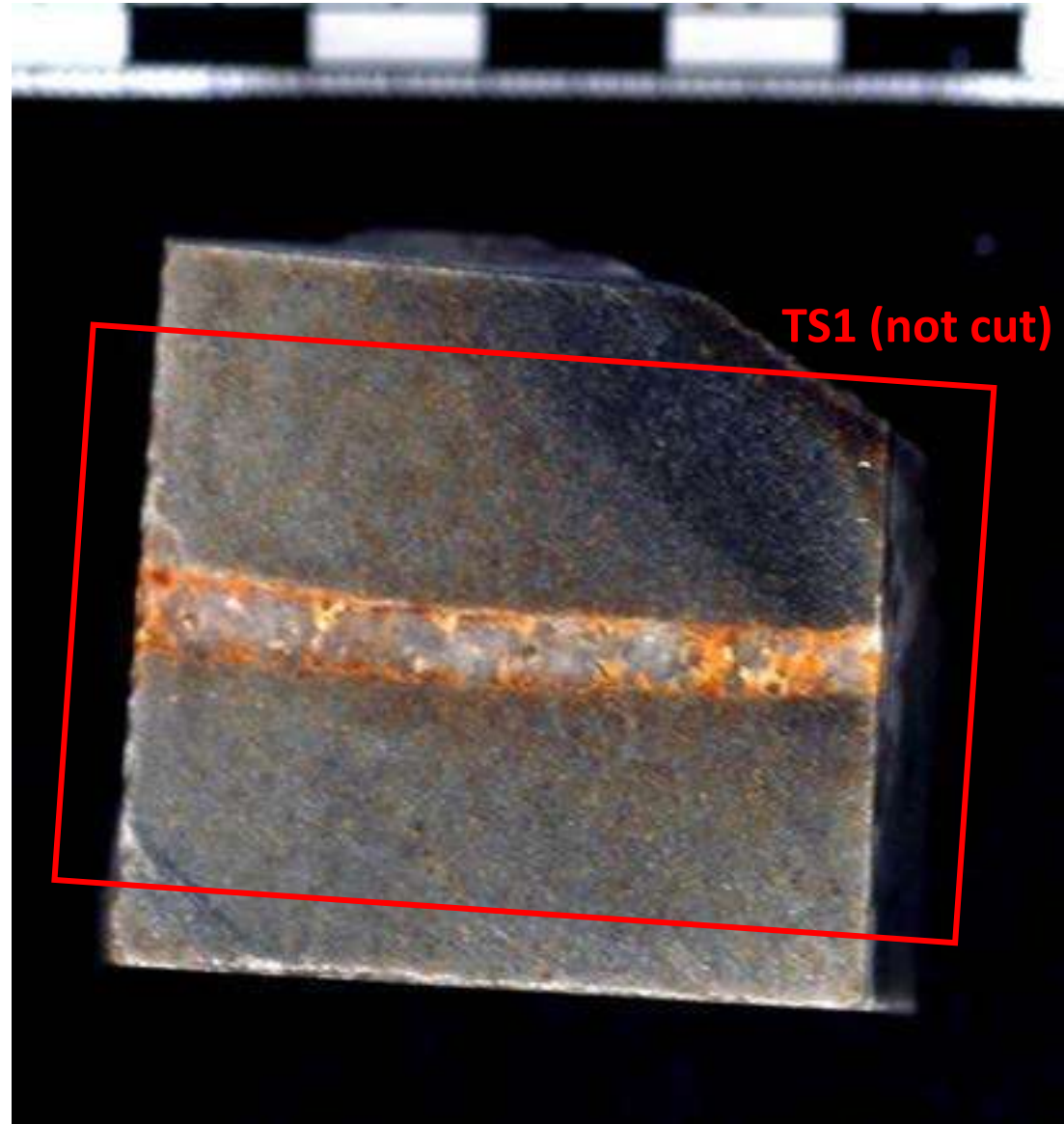
2020-KELL-10-A



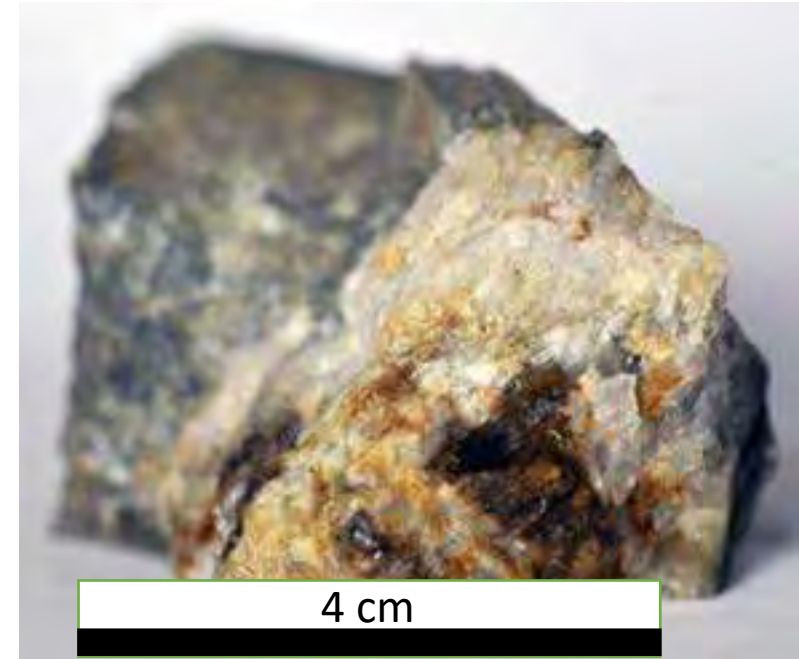
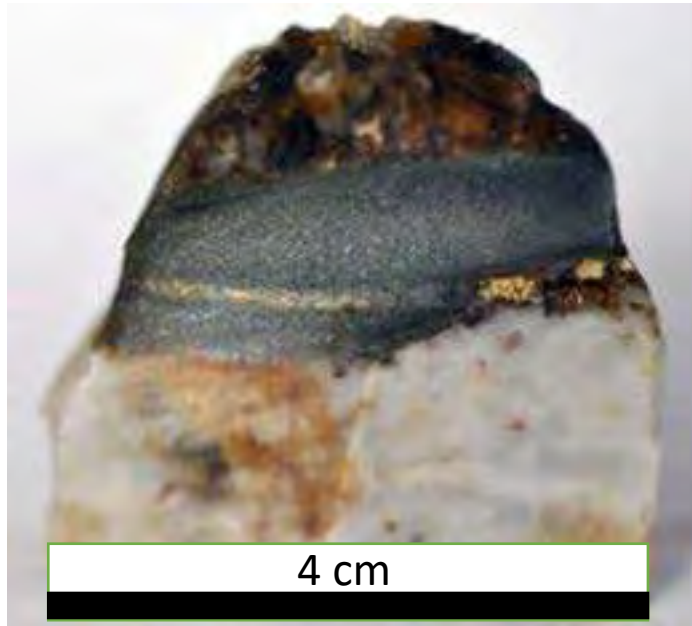
Vein hosted by Catavi Fm. quartzites.

The vein is approximately 0.5 cm thick and consists largely of quartz and carbonates along with lesser amounts of pyrite. Vein quartz is milky and massive. Yellow to pale-brown carbonates are subhedral and concentrate along the vein contact with the host rock. Euhedral to subhedral pyrite crystals (<1mm) occur mostly intergrown with vein carbonates along the rims of the veins, although some pyrite crystals and aggregates are observed within vein quartz. The host rock shows a dissemination of randomly distributed minute (<1 mm) euhedral pyrite crystals as well.

2020-KELL-10-A



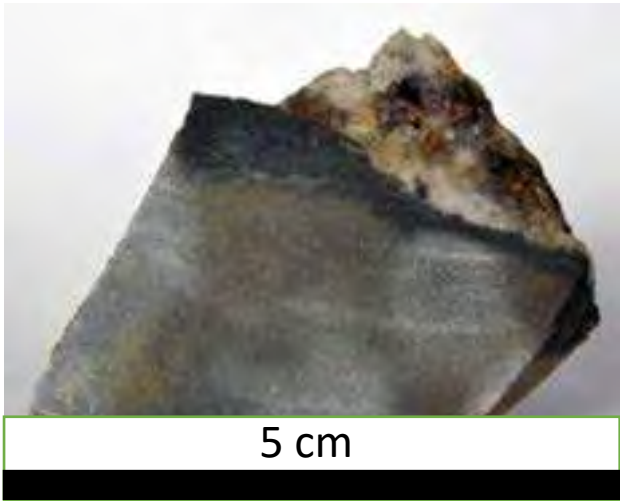
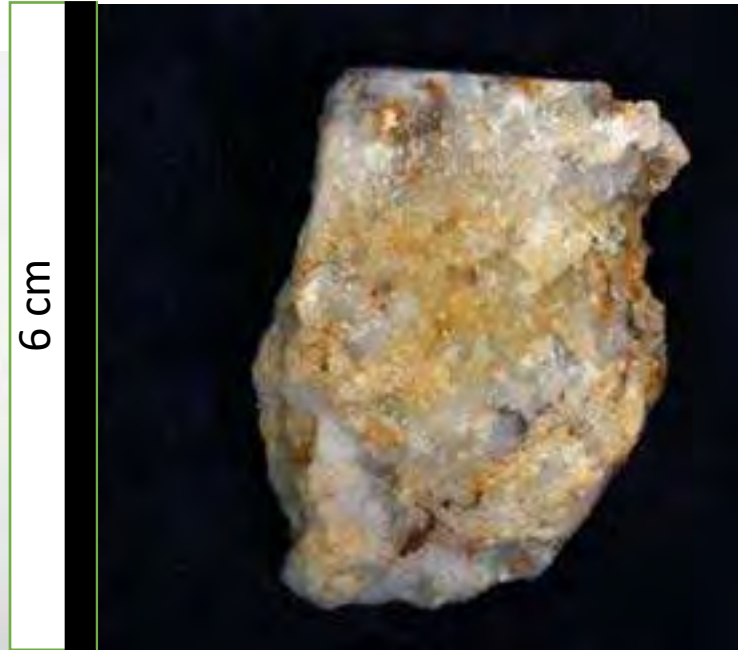
2020-KELL-10-B



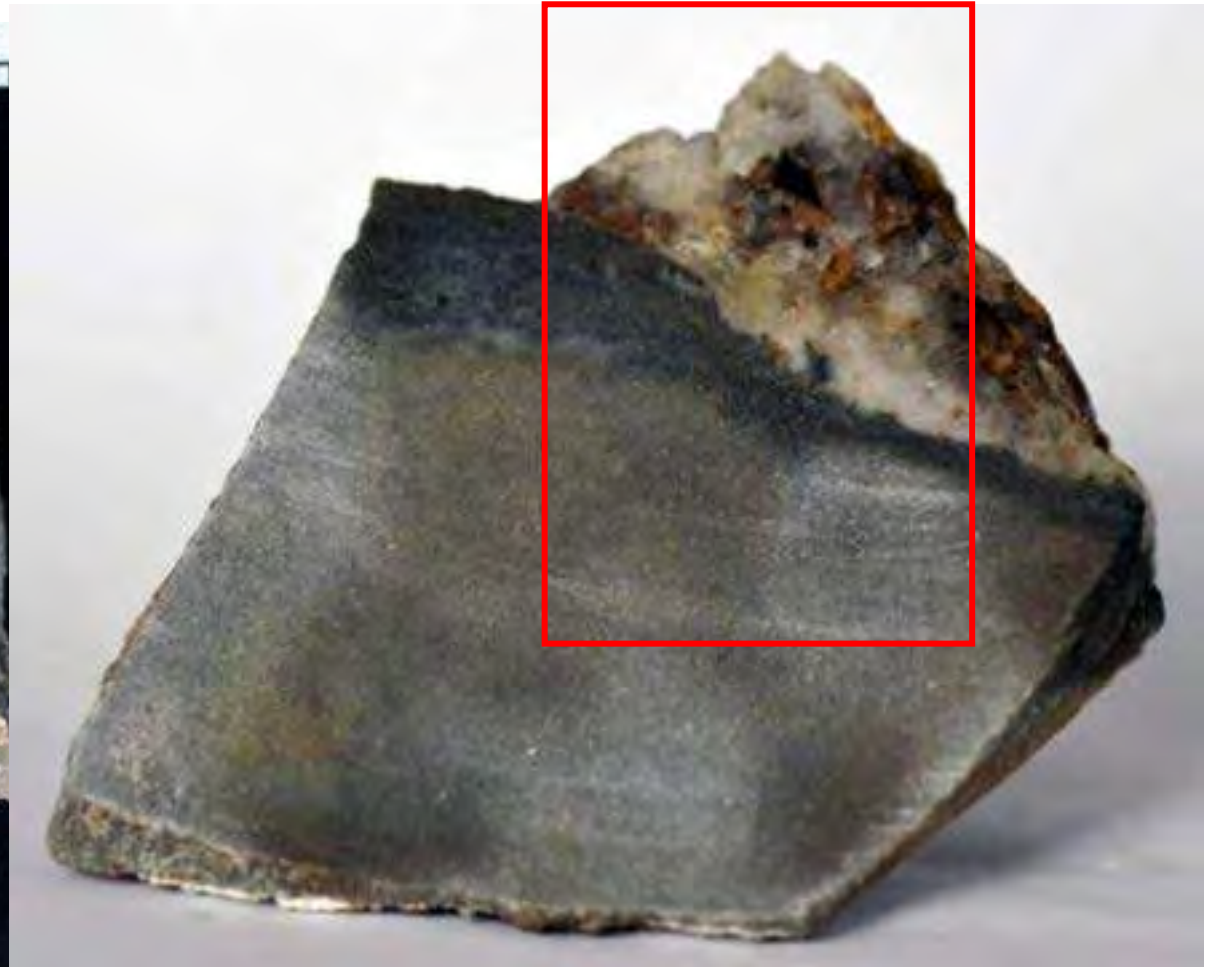
Veins hosted by Catavi Fm. quartzites.

The main vein is approximately 3.5 cm thick and contains a mineralization of quartz with lesser proportions of cassiterite, carbonates and, pyrite. Massive milky quartz is locally overgrown by euhedral translucent quartz crystals up to 1 cm long. Cassiterite crystals are brown in color and mm-sized, and appear intergrown with vein quartz. Carbonates are anhedral, with yellowish to dark-brown colors. Pyrite is scarce and appear forming individual crystals and aggregates <2 mm across along with vein carbonates.

2020-KELL-10-B



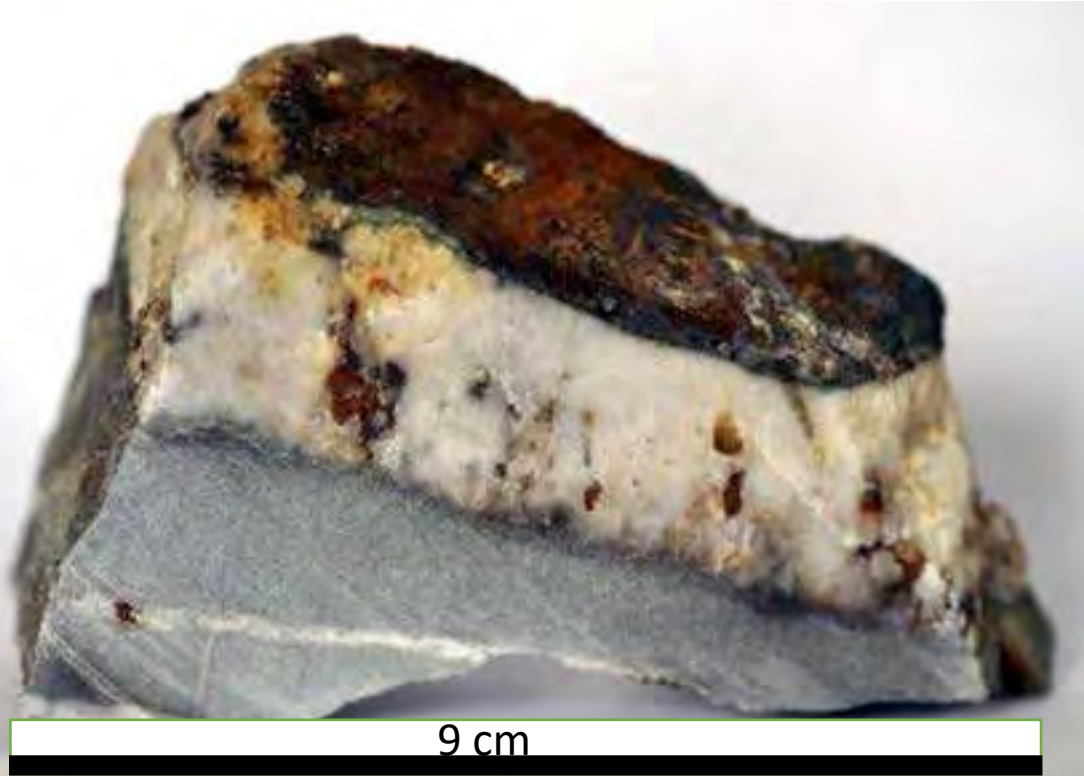
2020-KELL-10-B



2020-KELL-11

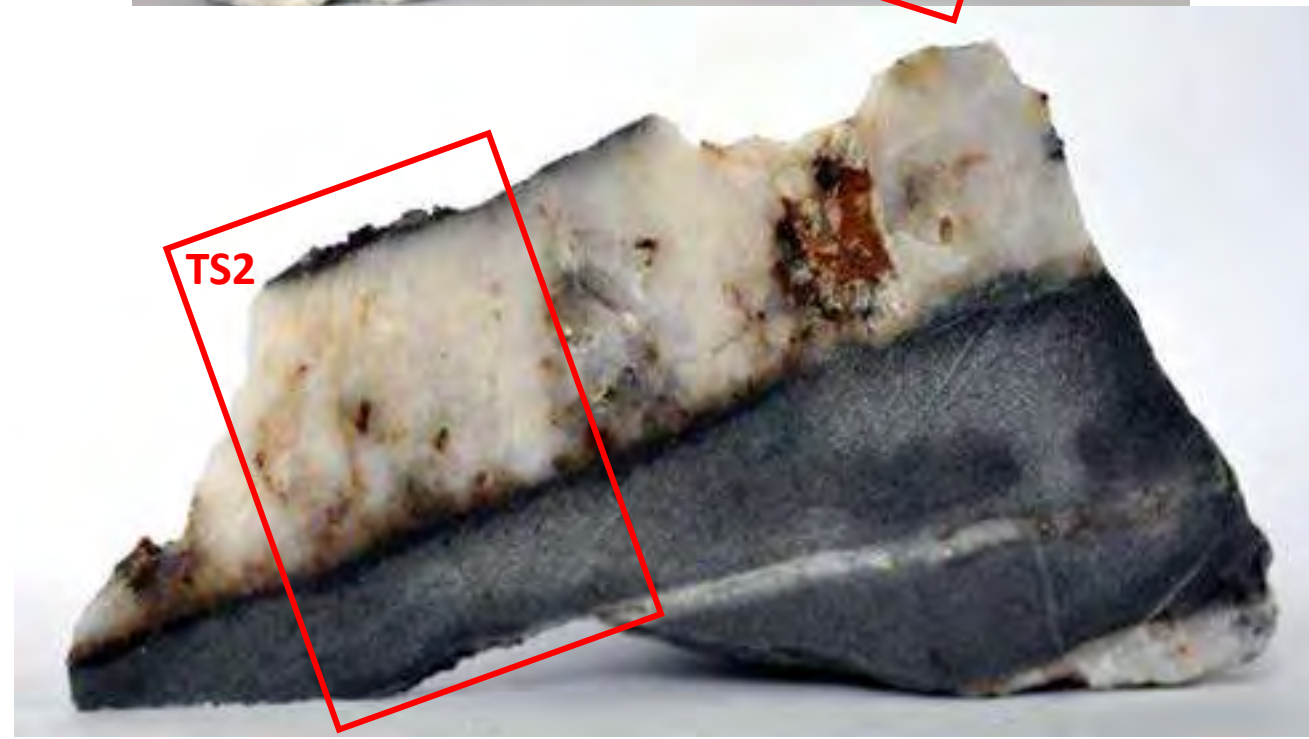
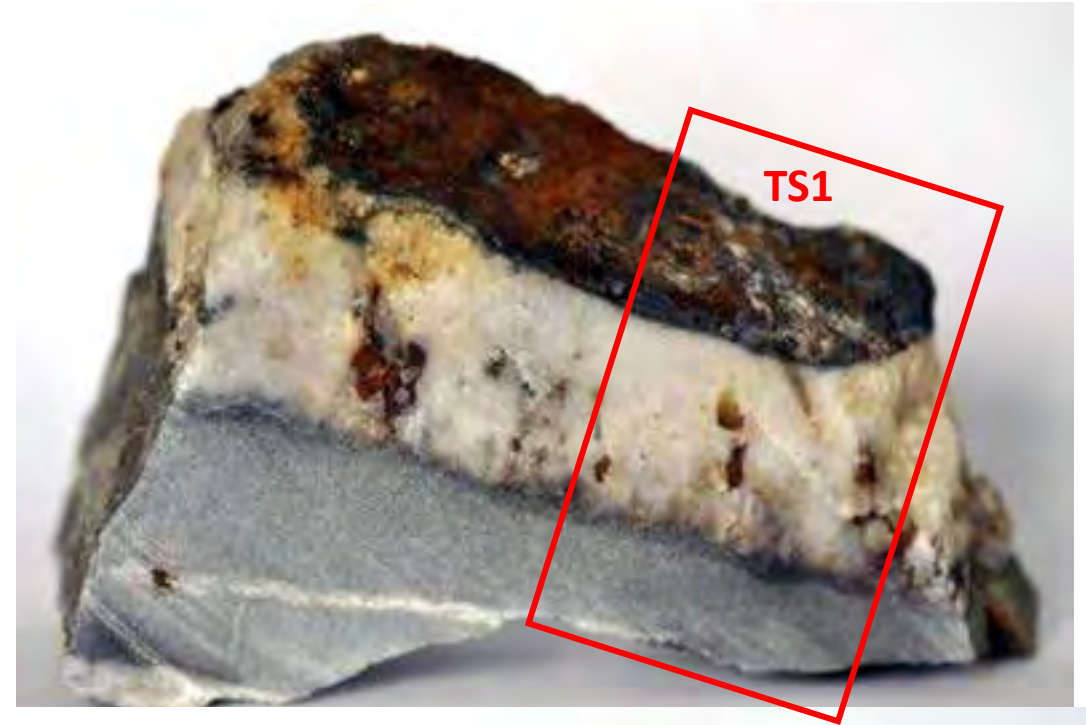


2020-KELL-11



Quartz-cassiterite veins hosted by Catavi Fm. quartzites. The main vein is approximately 3 cm thick and contains a mineralization of quartz with lesser proportions of sulfides, carbonates and very local white mica. Two types of quartz have been distinguished: i) milky massive granular quartz, and ii) hyaline euhedral quartz. Hyaline euhedral quartz crystals are up to 1 cm long and appear mostly as geodes in secondary porosity in milky quartz. Fe-rich carbonates appear mostly occupying interstitial space between hyaline quartz within geodes in milky quartz. Sulfide mineralization (pyrite and probably also brown sphalerite) occurs mostly as scattered subhedral grains within or close to vein carbonate. Interstitial to the quartz vein there is a white-grey micaceous mineral (muscovite?). Scattered mm-sized subhedral pyrite crystals appear along the host quartzite. In the vein selvage there is a narrow (about 1 mm thick) dark-green band (alteration halo of tourmaline?). Other veins in the sample are around 2 mm of wide and show similar paragenesis as the vein described above.

2020-KELL-11



2020-KELL-12-A

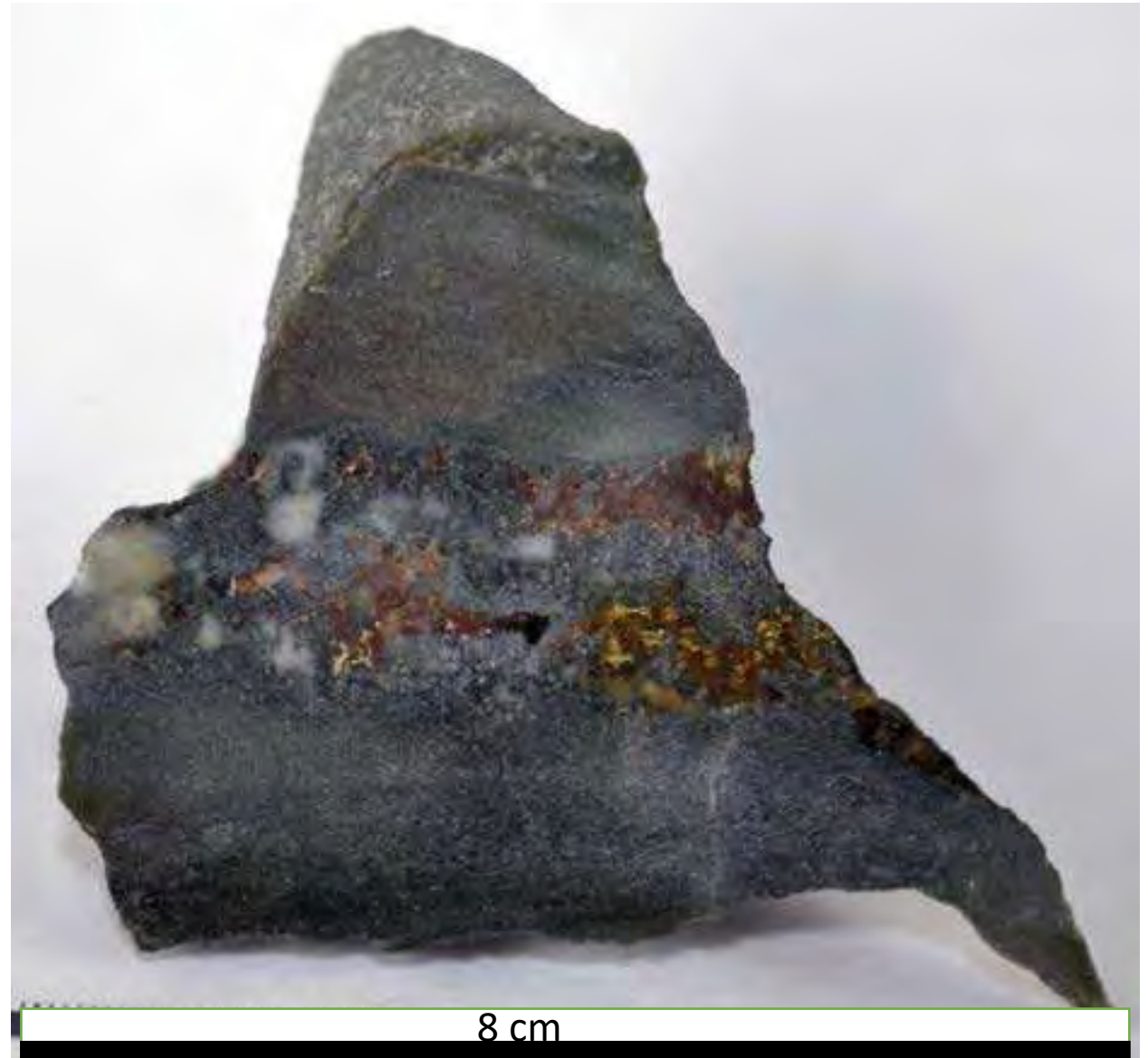


Quartz-pyrite vein hosted by Catavi Fm. quartzites. The vein is approximately 4 cm thick and contains a mineralization of quartz, pyrite and lesser proportions of Fe-rich carbonates. Pyrite crystals are mm-sized, and occur mostly as anhedral-subhedral grains forming massive aggregates towards the central part of the vein. Pyrite crystals are intergrown with dusty to bladed Fe-rich carbonate. Some euhedral pyritohedral crystals are observed. Quartz is milky and massive.

2020-KELL-12-B

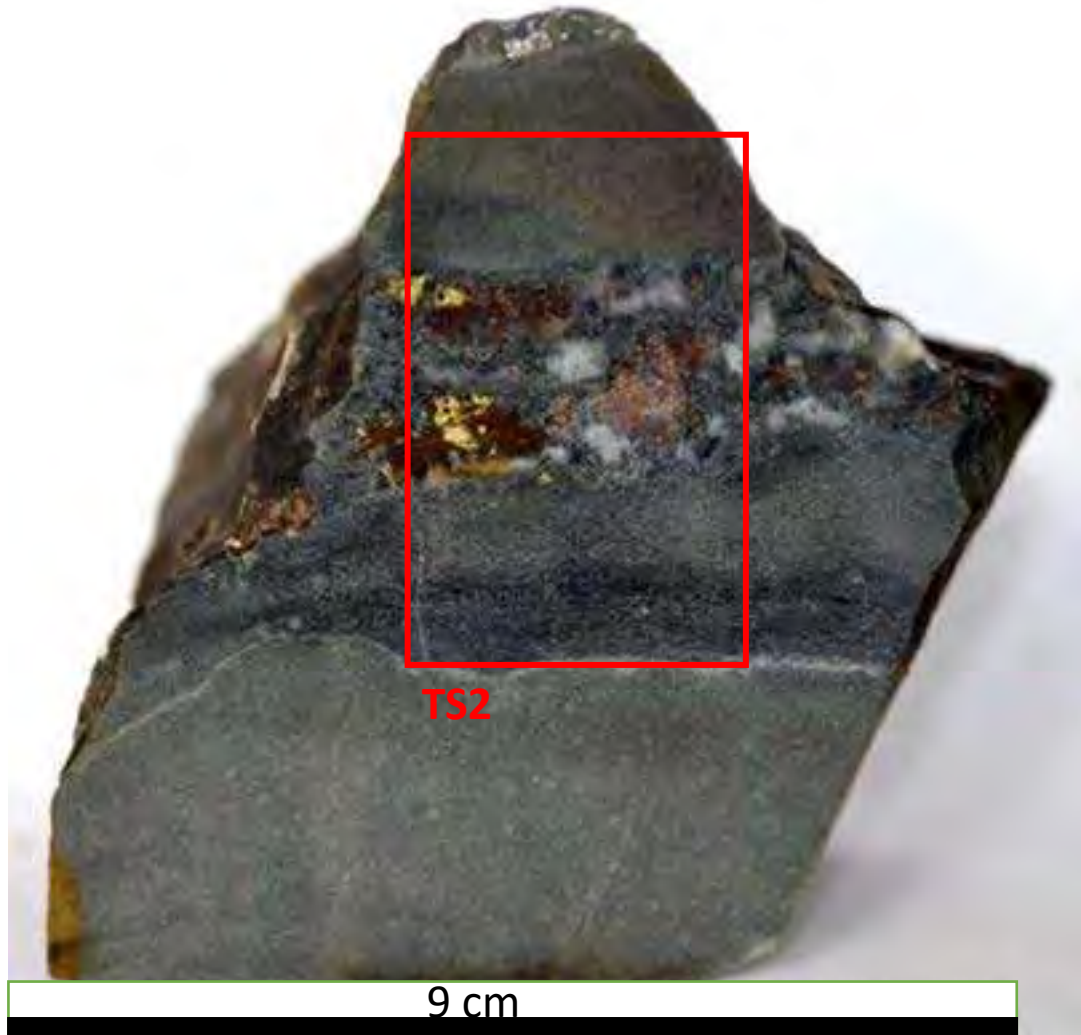


2020-KELL-12-B

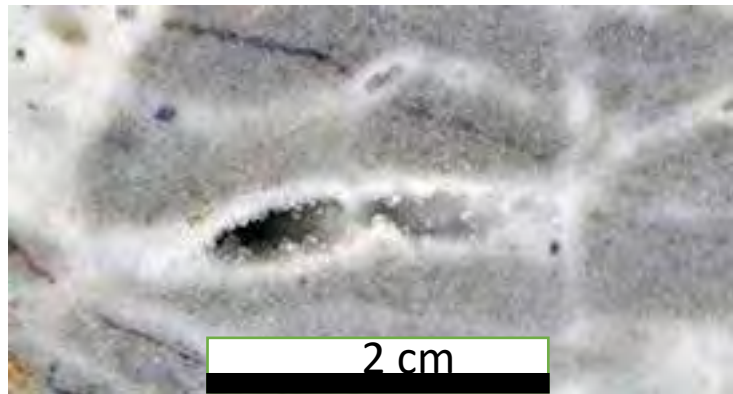


Veins hosted by Catavi Fm. quartzites. The main vein is approximately 3 cm wide and contains a mineralization of quartz, sulfides, carbonates, and tourmaline (\pm chlorite?). Quartz crystals are milky and up to 1 cm long. The sulfide mineralization comprises sphalerite, pyrite, and chalcopyrite. These sulfides appear as anhedral grains and patches mostly occupying interstitial space between quartz. Fe-rich carbonates are anhedral and occur interstitial to quartz as well. A dark green mineralization (probably tourmaline \pm chlorite) is ubiquitous in the sample and appear cementing the above described phases as well as along the rims of the vein.

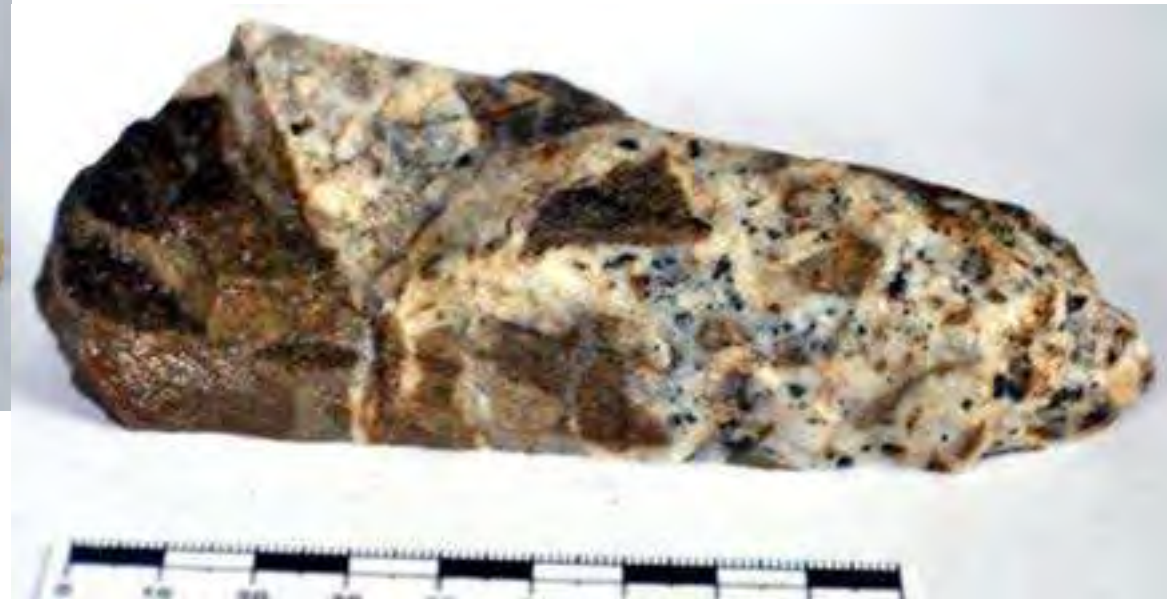
2020-KELL-12-B



2020-KELL-13-A



2020-KELL-13-A



Hydrothermal breccia. The breccia is composed of centimetric angular rock clasts derived from hosting Catavi Fm. quartzite. Often, clasts draw jigsaw-fit textures. The clasts are altered to an assemblage of muscovite(?) and a brown mineral that has not been identified in hand sample. These clasts are cemented by milky quartz. Geodes in milky quartz cement are lined with elongated euhedral quartz crystals (up to 2 mm long). Sulfide (mostly pyrite) occur as mm-sized euhedral grains within the milky quartz cement.

2020-KELL-13-A



2020-KELL-13-B



5 cm



5 cm

2020-KELL-13-B



Vein hosted by Catavi Fm. quartzites. The main vein is approximately 2 cm wide and contains a mineralization of quartz with lesser proportions of sphalerite and pyrite. Granular milky quartz is up to 2 cm long. Sphalerite crystals are dark brown in color and mm-sized, and occur mostly occupying interstitial space between quartz crystals. Pyrite crystals are mm-sized, and occur mostly as subhedral grains. This contact of the vein with the host rock is very sharp. The sulfide minerals are partially oxidized and lixiviated.

2020-KELL-14-A



2020-KELL-14-A

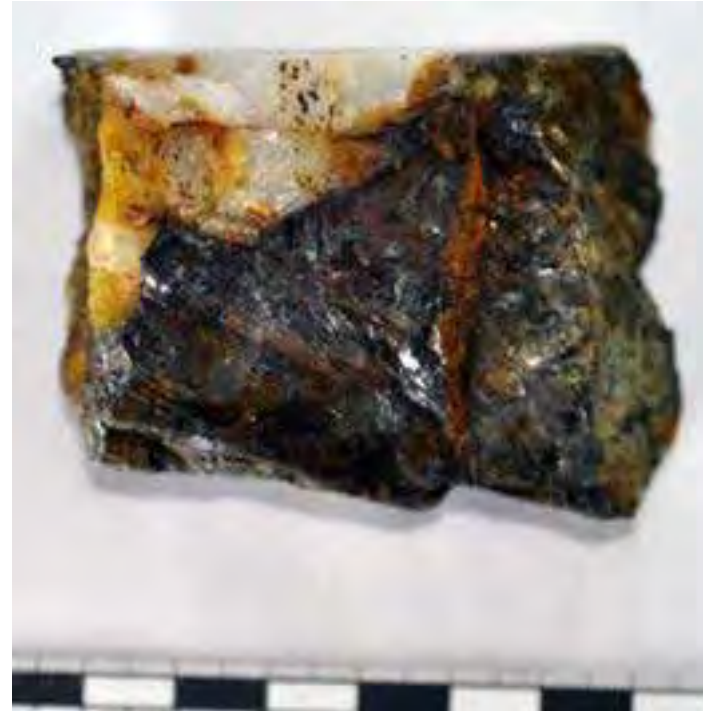
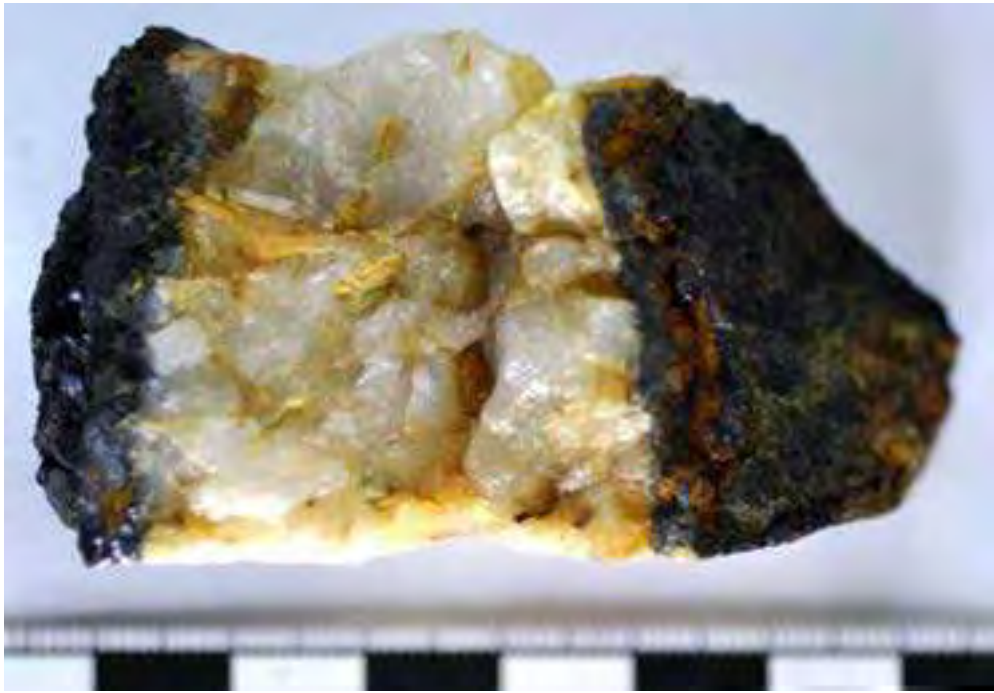


Sphalerite vein hosted by Catavi Fm. quartzites. A centimetric vein contains sphalerite-rich mineralization with lesser proportions of quartz and pyrite. Sphalerite anhedral crystals are dark brown to almost black in color and mm-sized. Vein quartz forms translucent euhedral elongated crystals (up to 5 cm long). Pyrite crystals are subhedral to anhedral and often form stringers (<1mm wide) and patches that cut sphalerite. Interstitial to sphalerite is a massive microgranular green mineralization (chlorite?) patches.

2020-KELL-14-B



2020-KELL-14-B



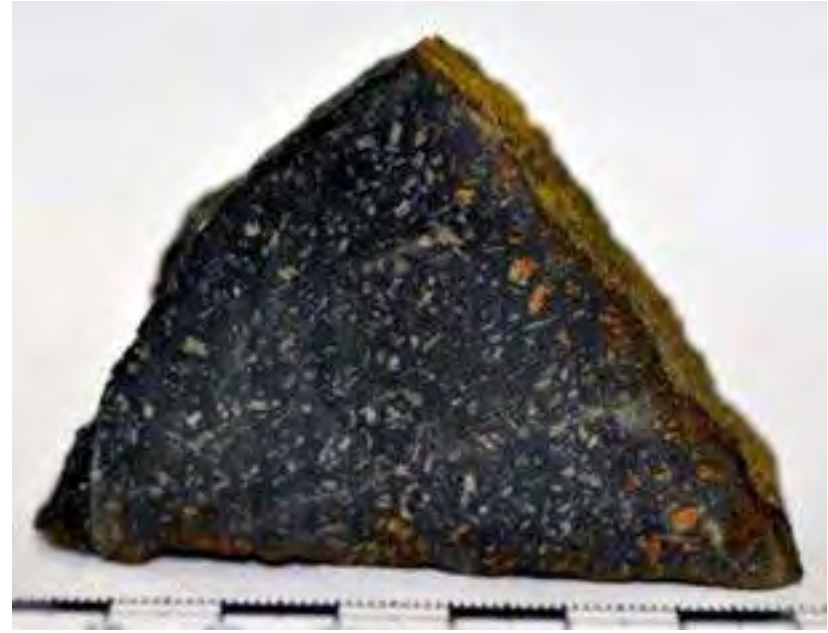
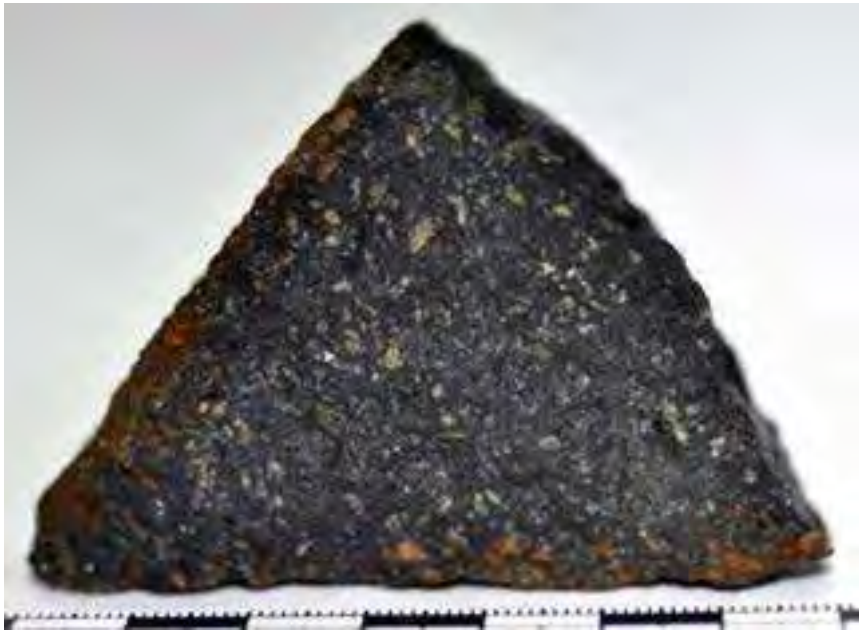
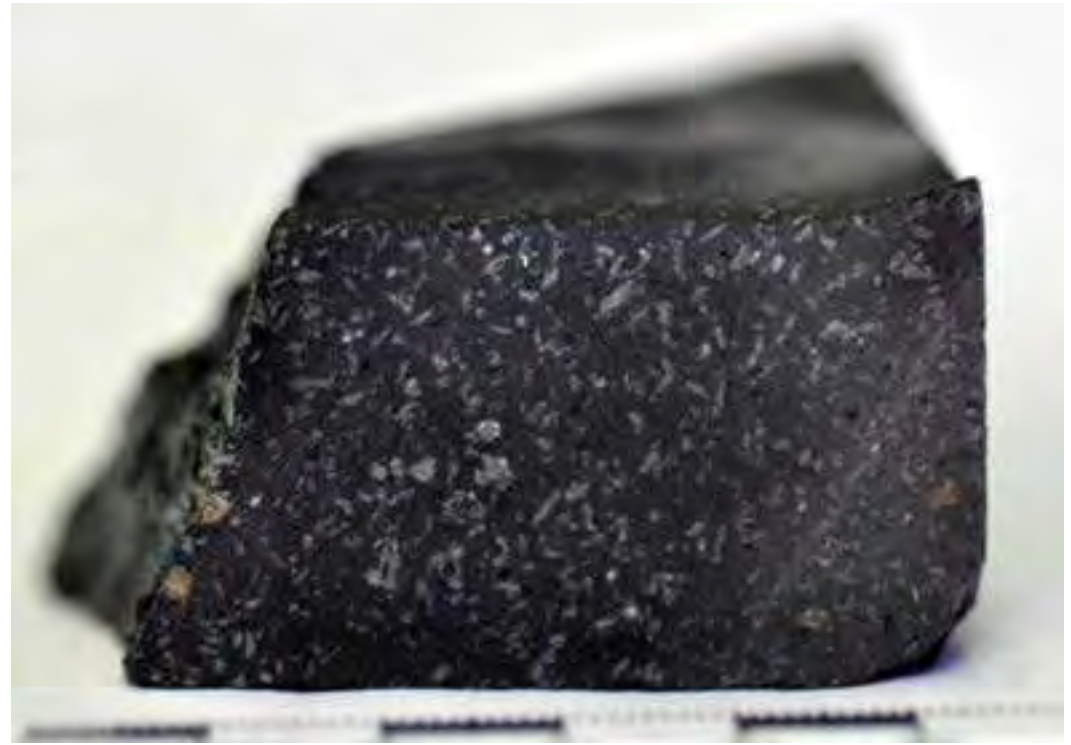
Sphalerite and quartz veins hosted by Catavi Fm. quartzites. The quartz vein is 4 cm wide and contains a mineralization composed largely of milky granular quartz and scattered minute (< 1mm) pyrite crystal; the vein is surrounded by a narrow (<1mm) green halo (chorite?). The sphalerite vein cut the quartz vein. Sphalerite is massive, dark brown in color, and occur along with scattered mm-sized subhedral pyrite grains. In both veins, fractures (<1mm width) are lined with sulfides and a pale-yellow mineral (carbonate?).

2020-KELL-15

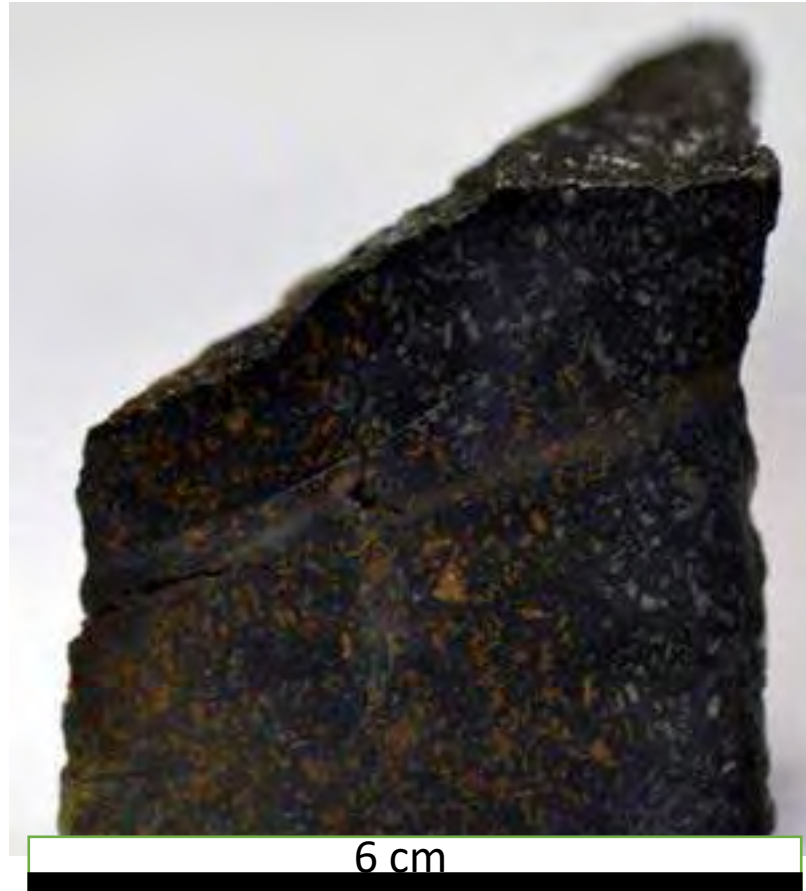


Black shale (low-grade metamorphism). Uncía Fm.

2020-KELL-16



2020-KELL-16



Dike of andesitic composition. Porphyritic textures describe by plagioclase and biotite phenocrysts in a cryptocrystalline groundmass of pale greenish gray color. Plagioclase phenocrysts are white, euhedral to subhedral and show tabular-prismatic habit and lengths up up to 4 mm. Biotite phenocrysts are less abundant than plagioclase phenocrysts, subhedral and up to <1mm across. mm-sized subhedral pyrite crystals appear scattered, in very low proportions, in the rock.

2020-KELL-16



2020-KELL-17-A



2020-KELL-17-A

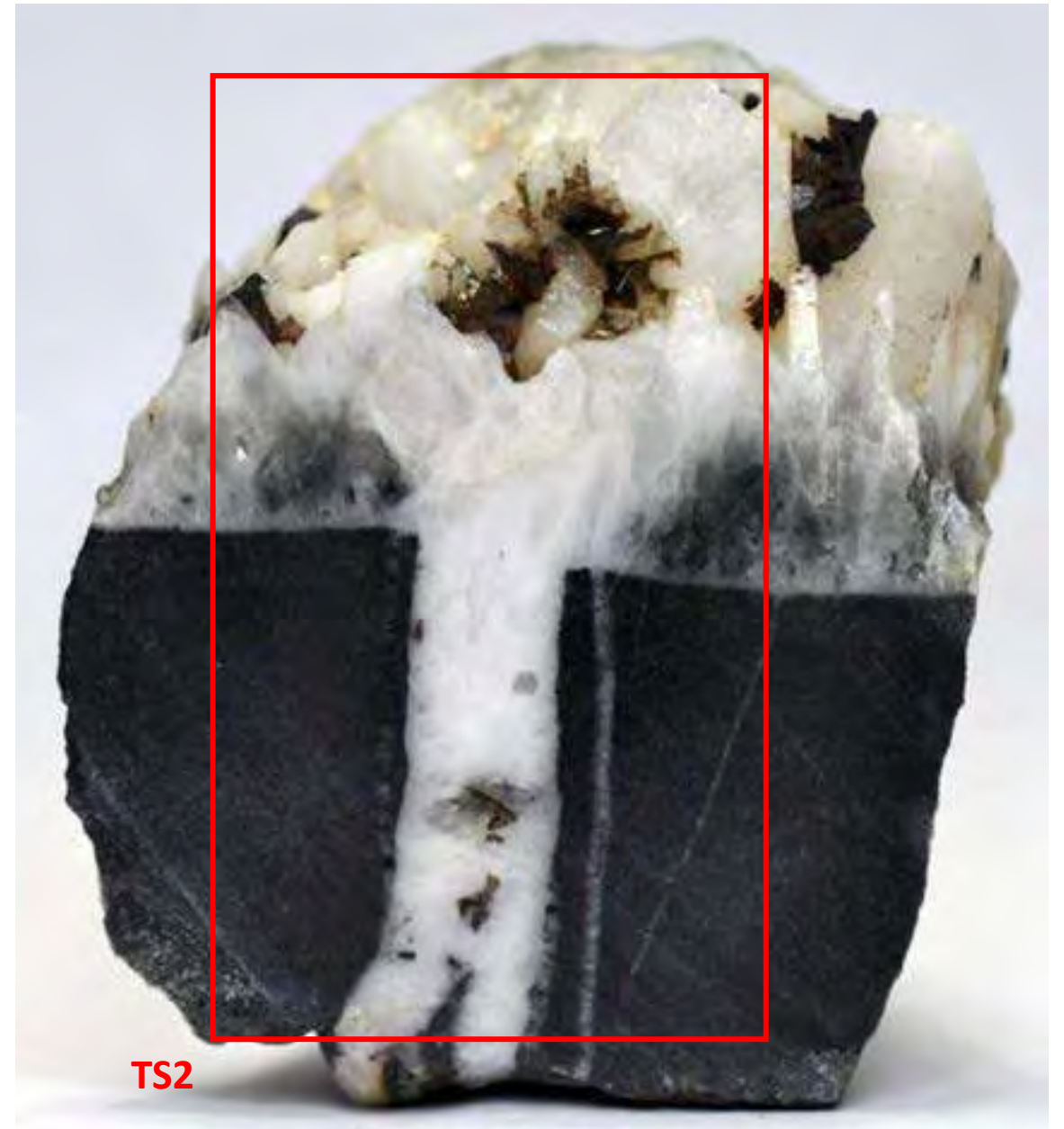
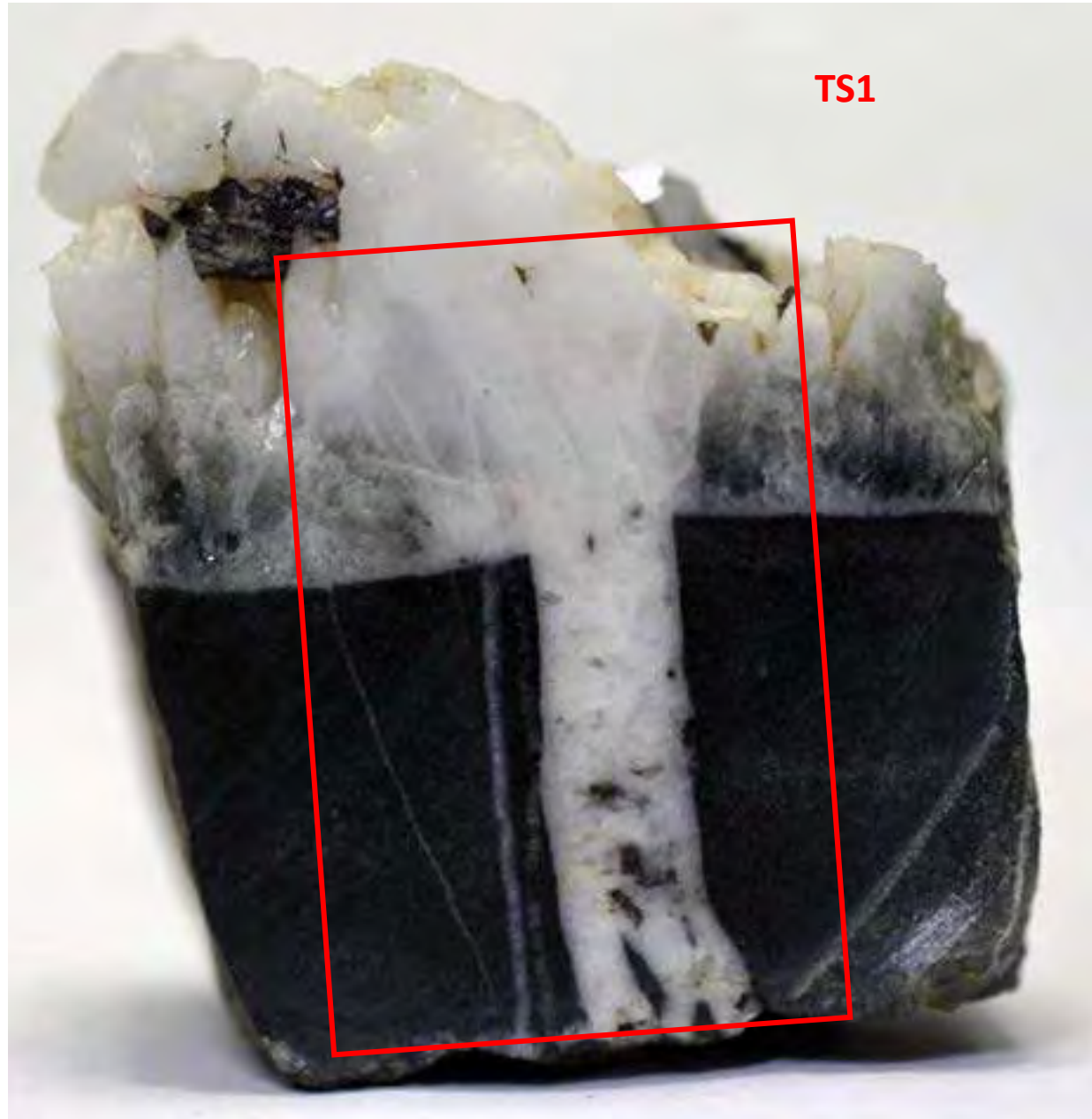


Quartz-cassiterite veins hosted by Catavi Fm. quartzites.

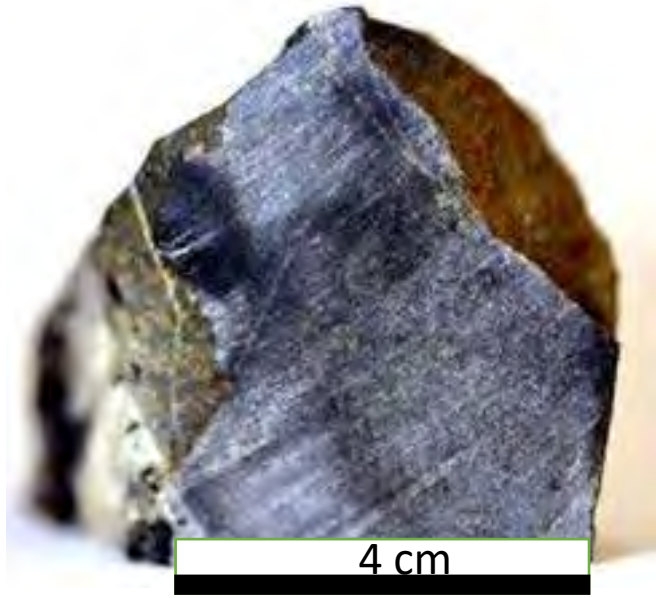
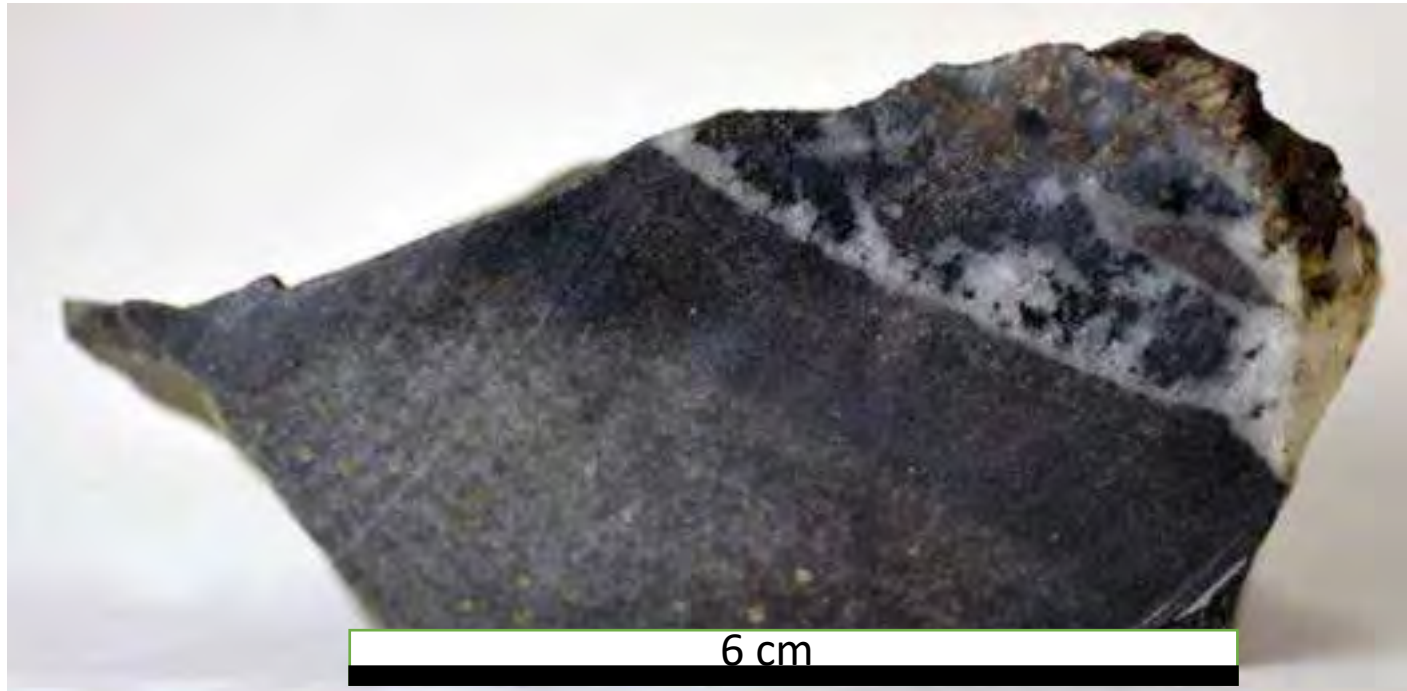
The main vein is approximately 3.5 cm wide and contains a mineralization of quartz with lesser proportions of cassiterite and Fe-rich carbonates. Euhedral to subhedral translucent quartz crystals up to 2 cm long describe comb textures. Cassiterite and Fe-rich carbonate grains appear mostly occupying interstitial space between comb quartz crystals. Cassiterite crystals are dark brown in color and mm-sized. Fe-rich carbonate grains are reddish brown in color and mm-sized, and often show platy to lens-shaped habits. In addition, the sample contains a series of veins that are oriented perpendicular to the main one (and which probably acted as feeders of this), are around 1cm thick, and show a similar paragenesis as that described for the main vein. These secondary veins are composed mostly of euhedral milky quartz crystals with mm to cm sizes. Geodes of euhedral, translucent quartz crystals >1 mm in length, and mm-sized cassiterite crystals occur towards the central part of the veins.

A further set of veins comprises stringers that are around 1mm wide and contain mineralization of quartz and tourmaline. Tourmaline mineralization shows as acicular crystals perpendicular to the growth of the veinlets.

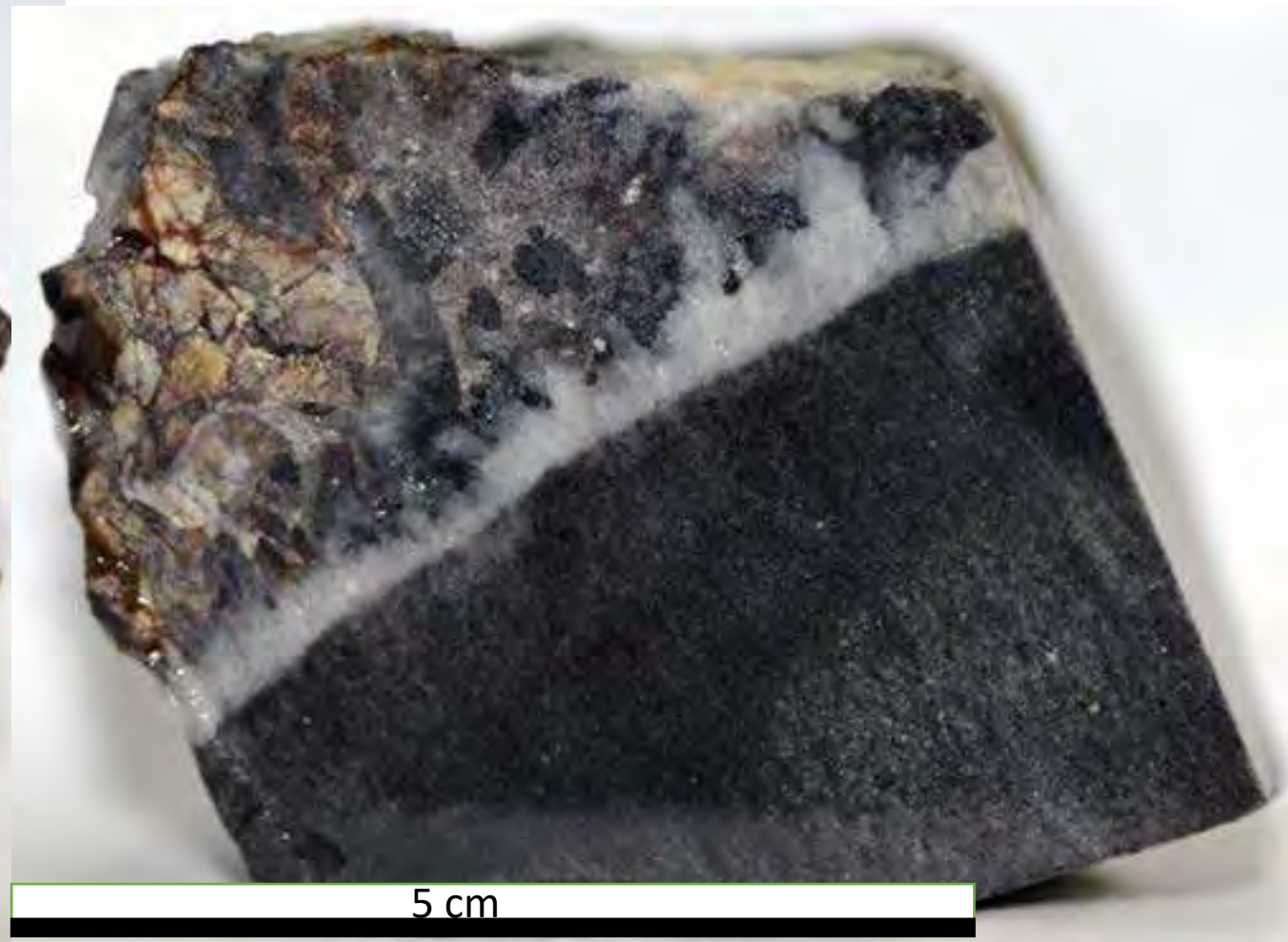
2020-KELL-17-A



2020-KELL-17-B



2020-KELL-17-B



2020-KELL-17-B



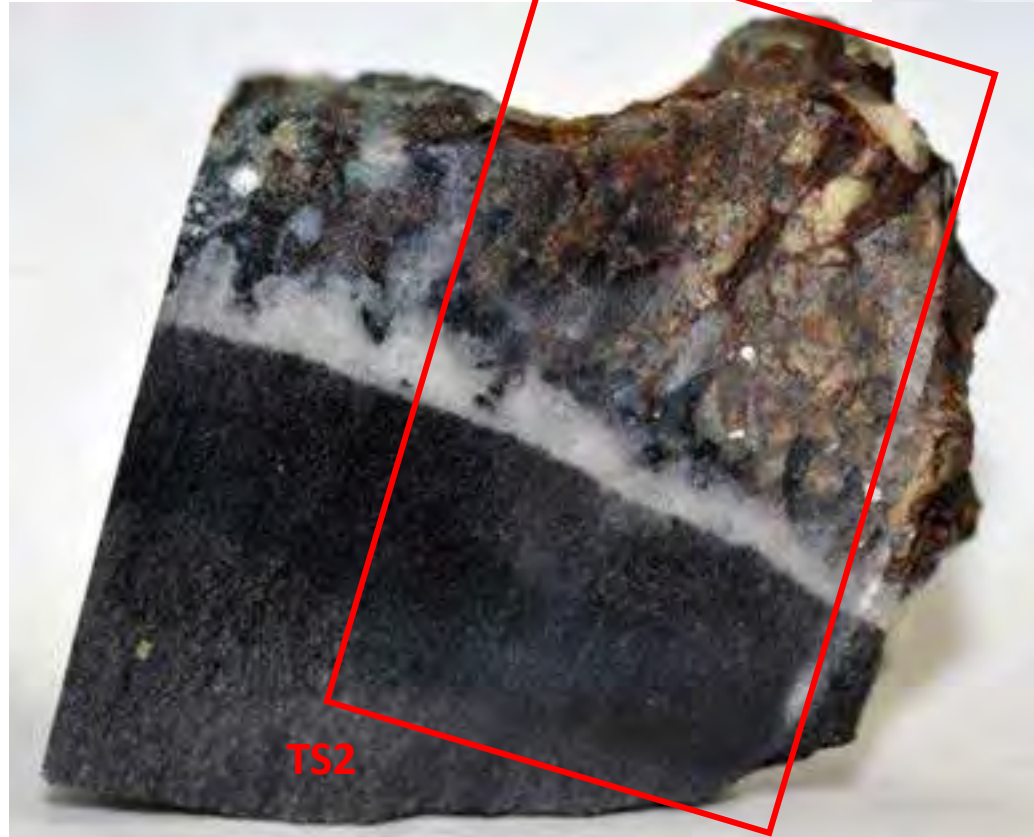
3 cm



5 cm

Quartz-carbonate veins hosted by Catavi Fm. quartzites. The main vein is approximately 4 cm wide. Two types of quartz have been distinguished: i) milky massive granular quartz (mostly to the borders of the vein), and ii) hyaline euhedral quartz, with individual crystals up to 2 cm long and describing comb textures. Fe-rich carbonate, with pale- and dark-brown colors, appear towards the central part of the vein and is mostly interstitial to comb quartz crystals. mm-sized elongated to acicular tourmaline crystals occur mostly along with milky quartz along the rims of the vein, or directly along the contact between the vein and the host rock. Radial aggregates of acicular tourmaline crystals intergrown with milky quartz are common.

2020-KELL-17-B



2020-KELL-17-C

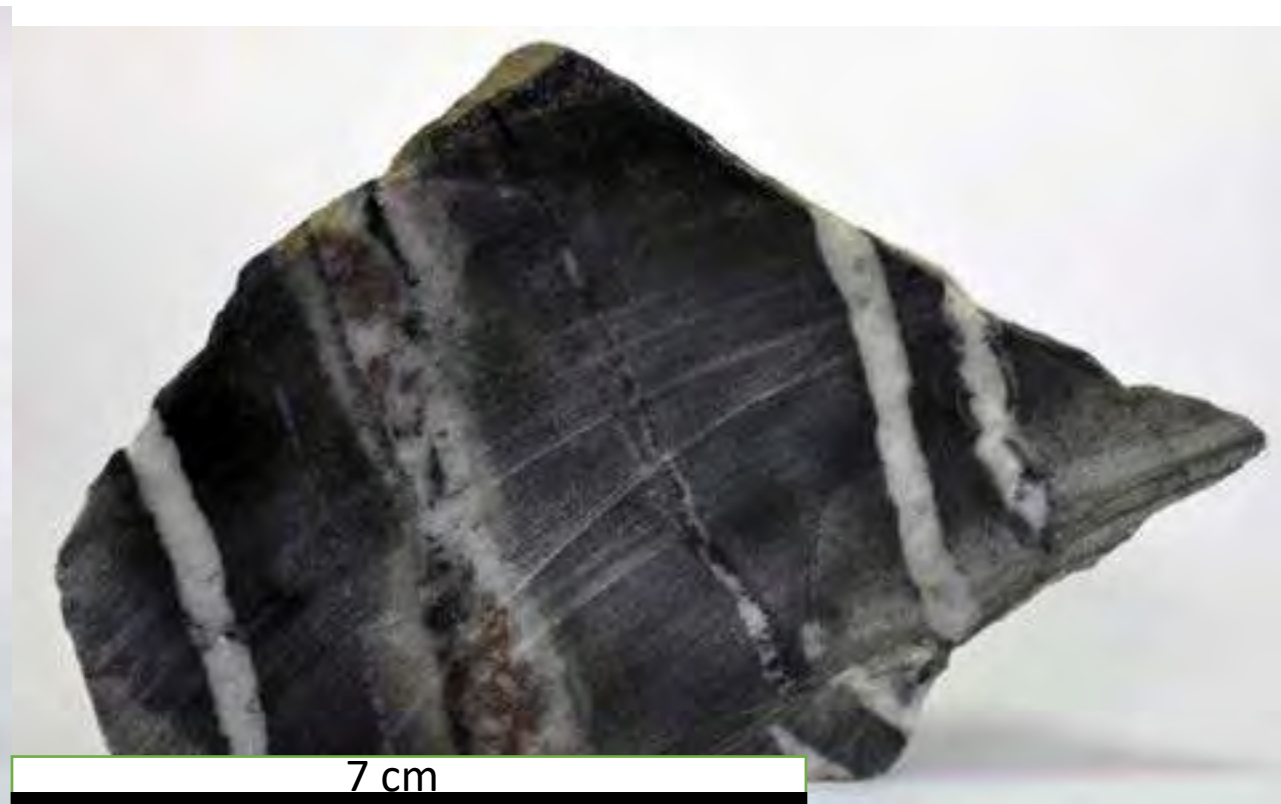
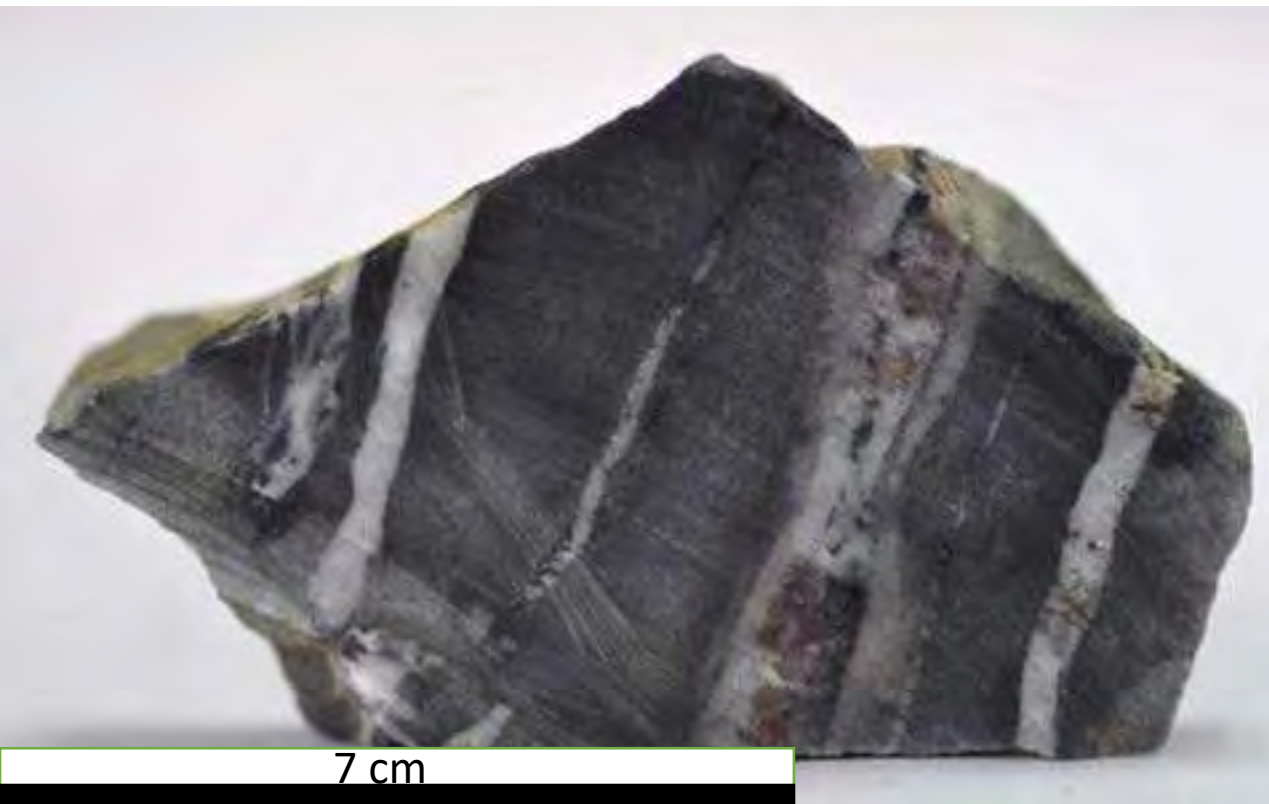


7 cm



7 cm

2020-KELL-17-C



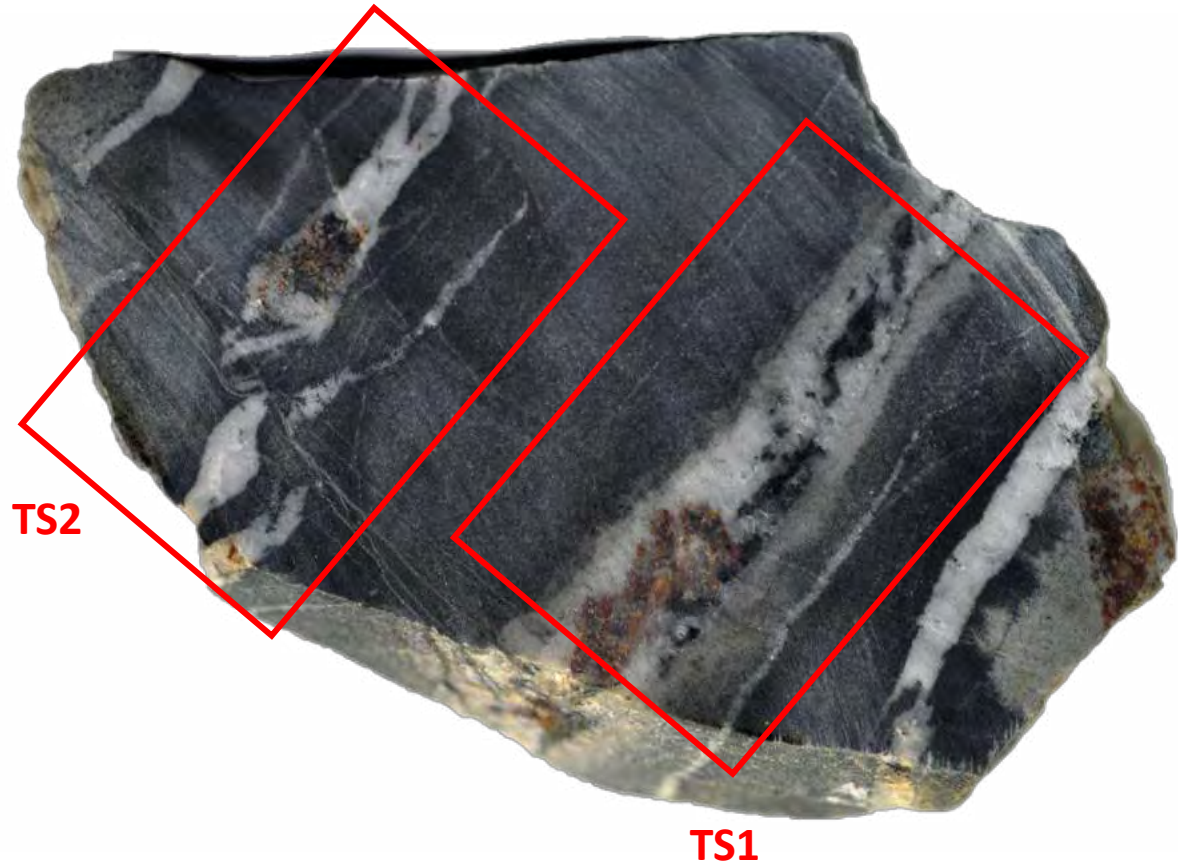
2020-KELL-17-C



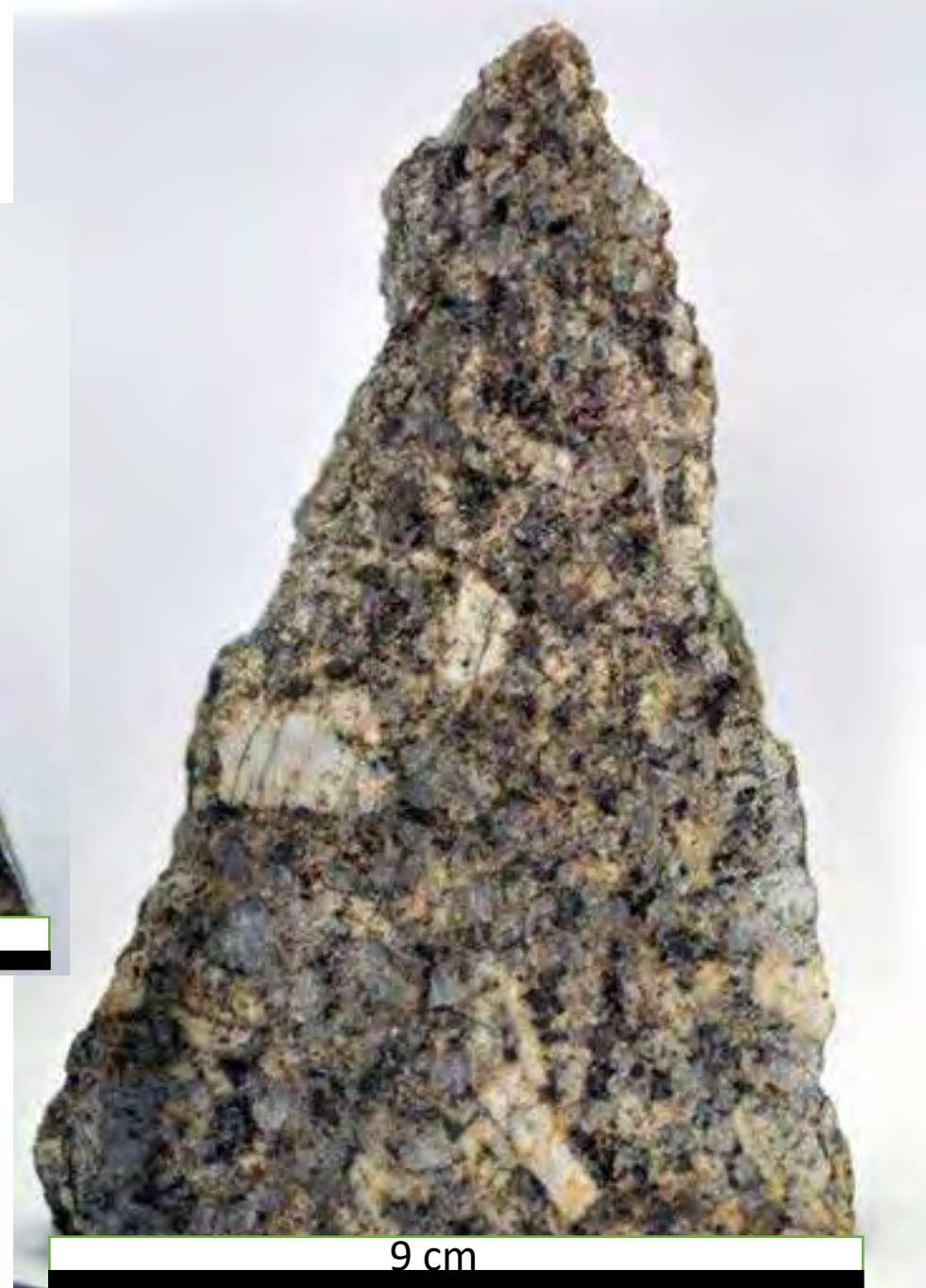
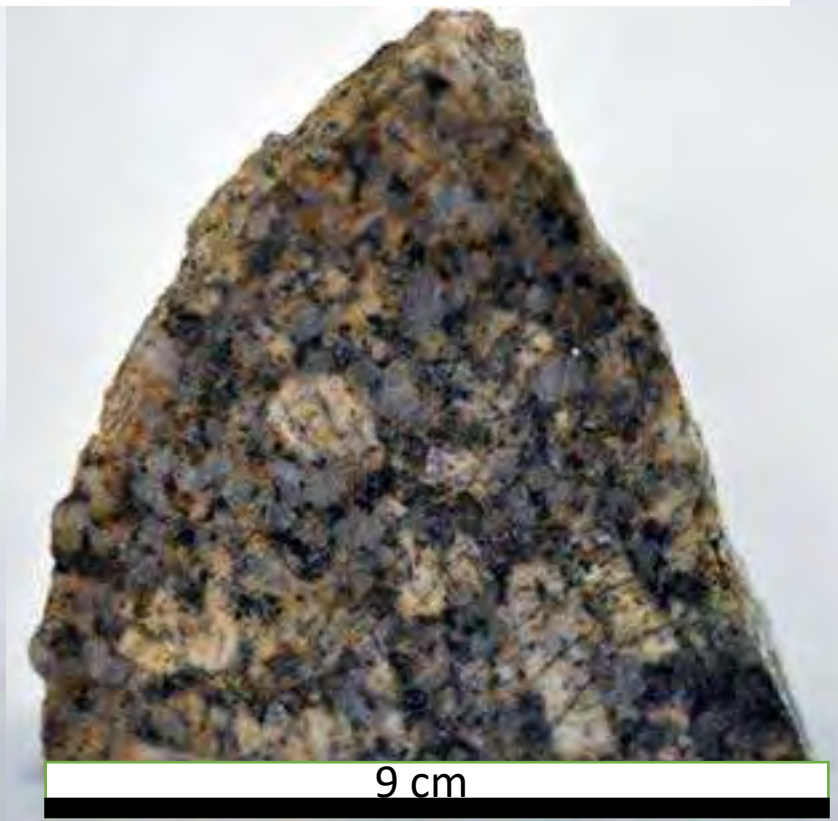
Veins hosted by Catavi Fm. quartzites.

Veins are approximately 1 cm wide and mostly composed of quartz, tourmaline, and cassiterite. Milky massive granular quartz is the major component and is surrounded and intergrown with black (<1 mm) crystals of tourmaline that appear as individual specimens mostly oriented perpendicular to the vein contacts. Cassiterite crystals are reddish-brown and yellowish in color, mm-sized, and their abundance increases towards the central part of the vein. Veins show irregular (varying from 2 to 5 mm in width) white-pale grey alteration haloes. mm-sized, angular fragments of the host rock are often incorporated within the veins.

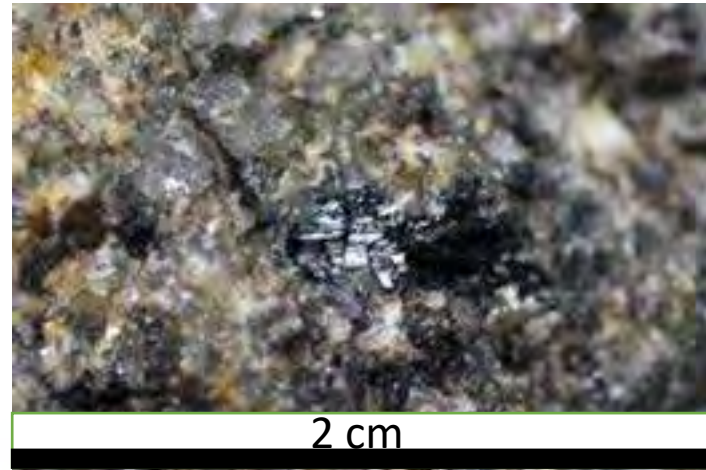
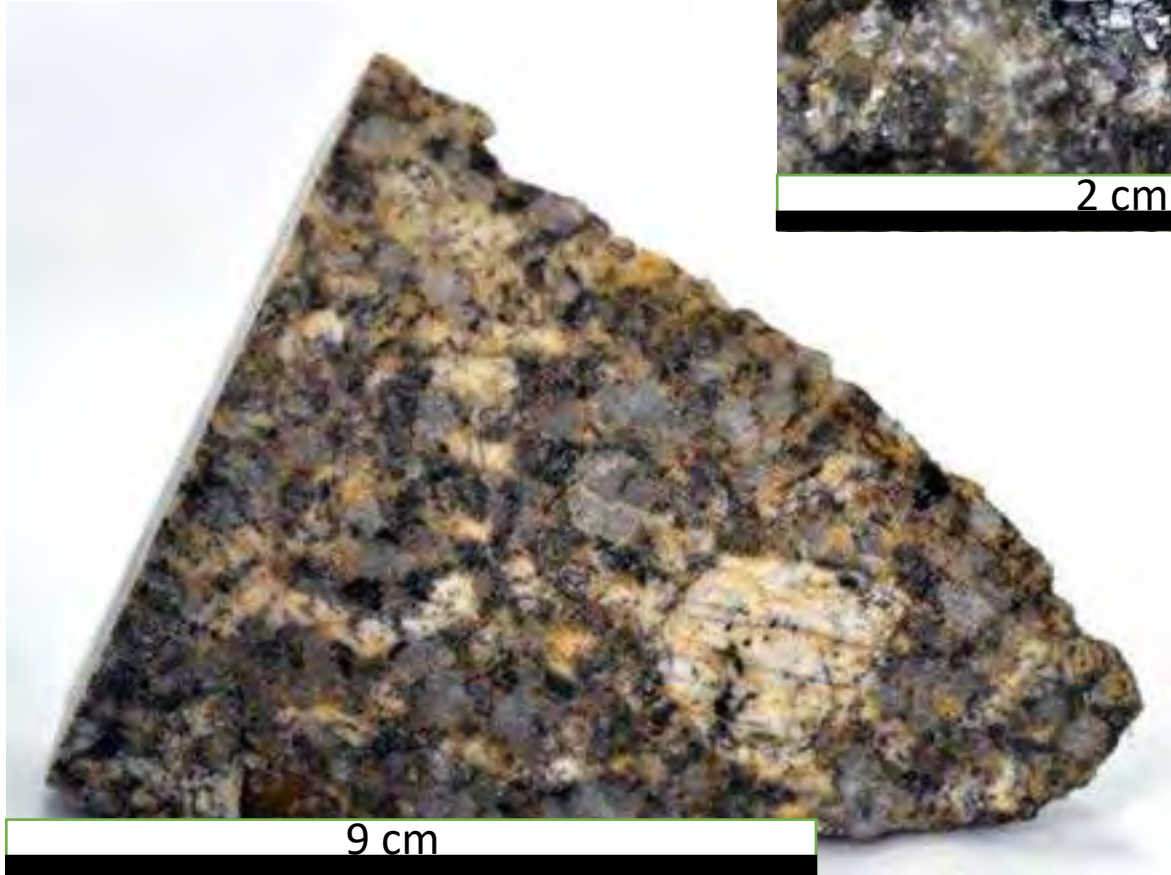
2020-KELL-17-C



2020-KELL-19

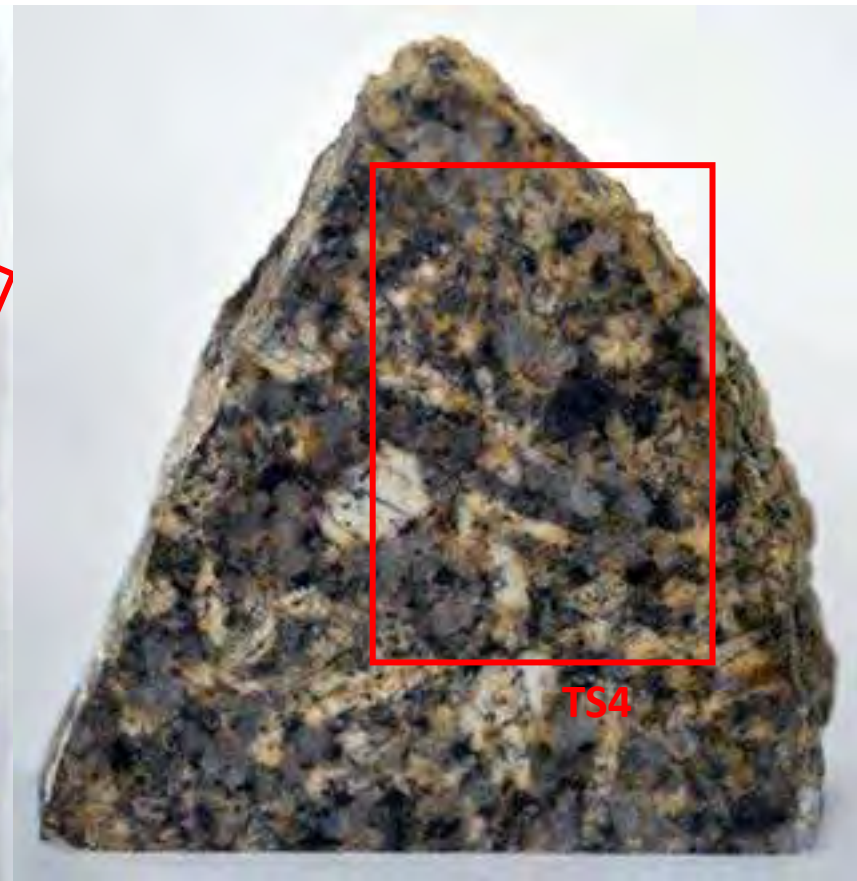


2020-KELL-19



Granitic porphyry stock. Euhedral to subhedral white megacrysts of K-feldspar, up to 4.5 cm in length, are surrounded by a groundmass composed of mm-sized crystals of K-feldspar, quartz, biotite, and cordierite. Quartz crystals are equant, translucent, and grey in color. Biotite crystals are dark-brown in color, subhedral, and have sizes up to 3 mm. Cordierite is bright blue in color, anhedral to subhedral, and up to 1 cm. K-feldspar megacrysts host black vitreous elongated to acicular crystals, which often concentrate along certain crystal growth faces (biotite? tourmaline?). K-feldspar megacrysts are cut by stringers (<1m wide) composed of a brown to pinkish-brown color.

2020-KELL-19



Total: 6 TS

2020-KELL-20



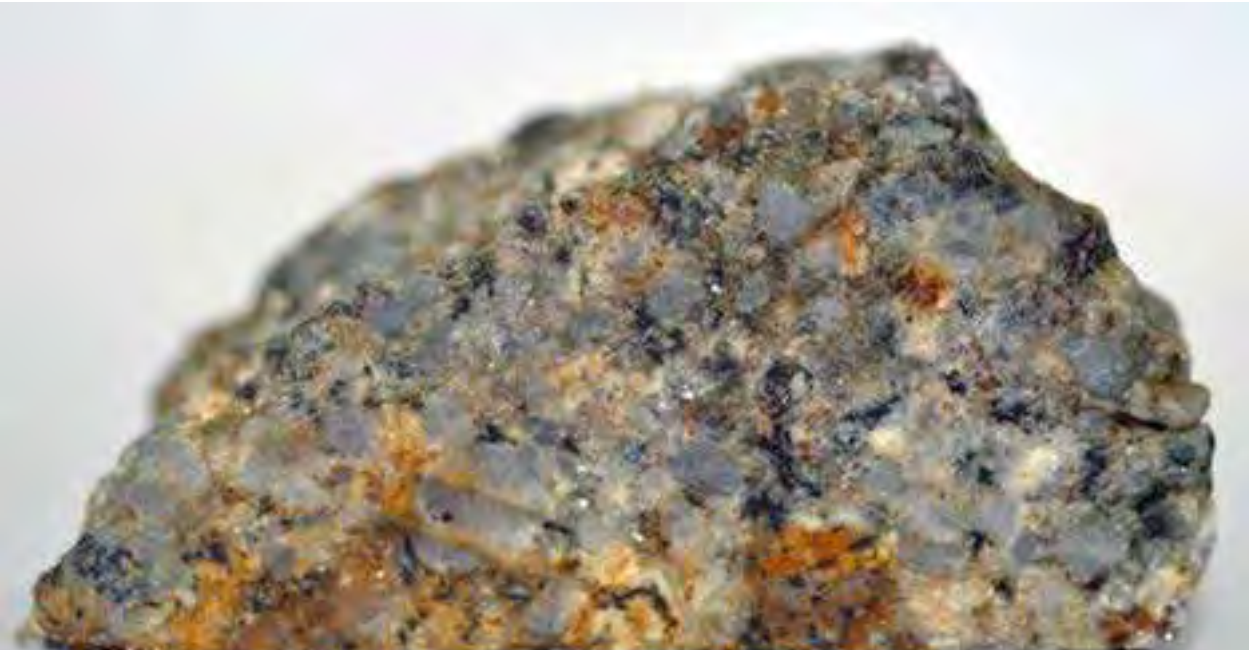
5 cm



8 cm

2020-KELL-20

TOTAL: 2 TS



7 cm



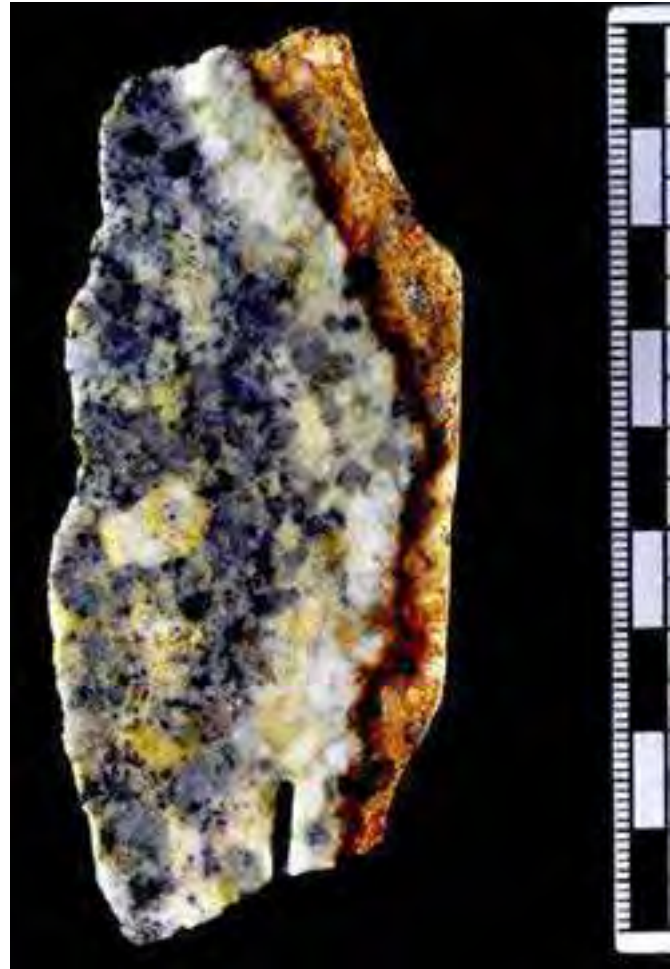
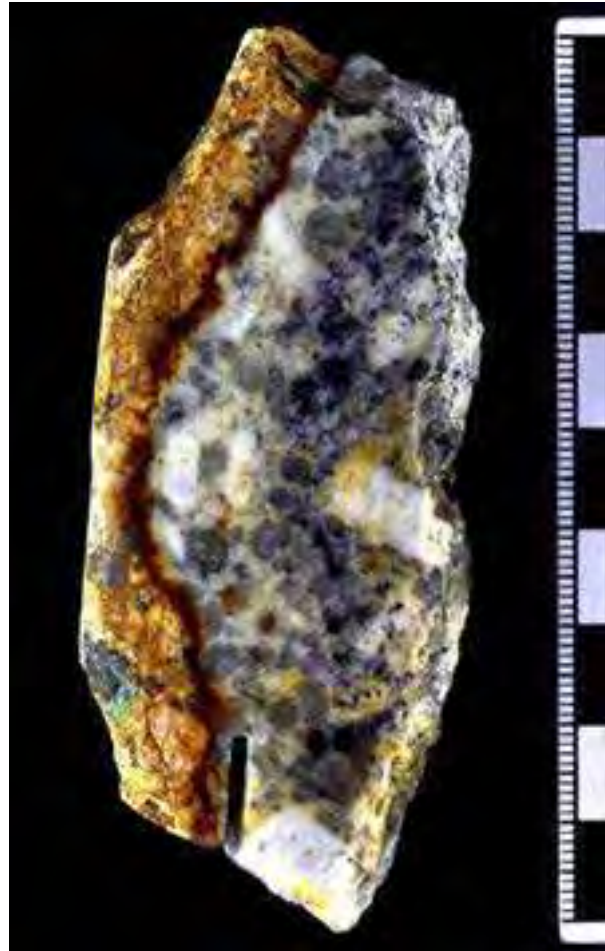
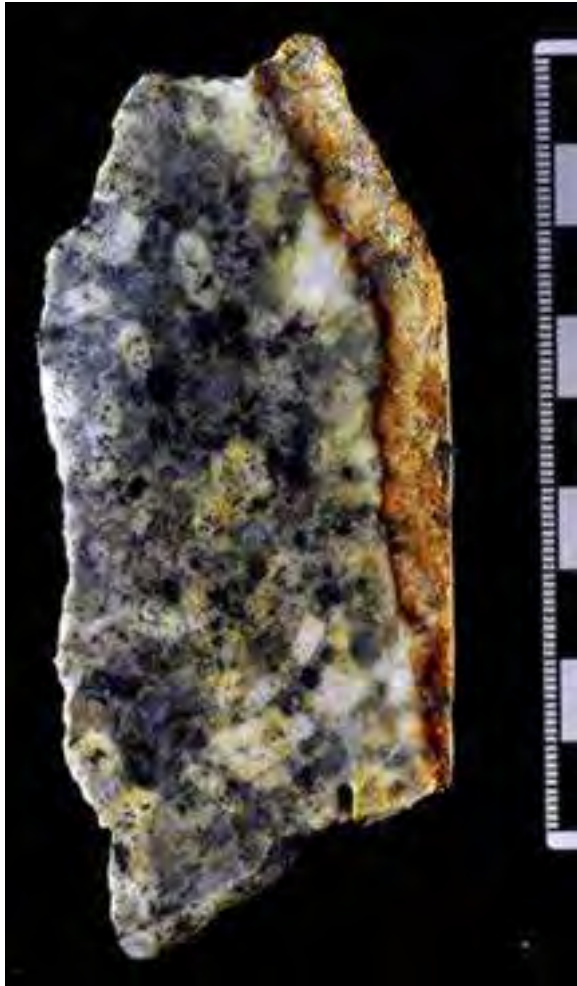
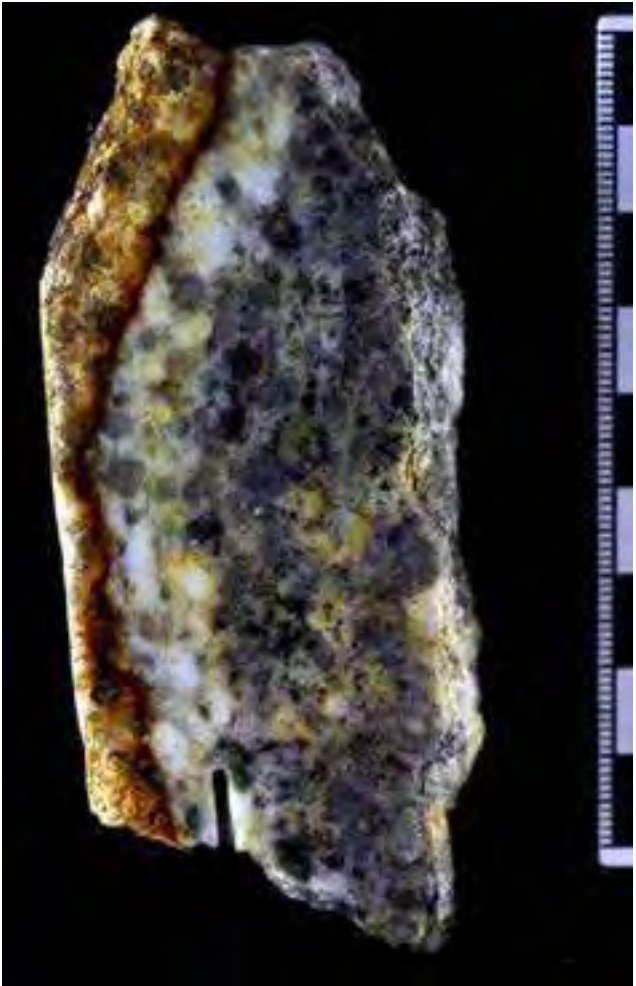
7 cm



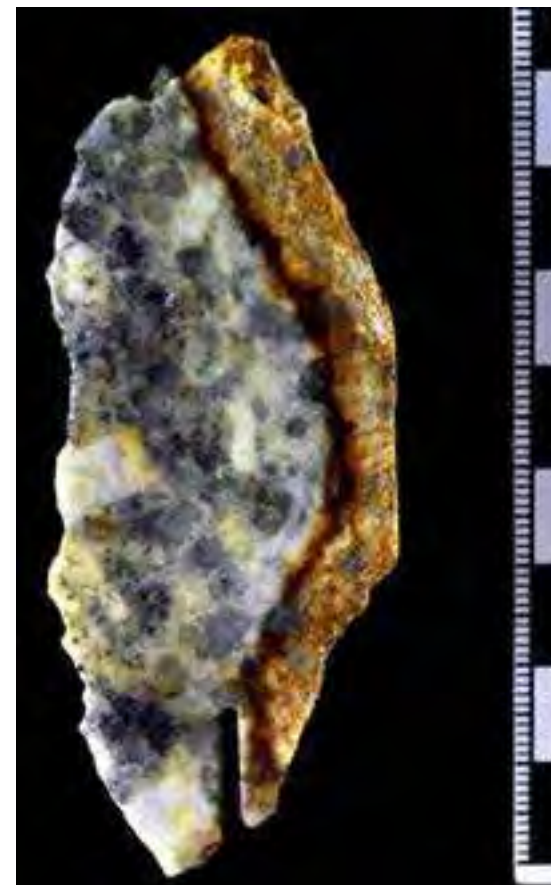
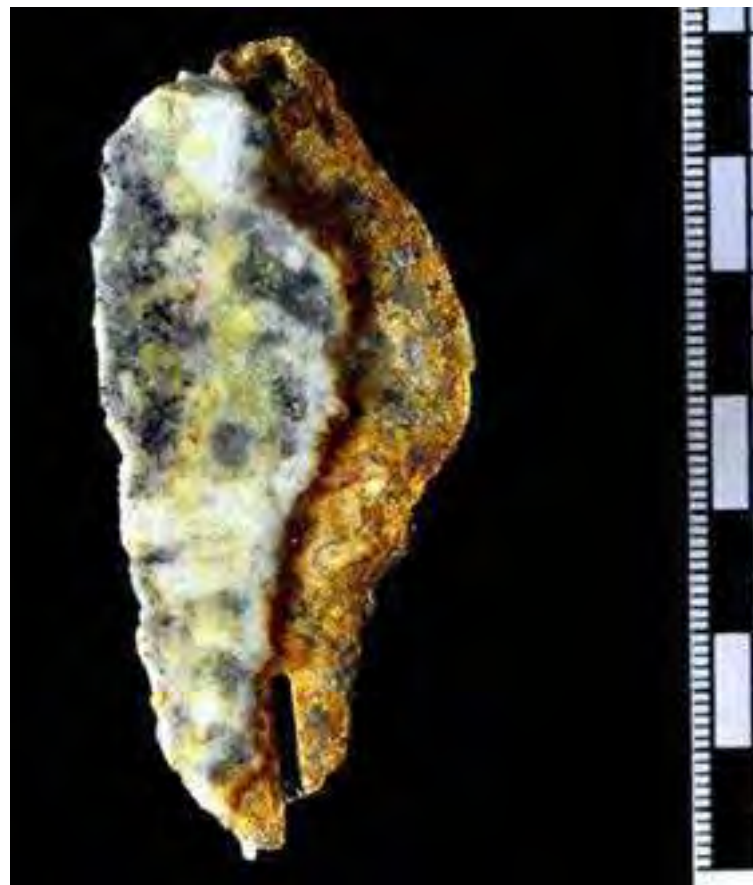
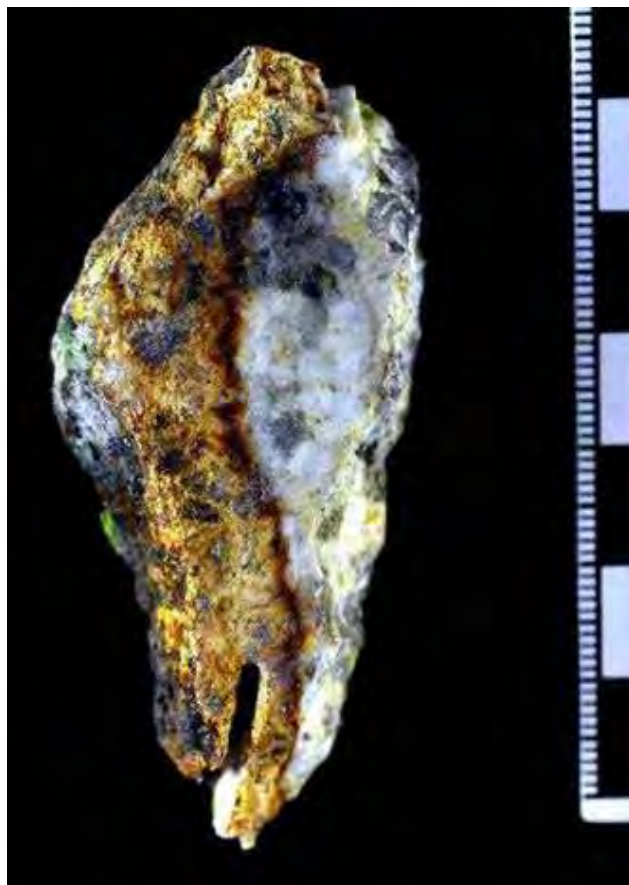
7 cm

Altered/oxidized equigranular intrusive granitic rock consisting of feldspar, quartz, biotite, muscovite and sulfides. Quartz subhedral translucent to milky granular crystals are up to 1 cm in length. Subhedral white crystals of feldspar are up to 1.5 cm in length and show a tabular and prismatic habit. Biotite (and other mafic minerals?) form subhedral and anhedral black crystals.

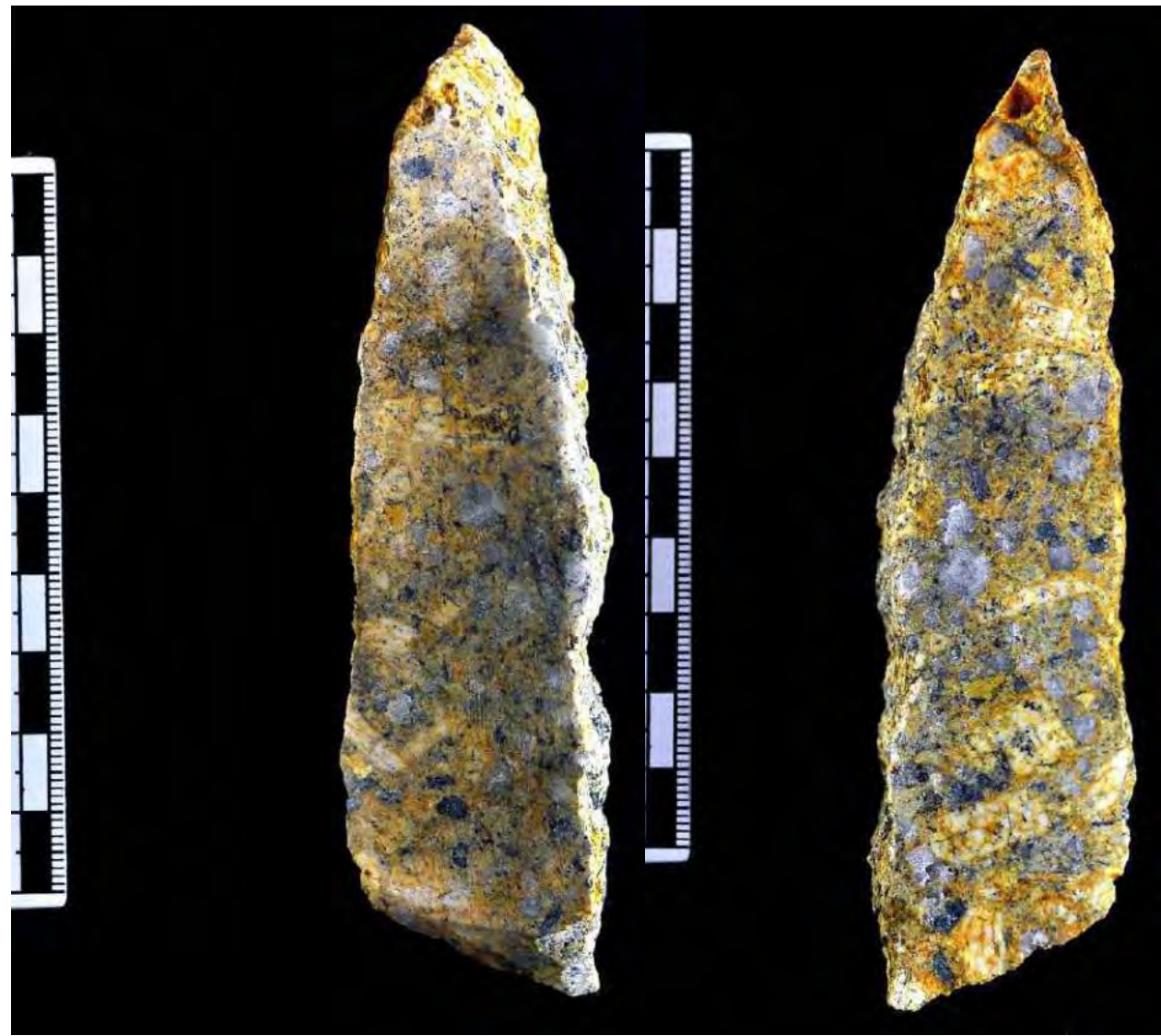
2020-KELL-21



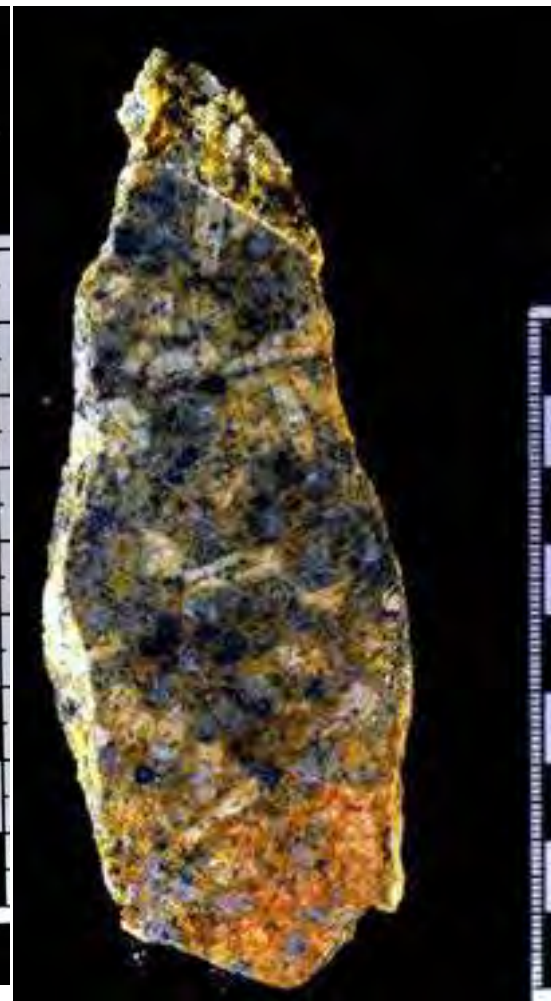
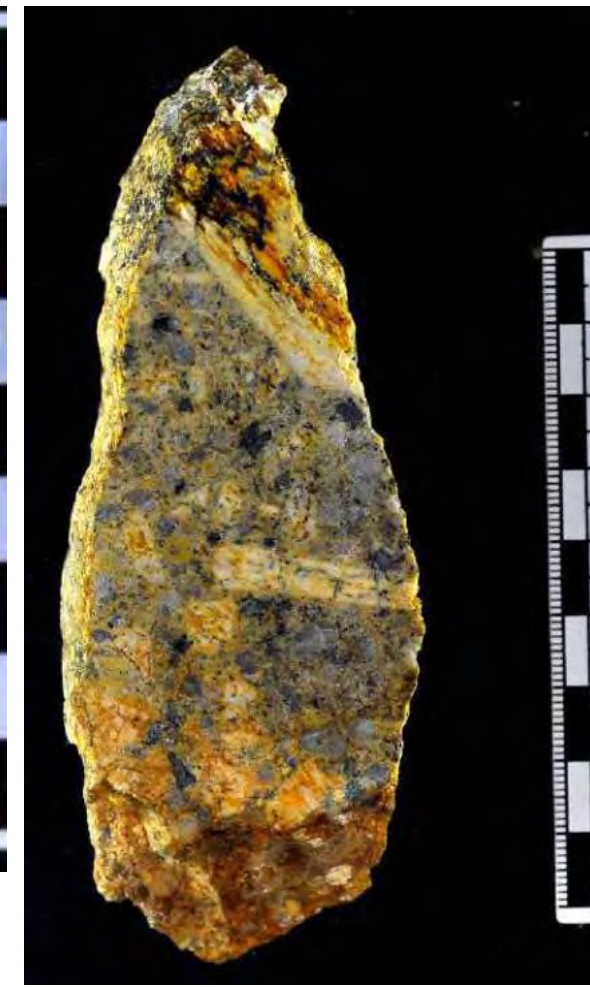
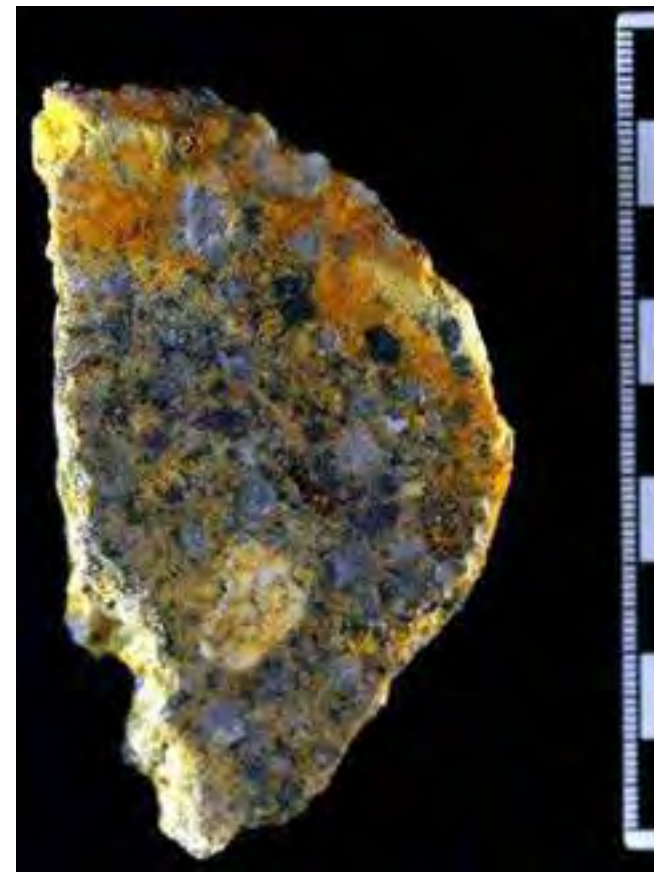
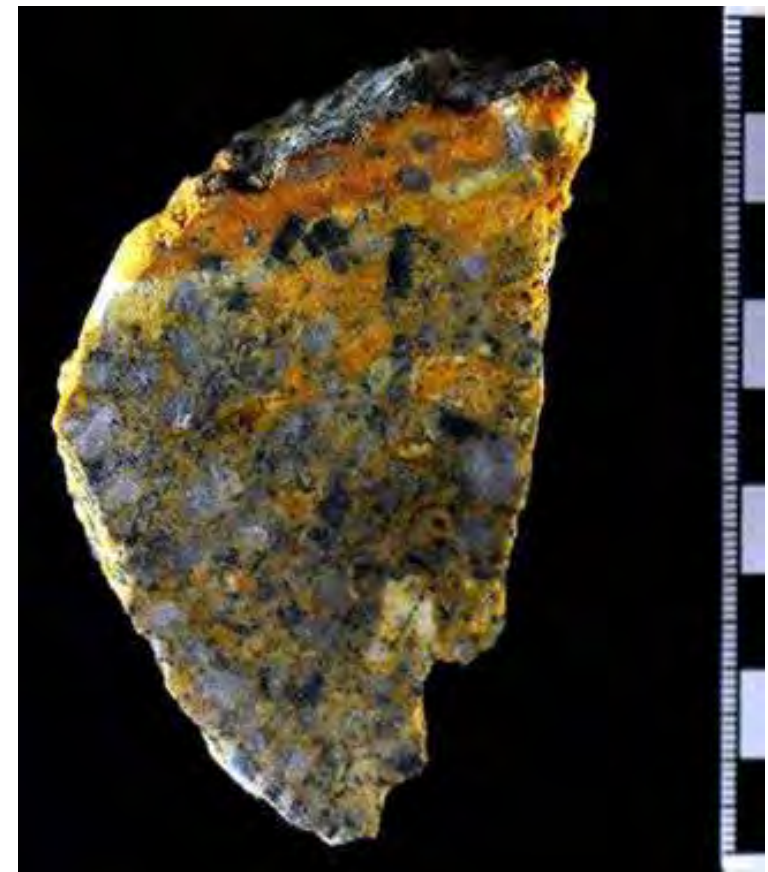
2020-KELL-21



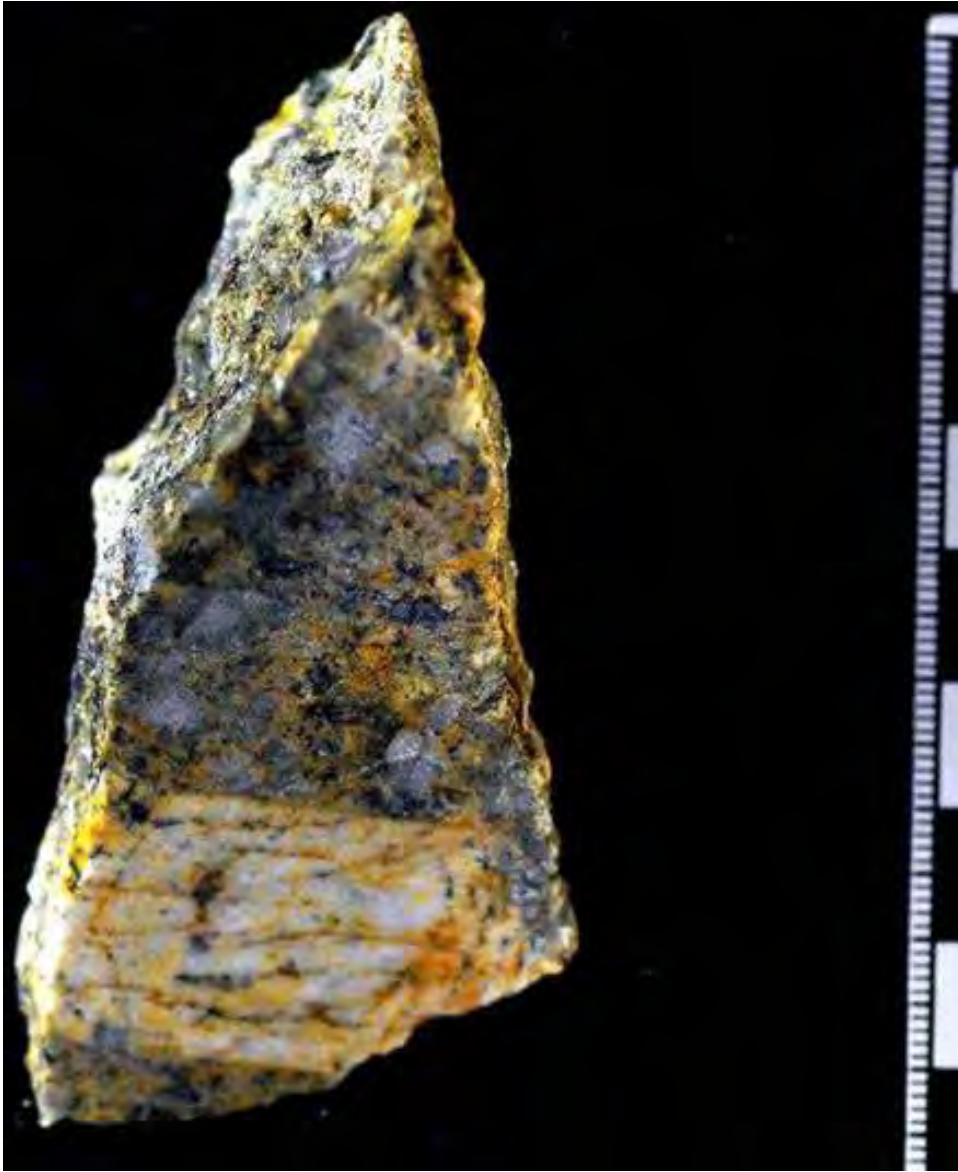
2020-KELL-21



2020-KELL-21

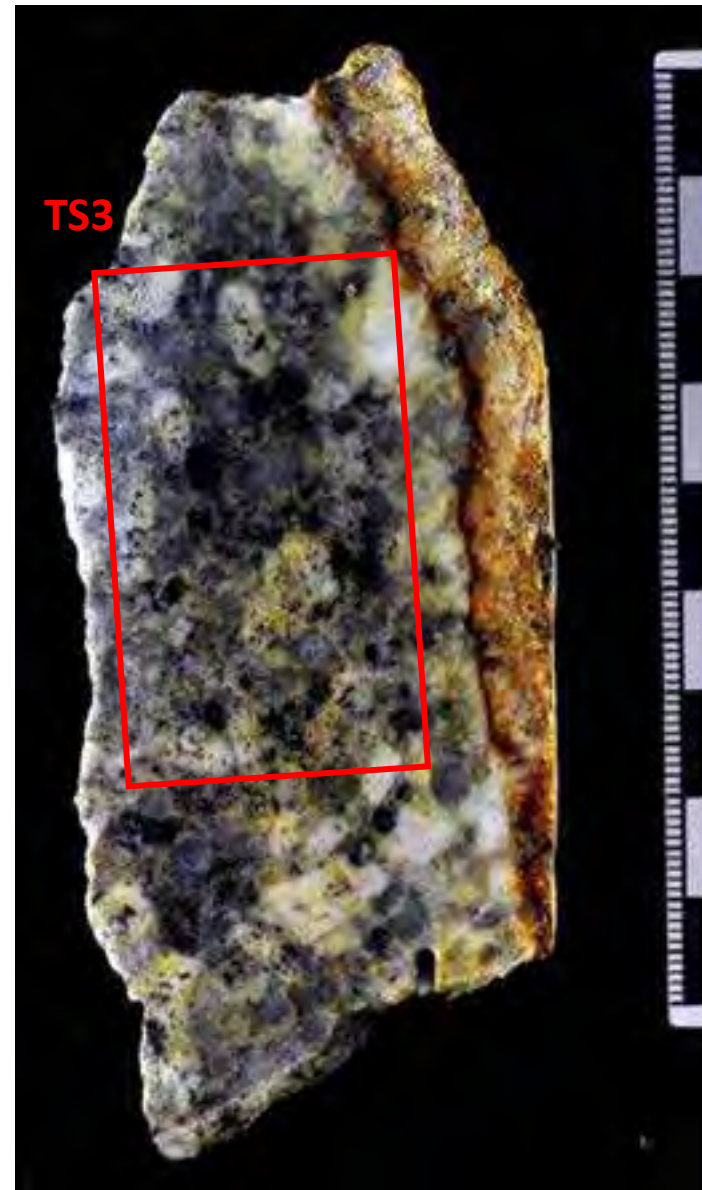
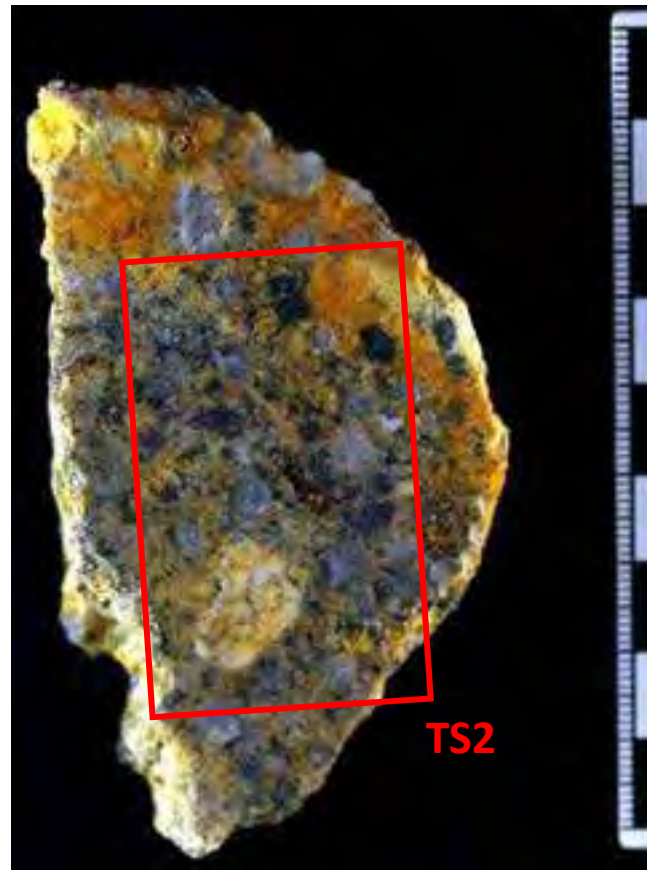
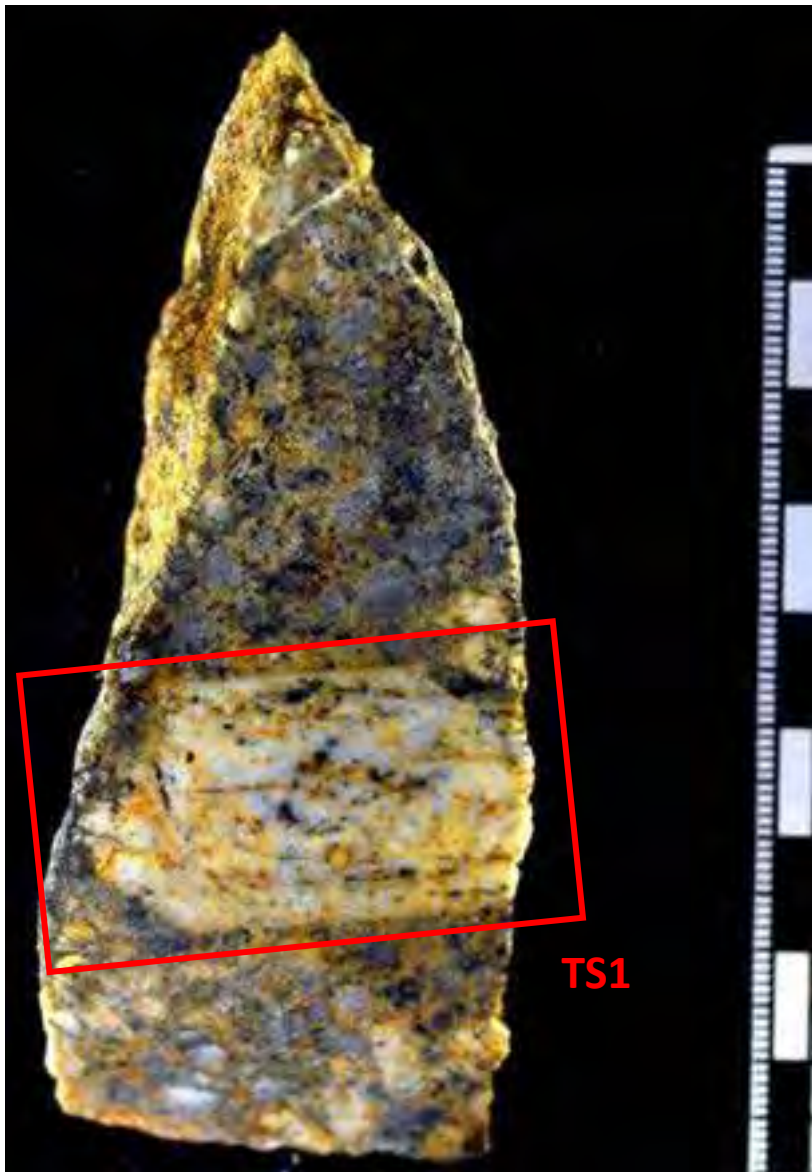


2020-KELL-21

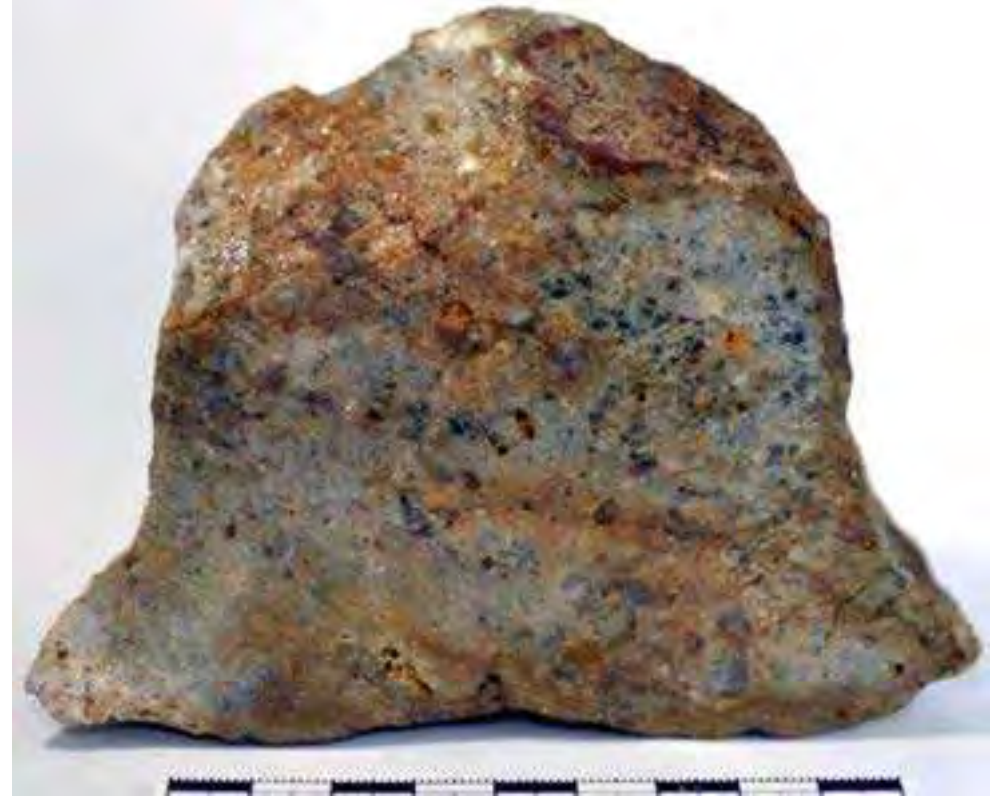


Phaneritic, porphyritic felsic intrusive rock. The rock is composed of a phaneritic, medium grained groundmass with feldspar and quartz and lesser proportions of biotite and cordierite. Quartz forms subhedral-anhedral, grey translucent crystals up to 1 cm long. Feldspar in the groundmass show tabular to elongated habit and a white-cream color. Biotite forms <1 mm euhedral and subhedral laths that are brown red in color, probably due to oxidation, and appears randomly distributed within cordierite, feldspar, and quartz crystals or across their crystal boundaries. Cordierite forms subhedral crystals up to 1 cm long, is grey-blue to grey-greenish in color, and have a vitreous lustre. The rock contain fairly abundant euhedral tabular megacrysts of feldspar, which are up to 4 cm long and white-creamy in color.

2020-KELL-21



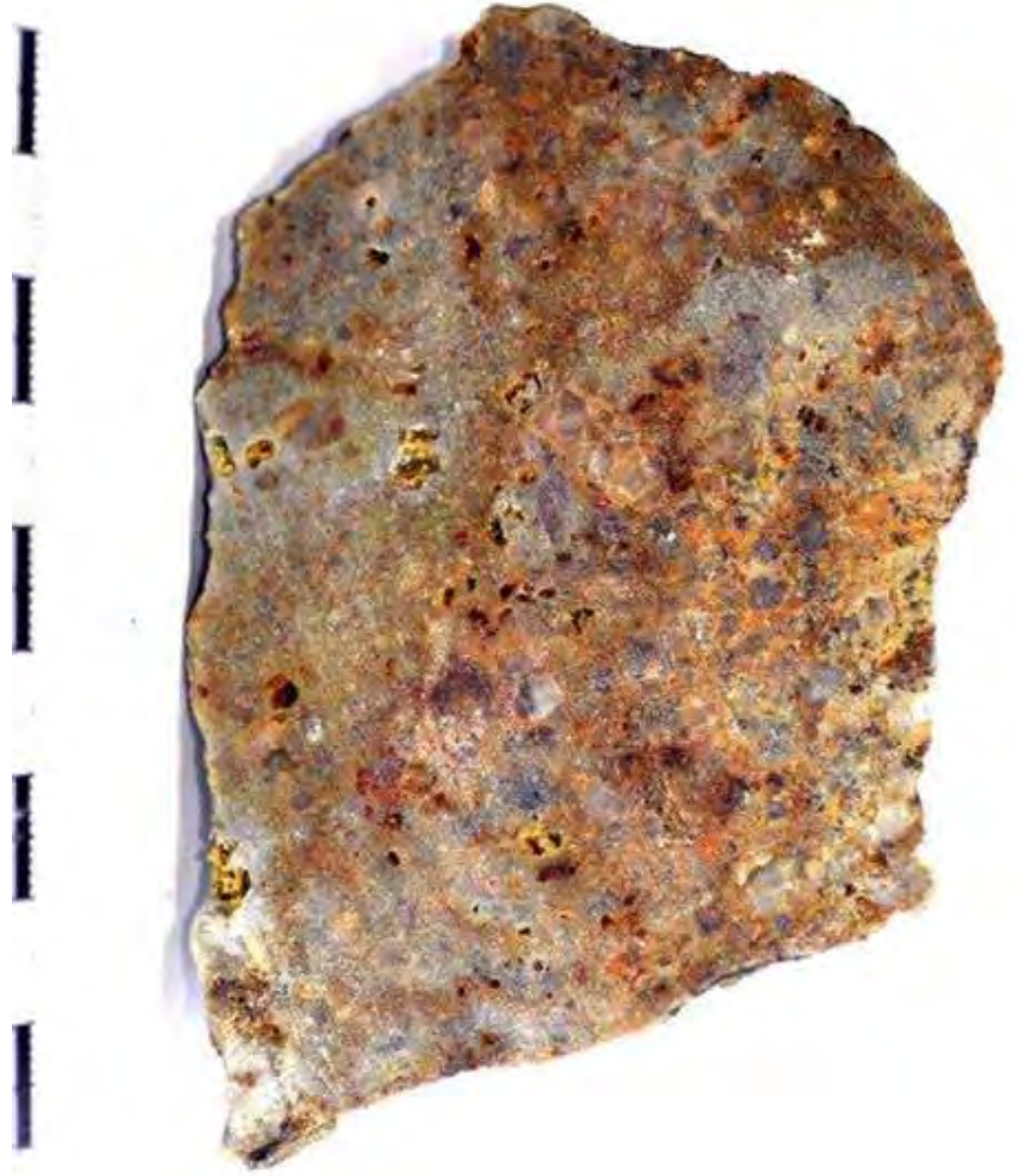
2020-KELL-22-A



2020-KELL-22-A

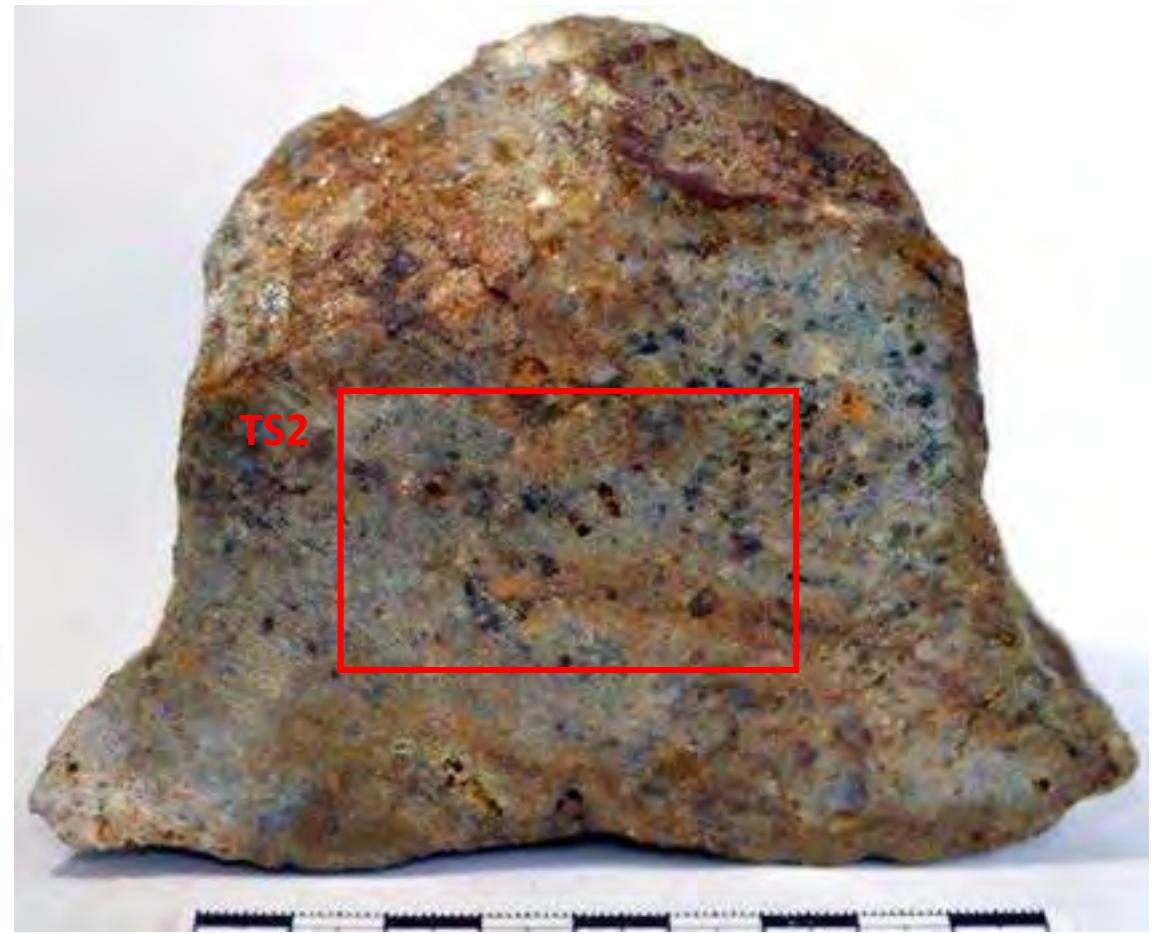


2020-KELL-22-A

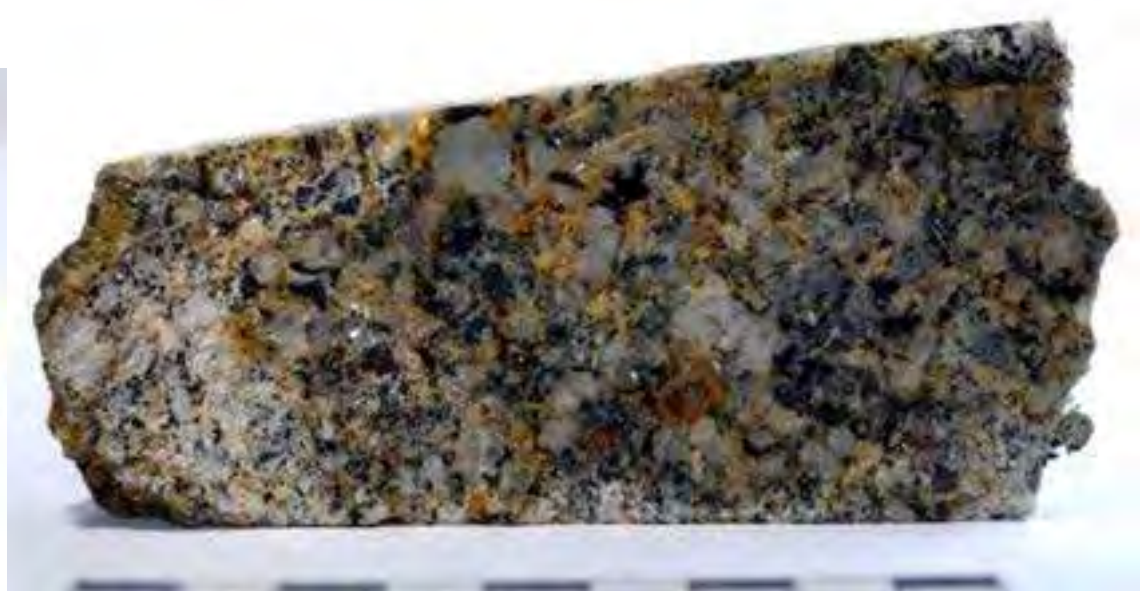
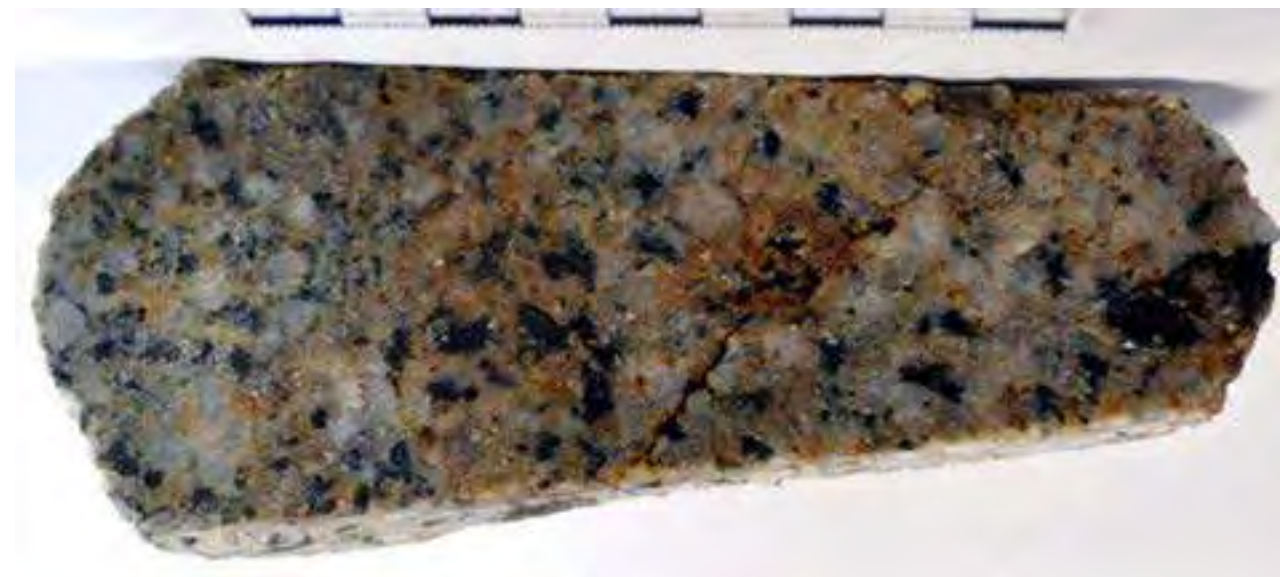


Greisen, mostly constituted of quartz. Two types of quartz have been distinguished: i) milky massive quartz (probably, of hydrothermal origin), and ii) hyaline, subhedral quartz (probably of magmatic origin) up to 1 cm long. Crystals of hyaline quartz are fractured and cemented by milky quartz. Muscovite occurs as disseminated subhedral crystals up to two mm long. The rock show abundant secondary porosity after the dissolution of former mineral elements. Cavities are filled with a subhedral pale yellow and red powdery mineral (Fe-oxides?).

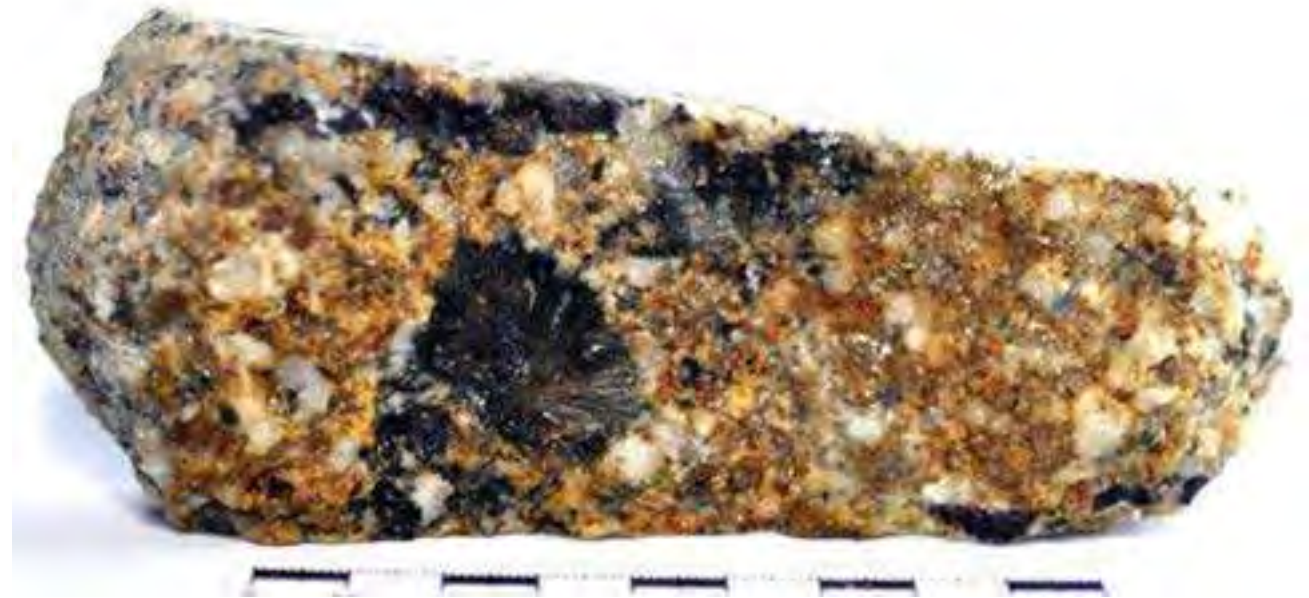
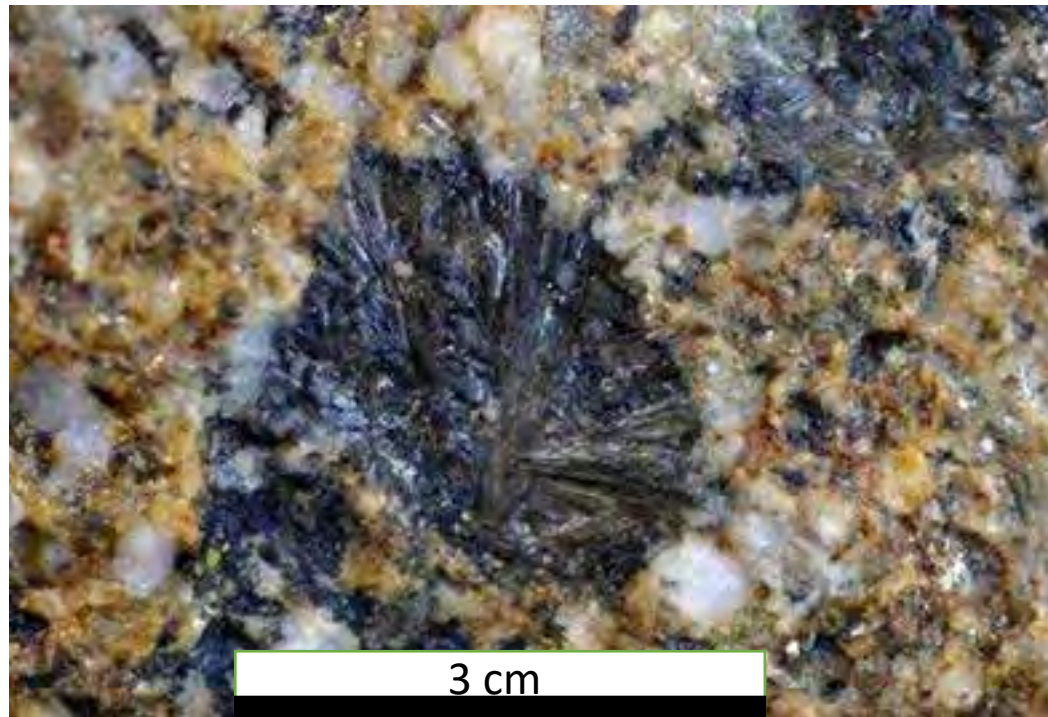
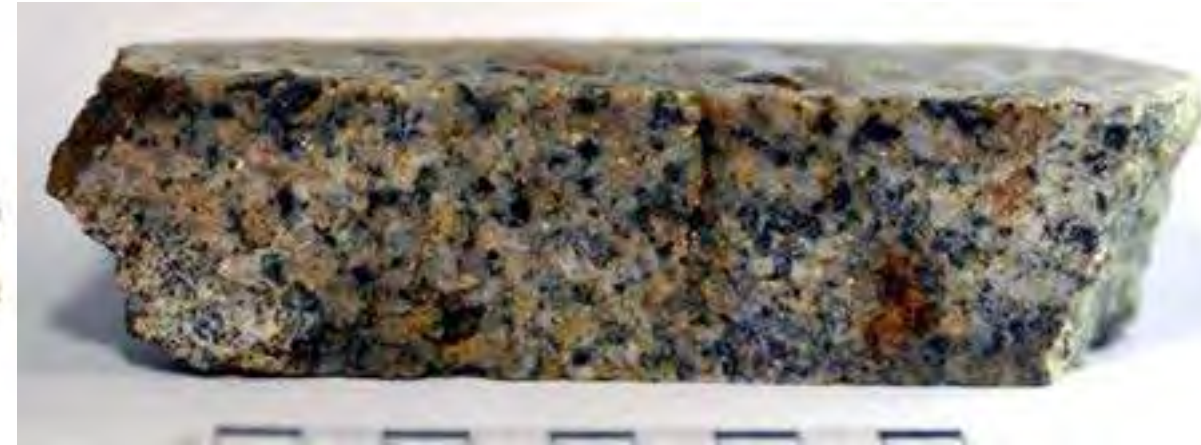
2020-KELL-22-A



2020-KELL-22-B



2020-KELL-22-B

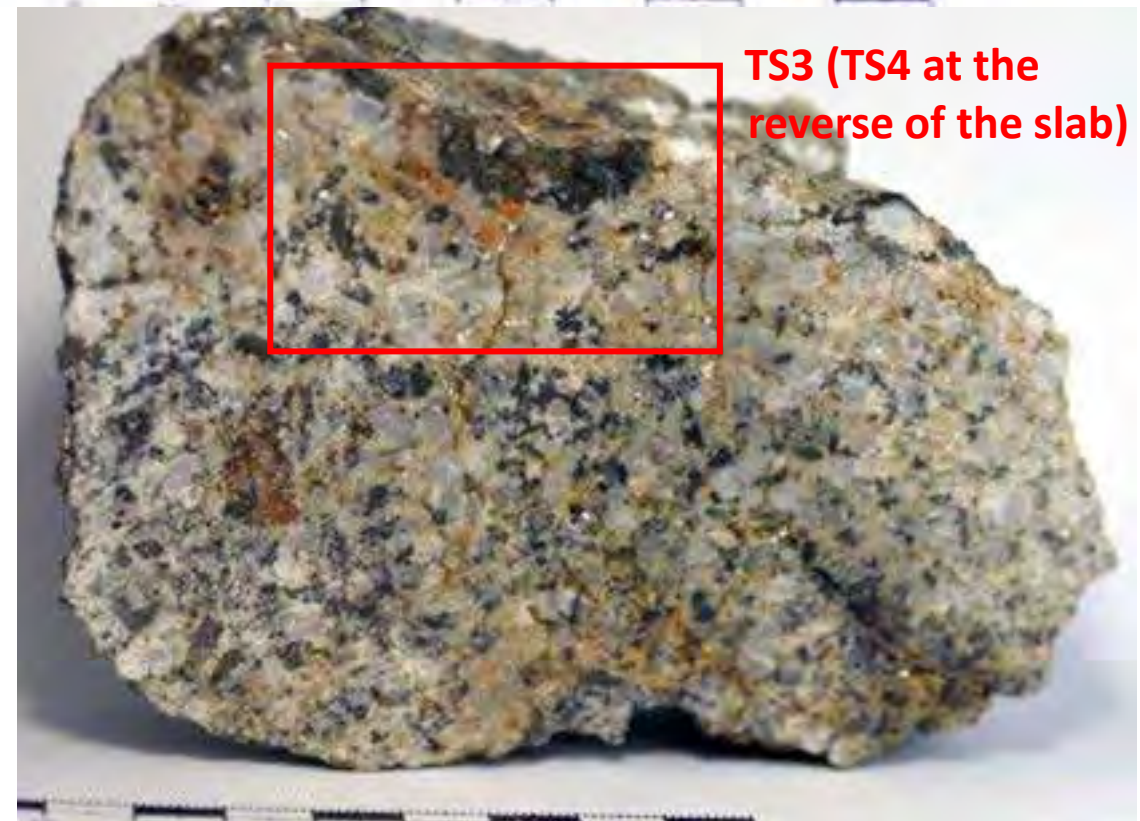
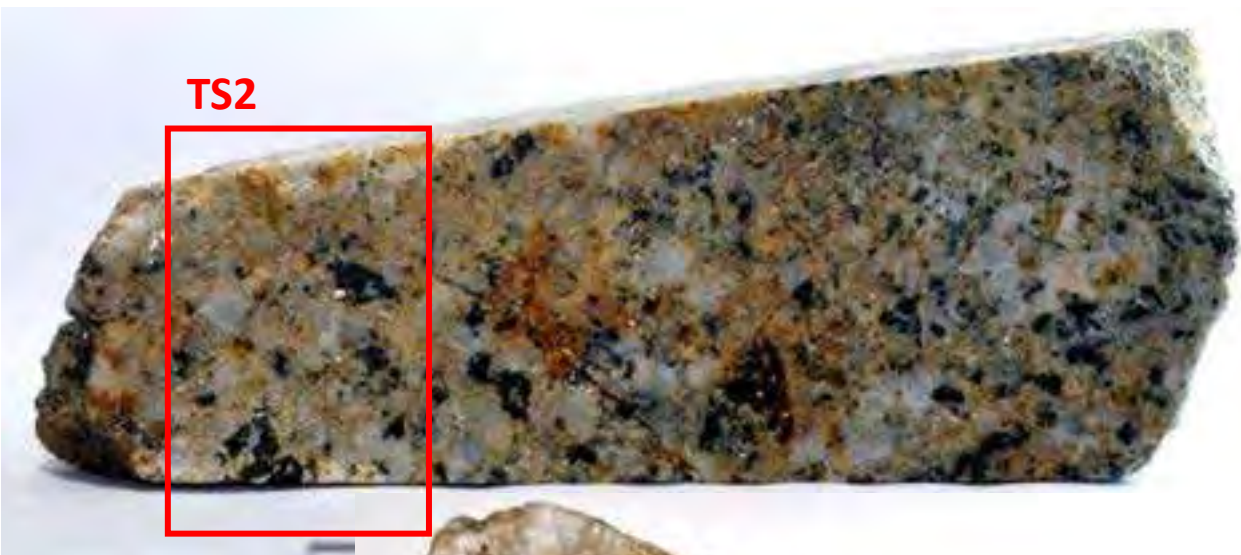


2020-KELL-22-B



Greisen/greisenized granitic rock mostly constituted of quartz, tourmaline, and muscovite. Two types of quartz have been distinguished: i) milky massive quartz (probably of hydrothermal origin), and ii) hyaline, subhedral quartz (probably, of magmatic origin). Hyaline subhedral quartz crystals are up to 2 cm long, fractured, and cemented by the milky quartz. Tourmaline is relatively abundant in the sample and appear as euhedral-subhedral elongated to acicular crystals with lengths up to 2 cm and often forms radial aggregates. Their color is brownish-black. Muscovite crystals are disseminated and up to two mm long. In addition, the rock contains other phases that have not been identified and that may correspond to Fe- and Mn- oxides.

2020-KELL-22-B



TS6 and TS7
in other 2
slabs not
shown in the
pictures

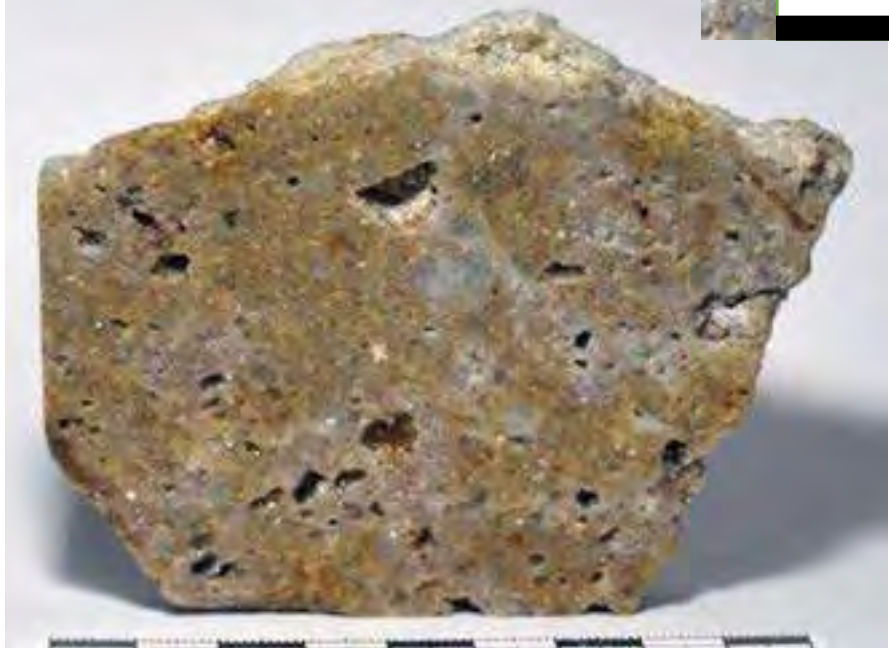
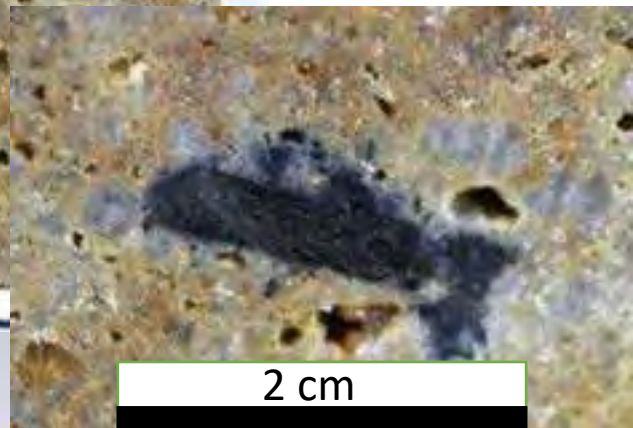
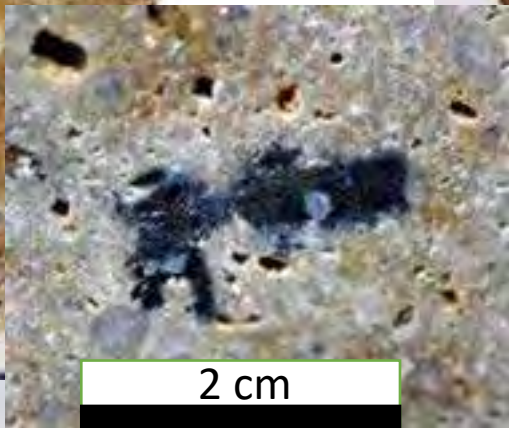
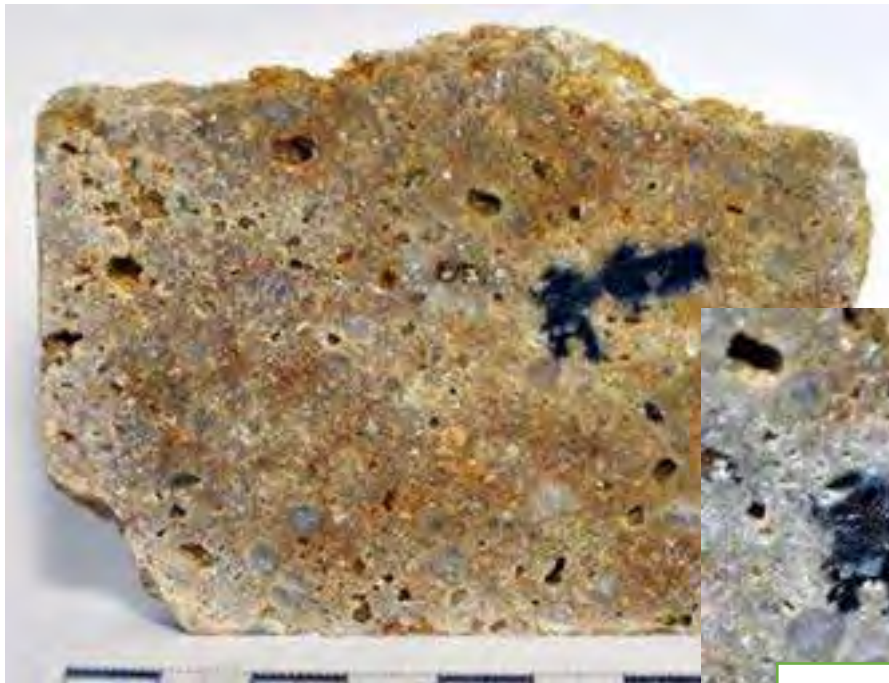
2020-KELL-23



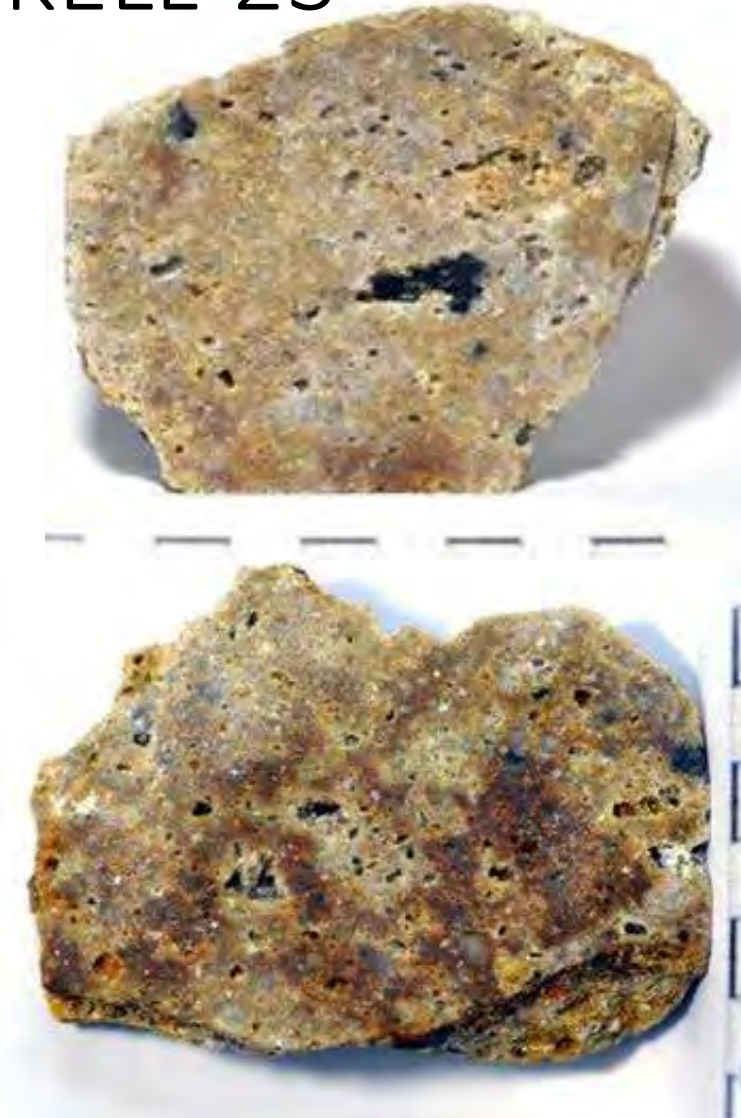
2020-KELL-23



2020-KELL-23

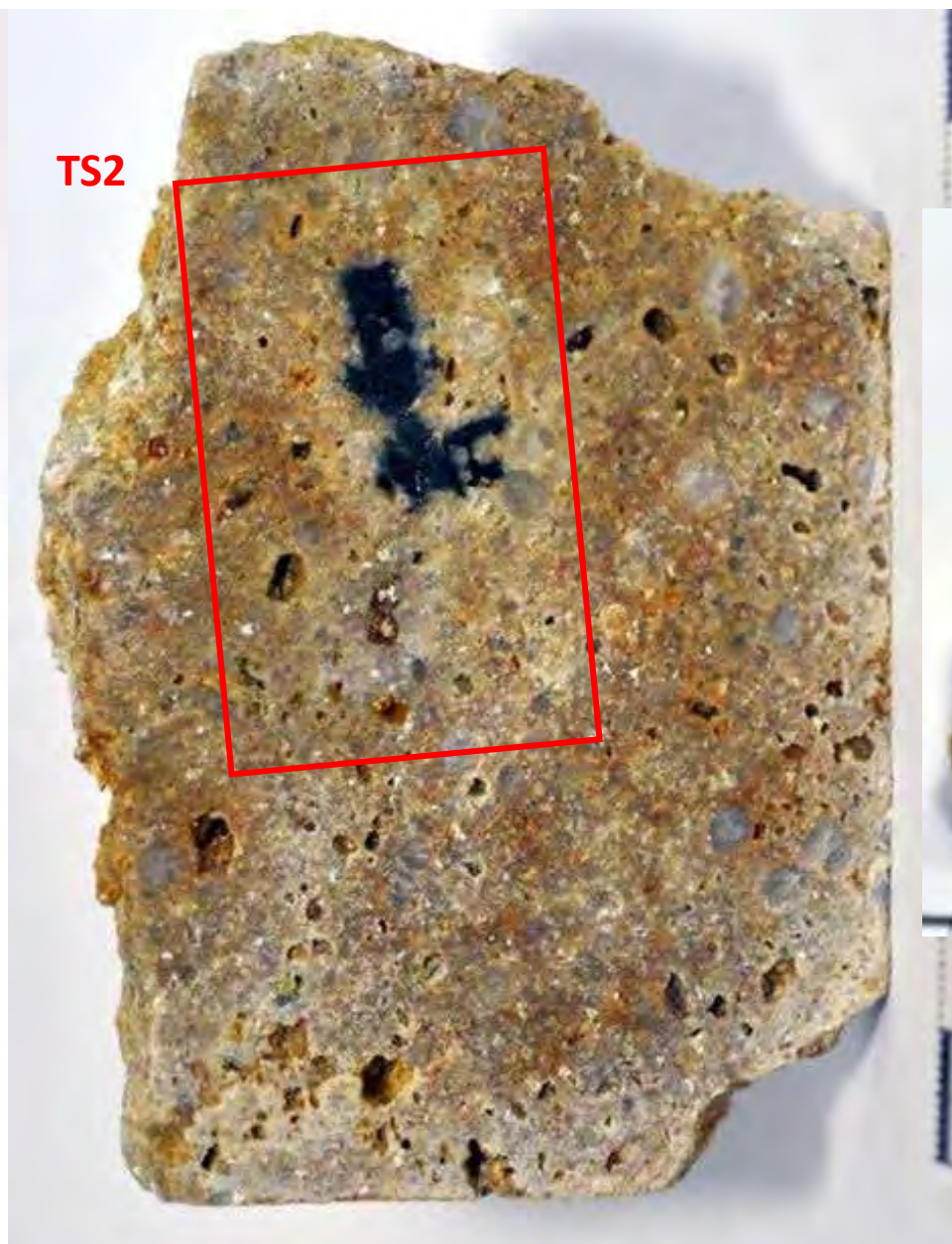


2020-KELL-23

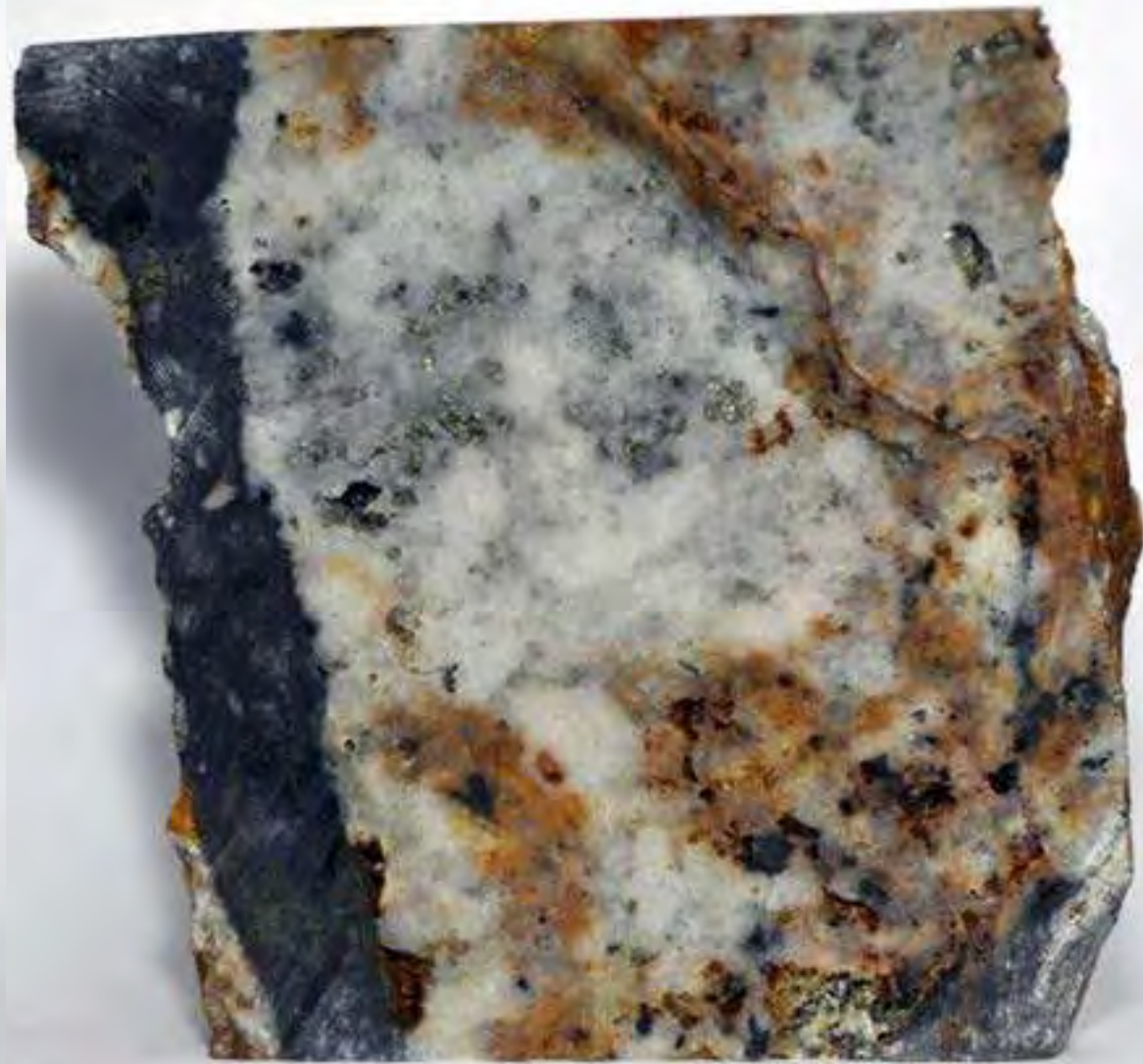
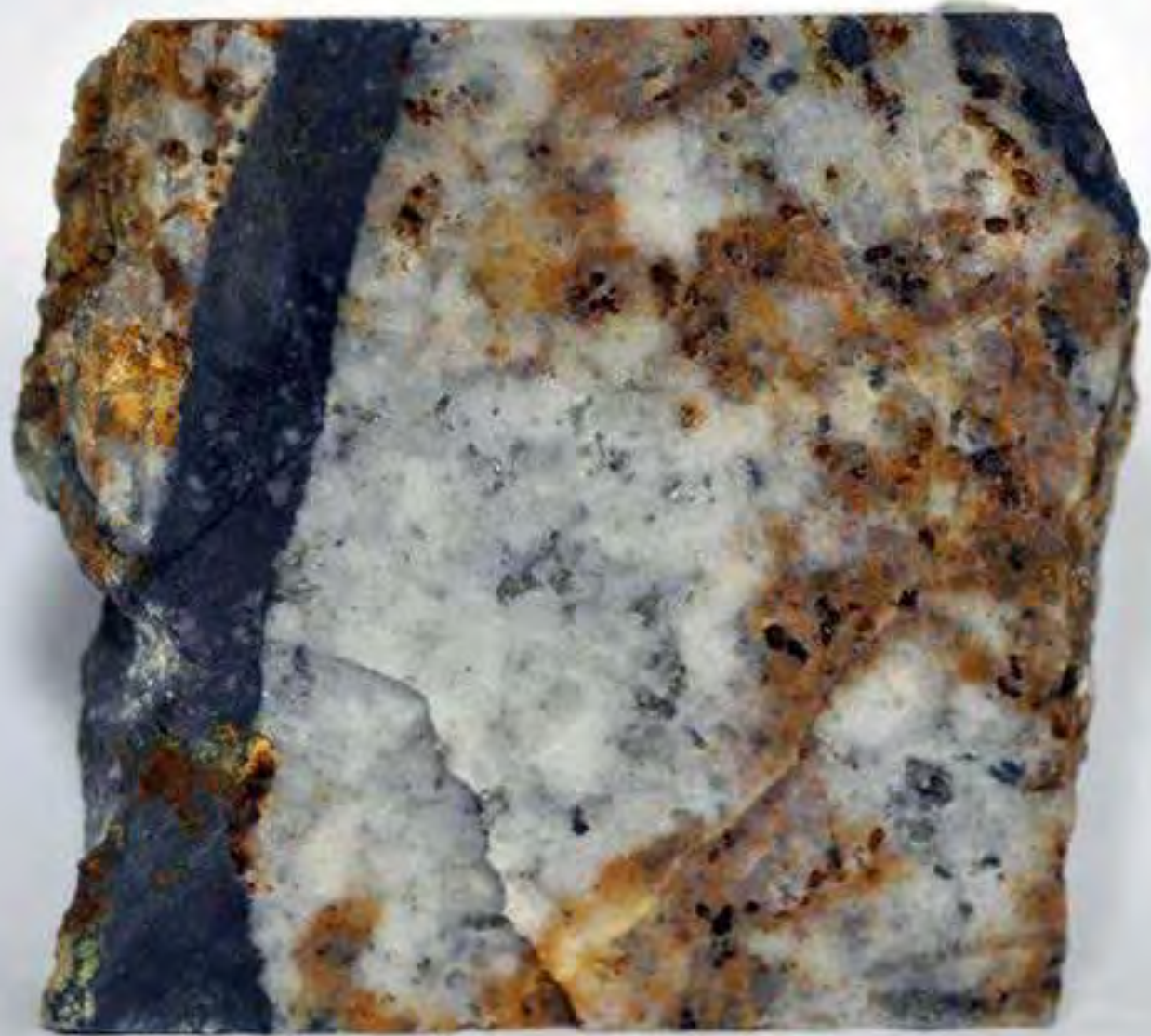


Greisen mostly constituted of quartz, tourmaline, and muscovite. The rock shows abundant cavities, probably after tabular feldspar. Two types of quartz have been distinguished: i) milky massive quartz (probably of hydrothermal origin), and ii) hyaline, subhedral quartz (probably, of magmatic origin). Hyaline subhedral quartz crystals are up to 1 cm long, fractured, and cemented by the milky quartz. Tourmaline, which is relatively abundant in this sample, forms acicular crystals up to 2 cm long and brownish-black color. Tourmaline acicular crystals form radial aggregates often adapting to the tabular cavities previously described. Muscovite occurs as disseminated subhedral platy crystals up to 5 mm across.

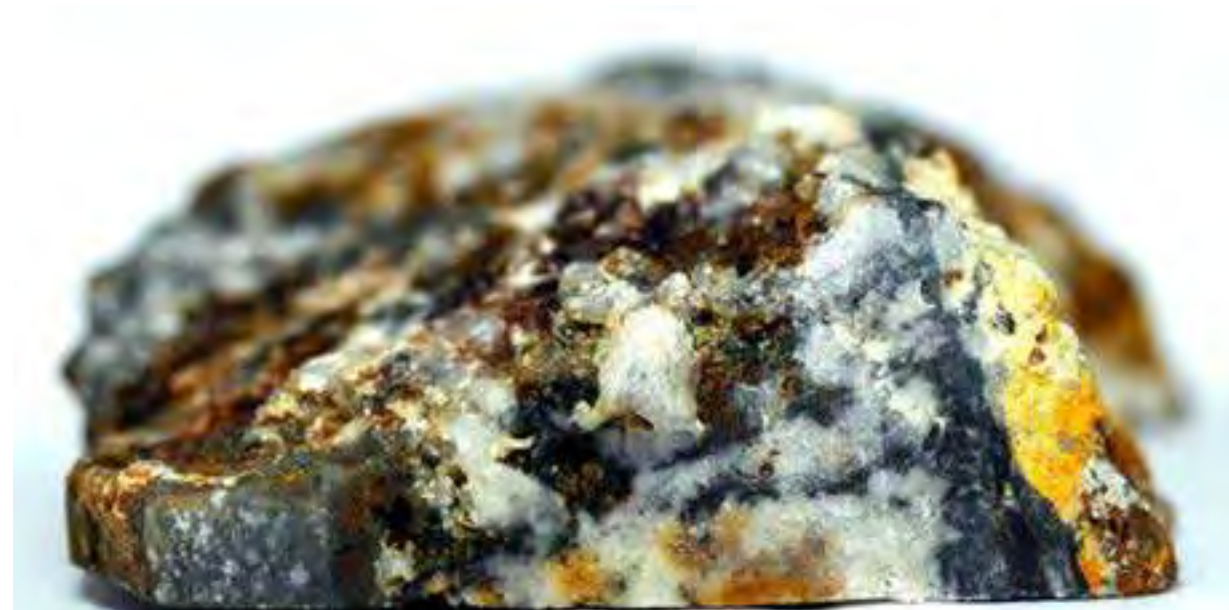
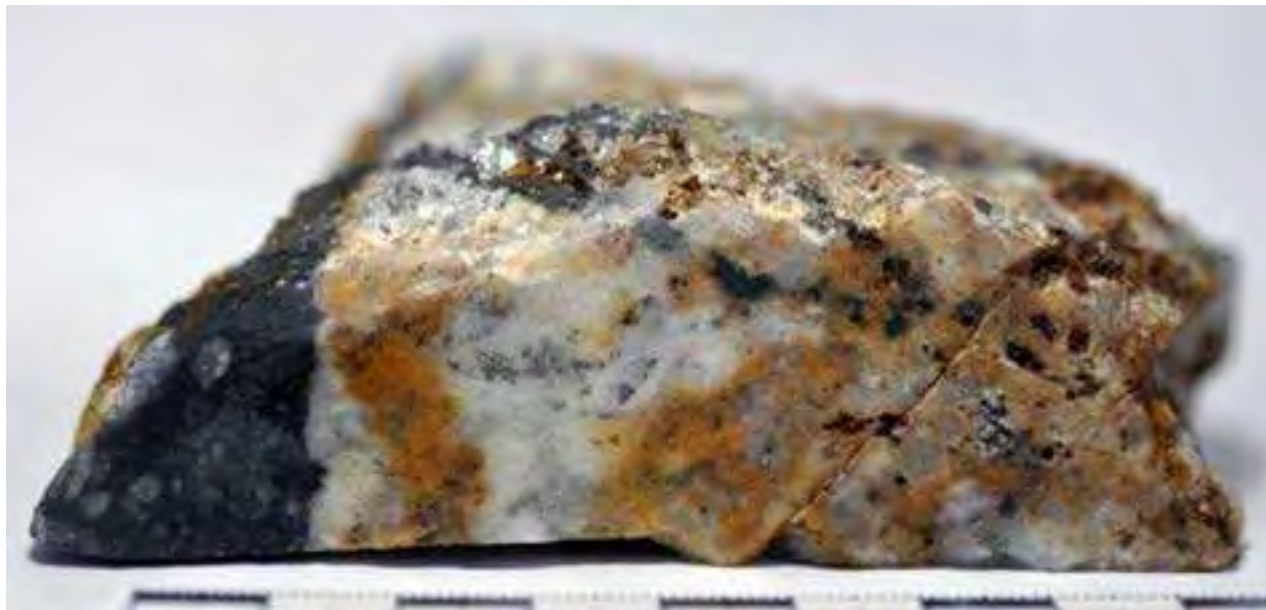
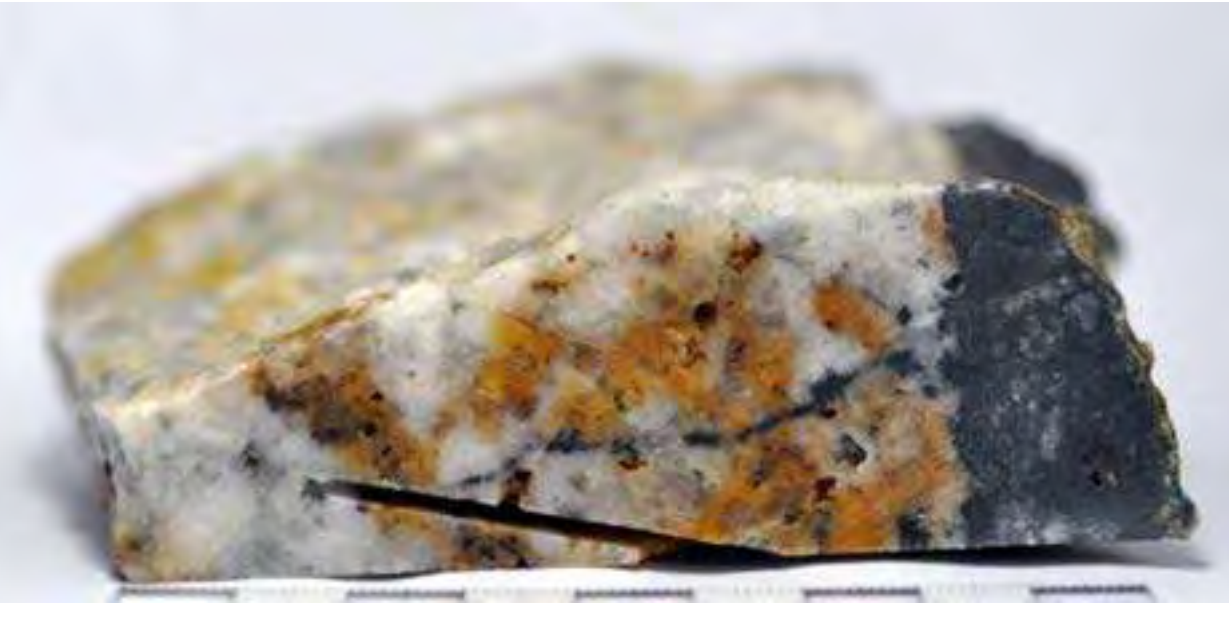
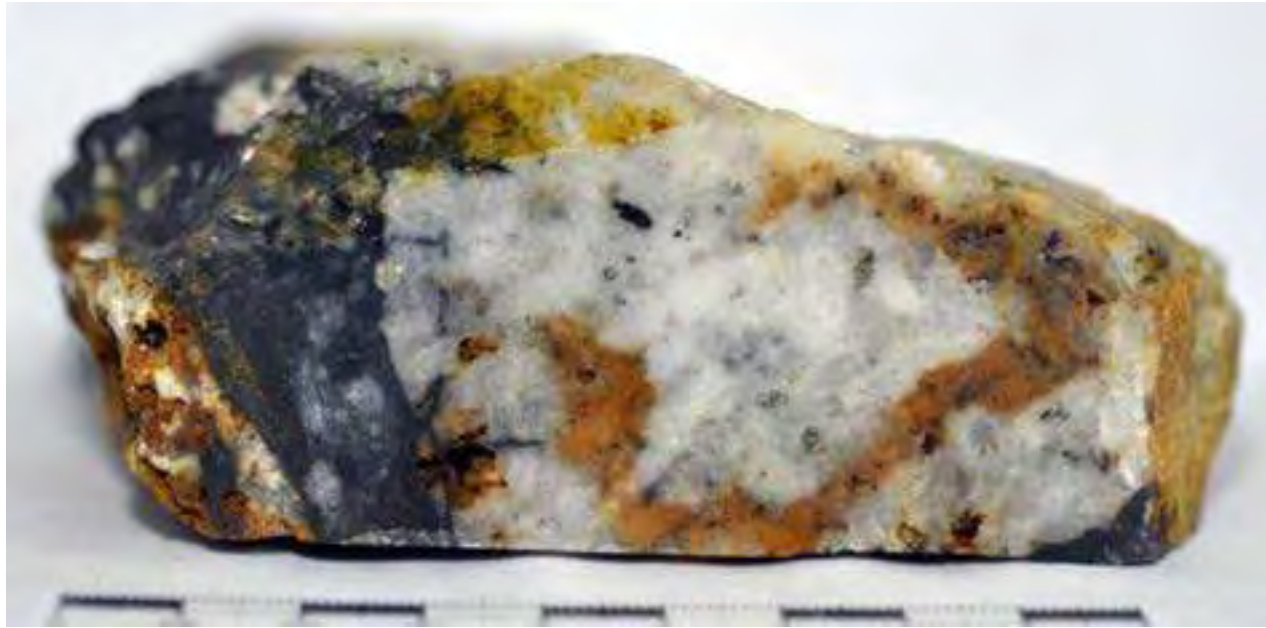
2020-KELL-23



2020-KELL-24



2020-KELL-24



2020-KELL-24



2020-KELL-24



2020-KELL-24



2020-KELL-24

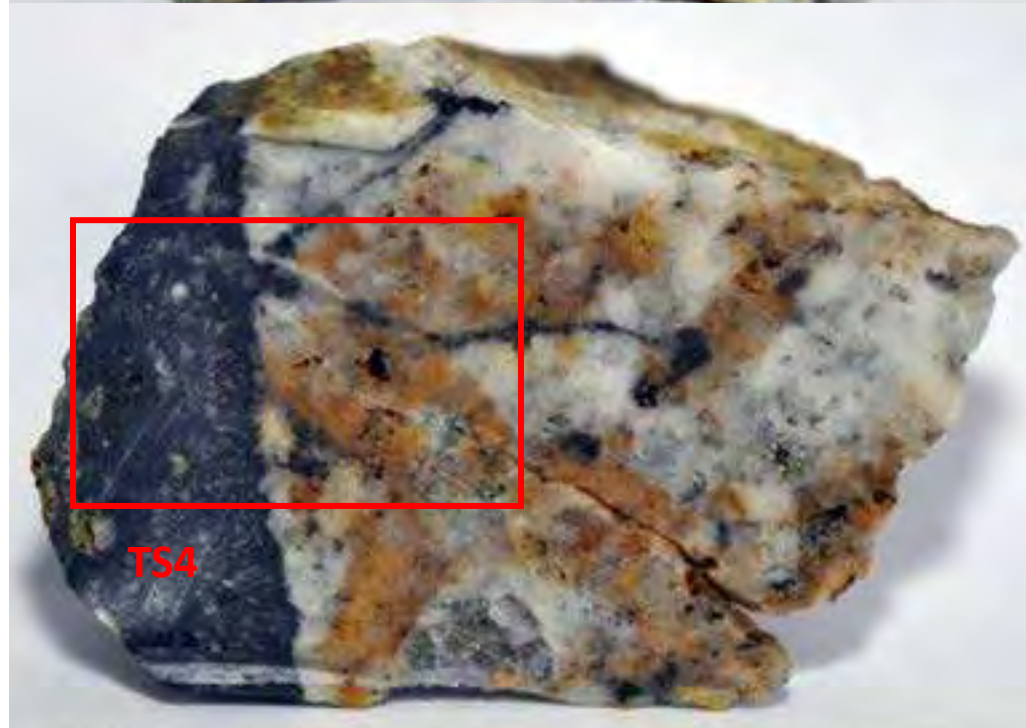
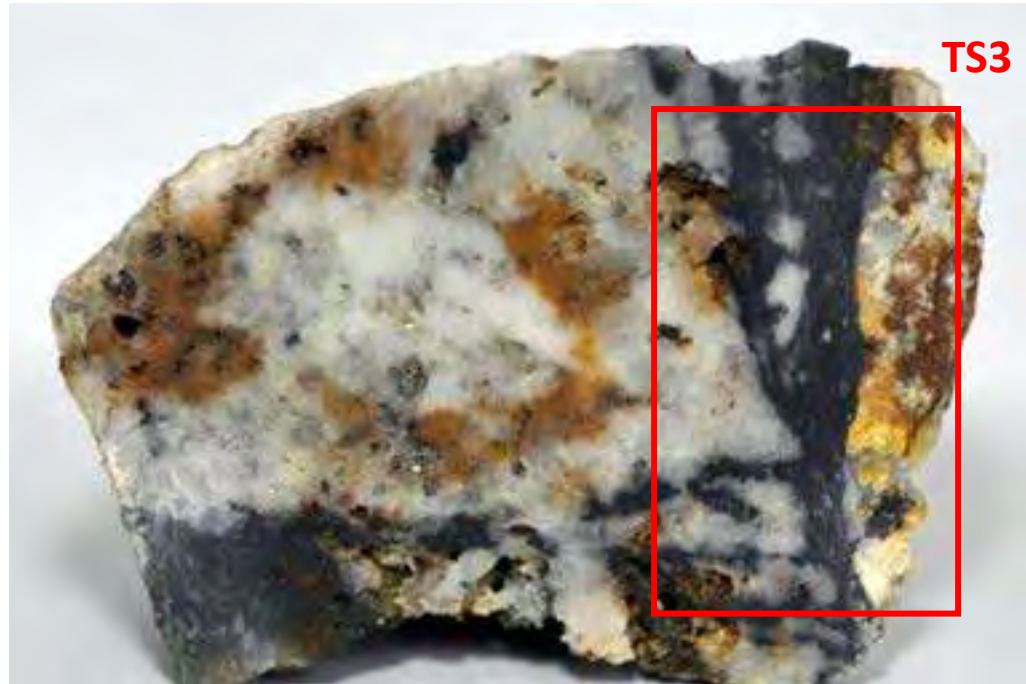


2020-KELL-24

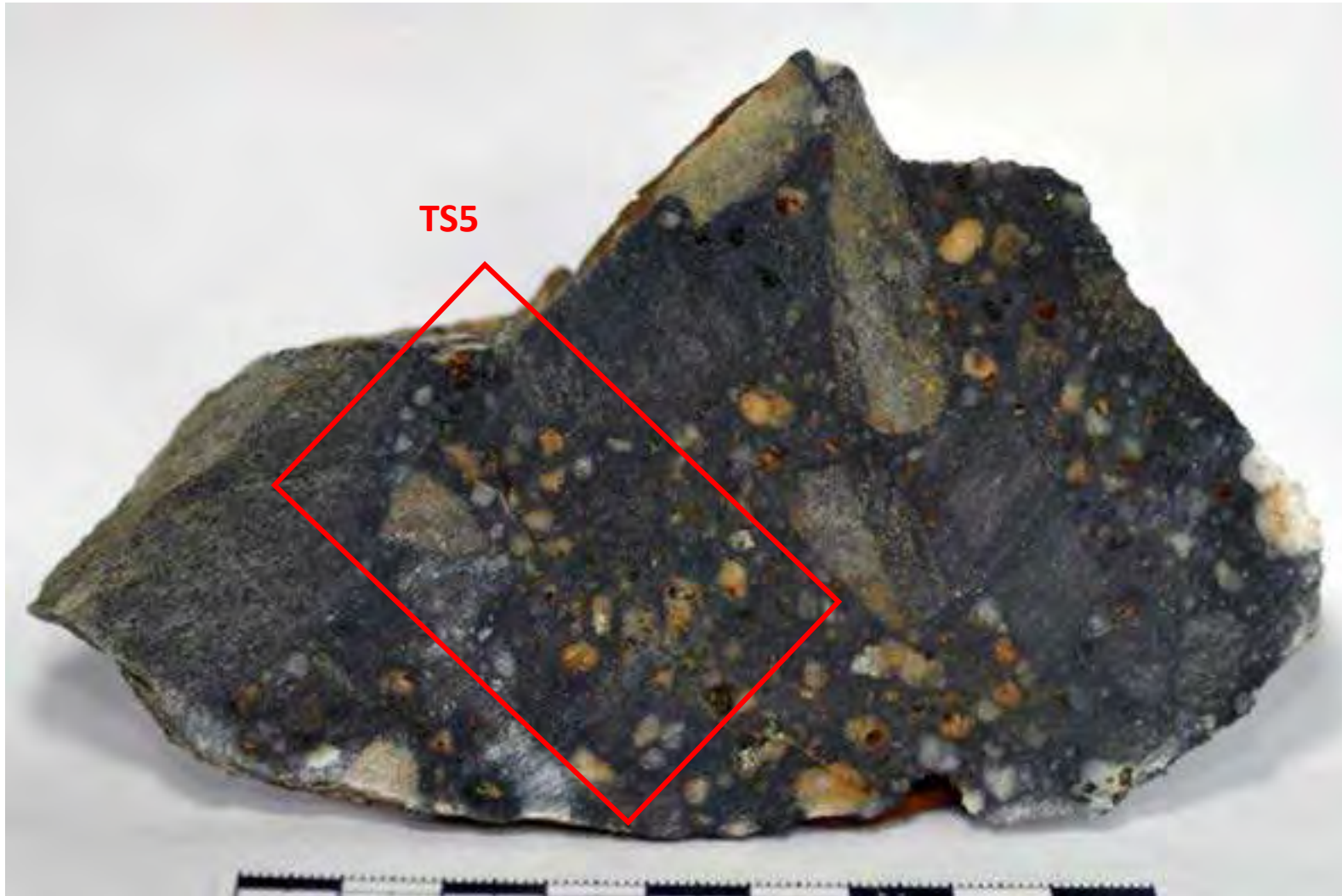


Tourmaline breccia hosting silicified granite and quartzite angular clasts. Silicified granite clasts are up to 8 cm across, composed almost exclusively of quartz, and show abundant secondary irregular cavities with sulfide mineralization within. Two types of quartz have been distinguished: i) milky massive quartz (probably of hydrothermal origin), and ii) hyaline, subhedral quartz (probably, of magmatic origin). Hyaline subhedral quartz crystals are up to 1 cm long, fractured, and cemented by the milky quartz. Muscovite occurs as disseminated subhedral platy crystals up to 2 mm across. Sulfides are mostly subhedral and euhedral pyrite grains < 1mm in size and partly line the secondary porosity in these clasts. Quartzite clasts are up to 4 cm and do not show sulfide mineralization. The tourmaline cement is massive, black in color, and show a fine sulfide (pyrite, arsenopyrite) and cassiterite dissemination.

2020-KELL-24



2020-KELL-24



2020-KELL-25



2020-KELL-25

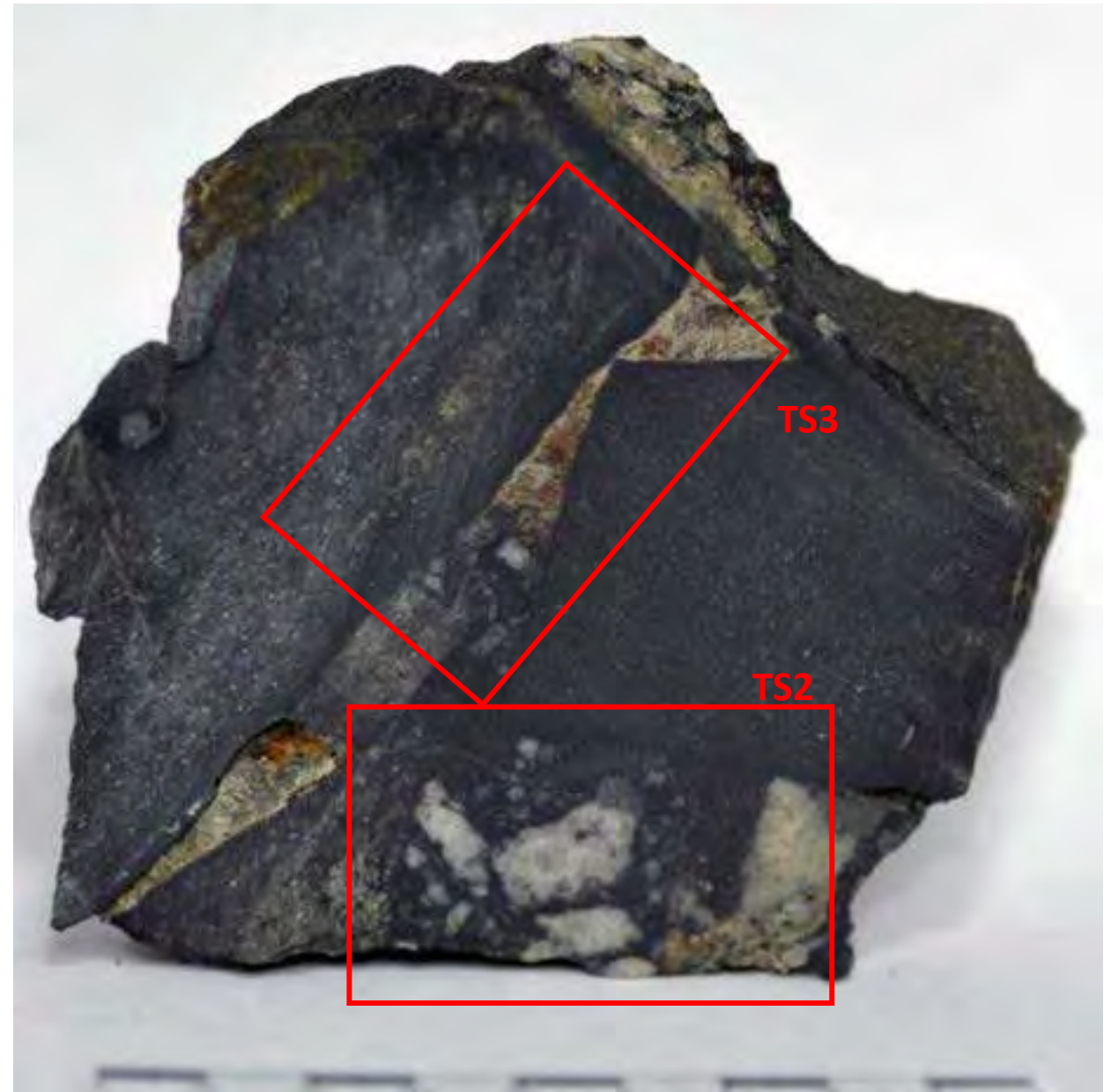


2020-KELL-25

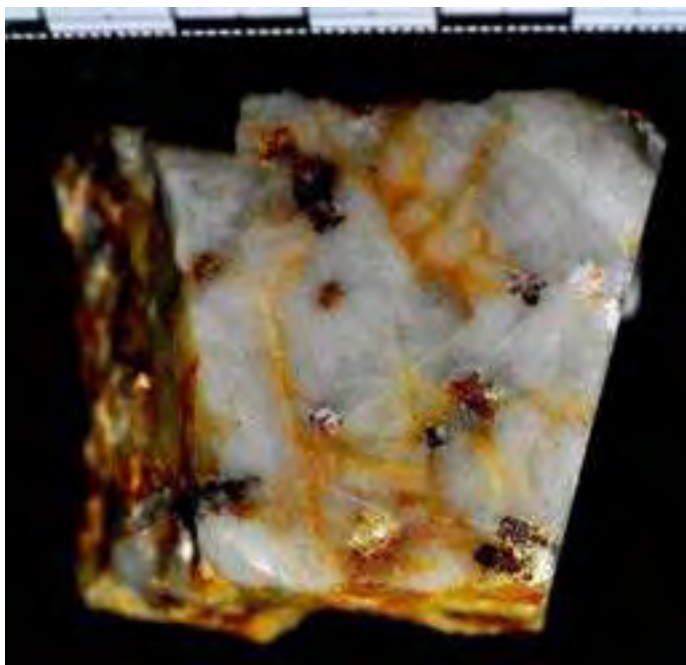
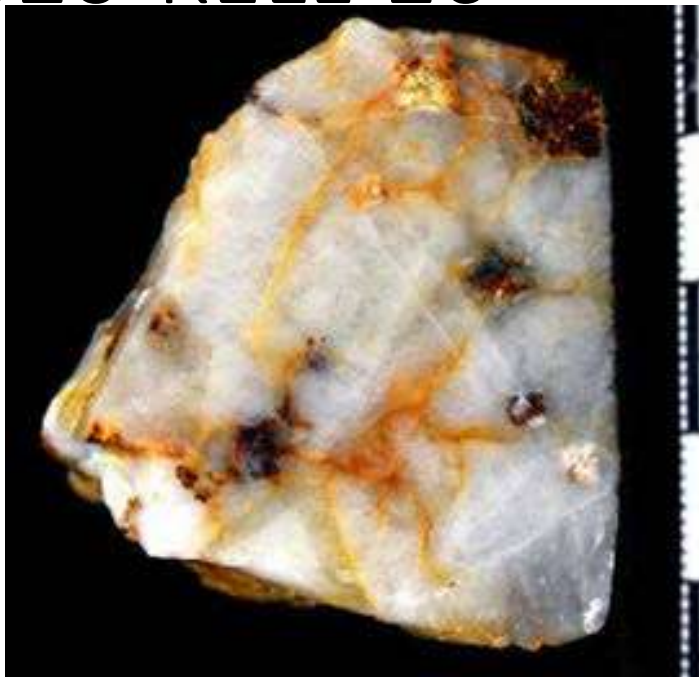


Mineralized tourmaline breccia. The breccia hosts angular clasts of variable size, mostly between 0.5 and 15 cm, cemented by a black matrix made up of tourmaline and sulfides. The origin of the clasts is diverse including white silicified granitic rocks and black quartzites (probably derived from the hosting Catavi Fm.). Silicified granite clasts are up to 6 cm across, composed almost exclusively of quartz, variably porous, and hosting locally abundant sulfide grains (mostly pyrite and arsenopyrite). Two types of quartz have been distinguished: i) milky massive quartz (probably of hydrothermal origin), and ii) hyaline, subhedral quartz up to 0.5 cm across (probably, of magmatic origin). Some of the granite clasts host muscovite subhedral platy crystals up to 2 mm across (probably derived from greisenized granitic rock). Quartzized rock clasts are relatively internally homogeneous; however, some of the fragments show dissemination of pyrite crystals, and some are cut by sulfide veinlets (<3 mm wide). mm-sized, subhedral pyrite, arsenopyrite, and cassiterite crystals occur scattered within the tourmaline groundmass.

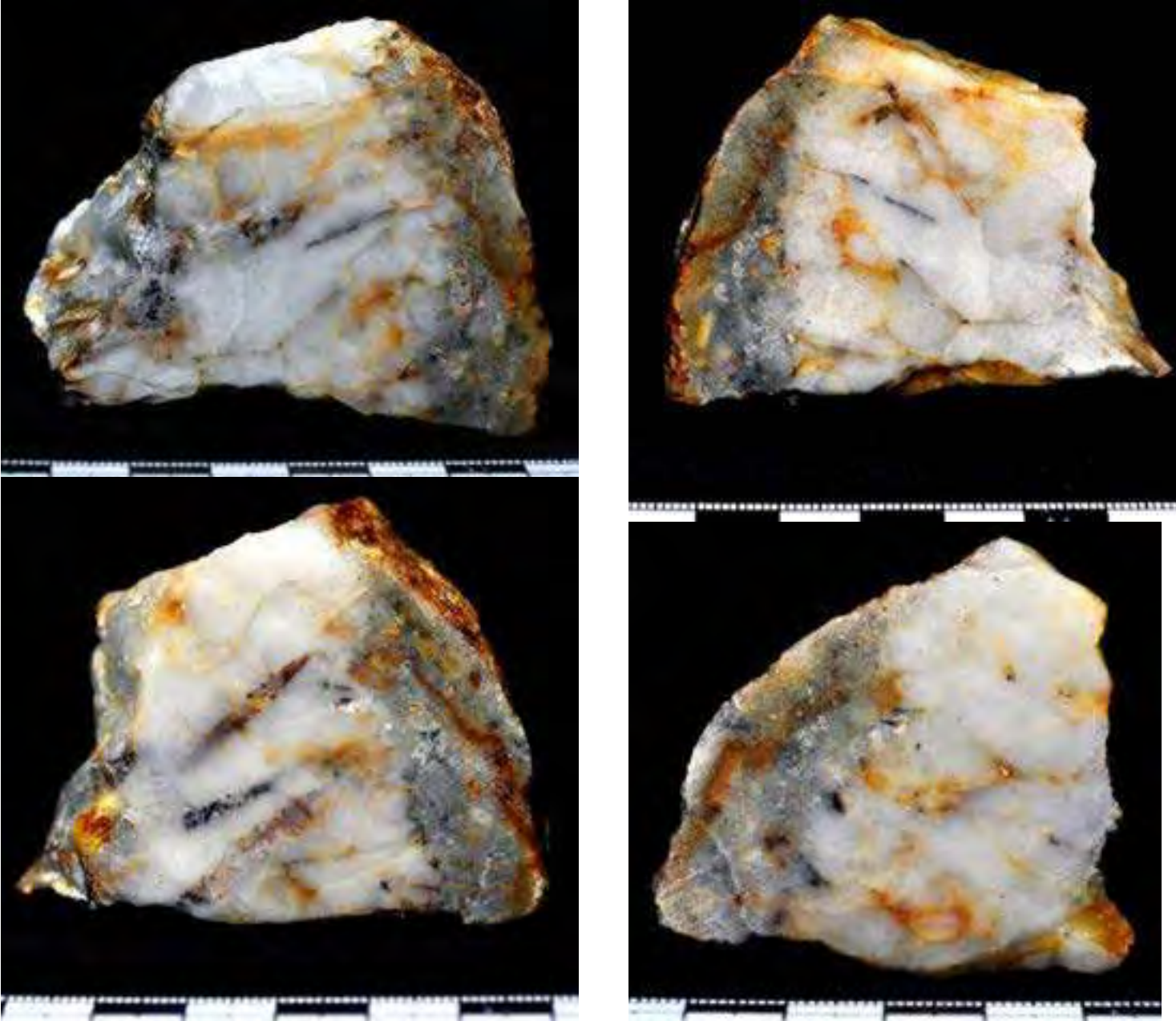
2020-KELL-25



2020-KELL-26

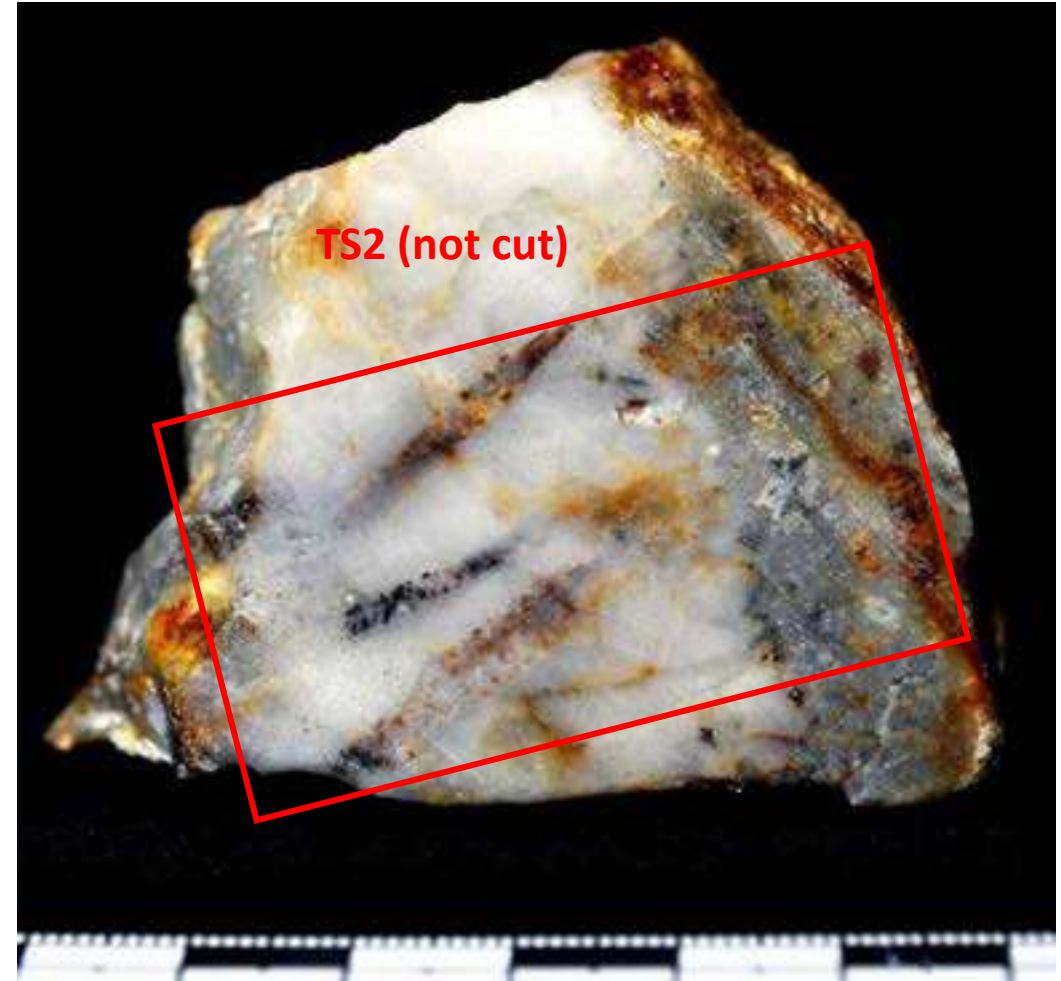


2020-KELL-26



Mineralized quartz vein with a thickness of approximately 6 cm in greisen. In addition to quartz, it is composed by lower proportions of tourmaline (?), muscovite, cassiterite, and sulfide (mostly oxidized) minerals. Quartz is milky and massive. Tourmaline crystals are black in color, acicular, mm-sized, and appear intergrown with muscovite. Muscovite occurs as disseminated subhedral platy crystals up to 2 mm across. Pyrite occurs as disseminated individual crystals <1mm. Cassiterite occurs as subhedral brown crystals intergrown with vein quartz.

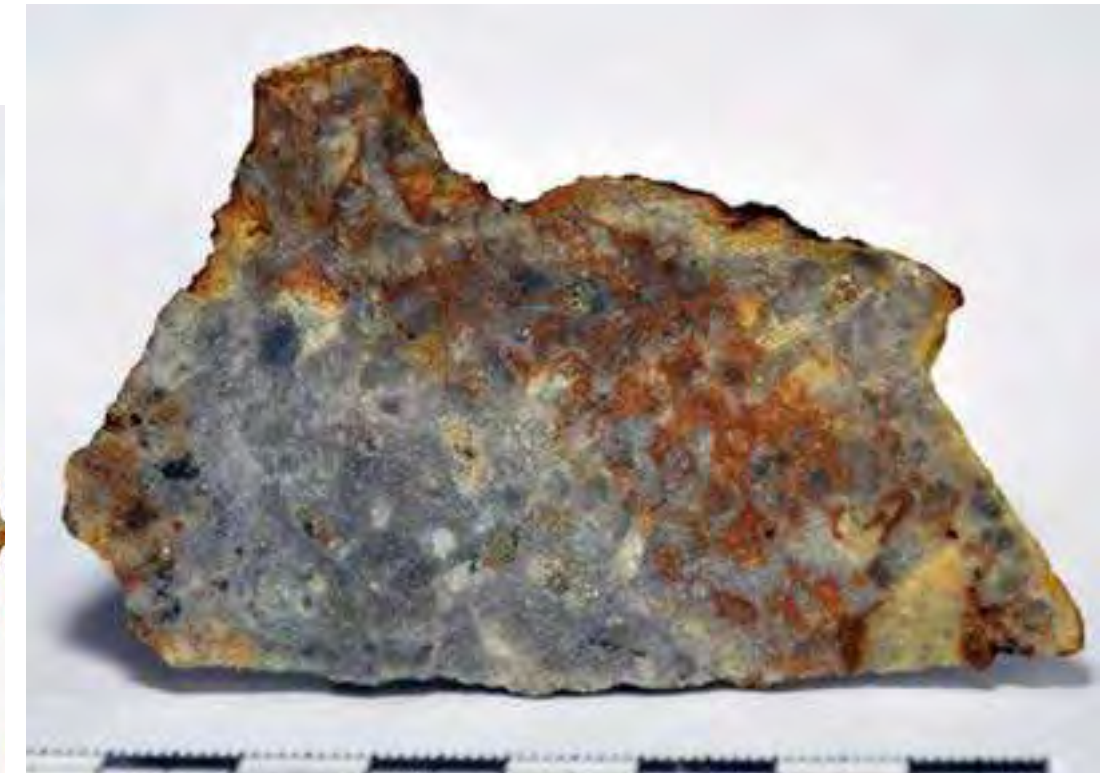
2020-KELL-26



2020-KELL-27



2020-KELL-27

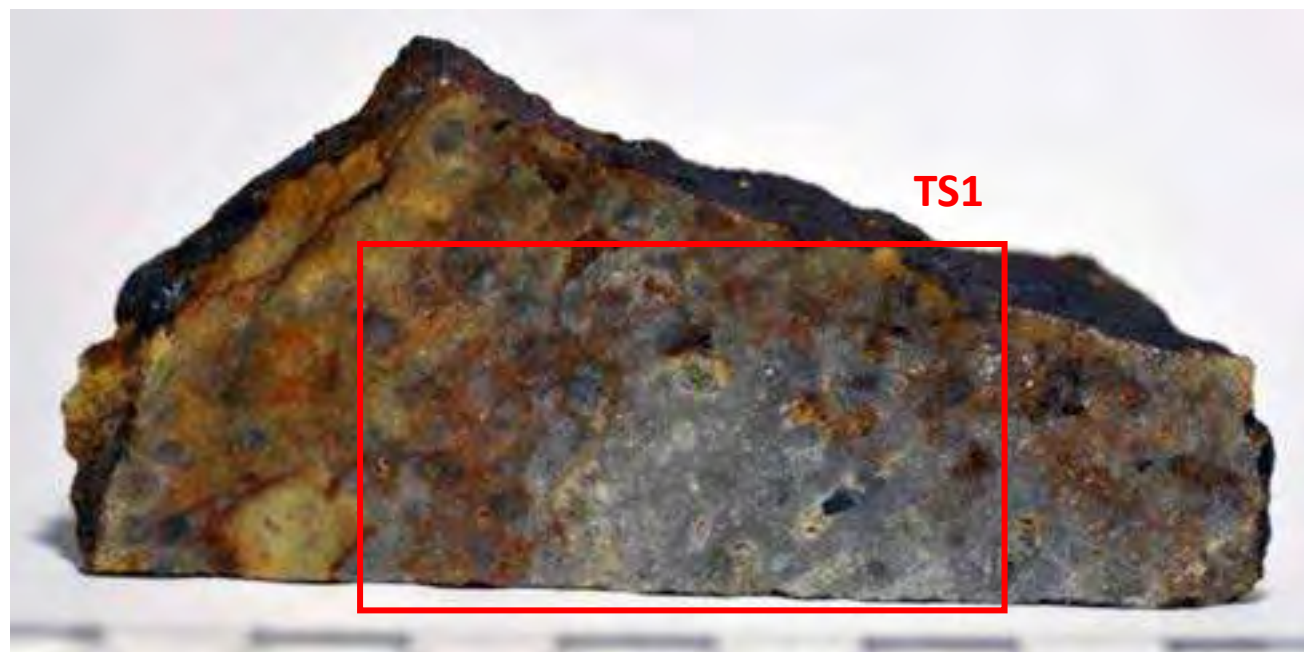


2020-KELL-27

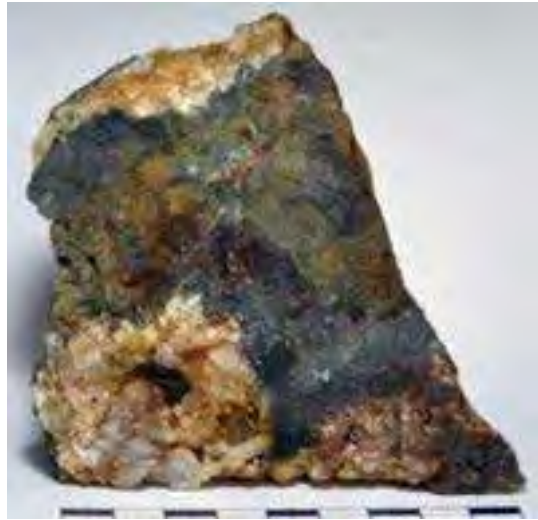


Mineralized greisen mostly constituted of quartz, muscovite, feldspar, tourmaline, and sulfides. Two types of quartz have been distinguished: i) milky massive quartz (probably of hydrothermal origin), and ii) hyaline, subhedral quartz (probably, of magmatic origin). Hyaline subhedral quartz crystals are up to 1 cm in size, fractured, and cemented by the milky quartz. Muscovite crystals are disseminated and up to two mm long. The rock shows abundant cavities, probably after tabular feldspar, which are also partially replaced by a black mineral (tourmaline?); however, some feldspar phenocrysts have not been completely destroyed/obliterated. Feldspar phenocrysts, or their ghosts, show tabular habit and lengths up to 1 cm. Pyrite forms individual euhedral crystals up to 1mm in size.

2020-KELL-27



2020-KELL-28-A



2020-KELL-28-A



Quartz vein hosted by Catavi Fm. quartzites. The vein is approximately 4 cm wide and contains a mineralization of quartz with lesser proportions of sulfides. Subhedral translucent quartz crystals up to 2 cm long describe comb textures. Pyrite subhedral crystals are scarce and appear forming individual crystals and aggregates <1 cm filling interstitial space between quartz crystals. Brown translucent crystals (cassiterite?) are scarce and occupy interstitial space between comb quartz crystals.

2020-KELL-28-B

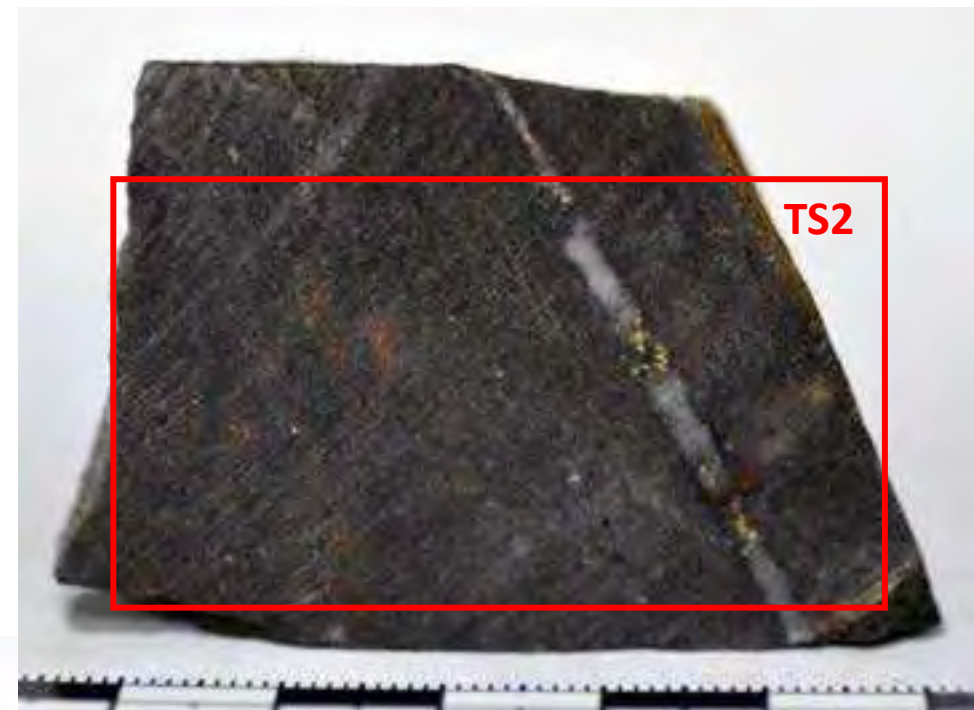
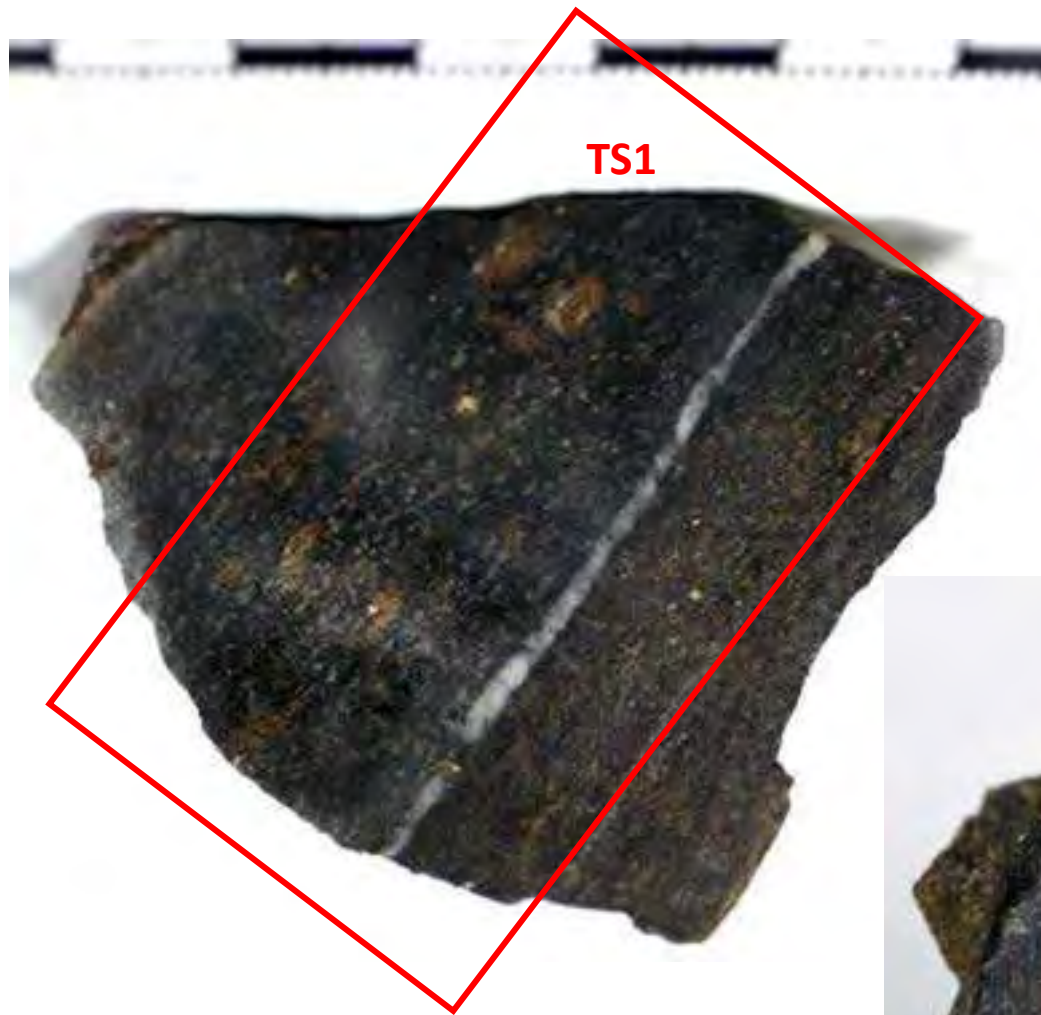


2020-KELL-28-B

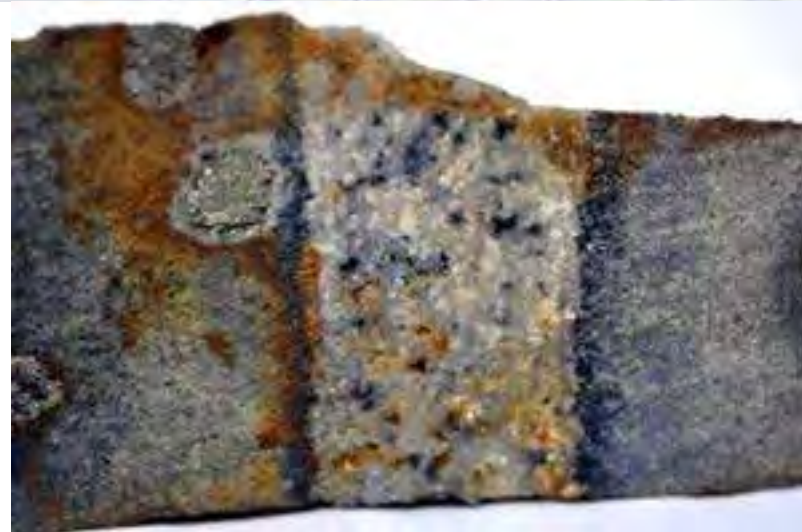
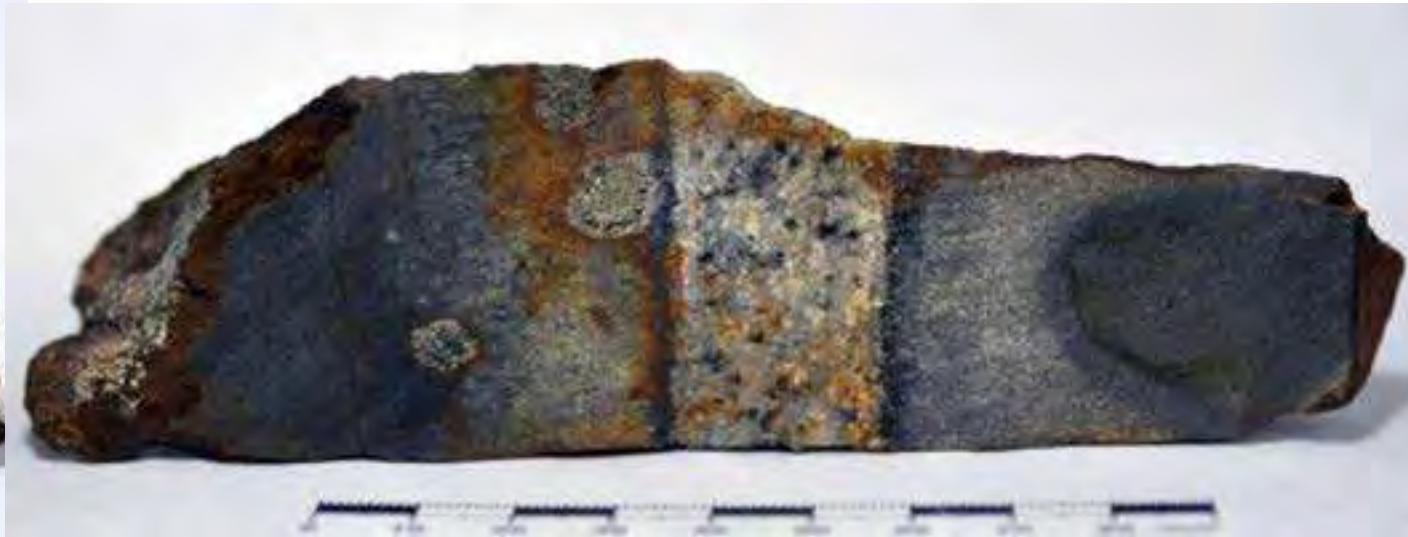


Quartz-tourmaline veinlets hosted by Catavi Fm. quartzites. Veinlets are up to 2 mm wide and are mostly composed of milky quartz and dark rims of tourmaline (<1mm wide). Oxidized pyrite is scarce and appears forming aggregates <4 mm across along with vein quartz.

2020-KELL-28-B



2020-KELL-28-C



Vein hosted by Catavi Fm. quartzites. The main vein is approximately 2 cm wide and contains a mineralization of quartz, pyrite, and tourmaline. Within the vein, massive milky quartz are intergrown with mm-sized subhedral, black tourmaline crystals. Pyrite forms individual subhedral crystals and aggregates <4mm in both the vein and host rock. The vein selvage contains black subhedral short-prismatic tourmaline crystals. These short-prismatic black crystals are mostly oriented perpendicular to the vein contact.

2020-KELL-28-C



2020-KELL-29



2020-KELL-29



Massive sulfide mineralization in tourmaline breccia; other clasts include silicified granite and quartzite. The sulfide mineralization is mostly composed of pyrite and arsenopyrite intergrown with subhedral, black crystals (tourmaline?) and partly oxidized. Silicified granite clasts are up to 1 cm across composed almost exclusively of quartz and muscovite.

2020-KELL-30-A



2020-KELL-30-A



Massive pyrite vein hosted by greisenized granitic rock. The host rock is mostly constituted of quartz, muscovite, and probably, tourmaline. Hyaline subhedral quartz crystals are up to 1 cm long, fractured, and cemented by milky quartz. Milky quartz pseudomorphically replaced some tabular crystals of feldspar. Muscovite crystals are disseminated and up to 1 mm long. Pyrite is scarce and appears forming individual euhedral crystals up to 1mm in size. Tourmaline crystals are scarce and show as aggregates of acicular crystals (<1mm). The massive pyrite vein is up to 1 cm wide is cut by a vein composed of green cubic subhedral crystals of fluorite.

2020-KELL-30-B

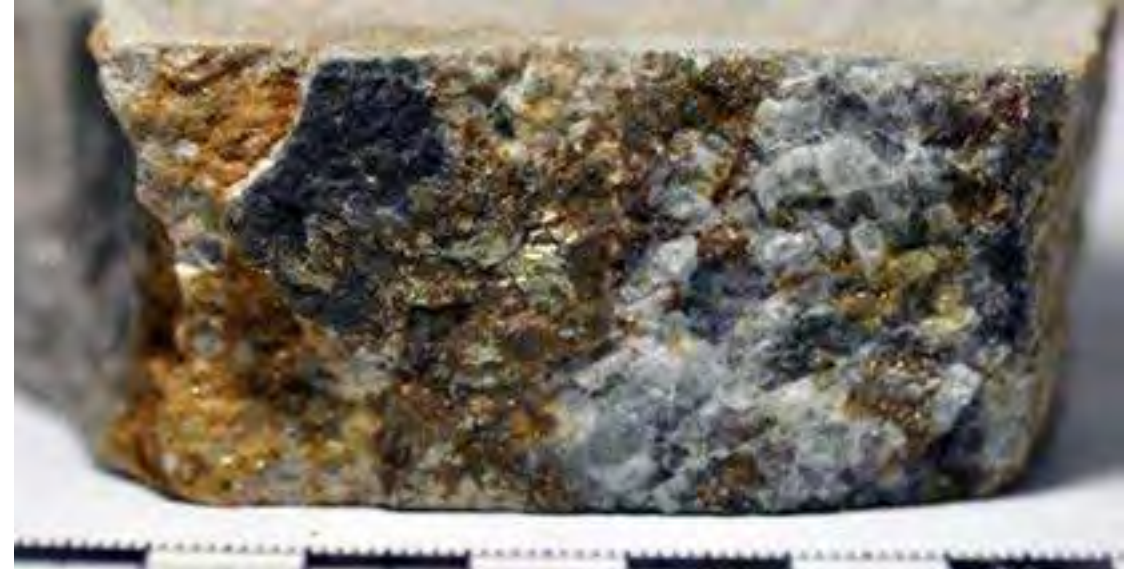
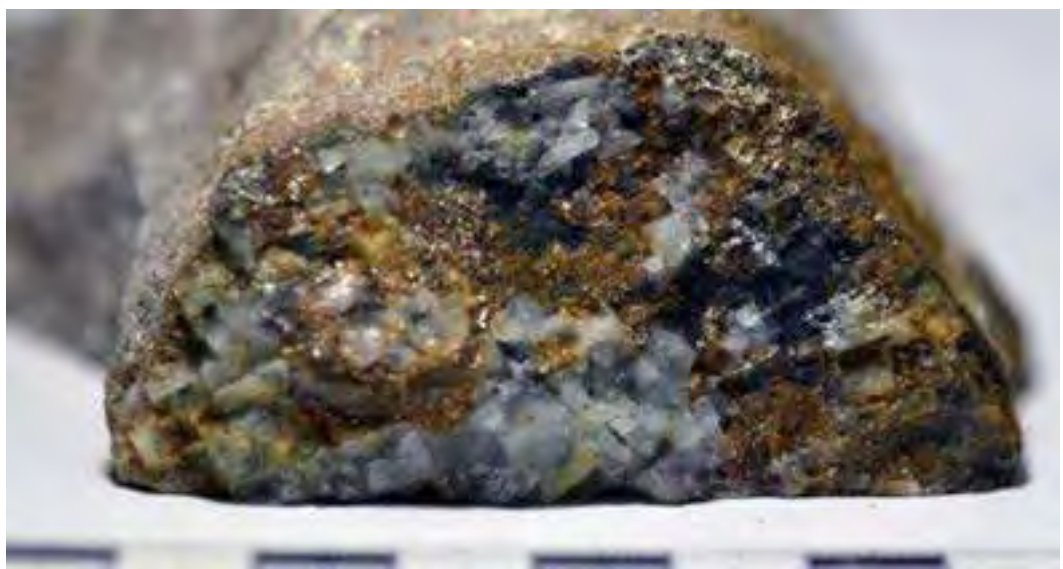


Greisenized granitic rock mostly constituted of quartz, muscovite, tourmaline, and pyrite. Hyaline subhedral quartz crystals are up to 1 cm long, fractured, and cemented by milky quartz. Feldspar phenocrysts have been pseudomorphically replaced by quartz. Muscovite crystals are disseminated and up to one mm long. Pyrite appears as subhedral crystals up to 1mm in size and forming patches up to 5 mm across. Tourmaline crystals are scarce and forms aggregates of acicular crystals (<1mm). The rock is cut by veins of massive pyrite and locally, by veins/coatings composed of green cubic subhedral crystals of fluorite.

2020-KELL-30-B



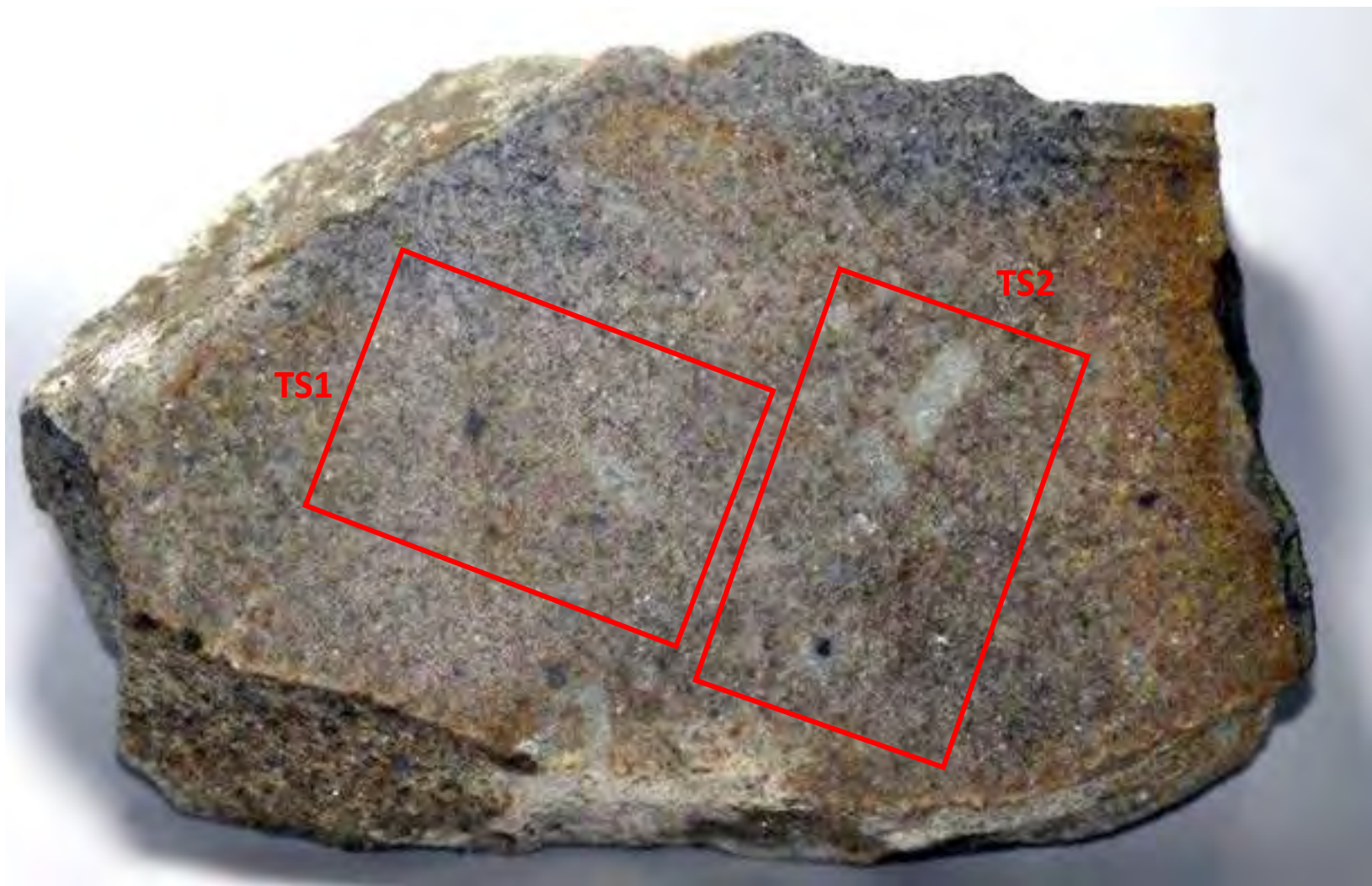
2020-KELL-30-B



2020-KELL-30-B



2020-KELL-30-B



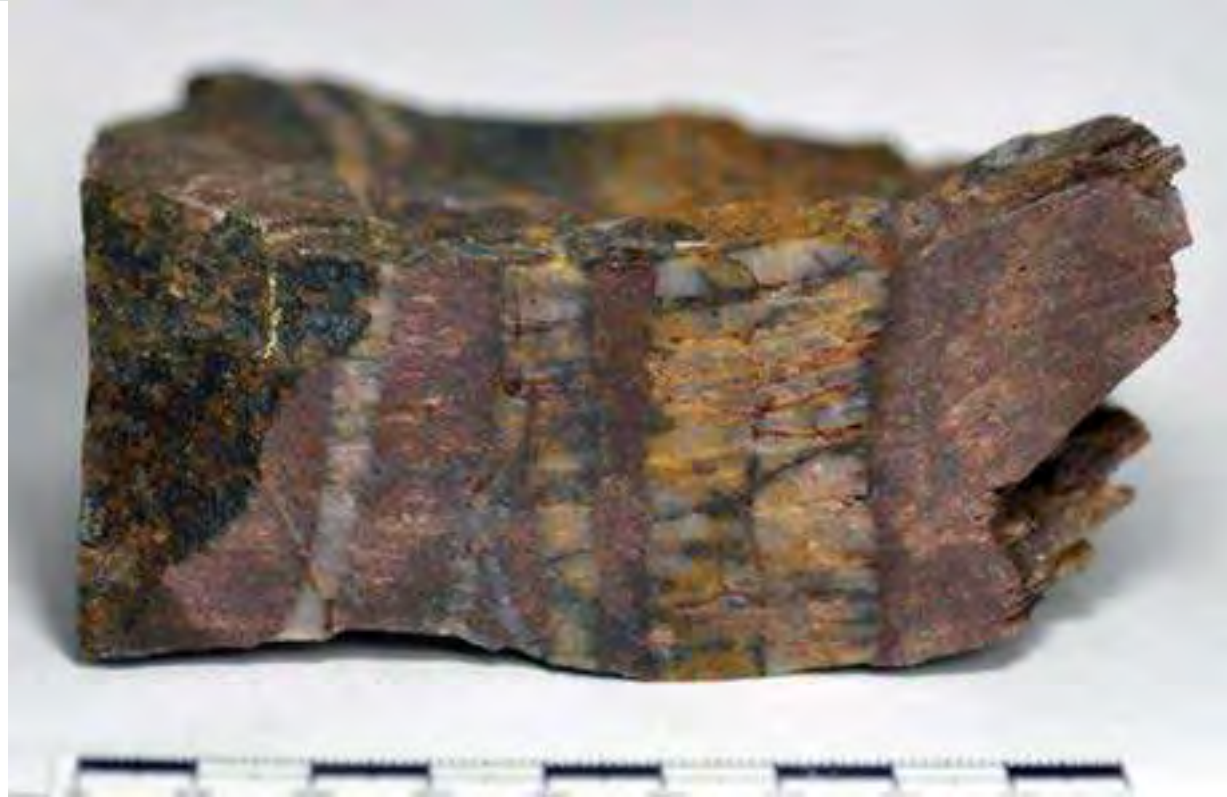
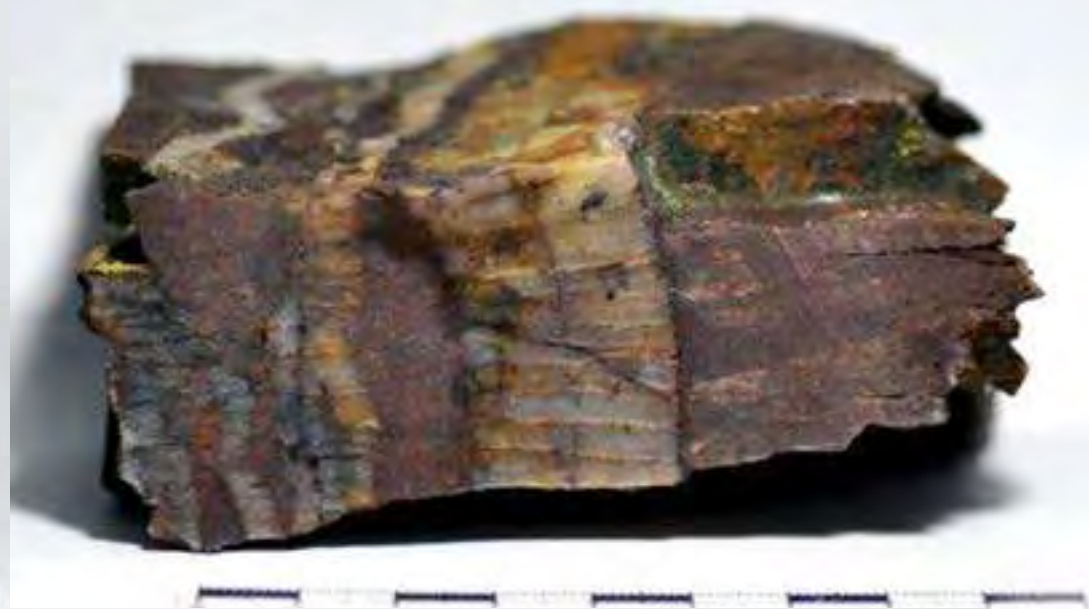
2020-KELL-31



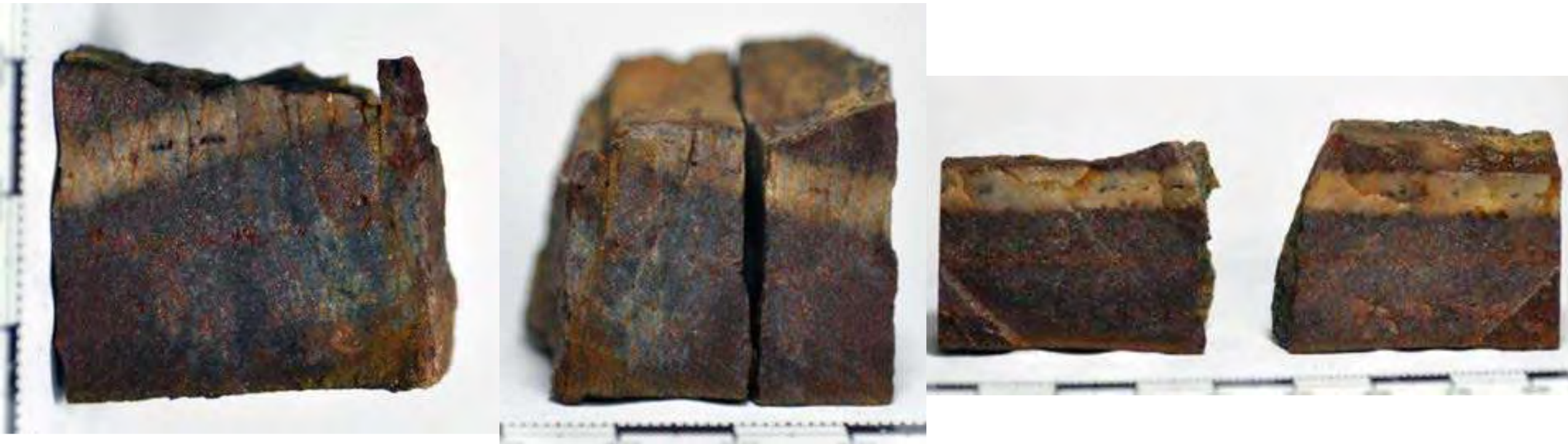
2020-KELL-31



2020-KELL-31



2020-KELL-31



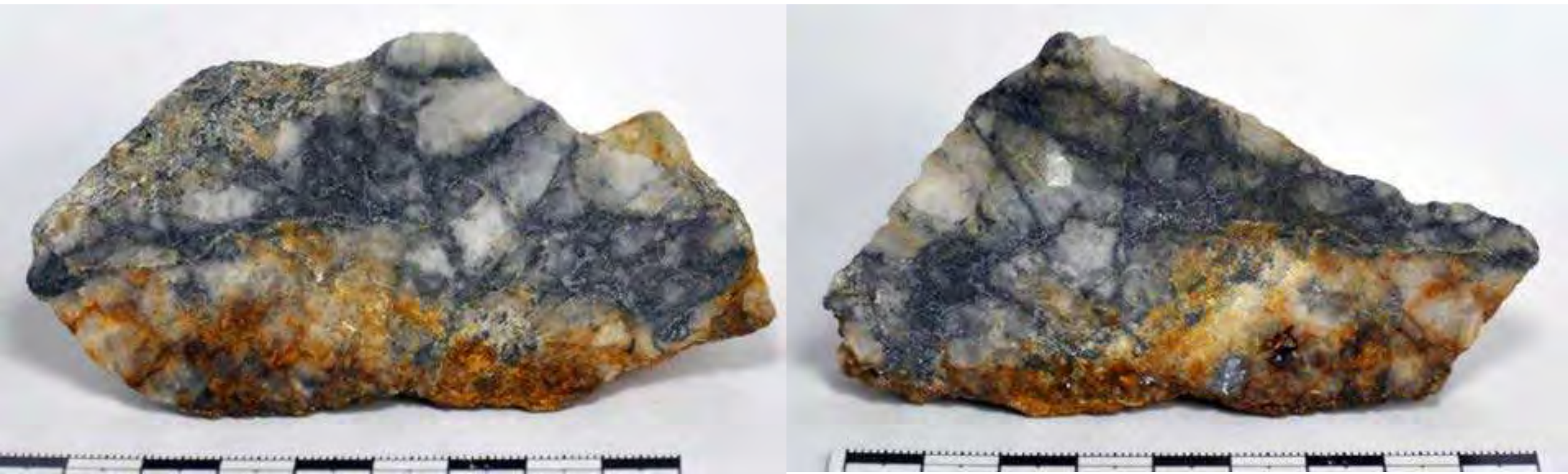
Vein system composed of centimetric-millimetric quartz-rich veins. Milky quartz is the main phase, and appear along with lesser proportions of cassiterite (?) and muscovite. Cassiterite (?) crystals are brown in color and mm-sized, and occur as scattered subhedral grains towards the central part of the veins. Muscovite occurs as scattered crystals within the vein and filling fractures in the host rock. Often, the veins contain mm- to cm-sized angular fragments of the host rocks.

2020-KELL-32-A



Quartz-rich veins composed largely of quartz, fluorite, cassiterite, and sulfides hosted by Catavi Fm. quartzites. Quartz is milky and massive. Fairly abundant fluorite euhedral cubic, translucent crystals (<5mm) overgrow quartz. Cassiterite crystals are dark brown in color and mm-sized. Sulfide minerals (pyrite and sphalerite?) also occur in the vein and are largely oxidized.

2020-KELL-32-B



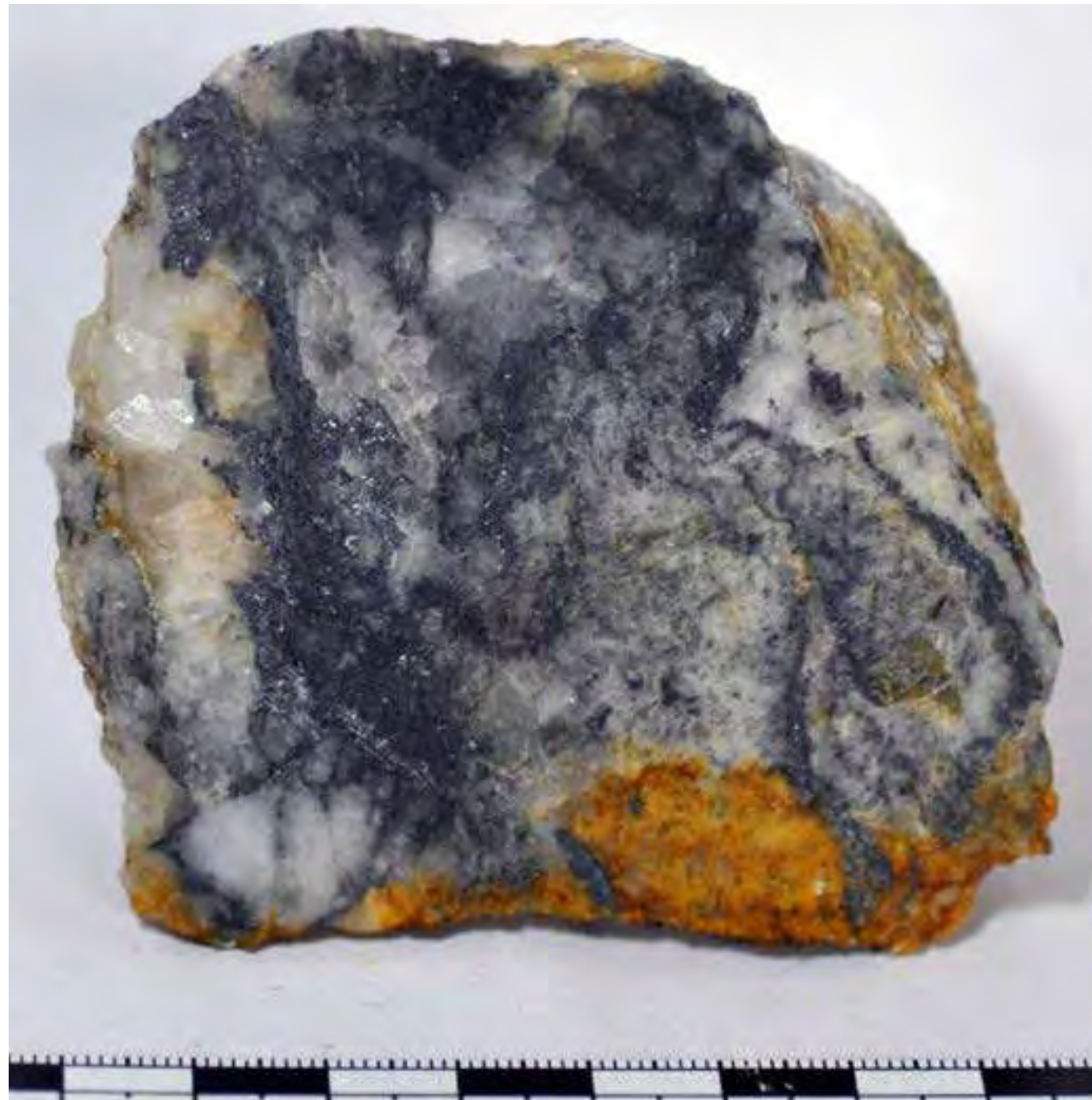
Mineralized hydrothermal breccia. Silicified clasts and milky quartz crystals up to 5 cm long are cemented by galena. Galena veinlets (<1mm wide) also cut quartz crystals.

2020-KELL-32-C



Galena- and quartz-rich vein. Quartz shows a massive milky aspect. Patches of a white, soft unidentified mineral also occur within the vein.

2020-KELL-32-D



2020-KELL-32-D



Quartz- and galena-rich vein. Quartz and galena form crustiform textures. Galena is massive. Quartz forms subhedral milky crystals up to 1 cm long. Black crystals (<1mm) (cassiterite?) appear scattered in both the quartz and galena.

2020-KELL-32-E



Mineralized hydrothermal breccia. Angular to sub-angular rock clasts up to 1 cm long, presumably from the hosting Catavi Fm., are cemented by semi-massive milky quartz. Some rock clasts have a porphyritic texture with white phenocrysts (<1mm), probably quartz or feldspars. The breccia is cut by a quartz-galena vein. Vein quartz crystals (1mm) are subhedral and translucent.

2020-KELL-32-F



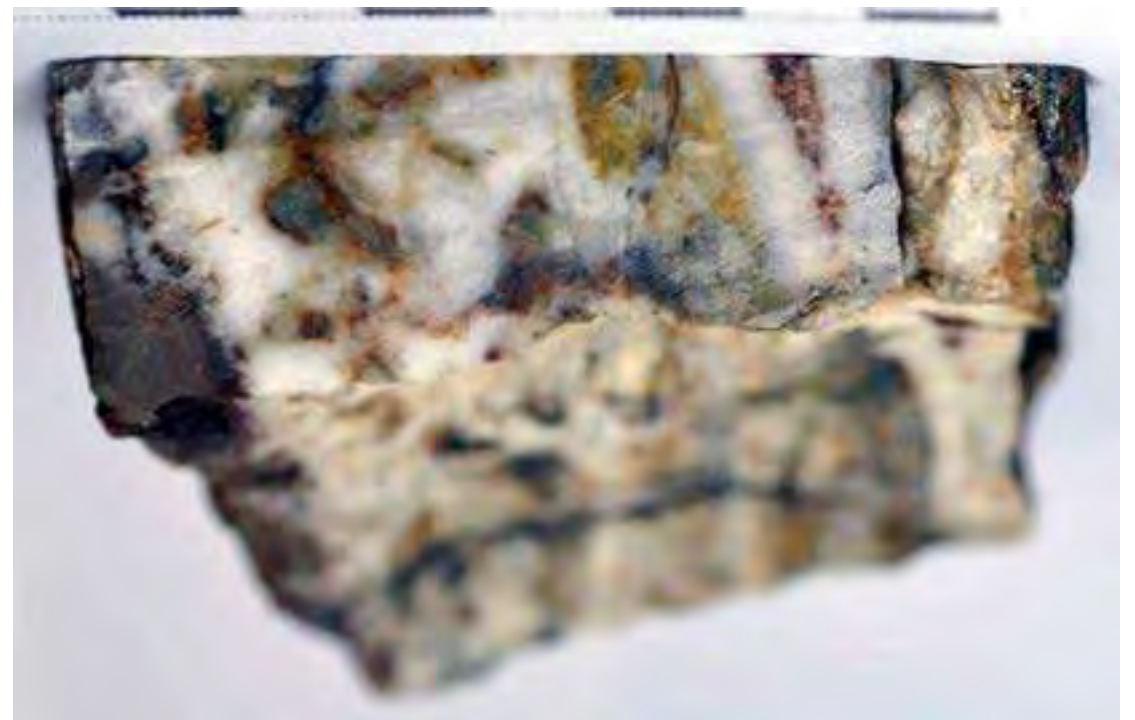
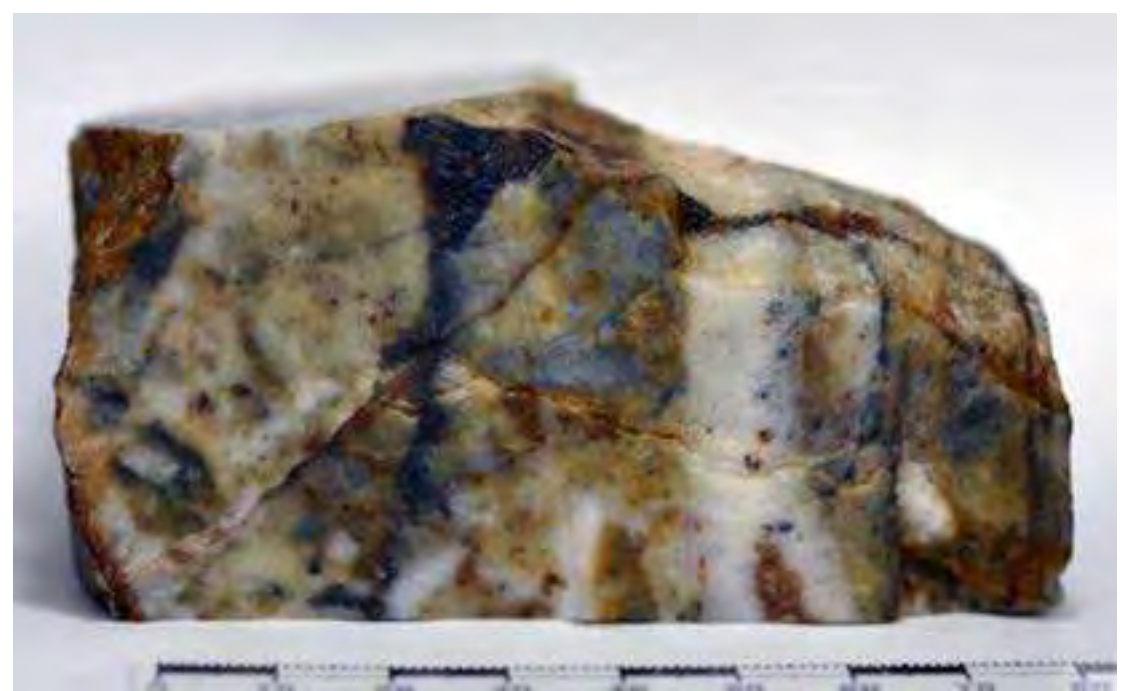
Quartz- and galena-rich vein. Intergrown quartz and galena forming a crustiform texture. Galena is massive in this sample. Quartz forms subhedral semi-translucent crystals up to 1 cm long. Black crystals (<1mm) (cassiterite?) appear scattered in the quartz and galena.

2020-KELL-32-G

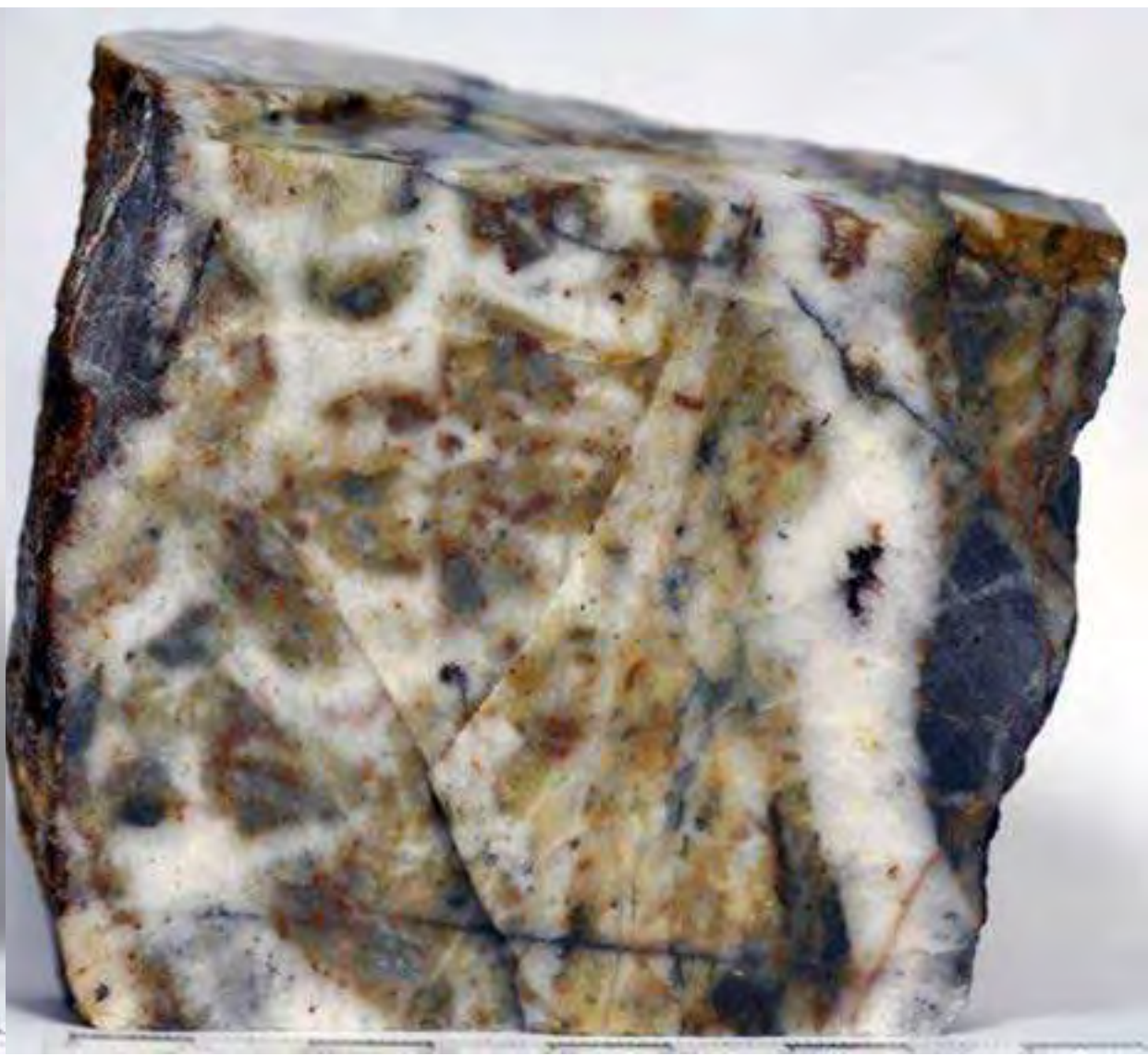


Quartz- and galena-rich vein. Quartz forms euhedral-subhedral translucent crystals up to 1 cm long. Black crystals (<1mm) (cassiterite?) appear scattered in the quartz and galena.

2020-KELL-33-A



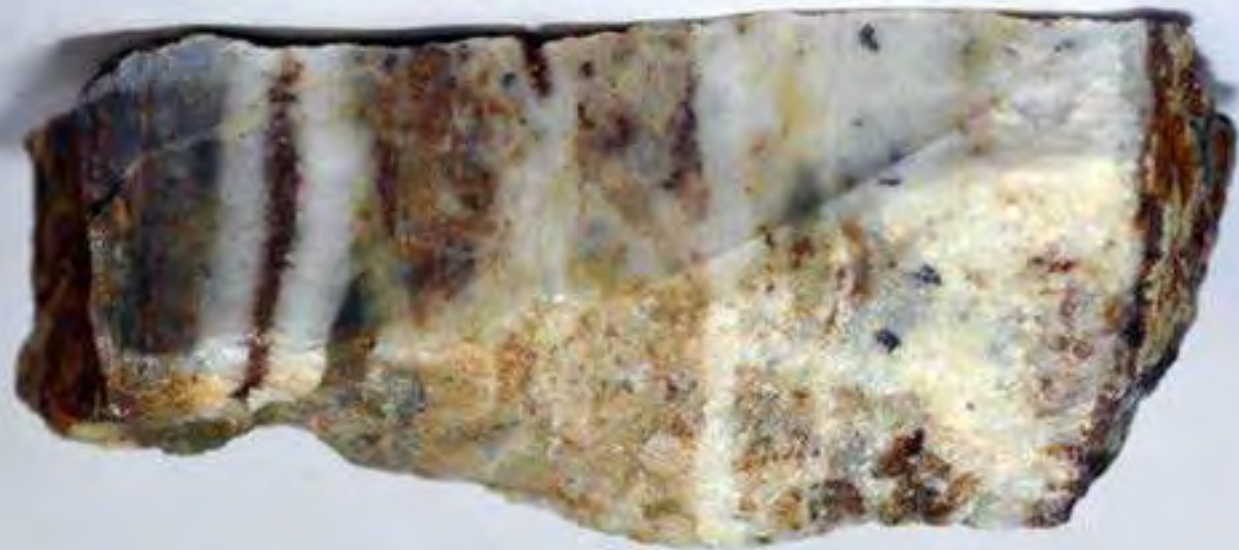
2020-KELL-33-A



2020-KELL-33-A



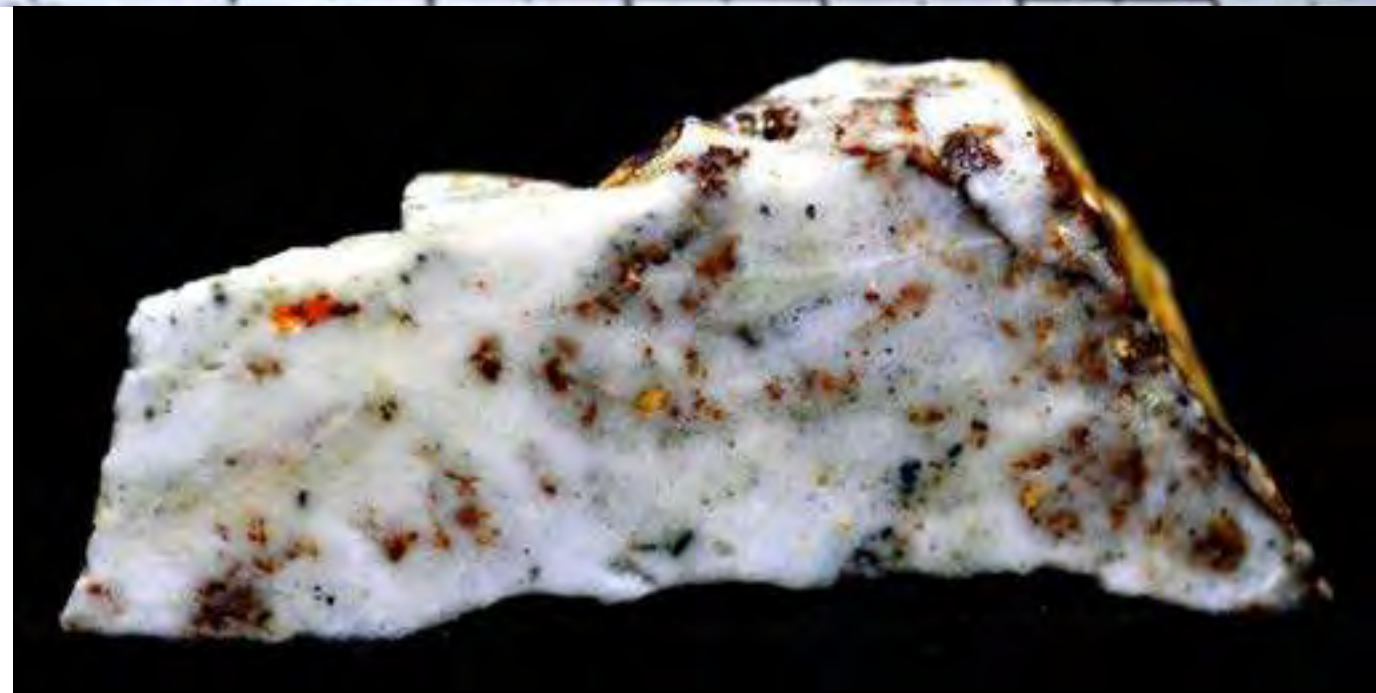
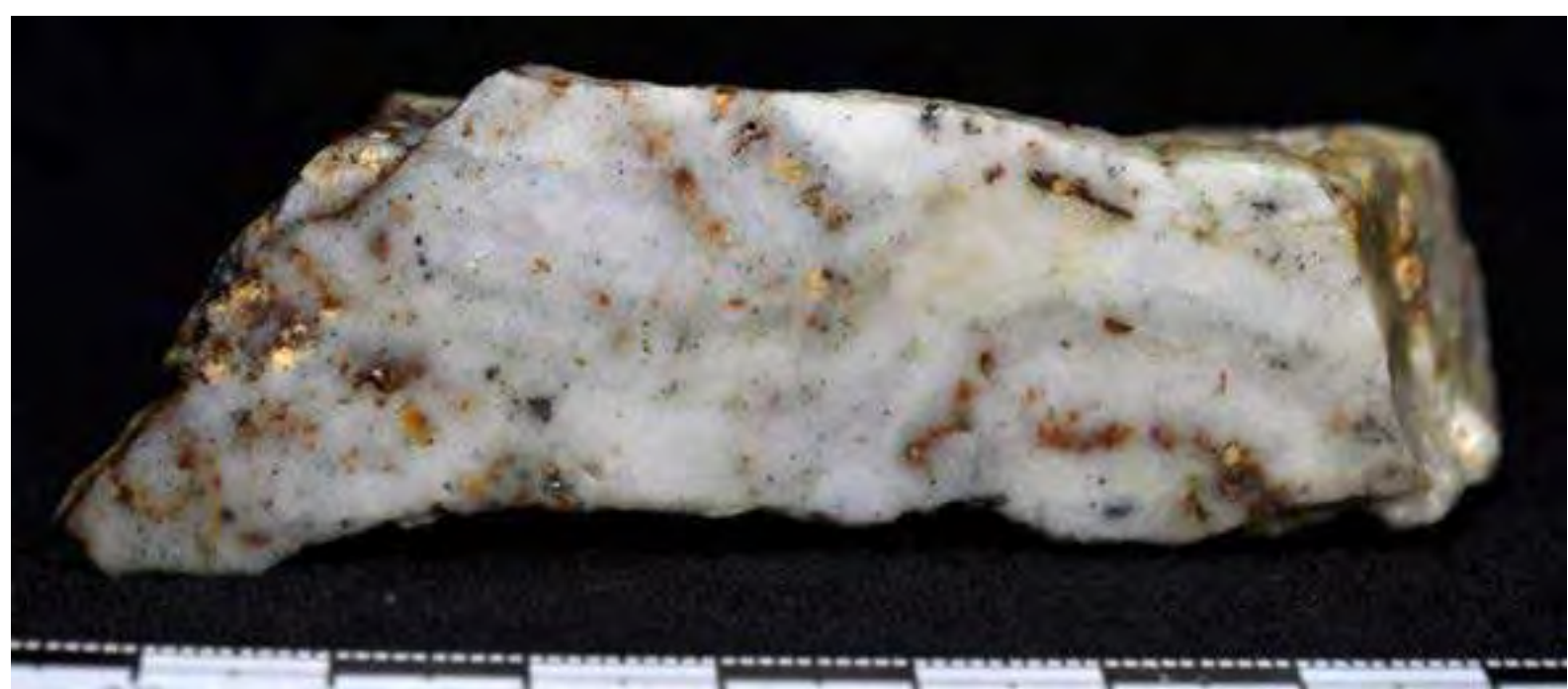
2020-KELL-33-A



6 cm

Complex vein with an internal brecciated texture. It is composed mostly of a cement of milky quartz with lesser proportions of sphalerite, galena and Fe-rich carbonates that host mm- to cm-sized angular to sub-angular quartzite fragments. Euhedral to subhedral translucent quartz crystals up to 0.5 cm long describe comb textures, and are often overgrown by a central suture of Fe-rich carbonate in some parts of the vein. Sphalerite (?) crystals are brown in color and mm-sized, and occur as aggregates towards the central part of the vein. Galena crystals are grey in color and mm-sized, and occur scattered in vein quartz or as thin veinlets (<1mm wide) that cut vein quartz.

2020-KELL-33-B



2020-KELL-33-B



Cockade texture described by host-rock angular fragments and a mineralization of quartz and lesser proportions of sphalerite \pm galena. Euhedral to subhedral translucent quartz crystals up to 0.5 cm long describe cockade textures on host-rock fragments. Sphalerite crystals are brown in color and mm-sized and forms aggregates.

2020-KELL-33-C



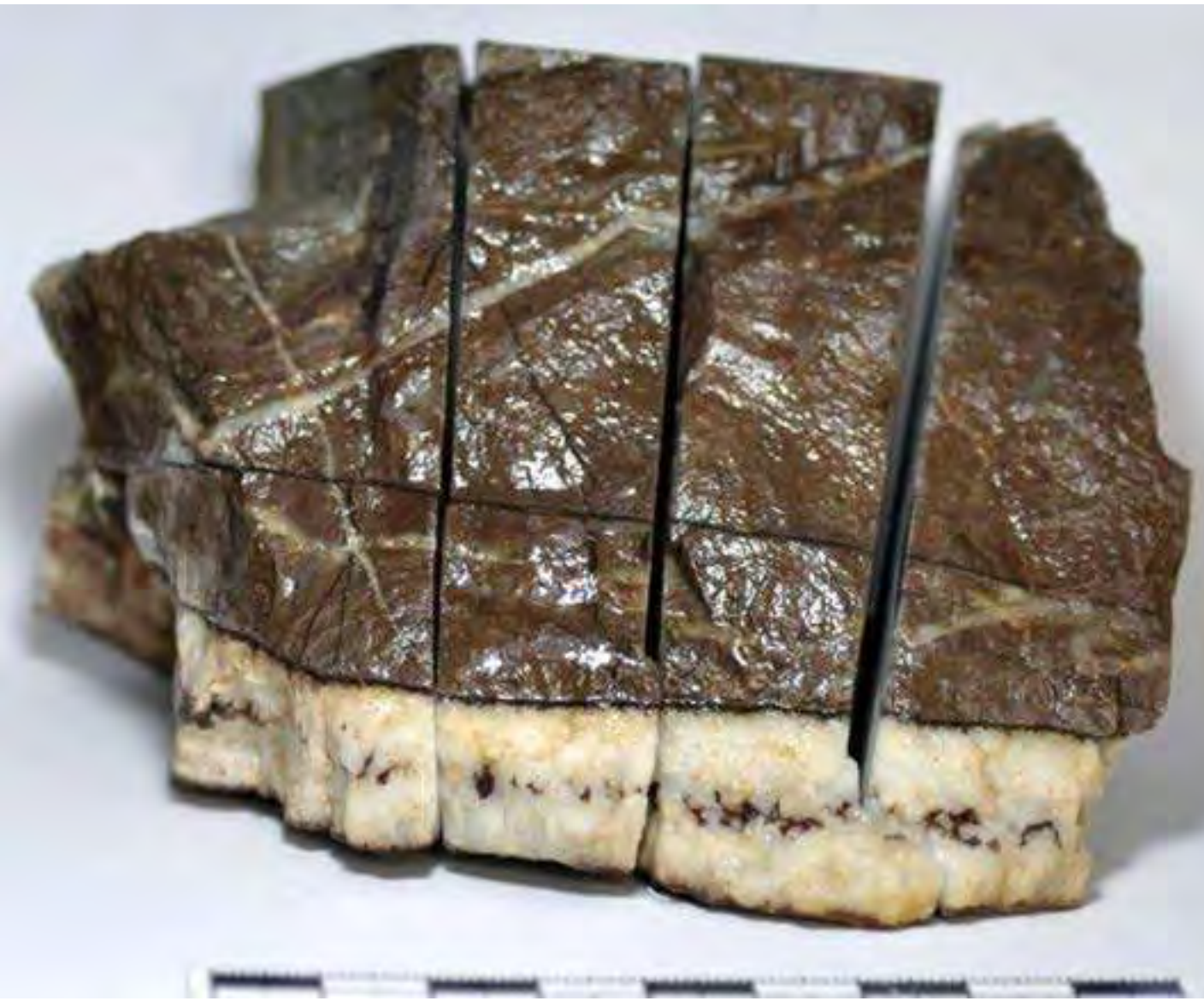
Mineralized breccia. The breccia is composed of dark quartzite (probably derived from hosting Catavi Fm.) and white, angular silicified (quartz) clasts with sizes up to 5 cm that are veined and cemented by massive galena. Silicified clasts often show internal comb and crustiform structures/textures suggesting continuous brecciation during hydrothermal mineralization. Some dark brown subhedral crystals (sphalerite ?) occupy the interstitial space between quartz crystals and in the center of the clasts. Lesser amounts of pyrite form local aggregates.

2020-KELL-33-D



Sphalerite-rich vein. Sphalerite is brown in color and largely massive, although some mm-sized subhedral crystals are observed. Sphalerite is intergrown with milky, massive quartz.

2020-KELL-33-E



2020-KELL-33-E



2020-KELL-33-E

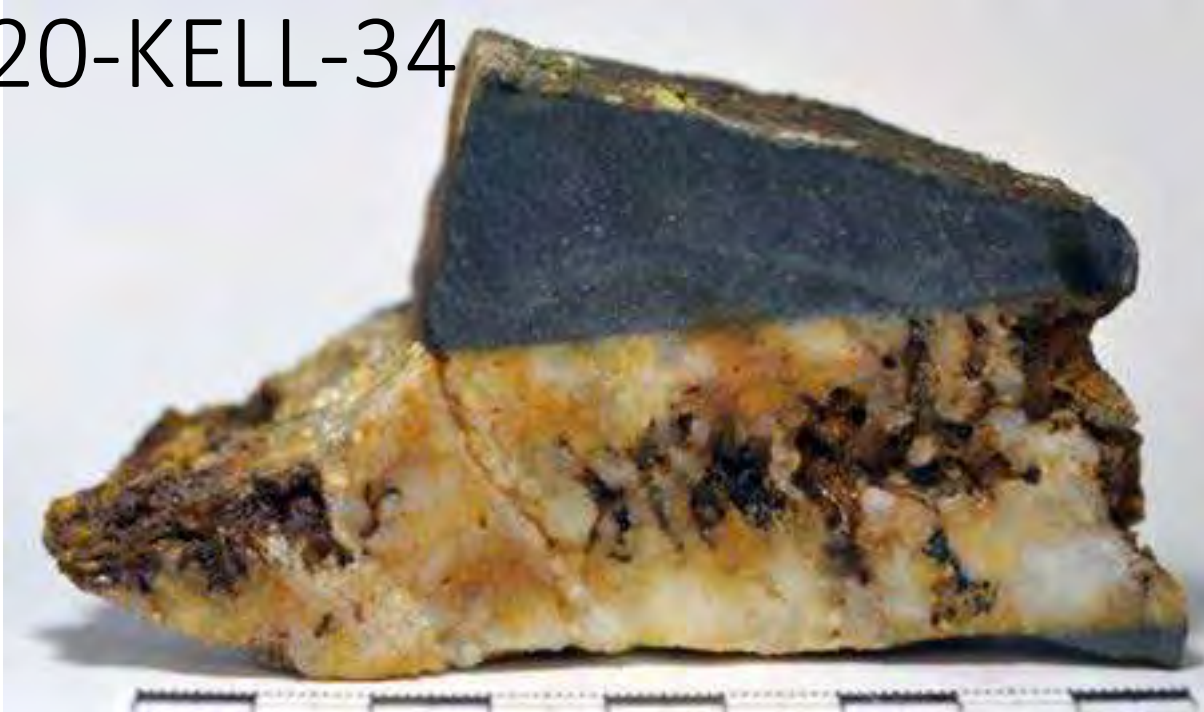


Quartz-rich veins hosted by Catavi Fm. quartzite. Thicker veins are up to 1.5 cm wide and appear along with a network of thinner irregular veins < 3 mm wide. The veins are mostly composed of milky quartz. The central sutures of the veins are occupied by a brown mineral (most probably, Fe-rich carbonates). Thicker veins show narrow halos (< 1mm) with a brown mineralization. The host rock shows pyrite dissemination.

2020-KELL-34



2020-KELL-34



2020-KELL-34



Quartz-rich veins hosted by Catavi Fm. quartzites. The main vein is approximately 3 cm wide and contains a mineralization of quartz and lesser proportions of Fe-rich carbonates and sulfides. Massive milky quartz is locally overgrown by euhedral quartz crystals up to 2 cm long. Anhedra Fe-rich carbonates and pyrite occur as fine aggregates that line secondary cavities towards the central part of the vein.

2020-KELL-35-A



Nice quartz crystals up to 5 cm long. These crystals are euhedral and translucent. A dark grey sulfide (galena?) is found in the base of the quartz crystals.

2020-KELL-35-A

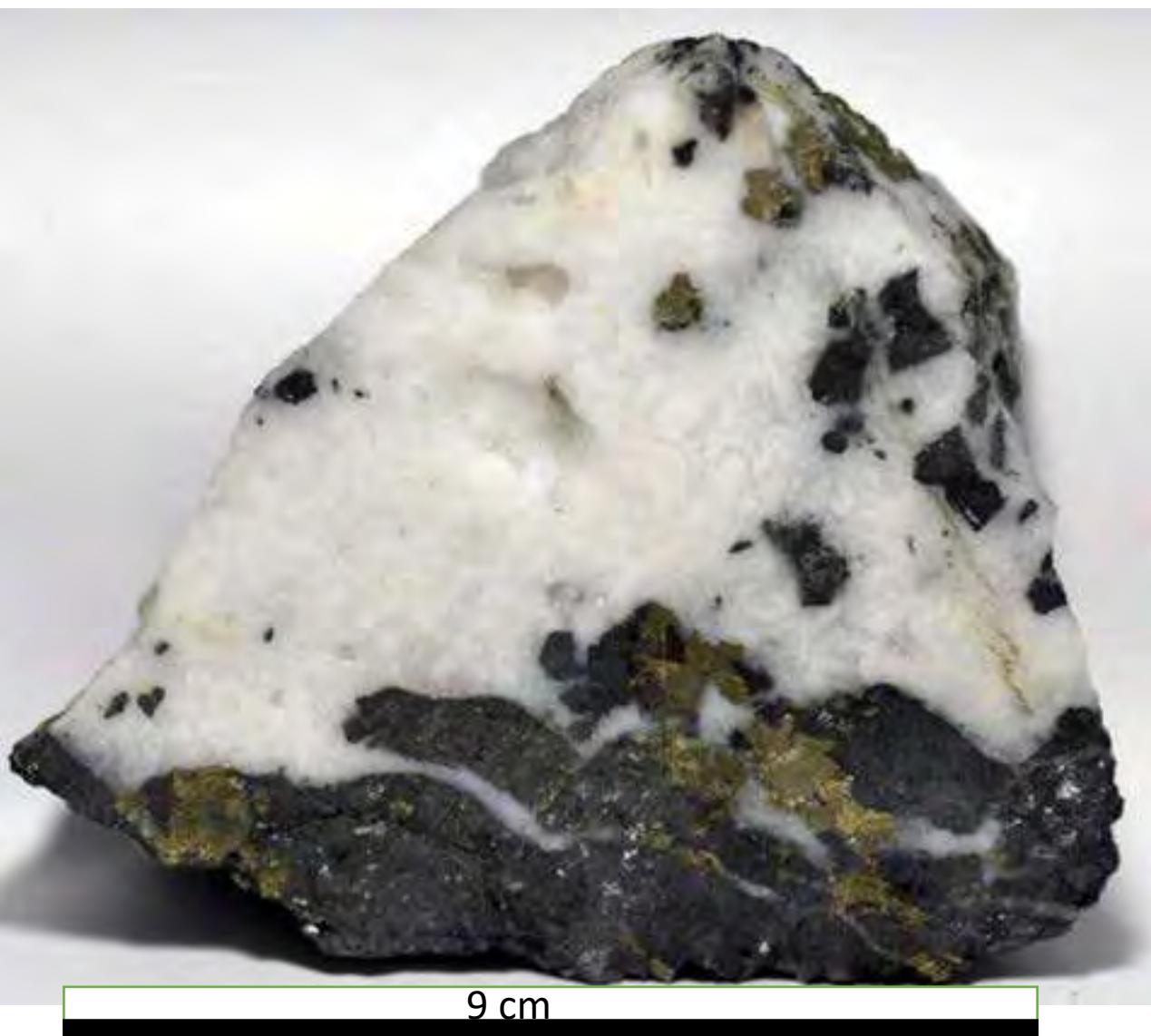


10 cm



10 cm

2020-KELL-35-B



2020-KELL-35-B



Vein composed of sphalerite, galena, quartz, siderite, chalcopyrite and pyrite. Massive sphalerite and galena is veined and cemented by milky quartz veins. Quartz forms euhedral-subhedral semi-translucent crystals with lengths up to 1.5 cm. Pale brown platy crystals of siderite occupy the interstitial space between quartz crystals. Pyrite \pm chalcopyrite form mm-sized patches and thin veinlets that cut the previously described mineral textures.

2020-KELL-36-A



Cockade and botryoidal textures in hydrothermal breccia. Clasts containing subangular mm-to cm-sized dark quartzite and massive milky quartz fragments cemented by pale brown sphalerite are overgrown by abundant botryoidal aggregates of platy siderite. Pyrite is scarce and appears as patches <5 mm across within clasts, cutting contacts between the rock fragments and the sphalerite cement. These textural relations suggest early milky quartz deposition, probably as veins hosted by quartzite, brecciation and sphalerite mineralization, pyrite mineralization, and final siderite deposition.

2020-KELL-36-B



Massive black sphalerite (*var.* marmatite) cut by thin quartz and pyrite-carbonate veinlets. The sample is composed in its great majority by massive sphalerite. Quartz veinlets (<1mm wide) cut the sphalerite. The veins contain scarce minute pyrite crystals (<1mm). A second vein system is composed of pale brown (carbonates?) and pyrite. Pyrite and quartz also form irregular aggregates in sphalerite. Pyrite crystals are mm-sized, and occur mostly as anhedral-subhedral grains forming millimetric aggregates.

2020-KELL-36-C



2020-KELL-36-C



Vein composed of massive sphalerite (*var.* marmatite) along with lesser proportions of pyrite and milky quartz. Pyrite forms subhedral-anhedral grains often forming millimetric aggregates that occupy interstitial space between sphalerite grains of thin veinlets that cut sphalerite.

2020-KELL-37



Black massive sphalerite (*var.* marmatite) with lesser proportions of pyrite \pm chalcopyrite. The sample is composed in its great majority by black massive sphalerite although individual sphalerite subhedral millimetric grains are also observed. Subhedral-anhedral pyrite \pm chalcopyrite crystals appear forming mm-sized aggregates or thin veinlets across the sphalerite.

2020-KELL-38



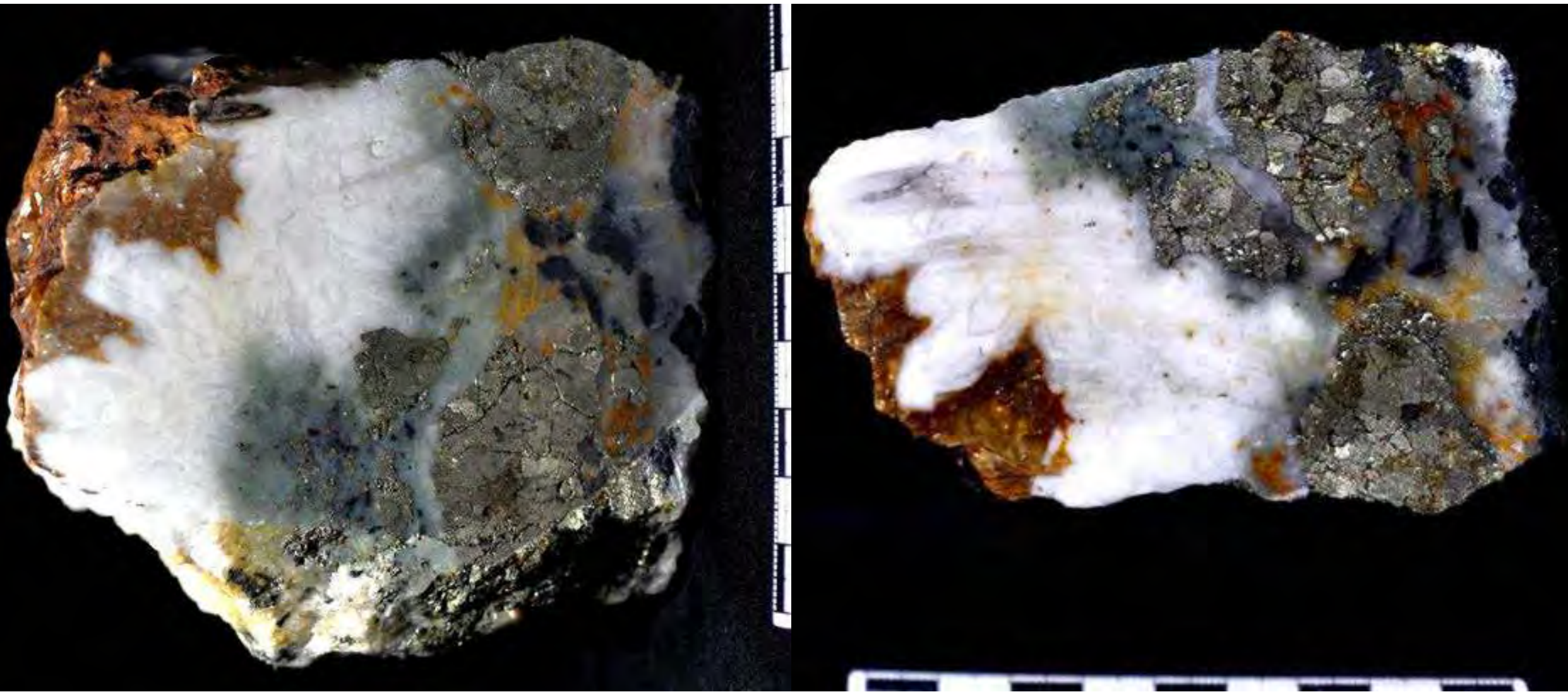
Gossan. Highly porous and orange-yellow in color. A yellow powdery mineral can correspond to a supergene Zn-rich mineralization (varlamoffite?).

2020-KELL-39



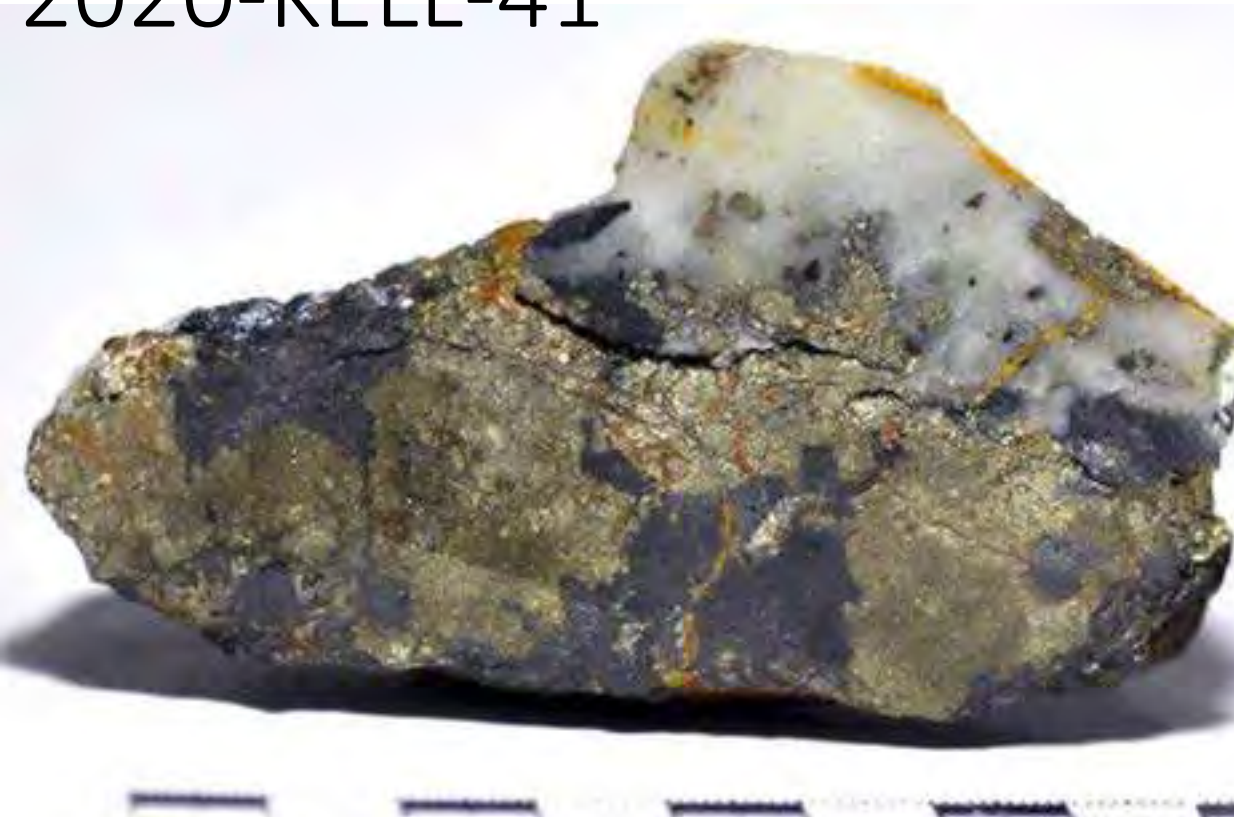
Quartz- and sulfide-rich vein. Milky quartz cements arsenopyrite and sphalerite. Lesser proportions of green of fluorite overgrow quartz crystals. Arsenopyrite forms individual crystals and aggregates <4 cm across within quartz and fluorite. Sphalerite is massive and very dark (*var.* marmatite).

2020-KELL-40



Quartz- and sulfide-rich vein. Subhedral zoned quartz crystals up to 3 cm in length show alternating milky and translucent bands. These quartz crystals overgrow vein massive milky quartz, sphalerite and arsenopyrite. Green fluorite is locally abundant and appears intergrown with the subhedral quartz crystals. Sphalerite is massive, black in color. Arsenopyrite occurs as individual crystals or in centimetric aggregates. Pale brown subhedral siderite crystals occupy the interstitial space between the subhedral quartz crystals.

2020-KELL-41

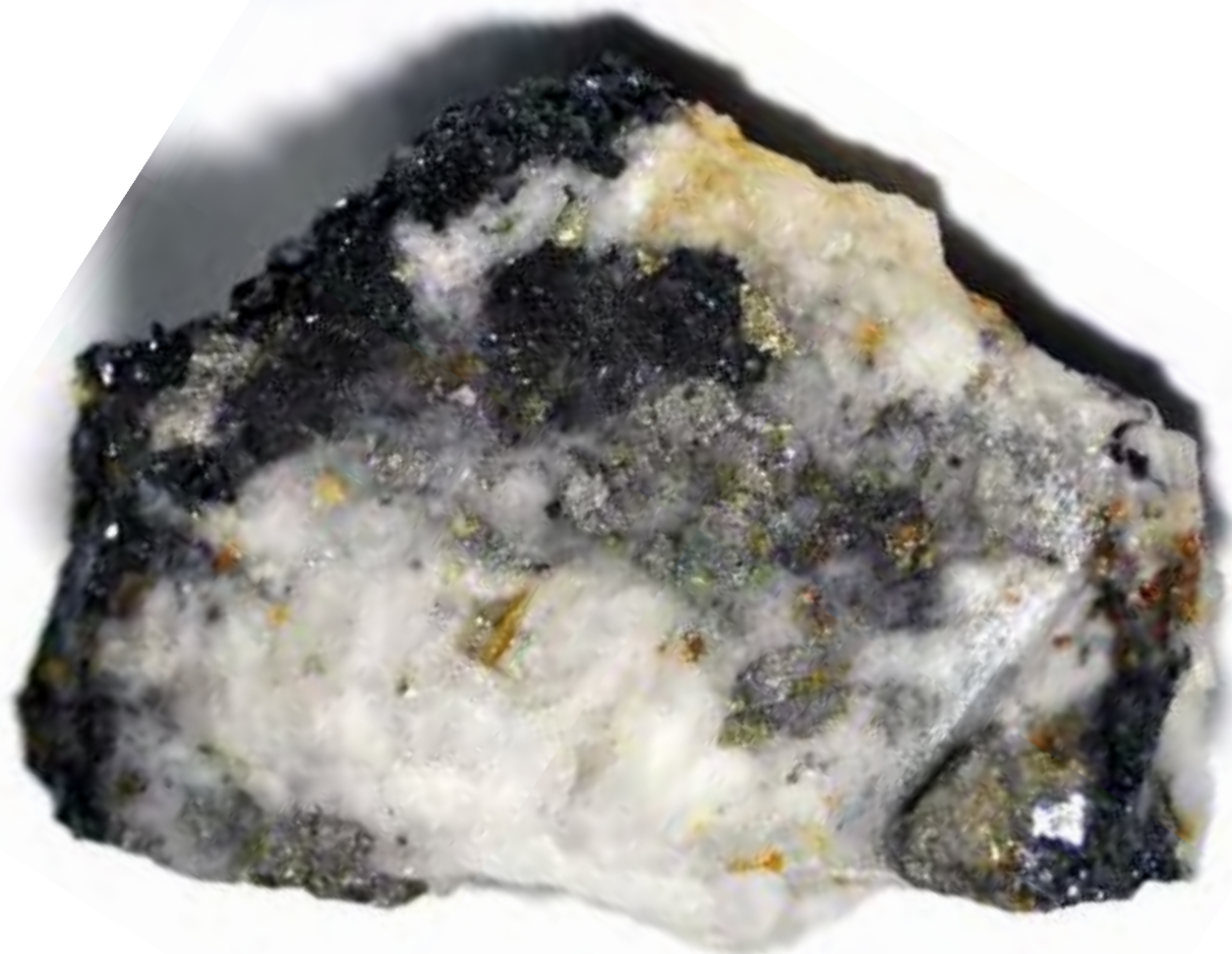


2020-KELL-41



Mineralized vein composed of sphalerite, pyrite, milky massive quartz, and siderite. Sphalerite is massive and dark grey-black in color (*var. marmatite*). Pyrite forms millimetric- centimetric aggregates of subhedral-euhedral millimetric crystals and is intergrown with mm-sized subhedral platy siderite crystals. Veinlets of siderite-pyrite cut across sphalerite and milky quartz.

2020-KELL-42



4 cm



2020-KELL-42



2020-KELL-42



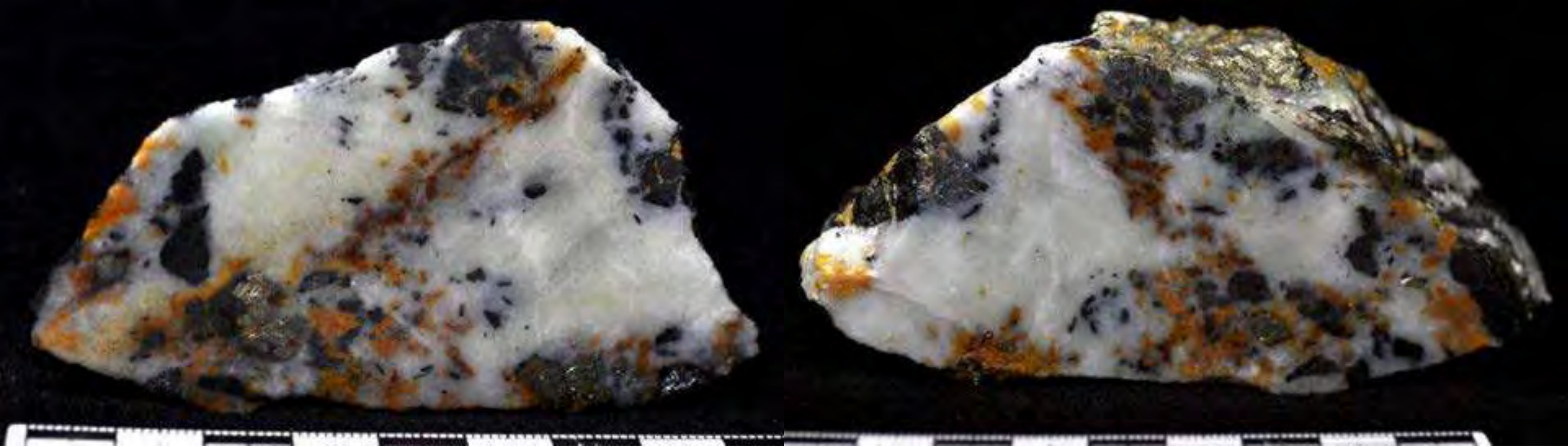
Mineralized vein composed of sphalerite, quartz, pyrite, siderite and lesser proportions of arsenopyrite, and fluorite. Sphalerite in the sample is massive and black in color. Arsenopyrite forms millimetric aggregates of subhedral crystals. Quartz is milky and forms mm- to cm-sized euhedral to subhedral crystals that are intergrown and grow on top of the sphalerite and arsenopyrite. Locally, quartz seem to grow over green fluorite, but the textural relationship is unclear in this sample. Pyrite forms mm- to cm-sized aggregates of subhedral-euhedral millimetric crystals which replaced and vein sphalerite and arsenopyrite. Veins of pale brown subhedral siderite crystals cut the whole assemblage described before.

2020-KELL-43



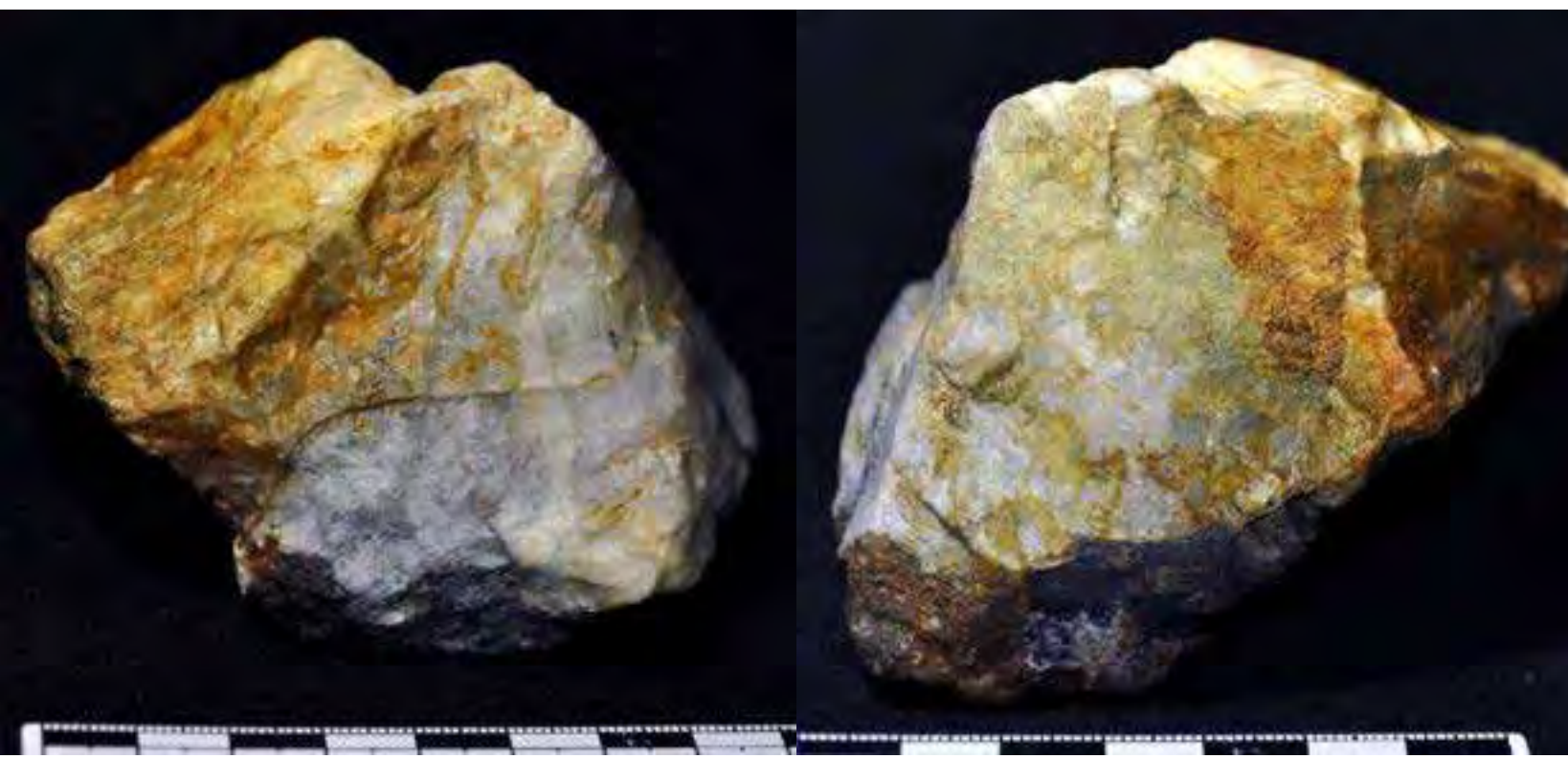
Mineralized vein composed mostly of quartz, pyrite, and lesser amounts of arsenopyrite. Massive milky quartz is locally overgrown by subhedral semi-translucent quartz crystals up to 0.5 cm long. Pyrite appear forming individual crystals and centimetric aggregates within secondary porosity in quartz. Arsenopyrite is intergrown with the quartz and forms millimetric aggregates of subhedral crystals.

2020-KELL-44

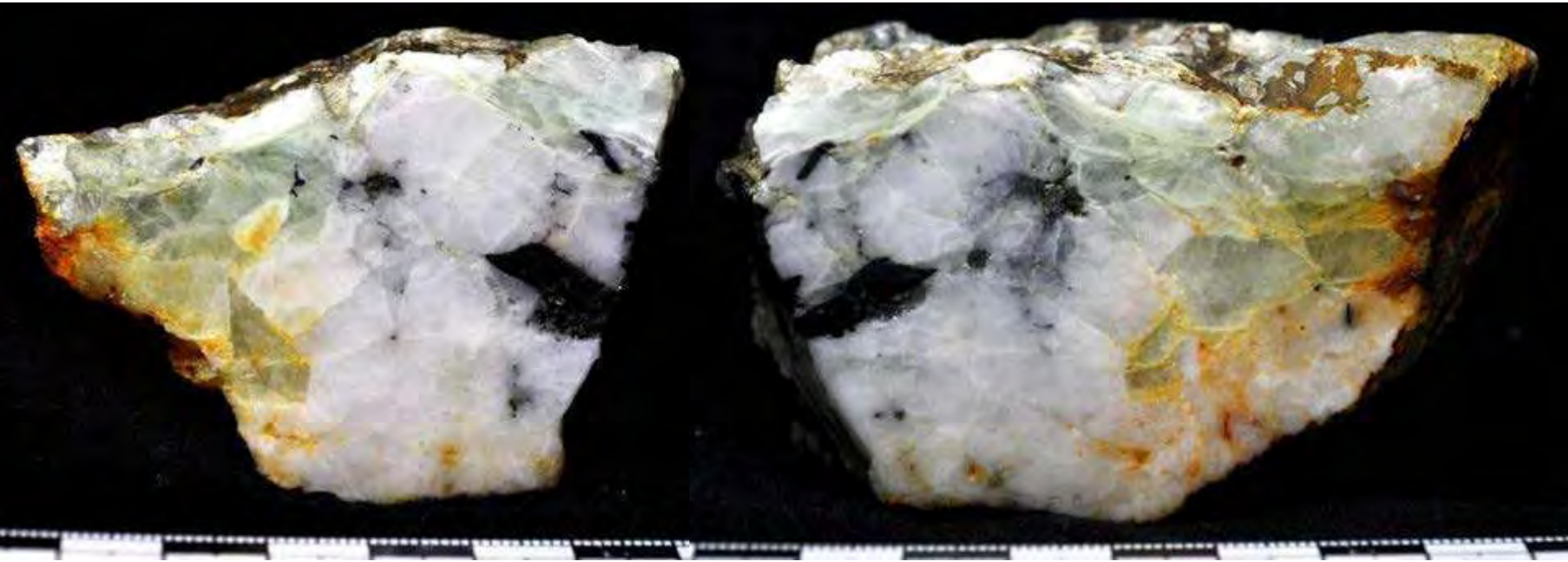


Mineralized vein with internal brecciated texture composed mostly of quartz, sphalerite, pyrite, and carbonates. Quartz is the most abundant phase in the sample and is granular, milky and massive. Quartz cements grains and fragments of sulfide minerals. Sphalerite is massive, black, and appears as mm- to cm-sized angular clasts. Some sphalerite clasts are cut by milky quartz veinlets. Pyrite is less abundant than sphalerite, forms individual crystals and centimetric aggregates of subhedral millimetric crystals, and partially replaced sphalerite. Patches of pale brown subhedral siderite crystals cut the whole assemblage described before.

2020-KELL-45-A



2020-KELL-45-A



Mineralized vein sample composed largely of quartz and fluorite and lesser amounts of sulfides, and carbonates. Quartz is milky and massive. Green fluorite is intergrown with the quartz with some distinguishable subhedral millimetric crystals. A greyish sulfide forms centimetric aggregates (arsenopyrite?) with a blue patina of oxidation. Elongated to bladed black crystals up to 1 cm long, probably of wolframite, are intergrown with the milky quartz. Pale brown subhedral siderite crystals line local secondary porosity in quartz.

2020-KELL-45-B



2020-KELL-45-B

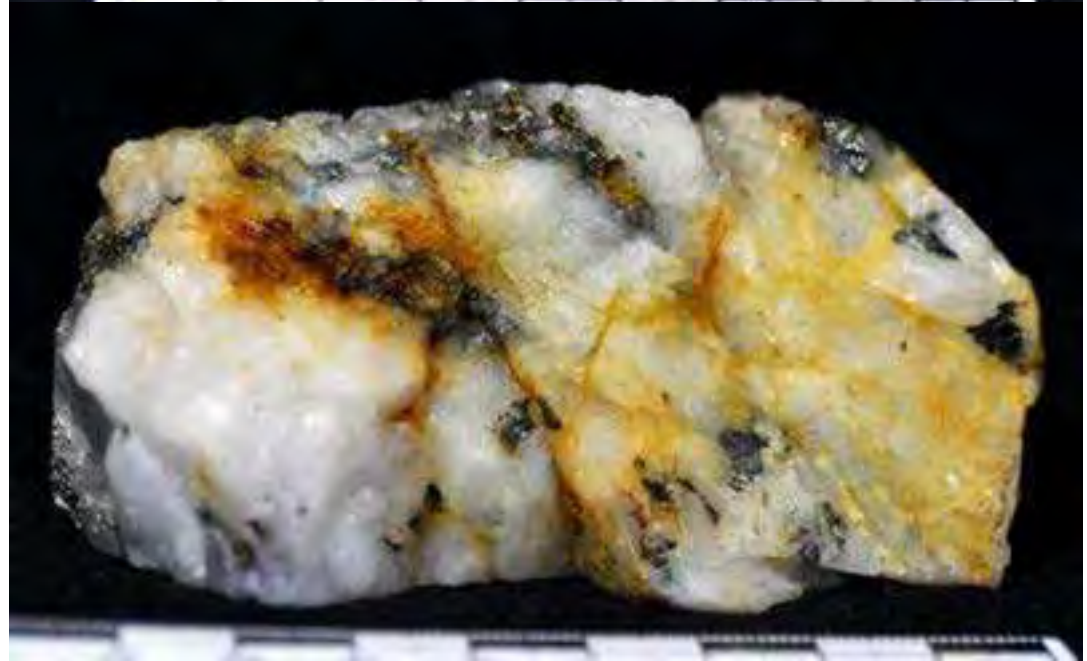


Mineralized vein composed mostly of quartz and lesser amounts of sulfides and Fe-rich carbonates. Milky quartz forms subhedral to euhedral crystals with basal sections up to 1 cm across. A greyish sulfide forms centimetric aggregates (arsenopyrite?) and is partly replaced by pyrite. Fe-rich carbonate (siderite) is pale-brown in color and appears mostly occupying interstitial space between quartz crystals.

2020-KELL-45-C



2020-KELL-45-C



2020-KELL-45-C

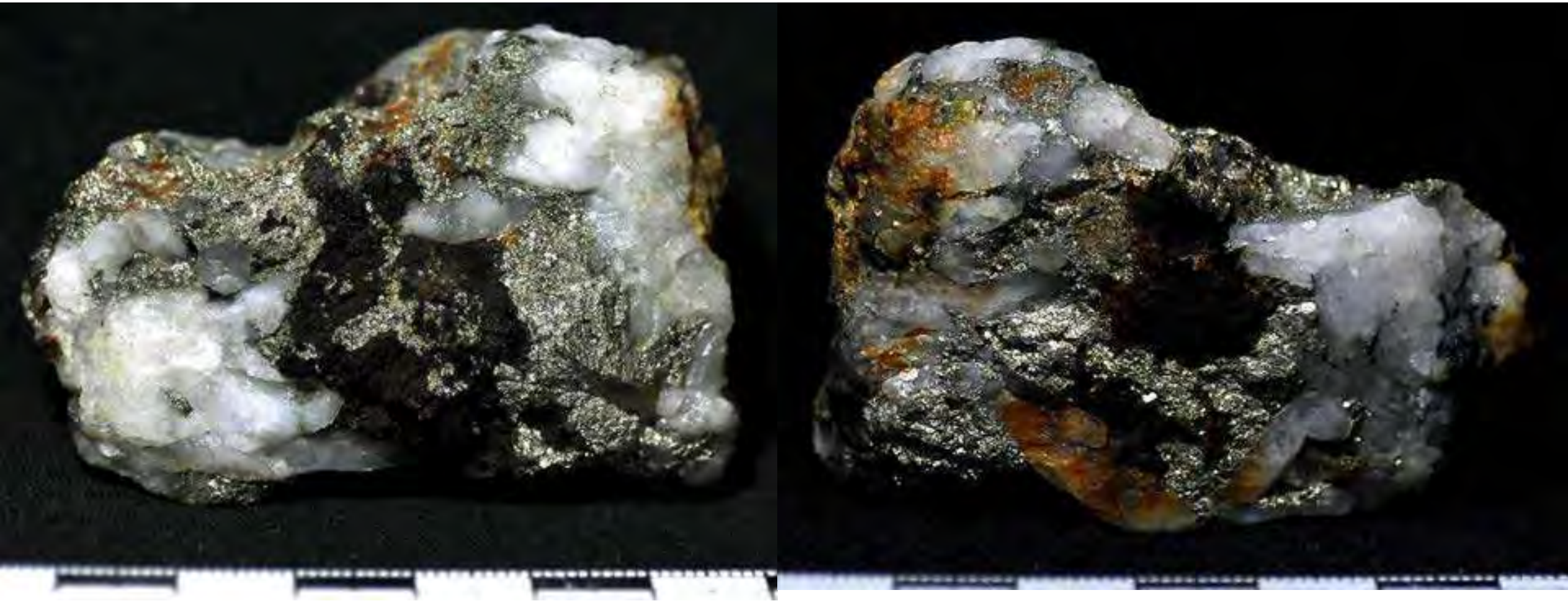


Mineralized vein composed largely of quartz, pyrite and Fe-rich carbonates. Quartz is milky and forms mm- to cm-sized subhedral to euhedral crystals. Pyrite and Fe-rich carbonates appear lining fractures and interstitial space between the quartz crystals. Pyrite forms mm- to cm-sized aggregates of mm-sized subhedral to euhedral grains.

2020-KELL-46



2020-KELL-46



Mineralized vein composed of quartz, pyrite, arsenopyrite, and Fe-rich carbonates. Quartz crystals are subhedral and prismatic (up to 5 cm long) with a semi-translucent white color. Quartz forms aggregates of several prismatic crystals. Pyrite, arsenopyrite and Fe-rich carbonates appear mostly occupying interstitial space between quartz crystals. Arsenopyrite is massive, and pyrite is mostly massive but forms some millimetric subhedral crystals.

2020-KELL-47



2020-KELL-47

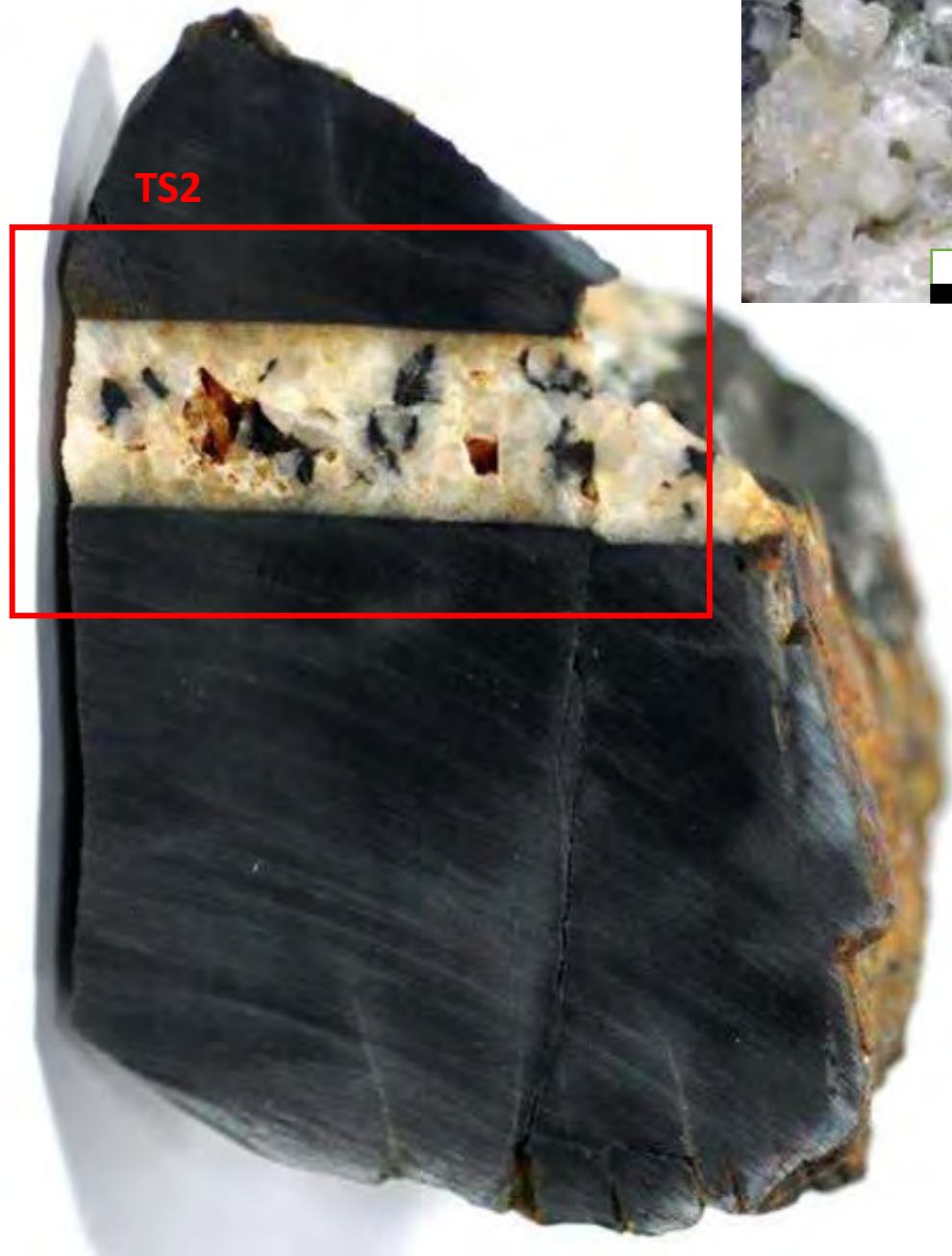


Quartz-cassiterite vein. Quartz shows centimetric-millimetric subhedral prismatic crystals. Cassiterite, which is particularly abundant in this sample, forms crystals that are subhedral-euhedral and intergrown with quartz. The cassiterite crystals are prismatic, millimetric, and show two different colors: black and brownish. The black cassiterite crystals show a semi-metallic lustre, while the brownish cassiterite crystals are translucent and show a more adamantine lustre.

2020-KELL-48



2020-KELL-48



2020-KELL-48



Quartz-tourmaline-cassiterite vein. The vein is 1.3 cm thick. Quartz forms mm- to cm-sized subhedral-euhedral prismatic crystals. There is a geode of subhedral quartz crystals. Cassiterite crystals are up to 5 mm across, subhedral-euhedral, prismatic, and brownish in color, and are intergrown with quartz crystals. Tourmaline forms millimetric aggregates of very fine needles of dark greenish color and that are intergrown with vein quartz.

2020-KELL-49



2020-KELL-49



Quartz-pyrite-arsenopyrite vein. Quartz crystals are subhedral, prismatic (up to 5 cm long), white in color, and translucent. Quartz crystals form aggregates of several prismatic crystals. Pyrite and arsenopyrite appear mostly occupying interstitial space between quartz crystals. Pyrite is massive with some distinguishable millimetric subhedral crystals. Arsenopyrite is found in lesser proportions than pyrite and form some subhedral crystals.

2020-KELL-50-A



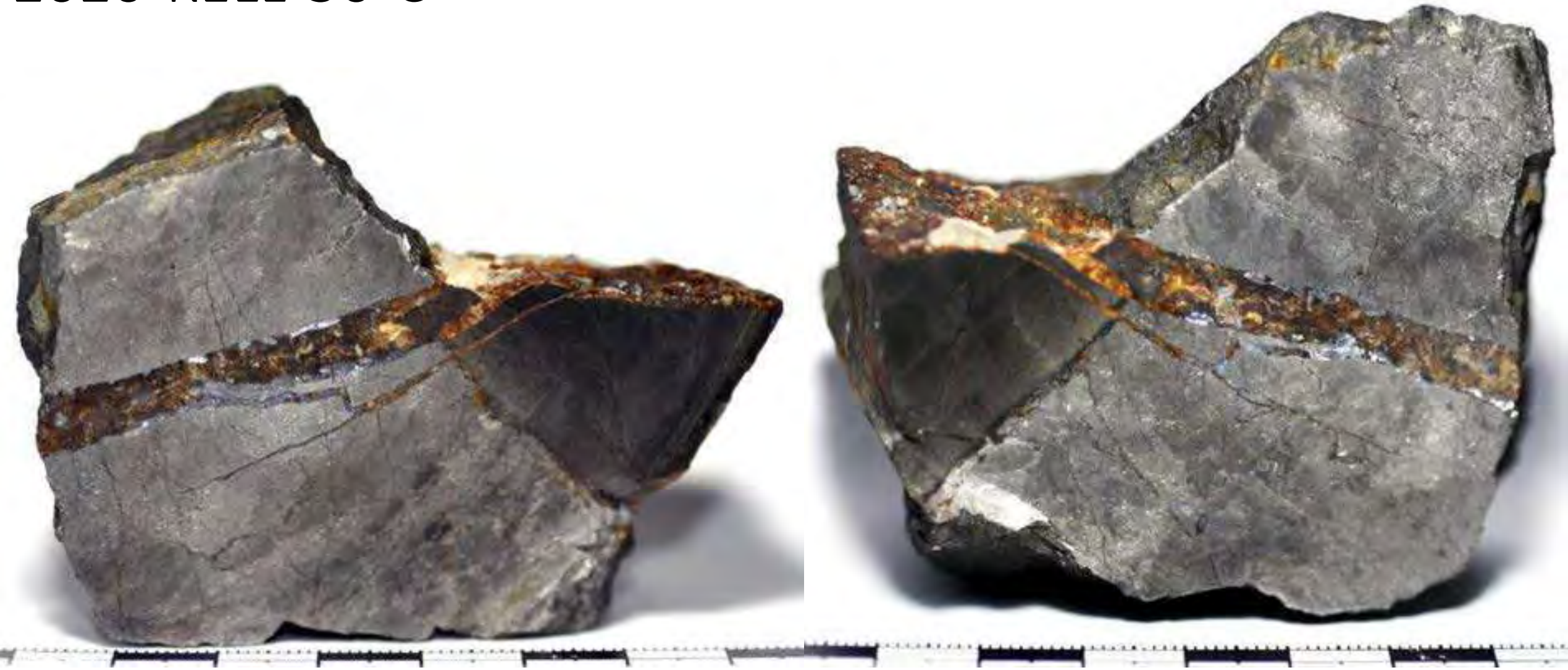
Mineralized vein composed of arsenopyrite and fluorite, along with lesser proportions of pyrite and quartz. The sample is mainly composed by massive arsenopyrite with some prismatic subhedral millimetric crystals that can be distinguished. Green fluorite millimetric subhedral crystals are intergrown with arsenopyrite. Granular quartz is much less abundant than fluorite. Pyrite is scarce and appear forming aggregates <5 mm across along with the arsenopyrite.

2020-KELL-50-B



Mineralized vein composed of quartz and arsenopyrite. Quartz forms translucent subhedral crystals up to 1 cm in length. Arsenopyrite forms subhedral-euhedral prismatic crystals (up to two cm long), which appear intergrown with quartz.

2020-KELL-50-C



Massive arsenopyrite is cut by a galena-Fe-rich carbonate vein. The vein contact is sharp. Galena concentrates mostly at the rims of the vein; some euhedral cubic galena crystals are distinguished. Fe-rich carbonates are the most abundant phases in the veinlet and form millimetric subhedral brownish translucent crystals. Quartz, which is relatively scarce in the vein, forms millimetric aggregates of subhedral crystals towards the central part of the vein.

2020-KELL-51-A



Mineralized quartz-cassiterite-Fe-rich carbonate vein. Euhedral-subhedral semi-translucent quartz crystals are up to 1.5 cm in length. Iron-rich carbonates form mm-sized brown, platy crystals that form aggregates on top of vein quartz. Pyrite forms millimetric aggregates of <1mm crystals.

2020-KELL-51-B



Quartz- and carbonate-rich vein with internal cockade textures. Translucent euhedral quartz crystals up to 1.5 cm long commonly show zoning. These quartz crystals form radial aggregates around host rock clasts. Iron -rich carbonate grains are reddish brown in color and mm-sized, often show platy to lens-shaped habits, and appear occupying interstitial space between vein quartz crystals. Pyrite is scarce and appear forming individual crystals (up to 0.5cm) and aggregates <2 cm in the host-rock and in the vein.

2020-KELL-51-C

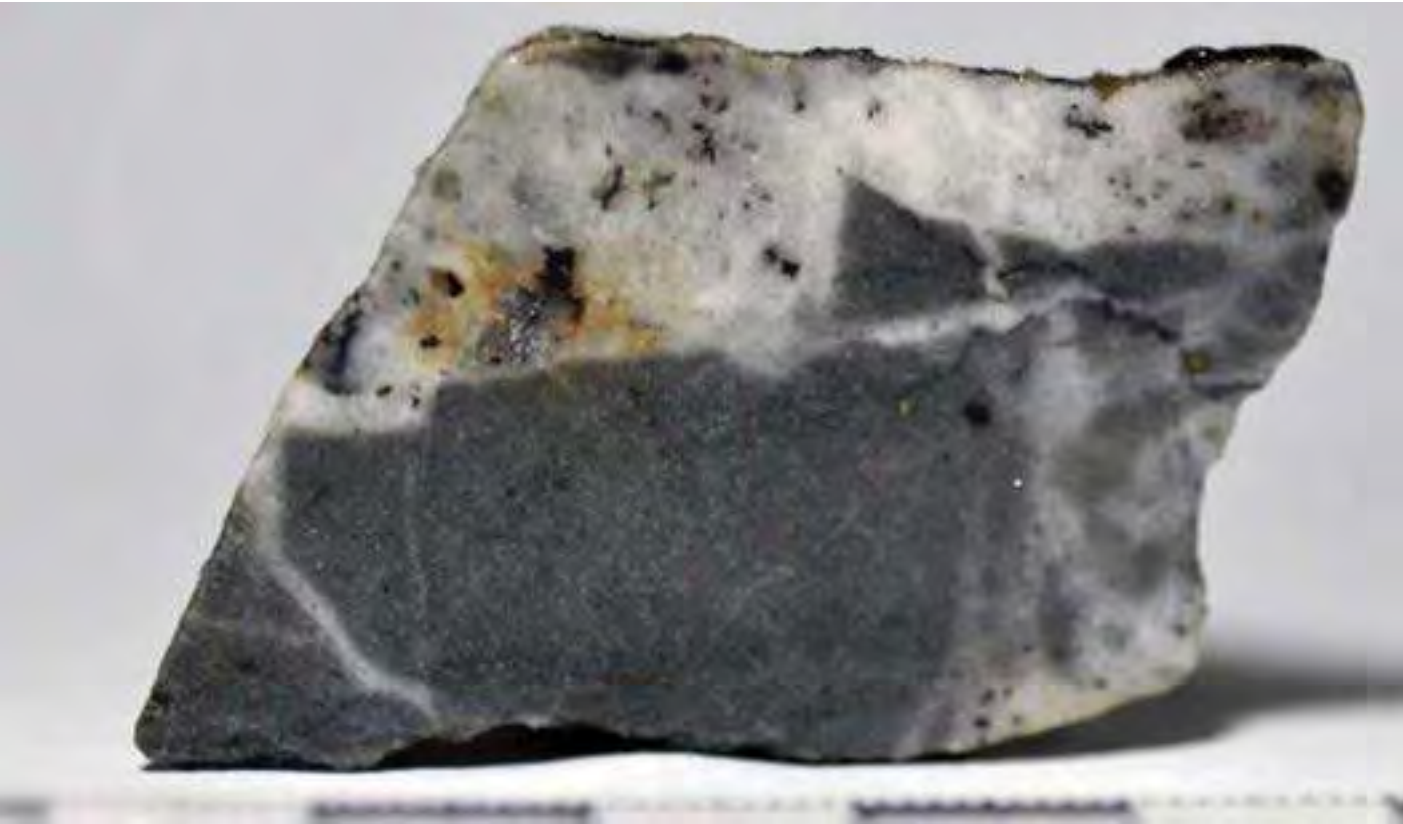


2020-KELL-51-C

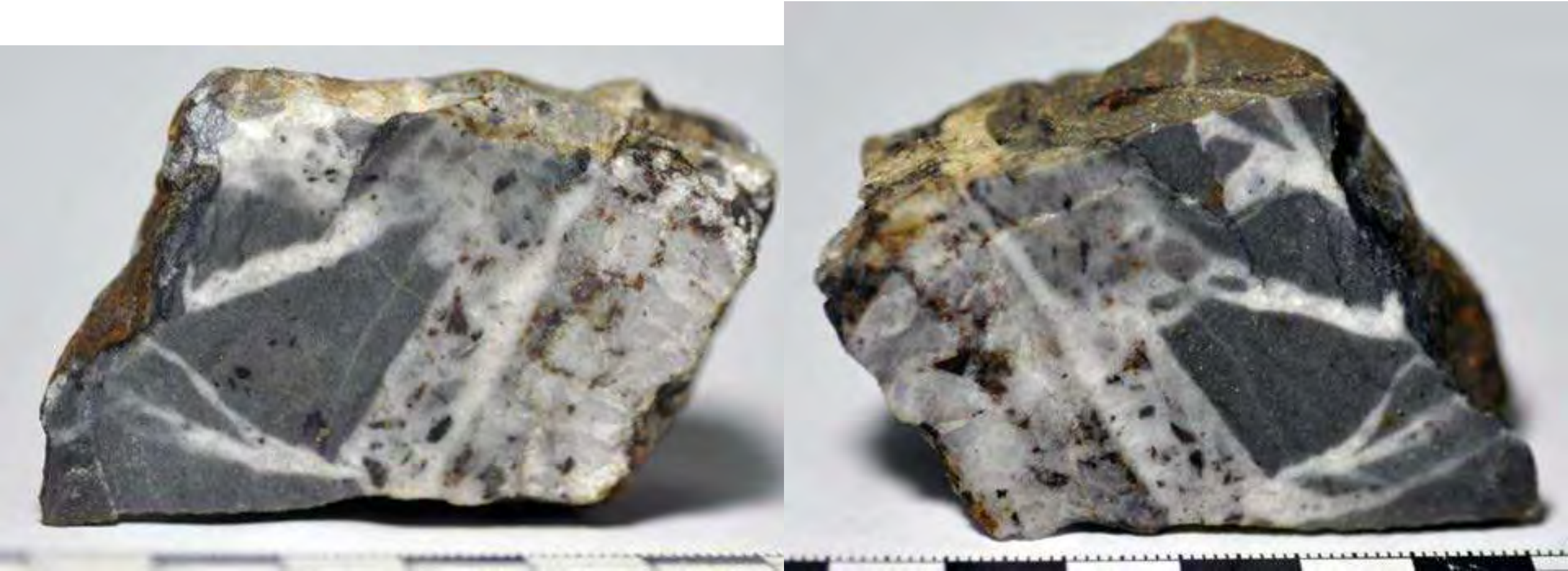


Quartz-cassiterite-tourmaline veinlets (~1mm thick). In the veinlets, milky quartz is the most abundant phase and cements cassiterite crystals (<1mm). The veinlets are surrounded by a dark (almost black) halo which is probably composed of tourmalines. Pyrite, which is scarce in the sample, forms euhedral millimetric crystals disseminated in the host- rock.

2020-KELL-52-A



2020-KELL-52-A



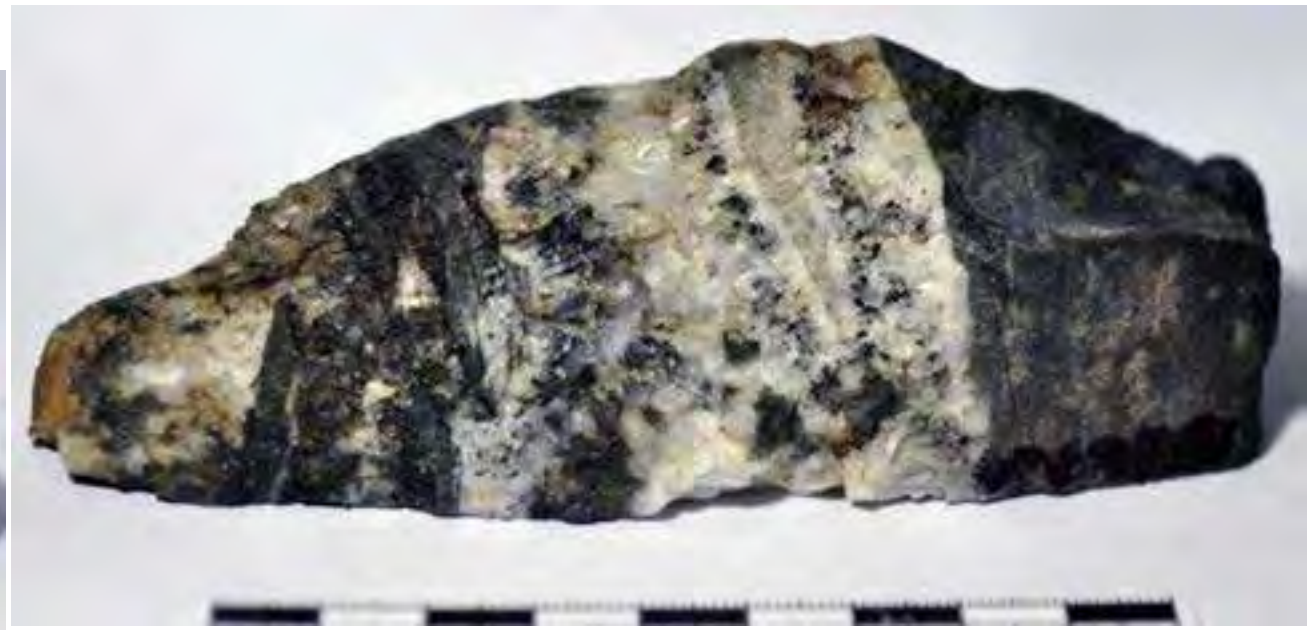
Hydrothermal breccia. The breccia is composed of centimetric angular rock clasts derived from hosting Catavi Fm. quartzite. Often, clasts show jigsaw-fit textures. These clasts are cemented by milky quartz. The breccia is cut by a centimetric quartz vein. In the vein, euhedral to subhedral translucent quartz crystals up to 1 cm long are intergrown with sphalerite subhedral black crystals. Pyrite and cassiterite occur as mm-sized euhedral/subhedral grains disseminated within both the rock clasts and vein quartz.

2020-KELL-52-B

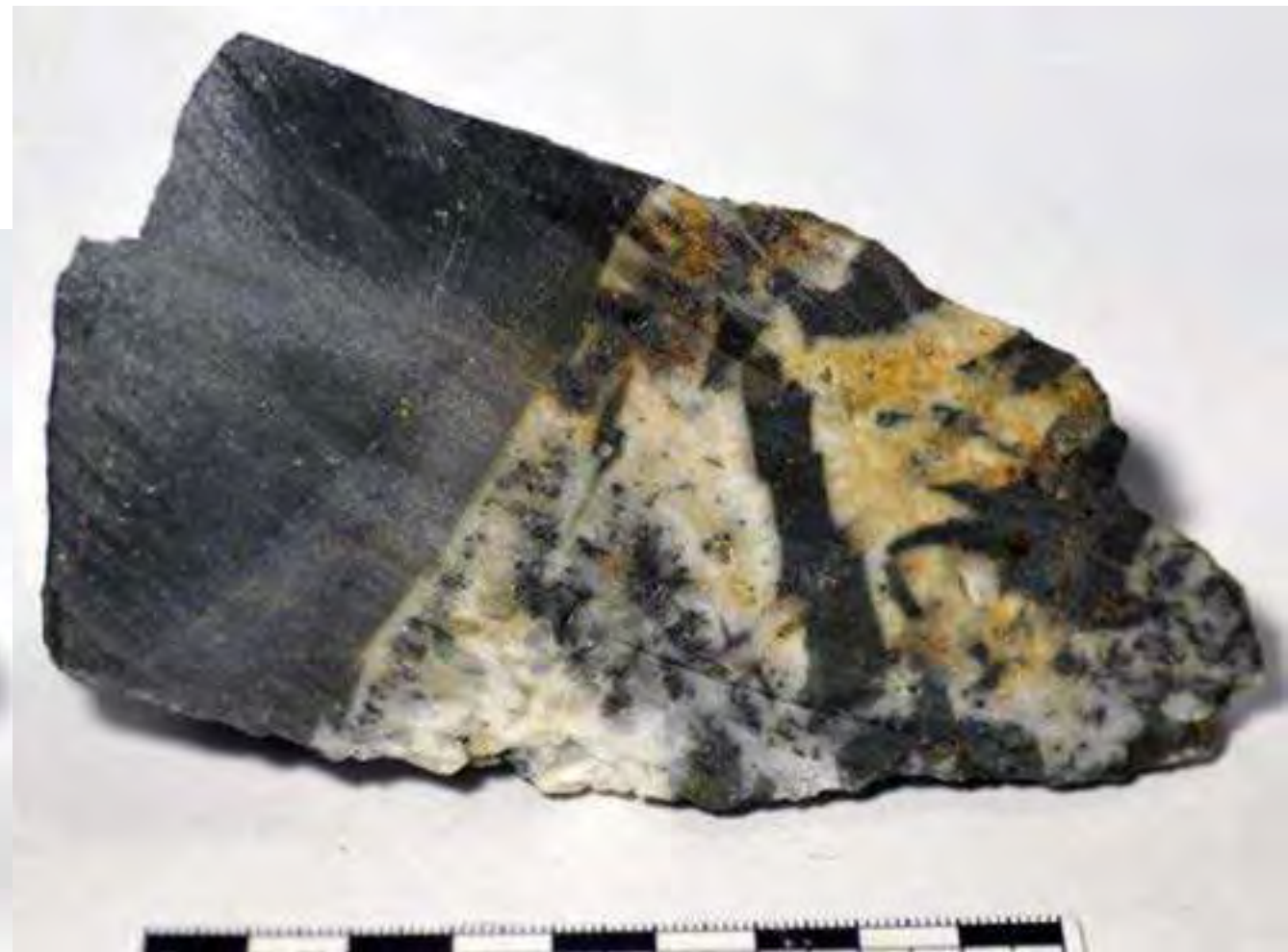


Mineralized quartz-carbonate-sulfide vein. From the contact with the host rock to the core of the vein, there is a gradation from euhedral to subhedral translucent quartz crystals up to 2 cm long depicting comb textures to Fe-rich carbonates. Quartz crystals show well-defined growth. Iron-rich carbonates form dark brown (partially oxidized), mm-sized, lens-shaped crystals. Pyrite and chalcopyrite are scarce and appear forming aggregates <0.5 cm intergrown with carbonates in the central suture of the vein.

2020-KELL-52-C



2020-KELL-52-C



Internally brecciated vein. It is composed mostly by quartz, along with lesser proportions of cassiterite and sulfides. Quartz forms euhedral to subhedral translucent crystals up to 0.5 cm in length. Tourmaline (?) acicular black crystals are observed towards the central part of the vein. Cassiterite crystals are brown in color and mm-sized and occur as aggregates towards the central part of the vein. Pyrite is scarce and appear forming aggregates <0.5 cm.

2020-KELL-52-D



2020-KELL-52-D

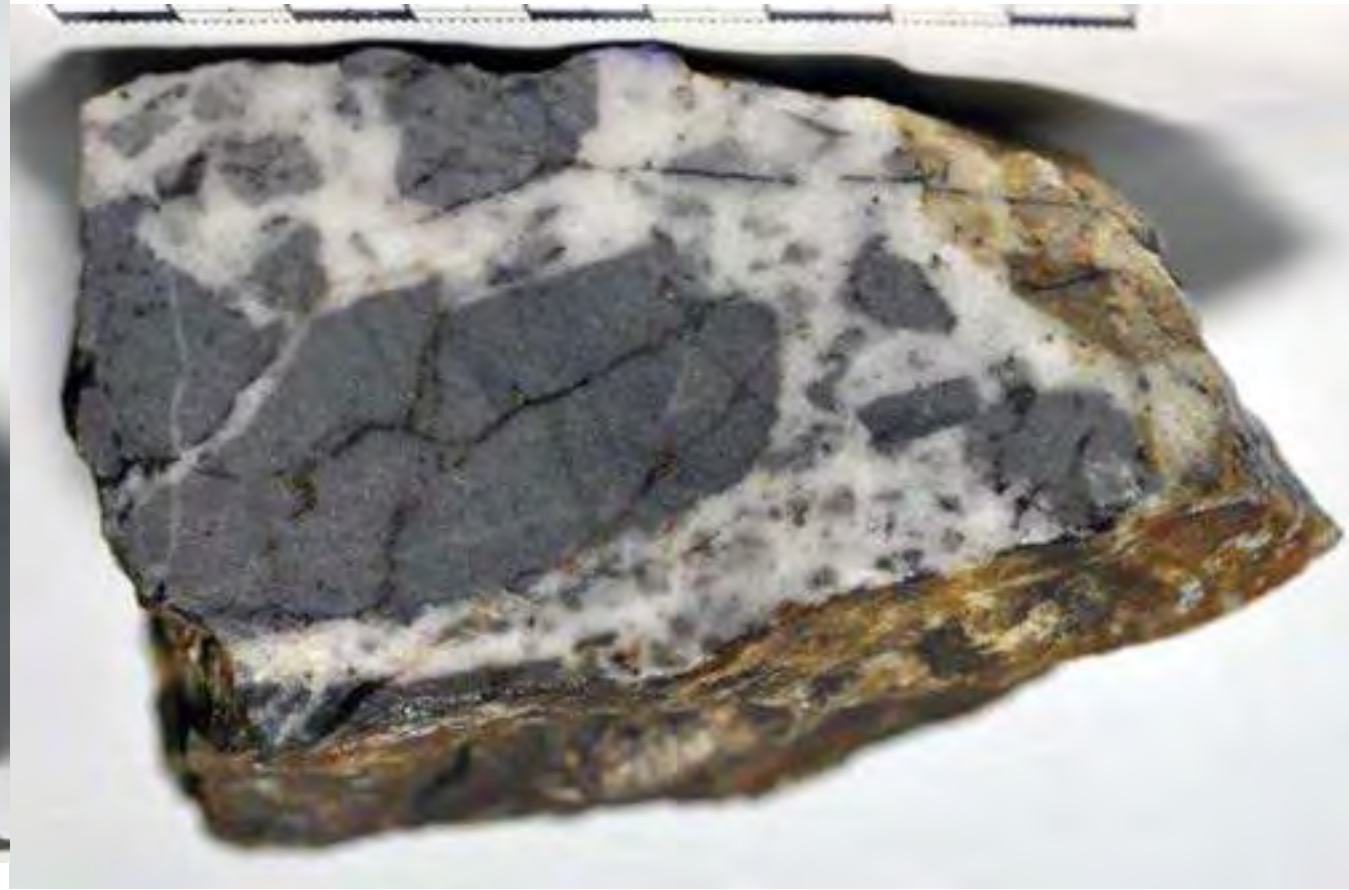


Mineralized quartz- and carbonate-rich vein. Quartz crystals are milky, zoned, subhedral, and up to 2 cm long. Scarce dark brown mm-sized cassiterite crystals occur intergrown with vein quartz. Pyrite is scarce and appears forming individual crystals and aggregates <2 mm in the vein quartz. Towards the core of the vein, quartz is overgrown by a thick band composed of Fe-rich, dark brown carbonate zoned crystals.

2020-KELL-52-E

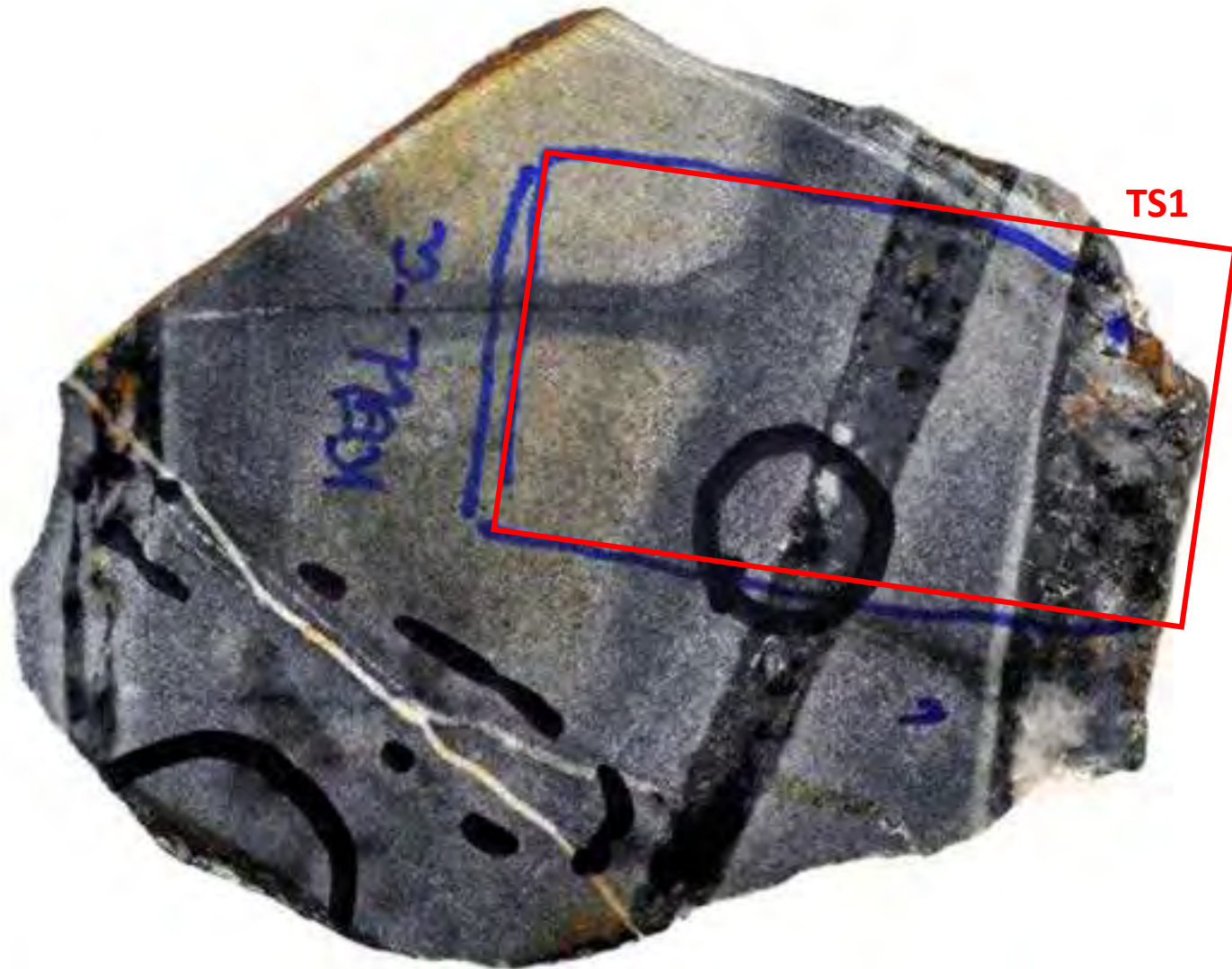


2020-KELL-52-E



Vein with internally brecciated texture. Centimetric angular rock clasts derived from hosting Catavi Fm. quartzite draw jigsaw-fit textures. Pyrite occurs in low amounts in the rock clasts as individual crystals and aggregates <2 mm. The clasts are cemented and veined by milky quartz. The whole assemblage is cut by thin stringers of Fe-rich carbonate.

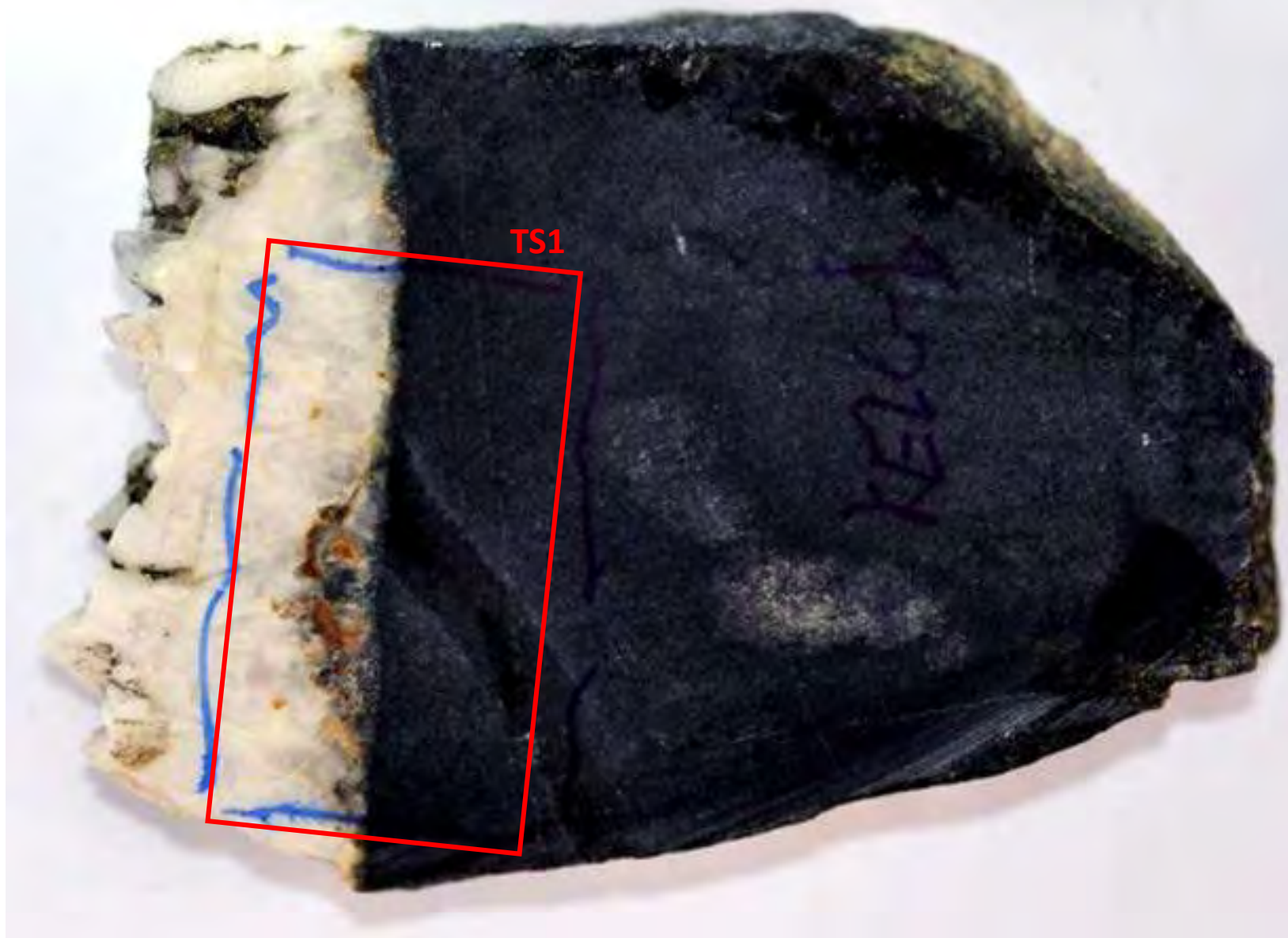
KELL-A



TS1

Tourmaline-, quartz-, and cassiterite-rich veins. The veins are centimetric and mainly composed by millimetric aggregates of radial acicular black tourmaline crystals. Translucent, subhedral millimetric quartz crystals are intergrown with tourmaline aggregates towards the central part of the vein. Cassiterite crystals are brown in color and sub-mm-sized. Veins show a 1-mm-wide white alteration halo.

KELL-B



Two different vein types are observed in the sample. The first are quartz-rich. In this vein type, euhedral to subhedral translucent quartz crystals up to 2 cm long are oriented perpendicular to the vein contacts thus drawing comb textures. Along the vein contact with the host rock, a <1-mm-thick band of black tourmaline (?) is observed. Carmel-colored sub-mm-sized cassiterite crystals concentrate along the vein borders. Comb quartz is overgrown by fine-grained arsenopyrite and pyrite towards the central section of the vein. The second vein type is almost monomineralic and composed of a black mass (tourmaline?).

Appendix C

Petrographic descriptions - Thin sections with tourmaline

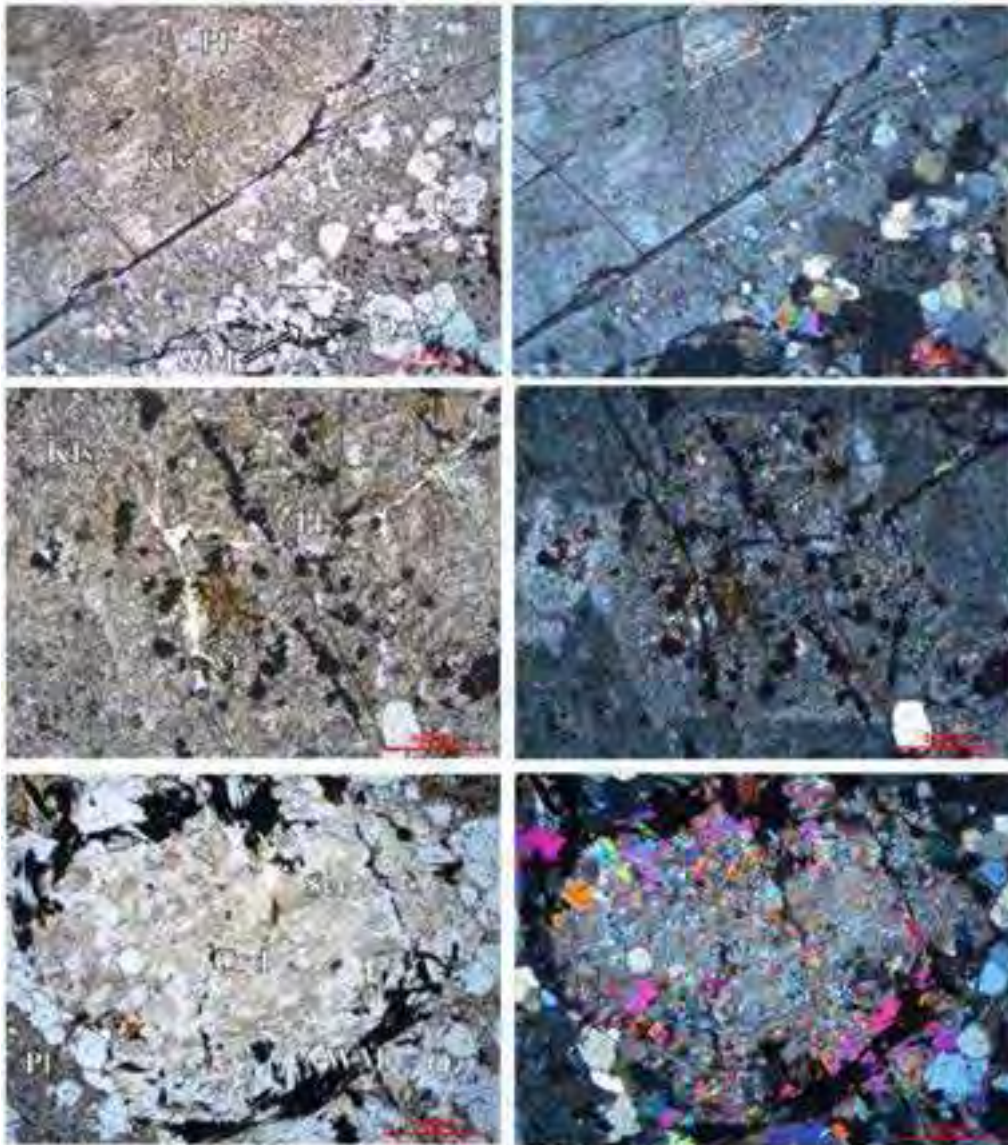


CHACALTAYA STOCK

2020-KELL-19-TS1

Minerals: quartz (Qz) + plagioclase (Pl) + white mica (WM) + sericite (Ser) + K-feldspar (Kfs) + cordierite (Crd)

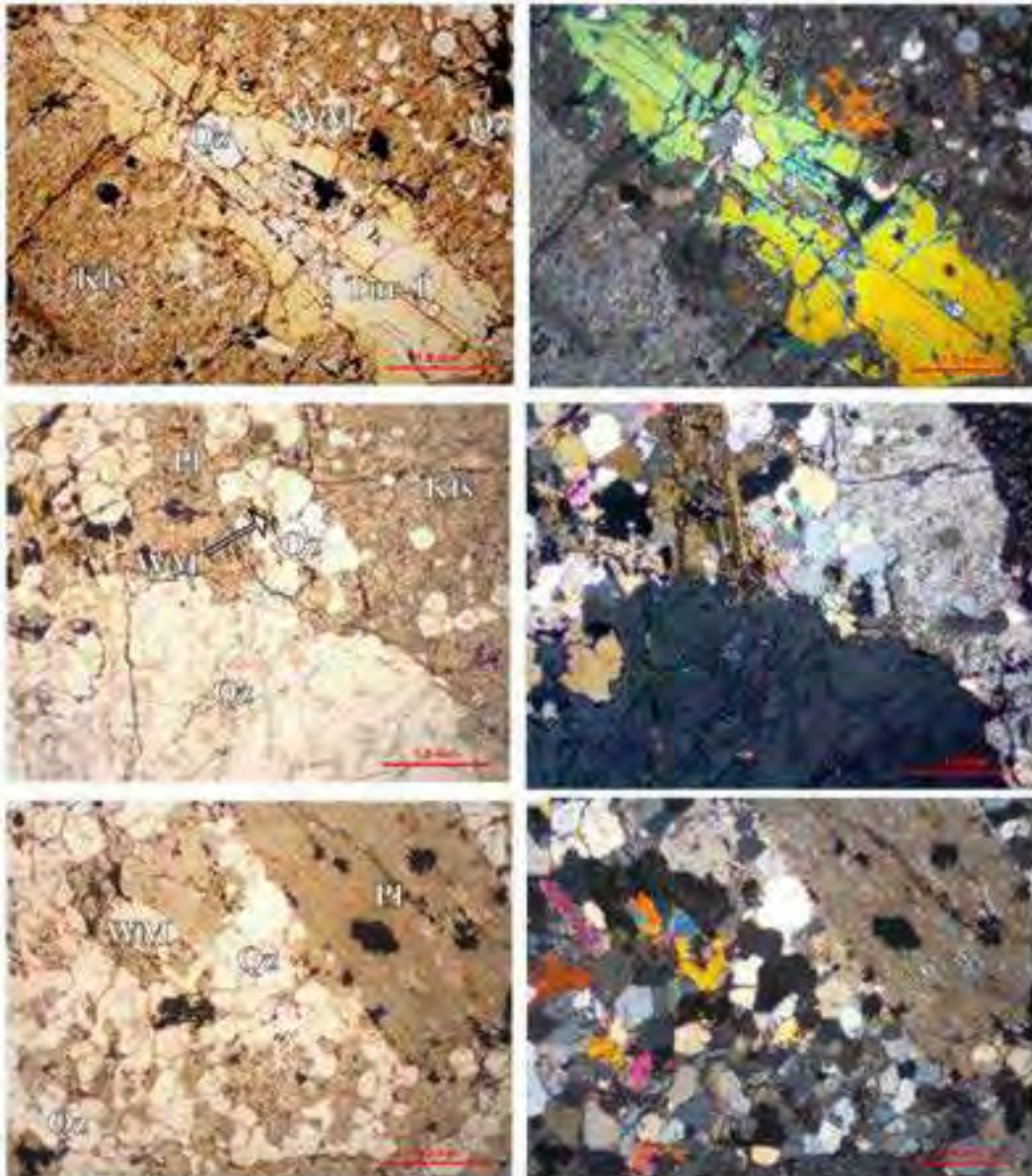
Granitic assemblage of quartz, plagioclase, and white mica. Inside this groundmass, K-feldspar megacrysts with sizes up to 5 cm show inclusions of quartz crystals mostly parallel to growth faces and more locally, plagioclase inclusions. Feldspars are partly altered to sericite. Cordierite crystals are pervasively altered to sericite (pinitization).

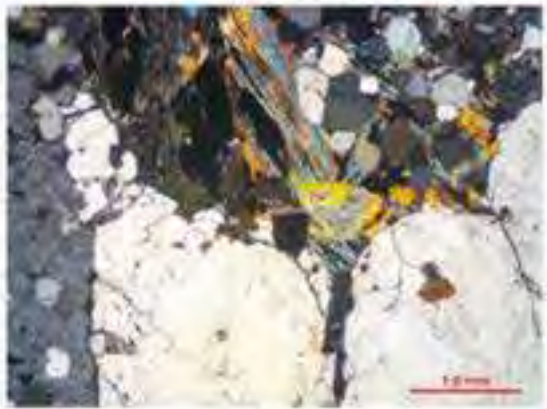
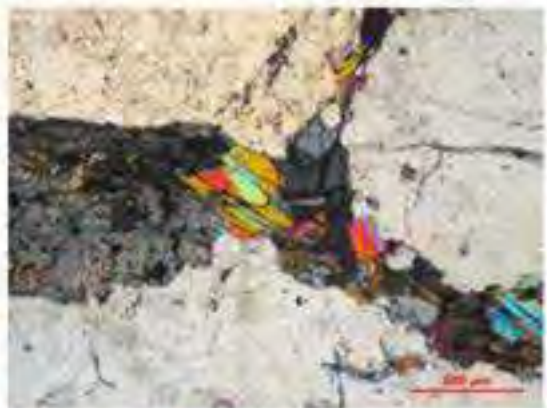
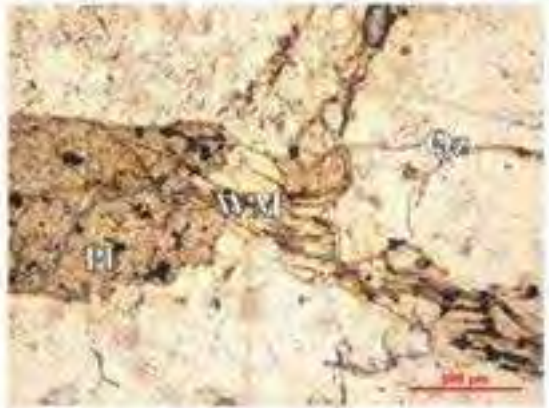
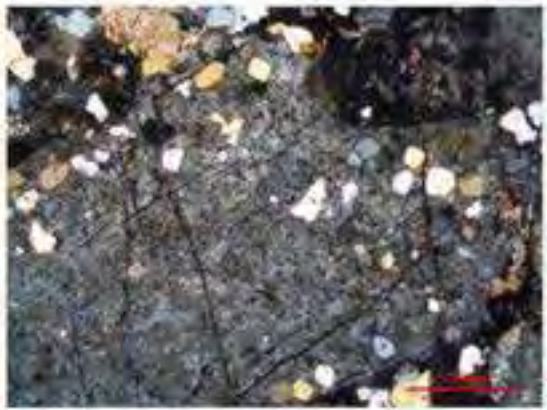
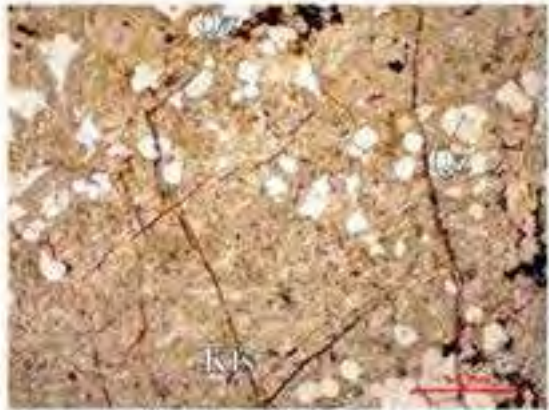


2020-KELL-19-TS6

Minerals: quartz (Qz) + plagioclase (Pl) + white mica (WM) + sericite (Ser) + K-feldspar (Kfs) + tourmaline-1 (Tur-1)

Granitic assemblage of quartz, plagioclase and white mica. Inside this groundmass, there are several megacrysts of K-feldspar, plagioclase crystals and quartz crystals. The K-feldspar megacrysts include quartz and plagioclase inclusions. Feldspars are partly altered to coarse and fine-grained (sericite) white mica, quartz and locally, tourmaline.



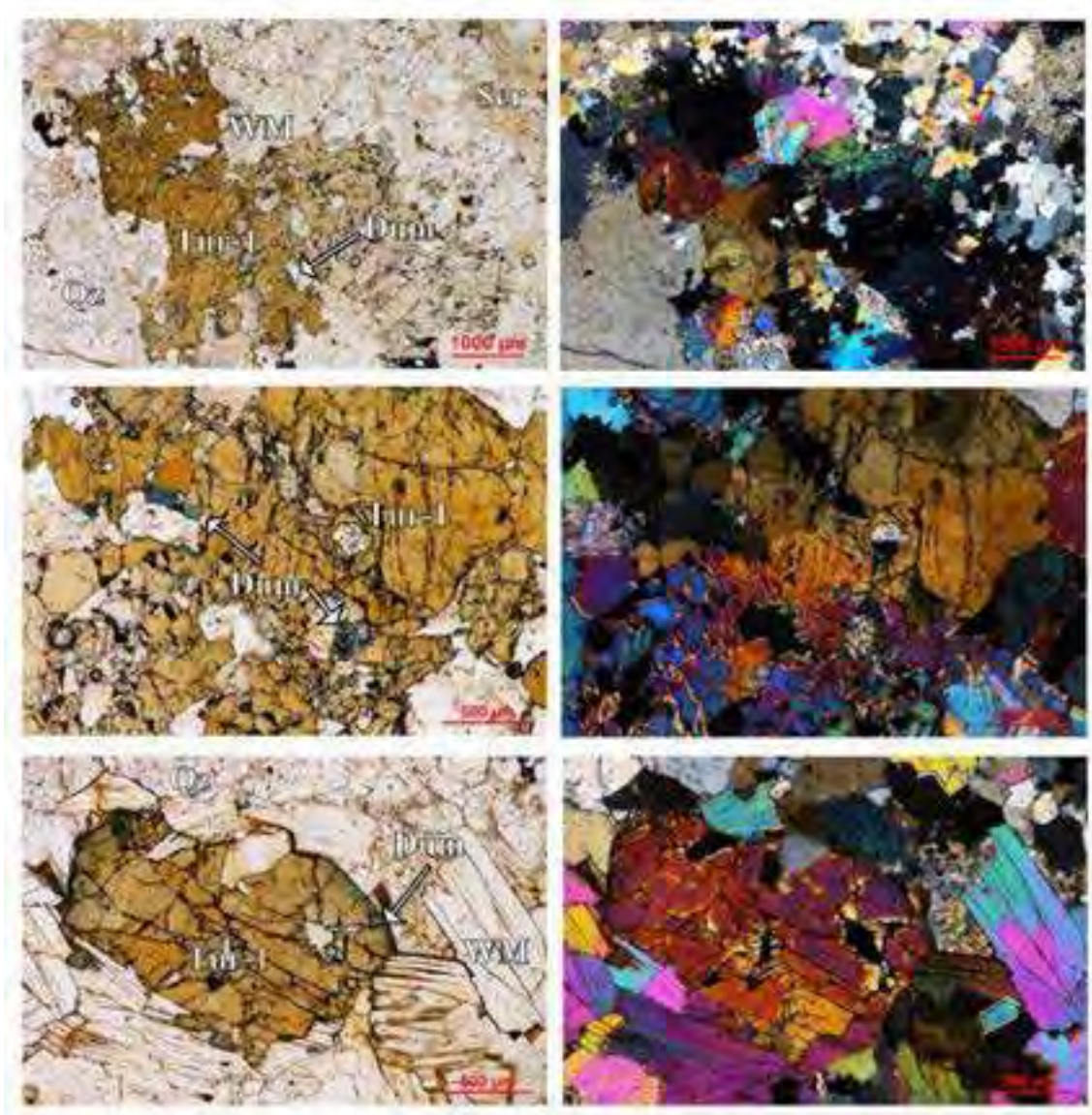


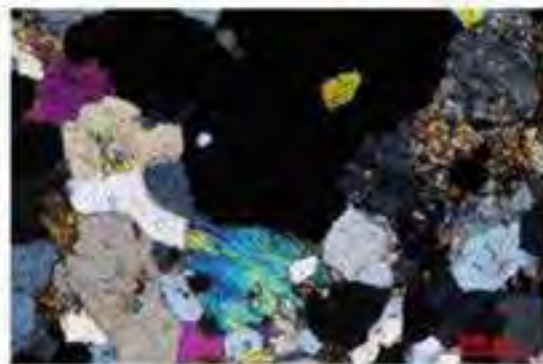
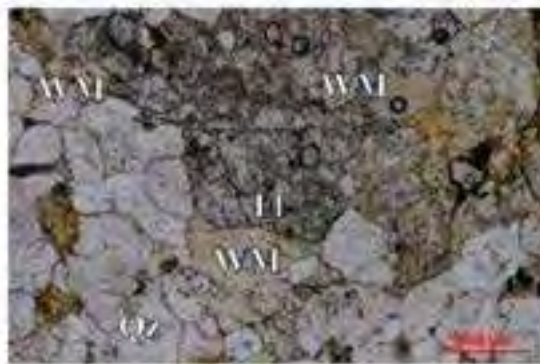
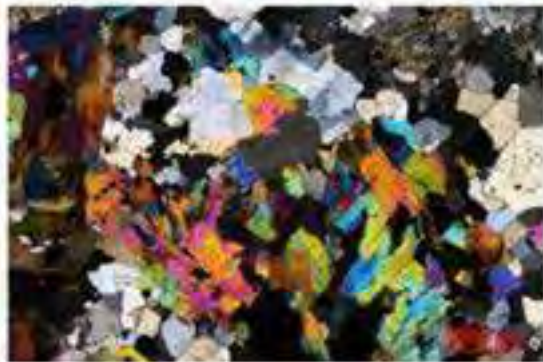
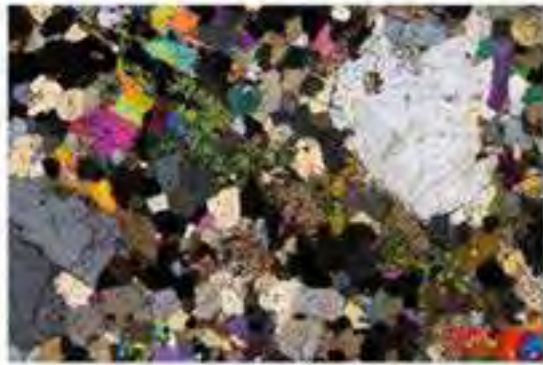
CHACALTAYA GREISEN

2020-KELL-22-B-TS1

Minerals: quartz (Qz) + tourmaline-1 (Tur-1) + white mica (WM) + sericite (Ser) + fluorite (Fl) + dumortierite (Dum)

Rock sample with conspicuous secondary porosity as a product of alteration. Coarse-grained anhedral to subhedral skeletal orange tourmaline crystals are locally overgrown by dumortierite and intergrown with medium-grained white mica and quartz. White mica tablets have a decussate texture. Sericite replacing the aforementioned assemblage occurs only locally. Fluorite appears lining secondary rock porosity.



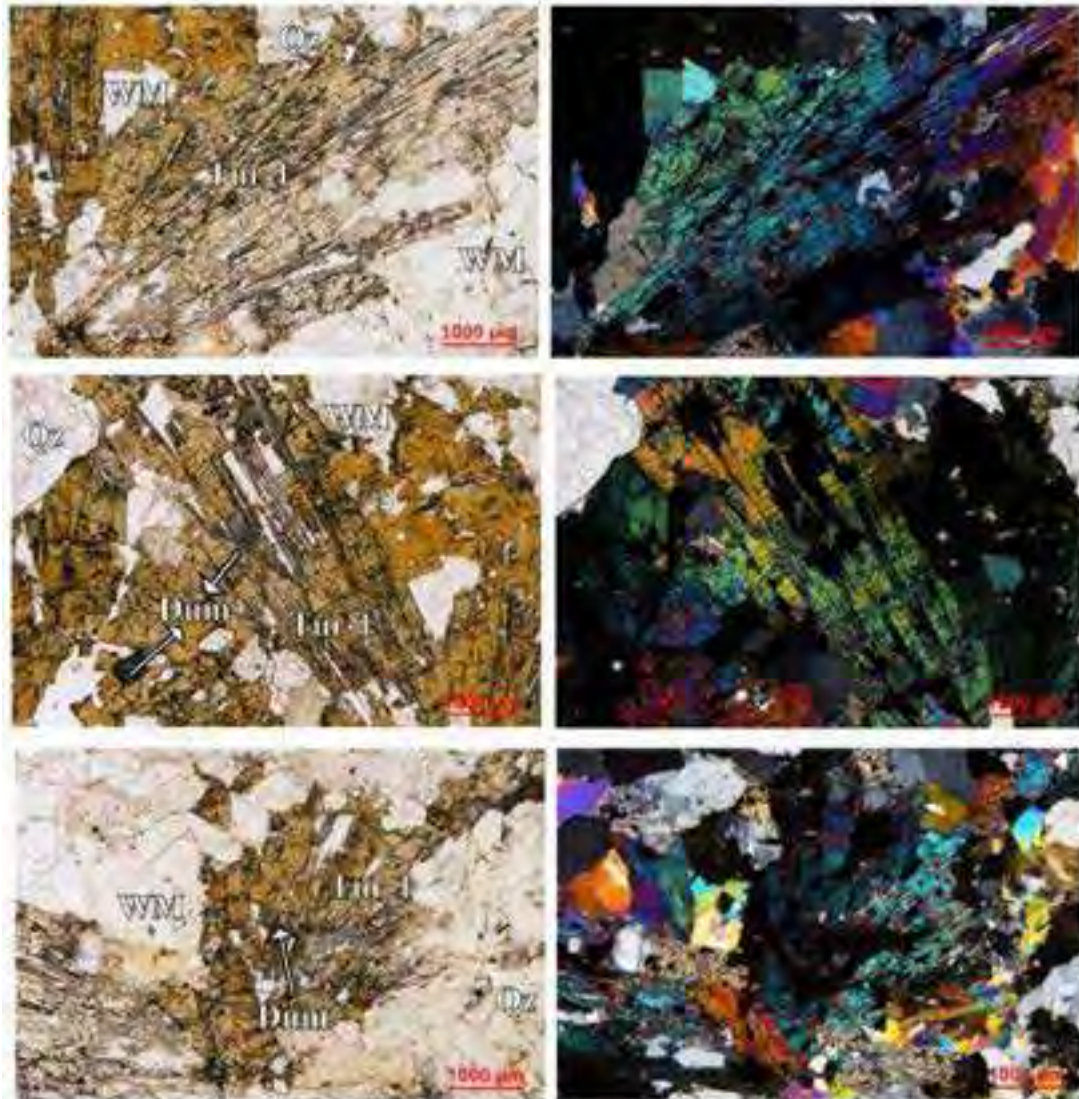


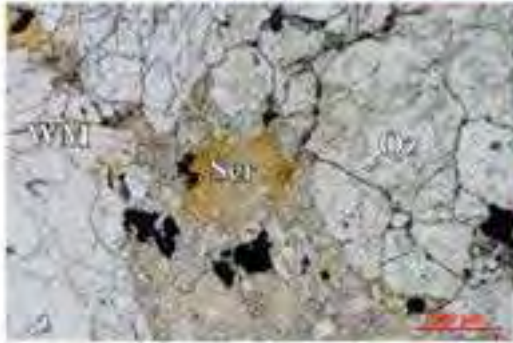
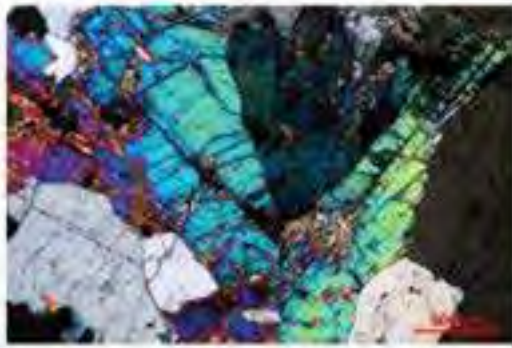
TCMX

2020-KELL-22-B-T6

Minerals: quartz (Qz) + tourmaline-1 (Tur-1) + white mica (WM) + sericite (Ser) + dumortierite (Dum)

Rock sample with conspicuous secondary porosity due to hydrothermal alteration. Skeletal to elongated orange tourmaline crystals appear forming radial aggregates that are up to 3 cm in length. Locally, tourmaline is overgrown by dumortierite. Medium-grained quartz and white mica are intergrown with tourmaline. White mica tablets have a decussate texture and are partly replaced by sericite.



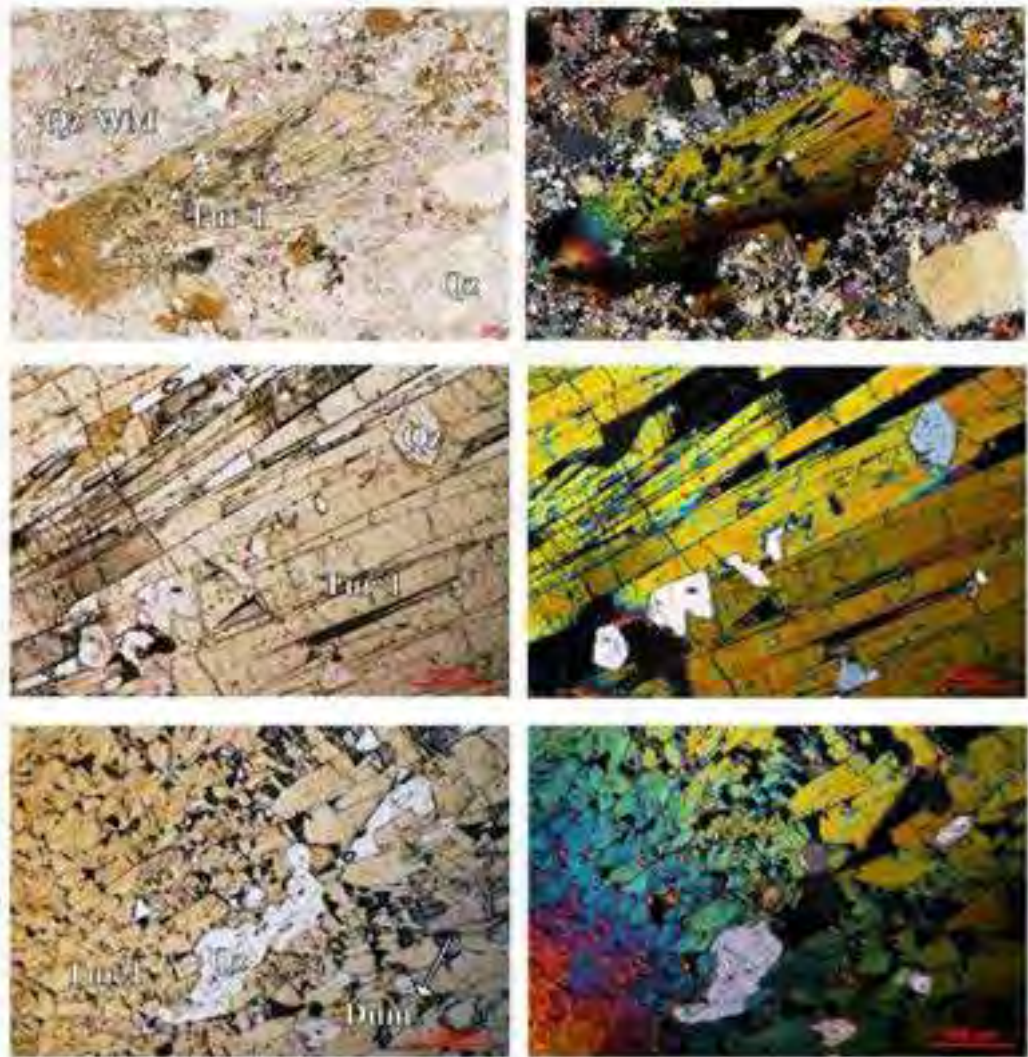


MCMXVII

2020-KELL-23-TS1

Minerals: quartz (Qz) + tourmaline-1 (Tur-1) + white mica (WM) + dumortierite (Dum)

Subhedral crystal of orange tourmaline up to 3 cm in length appear forming radial aggregates. Some crystals present a color zonation from the core to the rim and are partly overgrown by dumortierite (Dum). Quartz phenocrysts have irregular outlines with engulfment filled with the intergrowing assemblage of fine-grained quartz and white mica making up the groundmass of the sample.



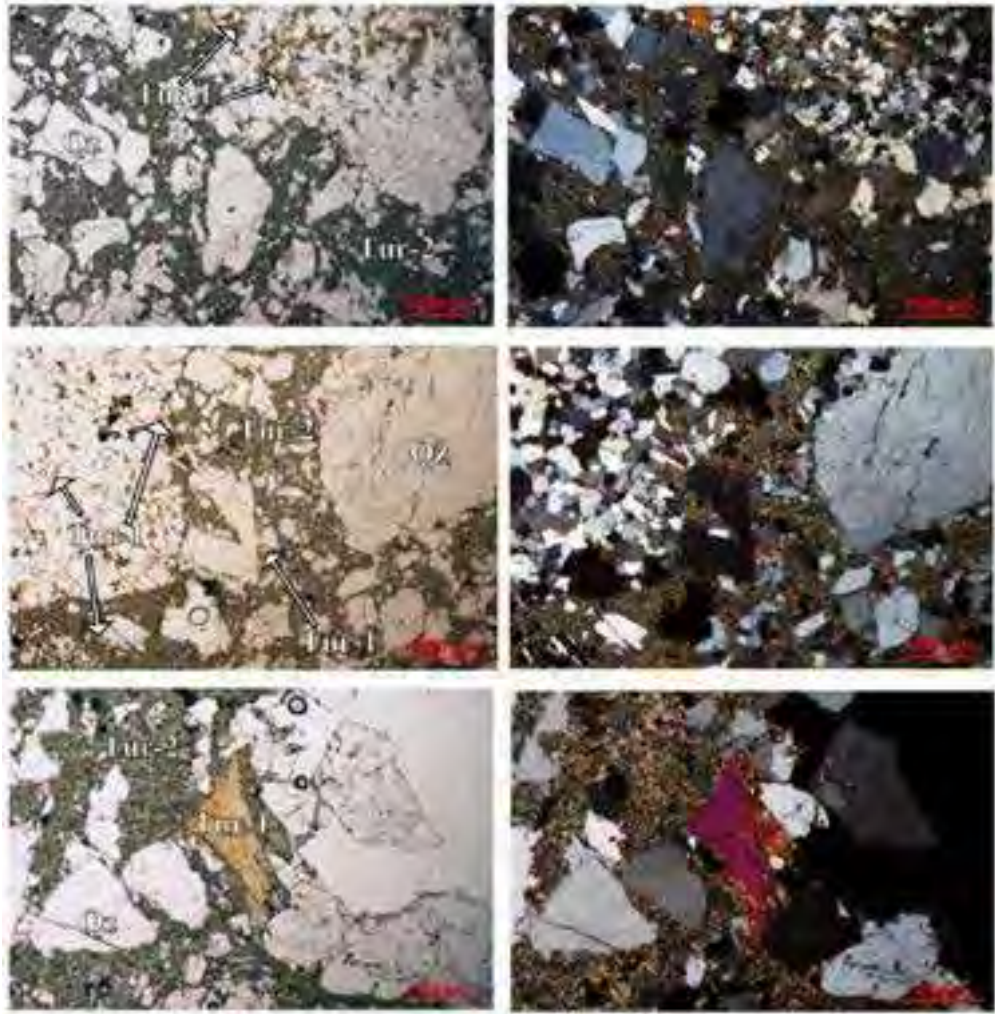


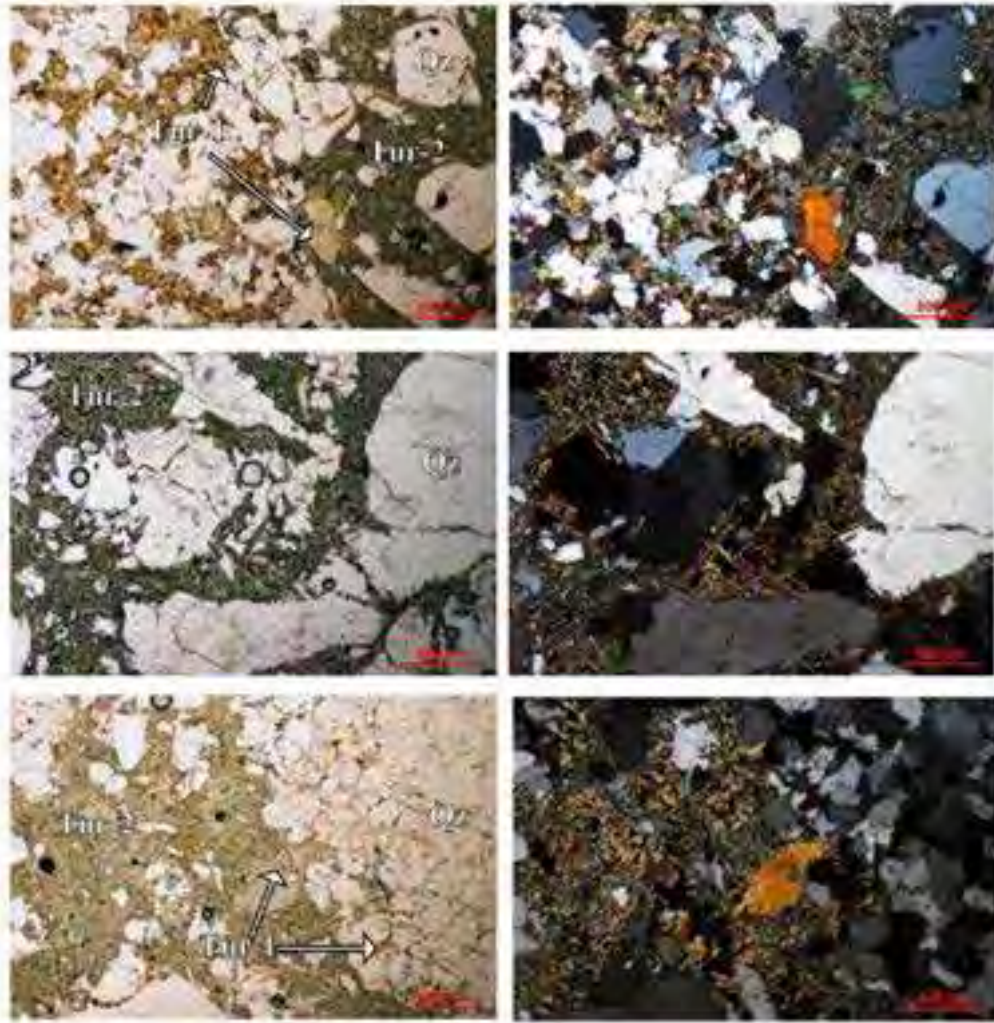
TOURMALINE BRECCIA

2020-KELL-24-TS1

Minerals: quartz (Qz) + tourmaline-1 (Tur-1) + tourmaline-2 (Tur-2)

Tourmaline breccia. The nature of clasts is diverse and include host quartzites, greisen, quartz, and tourmaline-1 fragments with angular and sub-angular outlines. Greisen clasts are fine-grained and composed of quartz and tourmaline-1 crystals. The matrix is composed of green acicular crystals of tourmaline-2.

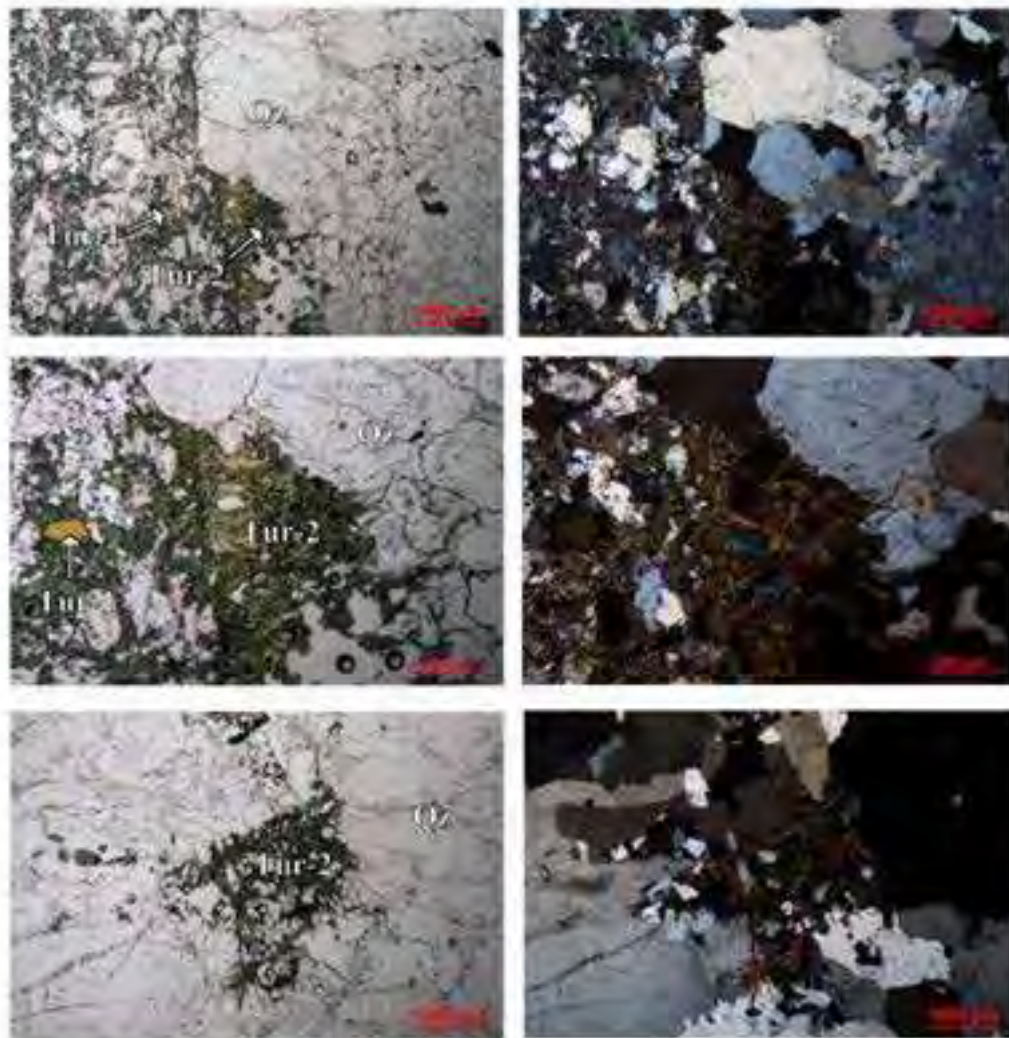


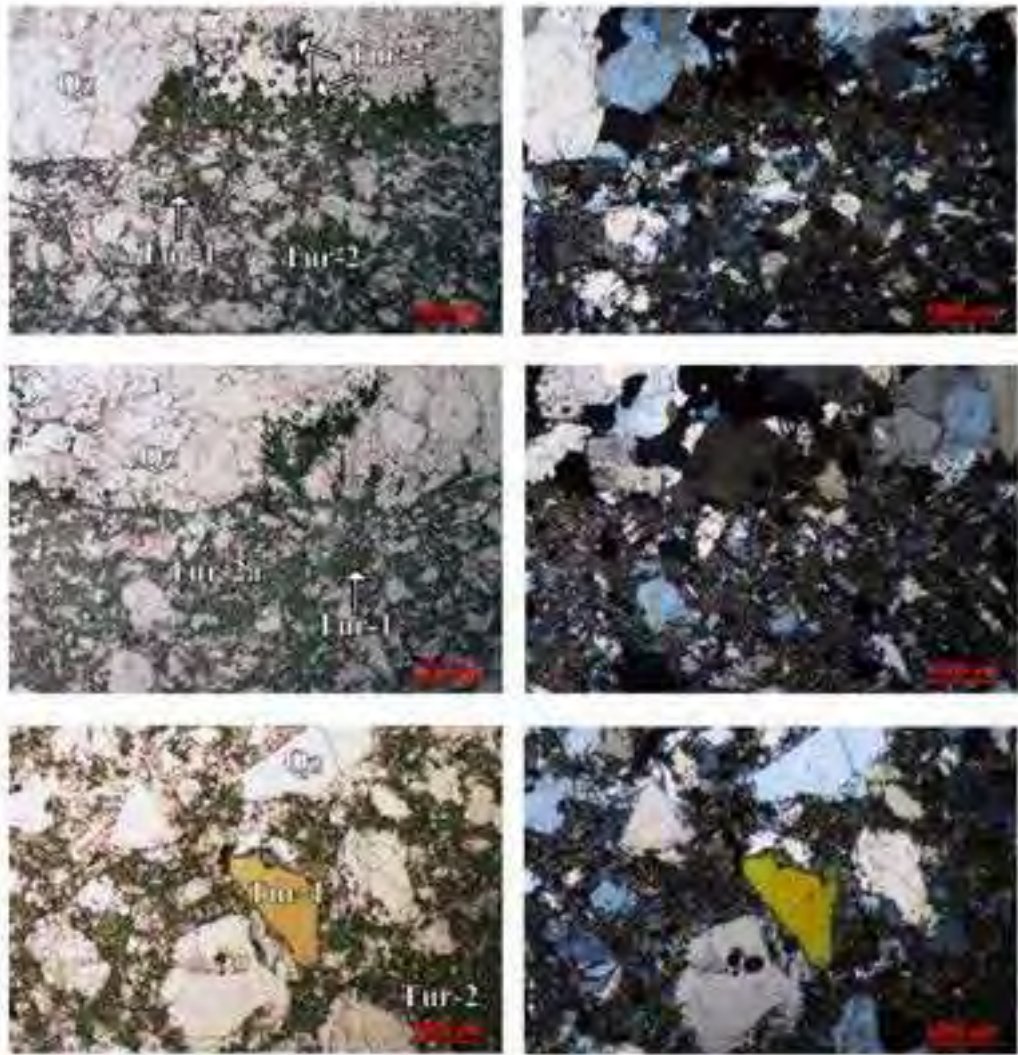


2020-KELL-24-TS4

Minerals: quartz (Qz) + tourmaline-1 (Tur-1) + tourmaline-2 (Tur-2)

Tourmaline breccia. The nature of clasts is diverse and include host quartzites, greisen, quartz, and tourmaline-1 fragments with angular and sub-angular outlines. Greisen clasts are fine-grained and composed of quartz and tourmaline-1 crystals. The matrix is composed of green acicular crystals of tourmaline-2. Acicular crystals of tourmaline-2 also appear as perpendicular growth on rock fragments as infill of acute-angle triangular spaces intergrown with cassiterite.



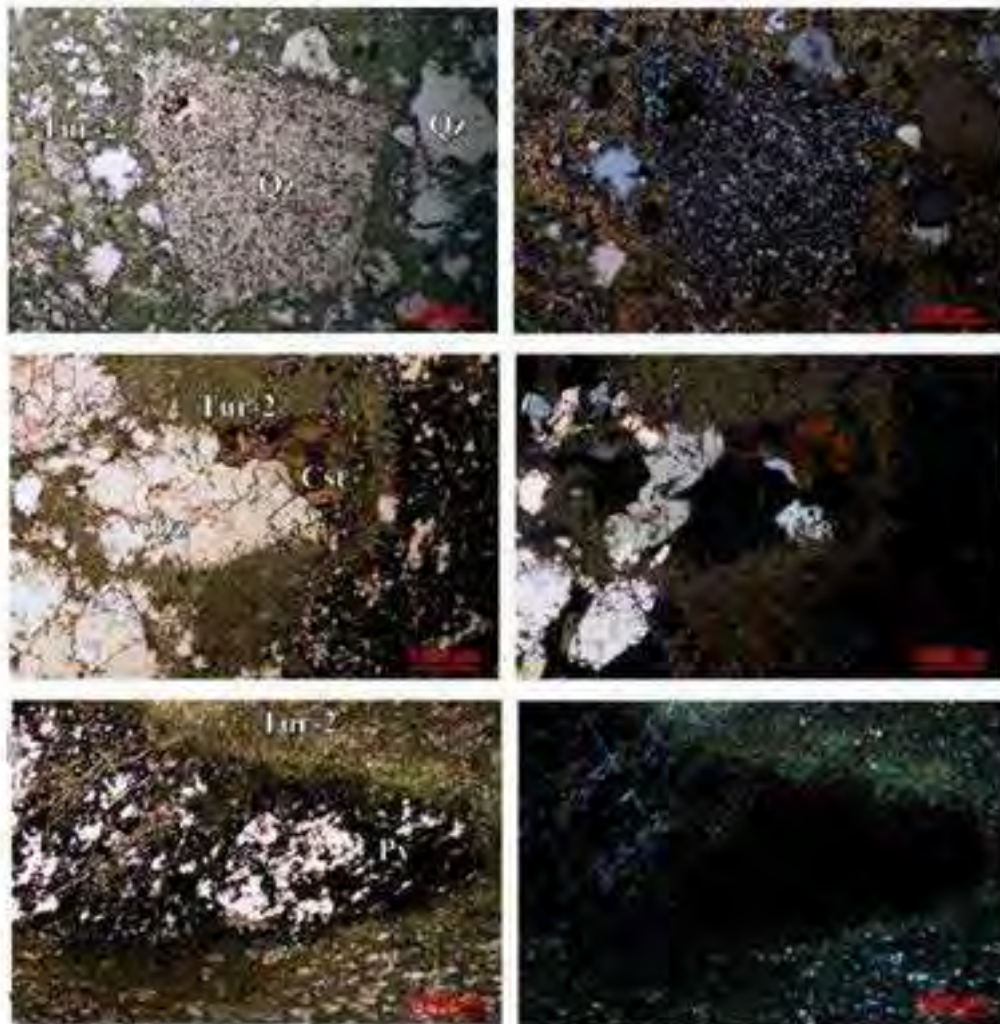


MCMXVII

2020-KELL-25-TS3

Minerals: quartz (Qz) + tourmaline-1 (Tur-1) + tourmaline-2 (Tur-2) + cassiterite (Cst) + pyrite (Py) + goethite (Ght)

Tourmaline breccia. The nature of clasts is diverse and include host quartzites, greisen, quartz, and tourmaline-1 fragments with angular and sub-angular outlines. Greisen clasts are fine-grained and composed of quartz Tur-1 crystals. The matrix is composed of green acicular crystals of tourmaline-2. Locally, tourmaline-2 is also found as very dark green acicular crystals finely intergrown with quartz, cassiterite, and sulfide lining interstitial space between clasts. Goethite appears as an alteration product of pyrite.



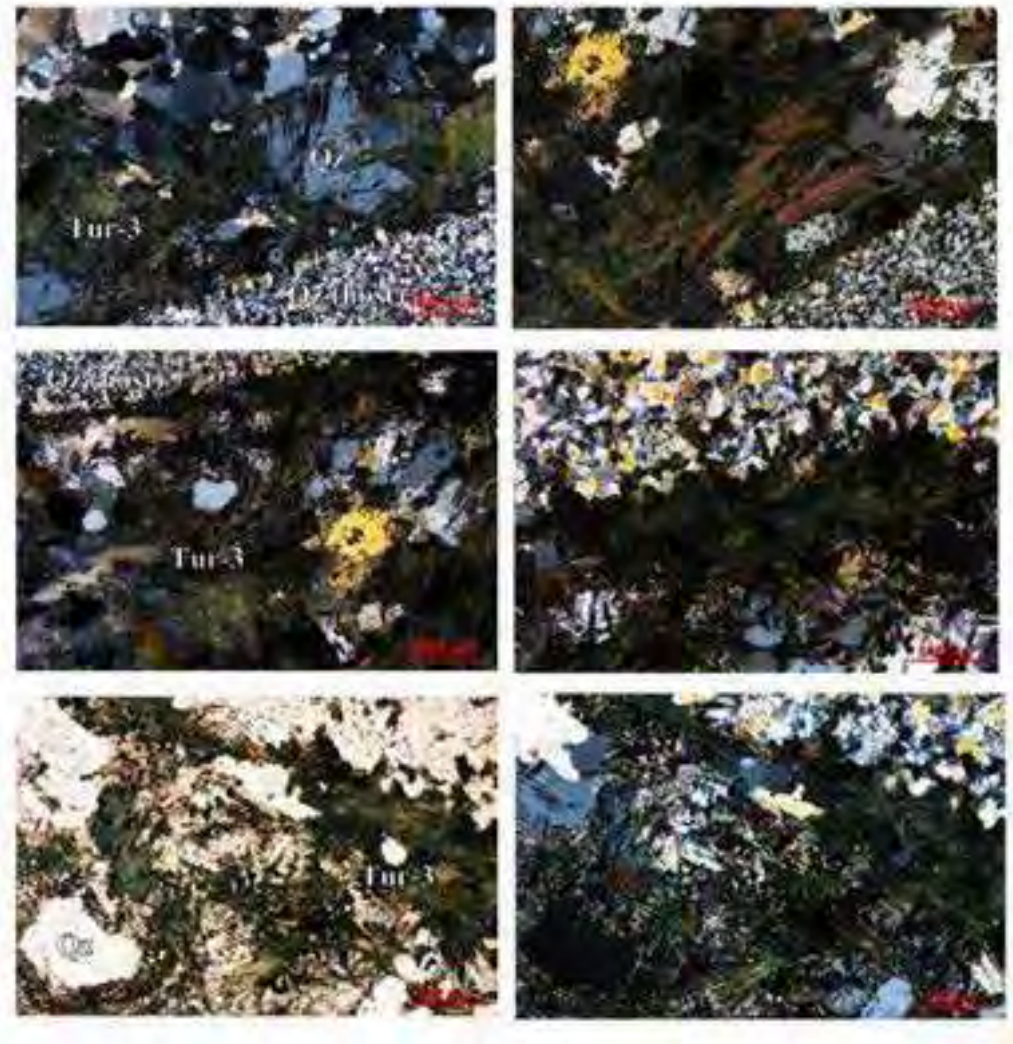


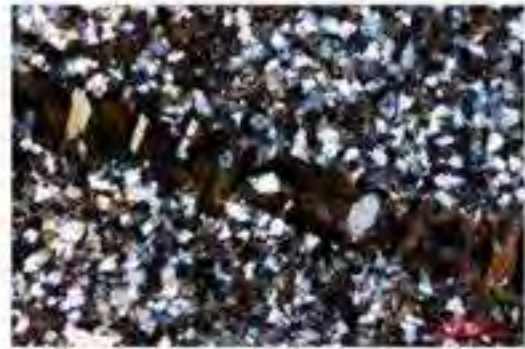
CASSITERITE-BEARING QUARTZ-TOURMALINE VEINS

KELL-A-TS

Minerals: quartz (Qz) + tourmaline-3 (Tur-3)

Within the vein, tourmaline-3 forms brownish-green acicular crystals that are intergrown with coarse-grained quartz. Vein-quartz is contrastingly larger than quartz grains in host quartzite. Along vein selvages, very fine-grained tourmaline-3 lines spaces between quartzite quartz grains. Some secondary veinlets of tourmaline across the host rock and rooted in the main quartz veins are observed.



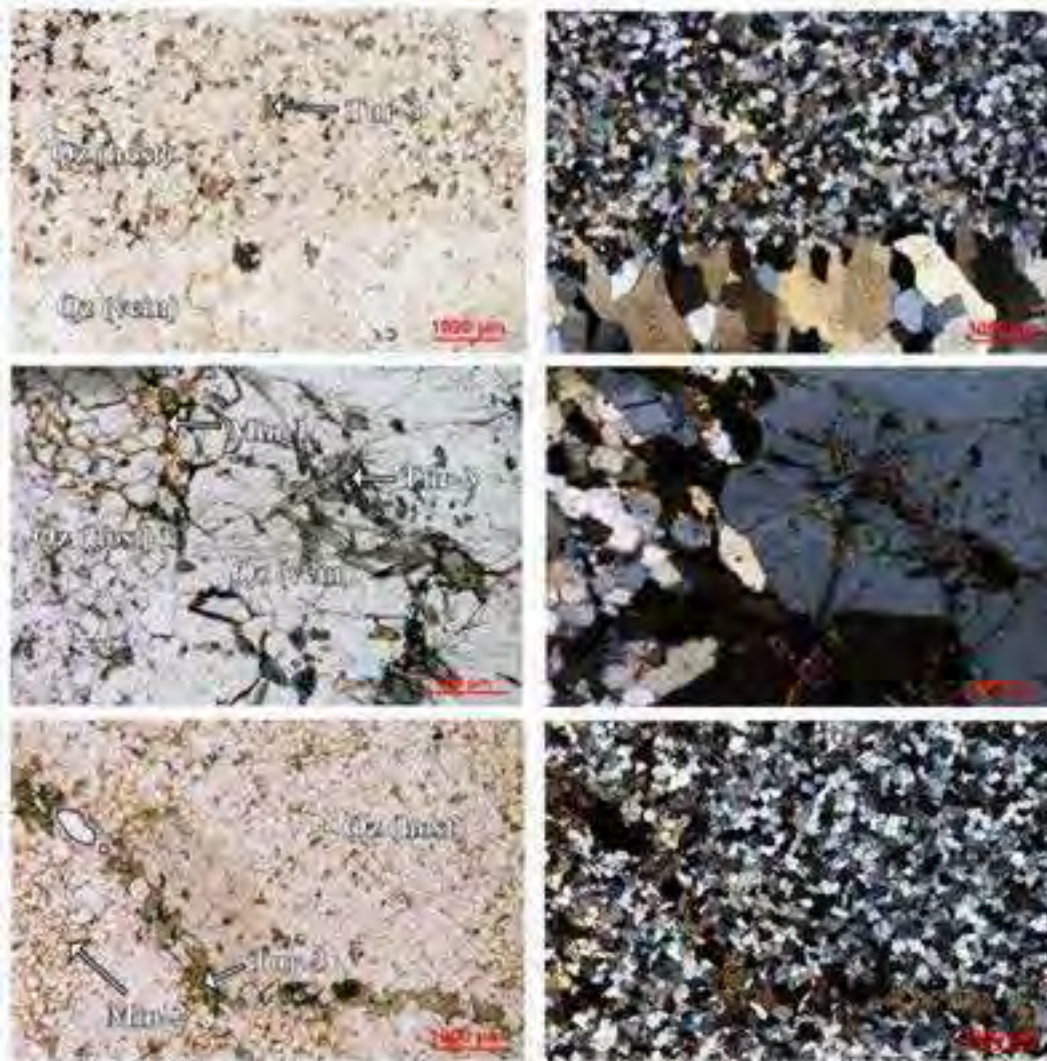


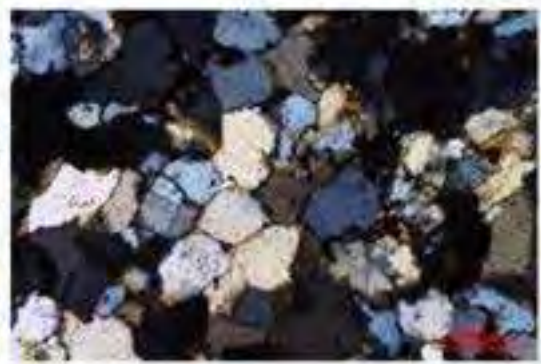
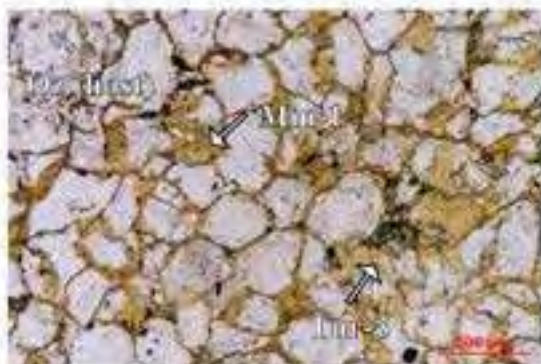
MCMXVII

2020-KELL-01-A-TS1

Minerals: quartz (Qz) + tourmaline-3 (Tur-3) + carbonates (Cb) + unidentified mineral (Min-1)

Tourmaline-3 and quartz veins hosted by quartzite. Tourmaline-3 is green to brownish-green and forms acicular crystals. In veins, tourmaline-3 is intergrown with coarse-grained quartz. Iron-rich carbonates line interstitial space between comb-textured quartz crystals in the central strip of the vein. The alteration halo is enriched in tourmaline-3, which occurs as very fine-grained crystals filling interstices between fine-grained quartzite quartz. The vein selvage also contains interdigitating dark-brown domains formed by an unidentified amorphous mineral that fills interstitial space between quartzite quartz grains.

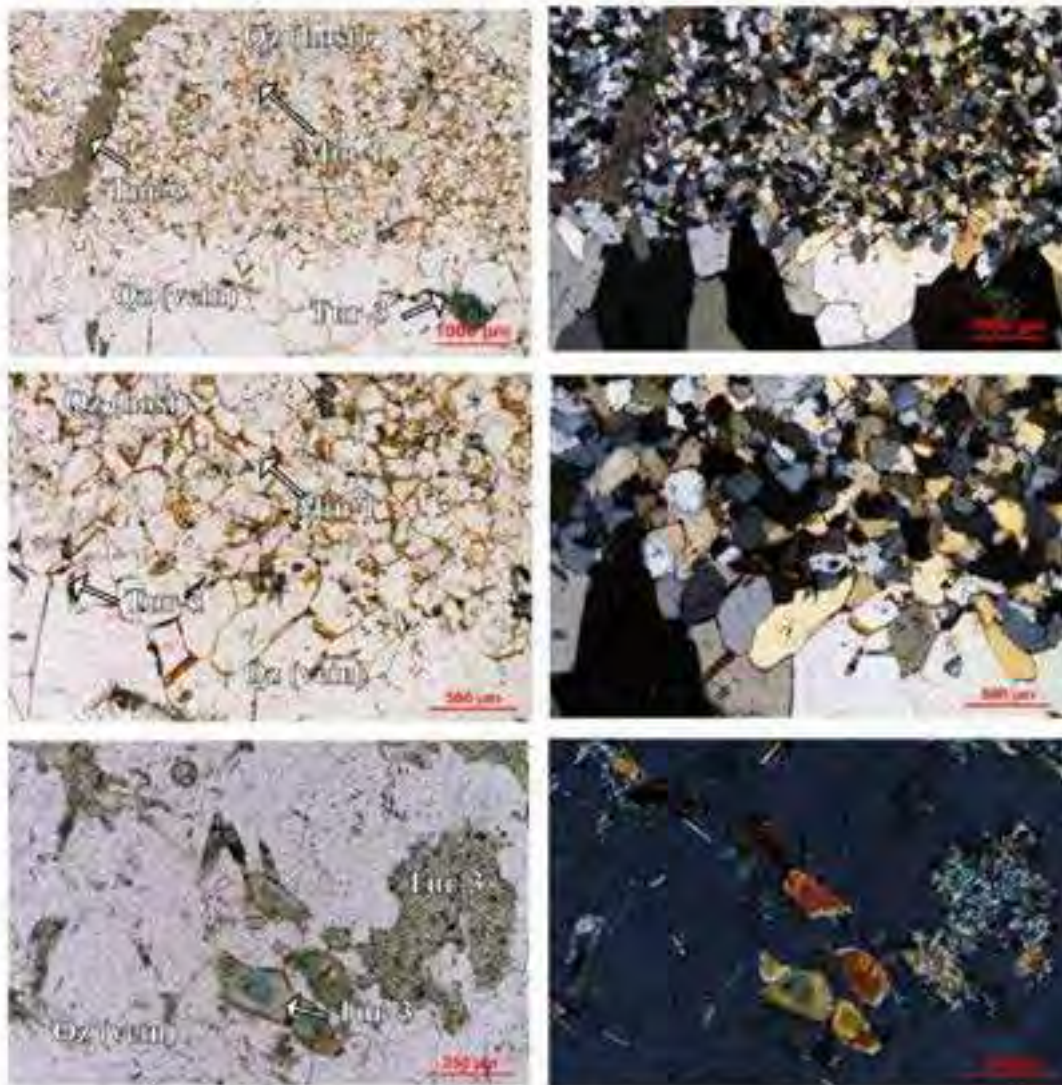


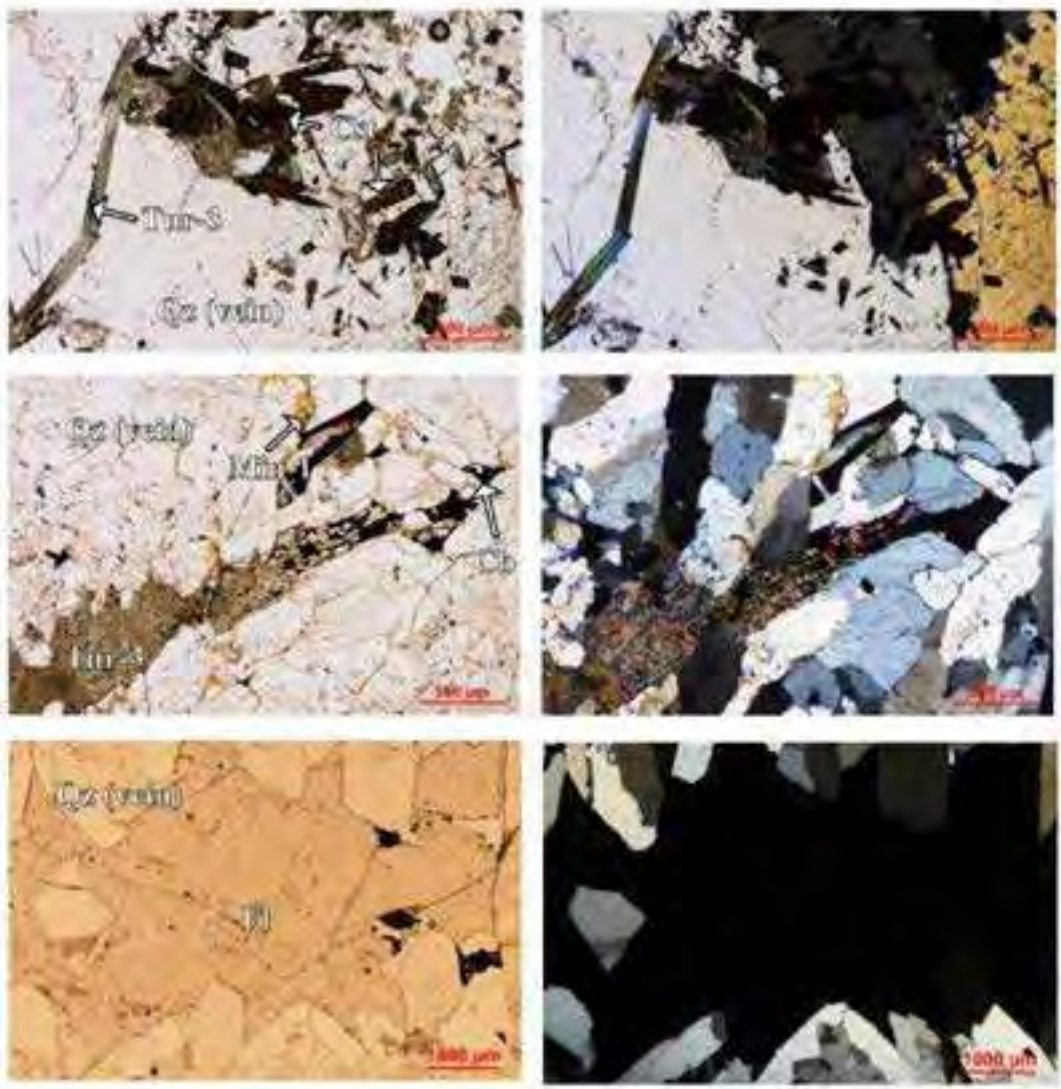


2020-KELL-01-A-TS3

Minerals: quartz (Qz) + tourmaline-3 (Tur-3) + carbonates (Cb) + mineral-1 (Min-1) + cassiterite (Cst) + fluorite (Fl)

Quartz veins hosted by quartzite. Tourmaline-3 is green-brown in color and appears as acicular crystals finely intergrown with quartz in the veins. Within veins, some tourmaline-3 crystals show color zoning from blue to green from core to rims. Cassiterite crystals are intergrown with tourmaline-3 close to the borders of the vein. Iron-rich carbonates and fluorite line interstitial space between comb-textured quartz crystals in the central portion of the vein. The alteration halo is enriched in tourmaline-3, which appear lining quartzite quartz. The vein selvage also contains a dark brown unidentified mineral.



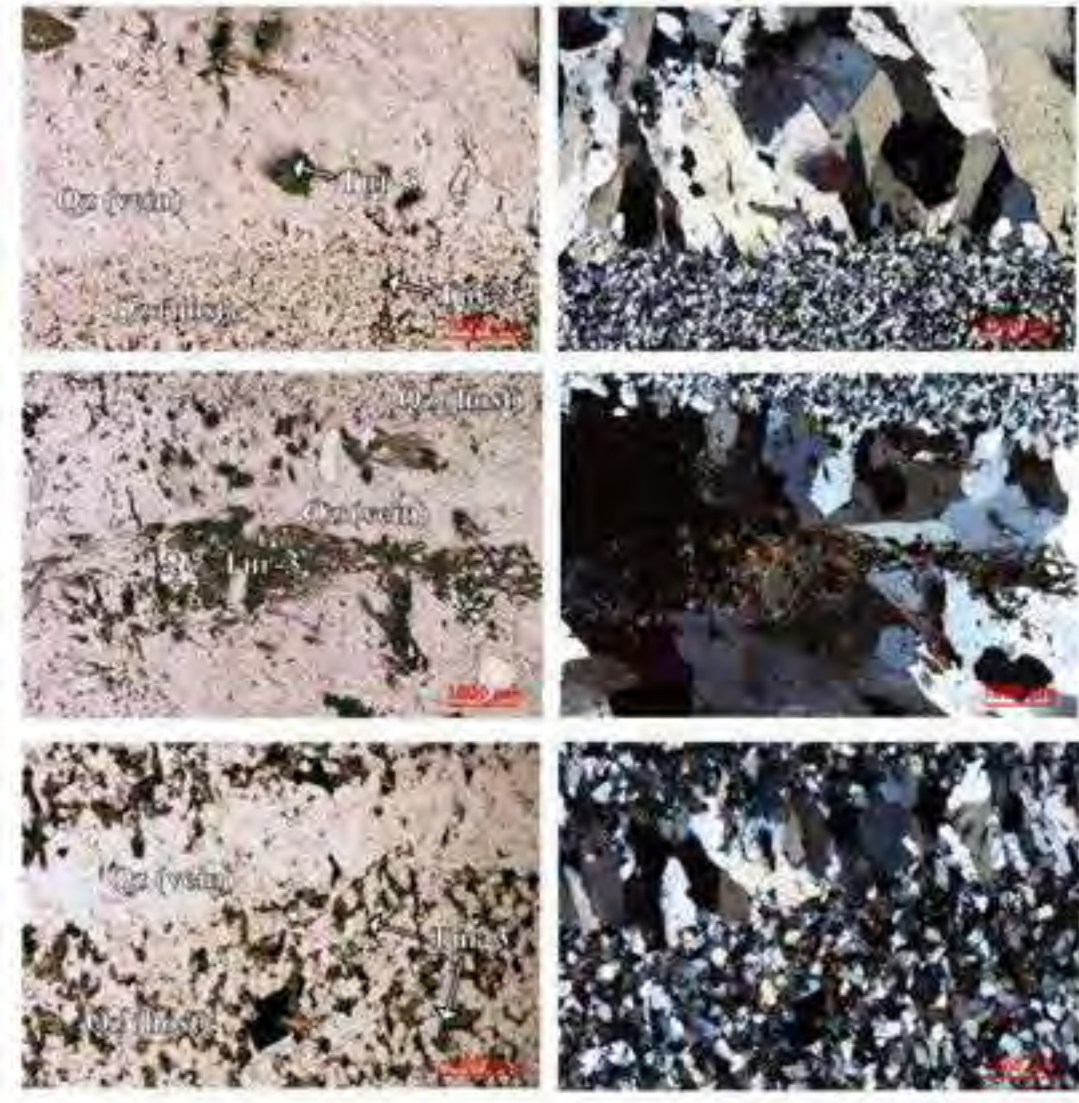


MCMXVII

2020-KELL-17-C-TS2

Minerals: quartz (Qz) + tourmaline-3 (Tur-3) + carbonates (Cb)

Quartz veins hosted by quartzite. Tourmaline-3 is green-brown in color and appears as acicular crystals finely intergrown with quartz in the veins. Within veins, some tourmaline-3 crystals show color zoning from blue to green from core to rims. Cassiterite crystals are intergrown with tourmaline-3 close to the borders of the vein. Iron-rich carbonates line interstitial space between comb-textured quartz crystals in the central portion of the vein. The alteration halo is enriched in tourmaline-3, which appear lining quartzite quartz. The vein selvage also contains a dark brown unidentified mineral.



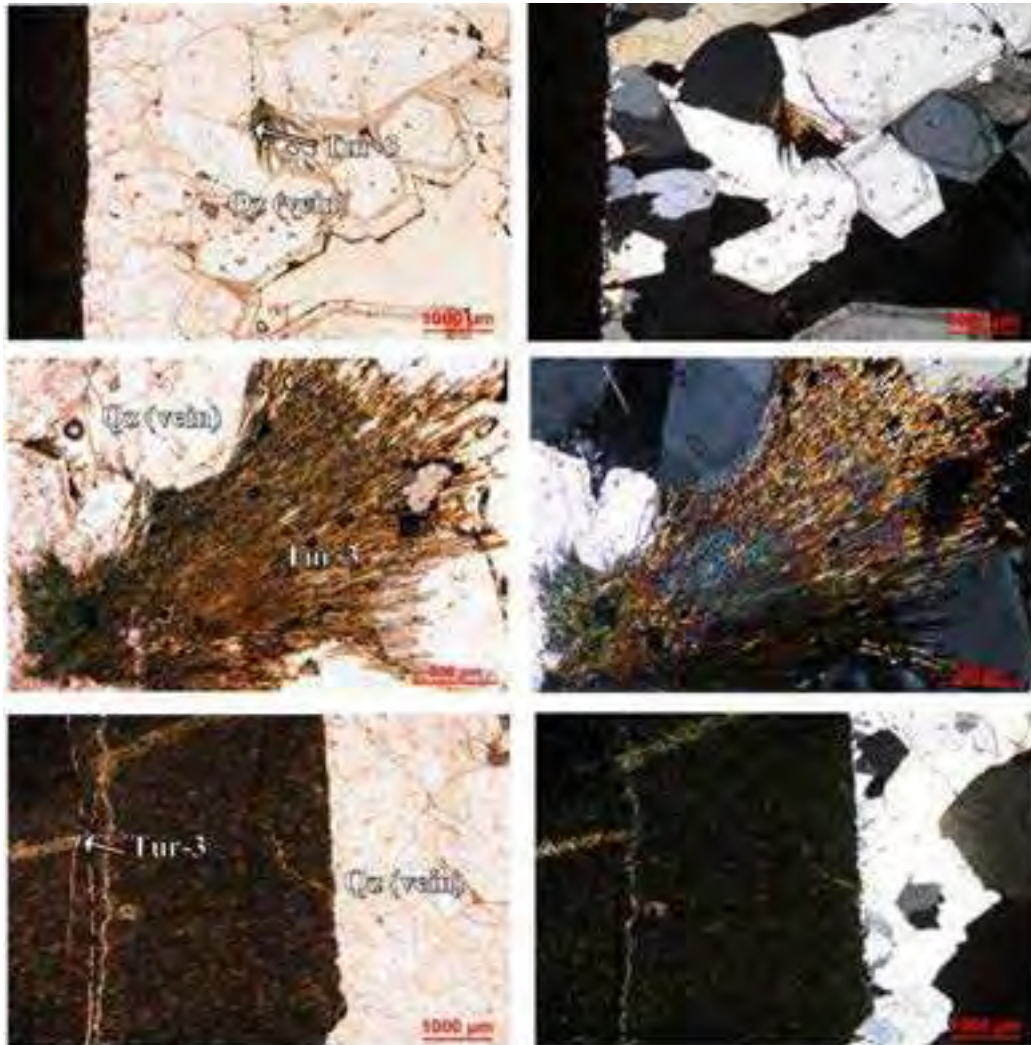


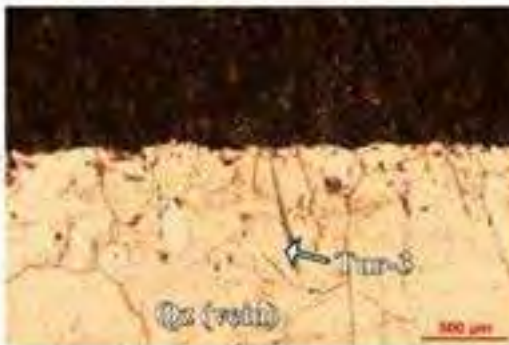
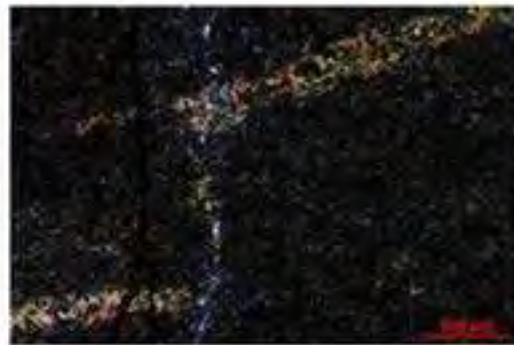
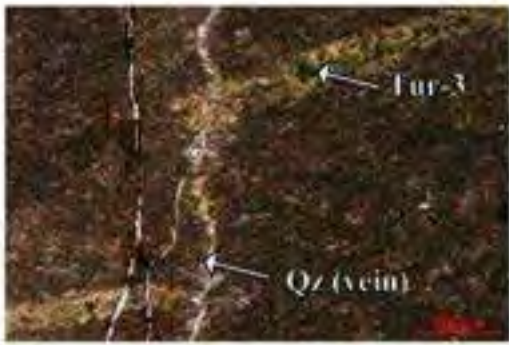
MCMXVII

2020-KELL-48-TS1

Minerals: quartz (Qz) + tourmaline-3 (Tur-3)

Quartz veins hosted by quartzite. Within veins, tourmaline-3 forms green-brown acicular crystals intergrown with coarse-grained quartz. Tourmaline-3 crystals form radial aggregates that are up to 3 mm in length. Quartz grains in veins define comb textures and are rich in primary fluid inclusions forming trails parallel to growth faces. The alteration halo is enriched in very fine-grained tourmaline-3 lining fine-grained quartzite quartz grains. Around the main vein, secondary veinlets of tourmaline-3 are cut by veinlets of quartz.





ICMXV

Appendix D

Electron microprobe (EPMA) tourmaline data



EMPA label	Type	Sample	Host-rock	Description	Locality	Zone	Color
2020-KELL-22-B-TS1-Circle A-TUR1A-001	Tur-1	2020-KELL-22-B	Greisen	Coarse-grained quartz-muscovite-tourmaline greisen	Chalcataya	Optically unzoned	Orange
2020-KELL-22-B-TS1-Circle A-TUR1A-002	Tur-1	2020-KELL-22-B	Greisen	Coarse-grained quartz-muscovite-tourmaline greisen	Chalcataya	Optically unzoned	Orange
2020-KELL-22-B-TS1-Circle A-TUR1A-003	Tur-1	2020-KELL-22-B	Greisen	Coarse-grained quartz-muscovite-tourmaline greisen	Chalcataya	Optically unzoned	Orange
2020-KELL-22-B-TS1-Circle A-TUR1A-004	Tur-1	2020-KELL-22-B	Greisen	Coarse-grained quartz-muscovite-tourmaline greisen	Chalcataya	Optically unzoned	Orange
2020-KELL-22-B-TS1-Circle A-TUR1A-005	Tur-1	2020-KELL-22-B	Greisen	Coarse-grained quartz-muscovite-tourmaline greisen	Chalcataya	Optically unzoned	Orange
2020-KELL-22-B-TS1-Circle A-TUR1A-006	Tur-1	2020-KELL-22-B	Greisen	Coarse-grained quartz-muscovite-tourmaline greisen	Chalcataya	Optically unzoned	Orange
2020-KELL-22-B-TS1-Circle A-TUR1A-007	Tur-1	2020-KELL-22-B	Greisen	Coarse-grained quartz-muscovite-tourmaline greisen	Chalcataya	Optically unzoned	Orange
2020-KELL-22-B-TS1-Circle A-TUR1A-008	Tur-1	2020-KELL-22-B	Greisen	Coarse-grained quartz-muscovite-tourmaline greisen	Chalcataya	Optically unzoned	Orange
2020-KELL-22-B-TS1-Circle A-TUR1A-009	Tur-1	2020-KELL-22-B	Greisen	Coarse-grained quartz-muscovite-tourmaline greisen	Chalcataya	Optically unzoned	Orange
2020-KELL-22-B-TS1-Circle A-TUR1A-010	Tur-1	2020-KELL-22-B	Greisen	Coarse-grained quartz-muscovite-tourmaline greisen	Chalcataya	Optically unzoned	Orange
2020-KELL-22-B-TS1-Circle A-TUR1A-011	Tur-1	2020-KELL-22-B	Greisen	Coarse-grained quartz-muscovite-tourmaline greisen	Chalcataya	Optically unzoned	Orange
2020-KELL-22-B-TS1-Circle A-TUR1A-012	Tur-1	2020-KELL-22-B	Greisen	Coarse-grained quartz-muscovite-tourmaline greisen	Chalcataya	Optically unzoned	Orange
2020-KELL-22-B-TS1-Circle A-TUR1A-013	Tur-1	2020-KELL-22-B	Greisen	Coarse-grained quartz-muscovite-tourmaline greisen	Chalcataya	Optically unzoned	Orange
2020-KELL-22-B-TS1-Circle A-TUR1A-014	Tur-1	2020-KELL-22-B	Greisen	Coarse-grained quartz-muscovite-tourmaline greisen	Chalcataya	Optically unzoned	Orange
2020-KELL-22-B-TS1-Circle A-TUR1A-015	Tur-1	2020-KELL-22-B	Greisen	Coarse-grained quartz-muscovite-tourmaline greisen	Chalcataya	Optically unzoned	Orange
2020-KELL-22-B-TS1-Circle A-TUR1A-016	Tur-1	2020-KELL-22-B	Greisen	Coarse-grained quartz-muscovite-tourmaline greisen	Chalcataya	Optically unzoned	Orange
2020-KELL-22-B-TS1-Circle A-TUR1A-017	Tur-1	2020-KELL-22-B	Greisen	Coarse-grained quartz-muscovite-tourmaline greisen	Chalcataya	Optically unzoned	Orange
2020-KELL-22-B-TS1-Circle B-TUR1A-001	Tur-1	2020-KELL-22-B	Greisen	Coarse-grained quartz-muscovite-tourmaline greisen	Chalcataya	Optically unzoned	Orange

EMPA label	Type	Sample	Host-rock	Description	Locality	Zone	Color
2020-KELL-22-B-TS1-Circle B-TUR1A-002	Tur-1	2020-KELL-22-B	Greisen	Coarse-grained quartz-muscovite-tourmaline greisen	Chalcataya	Optically unzoned	Orange
2020-KELL-22-B-TS1-Circle B-TUR1A-003	Tur-1	2020-KELL-22-B	Greisen	Coarse-grained quartz-muscovite-tourmaline greisen	Chalcataya	Optically unzoned	Orange
2020-KELL-22-B-TS1-Circle B-TUR1A-004	Tur-1	2020-KELL-22-B	Greisen	Coarse-grained quartz-muscovite-tourmaline greisen	Chalcataya	Optically unzoned	Orange
2020-KELL-22-B-TS1-Circle B-TUR1A-005	Tur-1	2020-KELL-22-B	Greisen	Coarse-grained quartz-muscovite-tourmaline greisen	Chalcataya	Optically unzoned	Orange
2020-KELL-22-B-TS1-Circle B-TUR1A-006	Tur-1	2020-KELL-22-B	Greisen	Coarse-grained quartz-muscovite-tourmaline greisen	Chalcataya	Optically unzoned	Orange
2020-KELL-22-B-TS1-Circle B-TUR1A-008	Tur-1	2020-KELL-22-B	Greisen	Coarse-grained quartz-muscovite-tourmaline greisen	Chalcataya	Optically unzoned	Orange
2020-KELL-22-B-TS1-Circle B-TUR1A-009	Tur-1	2020-KELL-22-B	Greisen	Coarse-grained quartz-muscovite-tourmaline greisen	Chalcataya	Optically unzoned	Orange
2020-KELL-22-B-TS1-Circle B-TUR1A-010	Tur-1	2020-KELL-22-B	Greisen	Coarse-grained quartz-muscovite-tourmaline greisen	Chalcataya	Optically unzoned	Orange
2020-KELL-22-B-TS1-Circle B-TUR1A-011	Tur-1	2020-KELL-22-B	Greisen	Coarse-grained quartz-muscovite-tourmaline greisen	Chalcataya	Optically unzoned	Orange
2020-KELL-22-B-TS1-Circle C-TUR1A-001	Tur-1	2020-KELL-22-B	Greisen	Coarse-grained quartz-muscovite-tourmaline greisen	Chalcataya	Optically unzoned	Orange
2020-KELL-22-B-TS1-Circle C-TUR1A-002	Tur-1	2020-KELL-22-B	Greisen	Coarse-grained quartz-muscovite-tourmaline greisen	Chalcataya	Optically unzoned	Orange
2020-KELL-22-B-TS1-Circle C-TUR1A-003	Tur-1	2020-KELL-22-B	Greisen	Coarse-grained quartz-muscovite-tourmaline greisen	Chalcataya	Optically unzoned	Orange
2020-KELL-22-B-TS1-Circle C-TUR1A-004	Tur-1	2020-KELL-22-B	Greisen	Coarse-grained quartz-muscovite-tourmaline greisen	Chalcataya	Optically unzoned	Orange
2020-KELL-22-B-TS1-Circle C-TUR1A-005	Tur-1	2020-KELL-22-B	Greisen	Coarse-grained quartz-muscovite-tourmaline greisen	Chalcataya	Optically unzoned	Orange
2020-KELL-22-B-TS1-Circle C-TUR1A-006	Tur-1	2020-KELL-22-B	Greisen	Coarse-grained quartz-muscovite-tourmaline greisen	Chalcataya	Optically unzoned	Orange
2020-KELL-22-B-TS1-Circle C-TUR1A-007	Tur-1	2020-KELL-22-B	Greisen	Coarse-grained quartz-muscovite-tourmaline greisen	Chalcataya	Optically unzoned	Orange
2020-KELL-22-B-TS1-Circle C-TUR1A-008	Tur-1	2020-KELL-22-B	Greisen	Coarse-grained quartz-muscovite-tourmaline greisen	Chalcataya	Optically unzoned	Orange
2020-KELL-22-B-TS1-Circle C-TUR1A-009	Tur-1	2020-KELL-22-B	Greisen	Coarse-grained quartz-muscovite-tourmaline greisen	Chalcataya	Optically unzoned	Orange

EMPA label	Type	Sample	Host-rock	Description	Locality	Zone	Color
2020-KELL-22-B-TS1-Circle C-TUR1A-010	Tur-1	2020-KELL-22-B	Greisen	Coarse-grained quartz-muscovite-tourmaline greisen	Chalcataya	Optically unzoned	Orange
2020-KELL-22-B-TS1-Circle C-TUR1A-011	Tur-1	2020-KELL-22-B	Greisen	Coarse-grained quartz-muscovite-tourmaline greisen	Chalcataya	Optically unzoned	Orange
2020-KELL-22-B-TS1-Circle C-TUR1A-012	Tur-1	2020-KELL-22-B	Greisen	Coarse-grained quartz-muscovite-tourmaline greisen	Chalcataya	Optically unzoned	Orange
2020-KELL-22-B-TS1-Circle C-TUR1A-013	Tur-1	2020-KELL-22-B	Greisen	Coarse-grained quartz-muscovite-tourmaline greisen	Chalcataya	Optically unzoned	Orange
2020-KELL-22-B-TS1-Circle C-TUR1A-014	Tur-1	2020-KELL-22-B	Greisen	Coarse-grained quartz-muscovite-tourmaline greisen	Chalcataya	Optically unzoned	Orange
2020-KELL-22-B-TS1-Circle D-TUR1A-001	Tur-1	2020-KELL-22-B	Greisen	Coarse-grained quartz-muscovite-tourmaline greisen	Chalcataya	Core	Orange
2020-KELL-22-B-TS1-Circle D-TUR1A-002	Tur-1	2020-KELL-22-B	Greisen	Coarse-grained quartz-muscovite-tourmaline greisen	Chalcataya	Core	Orange
2020-KELL-22-B-TS1-Circle D-TUR1A-003	Tur-1	2020-KELL-22-B	Greisen	Coarse-grained quartz-muscovite-tourmaline greisen	Chalcataya	Core	Orange
2020-KELL-22-B-TS1-Circle D-TUR1A-004	Tur-1	2020-KELL-22-B	Greisen	Coarse-grained quartz-muscovite-tourmaline greisen	Chalcataya	Core	Orange
2020-KELL-22-B-TS1-Circle D-TUR1A-005	Tur-1	2020-KELL-22-B	Greisen	Coarse-grained quartz-muscovite-tourmaline greisen	Chalcataya	Core	Orange
2020-KELL-22-B-TS1-Circle D-TUR1A-006	Tur-1	2020-KELL-22-B	Greisen	Coarse-grained quartz-muscovite-tourmaline greisen	Chalcataya	Core	Orange
2020-KELL-22-B-TS1-Circle D-TUR1A-007	Tur-1	2020-KELL-22-B	Greisen	Coarse-grained quartz-muscovite-tourmaline greisen	Chalcataya	Core	Orange
2020-KELL-22-B-TS1-Circle D-TUR1A-008	Tur-1	2020-KELL-22-B	Greisen	Coarse-grained quartz-muscovite-tourmaline greisen	Chalcataya	Core	Orange
2020-KELL-22-B-TS1-Circle D-TUR1A-009	Tur-1	2020-KELL-22-B	Greisen	Coarse-grained quartz-muscovite-tourmaline greisen	Chalcataya	Rim	Orange
2020-KELL-22-B-TS1-Circle D-TUR1A-010	Tur-1	2020-KELL-22-B	Greisen	Coarse-grained quartz-muscovite-tourmaline greisen	Chalcataya	Rim	Orange
2020-KELL-22-B-TS1-Circle D-TUR1A-011	Tur-1	2020-KELL-22-B	Greisen	Coarse-grained quartz-muscovite-tourmaline greisen	Chalcataya	Rim	Orange
2020-KELL-22-B-TS1-Circle D-TUR1A-012	Tur-1	2020-KELL-22-B	Greisen	Coarse-grained quartz-muscovite-tourmaline greisen	Chalcataya	Rim	Orange
2020-KELL-22-B-TS1-Circle D-TUR1A-013	Tur-1	2020-KELL-22-B	Greisen	Coarse-grained quartz-muscovite-tourmaline greisen	Chalcataya	Rim	Orange

EMPA label	Type	Sample	Host-rock	Description	Locality	Zone	Color
2020-KELL-22-B-TS1-Circle D-TUR1A-014	Tur-1	2020-KELL-22-B	Greisen	Coarse-grained quartz-muscovite-tourmaline greisen	Chalcataya	Rim	Orange
2020-KELL-22-B-TS1-Circle D-TUR1A-015	Tur-1	2020-KELL-22-B	Greisen	Coarse-grained quartz-muscovite-tourmaline greisen	Chalcataya	Rim	Orange
2020-KELL-22-B-TS1-Circle D-TUR1A-016	Tur-1	2020-KELL-22-B	Greisen	Coarse-grained quartz-muscovite-tourmaline greisen	Chalcataya	Rim	Orange
2020-KELL-22-B-TS1-Circle D-TUR1A-017	Tur-1	2020-KELL-22-B	Greisen	Coarse-grained quartz-muscovite-tourmaline greisen	Chalcataya	Rim	Orange
2020-KELL-22-B-TS1-Circle D-TUR1A-018	Tur-1	2020-KELL-22-B	Greisen	Coarse-grained quartz-muscovite-tourmaline greisen	Chalcataya	Core	Orange
2020-KELL-22-B-TS1-Circle E-TUR1A-001	Tur-1	2020-KELL-22-B	Greisen	Coarse-grained quartz-muscovite-tourmaline greisen	Chalcataya	Optically unzoned	Orange
2020-KELL-22-B-TS1-Circle E-TUR1A-002	Tur-1	2020-KELL-22-B	Greisen	Coarse-grained quartz-muscovite-tourmaline greisen	Chalcataya	Optically unzoned	Orange
2020-KELL-22-B-TS1-Circle E-TUR1A-003	Tur-1	2020-KELL-22-B	Greisen	Coarse-grained quartz-muscovite-tourmaline greisen	Chalcataya	Optically unzoned	Orange
2020-KELL-22-B-TS1-Circle E-TUR1A-004	Tur-1	2020-KELL-22-B	Greisen	Coarse-grained quartz-muscovite-tourmaline greisen	Chalcataya	Optically unzoned	Orange
2020-KELL-22-B-TS1-Circle E-TUR1A-005	Tur-1	2020-KELL-22-B	Greisen	Coarse-grained quartz-muscovite-tourmaline greisen	Chalcataya	Optically unzoned	Orange
2020-KELL-22-B-TS1-Circle E-TUR1A-006	Tur-1	2020-KELL-22-B	Greisen	Coarse-grained quartz-muscovite-tourmaline greisen	Chalcataya	Optically unzoned	Orange
2020-KELL-22-B-TS1-Circle E-TUR1A-007	Tur-1	2020-KELL-22-B	Greisen	Coarse-grained quartz-muscovite-tourmaline greisen	Chalcataya	Optically unzoned	Orange
2020-KELL-22-B-TS1-Circle E-TUR1A-008	Tur-1	2020-KELL-22-B	Greisen	Coarse-grained quartz-muscovite-tourmaline greisen	Chalcataya	Optically unzoned	Orange
2020-KELL-22-B-TS1-Circle E-TUR1A-009	Tur-1	2020-KELL-22-B	Greisen	Coarse-grained quartz-muscovite-tourmaline greisen	Chalcataya	Optically unzoned	Orange
2020-KELL-22-B-TS6-Circle A-Tur1a-001	Tur-1	2020-KELL-22-B	Greisen	Coarse-grained quartz-muscovite-tourmaline greisen	Chalcataya	Optically unzoned	Orange
2020-KELL-22-B-TS6-Circle A-Tur1a-002	Tur-1	2020-KELL-22-B	Greisen	Coarse-grained quartz-muscovite-tourmaline greisen	Chalcataya	Optically unzoned	Orange
2020-KELL-22-B-TS6-Circle A-Tur1a-003	Tur-1	2020-KELL-22-B	Greisen	Coarse-grained quartz-muscovite-tourmaline greisen	Chalcataya	Optically unzoned	Orange
2020-KELL-22-B-TS6-Circle A-Tur1a-004	Tur-1	2020-KELL-22-B	Greisen	Coarse-grained quartz-muscovite-tourmaline greisen	Chalcataya	Optically unzoned	Orange

EMPA label	Type	Sample	Host-rock	Description	Locality	Zone	Color
2020-KELL-22-B-TS6-Circle A-Tur1a-005	Tur-1	2020-KELL-22-B	Greisen	Coarse-grained quartz-muscovite-tourmaline greisen	Chalcataya	Optically unzoned	Orange
2020-KELL-22-B-TS6-Circle A-Tur1a-006	Tur-1	2020-KELL-22-B	Greisen	Coarse-grained quartz-muscovite-tourmaline greisen	Chalcataya	Optically unzoned	Orange
2020-KELL-22-B-TS6-Circle A-Tur1a-007	Tur-1	2020-KELL-22-B	Greisen	Coarse-grained quartz-muscovite-tourmaline greisen	Chalcataya	Optically unzoned	Orange
2020-KELL-22-B-TS6-Circle A-Tur1a-008	Tur-1	2020-KELL-22-B	Greisen	Coarse-grained quartz-muscovite-tourmaline greisen	Chalcataya	Optically unzoned	Orange
2020-KELL-22-B-TS6-Circle C-TUR1A-001	Tur-1	2020-KELL-22-B	Greisen	Coarse-grained quartz-muscovite-tourmaline greisen	Chalcataya	Optically unzoned	Orange
2020-KELL-22-B-TS6-Circle C-TUR1A-002	Tur-1	2020-KELL-22-B	Greisen	Coarse-grained quartz-muscovite-tourmaline greisen	Chalcataya	Optically unzoned	Orange
2020-KELL-22-B-TS6-Circle D-TUR1A-001	Tur-1	2020-KELL-22-B	Greisen	Coarse-grained quartz-muscovite-tourmaline greisen	Chalcataya	Optically unzoned	Orange
2020-KELL-22-B-TS6-Circle D-TUR1A-002	Tur-1	2020-KELL-22-B	Greisen	Coarse-grained quartz-muscovite-tourmaline greisen	Chalcataya	Optically unzoned	Orange
2020-KELL-22-B-TS6-Circle D-TUR1A-004	Tur-1	2020-KELL-22-B	Greisen	Coarse-grained quartz-muscovite-tourmaline greisen	Chalcataya	Optically unzoned	Orange
2020-KELL-22-B-TS6-Circle D-TUR1A-005	Tur-1	2020-KELL-22-B	Greisen	Coarse-grained quartz-muscovite-tourmaline greisen	Chalcataya	Optically unzoned	Orange
2020-KELL-22-B-TS6-Circle D-TUR1A-006	Tur-1	2020-KELL-22-B	Greisen	Coarse-grained quartz-muscovite-tourmaline greisen	Chalcataya	Optically unzoned	Orange
2020-KELL-22-B-TS6-Circle D-TUR1A-007	Tur-1	2020-KELL-22-B	Greisen	Coarse-grained quartz-muscovite-tourmaline greisen	Chalcataya	Optically unzoned	Orange
2020-KELL-22-B-TS6-Circle D-TUR1A-008	Tur-1	2020-KELL-22-B	Greisen	Coarse-grained quartz-muscovite-tourmaline greisen	Chalcataya	Optically unzoned	Orange
2020-KELL-22-B-TS6-Circle D-TUR1A-009	Tur-1	2020-KELL-22-B	Greisen	Coarse-grained quartz-muscovite-tourmaline greisen	Chalcataya	Optically unzoned	Orange
2020-KELL-22-B-TS6-Circle E-TUR1A-001	Tur-1	2020-KELL-22-B	Greisen	Coarse-grained quartz-muscovite-tourmaline greisen	Chalcataya	Optically unzoned	Orange
2020-KELL-22-B-TS6-Circle E-TUR1A-002	Tur-1	2020-KELL-22-B	Greisen	Coarse-grained quartz-muscovite-tourmaline greisen	Chalcataya	Optically unzoned	Orange
2020-KELL-22-B-TS6-Circle E-TUR1A-003	Tur-1	2020-KELL-22-B	Greisen	Coarse-grained quartz-muscovite-tourmaline greisen	Chalcataya	Optically unzoned	Orange
2020-KELL-22-B-TS6-Circle E-TUR1A-004	Tur-1	2020-KELL-22-B	Greisen	Coarse-grained quartz-muscovite-tourmaline greisen	Chalcataya	Optically unzoned	Orange

EMPA label	Type	Sample	Host-rock	Description	Locality	Zone	Color
2020-KELL-22-B-TS6-Circle E-TUR1A-005	Tur-1	2020-KELL-22-B	Greisen	Coarse-grained quartz-muscovite-tourmaline greisen	Chalcataya	Optically unzoned	Orange
2020-KELL-22-B-TS6-Circle F-TUR1A-001	Tur-1	2020-KELL-22-B	Greisen	Coarse-grained quartz-muscovite-tourmaline greisen	Chalcataya	Optically unzoned	Orange
2020-KELL-22-B-TS6-Circle F-TUR1A-002	Tur-1	2020-KELL-22-B	Greisen	Coarse-grained quartz-muscovite-tourmaline greisen	Chalcataya	Optically unzoned	Orange
2020-KELL-22-B-TS6-Circle F-TUR1A-003	Tur-1	2020-KELL-22-B	Greisen	Coarse-grained quartz-muscovite-tourmaline greisen	Chalcataya	Optically unzoned	Orange
2020-KELL-22-B-TS6-Circle F-TUR1A-004	Tur-1	2020-KELL-22-B	Greisen	Coarse-grained quartz-muscovite-tourmaline greisen	Chalcataya	Optically unzoned	Orange
2020-KELL-22-B-TS6-Circle F-TUR1A-005	Tur-1	2020-KELL-22-B	Greisen	Coarse-grained quartz-muscovite-tourmaline greisen	Chalcataya	Optically unzoned	Orange
2020-KELL-22-B-TS6-Circle F-TUR1A-006	Tur-1	2020-KELL-22-B	Greisen	Coarse-grained quartz-muscovite-tourmaline greisen	Chalcataya	Optically unzoned	Orange
2020-KELL-22-B-TS6-Circle G-TUR1A-001	Tur-1	2020-KELL-22-B	Greisen	Coarse-grained quartz-muscovite-tourmaline greisen	Chalcataya	Optically unzoned	Orange
2020-KELL-22-B-TS6-Circle G-TUR1A-002	Tur-1	2020-KELL-22-B	Greisen	Coarse-grained quartz-muscovite-tourmaline greisen	Chalcataya	Optically unzoned	Orange
2020-KELL-22-B-TS6-Circle G-TUR1A-003	Tur-1	2020-KELL-22-B	Greisen	Coarse-grained quartz-muscovite-tourmaline greisen	Chalcataya	Optically unzoned	Orange
2020-KELL-22-B-TS6-Circle G-TUR1A-004	Tur-1	2020-KELL-22-B	Greisen	Coarse-grained quartz-muscovite-tourmaline greisen	Chalcataya	Optically unzoned	Orange
2020-KELL-22-B-TS6-Circle G-TUR1A-005	Tur-1	2020-KELL-22-B	Greisen	Coarse-grained quartz-muscovite-tourmaline greisen	Chalcataya	Optically unzoned	Orange
2020-KELL-22-B-TS6-Circle G-TUR1A-006	Tur-1	2020-KELL-22-B	Greisen	Coarse-grained quartz-muscovite-tourmaline greisen	Chalcataya	Optically unzoned	Orange
2020-KELL-22-B-TS6-Circle G-TUR1A-007	Tur-1	2020-KELL-22-B	Greisen	Coarse-grained quartz-muscovite-tourmaline greisen	Chalcataya	Optically unzoned	Orange
2020-KELL-22-B-TS6-Circle G-TUR1A-008	Tur-1	2020-KELL-22-B	Greisen	Coarse-grained quartz-muscovite-tourmaline greisen	Chalcataya	Optically unzoned	Orange
2020-KELL-22-B-TS6-Circle H-TUR1A-001	Tur-1	2020-KELL-22-B	Greisen	Coarse-grained quartz-muscovite-tourmaline greisen	Chalcataya	Optically unzoned	Orange
2020-KELL-22-B-TS6-Circle H-TUR1A-002	Tur-1	2020-KELL-22-B	Greisen	Coarse-grained quartz-muscovite-tourmaline greisen	Chalcataya	Optically unzoned	Orange
2020-KELL-22-B-TS6-Circle H-TUR1A-003	Tur-1	2020-KELL-22-B	Greisen	Coarse-grained quartz-muscovite-tourmaline greisen	Chalcataya	Optically unzoned	Orange

EMPA label	Type	Sample	Host-rock	Description	Locality	Zone	Color
2020-KELL-22-B-TS6-Circle H-TUR1A-004	Tur-1	2020-KELL-22-B	Greisen	Coarse-grained quartz-muscovite-tourmaline greisen	Chalcataya	Optically unzoned	Orange
2020-KELL-22-B-TS6-Circle H-TUR1A-005	Tur-1	2020-KELL-22-B	Greisen	Coarse-grained quartz-muscovite-tourmaline greisen	Chalcataya	Optically unzoned	Orange
2020-KELL-22-B-TS6-Circle J-TUR1A-001	Tur-1	2020-KELL-22-B	Greisen	Coarse-grained quartz-muscovite-tourmaline greisen	Chalcataya	Optically unzoned	Orange
2020-KELL-22-B-TS6-Circle J-TUR1A-002	Tur-1	2020-KELL-22-B	Greisen	Coarse-grained quartz-muscovite-tourmaline greisen	Chalcataya	Optically unzoned	Orange
2020-KELL-22-B-TS6-Circle J-TUR1A-003	Tur-1	2020-KELL-22-B	Greisen	Coarse-grained quartz-muscovite-tourmaline greisen	Chalcataya	Optically unzoned	Orange
2020-KELL-22-B-TS6-Circle J-TUR1A-004	Tur-1	2020-KELL-22-B	Greisen	Coarse-grained quartz-muscovite-tourmaline greisen	Chalcataya	Optically unzoned	Orange
2020-KELL-22-B-TS6-Circle J-TUR1A-005	Tur-1	2020-KELL-22-B	Greisen	Coarse-grained quartz-muscovite-tourmaline greisen	Chalcataya	Optically unzoned	Orange
2020-KELL-22-B-TS6-Circle J-TUR1A-006	Tur-1	2020-KELL-22-B	Greisen	Coarse-grained quartz-muscovite-tourmaline greisen	Chalcataya	Optically unzoned	Orange
2020-KELL-22-B-TS6-Circle K-TUR1A-001	Tur-1	2020-KELL-22-B	Greisen	Coarse-grained quartz-muscovite-tourmaline greisen	Chalcataya	Optically unzoned	Orange
2020-KELL-22-B-TS6-Circle K-TUR1A-002	Tur-1	2020-KELL-22-B	Greisen	Coarse-grained quartz-muscovite-tourmaline greisen	Chalcataya	Optically unzoned	Orange
2020-KELL-22-B-TS6-Circle K-TUR1A-003	Tur-1	2020-KELL-22-B	Greisen	Coarse-grained quartz-muscovite-tourmaline greisen	Chalcataya	Optically unzoned	Orange
2020-KELL-22-B-TS6-Circle K-TUR1A-004	Tur-1	2020-KELL-22-B	Greisen	Coarse-grained quartz-muscovite-tourmaline greisen	Chalcataya	Optically unzoned	Orange
2020-KELL-22-B-TS6-Circle K-TUR1A-005	Tur-1	2020-KELL-22-B	Greisen	Coarse-grained quartz-muscovite-tourmaline greisen	Chalcataya	Optically unzoned	Orange
2020-KELL-22-B-TS6-Circle K-TUR1A-006	Tur-1	2020-KELL-22-B	Greisen	Coarse-grained quartz-muscovite-tourmaline greisen	Chalcataya	Optically unzoned	Orange
2020-KELL-22-B-TS6-Circle L-TUR1A-001	Tur-1	2020-KELL-22-B	Greisen	Coarse-grained quartz-muscovite-tourmaline greisen	Chalcataya	Optically unzoned	Orange
2020-KELL-22-B-TS6-Circle L-TUR1A-002	Tur-1	2020-KELL-22-B	Greisen	Coarse-grained quartz-muscovite-tourmaline greisen	Chalcataya	Optically unzoned	Orange
2020-KELL-22-B-TS6-Circle L-TUR1A-003	Tur-1	2020-KELL-22-B	Greisen	Coarse-grained quartz-muscovite-tourmaline greisen	Chalcataya	Optically unzoned	Orange
2020-KELL-22-B-TS6-Circle L-TUR1A-004	Tur-1	2020-KELL-22-B	Greisen	Coarse-grained quartz-muscovite-tourmaline greisen	Chalcataya	Optically unzoned	Orange

EMPA label	Type	Sample	Host-rock	Description	Locality	Zone	Color
2020-KELL-22-B-TS6-Circle L-TUR1A-005	Tur-1	2020-KELL-22-B	Greisen	Coarse-grained quartz-muscovite-tourmaline greisen	Chalcataya	Optically unzoned	Orange
2020-KELL-22-B-TS6-Circle L-TUR1A-006	Tur-1	2020-KELL-22-B	Greisen	Coarse-grained quartz-muscovite-tourmaline greisen	Chalcataya	Optically unzoned	Orange
2020-KELL-23-TS1-Circle A-TUR1A-001	Tur-1	2020-KELL-23	Greisen	Coarse-grained quartz-muscovite-tourmaline greisen	Chalcataya	Optically unzoned	Orange
2020-KELL-23-TS1-Circle A-TUR1A-002	Tur-1	2020-KELL-23	Greisen	Coarse-grained quartz-muscovite-tourmaline greisen	Chalcataya	Optically unzoned	Orange
2020-KELL-23-TS1-Circle A-TUR1A-003	Tur-1	2020-KELL-23	Greisen	Coarse-grained quartz-muscovite-tourmaline greisen	Chalcataya	Optically unzoned	Orange
2020-KELL-23-TS1-Circle A-TUR1A-004	Tur-1	2020-KELL-23	Greisen	Coarse-grained quartz-muscovite-tourmaline greisen	Chalcataya	Optically unzoned	Orange
2020-KELL-23-TS1-Circle A-TUR1A-005	Tur-1	2020-KELL-23	Greisen	Coarse-grained quartz-muscovite-tourmaline greisen	Chalcataya	Optically unzoned	Orange
2020-KELL-23-TS1-Circle A-TUR1A-006	Tur-1	2020-KELL-23	Greisen	Coarse-grained quartz-muscovite-tourmaline greisen	Chalcataya	Optically unzoned	Orange
2020-KELL-23-TS1-Circle A-TUR1A-007	Tur-1	2020-KELL-23	Greisen	Coarse-grained quartz-muscovite-tourmaline greisen	Chalcataya	Optically unzoned	Orange
2020-KELL-23-TS1-Circle A-TUR1A-008	Tur-1	2020-KELL-23	Greisen	Coarse-grained quartz-muscovite-tourmaline greisen	Chalcataya	Optically unzoned	Orange
2020-KELL-23-TS1-Circle A-TUR1A-009	Tur-1	2020-KELL-23	Greisen	Coarse-grained quartz-muscovite-tourmaline greisen	Chalcataya	Optically unzoned	Orange
2020-KELL-23-TS1-Circle A-TUR1A-010	Tur-1	2020-KELL-23	Greisen	Coarse-grained quartz-muscovite-tourmaline greisen	Chalcataya	Optically unzoned	Orange
2020-KELL-23-TS1-Circle A-TUR1A-011	Tur-1	2020-KELL-23	Greisen	Coarse-grained quartz-muscovite-tourmaline greisen	Chalcataya	Optically unzoned	Orange
2020-KELL-23-TS1-Circle A-TUR1A-012	Tur-1	2020-KELL-23	Greisen	Coarse-grained quartz-muscovite-tourmaline greisen	Chalcataya	Optically unzoned	Orange
2020-KELL-23-TS1-Circle B-TUR1A-001	Tur-1	2020-KELL-23	Greisen	Coarse-grained quartz-muscovite-tourmaline greisen	Chalcataya	Optically unzoned	Orange
2020-KELL-23-TS1-Circle B-TUR1A-002	Tur-1	2020-KELL-23	Greisen	Coarse-grained quartz-muscovite-tourmaline greisen	Chalcataya	Optically unzoned	Orange
2020-KELL-23-TS1-Circle B-TUR1A-003	Tur-1	2020-KELL-23	Greisen	Coarse-grained quartz-muscovite-tourmaline greisen	Chalcataya	Optically unzoned	Orange
2020-KELL-23-TS1-Circle B-TUR1A-004	Tur-1	2020-KELL-23	Greisen	Coarse-grained quartz-muscovite-tourmaline greisen	Chalcataya	Optically unzoned	Orange

EMPA label	Type	Sample	Host-rock	Description	Locality	Zone	Color
2020-KELL-23-TS1-Circle B-TUR1A-005	Tur-1	2020-KELL-23	Greisen	Coarse-grained quartz-muscovite-tourmaline greisen	Chalcataya	Optically unzoned	Orange
2020-KELL-23-TS1-Circle B-TUR1A-006	Tur-1	2020-KELL-23	Greisen	Coarse-grained quartz-muscovite-tourmaline greisen	Chalcataya	Optically unzoned	Orange
2020-KELL-23-TS1-Circle B-TUR1A-007	Tur-1	2020-KELL-23	Greisen	Coarse-grained quartz-muscovite-tourmaline greisen	Chalcataya	Optically unzoned	Orange
2020-KELL-23-TS1-Circle B-TUR1A-008	Tur-1	2020-KELL-23	Greisen	Coarse-grained quartz-muscovite-tourmaline greisen	Chalcataya	Optically unzoned	Orange
2020-KELL-23-TS1-Circle B-TUR1A-009	Tur-1	2020-KELL-23	Greisen	Coarse-grained quartz-muscovite-tourmaline greisen	Chalcataya	Optically unzoned	Orange
2020-KELL-23-TS1-Circle B-TUR1A-010	Tur-1	2020-KELL-23	Greisen	Coarse-grained quartz-muscovite-tourmaline greisen	Chalcataya	Optically unzoned	Orange
2020-KELL-23-TS1-Circle B-TUR1A-011	Tur-1	2020-KELL-23	Greisen	Coarse-grained quartz-muscovite-tourmaline greisen	Chalcataya	Optically unzoned	Orange
2020-KELL-23-TS1-Circle B-TUR1A-012	Tur-1	2020-KELL-23	Greisen	Coarse-grained quartz-muscovite-tourmaline greisen	Chalcataya	Optically unzoned	Orange
2020-KELL-23-TS1-Circle B-TUR1A-013	Tur-1	2020-KELL-23	Greisen	Coarse-grained quartz-muscovite-tourmaline greisen	Chalcataya	Optically unzoned	Orange
2020-KELL-23-TS1-Circle B-TUR1A-014	Tur-1	2020-KELL-23	Greisen	Coarse-grained quartz-muscovite-tourmaline greisen	Chalcataya	Optically unzoned	Orange
2020-KELL-23-TS1-Circle B-TUR1A-015	Tur-1	2020-KELL-23	Greisen	Coarse-grained quartz-muscovite-tourmaline greisen	Chalcataya	Optically unzoned	Orange
2020-KELL-23-TS1-Circle B-TUR1A-016	Tur-1	2020-KELL-23	Greisen	Coarse-grained quartz-muscovite-tourmaline greisen	Chalcataya	Optically unzoned	Orange
2020-KELL-23-TS1-Circle B-TUR1A-017	Tur-1	2020-KELL-23	Greisen	Coarse-grained quartz-muscovite-tourmaline greisen	Chalcataya	Optically unzoned	Orange
2020-KELL-23-TS1-Circle B-TUR1A-018	Tur-1	2020-KELL-23	Greisen	Coarse-grained quartz-muscovite-tourmaline greisen	Chalcataya	Optically unzoned	Orange
2020-KELL-23-TS1-Circle B-TUR1A-019	Tur-1	2020-KELL-23	Greisen	Coarse-grained quartz-muscovite-tourmaline greisen	Chalcataya	Optically unzoned	Orange
2020-KELL-23-TS1-Circle B-TUR1A-020	Tur-1	2020-KELL-23	Greisen	Coarse-grained quartz-muscovite-tourmaline greisen	Chalcataya	Optically unzoned	Orange
2020-KELL-23-TS1-Circle B-TUR1A-021	Tur-1	2020-KELL-23	Greisen	Coarse-grained quartz-muscovite-tourmaline greisen	Chalcataya	Optically unzoned	Orange
2020-KELL-23-TS1-Circle B-TUR1A-023	Tur-1	2020-KELL-23	Greisen	Coarse-grained quartz-muscovite-tourmaline greisen	Chalcataya	Optically unzoned	Orange

EMPA label	Type	Sample	Host-rock	Description	Locality	Zone	Color
2020-KELL-23-TS1-Circle B-TUR1A-024	Tur-1	2020-KELL-23	Greisen	Coarse-grained quartz-muscovite-tourmaline greisen	Chalcataya	Optically unzoned	Orange
2020-KELL-23-TS1-Circle B-TUR1A-025	Tur-1	2020-KELL-23	Greisen	Coarse-grained quartz-muscovite-tourmaline greisen	Chalcataya	Optically unzoned	Orange
2020-KELL-23-TS1-Circle B-TUR1A-026	Tur-1	2020-KELL-23	Greisen	Coarse-grained quartz-muscovite-tourmaline greisen	Chalcataya	Optically unzoned	Orange
2020-KELL-23-TS1-Circle B-TUR1A-027	Tur-1	2020-KELL-23	Greisen	Coarse-grained quartz-muscovite-tourmaline greisen	Chalcataya	Optically unzoned	Orange
2020-KELL-23-TS1-Circle B-TUR1A-028	Tur-1	2020-KELL-23	Greisen	Coarse-grained quartz-muscovite-tourmaline greisen	Chalcataya	Optically unzoned	Orange
2020-KELL-23-TS1-Circle B-TUR1A-029	Tur-1	2020-KELL-23	Greisen	Coarse-grained quartz-muscovite-tourmaline greisen	Chalcataya	Optically unzoned	Orange
2020-KELL-23-TS1-Circle B-TUR1A-030	Tur-1	2020-KELL-23	Greisen	Coarse-grained quartz-muscovite-tourmaline greisen	Chalcataya	Optically unzoned	Orange
2020-KELL-23-TS1-Circle B-TUR1A-031	Tur-1	2020-KELL-23	Greisen	Coarse-grained quartz-muscovite-tourmaline greisen	Chalcataya	Optically unzoned	Orange
2020-KELL-23-TS1-Circle B-TUR1A-032	Tur-1	2020-KELL-23	Greisen	Coarse-grained quartz-muscovite-tourmaline greisen	Chalcataya	Optically unzoned	Orange
2020-KELL-23-TS1-Circle B-TUR1A-033	Tur-1	2020-KELL-23	Greisen	Coarse-grained quartz-muscovite-tourmaline greisen	Chalcataya	Optically unzoned	Orange
2020-KELL-24-TS1-Circle A-Tur1a-001	Tur-1	2020-KELL-24	Catavi Fm. quartzites	Tourmaline breccia hosting angular clasts of Catavi Fm. quartzites and greisen	Chalcataya	Optically unzoned	Orange
2020-KELL-24-TS1-Circle A-Tur1a-001	Tur-1	2020-KELL-24	Catavi Fm. quartzites	Tourmaline breccia hosting angular clasts of Catavi Fm. quartzites and greisen	Chalcataya	Optically unzoned	Orange
2020-KELL-24-TS1-Circle A-Tur1a-002	Tur-1	2020-KELL-24	Catavi Fm. quartzites	Tourmaline breccia hosting angular clasts of Catavi Fm. quartzites and greisen	Chalcataya	Optically unzoned	Orange
2020-KELL-24-TS1-Circle A-Tur1a-003	Tur-1	2020-KELL-24	Catavi Fm. quartzites	Tourmaline breccia hosting angular clasts of Catavi Fm. quartzites and greisen	Chalcataya	Optically unzoned	Orange
2020-KELL-24-TS1-Circle A-Tur1a-004	Tur-1	2020-KELL-24	Catavi Fm. quartzites	Tourmaline breccia hosting angular clasts of Catavi Fm. quartzites and greisen	Chalcataya	Optically unzoned	Orange

EMPA label	Type	Sample	Host-rock	Description	Locality	Zone	Color
2020-KELL-24-TS1-Circle A-Tur2-core001	Tur-2	2020-KELL-24	Catavi Fm. quartzites	Tourmaline breccia hosting angular clasts of Catavi Fm. quartzites and greisen	Chalcataya	Core	Bluish green
2020-KELL-24-TS1-Circle A-Tur2-core002	Tur-2	2020-KELL-24	Catavi Fm. quartzites	Tourmaline breccia hosting angular clasts of Catavi Fm. quartzites and greisen	Chalcataya	Core	Bluish green
2020-KELL-24-TS1-Circle A-Tur2-core003	Tur-2	2020-KELL-24	Catavi Fm. quartzites	Tourmaline breccia hosting angular clasts of Catavi Fm. quartzites and greisen	Chalcataya	Core	Bluish green
2020-KELL-24-TS1-Circle A-Tur2-core004	Tur-2	2020-KELL-24	Catavi Fm. quartzites	Tourmaline breccia hosting angular clasts of Catavi Fm. quartzites and greisen	Chalcataya	Core	Bluish green
2020-KELL-24-TS1-Circle A-Tur2-rim001	Tur-2	2020-KELL-24	Catavi Fm. quartzites	Tourmaline breccia hosting angular clasts of Catavi Fm. quartzites and greisen	Chalcataya	Rim	Bluish green
2020-KELL-24-TS1-Circle A-Tur2-rim002	Tur-2	2020-KELL-24	Catavi Fm. quartzites	Tourmaline breccia hosting angular clasts of Catavi Fm. quartzites and greisen	Chalcataya	Rim	Bluish green
2020-KELL-24-TS1-Circle A-Tur2-001	Tur-2	2020-KELL-24	Catavi Fm. quartzites	Tourmaline breccia hosting angular clasts of Catavi Fm. quartzites and greisen	Chalcataya	Optically unzoned	Bluish green
2020-KELL-24-TS1-Circle A-Tur2-002	Tur-2	2020-KELL-24	Catavi Fm. quartzites	Tourmaline breccia hosting angular clasts of Catavi Fm. quartzites and greisen	Chalcataya	Core	Bluish green
2020-KELL-24-TS1-Circle A-Tur2-003	Tur-2	2020-KELL-24	Catavi Fm. quartzites	Tourmaline breccia hosting angular clasts of Catavi Fm. quartzites and greisen	Chalcataya	Optically unzoned	Bluish green
2020-KELL-24-TS1-Circle A-Tur2-004	Tur-2	2020-KELL-24	Catavi Fm. quartzites	Tourmaline breccia hosting angular clasts of Catavi Fm. quartzites and greisen	Chalcataya	Core-2	Bluish green
2020-KELL-24-TS1-Circle A-Tur2-005	Tur-2	2020-KELL-24	Catavi Fm. quartzites	Tourmaline breccia hosting angular clasts of Catavi Fm. quartzites and greisen	Chalcataya	Core-1	Bluish green
2020-KELL-24-TS1-Circle A-Tur2-006	Tur-2	2020-KELL-24	Catavi Fm. quartzites	Tourmaline breccia hosting angular clasts of Catavi Fm. quartzites and greisen	Chalcataya	Core	Bluish green

EMPA label	Type	Sample	Host-rock	Description	Locality	Zone	Color
2020-KELL-24-TS1-Circle A-Tur2-007	Tur-2	2020-KELL-24	Catavi Fm. quartzites	Tourmaline breccia hosting angular clasts of Catavi Fm. quartzites and greisen	Chalcataya	Rim	Bluish green
2020-KELL-24-TS1-Circle B-Tur1a-001	Tur-1	2020-KELL-24	Catavi Fm. quartzites	Tourmaline breccia hosting angular clasts of Catavi Fm. quartzites and greisen	Chalcataya	Optically unzoned	Orange
2020-KELL-24-TS1-Circle B-Tur1a-002	Tur-1	2020-KELL-24	Catavi Fm. quartzites	Tourmaline breccia hosting angular clasts of Catavi Fm. quartzites and greisen	Chalcataya	Optically unzoned	Orange
2020-KELL-24-TS1-Circle B-Tur2-001	Tur-2	2020-KELL-24	Catavi Fm. quartzites	Tourmaline breccia hosting angular clasts of Catavi Fm. quartzites and greisen	Chalcataya	Optically unzoned	Bluish green
2020-KELL-24-TS1-Circle B-Tur2-002	Tur-2	2020-KELL-24	Catavi Fm. quartzites	Tourmaline breccia hosting angular clasts of Catavi Fm. quartzites and greisen	Chalcataya	Optically unzoned	Bluish green
2020-KELL-24-TS1-Circle B-Tur2-003	Tur-2	2020-KELL-24	Catavi Fm. quartzites	Tourmaline breccia hosting angular clasts of Catavi Fm. quartzites and greisen	Chalcataya	Optically unzoned	Bluish green
2020-KELL-24-TS1-Circle B-Tur2-004	Tur-2	2020-KELL-24	Catavi Fm. quartzites	Tourmaline breccia hosting angular clasts of Catavi Fm. quartzites and greisen	Chalcataya	Optically unzoned	Bluish green
2020-KELL-24-TS1-Circle B-Tur2-005	Tur-2	2020-KELL-24	Catavi Fm. quartzites	Tourmaline breccia hosting angular clasts of Catavi Fm. quartzites and greisen	Chalcataya	Optically unzoned	Bluish green
2020-KELL-24-TS1-Circle B-Tur2-006	Tur-2	2020-KELL-24	Catavi Fm. quartzites	Tourmaline breccia hosting angular clasts of Catavi Fm. quartzites and greisen	Chalcataya	Optically unzoned	Bluish green
2020-KELL-24-TS1-Circle B-Tur2-007	Tur-2	2020-KELL-24	Catavi Fm. quartzites	Tourmaline breccia hosting angular clasts of Catavi Fm. quartzites and greisen	Chalcataya	Optically unzoned	Bluish green
2020-KELL-24-TS1-Circle C-Tur2-001	Tur-2	2020-KELL-24	Catavi Fm. quartzites	Tourmaline breccia hosting angular clasts of Catavi Fm. quartzites and greisen	Chalcataya	Optically unzoned	Bluish green
2020-KELL-24-TS1-Circle C-Tur2-002	Tur-2	2020-KELL-24	Catavi Fm. quartzites	Tourmaline breccia hosting angular clasts of Catavi Fm. quartzites and greisen	Chalcataya	Optically unzoned	Bluish green

EMPA label	Type	Sample	Host-rock	Description	Locality	Zone	Color
2020-KELL-24-TS1-Circle C-Tur2-003	Tur-2	2020-KELL-24	Catavi Fm. quartzites	Tourmaline breccia hosting angular clasts of Catavi Fm. quartzites and greisen	Chalcataya	Optically unzoned	Bluish green
2020-KELL-24-TS1-Circle C-Tur2-004	Tur-2	2020-KELL-24	Catavi Fm. quartzites	Tourmaline breccia hosting angular clasts of Catavi Fm. quartzites and greisen	Chalcataya	Optically unzoned	Bluish green
2020-KELL-24-TS1-Circle C-Tur2-005	Tur-2	2020-KELL-24	Catavi Fm. quartzites	Tourmaline breccia hosting angular clasts of Catavi Fm. quartzites and greisen	Chalcataya	Optically unzoned	Bluish green
2020-KELL-24-TS1-Circle C-Tur2-006	Tur-2	2020-KELL-24	Catavi Fm. quartzites	Tourmaline breccia hosting angular clasts of Catavi Fm. quartzites and greisen	Chalcataya	Optically unzoned	Bluish green
2020-KELL-24-TS1-Circle C-Tur2-007	Tur-2	2020-KELL-24	Catavi Fm. quartzites	Tourmaline breccia hosting angular clasts of Catavi Fm. quartzites and greisen	Chalcataya	Optically unzoned	Bluish green
2020-KELL-24-TS1-Circle C-Tur2-008	Tur-2	2020-KELL-24	Catavi Fm. quartzites	Tourmaline breccia hosting angular clasts of Catavi Fm. quartzites and greisen	Chalcataya	Optically unzoned	Bluish green
2020-KELL-24-TS1-Circle D-Tur1a-001	Tur-1	2020-KELL-24	Catavi Fm. quartzites	Tourmaline breccia hosting angular clasts of Catavi Fm. quartzites and greisen	Chalcataya	Optically unzoned	Orange
2020-KELL-24-TS1-Circle D-Tur1a-002	Tur-1	2020-KELL-24	Catavi Fm. quartzites	Tourmaline breccia hosting angular clasts of Catavi Fm. quartzites and greisen	Chalcataya	Optically unzoned	Orange
2020-KELL-24-TS1-Circle D-Tur1a-003	Tur-1	2020-KELL-24	Catavi Fm. quartzites	Tourmaline breccia hosting angular clasts of Catavi Fm. quartzites and greisen	Chalcataya	Optically unzoned	Orange
2020-KELL-24-TS1-Circle E-Tur1a-004	Tur-1	2020-KELL-24	Catavi Fm. quartzites	Tourmaline breccia hosting angular clasts of Catavi Fm. quartzites and greisen	Chalcataya	Optically unzoned	Orange
2020-KELL-24-TS1-Circle E-Tur1a-005	Tur-1	2020-KELL-24	Catavi Fm. quartzites	Tourmaline breccia hosting angular clasts of Catavi Fm. quartzites and greisen	Chalcataya	Optically unzoned	Orange
2020-KELL-24-TS1-Circle E-Tur1a-006	Tur-1	2020-KELL-24	Catavi Fm. quartzites	Tourmaline breccia hosting angular clasts of Catavi Fm. quartzites and greisen	Chalcataya	Optically unzoned	Orange

EMPA label	Type	Sample	Host-rock	Description	Locality	Zone	Color
2020-KELL-24-TS1-Circle E-Tur1a-007	Tur-1	2020-KELL-24	Catavi Fm. quartzites	Tourmaline breccia hosting angular clasts of Catavi Fm. quartzites and greisen	Chalcataya	Optically unzoned	Orange
2020-KELL-24-TS1-Circle F-Tur1a-001	Tur-1	2020-KELL-24	Catavi Fm. quartzites	Tourmaline breccia hosting angular clasts of Catavi Fm. quartzites and greisen	Chalcataya	Optically unzoned	Orange
2020-KELL-24-TS1-Circle F-Tur1a-002	Tur-1	2020-KELL-24	Catavi Fm. quartzites	Tourmaline breccia hosting angular clasts of Catavi Fm. quartzites and greisen	Chalcataya	Optically unzoned	Orange
2020-KELL-24-TS1-Circle F-Tur2-001	Tur-2	2020-KELL-24	Catavi Fm. quartzites	Tourmaline breccia hosting angular clasts of Catavi Fm. quartzites and greisen	Chalcataya	Optically unzoned	Bluish green
2020-KELL-24-TS1-Circle F-Tur2-002	Tur-2	2020-KELL-24	Catavi Fm. quartzites	Tourmaline breccia hosting angular clasts of Catavi Fm. quartzites and greisen	Chalcataya	Optically unzoned	Bluish green
2020-KELL-24-TS1-Circle G-Tur2-001	Tur-2	2020-KELL-24	Catavi Fm. quartzites	Tourmaline breccia hosting angular clasts of Catavi Fm. quartzites and greisen	Chalcataya	Optically unzoned	Bluish green
2020-KELL-24-TS1-Circle G-Tur2-002	Tur-2	2020-KELL-24	Catavi Fm. quartzites	Tourmaline breccia hosting angular clasts of Catavi Fm. quartzites and greisen	Chalcataya	Optically unzoned	Bluish green
2020-KELL-24-TS1-Circle G-Tur2-003	Tur-2	2020-KELL-24	Catavi Fm. quartzites	Tourmaline breccia hosting angular clasts of Catavi Fm. quartzites and greisen	Chalcataya	Optically unzoned	Bluish green
2020-KELL-24-TS1-Circle H-Tur1a-001	Tur-1	2020-KELL-24	Catavi Fm. quartzites	Tourmaline breccia hosting angular clasts of Catavi Fm. quartzites and greisen	Chalcataya	Optically unzoned	Orange
2020-KELL-24-TS1-Circle H-Tur2-001	Tur-2	2020-KELL-24	Catavi Fm. quartzites	Tourmaline breccia hosting angular clasts of Catavi Fm. quartzites and greisen	Chalcataya	Optically unzoned	Bluish green
2020-KELL-24-TS1-Circle H-Tur2-002	Tur-2	2020-KELL-24	Catavi Fm. quartzites	Tourmaline breccia hosting angular clasts of Catavi Fm. quartzites and greisen	Chalcataya	Optically unzoned	Bluish green
2020-KELL-24-TS1-Circle H-Tur2-003	Tur-2	2020-KELL-24	Catavi Fm. quartzites	Tourmaline breccia hosting angular clasts of Catavi Fm. quartzites and greisen	Chalcataya	Optically unzoned	Bluish green

EMPA label	Type	Sample	Host-rock	Description	Locality	Zone	Color
2020-KELL-24-TS1-Circle I-Tur1a-001	Tur-1	2020-KELL-24	Catavi Fm. quartzites	Tourmaline breccia hosting angular clasts of Catavi Fm. quartzites and greisen	Chalcataya	Optically unzoned	Orange
2020-KELL-24-TS1-Circle I-Tur1a-002	Tur-1	2020-KELL-24	Catavi Fm. quartzites	Tourmaline breccia hosting angular clasts of Catavi Fm. quartzites and greisen	Chalcataya	Optically unzoned	Orange
2020-KELL-24-TS1-Circle I-Tur1a-003	Tur-1	2020-KELL-24	Catavi Fm. quartzites	Tourmaline breccia hosting angular clasts of Catavi Fm. quartzites and greisen	Chalcataya	Optically unzoned	Orange
2020-KELL-24-TS1-Circle I-Tur1a-004	Tur-1	2020-KELL-24	Catavi Fm. quartzites	Tourmaline breccia hosting angular clasts of Catavi Fm. quartzites and greisen	Chalcataya	Optically unzoned	Orange
2020-KELL-24-TS1-Circle I-Tur2-001	Tur-2	2020-KELL-24	Catavi Fm. quartzites	Tourmaline breccia hosting angular clasts of Catavi Fm. quartzites and greisen	Chalcataya	Optically unzoned	Bluish green
2020-KELL-24-TS1-Circle I-Tur2-002	Tur-2	2020-KELL-24	Catavi Fm. quartzites	Tourmaline breccia hosting angular clasts of Catavi Fm. quartzites and greisen	Chalcataya	Optically unzoned	Bluish green
2020-KELL-24-TS1-Circle J-Tur2-001	Tur-2	2020-KELL-24	Catavi Fm. quartzites	Tourmaline breccia hosting angular clasts of Catavi Fm. quartzites and greisen	Chalcataya	Optically unzoned	Bluish green
2020-KELL-24-TS1-Circle J-Tur2-002	Tur-2	2020-KELL-24	Catavi Fm. quartzites	Tourmaline breccia hosting angular clasts of Catavi Fm. quartzites and greisen	Chalcataya	Optically unzoned	Bluish green
2020-KELL-24-TS1-Circle J-Tur2-003	Tur-2	2020-KELL-24	Catavi Fm. quartzites	Tourmaline breccia hosting angular clasts of Catavi Fm. quartzites and greisen	Chalcataya	Optically unzoned	Bluish green
2020-KELL-24-TS1-Circle J-Tur2-004	Tur-2	2020-KELL-24	Catavi Fm. quartzites	Tourmaline breccia hosting angular clasts of Catavi Fm. quartzites and greisen	Chalcataya	Optically unzoned	Bluish green
2020-KELL-24-TS1-Circle K-Tur2-001	Tur-2	2020-KELL-24	Catavi Fm. quartzites	Tourmaline breccia hosting angular clasts of Catavi Fm. quartzites and greisen	Chalcataya	Optically unzoned	Bluish green
2020-KELL-24-TS1-Circle K-Tur2-002	Tur-2	2020-KELL-24	Catavi Fm. quartzites	Tourmaline breccia hosting angular clasts of Catavi Fm. quartzites and greisen	Chalcataya	Optically unzoned	Bluish green

EMPA label	Type	Sample	Host-rock	Description	Locality	Zone	Color
2020-KELL-24-TS1-Circle K-Tur2-003	Tur-2	2020-KELL-24	Catavi Fm. quartzites	Tourmaline breccia hosting angular clasts of Catavi Fm. quartzites and greisen	Chalcataya	Optically unzoned	Bluish green
2020-KELL-24-TS1-Circle K-Tur2-004	Tur-2	2020-KELL-24	Catavi Fm. quartzites	Tourmaline breccia hosting angular clasts of Catavi Fm. quartzites and greisen	Chalcataya	Optically unzoned	Bluish green
2020-KELL-24-TS1-Circle L-Tur2-001	Tur-2	2020-KELL-24	Catavi Fm. quartzites	Tourmaline breccia hosting angular clasts of Catavi Fm. quartzites and greisen	Chalcataya	Optically unzoned	Bluish green
2020-KELL-24-TS1-Circle L-Tur2-002	Tur-2	2020-KELL-24	Catavi Fm. quartzites	Tourmaline breccia hosting angular clasts of Catavi Fm. quartzites and greisen	Chalcataya	Optically unzoned	Bluish green
2020-KELL-24-TS1-Circle L-Tur2-003	Tur-2	2020-KELL-24	Catavi Fm. quartzites	Tourmaline breccia hosting angular clasts of Catavi Fm. quartzites and greisen	Chalcataya	Optically unzoned	Bluish green
2020-KELL-24-TS1-Circle L-Tur2-004	Tur-2	2020-KELL-24	Catavi Fm. quartzites	Tourmaline breccia hosting angular clasts of Catavi Fm. quartzites and greisen	Chalcataya	Optically unzoned	Bluish green
2020-KELL-24-TS1-Circle L-Tur2-005	Tur-2	2020-KELL-24	Catavi Fm. quartzites	Tourmaline breccia hosting angular clasts of Catavi Fm. quartzites and greisen	Chalcataya	Optically unzoned	Bluish green
2020-KELL-24-TS1-Circle L-Tur2-006	Tur-2	2020-KELL-24	Catavi Fm. quartzites	Tourmaline breccia hosting angular clasts of Catavi Fm. quartzites and greisen	Chalcataya	Optically unzoned	Bluish green
2020-KELL-24-TS4-Circle A-Tur2-001	Tur-2	2020-KELL-24	Catavi Fm. quartzites	Tourmaline breccia hosting angular clasts of Catavi Fm. quartzites and greisen	Chalcataya	Optically unzoned	Bluish green
2020-KELL-24-TS4-Circle A-Tur2-002	Tur-2	2020-KELL-24	Catavi Fm. quartzites	Tourmaline breccia hosting angular clasts of Catavi Fm. quartzites and greisen	Chalcataya	Optically unzoned	Bluish green
2020-KELL-24-TS4-Circle A-Tur2-003	Tur-2	2020-KELL-24	Catavi Fm. quartzites	Tourmaline breccia hosting angular clasts of Catavi Fm. quartzites and greisen	Chalcataya	Optically unzoned	Bluish green
2020-KELL-24-TS4-Circle A-Tur2-004	Tur-2	2020-KELL-24	Catavi Fm. quartzites	Tourmaline breccia hosting angular clasts of Catavi Fm. quartzites and greisen	Chalcataya	Optically unzoned	Bluish green

EMPA label	Type	Sample	Host-rock	Description	Locality	Zone	Color
2020-KELL-24-TS4-Circle A-Tur2-005	Tur-2	2020-KELL-24	Catavi Fm. quartzites	Tourmaline breccia hosting angular clasts of Catavi Fm. quartzites and greisen	Chalcataya	Optically unzoned	Bluish green
2020-KELL-24-TS4-Circle A-Tur2-006	Tur-2	2020-KELL-24	Catavi Fm. quartzites	Tourmaline breccia hosting angular clasts of Catavi Fm. quartzites and greisen	Chalcataya	Optically unzoned	Bluish green
2020-KELL-24-TS4-Circle A-Tur2-007	Tur-2	2020-KELL-24	Catavi Fm. quartzites	Tourmaline breccia hosting angular clasts of Catavi Fm. quartzites and greisen	Chalcataya	Optically unzoned	Bluish green
2020-KELL-24-TS4-Circle A-Tur2-008	Tur-2	2020-KELL-24	Catavi Fm. quartzites	Tourmaline breccia hosting angular clasts of Catavi Fm. quartzites and greisen	Chalcataya	Optically unzoned	Bluish green
2020-KELL-24-TS4-Circle A-Tur2-009	Tur-2	2020-KELL-24	Catavi Fm. quartzites	Tourmaline breccia hosting angular clasts of Catavi Fm. quartzites and greisen	Chalcataya	Optically unzoned	Bluish green
2020-KELL-24-TS4-Circle A-Tur2-010	Tur-2	2020-KELL-24	Catavi Fm. quartzites	Tourmaline breccia hosting angular clasts of Catavi Fm. quartzites and greisen	Chalcataya	Optically unzoned	Bluish green
2020-KELL-24-TS4-Circle B-Tur2-001	Tur-2	2020-KELL-24	Catavi Fm. quartzites	Tourmaline breccia hosting angular clasts of Catavi Fm. quartzites and greisen	Chalcataya	Optically unzoned	Bluish green
2020-KELL-24-TS4-Circle B-Tur2-002	Tur-2	2020-KELL-24	Catavi Fm. quartzites	Tourmaline breccia hosting angular clasts of Catavi Fm. quartzites and greisen	Chalcataya	Optically unzoned	Bluish green
2020-KELL-24-TS4-Circle B-Tur2-003	Tur-2	2020-KELL-24	Catavi Fm. quartzites	Tourmaline breccia hosting angular clasts of Catavi Fm. quartzites and greisen	Chalcataya	Optically unzoned	Bluish green
2020-KELL-24-TS4-Circle B-Tur2-004	Tur-2	2020-KELL-24	Catavi Fm. quartzites	Tourmaline breccia hosting angular clasts of Catavi Fm. quartzites and greisen	Chalcataya	Optically unzoned	Bluish green
2020-KELL-24-TS4-Circle B-Tur2-005	Tur-2	2020-KELL-24	Catavi Fm. quartzites	Tourmaline breccia hosting angular clasts of Catavi Fm. quartzites and greisen	Chalcataya	Optically unzoned	Bluish green
2020-KELL-24-TS4-Circle C-Tur2-001	Tur-2	2020-KELL-24	Catavi Fm. quartzites	Tourmaline breccia hosting angular clasts of Catavi Fm. quartzites and greisen	Chalcataya	Optically unzoned	Bluish green

EMPA label	Type	Sample	Host-rock	Description	Locality	Zone	Color
2020-KELL-24-TS4-Circle C-Tur2-002	Tur-2	2020-KELL-24	Catavi Fm. quartzites	Tourmaline breccia hosting angular clasts of Catavi Fm. quartzites and greisen	Chalcataya	Optically unzoned	Bluish green
2020-KELL-24-TS4-Circle C-Tur2-003	Tur-2	2020-KELL-24	Catavi Fm. quartzites	Tourmaline breccia hosting angular clasts of Catavi Fm. quartzites and greisen	Chalcataya	Optically unzoned	Bluish green
2020-KELL-24-TS4-Circle C-Tur2-004	Tur-2	2020-KELL-24	Catavi Fm. quartzites	Tourmaline breccia hosting angular clasts of Catavi Fm. quartzites and greisen	Chalcataya	Optically unzoned	Bluish green
2020-KELL-24-TS4-Circle C-Tur2-005	Tur-2	2020-KELL-24	Catavi Fm. quartzites	Tourmaline breccia hosting angular clasts of Catavi Fm. quartzites and greisen	Chalcataya	Optically unzoned	Bluish green
2020-KELL-24-TS4-Circle D-Tur2-001	Tur-2	2020-KELL-24	Catavi Fm. quartzites	Tourmaline breccia hosting angular clasts of Catavi Fm. quartzites and greisen	Chalcataya	Optically unzoned	Bluish green
2020-KELL-24-TS4-Circle D-Tur2-002	Tur-2	2020-KELL-24	Catavi Fm. quartzites	Tourmaline breccia hosting angular clasts of Catavi Fm. quartzites and greisen	Chalcataya	Optically unzoned	Bluish green
2020-KELL-24-TS4-Circle D-Tur2-003	Tur-2	2020-KELL-24	Catavi Fm. quartzites	Tourmaline breccia hosting angular clasts of Catavi Fm. quartzites and greisen	Chalcataya	Optically unzoned	Bluish green
2020-KELL-24-TS4-Circle D-Tur2-004	Tur-2	2020-KELL-24	Catavi Fm. quartzites	Tourmaline breccia hosting angular clasts of Catavi Fm. quartzites and greisen	Chalcataya	Optically unzoned	Bluish green
2020-KELL-24-TS4-Circle D-Tur2-005	Tur-2	2020-KELL-24	Catavi Fm. quartzites	Tourmaline breccia hosting angular clasts of Catavi Fm. quartzites and greisen	Chalcataya	Optically unzoned	Bluish green
2020-KELL-24-TS4-Circle D-Tur2-006	Tur-2	2020-KELL-24	Catavi Fm. quartzites	Tourmaline breccia hosting angular clasts of Catavi Fm. quartzites and greisen	Chalcataya	Optically unzoned	Bluish green
2020-KELL-24-TS4-Circle E-Tur1a-001	Tur-1	2020-KELL-24	Catavi Fm. quartzites	Tourmaline breccia hosting angular clasts of Catavi Fm. quartzites and greisen	Chalcataya	Optically unzoned	Orange
2020-KELL-24-TS4-Circle E-Tur1a-002	Tur-1	2020-KELL-24	Catavi Fm. quartzites	Tourmaline breccia hosting angular clasts of Catavi Fm. quartzites and greisen	Chalcataya	Optically unzoned	Orange

EMPA label	Type	Sample	Host-rock	Description	Locality	Zone	Color
2020-KELL-24-TS4-Circle E-Tur1a-003	Tur-1	2020-KELL-24	Catavi Fm. quartzites	Tourmaline breccia hosting angular clasts of Catavi Fm. quartzites and greisen	Chalcataya	Optically unzoned	Orange
2020-KELL-24-TS4-Circle E-Tur1a-004	Tur-1	2020-KELL-24	Catavi Fm. quartzites	Tourmaline breccia hosting angular clasts of Catavi Fm. quartzites and greisen	Chalcataya	Optically unzoned	Orange
2020-KELL-24-TS4-Circle E-Tur2-001	Tur-2	2020-KELL-24	Catavi Fm. quartzites	Tourmaline breccia hosting angular clasts of Catavi Fm. quartzites and greisen	Chalcataya	Optically unzoned	Bluish green
2020-KELL-24-TS4-Circle E-Tur2-002	Tur-2	2020-KELL-24	Catavi Fm. quartzites	Tourmaline breccia hosting angular clasts of Catavi Fm. quartzites and greisen	Chalcataya	Optically unzoned	Bluish green
2020-KELL-24-TS4-Circle E-Tur2-003	Tur-2	2020-KELL-24	Catavi Fm. quartzites	Tourmaline breccia hosting angular clasts of Catavi Fm. quartzites and greisen	Chalcataya	Optically unzoned	Bluish green
2020-KELL-24-TS4-Circle E-Tur2-004	Tur-2	2020-KELL-24	Catavi Fm. quartzites	Tourmaline breccia hosting angular clasts of Catavi Fm. quartzites and greisen	Chalcataya	Optically unzoned	Bluish green
2020-KELL-24-TS4-Circle E-Tur2-005	Tur-2	2020-KELL-24	Catavi Fm. quartzites	Tourmaline breccia hosting angular clasts of Catavi Fm. quartzites and greisen	Chalcataya	Optically unzoned	Bluish green
2020-KELL-24-TS4-Circle E-Tur2-006	Tur-2	2020-KELL-24	Catavi Fm. quartzites	Tourmaline breccia hosting angular clasts of Catavi Fm. quartzites and greisen	Chalcataya	Optically unzoned	Bluish green
2020-KELL-24-TS4-Circle E-Tur2-007	Tur-2	2020-KELL-24	Catavi Fm. quartzites	Tourmaline breccia hosting angular clasts of Catavi Fm. quartzites and greisen	Chalcataya	Optically unzoned	Bluish green
2020-KELL-24-TS4-Circle E-Tur2-008	Tur-2	2020-KELL-24	Catavi Fm. quartzites	Tourmaline breccia hosting angular clasts of Catavi Fm. quartzites and greisen	Chalcataya	Optically unzoned	Bluish green
2020-KELL-24-TS4-Circle F-Tur2-001	Tur-2	2020-KELL-24	Catavi Fm. quartzites	Tourmaline breccia hosting angular clasts of Catavi Fm. quartzites and greisen	Chalcataya	Optically unzoned	Bluish green
2020-KELL-24-TS4-Circle F-Tur2-002	Tur-2	2020-KELL-24	Catavi Fm. quartzites	Tourmaline breccia hosting angular clasts of Catavi Fm. quartzites and greisen	Chalcataya	Optically unzoned	Bluish green

EMPA label	Type	Sample	Host-rock	Description	Locality	Zone	Color
2020-KELL-24-TS4-Circle F-Tur2-003	Tur-2	2020-KELL-24	Catavi Fm. quartzites	Tourmaline breccia hosting angular clasts of Catavi Fm. quartzites and greisen	Chalcataya	Optically unzoned	Bluish green
2020-KELL-24-TS4-Circle F-Tur2-004	Tur-2	2020-KELL-24	Catavi Fm. quartzites	Tourmaline breccia hosting angular clasts of Catavi Fm. quartzites and greisen	Chalcataya	Optically unzoned	Bluish green
2020-KELL-24-TS4-Circle G-Tur2-001	Tur-2	2020-KELL-24	Catavi Fm. quartzites	Tourmaline breccia hosting angular clasts of Catavi Fm. quartzites and greisen	Chalcataya	Optically unzoned	Bluish green
2020-KELL-24-TS4-Circle G-Tur2-002	Tur-2	2020-KELL-24	Catavi Fm. quartzites	Tourmaline breccia hosting angular clasts of Catavi Fm. quartzites and greisen	Chalcataya	Optically unzoned	Bluish green
2020-KELL-24-TS4-Circle G-Tur2-003	Tur-2	2020-KELL-24	Catavi Fm. quartzites	Tourmaline breccia hosting angular clasts of Catavi Fm. quartzites and greisen	Chalcataya	Optically unzoned	Bluish green
2020-KELL-24-TS4-Circle G-Tur2-004	Tur-2	2020-KELL-24	Catavi Fm. quartzites	Tourmaline breccia hosting angular clasts of Catavi Fm. quartzites and greisen	Chalcataya	Optically unzoned	Bluish green
2020-KELL-24-TS4-Circle G-Tur1a-001	Tur-1	2020-KELL-24	Catavi Fm. quartzites	Tourmaline breccia hosting angular clasts of Catavi Fm. quartzites and greisen	Chalcataya	Optically unzoned	Orange
2020-KELL-24-TS4-Circle G-Tur1a-002	Tur-1	2020-KELL-24	Catavi Fm. quartzites	Tourmaline breccia hosting angular clasts of Catavi Fm. quartzites and greisen	Chalcataya	Optically unzoned	Orange
2020-KELL-24-TS4-Circle H-Tur2-001	Tur-2	2020-KELL-24	Catavi Fm. quartzites	Tourmaline breccia hosting angular clasts of Catavi Fm. quartzites and greisen	Chalcataya	Optically unzoned	Bluish green
2020-KELL-24-TS4-Circle I-Tur1a-001	Tur-1	2020-KELL-24	Catavi Fm. quartzites	Tourmaline breccia hosting angular clasts of Catavi Fm. quartzites and greisen	Chalcataya	Optically unzoned	Orange
2020-KELL-24-TS4-Circle I-Tur1a-002	Tur-1	2020-KELL-24	Catavi Fm. quartzites	Tourmaline breccia hosting angular clasts of Catavi Fm. quartzites and greisen	Chalcataya	Optically unzoned	Orange
2020-KELL-24-TS4-Circle I-Tur1a-003	Tur-1	2020-KELL-24	Catavi Fm. quartzites	Tourmaline breccia hosting angular clasts of Catavi Fm. quartzites and greisen	Chalcataya	Optically unzoned	Orange

EMPA label	Type	Sample	Host-rock	Description	Locality	Zone	Color
2020-KELL-24-TS4-Circle J-Tur2-001	Tur-2	2020-KELL-24	Catavi Fm. quartzites	Tourmaline breccia hosting angular clasts of Catavi Fm. quartzites and greisen	Chalcataya	Core	Bright orange - pale green
2020-KELL-24-TS4-Circle J-Tur2-002	Tur-2	2020-KELL-24	Catavi Fm. quartzites	Tourmaline breccia hosting angular clasts of Catavi Fm. quartzites and greisen	Chalcataya	Overgrowth	Bluish green
2020-KELL-24-TS4-Circle J-Tur2-003	Tur-2	2020-KELL-24	Catavi Fm. quartzites	Tourmaline breccia hosting angular clasts of Catavi Fm. quartzites and greisen	Chalcataya	Overgrowth	Bluish green
2020-KELL-24-TS4-Circle K-Tur1a-001	Tur-1	2020-KELL-24	Catavi Fm. quartzites	Tourmaline breccia hosting angular clasts of Catavi Fm. quartzites and greisen	Chalcataya	Rim	Orange
2020-KELL-24-TS4-Circle K-Tur1a-002	Tur-1	2020-KELL-24	Catavi Fm. quartzites	Tourmaline breccia hosting angular clasts of Catavi Fm. quartzites and greisen	Chalcataya	Rim	Orange
2020-KELL-24-TS4-Circle K-Tur1a-003	Tur-1	2020-KELL-24	Catavi Fm. quartzites	Tourmaline breccia hosting angular clasts of Catavi Fm. quartzites and greisen	Chalcataya	Core	Orange
2020-KELL-24-TS4-Circle K-Tur1a-004	Tur-1	2020-KELL-24	Catavi Fm. quartzites	Tourmaline breccia hosting angular clasts of Catavi Fm. quartzites and greisen	Chalcataya	Core	Orange
2020-KELL-24-TS4-Circle K-Tur1a-005	Tur-1	2020-KELL-24	Catavi Fm. quartzites	Tourmaline breccia hosting angular clasts of Catavi Fm. quartzites and greisen	Chalcataya	Core	Orange
2020-KELL-24-TS4-Circle K-Tur2-001	Tur-2	2020-KELL-24	Catavi Fm. quartzites	Tourmaline breccia hosting angular clasts of Catavi Fm. quartzites and greisen	Chalcataya	Optically unzoned	Bluish green
2020-KELL-24-TS4-Circle K-Tur2-002	Tur-2	2020-KELL-24	Catavi Fm. quartzites	Tourmaline breccia hosting angular clasts of Catavi Fm. quartzites and greisen	Chalcataya	Optically unzoned	Bluish green
2020-KELL-24-TS4-Circle K-Tur2-003	Tur-2	2020-KELL-25	Catavi Fm. quartzites	Tourmaline breccia hosting angular clasts of Catavi Fm. quartzites and greisen	Chalcataya	Optically unzoned	Bluish green
2020-KELL-25-TS3-Circle A-Tur2-001	Tur-2	2020-KELL-25	Catavi Fm. quartzites	Tourmaline breccia hosting angular clasts of Catavi Fm. quartzites and greisen	Chalcataya	Optically unzoned	Bluish green

EMPA label	Type	Sample	Host-rock	Description	Locality	Zone	Color
2020-KELL-25-TS3-Circle A-Tur2-002	Tur-2	2020-KELL-25	Catavi Fm. quartzites	Tourmaline breccia hosting angular clasts of Catavi Fm. quartzites and greisen	Chalcataya	Optically unzoned	Bluish green
2020-KELL-25-TS3-Circle A-Tur2-003	Tur-2	2020-KELL-25	Catavi Fm. quartzites	Tourmaline breccia hosting angular clasts of Catavi Fm. quartzites and greisen	Chalcataya	Optically unzoned	Bluish green
2020-KELL-25-TS3-Circle B-Tur2-001	Tur-2	2020-KELL-25	Catavi Fm. quartzites	Tourmaline breccia hosting angular clasts of Catavi Fm. quartzites and greisen	Chalcataya	Optically unzoned	Bluish green
2020-KELL-25-TS3-Circle B-Tur2-002	Tur-2	2020-KELL-25	Catavi Fm. quartzites	Tourmaline breccia hosting angular clasts of Catavi Fm. quartzites and greisen	Chalcataya	Optically unzoned	Bluish green
2020-KELL-25-TS3-Circle B-Tur2-003	Tur-2	2020-KELL-25	Catavi Fm. quartzites	Tourmaline breccia hosting angular clasts of Catavi Fm. quartzites and greisen	Chalcataya	Optically unzoned	Bluish green
2020-KELL-25-TS3-Circle C-Tur2-001	Tur-2	2020-KELL-25	Catavi Fm. quartzites	Tourmaline breccia hosting angular clasts of Catavi Fm. quartzites and greisen	Chalcataya	Optically unzoned	Bluish green
2020-KELL-25-TS3-Circle D-Tur2-001	Tur-2	2020-KELL-25	Catavi Fm. quartzites	Tourmaline breccia hosting angular clasts of Catavi Fm. quartzites and greisen	Chalcataya	Optically unzoned	Bluish green
2020-KELL-25-TS3-Circle D-Tur2-002	Tur-2	2020-KELL-25	Catavi Fm. quartzites	Tourmaline breccia hosting angular clasts of Catavi Fm. quartzites and greisen	Chalcataya	Optically unzoned	Bluish green
2020-KELL-25-TS3-Circle D-Tur2-003	Tur-2	2020-KELL-25	Catavi Fm. quartzites	Tourmaline breccia hosting angular clasts of Catavi Fm. quartzites and greisen	Chalcataya	Optically unzoned	Bluish green
2020-KELL-25-TS3-Circle E-Tur2-001	Tur-2	2020-KELL-25	Catavi Fm. quartzites	Tourmaline breccia hosting angular clasts of Catavi Fm. quartzites and greisen	Chalcataya	Optically unzoned	Bluish green
2020-KELL-25-TS3-Circle E-Tur2-002	Tur-2	2020-KELL-25	Catavi Fm. quartzites	Tourmaline breccia hosting angular clasts of Catavi Fm. quartzites and greisen	Chalcataya	Optically unzoned	Bluish green
2020-KELL-25-TS3-Circle F-Tur2-001	Tur-2	2020-KELL-25	Catavi Fm. quartzites	Tourmaline breccia hosting angular clasts of Catavi Fm. quartzites and greisen	Chalcataya	Optically unzoned	Bluish green

EMPA label	Type	Sample	Host-rock	Description	Locality	Zone	Color
2020-KELL-25-TS3-Circle F-Tur2-002	Tur-2	2020-KELL-25	Catavi Fm. quartzites	Tourmaline breccia hosting angular clasts of Catavi Fm. quartzites and greisen	Chalcataya	Optically unzoned	Bluish green
2020-KELL-25-TS3-Circle F-Tur2-003	Tur-2	2020-KELL-25	Catavi Fm. quartzites	Tourmaline breccia hosting angular clasts of Catavi Fm. quartzites and greisen	Chalcataya	Optically unzoned	Bluish green
2020-KELL-25-TS3-Circle H-Tur2-001	Tur-2	2020-KELL-25	Catavi Fm. quartzites	Tourmaline breccia hosting angular clasts of Catavi Fm. quartzites and greisen	Chalcataya	Optically unzoned	Bluish green
2020-KELL-25-TS3-Circle H-Tur2-002	Tur-2	2020-KELL-25	Catavi Fm. quartzites	Tourmaline breccia hosting angular clasts of Catavi Fm. quartzites and greisen	Chalcataya	Optically unzoned	Bluish green
2020-KELL-25-TS3-Circle H-Tur2-003	Tur-2	2020-KELL-25	Catavi Fm. quartzites	Tourmaline breccia hosting angular clasts of Catavi Fm. quartzites and greisen	Chalcataya	Optically unzoned	Bluish green
2020-KELL-25-TS3-Circle J-Tur2-001	Tur-2	2020-KELL-25	Catavi Fm. quartzites	Tourmaline breccia hosting angular clasts of Catavi Fm. quartzites and greisen	Chalcataya	Optically unzoned	Bluish green
2020-KELL-25-TS3-Circle J-Tur2-002	Tur-2	2020-KELL-25	Catavi Fm. quartzites	Tourmaline breccia hosting angular clasts of Catavi Fm. quartzites and greisen	Chalcataya	Optically unzoned	Bluish green
2020-KELL-25-TS3-Circle J-Tur2-003	Tur-2	KELL-A	Catavi Fm. quartzites	Tourmaline breccia hosting angular clasts of Catavi Fm. quartzites and greisen	Chalcataya	Optically unzoned	Bluish green
KELL-A-TS-Circle A-Tur3-001	Tur-3	KELL-A	Veins in Catavi Fm. quartzites	Quartz-tourmaline-cassiterite veins in quartzites	Kellhuani	Optically unzoned	Bluish green
KELL-A-TS-Circle A-Tur3-002	Tur-3	KELL-A	Veins in Catavi Fm. quartzites	Quartz-tourmaline-cassiterite veins in quartzites	Kellhuani	Optically unzoned	Bluish green
KELL-A-TS-Circle A-Tur3-003	Tur-3	KELL-A	Veins in Catavi Fm. quartzites	Quartz-tourmaline-cassiterite veins in quartzites	Kellhuani	Optically unzoned	Bluish green
KELL-A-TS-Circle A-Tur3-004	Tur-3	KELL-A	Veins in Catavi Fm. quartzites	Quartz-tourmaline-cassiterite veins in quartzites	Kellhuani	Optically unzoned	Bluish green

EMPA label	Type	Sample	Host-rock	Description	Locality	Zone	Color
KELL-A-TS-Circle B-Tur3-001	Tur-3	KELL-A	Veins in Catavi Fm. quartzites	Quartz-tourmaline-cassiterite veins in quartzites	Kellhuani	Optically unzoned	Bluish green
KELL-A-TS-Circle B-Tur3-002	Tur-3	KELL-A	Veins in Catavi Fm. quartzites	Quartz-tourmaline-cassiterite veins in quartzites	Kellhuani	Optically unzoned	Bluish green
KELL-A-TS-Circle B-Tur3-003	Tur-3	KELL-A	Veins in Catavi Fm. quartzites	Quartz-tourmaline-cassiterite veins in quartzites	Kellhuani	Optically unzoned	Bluish green
KELL-A-TS-Circle B-Tur3-004	Tur-3	KELL-A	Veins in Catavi Fm. quartzites	Quartz-tourmaline-cassiterite veins in quartzites	Kellhuani	Optically unzoned	Bluish green
KELL-A-TS-Circle B-Tur3-005	Tur-3	KELL-A	Veins in Catavi Fm. quartzites	Quartz-tourmaline-cassiterite veins in quartzites	Kellhuani	Optically unzoned	Bluish green
KELL-A-TS-Circle C-Tur3-001	Tur-3	KELL-A	Veins in Catavi Fm. quartzites	Quartz-tourmaline-cassiterite veins in quartzites	Kellhuani	Optically unzoned	Bluish green
KELL-A-TS-Circle C-Tur3-002	Tur-3	KELL-A	Veins in Catavi Fm. quartzites	Quartz-tourmaline-cassiterite veins in quartzites	Kellhuani	Optically unzoned	Bluish green
KELL-A-TS-Circle C-Tur3-003	Tur-3	KELL-A	Veins in Catavi Fm. quartzites	Quartz-tourmaline-cassiterite veins in quartzites	Kellhuani	Optically unzoned	Bluish green
KELL-A-TS-Circle C-Tur3-004	Tur-3	KELL-A	Veins in Catavi Fm. quartzites	Quartz-tourmaline-cassiterite veins in quartzites	Kellhuani	Optically unzoned	Bluish green
KELL-A-TS-Circle C-Tur3-005	Tur-3	KELL-A	Veins in Catavi Fm. quartzites	Quartz-tourmaline-cassiterite veins in quartzites	Kellhuani	Optically unzoned	Bluish green
KELL-A-TS-Circle C-Tur3-006	Tur-3	KELL-A	Veins in Catavi Fm. quartzites	Quartz-tourmaline-cassiterite veins in quartzites	Kellhuani	Optically unzoned	Bluish green
KELL-A-TS-Circle D-Tur3-001	Tur-3	KELL-A	Veins in Catavi Fm. quartzites	Quartz-tourmaline-cassiterite veins in quartzites	Kellhuani	Optically unzoned	Bluish green

EMPA label	Type	Sample	Host-rock	Description	Locality	Zone	Color
KELL-A-TS-Circle D-Tur3-002	Tur-3	KELL-A	Veins in Catavi Fm. quartzites	Quartz-tourmaline-cassiterite veins in quartzites	Kellhuani	Optically unzoned	Bluish green
KELL-A-TS-Circle D-Tur3-003	Tur-3	KELL-A	Veins in Catavi Fm. quartzites	Quartz-tourmaline-cassiterite veins in quartzites	Kellhuani	Optically unzoned	Bluish green
KELL-A-TS-Circle D-Tur3-004	Tur-3	KELL-A	Veins in Catavi Fm. quartzites	Quartz-tourmaline-cassiterite veins in quartzites	Kellhuani	Optically unzoned	Bluish green
KELL-A-TS-Circle E-Tur3-001	Tur-3	KELL-A	Veins in Catavi Fm. quartzites	Quartz-tourmaline-cassiterite veins in quartzites	Kellhuani	Optically unzoned	Bluish green
KELL-A-TS-Circle E-Tur3-002	Tur-3	KELL-A	Veins in Catavi Fm. quartzites	Quartz-tourmaline-cassiterite veins in quartzites	Kellhuani	Optically unzoned	Bluish green
KELL-A-TS-Circle E-Tur3-003	Tur-3	KELL-A	Veins in Catavi Fm. quartzites	Quartz-tourmaline-cassiterite veins in quartzites	Kellhuani	Optically unzoned	Bluish green
KELL-A-TS-Circle E-Tur3-004	Tur-3	KELL-A	Veins in Catavi Fm. quartzites	Quartz-tourmaline-cassiterite veins in quartzites	Kellhuani	Optically unzoned	Bluish green
KELL-A-TS-Circle E-Tur3-005	Tur-3	KELL-A	Veins in Catavi Fm. quartzites	Quartz-tourmaline-cassiterite veins in quartzites	Kellhuani	Optically unzoned	Bluish green
KELL-A-TS-Circle E-Tur3-006	Tur-3	KELL-A	Veins in Catavi Fm. quartzites	Quartz-tourmaline-cassiterite veins in quartzites	Kellhuani	Optically unzoned	Bluish green
KELL-A-TS-Circle E-Tur3-007	Tur-3	KELL-A	Veins in Catavi Fm. quartzites	Quartz-tourmaline-cassiterite veins in quartzites	Kellhuani	Optically unzoned	Bluish green
KELL-A-TS-Circle E-Tur3-008	Tur-3	KELL-A	Veins in Catavi Fm. quartzites	Quartz-tourmaline-cassiterite veins in quartzites	Kellhuani	Optically unzoned	Bluish green
KELL-A-TS-Circle E-Tur3-009	Tur-3	KELL-A	Veins in Catavi Fm. quartzites	Quartz-tourmaline-cassiterite veins in quartzites	Kellhuani	Optically unzoned	Bluish green

EMPA label	Type	Sample	Host-rock	Description	Locality	Zone	Color
KELL-A-TS-Circle E-Tur3-010	Tur-3	KELL-A	Veins in Catavi Fm. quartzites	Quartz-tourmaline-cassiterite veins in quartzites	Kellhuani	Optically unzoned	Bluish green
KELL-A-TS-Circle F-Tur3-001	Tur-3	KELL-A	Veins in Catavi Fm. quartzites	Quartz-tourmaline-cassiterite veins in quartzites	Kellhuani	Optically unzoned	Bluish green
KELL-A-TS-Circle F-Tur3-002	Tur-3	KELL-A	Veins in Catavi Fm. quartzites	Quartz-tourmaline-cassiterite veins in quartzites	Kellhuani	Optically unzoned	Bluish green
KELL-A-TS-Circle F-Tur3-003	Tur-3	KELL-A	Veins in Catavi Fm. quartzites	Quartz-tourmaline-cassiterite veins in quartzites	Kellhuani	Optically unzoned	Bluish green
KELL-A-TS-Circle F-Tur3-004	Tur-3	KELL-A	Veins in Catavi Fm. quartzites	Quartz-tourmaline-cassiterite veins in quartzites	Kellhuani	Optically unzoned	Bluish green
KELL-A-TS-Circle F-Tur3-005	Tur-3	KELL-A	Veins in Catavi Fm. quartzites	Quartz-tourmaline-cassiterite veins in quartzites	Kellhuani	Optically unzoned	Bluish green
KELL-A-TS-Circle F-Tur3-006	Tur-3	KELL-A	Veins in Catavi Fm. quartzites	Quartz-tourmaline-cassiterite veins in quartzites	Kellhuani	Optically unzoned	Bluish green
KELL-A-TS-Circle F-Tur3-007	Tur-3	KELL-A	Veins in Catavi Fm. quartzites	Quartz-tourmaline-cassiterite veins in quartzites	Kellhuani	Optically unzoned	Bluish green
KELL-A-TS-Circle G-Tur3-001	Tur-3	KELL-A	Veins in Catavi Fm. quartzites	Quartz-tourmaline-cassiterite veins in quartzites	Kellhuani	Optically unzoned	Bluish green
KELL-A-TS-Circle G-Tur3-002	Tur-3	KELL-A	Veins in Catavi Fm. quartzites	Quartz-tourmaline-cassiterite veins in quartzites	Kellhuani	Optically unzoned	Bluish green
KELL-A-TS-Circle G-Tur3-003	Tur-3	KELL-A	Veins in Catavi Fm. quartzites	Quartz-tourmaline-cassiterite veins in quartzites	Kellhuani	Optically unzoned	Bluish green
KELL-A-TS-Circle G-Tur3-004	Tur-3	KELL-A	Veins in Catavi Fm. quartzites	Quartz-tourmaline-cassiterite veins in quartzites	Kellhuani	Optically unzoned	Bluish green

EMPA label	Type	Sample	Host-rock	Description	Locality	Zone	Color
KELL-A-TS-Circle G-Tur3-005	Tur-3	KELL-A	Veins in Catavi Fm. quartzites	Quartz-tourmaline-cassiterite veins in quartzites	Kellhuani	Optically unzoned	Bluish green
KELL-A-TS-Circle G-Tur3-006	Tur-3	KELL-A	Veins in Catavi Fm. quartzites	Quartz-tourmaline-cassiterite veins in quartzites	Kellhuani	Optically unzoned	Bluish green
KELL-A-TS-Circle G-Tur3-007	Tur-3	KELL-A	Veins in Catavi Fm. quartzites	Quartz-tourmaline-cassiterite veins in quartzites	Kellhuani	Optically unzoned	Bluish green
KELL-A-TS-Circle G-Tur3-008	Tur-3	KELL-A	Veins in Catavi Fm. quartzites	Quartz-tourmaline-cassiterite veins in quartzites	Kellhuani	Optically unzoned	Bluish green
KELL-A-TS-Circle G-Tur3-009	Tur-3	KELL-A	Veins in Catavi Fm. quartzites	Quartz-tourmaline-cassiterite veins in quartzites	Kellhuani	Optically unzoned	Bluish green
KELL-A-TS-Circle G-Tur3-010	Tur-3	KELL-A	Veins in Catavi Fm. quartzites	Quartz-tourmaline-cassiterite veins in quartzites	Kellhuani	Optically unzoned	Bluish green
KELL-A-TS-Circle G-Tur3-011	Tur-3	KELL-A	Veins in Catavi Fm. quartzites	Quartz-tourmaline-cassiterite veins in quartzites	Kellhuani	Optically unzoned	Bluish green
KELL-A-TS-Circle G-Tur3-012	Tur-3	KELL-A	Veins in Catavi Fm. quartzites	Quartz-tourmaline-cassiterite veins in quartzites	Kellhuani	Optically unzoned	Bluish green
KELL-A-TS-Circle G-Tur3-013	Tur-3	KELL-A	Veins in Catavi Fm. quartzites	Quartz-tourmaline-cassiterite veins in quartzites	Kellhuani	Optically unzoned	Bluish green
KELL-A-TS-Circle H-Tur3-001	Tur-3	KELL-A	Veins in Catavi Fm. quartzites	Quartz-tourmaline-cassiterite veins in quartzites	Kellhuani	Optically unzoned	Bluish green
KELL-A-TS-Circle H-Tur3-002	Tur-3	KELL-A	Veins in Catavi Fm. quartzites	Quartz-tourmaline-cassiterite veins in quartzites	Kellhuani	Optically unzoned	Bluish green
KELL-A-TS-Circle H-Tur3-003	Tur-3	KELL-A	Veins in Catavi Fm. quartzites	Quartz-tourmaline-cassiterite veins in quartzites	Kellhuani	Optically unzoned	Bluish green

EMPA label	Type	Sample	Host-rock	Description	Locality	Zone	Color
KELL-A-TS-Circle H-Tur3-004	Tur-3	KELL-A	Veins in Catavi Fm. quartzites	Quartz-tourmaline-cassiterite veins in quartzites	Kellhuani	Optically unzoned	Bluish green
KELL-A-TS-Circle H-Tur3-005	Tur-3	KELL-A	Veins in Catavi Fm. quartzites	Quartz-tourmaline-cassiterite veins in quartzites	Kellhuani	Optically unzoned	Bluish green
KELL-A-TS-Circle H-Tur3-006	Tur-3	KELL-A	Veins in Catavi Fm. quartzites	Quartz-tourmaline-cassiterite veins in quartzites	Kellhuani	Optically unzoned	Bluish green
KELL-A-TS-Circle H-Tur3-007	Tur-3	KELL-A	Veins in Catavi Fm. quartzites	Quartz-tourmaline-cassiterite veins in quartzites	Kellhuani	Optically unzoned	Bluish green
KELL-A-TS-Circle H-Tur3-008	Tur-3	KELL-A	Veins in Catavi Fm. quartzites	Quartz-tourmaline-cassiterite veins in quartzites	Kellhuani	Optically unzoned	Bluish green
KELL-A-TS-Circle I-Tur3-001	Tur-3	KELL-A	Veins in Catavi Fm. quartzites	Quartz-tourmaline-cassiterite veins in quartzites	Kellhuani	Optically unzoned	Bluish green
KELL-A-TS-Circle I-Tur3-002	Tur-3	KELL-A	Veins in Catavi Fm. quartzites	Quartz-tourmaline-cassiterite veins in quartzites	Kellhuani	Optically unzoned	Bluish green
KELL-A-TS-Circle I-Tur3-003	Tur-3	KELL-A	Veins in Catavi Fm. quartzites	Quartz-tourmaline-cassiterite veins in quartzites	Kellhuani	Optically unzoned	Bluish green
KELL-A-TS-Circle I-Tur3-004	Tur-3	KELL-A	Veins in Catavi Fm. quartzites	Quartz-tourmaline-cassiterite veins in quartzites	Kellhuani	Optically unzoned	Bluish green
KELL-A-TS-Circle I-Tur3-005	Tur-3	KELL-A	Veins in Catavi Fm. quartzites	Quartz-tourmaline-cassiterite veins in quartzites	Kellhuani	Optically unzoned	Bluish green
KELL-A-TS-Circle I-Tur3-006	Tur-3	KELL-A	Veins in Catavi Fm. quartzites	Quartz-tourmaline-cassiterite veins in quartzites	Kellhuani	Optically unzoned	Bluish green
KELL-A-TS-Circle I-Tur3-007	Tur-3	KELL-A	Veins in Catavi Fm. quartzites	Quartz-tourmaline-cassiterite veins in quartzites	Kellhuani	Optically unzoned	Bluish green

EMPA label	Type	Sample	Host-rock	Description	Locality	Zone	Color
KELL-A-TS-Circle I-Tur3-008	Tur-3	KELL-A	Veins in Catavi Fm. quartzites	Quartz-tourmaline-cassiterite veins in quartzites	Kellhuani	Optically unzoned	Bluish green
KELL-A-TS-Circle I-Tur3-009	Tur-3	KELL-A	Veins in Catavi Fm. quartzites	Quartz-tourmaline-cassiterite veins in quartzites	Kellhuani	Optically unzoned	Bluish green
KELL-A-TS-Circle I-Tur3-010	Tur-3	KELL-A	Veins in Catavi Fm. quartzites	Quartz-tourmaline-cassiterite veins in quartzites	Kellhuani	Optically unzoned	Bluish green
KELL-A-TS-Circle I-Tur3-011	Tur-3	KELL-A	Veins in Catavi Fm. quartzites	Quartz-tourmaline-cassiterite veins in quartzites	Kellhuani	Optically unzoned	Bluish green
KELL-A-TS-Circle I-Tur3-012	Tur-3	KELL-A	Veins in Catavi Fm. quartzites	Quartz-tourmaline-cassiterite veins in quartzites	Kellhuani	Optically unzoned	Bluish green
2020-KELL-1-A-TS1-Circle A-tur3-002	Tur-3	2020-KELL-1-A	Veins in Catavi Fm. quartzites	Quartz-tourmaline-cassiterite veins in quartzites	Kellhuani	Optically unzoned	Bluish green
2020-KELL-1-A-TS1-Circle A-tur3-003	Tur-3	2020-KELL-1-A	Veins in Catavi Fm. quartzites	Quartz-tourmaline-cassiterite veins in quartzites	Kellhuani	Optically unzoned	Bluish green
2020-KELL-1-A-TS1-Circle A-tur3-004	Tur-3	2020-KELL-1-A	Veins in Catavi Fm. quartzites	Quartz-tourmaline-cassiterite veins in quartzites	Kellhuani	Optically unzoned	Bluish green
2020-KELL-1-A-TS1-Circle A-tur3-005	Tur-3	2020-KELL-1-A	Veins in Catavi Fm. quartzites	Quartz-tourmaline-cassiterite veins in quartzites	Kellhuani	Optically unzoned	Bluish green
2020-KELL-1-A-TS1-Circle A-tur3-006	Tur-3	2020-KELL-1-A	Veins in Catavi Fm. quartzites	Quartz-tourmaline-cassiterite veins in quartzites	Kellhuani	Optically unzoned	Bluish green
2020-KELL-1-A-TS1-Circle A-tur3-007	Tur-3	2020-KELL-1-A	Veins in Catavi Fm. quartzites	Quartz-tourmaline-cassiterite veins in quartzites	Kellhuani	Optically unzoned	Bluish green
2020-KELL-1-A-TS1-Circle A-tur3-008	Tur-3	2020-KELL-1-A	Veins in Catavi Fm. quartzites	Quartz-tourmaline-cassiterite veins in quartzites	Kellhuani	Optically unzoned	Bluish green

EMPA label	Type	Sample	Host-rock	Description	Locality	Zone	Color
2020-KELL-1-A-TS1-Circle B-tur3-core-00	Tur-3	2020-KELL-1-A	Veins in Catavi Fm. quartzites	Quartz-tourmaline-cassiterite veins in quartzites	Kellhuani	Core	Bluish green
2020-KELL-1-A-TS1-Circle B-tur3-core-00	Tur-3	2020-KELL-1-A	Veins in Catavi Fm. quartzites	Quartz-tourmaline-cassiterite veins in quartzites	Kellhuani	Core	Bluish green
2020-KELL-1-A-TS1-Circle B-tur3-core-00	Tur-3	2020-KELL-1-A	Veins in Catavi Fm. quartzites	Quartz-tourmaline-cassiterite veins in quartzites	Kellhuani	Core	Bluish green
2020-KELL-1-A-TS1-Circle B-tur3-rim-001	Tur-3	2020-KELL-1-A	Veins in Catavi Fm. quartzites	Quartz-tourmaline-cassiterite veins in quartzites	Kellhuani	Rim	Bluish green
2020-KELL-1-A-TS1-Circle B-tur3-rim-002	Tur-3	2020-KELL-1-A	Veins in Catavi Fm. quartzites	Quartz-tourmaline-cassiterite veins in quartzites	Kellhuani	Rim	Bluish green
2020-KELL-1-A-TS1-Circle B-tur3-rim-003	Tur-3	2020-KELL-1-A	Veins in Catavi Fm. quartzites	Quartz-tourmaline-cassiterite veins in quartzites	Kellhuani	Rim	Bluish green
2020-KELL-1-A-TS1-Circle B-tur3-rim-004	Tur-3	2020-KELL-1-A	Veins in Catavi Fm. quartzites	Quartz-tourmaline-cassiterite veins in quartzites	Kellhuani	Rim	Bluish green
2020-KELL-1-A-TS1-Circle C-tur3-001	Tur-3	2020-KELL-1-A	Veins in Catavi Fm. quartzites	Quartz-tourmaline-cassiterite veins in quartzites	Kellhuani	Optically unzoned	Bluish green
2020-KELL-1-A-TS1-Circle C-tur3-002	Tur-3	2020-KELL-1-A	Veins in Catavi Fm. quartzites	Quartz-tourmaline-cassiterite veins in quartzites	Kellhuani	Optically unzoned	Bluish green
2020-KELL-1-A-TS1-Circle C-tur3-003	Tur-3	2020-KELL-1-A	Veins in Catavi Fm. quartzites	Quartz-tourmaline-cassiterite veins in quartzites	Kellhuani	Optically unzoned	Bluish green
2020-KELL-1-A-TS1-Circle C-tur3-004	Tur-3	2020-KELL-1-A	Veins in Catavi Fm. quartzites	Quartz-tourmaline-cassiterite veins in quartzites	Kellhuani	Optically unzoned	Bluish green
2020-KELL-1-A-TS1-Circle C-tur3-005	Tur-3	2020-KELL-1-A	Veins in Catavi Fm. quartzites	Quartz-tourmaline-cassiterite veins in quartzites	Kellhuani	Optically unzoned	Bluish green

EMPA label	Type	Sample	Host-rock	Description	Locality	Zone	Color
2020-KELL-1-A-TS1-Circle C-tur3-006	Tur-3	2020-KELL-1-A	Veins in Catavi Fm. quartzites	Quartz-tourmaline-cassiterite veins in quartzites	Kellhuani	Optically unzoned	Bluish green
2020-KELL-1-A-TS1-Circle C-tur3-007	Tur-3	2020-KELL-1-A	Veins in Catavi Fm. quartzites	Quartz-tourmaline-cassiterite veins in quartzites	Kellhuani	Optically unzoned	Bluish green
2020-KELL-1-A-TS1-Circle C-tur3-008	Tur-3	2020-KELL-1-A	Veins in Catavi Fm. quartzites	Quartz-tourmaline-cassiterite veins in quartzites	Kellhuani	Optically unzoned	Bluish green
2020-KELL-1-A-TS1-Circle C-tur3-core-00	Tur-3	2020-KELL-1-A	Veins in Catavi Fm. quartzites	Quartz-tourmaline-cassiterite veins in quartzites	Kellhuani	Core	Bluish green
2020-KELL-1-A-TS1-Circle C-tur3-core-00	Tur-3	2020-KELL-1-A	Veins in Catavi Fm. quartzites	Quartz-tourmaline-cassiterite veins in quartzites	Kellhuani	Core	Bluish green
2020-KELL-1-A-TS1-Circle C-tur3-core-00	Tur-3	2020-KELL-1-A	Veins in Catavi Fm. quartzites	Quartz-tourmaline-cassiterite veins in quartzites	Kellhuani	Core	Bluish green
2020-KELL-1-A-TS1-Circle C-tur3-rim-001	Tur-3	2020-KELL-1-A	Veins in Catavi Fm. quartzites	Quartz-tourmaline-cassiterite veins in quartzites	Kellhuani	Rim	Bluish green
2020-KELL-1-A-TS1-Circle C-tur3-rim-002	Tur-3	2020-KELL-1-A	Veins in Catavi Fm. quartzites	Quartz-tourmaline-cassiterite veins in quartzites	Kellhuani	Rim	Bluish green
2020-KELL-1-A-TS1-Circle D-tur3-core-00	Tur-3	2020-KELL-1-A	Veins in Catavi Fm. quartzites	Quartz-tourmaline-cassiterite veins in quartzites	Kellhuani	Core	Bluish green
2020-KELL-1-A-TS1-Circle D-tur3-core-00	Tur-3	2020-KELL-1-A	Veins in Catavi Fm. quartzites	Quartz-tourmaline-cassiterite veins in quartzites	Kellhuani	Core	Bluish green
2020-KELL-1-A-TS1-Circle D-tur3-core-00	Tur-3	2020-KELL-1-A	Veins in Catavi Fm. quartzites	Quartz-tourmaline-cassiterite veins in quartzites	Kellhuani	Core	Bluish green
2020-KELL-1-A-TS1-Circle D-tur3-rim-001	Tur-3	2020-KELL-1-A	Veins in Catavi Fm. quartzites	Quartz-tourmaline-cassiterite veins in quartzites	Kellhuani	Rim	Bluish green

EMPA label	Type	Sample	Host-rock	Description	Locality	Zone	Color
2020-KELL-1-A-TS1-Circle D-tur3-rim-002	Tur-3	2020-KELL-1-A	Veins in Catavi Fm. quartzites	Quartz-tourmaline-cassiterite veins in quartzites	Kellhuani	Rim	Bluish green
2020-KELL-1-A-TS1-Circle D-tur3-rim-003	Tur-3	2020-KELL-1-A	Veins in Catavi Fm. quartzites	Quartz-tourmaline-cassiterite veins in quartzites	Kellhuani	Rim	Bluish green
2020-KELL-1-A-TS1-Circle D-tur3-001	Tur-3	2020-KELL-1-A	Veins in Catavi Fm. quartzites	Quartz-tourmaline-cassiterite veins in quartzites	Kellhuani	Optically unzoned	Bluish green
2020-KELL-1-A-TS1-Circle D-tur3-002	Tur-3	2020-KELL-1-A	Veins in Catavi Fm. quartzites	Quartz-tourmaline-cassiterite veins in quartzites	Kellhuani	Optically unzoned	Bluish green
2020-KELL-1-A-TS1-Circle D-tur3-003	Tur-3	2020-KELL-1-A	Veins in Catavi Fm. quartzites	Quartz-tourmaline-cassiterite veins in quartzites	Kellhuani	Optically unzoned	Bluish green
2020-KELL-1-A-TS1-Circle D-tur3-004	Tur-3	2020-KELL-1-A	Veins in Catavi Fm. quartzites	Quartz-tourmaline-cassiterite veins in quartzites	Kellhuani	Optically unzoned	Bluish green
2020-KELL-1-A-TS1-Circle D-tur3-005	Tur-3	2020-KELL-1-A	Veins in Catavi Fm. quartzites	Quartz-tourmaline-cassiterite veins in quartzites	Kellhuani	Optically unzoned	Bluish green
2020-KELL-1-A-TS1-Circle D-tur3-006	Tur-3	2020-KELL-1-A	Veins in Catavi Fm. quartzites	Quartz-tourmaline-cassiterite veins in quartzites	Kellhuani	Optically unzoned	Bluish green
2020-KELL-1-A-TS1-Circle D-tur3-007	Tur-3	2020-KELL-1-A	Veins in Catavi Fm. quartzites	Quartz-tourmaline-cassiterite veins in quartzites	Kellhuani	Optically unzoned	Bluish green
2020-KELL-1-A-TS1-Circle D-tur3-008	Tur-3	2020-KELL-1-A	Veins in Catavi Fm. quartzites	Quartz-tourmaline-cassiterite veins in quartzites	Kellhuani	Optically unzoned	Bluish green
2020-KELL-1-A-TS1-Circle D-tur3-009	Tur-3	2020-KELL-1-A	Veins in Catavi Fm. quartzites	Quartz-tourmaline-cassiterite veins in quartzites	Kellhuani	Optically unzoned	Bluish green
2020-KELL-1-A-TS1-Circle D-tur3-010	Tur-3	2020-KELL-1-A	Veins in Catavi Fm. quartzites	Quartz-tourmaline-cassiterite veins in quartzites	Kellhuani	Optically unzoned	Bluish green

EMPA label	Type	Sample	Host-rock	Description	Locality	Zone	Color
2020-KELL-1-A-TS1-Circle D-tur3-011	Tur-3	2020-KELL-1-A	Veins in Catavi Fm. quartzites	Quartz-tourmaline-cassiterite veins in quartzites	Kellhuani	Optically unzoned	Bluish green
2020-KELL-1-A-TS1-Circle E-tur3-001	Tur-3	2020-KELL-1-A	Veins in Catavi Fm. quartzites	Quartz-tourmaline-cassiterite veins in quartzites	Kellhuani	Optically unzoned	Bluish green
2020-KELL-1-A-TS1-Circle F-tur3-002	Tur-3	2020-KELL-1-A	Veins in Catavi Fm. quartzites	Quartz-tourmaline-cassiterite veins in quartzites	Kellhuani	Optically unzoned	Bluish green
2020-KELL-1-A-TS1-Circle E-tur3-002	Tur-3	2020-KELL-1-A	Veins in Catavi Fm. quartzites	Quartz-tourmaline-cassiterite veins in quartzites	Kellhuani	Optically unzoned	Bluish green
2020-KELL-1-A-TS1-Circle E-tur3-rim-002	Tur-3	2020-KELL-1-A	Veins in Catavi Fm. quartzites	Quartz-tourmaline-cassiterite veins in quartzites	Kellhuani	Rim	Bluish green
2020-KELL-1-A-TS1-Circle E-tur3-001	Tur-3	2020-KELL-1-A	Veins in Catavi Fm. quartzites	Quartz-tourmaline-cassiterite veins in quartzites	Kellhuani	Optically unzoned	Bluish green
2020-KELL-1-A-TS1-Circle E-tur3-002	Tur-3	2020-KELL-1-A	Veins in Catavi Fm. quartzites	Quartz-tourmaline-cassiterite veins in quartzites	Kellhuani	Optically unzoned	Bluish green
2020-KELL-1-A-TS1-Circle E-tur3-003	Tur-3	2020-KELL-1-A	Veins in Catavi Fm. quartzites	Quartz-tourmaline-cassiterite veins in quartzites	Kellhuani	Optically unzoned	Bluish green
2020-KELL-1-A-TS1-Circle E-tur3-core2-0	Tur-3	2020-KELL-1-A	Veins in Catavi Fm. quartzites	Quartz-tourmaline-cassiterite veins in quartzites	Kellhuani	Core	Bluish green
2020-KELL-1-A-TS1-Circle E-tur3-rim2-00	Tur-3	2020-KELL-1-A	Veins in Catavi Fm. quartzites	Quartz-tourmaline-cassiterite veins in quartzites	Kellhuani	Rim	Bluish green
2020-KELL-1-A-TS1-Circle E-tur3-rim2-00	Tur-3	2020-KELL-1-A	Veins in Catavi Fm. quartzites	Quartz-tourmaline-cassiterite veins in quartzites	Kellhuani	Rim	Bluish green
2020-KELL-1-A-TS1-Circle E-tur3-rim2-00	Tur-3	2020-KELL-1-A	Veins in Catavi Fm. quartzites	Quartz-tourmaline-cassiterite veins in quartzites	Kellhuani	Rim	Bluish green

EMPA label	Type	Sample	Host-rock	Description	Locality	Zone	Color
2020-KELL-1-A-TS1-Circle F-tur3-core-00	Tur-3	2020-KELL-1-A	Veins in Catavi Fm. quartzites	Quartz-tourmaline-cassiterite veins in quartzites	Kellhuani	Core	Bluish green
2020-KELL-1-A-TS1-Circle F-tur3-core-00	Tur-3	2020-KELL-1-A	Veins in Catavi Fm. quartzites	Quartz-tourmaline-cassiterite veins in quartzites	Kellhuani	Core	Bluish green
2020-KELL-1-A-TS1-Circle F-tur3-core-00	Tur-3	2020-KELL-1-A	Veins in Catavi Fm. quartzites	Quartz-tourmaline-cassiterite veins in quartzites	Kellhuani	Core	Bluish green
2020-KELL-1-A-TS1-Circle F-tur3-rim-004	Tur-3	2020-KELL-1-A	Veins in Catavi Fm. quartzites	Quartz-tourmaline-cassiterite veins in quartzites	Kellhuani	Rim	Bluish green
2020-KELL-1-A-TS1-Circle F-tur3-rim-005	Tur-3	2020-KELL-1-A	Veins in Catavi Fm. quartzites	Quartz-tourmaline-cassiterite veins in quartzites	Kellhuani	Rim	Bluish green
2020-KELL-1-A-TS1-Circle F-tur3-rim-006	Tur-3	2020-KELL-1-A	Veins in Catavi Fm. quartzites	Quartz-tourmaline-cassiterite veins in quartzites	Kellhuani	Rim	Bluish green
2020-KELL-1-A-TS1-Circle F-tur3-007	Tur-3	2020-KELL-1-A	Veins in Catavi Fm. quartzites	Quartz-tourmaline-cassiterite veins in quartzites	Kellhuani	Optically unzoned	Bluish green
2020-KELL-1-A-TS1-Circle H-tur3-core-00	Tur-3	2020-KELL-1-A	Veins in Catavi Fm. quartzites	Quartz-tourmaline-cassiterite veins in quartzites	Kellhuani	Core	Bluish green
2020-KELL-1-A-TS1-Circle H-tur3-core-00	Tur-3	2020-KELL-1-A	Veins in Catavi Fm. quartzites	Quartz-tourmaline-cassiterite veins in quartzites	Kellhuani	Core	Bluish green
2020-KELL-1-A-TS1-Circle H-tur3-core-00	Tur-3	2020-KELL-1-A	Veins in Catavi Fm. quartzites	Quartz-tourmaline-cassiterite veins in quartzites	Kellhuani	Core	Bluish green
2020-KELL-1-A-TS1-Circle H-tur3-core-00	Tur-3	2020-KELL-1-A	Veins in Catavi Fm. quartzites	Quartz-tourmaline-cassiterite veins in quartzites	Kellhuani	Core	Bluish green
2020-KELL-1-A-TS1-Circle H-tur3-core-00	Tur-3	2020-KELL-1-A	Veins in Catavi Fm. quartzites	Quartz-tourmaline-cassiterite veins in quartzites	Kellhuani	Core	Bluish green

EMPA label	Type	Sample	Host-rock	Description	Locality	Zone	Color
2020-KELL-1-A-TS1-Circle H-tur3-core-00	Tur-3	2020-KELL-1-A	Veins in Catavi Fm. quartzites	Quartz-tourmaline-cassiterite veins in quartzites	Kellhuani	Core	Bluish green
2020-KELL-1-A-TS1-Circle H-tur3-rim-007	Tur-3	2020-KELL-1-A	Veins in Catavi Fm. quartzites	Quartz-tourmaline-cassiterite veins in quartzites	Kellhuani	Rim	Bluish green
2020-KELL-1-A-TS1-Circle H-tur3-rim-008	Tur-3	2020-KELL-1-A	Veins in Catavi Fm. quartzites	Quartz-tourmaline-cassiterite veins in quartzites	Kellhuani	Rim	Bluish green
2020-KELL-1-A-TS1-Circle H-tur3-rim-009	Tur-3	2020-KELL-1-A	Veins in Catavi Fm. quartzites	Quartz-tourmaline-cassiterite veins in quartzites	Kellhuani	Rim	Bluish green
2020-KELL-1-A-TS1-Circle H-tur3-rim-010	Tur-3	2020-KELL-1-A	Veins in Catavi Fm. quartzites	Quartz-tourmaline-cassiterite veins in quartzites	Kellhuani	Rim	Bluish green
2020-KELL-1-A-TS1-Circle H-tur3-rim-011	Tur-3	2020-KELL-1-A	Veins in Catavi Fm. quartzites	Quartz-tourmaline-cassiterite veins in quartzites	Kellhuani	Rim	Bluish green
2020-KELL-1-A-TS1-Circle H-tur3-rim-012	Tur-3	2020-KELL-1-A	Veins in Catavi Fm. quartzites	Quartz-tourmaline-cassiterite veins in quartzites	Kellhuani	Rim	Bluish green
2020-KELL-1-A-TS1-Circle H-tur3-013	Tur-3	2020-KELL-1-A	Veins in Catavi Fm. quartzites	Quartz-tourmaline-cassiterite veins in quartzites	Kellhuani	Optically unzoned	Bluish green
2020-KELL-1-A-TS3-Circle A-tur3-001	Tur-3	2020-KELL-1-A	Veins in Catavi Fm. quartzites	Quartz-tourmaline-cassiterite veins in quartzites	Kellhuani	Optically unzoned	Bluish green
2020-KELL-1-A-TS3-Circle A-tur3-002	Tur-3	2020-KELL-1-A	Veins in Catavi Fm. quartzites	Quartz-tourmaline-cassiterite veins in quartzites	Kellhuani	Optically unzoned	Bluish green
2020-KELL-1-A-TS3-Circle A-tur3-003	Tur-3	2020-KELL-1-A	Veins in Catavi Fm. quartzites	Quartz-tourmaline-cassiterite veins in quartzites	Kellhuani	Optically unzoned	Bluish green
2020-KELL-1-A-TS3-Circle B-tur3-001	Tur-3	2020-KELL-1-A	Veins in Catavi Fm. quartzites	Quartz-tourmaline-cassiterite veins in quartzites	Kellhuani	Optically unzoned	Bluish green

EMPA label	Type	Sample	Host-rock	Description	Locality	Zone	Color
2020-KELL-1-A-TS3-Circle B-tur3-002	Tur-3	2020-KELL-1-A	Veins in Catavi Fm. quartzites	Quartz-tourmaline-cassiterite veins in quartzites	Kellhuani	Optically unzoned	Bluish green
2020-KELL-1-A-TS3-Circle B-tur3-003	Tur-3	2020-KELL-1-A	Veins in Catavi Fm. quartzites	Quartz-tourmaline-cassiterite veins in quartzites	Kellhuani	Optically unzoned	Bluish green
2020-KELL-1-A-TS3-Circle B-tur3-004	Tur-3	2020-KELL-1-A	Veins in Catavi Fm. quartzites	Quartz-tourmaline-cassiterite veins in quartzites	Kellhuani	Optically unzoned	Bluish green
2020-KELL-1-A-TS3-Circle B-tur3-005	Tur-3	2020-KELL-1-A	Veins in Catavi Fm. quartzites	Quartz-tourmaline-cassiterite veins in quartzites	Kellhuani	Optically unzoned	Bluish green
2020-KELL-1-A-TS3-Circle C-tur3-core-00	Tur-3	2020-KELL-1-A	Veins in Catavi Fm. quartzites	Quartz-tourmaline-cassiterite veins in quartzites	Kellhuani	Core	Bluish green
2020-KELL-1-A-TS3-Circle C-tur3-core-00	Tur-3	2020-KELL-1-A	Veins in Catavi Fm. quartzites	Quartz-tourmaline-cassiterite veins in quartzites	Kellhuani	Core	Bluish green
2020-KELL-1-A-TS3-Circle C-tur3-core-00	Tur-3	2020-KELL-1-A	Veins in Catavi Fm. quartzites	Quartz-tourmaline-cassiterite veins in quartzites	Kellhuani	Core	Bluish green
2020-KELL-1-A-TS3-Circle C-tur3-rim-004	Tur-3	2020-KELL-1-A	Veins in Catavi Fm. quartzites	Quartz-tourmaline-cassiterite veins in quartzites	Kellhuani	Rim	Bluish green
2020-KELL-1-A-TS3-Circle C-tur3-rim-005	Tur-3	2020-KELL-1-A	Veins in Catavi Fm. quartzites	Quartz-tourmaline-cassiterite veins in quartzites	Kellhuani	Rim	Bluish green
2020-KELL-1-A-TS3-Circle C-tur3-rim-006	Tur-3	2020-KELL-1-A	Veins in Catavi Fm. quartzites	Quartz-tourmaline-cassiterite veins in quartzites	Kellhuani	Rim	Bluish green
2020-KELL-1-A-TS3-Circle D-tur3-001	Tur-3	2020-KELL-1-A	Veins in Catavi Fm. quartzites	Quartz-tourmaline-cassiterite veins in quartzites	Kellhuani	Optically unzoned	Bluish green
2020-KELL-1-A-TS3-Circle D-tur3-002	Tur-3	2020-KELL-1-A	Veins in Catavi Fm. quartzites	Quartz-tourmaline-cassiterite veins in quartzites	Kellhuani	Optically unzoned	Bluish green

EMPA label	Type	Sample	Host-rock	Description	Locality	Zone	Color
2020-KELL-1-A-TS3-Circle D-tur3-003	Tur-3	2020-KELL-1-A	Veins in Catavi Fm. quartzites	Quartz-tourmaline-cassiterite veins in quartzites	Kellhuani	Optically unzoned	Bluish green
2020-KELL-1-A-TS3-Circle D-tur3-004	Tur-3	2020-KELL-1-A	Veins in Catavi Fm. quartzites	Quartz-tourmaline-cassiterite veins in quartzites	Kellhuani	Optically unzoned	Bluish green
2020-KELL-1-A-TS3-Circle D-tur3-005	Tur-3	2020-KELL-1-A	Veins in Catavi Fm. quartzites	Quartz-tourmaline-cassiterite veins in quartzites	Kellhuani	Optically unzoned	Bluish green
2020-KELL-1-A-TS3-Circle E-tur3-core-00	Tur-3	2020-KELL-1-A	Veins in Catavi Fm. quartzites	Quartz-tourmaline-cassiterite veins in quartzites	Kellhuani	Core	Bluish green
2020-KELL-1-A-TS3-Circle E-tur3-core-00	Tur-3	2020-KELL-1-A	Veins in Catavi Fm. quartzites	Quartz-tourmaline-cassiterite veins in quartzites	Kellhuani	Core	Bluish green
2020-KELL-1-A-TS3-Circle E-tur3-rim-003	Tur-3	2020-KELL-1-A	Veins in Catavi Fm. quartzites	Quartz-tourmaline-cassiterite veins in quartzites	Kellhuani	Rim	Bluish green
2020-KELL-1-A-TS3-Circle E-tur3-rim-004	Tur-3	2020-KELL-1-A	Veins in Catavi Fm. quartzites	Quartz-tourmaline-cassiterite veins in quartzites	Kellhuani	Rim	Bluish green
2020-KELL-1-A-TS3-Circle E-tur3-rim-005	Tur-3	2020-KELL-1-A	Veins in Catavi Fm. quartzites	Quartz-tourmaline-cassiterite veins in quartzites	Kellhuani	Rim	Bluish green
2020-KELL-1-A-TS3-Circle E-tur3-rim-006	Tur-3	2020-KELL-1-A	Veins in Catavi Fm. quartzites	Quartz-tourmaline-cassiterite veins in quartzites	Kellhuani	Rim	Bluish green
2020-KELL-1-A-TS3-Circle E-tur3-core-00	Tur-3	2020-KELL-1-A	Veins in Catavi Fm. quartzites	Quartz-tourmaline-cassiterite veins in quartzites	Kellhuani	Core	Bluish green
2020-KELL-1-A-TS3-Circle F-tur3-core-00	Tur-3	2020-KELL-1-A	Veins in Catavi Fm. quartzites	Quartz-tourmaline-cassiterite veins in quartzites	Kellhuani	Core	Bluish green
2020-KELL-1-A-TS3-Circle F-tur3-core-00	Tur-3	2020-KELL-1-A	Veins in Catavi Fm. quartzites	Quartz-tourmaline-cassiterite veins in quartzites	Kellhuani	Core	Bluish green

EMPA label	Type	Sample	Host-rock	Description	Locality	Zone	Color
2020-KELL-1-A-TS3-Circle F-tur3-core-00	Tur-3	2020-KELL-1-A	Veins in Catavi Fm. quartzites	Quartz-tourmaline-cassiterite veins in quartzites	Kellhuani	Core	Bluish green
2020-KELL-1-A-TS3-Circle F-tur3-rim-004	Tur-3	2020-KELL-1-A	Veins in Catavi Fm. quartzites	Quartz-tourmaline-cassiterite veins in quartzites	Kellhuani	Rim	Bluish green
2020-KELL-1-A-TS3-Circle F-tur3-rim-005	Tur-3	2020-KELL-1-A	Veins in Catavi Fm. quartzites	Quartz-tourmaline-cassiterite veins in quartzites	Kellhuani	Rim	Bluish green
2020-KELL-1-A-TS3-Circle F-tur3-rim-006	Tur-3	2020-KELL-1-A	Veins in Catavi Fm. quartzites	Quartz-tourmaline-cassiterite veins in quartzites	Kellhuani	Rim	Bluish green
2020-KELL-1-A-TS3-Circle F-tur3-rim-007	Tur-3	2020-KELL-1-A	Veins in Catavi Fm. quartzites	Quartz-tourmaline-cassiterite veins in quartzites	Kellhuani	Rim	Bluish green
2020-KELL-1-A-TS3-Circle F-tur3-rim-008	Tur-3	2020-KELL-1-A	Veins in Catavi Fm. quartzites	Quartz-tourmaline-cassiterite veins in quartzites	Kellhuani	Rim	Bluish green
2020-KELL-1-A-TS3-Circle F-tur3-rim-009	Tur-3	2020-KELL-1-A	Veins in Catavi Fm. quartzites	Quartz-tourmaline-cassiterite veins in quartzites	Kellhuani	Rim	Bluish green
2020-KELL-1-A-TS3-Circle F-tur3-core-01	Tur-3	2020-KELL-1-A	Veins in Catavi Fm. quartzites	Quartz-tourmaline-cassiterite veins in quartzites	Kellhuani	Core	Bluish green
2020-KELL-1-A-TS3-Circle F-tur3-core-01	Tur-3	2020-KELL-1-A	Veins in Catavi Fm. quartzites	Quartz-tourmaline-cassiterite veins in quartzites	Kellhuani	Core	Bluish green
2020-KELL-1-A-TS3-Circle F-tur3-core-01	Tur-3	2020-KELL-1-A	Veins in Catavi Fm. quartzites	Quartz-tourmaline-cassiterite veins in quartzites	Kellhuani	Core	Bluish green
2020-KELL-1-A-TS3-Circle F-tur3-core-01	Tur-3	2020-KELL-1-A	Veins in Catavi Fm. quartzites	Quartz-tourmaline-cassiterite veins in quartzites	Kellhuani	Core	Bluish green
2020-KELL-1-A-TS3-Circle F-tur3-core-01	Tur-3	2020-KELL-1-A	Veins in Catavi Fm. quartzites	Quartz-tourmaline-cassiterite veins in quartzites	Kellhuani	Core	Bluish green

EMPA label	Type	Sample	Host-rock	Description	Locality	Zone	Color
2020-KELL-1-A-TS3-Circle F-tur3-core-01	Tur-3	2020-KELL-1-A	Veins in Catavi Fm. quartzites	Quartz-tourmaline-cassiterite veins in quartzites	Kellhuani	Core	Bluish green
2020-KELL-1-A-TS3-Circle G-tur3-core-00	Tur-3	2020-KELL-1-A	Veins in Catavi Fm. quartzites	Quartz-tourmaline-cassiterite veins in quartzites	Kellhuani	Core	Bluish green
2020-KELL-1-A-TS3-Circle G-tur3-rim-002	Tur-3	2020-KELL-1-A	Veins in Catavi Fm. quartzites	Quartz-tourmaline-cassiterite veins in quartzites	Kellhuani	Rim	Bluish green
2020-KELL-1-A-TS3-Circle G-tur3-core-00	Tur-3	2020-KELL-1-A	Veins in Catavi Fm. quartzites	Quartz-tourmaline-cassiterite veins in quartzites	Kellhuani	Core	Bluish green
2020-KELL-1-A-TS3-Circle G-tur3-core-00	Tur-3	2020-KELL-1-A	Veins in Catavi Fm. quartzites	Quartz-tourmaline-cassiterite veins in quartzites	Kellhuani	Core	Bluish green
2020-KELL-1-A-TS3-Circle G-tur3-core-00	Tur-3	2020-KELL-1-A	Veins in Catavi Fm. quartzites	Quartz-tourmaline-cassiterite veins in quartzites	Kellhuani	Core	Bluish green
2020-KELL-1-A-TS3-Circle G-tur3-core-00	Tur-3	2020-KELL-1-A	Veins in Catavi Fm. quartzites	Quartz-tourmaline-cassiterite veins in quartzites	Kellhuani	Core	Bluish green
2020-KELL-1-A-TS3-Circle G-tur3-core-00	Tur-3	2020-KELL-1-A	Veins in Catavi Fm. quartzites	Quartz-tourmaline-cassiterite veins in quartzites	Kellhuani	Core	Bluish green
2020-KELL-17-C-TS2-Circle A-tur3-001	Tur-3	2020-KELL-17-C	Veins in Catavi Fm. quartzites	Quartz-tourmaline-cassiterite veins in quartzites	Kellhuani	Optically unzoned	Bluish green
2020-KELL-17-C-TS2-Circle A-tur3-002	Tur-3	2020-KELL-17-C	Veins in Catavi Fm. quartzites	Quartz-tourmaline-cassiterite veins in quartzites	Kellhuani	Optically unzoned	Bluish green
2020-KELL-17-C-TS2-Circle A-tur3-003	Tur-3	2020-KELL-17-C	Veins in Catavi Fm. quartzites	Quartz-tourmaline-cassiterite veins in quartzites	Kellhuani	Optically unzoned	Bluish green
2020-KELL-17-C-TS2-Circle A-tur3-004	Tur-3	2020-KELL-17-C	Veins in Catavi Fm. quartzites	Quartz-tourmaline-cassiterite veins in quartzites	Kellhuani	Optically unzoned	Bluish green

EMPA label	Type	Sample	Host-rock	Description	Locality	Zone	Color
2020-KELL-17-C-TS2-Circle A-tur3-005	Tur-3	2020-KELL-17-C	Veins in Catavi Fm. quartzites	Quartz-tourmaline-cassiterite veins in quartzites	Kellhuani	Optically unzoned	Bluish green
2020-KELL-17-C-TS2-Circle A-tur3-006	Tur-3	2020-KELL-17-C	Veins in Catavi Fm. quartzites	Quartz-tourmaline-cassiterite veins in quartzites	Kellhuani	Optically unzoned	Bluish green
2020-KELL-17-C-TS2-Circle A-tur3-007	Tur-3	2020-KELL-17-C	Veins in Catavi Fm. quartzites	Quartz-tourmaline-cassiterite veins in quartzites	Kellhuani	Optically unzoned	Bluish green
2020-KELL-17-C-TS2-Circle A-tur3-008	Tur-3	2020-KELL-17-C	Veins in Catavi Fm. quartzites	Quartz-tourmaline-cassiterite veins in quartzites	Kellhuani	Optically unzoned	Bluish green
2020-KELL-17-C-TS2-Circle A-tur3-009	Tur-3	2020-KELL-17-C	Veins in Catavi Fm. quartzites	Quartz-tourmaline-cassiterite veins in quartzites	Kellhuani	Optically unzoned	Bluish green
2020-KELL-17-C-TS2-Circle B-tur3-001	Tur-3	2020-KELL-17-C	Veins in Catavi Fm. quartzites	Quartz-tourmaline-cassiterite veins in quartzites	Kellhuani	Optically unzoned	Bluish green
2020-KELL-17-C-TS2-Circle B-tur3-002	Tur-3	2020-KELL-17-C	Veins in Catavi Fm. quartzites	Quartz-tourmaline-cassiterite veins in quartzites	Kellhuani	Optically unzoned	Bluish green
2020-KELL-17-C-TS2-Circle B-tur3-003	Tur-3	2020-KELL-17-C	Veins in Catavi Fm. quartzites	Quartz-tourmaline-cassiterite veins in quartzites	Kellhuani	Optically unzoned	Bluish green
2020-KELL-17-C-TS2-Circle C-tur3-001	Tur-3	2020-KELL-17-C	Veins in Catavi Fm. quartzites	Quartz-tourmaline-cassiterite veins in quartzites	Kellhuani	Optically unzoned	Bluish green
2020-KELL-17-C-TS2-Circle C-tur3-002	Tur-3	2020-KELL-17-C	Veins in Catavi Fm. quartzites	Quartz-tourmaline-cassiterite veins in quartzites	Kellhuani	Optically unzoned	Bluish green
2020-KELL-17-C-TS2-Circle C-tur3-003	Tur-3	2020-KELL-17-C	Veins in Catavi Fm. quartzites	Quartz-tourmaline-cassiterite veins in quartzites	Kellhuani	Optically unzoned	Bluish green
2020-KELL-17-C-TS2-Circle C-tur3-004	Tur-3	2020-KELL-17-C	Veins in Catavi Fm. quartzites	Quartz-tourmaline-cassiterite veins in quartzites	Kellhuani	Optically unzoned	Bluish green

EMPA label	Type	Sample	Host-rock	Description	Locality	Zone	Color
2020-KELL-17-C-TS2-Circle C-tur3-005	Tur-3	2020-KELL-17-C	Veins in Catavi Fm. quartzites	Quartz-tourmaline-cassiterite veins in quartzites	Kellhuani	Optically unzoned	Bluish green
2020-KELL-17-C-TS2-Circle D-tur3-001	Tur-3	2020-KELL-17-C	Veins in Catavi Fm. quartzites	Quartz-tourmaline-cassiterite veins in quartzites	Kellhuani	Optically unzoned	Bluish green
2020-KELL-17-C-TS2-Circle D-tur3-002	Tur-3	2020-KELL-17-C	Veins in Catavi Fm. quartzites	Quartz-tourmaline-cassiterite veins in quartzites	Kellhuani	Optically unzoned	Bluish green
2020-KELL-17-C-TS2-Circle D-tur3-003	Tur-3	2020-KELL-17-C	Veins in Catavi Fm. quartzites	Quartz-tourmaline-cassiterite veins in quartzites	Kellhuani	Optically unzoned	Bluish green
2020-KELL-17-C-TS2-Circle D-tur3-004	Tur-3	2020-KELL-17-C	Veins in Catavi Fm. quartzites	Quartz-tourmaline-cassiterite veins in quartzites	Kellhuani	Optically unzoned	Bluish green
2020-KELL-17-C-TS2-Circle E-tur3-001	Tur-3	2020-KELL-17-C	Veins in Catavi Fm. quartzites	Quartz-tourmaline-cassiterite veins in quartzites	Kellhuani	Optically unzoned	Bluish green
2020-KELL-17-C-TS2-Circle E-tur3-002	Tur-3	2020-KELL-17-C	Veins in Catavi Fm. quartzites	Quartz-tourmaline-cassiterite veins in quartzites	Kellhuani	Optically unzoned	Bluish green
2020-KELL-17-C-TS2-Circle E-tur3-003	Tur-3	2020-KELL-17-C	Veins in Catavi Fm. quartzites	Quartz-tourmaline-cassiterite veins in quartzites	Kellhuani	Optically unzoned	Bluish green
2020-KELL-17-C-TS2-Circle E-tur3-004	Tur-3	2020-KELL-17-C	Veins in Catavi Fm. quartzites	Quartz-tourmaline-cassiterite veins in quartzites	Kellhuani	Optically unzoned	Bluish green
2020-KELL-17-C-TS2-Circle F-tur3-001	Tur-3	2020-KELL-17-C	Veins in Catavi Fm. quartzites	Quartz-tourmaline-cassiterite veins in quartzites	Kellhuani	Optically unzoned	Bluish green
2020-KELL-17-C-TS2-Circle F-tur3-002	Tur-3	2020-KELL-17-C	Veins in Catavi Fm. quartzites	Quartz-tourmaline-cassiterite veins in quartzites	Kellhuani	Optically unzoned	Bluish green
2020-KELL-17-C-TS2-Circle F-tur3-003	Tur-3	2020-KELL-17-C	Veins in Catavi Fm. quartzites	Quartz-tourmaline-cassiterite veins in quartzites	Kellhuani	Optically unzoned	Bluish green

EMPA label	Type	Sample	Host-rock	Description	Locality	Zone	Color
2020-KELL-17-C-TS2-Circle F-tur3-004	Tur-3	2020-KELL-17-C	Veins in Catavi Fm. quartzites	Quartz-tourmaline-cassiterite veins in quartzites	Kellhuani	Optically unzoned	Bluish green
2020-KELL-17-C-TS2-Circle F-tur3-005	Tur-3	2020-KELL-17-C	Veins in Catavi Fm. quartzites	Quartz-tourmaline-cassiterite veins in quartzites	Kellhuani	Optically unzoned	Bluish green
2020-KELL-17-C-TS2-Circle F-tur3-006	Tur-3	2020-KELL-17-C	Veins in Catavi Fm. quartzites	Quartz-tourmaline-cassiterite veins in quartzites	Kellhuani	Optically unzoned	Bluish green
2020-KELL-17-C-TS2-Circle G-tur3-001	Tur-3	2020-KELL-17-C	Veins in Catavi Fm. quartzites	Quartz-tourmaline-cassiterite veins in quartzites	Kellhuani	Optically unzoned	Bluish green
2020-KELL-17-C-TS2-Circle G-tur3-002	Tur-3	2020-KELL-17-C	Veins in Catavi Fm. quartzites	Quartz-tourmaline-cassiterite veins in quartzites	Kellhuani	Optically unzoned	Bluish green
2020-KELL-17-C-TS2-Circle G-tur3-003	Tur-3	2020-KELL-17-C	Veins in Catavi Fm. quartzites	Quartz-tourmaline-cassiterite veins in quartzites	Kellhuani	Optically unzoned	Bluish green
2020-KELL-17-C-TS2-Circle G-tur3-004	Tur-3	2020-KELL-17-C	Veins in Catavi Fm. quartzites	Quartz-tourmaline-cassiterite veins in quartzites	Kellhuani	Optically unzoned	Bluish green
2020-KELL-17-C-TS2-Circle H-tur3-001	Tur-3	2020-KELL-17-C	Veins in Catavi Fm. quartzites	Quartz-tourmaline-cassiterite veins in quartzites	Kellhuani	Optically unzoned	Bluish green
2020-KELL-17-C-TS2-Circle H-tur3-002	Tur-3	2020-KELL-17-C	Veins in Catavi Fm. quartzites	Quartz-tourmaline-cassiterite veins in quartzites	Kellhuani	Optically unzoned	Bluish green
2020-KELL-17-C-TS2-Circle H-tur3-003	Tur-3	2020-KELL-17-C	Veins in Catavi Fm. quartzites	Quartz-tourmaline-cassiterite veins in quartzites	Kellhuani	Optically unzoned	Bluish green
2020-KELL-17-C-TS2-Circle H-tur3-004	Tur-3	2020-KELL-17-C	Veins in Catavi Fm. quartzites	Quartz-tourmaline-cassiterite veins in quartzites	Kellhuani	Optically unzoned	Bluish green
2020-KELL-17-C-TS2-Circle H-tur3-005	Tur-3	2020-KELL-17-C	Veins in Catavi Fm. quartzites	Quartz-tourmaline-cassiterite veins in quartzites	Kellhuani	Optically unzoned	Bluish green

EMPA label	Type	Sample	Host-rock	Description	Locality	Zone	Color
2020-KELL-48-TS1-Circle A-tur3-001	Tur-3	2020-KELL-48	Veins in Catavi Fm. quartzites	Quartz-tourmaline-cassiterite veins in quartzites	Kellhuani	Optically unzoned	Bluish green
2020-KELL-48-TS1-Circle A-tur3-002	Tur-3	2020-KELL-48	Veins in Catavi Fm. quartzites	Quartz-tourmaline-cassiterite veins in quartzites	Kellhuani	Optically unzoned	Bluish green
2020-KELL-48-TS1-Circle B-tur3-001	Tur-3	2020-KELL-48	Veins in Catavi Fm. quartzites	Quartz-tourmaline-cassiterite veins in quartzites	Kellhuani	Optically unzoned	Bluish green
2020-KELL-48-TS1-Circle B-tur3-002	Tur-3	2020-KELL-48	Veins in Catavi Fm. quartzites	Quartz-tourmaline-cassiterite veins in quartzites	Kellhuani	Optically unzoned	Bluish green
2020-KELL-48-TS1-Circle B-tur3-003	Tur-3	2020-KELL-48	Veins in Catavi Fm. quartzites	Quartz-tourmaline-cassiterite veins in quartzites	Kellhuani	Optically unzoned	Bluish green
2020-KELL-48-TS1-Circle B-tur3-004	Tur-3	2020-KELL-48	Veins in Catavi Fm. quartzites	Quartz-tourmaline-cassiterite veins in quartzites	Kellhuani	Optically unzoned	Bluish green
2020-KELL-48-TS1-Circle B-tur3-005	Tur-3	2020-KELL-48	Veins in Catavi Fm. quartzites	Quartz-tourmaline-cassiterite veins in quartzites	Kellhuani	Optically unzoned	Bluish green
2020-KELL-48-TS1-Circle B-tur3-006	Tur-3	2020-KELL-48	Veins in Catavi Fm. quartzites	Quartz-tourmaline-cassiterite veins in quartzites	Kellhuani	Optically unzoned	Bluish green
2020-KELL-48-TS1-Circle C-tur3-001	Tur-3	2020-KELL-48	Veins in Catavi Fm. quartzites	Quartz-tourmaline-cassiterite veins in quartzites	Kellhuani	Optically unzoned	Bluish green
2020-KELL-48-TS1-Circle C-tur3-002	Tur-3	2020-KELL-48	Veins in Catavi Fm. quartzites	Quartz-tourmaline-cassiterite veins in quartzites	Kellhuani	Optically unzoned	Bluish green
2020-KELL-48-TS1-Circle C-tur3-003	Tur-3	2020-KELL-48	Veins in Catavi Fm. quartzites	Quartz-tourmaline-cassiterite veins in quartzites	Kellhuani	Optically unzoned	Bluish green
2020-KELL-48-TS1-Circle D-tur3-001	Tur-3	2020-KELL-48	Veins in Catavi Fm. quartzites	Quartz-tourmaline-cassiterite veins in quartzites	Kellhuani	Optically unzoned	Bluish green

EMPA label	Type	Sample	Host-rock	Description	Locality	Zone	Color
2020-KELL-48-TS1-Circle D-tur3-002	Tur-3	2020-KELL-48	Veins in Catavi Fm. quartzites	Quartz-tourmaline-cassiterite veins in quartzites	Kellhuani	Optically unzoned	Bluish green
2020-KELL-48-TS1-Circle D-tur3-003	Tur-3	2020-KELL-48	Veins in Catavi Fm. quartzites	Quartz-tourmaline-cassiterite veins in quartzites	Kellhuani	Optically unzoned	Bluish green
2020-KELL-48-TS1-Circle D-tur3-004	Tur-3	2020-KELL-48	Veins in Catavi Fm. quartzites	Quartz-tourmaline-cassiterite veins in quartzites	Kellhuani	Optically unzoned	Bluish green
2020-KELL-48-TS1-Circle E-tur3-001	Tur-3	2020-KELL-48	Veins in Catavi Fm. quartzites	Quartz-tourmaline-cassiterite veins in quartzites	Kellhuani	Optically unzoned	Bluish green
2020-KELL-48-TS1-Circle E-tur3-002	Tur-3	2020-KELL-48	Veins in Catavi Fm. quartzites	Quartz-tourmaline-cassiterite veins in quartzites	Kellhuani	Optically unzoned	Bluish green
2020-KELL-48-TS1-Circle E-tur3-003	Tur-3	2020-KELL-48	Veins in Catavi Fm. quartzites	Quartz-tourmaline-cassiterite veins in quartzites	Kellhuani	Optically unzoned	Bluish green
2020-KELL-48-TS1-Circle F-tur3-004	Tur-3	2020-KELL-48	Veins in Catavi Fm. quartzites	Quartz-tourmaline-cassiterite veins in quartzites	Kellhuani	Optically unzoned	Bluish green
2020-KELL-48-TS1-Circle F-tur3-005	Tur-3	2020-KELL-48	Veins in Catavi Fm. quartzites	Quartz-tourmaline-cassiterite veins in quartzites	Kellhuani	Optically unzoned	Bluish green
2020-KELL-48-TS1-Circle G-tur3-001	Tur-3	2020-KELL-48	Veins in Catavi Fm. quartzites	Quartz-tourmaline-cassiterite veins in quartzites	Kellhuani	Optically unzoned	Bluish green
2020-KELL-48-TS1-Circle G-tur3-002	Tur-3	2020-KELL-48	Veins in Catavi Fm. quartzites	Quartz-tourmaline-cassiterite veins in quartzites	Kellhuani	Optically unzoned	Bluish green
2020-KELL-48-TS1-Circle G-tur3-003	Tur-3	2020-KELL-48	Veins in Catavi Fm. quartzites	Quartz-tourmaline-cassiterite veins in quartzites	Kellhuani	Optically unzoned	Bluish green
2020-KELL-48-TS1-Circle G-tur3-004	Tur-3	2020-KELL-48	Veins in Catavi Fm. quartzites	Quartz-tourmaline-cassiterite veins in quartzites	Kellhuani	Optically unzoned	Bluish green

EMPA label	Type	Sample	Host-rock	Description	Locality	Zone	Color
2020-KELL-48-TS1-Circle H-tur3-001	Tur-3	2020-KELL-48	Veins in Catavi Fm. quartzites	Quartz-tourmaline-cassiterite veins in quartzites	Kellhuani	Optically unzoned	Bluish green
2020-KELL-48-TS1-Circle H-tur3-002	Tur-3	2020-KELL-48	Veins in Catavi Fm. quartzites	Quartz-tourmaline-cassiterite veins in quartzites	Kellhuani	Optically unzoned	Bluish green
2020-KELL-48-TS1-Circle I-tur3-001	Tur-3	2020-KELL-48	Veins in Catavi Fm. quartzites	Quartz-tourmaline-cassiterite veins in quartzites	Kellhuani	Optically unzoned	Bluish green
2020-KELL-48-TS1-Circle I-tur3-002	Tur-3	2020-KELL-48	Veins in Catavi Fm. quartzites	Quartz-tourmaline-cassiterite veins in quartzites	Kellhuani	Optically unzoned	Bluish green
2020-KELL-48-TS1-Circle I-tur3-003	Tur-3	2020-KELL-48	Veins in Catavi Fm. quartzites	Quartz-tourmaline-cassiterite veins in quartzites	Kellhuani	Optically unzoned	Bluish green
2020-KELL-48-TS1-Circle I-tur3-004	Tur-3	2020-KELL-48	Veins in Catavi Fm. quartzites	Quartz-tourmaline-cassiterite veins in quartzites	Kellhuani	Optically unzoned	Bluish green
2020-KELL-48-TS1-Circle I-tur3-005	Tur-3	2020-KELL-48	Veins in Catavi Fm. quartzites	Quartz-tourmaline-cassiterite veins in quartzites	Kellhuani	Optically unzoned	Bluish green

EMPA label	Type	SiO ₂	TiO ₂	Al ₂ O ₃	Cr ₂ O ₃	FeO	MnO	MgO	CaO	Na ₂ O	K ₂ O	F	Cl	H ₂ O*	B ₂ O ₃ *	O=F	O=Cl	Total
2020-KELL-22-B-TS1-Circle A-TUR1A-001	Tur-1	35.10	0.61	33.47	<d.l.	12.47	<d.l.	2.11	0.09	1.83	0.03	0.67	<d.l.	2.89	10.26	0.28	0.00	99.25
2020-KELL-22-B-TS1-Circle A-TUR1A-002	Tur-1	34.92	0.43	34.27	<d.l.	12.72	<d.l.	1.86	0.11	1.88	0.03	0.71	<d.l.	2.90	10.32	0.30	0.00	99.85
2020-KELL-22-B-TS1-Circle A-TUR1A-003	Tur-1	35.01	0.39	34.18	<d.l.	12.36	<d.l.	1.68	0.08	1.94	0.03	0.63	<d.l.	2.94	10.25	0.27	0.00	99.22
2020-KELL-22-B-TS1-Circle A-TUR1A-004	Tur-1	35.16	0.32	34.28	<d.l.	11.98	<d.l.	1.89	0.10	1.82	0.03	0.69	<d.l.	2.88	10.27	0.29	0.00	99.13
2020-KELL-22-B-TS1-Circle A-TUR1A-005	Tur-1	35.00	0.33	35.12	<d.l.	11.97	<d.l.	1.69	0.10	1.70	0.02	0.58	<d.l.	2.91	10.33	0.24	0.00	99.51
2020-KELL-22-B-TS1-Circle A-TUR1A-006	Tur-1	35.76	<d.l.	35.55	<d.l.	12.68	<d.l.	0.43	<d.l.	1.37	<d.l.	0.17	<d.l.	2.98	10.30	0.07	0.00	99.17
2020-KELL-22-B-TS1-Circle A-TUR1A-007	Tur-1	34.65	0.37	33.89	<d.l.	12.96	<d.l.	1.77	0.13	1.90	0.05	0.67	<d.l.	2.91	10.24	0.28	0.00	99.26
2020-KELL-22-B-TS1-Circle A-TUR1A-008	Tur-1	34.43	0.47	34.44	<d.l.	12.40	<d.l.	1.51	0.16	1.85	0.03	0.82	<d.l.	2.82	10.20	0.35	0.00	98.78
2020-KELL-22-B-TS1-Circle A-TUR1A-009	Tur-1	34.67	0.38	34.75	<d.l.	12.52	<d.l.	1.55	0.16	1.71	0.03	0.76	<d.l.	2.83	10.28	0.32	0.00	99.31
2020-KELL-22-B-TS1-Circle A-TUR1A-010	Tur-1	34.95	0.34	34.90	<d.l.	12.01	<d.l.	1.48	0.13	1.59	0.03	0.56	<d.l.	2.88	10.26	0.24	0.00	98.90
2020-KELL-22-B-TS1-Circle A-TUR1A-011	Tur-1	35.72	<d.l.	34.65	<d.l.	13.55	<d.l.	0.46	<d.l.	1.53	0.03	0.47	<d.l.	2.88	10.26	0.20	0.00	99.36
2020-KELL-22-B-TS1-Circle A-TUR1A-012	Tur-1	35.37	<d.l.	34.87	<d.l.	12.95	0.08	0.88	0.05	1.56	0.04	0.51	<d.l.	2.89	10.28	0.22	0.00	99.26
2020-KELL-22-B-TS1-Circle A-TUR1A-013	Tur-1	34.56	0.61	33.81	<d.l.	12.58	<d.l.	1.55	0.18	1.83	0.04	0.74	<d.l.	2.85	10.16	0.31	0.00	98.60
2020-KELL-22-B-TS1-Circle A-TUR1A-014	Tur-1	34.90	0.17	35.03	<d.l.	11.89	<d.l.	1.40	0.12	1.78	0.04	0.50	<d.l.	2.96	10.24	0.21	0.00	98.81
2020-KELL-22-B-TS1-Circle A-TUR1A-015	Tur-1	34.68	0.58	33.73	<d.l.	12.78	<d.l.	1.64	0.16	1.94	0.04	0.81	<d.l.	2.85	10.20	0.34	0.00	99.07
2020-KELL-22-B-TS1-Circle A-TUR1A-016	Tur-1	35.00	0.41	34.18	<d.l.	12.28	<d.l.	1.81	0.11	1.81	<d.l.	0.68	<d.l.	2.88	10.26	0.29	0.00	99.13
2020-KELL-22-B-TS1-Circle A-TUR1A-017	Tur-1	34.28	0.50	34.51	<d.l.	12.58	<d.l.	1.59	0.19	1.95	0.02	0.75	<d.l.	2.89	10.22	0.32	0.00	99.17
2020-KELL-22-B-TS1-Circle B-TUR1A-001	Tur-1	35.05	0.35	34.75	<d.l.	12.26	<d.l.	1.64	0.13	1.79	0.03	0.56	<d.l.	2.95	10.31	0.24	0.00	99.58
2020-KELL-22-B-TS1-Circle B-TUR1A-002	Tur-1	34.85	<d.l.	34.48	<d.l.	12.59	<d.l.	1.48	0.09	1.76	0.04	0.73	<d.l.	2.83	10.22	0.31	0.00	98.77
2020-KELL-22-B-TS1-Circle B-TUR1A-003	Tur-1	35.08	0.29	35.11	<d.l.	11.66	<d.l.	1.61	0.07	1.46	0.03	0.48	<d.l.	2.88	10.29	0.20	0.00	98.76
2020-KELL-22-B-TS1-Circle B-TUR1A-004	Tur-1	34.75	0.30	34.78	<d.l.	12.26	<d.l.	1.63	0.12	1.78	0.03	0.61	<d.l.	2.91	10.27	0.26	0.00	99.19
2020-KELL-22-B-TS1-Circle B-TUR1A-005	Tur-1	35.42	0.19	35.30	<d.l.	11.81	<d.l.	1.53	0.05	1.54	0.04	0.48	<d.l.	2.91	10.35	0.20	0.00	99.42
2020-KELL-22-B-TS1-Circle B-TUR1A-006	Tur-1	35.74	0.31	35.14	<d.l.	11.70	<d.l.	1.46	0.05	1.53	0.03	0.35	<d.l.	2.97	10.35	0.15	0.00	99.49
2020-KELL-22-B-TS1-Circle B-TUR1A-008	Tur-1	34.66	0.54	33.40	<d.l.	12.57	<d.l.	1.93	0.13	1.96	0.03	0.84	<d.l.	2.83	10.18	0.35	0.00	98.71
2020-KELL-22-B-TS1-Circle B-TUR1A-009	Tur-1	34.44	0.45	34.09	<d.l.	12.47	<d.l.	1.71	0.12	1.86	0.04	0.66	<d.l.	2.89	10.19	0.28	0.00	98.64
2020-KELL-22-B-TS1-Circle B-TUR1A-010	Tur-1	34.87	0.60	33.73	<d.l.	12.50	<d.l.	1.67	0.12	1.80	0.03	0.69	<d.l.	2.86	10.20	0.29	0.00	98.78
2020-KELL-22-B-TS1-Circle B-TUR1A-011	Tur-1	34.54	0.31	34.40	<d.l.	12.05	<d.l.	1.72	0.09	1.74	0.02	0.63	<d.l.	2.86	10.19	0.27	0.00	98.29
2020-KELL-22-B-TS1-Circle C-TUR1A-001	Tur-1	35.09	0.30	34.56	<d.l.	11.99	<d.l.	1.95	0.09	1.82	0.04	0.53	<d.l.	2.97	10.31	0.22	0.00	99.43
2020-KELL-22-B-TS1-Circle C-TUR1A-002	Tur-1	35.33	0.24	34.83	<d.l.	11.66	<d.l.	1.86	0.12	1.73	0.03	0.48	<d.l.	2.97	10.32	0.20	0.00	99.37
2020-KELL-22-B-TS1-Circle C-TUR1A-003	Tur-1	35.10	0.21	34.47	<d.l.	12.68	<d.l.	1.31	0.07	1.72	0.02	0.61	<d.l.	2.88	10.25	0.26	0.00	99.06
2020-KELL-22-B-TS1-Circle C-TUR1A-004	Tur-1	35.15	0.23	33.99	<d.l.	12.89	<d.l.	1.65	0.08	1.75	0.04	0.47	<d.l.	2.96	10.27	0.20	0.00	99.28
2020-KELL-22-B-TS1-Circle C-TUR1A-005	Tur-1	34.81	0.41	32.99	<d.l.	14.40	<d.l.	1.14	0.14	1.81	0.03	0.60	<d.l.	2.90	10.17	0.25	0.00	99.14
2020-KELL-22-B-TS1-Circle C-TUR1A-006	Tur-1	35.35	0.20	33.11	<d.l.	13.79	<d.l.	1.40	0.06	1.88	0.03	0.55	<d.l.	2.94	10.21	0.23	0.00	99.30
2020-KELL-22-B-TS1-Circle C-TUR1A-007	Tur-1	34.47	<d.l.	33.20	<d.l.	14.87	0.11	0.70	0.19	1.65	0.04	0.54	<d.l.	2.88	10.10	0.23	0.00	98.52
2020-KELL-22-B-TS1-Circle C-TUR1A-008	Tur-1	34.94	0.17	32.99	<d.l.	13.42	0.13	1.79	0.47	1.51	0.03	0.17	<d.l.	3.08	10.19	0.07	0.00	98.82
2020-KELL-22-B-TS1-Circle C-TUR1A-009	Tur-1	35.09	0.22	31.87	<d.l.	14.23	0.10	1.87	0.46	1.95	0.03	0.20	<d.l.	3.18	10.15	0.08	0.00	99.26
2020-KELL-22-B-TS1-Circle C-TUR1A-010	Tur-1	34.86	0.34	34.32	<d.l.	12.26	<d.l.	1.65	0.12	1.78	0.03	0.44	<d.l.	2.98	10.23	0.19	0.00	98.82
2020-KELL-22-B-TS1-Circle C-TUR1A-011	Tur-1	35.05	0.35	33.95	<d.l.	12.35	<d.l.	1.70	0.10	1.83	0.02	0.72	<d.l.	2.86	10.22	0.30	0.00	98.84
2020-KELL-22-B-TS1-Circle C-TUR1A-012	Tur-1	34.91	0.28	34.39	<d.l.	12.25	<d.l.	1.65	0.11	1.80	0.03	0.64	<d.l.	2.89	10.24	0.27	0.00	98.92

EMPA label	Type	SiO ₂	TiO ₂	Al ₂ O ₃	Cr ₂ O ₃	FeO	MnO	MgO	CaO	Na ₂ O	K ₂ O	F	Cl	H ₂ O*	B ₂ O ₃ *	O=F	O=Cl	Total
2020-KELL-22-B-TS1-Circle C-TUR1A-013	Tur-1	35.67	0.22	34.89	<d.l.	13.58	<d.l.	1.01	0.11	1.72	0.03	0.44	<d.l.	3.01	10.41	0.19	0.00	100.90
2020-KELL-22-B-TS1-Circle C-TUR1A-014	Tur-1	34.88	0.52	33.88	<d.l.	12.78	<d.l.	1.90	0.11	1.73	0.05	0.77	<d.l.	2.83	10.28	0.32	0.00	99.40
2020-KELL-22-B-TS1-Circle D-TUR1A-001	Tur-1	34.96	0.23	34.83	<d.l.	12.19	<d.l.	1.71	0.11	1.71	0.04	0.53	<d.l.	2.94	10.30	0.22	0.00	99.33
2020-KELL-22-B-TS1-Circle D-TUR1A-002	Tur-1	35.00	0.34	34.46	<d.l.	12.19	<d.l.	1.64	0.13	1.68	0.03	0.72	<d.l.	2.83	10.26	0.30	0.00	98.97
2020-KELL-22-B-TS1-Circle D-TUR1A-003	Tur-1	34.52	0.41	33.55	<d.l.	13.03	<d.l.	1.88	0.15	2.00	0.03	0.79	<d.l.	2.88	10.20	0.33	0.00	99.11
2020-KELL-22-B-TS1-Circle D-TUR1A-004	Tur-1	35.08	0.23	34.32	<d.l.	12.02	<d.l.	1.72	0.13	1.70	0.04	0.51	<d.l.	2.93	10.23	0.22	0.00	98.70
2020-KELL-22-B-TS1-Circle D-TUR1A-005	Tur-1	34.36	0.62	32.98	<d.l.	13.49	<d.l.	2.08	0.15	1.97	0.04	0.72	<d.l.	2.90	10.21	0.30	0.00	99.22
2020-KELL-22-B-TS1-Circle D-TUR1A-006	Tur-1	34.90	0.48	33.98	<d.l.	12.76	<d.l.	1.86	0.11	1.86	0.03	0.77	<d.l.	2.86	10.28	0.32	0.00	99.57
2020-KELL-22-B-TS1-Circle D-TUR1A-007	Tur-1	34.76	0.55	34.08	<d.l.	13.04	<d.l.	1.13	0.10	1.84	0.03	0.53	<d.l.	2.94	10.19	0.22	0.00	98.97
2020-KELL-22-B-TS1-Circle D-TUR1A-008	Tur-1	34.81	0.34	34.07	<d.l.	13.22	<d.l.	1.22	0.10	1.65	0.04	0.57	<d.l.	2.87	10.21	0.24	0.00	98.86
2020-KELL-22-B-TS1-Circle D-TUR1A-009	Tur-1	34.52	0.27	33.03	<d.l.	14.91	0.11	0.70	0.21	1.83	0.04	0.71	<d.l.	2.85	10.11	0.30	0.00	98.99
2020-KELL-22-B-TS1-Circle D-TUR1A-010	Tur-1	35.22	0.16	32.79	<d.l.	13.49	<d.l.	1.50	0.06	1.81	0.03	0.33	<d.l.	3.01	10.14	0.14	0.00	98.40
2020-KELL-22-B-TS1-Circle D-TUR1A-011	Tur-1	35.10	<d.l.	33.79	<d.l.	13.89	0.09	0.65	0.21	1.36	0.03	0.38	<d.l.	2.88	10.15	0.16	0.00	98.37
2020-KELL-22-B-TS1-Circle D-TUR1A-012	Tur-1	35.16	<d.l.	32.84	<d.l.	11.84	0.10	2.70	0.52	1.59	0.04	0.15	<d.l.	3.12	10.18	0.06	0.00	98.18
2020-KELL-22-B-TS1-Circle D-TUR1A-013	Tur-1	34.70	0.24	31.19	<d.l.	15.37	<d.l.	1.34	0.55	1.83	0.04	0.25	<d.l.	3.10	10.02	0.11	0.00	98.53
2020-KELL-22-B-TS1-Circle D-TUR1A-014	Tur-1	34.82	0.19	30.85	<d.l.	14.53	0.12	2.17	0.55	2.14	0.06	0.24	<d.l.	3.21	10.06	0.10	0.00	98.84
2020-KELL-22-B-TS1-Circle D-TUR1A-015	Tur-1	34.55	<d.l.	31.55	<d.l.	14.22	0.12	1.61	0.34	1.66	0.04	0.17	<d.l.	3.05	9.98	0.07	0.00	97.21
2020-KELL-22-B-TS1-Circle D-TUR1A-016	Tur-1	33.91	<d.l.	31.59	<d.l.	14.21	0.09	1.62	0.47	1.54	0.03	0.15	<d.l.	3.02	9.91	0.06	0.00	96.48
2020-KELL-22-B-TS1-Circle D-TUR1A-017	Tur-1	33.94	<d.l.	31.68	<d.l.	13.60	<d.l.	1.68	0.48	1.53	0.03	<d.l.	<d.l.	3.08	9.87	0.00	0.00	95.89
2020-KELL-22-B-TS1-Circle D-TUR1A-018	Tur-1	35.63	0.28	35.39	<d.l.	11.82	<d.l.	1.38	0.09	1.58	0.03	0.37	<d.l.	2.99	10.37	0.16	0.00	99.77
2020-KELL-22-B-TS1-Circle E-TUR1A-001	Tur-1	33.26	0.54	32.28	<d.l.	12.53	<d.l.	1.82	0.15	1.85	0.06	0.77	<d.l.	2.75	9.84	0.32	0.00	95.53
2020-KELL-22-B-TS1-Circle E-TUR1A-002	Tur-1	34.75	0.39	33.35	<d.l.	12.98	<d.l.	1.77	0.10	1.90	0.04	0.57	<d.l.	2.94	10.18	0.24	0.00	98.73
2020-KELL-22-B-TS1-Circle E-TUR1A-003	Tur-1	34.69	0.29	34.32	<d.l.	12.03	<d.l.	1.67	0.11	1.78	0.02	0.53	<d.l.	2.92	10.19	0.22	0.00	98.33
2020-KELL-22-B-TS1-Circle E-TUR1A-004	Tur-1	34.43	0.45	34.31	<d.l.	12.44	<d.l.	1.78	0.15	1.85	0.03	0.66	<d.l.	2.90	10.23	0.28	0.00	98.95
2020-KELL-22-B-TS1-Circle E-TUR1A-005	Tur-1	35.14	0.53	34.67	<d.l.	12.26	<d.l.	1.73	0.20	1.94	0.05	0.80	0.02	2.90	10.34	0.34	0.01	100.23
2020-KELL-22-B-TS1-Circle E-TUR1A-006	Tur-1	34.02	0.42	33.81	<d.l.	12.59	<d.l.	1.57	0.16	1.79	0.05	0.85	<d.l.	2.76	10.09	0.36	0.00	97.75
2020-KELL-22-B-TS1-Circle E-TUR1A-007	Tur-1	34.22	0.50	34.63	<d.l.	13.34	<d.l.	0.86	0.18	1.83	0.03	0.71	<d.l.	2.86	10.18	0.30	0.00	99.04
2020-KELL-22-B-TS1-Circle E-TUR1A-008	Tur-1	34.85	0.26	35.39	<d.l.	12.28	<d.l.	1.14	0.15	1.67	0.03	0.57	<d.l.	2.91	10.28	0.24	0.00	99.29
2020-KELL-22-B-TS1-Circle E-TUR1A-009	Tur-1	34.40	0.46	34.75	<d.l.	12.23	<d.l.	1.88	0.13	1.83	0.04	0.78	<d.l.	2.85	10.28	0.33	0.00	99.30
2020-KELL-22-B-TS6-Circle A-Tur1a-001	Tur-1	34.38	0.50	34.17	<d.l.	12.13	<d.l.	1.80	0.15	1.82	0.05	0.78	<d.l.	2.83	10.18	0.33	0.00	98.46
2020-KELL-22-B-TS6-Circle A-Tur1a-002	Tur-1	34.86	0.34	34.97	<d.l.	12.12	<d.l.	1.60	0.17	1.73	0.03	0.58	<d.l.	2.93	10.30	0.24	0.00	99.38
2020-KELL-22-B-TS6-Circle A-Tur1a-003	Tur-1	36.74	0.28	36.48	<d.l.	11.90	<d.l.	1.31	0.19	1.42	0.03	0.48	<d.l.	2.98	10.64	0.20	0.00	102.25
2020-KELL-22-B-TS6-Circle A-Tur1a-004	Tur-1	34.76	0.57	33.76	<d.l.	12.91	<d.l.	1.88	0.14	1.91	0.04	0.75	<d.l.	2.89	10.26	0.32	0.00	99.55
2020-KELL-22-B-TS6-Circle A-Tur1a-005	Tur-1	34.46	0.66	33.46	<d.l.	12.64	<d.l.	1.72	0.13	1.94	0.02	0.85	<d.l.	2.81	10.14	0.36	0.00	98.47
2020-KELL-22-B-TS6-Circle A-Tur1a-006	Tur-1	34.82	0.50	33.06	<d.l.	13.27	<d.l.	1.87	0.13	1.95	0.05	0.91	<d.l.	2.81	10.20	0.38	0.00	99.18
2020-KELL-22-B-TS6-Circle A-Tur1a-007	Tur-1	34.93	0.71	34.06	<d.l.	12.35	<d.l.	1.86	0.23	1.90	0.04	0.71	<d.l.	2.92	10.28	0.30	0.00	99.69
2020-KELL-22-B-TS6-Circle A-Tur1a-008	Tur-1	35.00	0.41	33.79	<d.l.	12.19	<d.l.	1.96	0.11	1.84	0.02	0.67	<d.l.	2.89	10.23	0.28	0.00	98.82
2020-KELL-22-B-TS6-Circle C-TUR1A-001	Tur-1	34.93	0.31	34.09	<d.l.	12.57	<d.l.	1.83	0.11	2.02	0.03	0.80	<d.l.	2.89	10.26	0.34	0.00	99.50
2020-KELL-22-B-TS6-Circle C-TUR1A-002	Tur-1	35.61	0.25	35.22	<d.l.	11.71	<d.l.	1.39	0.07	1.63	<d.l.	0.35	<d.l.	2.99	10.33	0.15	0.00	99.41

EMPA label	Type	SiO ₂	TiO ₂	Al ₂ O ₃	Cr ₂ O ₃	FeO	MnO	MgO	CaO	Na ₂ O	K ₂ O	F	Cl	H ₂ O*	B ₂ O ₃ *	O=F	O=Cl	Total
2020-KELL-22-B-TS6-Circle D-TUR1A-001	Tur-1	35.26	0.27	31.76	<d.l.	14.96	0.13	1.08	0.13	1.71	0.03	0.77	<d.l.	2.77	10.10	0.32	0.00	98.64
2020-KELL-22-B-TS6-Circle D-TUR1A-002	Tur-1	35.40	0.29	33.98	<d.l.	12.69	<d.l.	1.55	0.05	1.88	<d.l.	0.54	<d.l.	2.96	10.27	0.23	0.00	99.37
2020-KELL-22-B-TS6-Circle D-TUR1A-004	Tur-1	35.81	0.16	35.24	<d.l.	11.94	<d.l.	1.55	0.05	1.59	0.03	0.50	<d.l.	2.93	10.40	0.21	0.00	99.99
2020-KELL-22-B-TS6-Circle D-TUR1A-005	Tur-1	35.25	0.29	34.38	<d.l.	12.09	<d.l.	1.69	0.06	1.70	0.02	0.66	<d.l.	2.85	10.27	0.28	0.00	98.98
2020-KELL-22-B-TS6-Circle D-TUR1A-006	Tur-1	29.46	0.27	28.24	<d.l.	11.18	<d.l.	1.68	0.27	1.81	0.08	0.43	0.02	2.62	8.67	0.18	0.01	84.54
2020-KELL-22-B-TS6-Circle D-TUR1A-007	Tur-1	31.24	0.35	30.22	<d.l.	11.18	<d.l.	1.75	0.12	2.00	0.05	0.73	0.04	2.63	9.16	0.31	0.01	89.15
2020-KELL-22-B-TS6-Circle D-TUR1A-008	Tur-1	35.05	0.38	34.73	<d.l.	13.06	<d.l.	1.20	0.11	1.47	0.04	0.54	<d.l.	2.86	10.31	0.23	0.00	99.53
2020-KELL-22-B-TS6-Circle D-TUR1A-009	Tur-1	34.88	0.48	33.82	<d.l.	13.16	<d.l.	1.62	0.08	1.93	0.02	0.65	<d.l.	2.92	10.26	0.27	0.00	99.55
2020-KELL-22-B-TS6-Circle E-TUR1A-001	Tur-1	35.00	0.39	34.47	<d.l.	12.51	<d.l.	1.60	0.12	1.78	0.04	0.69	<d.l.	2.88	10.29	0.29	0.00	99.47
2020-KELL-22-B-TS6-Circle E-TUR1A-002	Tur-1	34.89	0.35	34.06	<d.l.	12.67	<d.l.	1.63	0.11	1.88	0.04	0.64	<d.l.	2.92	10.23	0.27	0.00	99.15
2020-KELL-22-B-TS6-Circle E-TUR1A-003	Tur-1	39.09	0.23	38.75	<d.l.	11.56	<d.l.	1.41	0.09	1.82	<d.l.	0.39	<d.l.	3.26	11.21	0.16	0.00	107.64
2020-KELL-22-B-TS6-Circle E-TUR1A-004	Tur-1	34.71	0.23	35.29	<d.l.	12.20	<d.l.	1.29	0.16	1.69	0.02	0.61	<d.l.	2.89	10.27	0.26	0.00	99.10
2020-KELL-22-B-TS6-Circle E-TUR1A-005	Tur-1	34.88	0.20	35.15	<d.l.	12.08	<d.l.	1.48	0.14	1.72	<d.l.	0.57	<d.l.	2.91	10.29	0.24	0.00	99.18
2020-KELL-22-B-TS6-Circle F-TUR1A-001	Tur-1	35.25	0.39	33.88	<d.l.	12.59	<d.l.	1.97	0.08	1.86	0.03	0.59	<d.l.	2.95	10.31	0.25	0.00	99.64
2020-KELL-22-B-TS6-Circle F-TUR1A-002	Tur-1	34.73	0.49	34.21	<d.l.	12.74	<d.l.	1.65	0.15	1.76	0.03	0.72	<d.l.	2.85	10.26	0.30	0.00	99.29
2020-KELL-22-B-TS6-Circle F-TUR1A-003	Tur-1	34.88	0.53	34.45	<d.l.	12.57	<d.l.	1.70	0.16	1.84	0.03	0.59	<d.l.	2.95	10.30	0.25	0.00	99.76
2020-KELL-22-B-TS6-Circle F-TUR1A-004	Tur-1	34.76	0.60	34.06	<d.l.	12.70	<d.l.	1.87	0.17	1.98	0.04	0.80	<d.l.	2.89	10.29	0.34	0.00	99.82
2020-KELL-22-B-TS6-Circle F-TUR1A-005	Tur-1	34.79	0.49	34.48	<d.l.	12.33	<d.l.	1.59	0.14	1.80	0.03	0.78	<d.l.	2.83	10.25	0.33	0.00	99.19
2020-KELL-22-B-TS6-Circle F-TUR1A-006	Tur-1	34.97	0.32	34.44	<d.l.	12.20	<d.l.	1.74	0.11	1.73	0.03	0.48	<d.l.	2.96	10.27	0.20	0.00	99.04
2020-KELL-22-B-TS6-Circle G-TUR1A-001	Tur-1	34.09	0.78	33.77	<d.l.	13.43	<d.l.	1.36	0.24	1.97	0.04	0.71	<d.l.	2.91	10.17	0.30	0.00	99.17
2020-KELL-22-B-TS6-Circle G-TUR1A-002	Tur-1	34.74	0.56	33.91	<d.l.	12.61	<d.l.	1.46	0.16	1.82	0.04	0.71	<d.l.	2.86	10.18	0.30	0.00	98.75
2020-KELL-22-B-TS6-Circle G-TUR1A-003	Tur-1	34.74	0.45	35.14	<d.l.	12.35	<d.l.	1.52	0.15	1.76	0.03	0.64	<d.l.	2.91	10.32	0.27	0.00	99.74
2020-KELL-22-B-TS6-Circle G-TUR1A-004	Tur-1	34.86	0.56	34.13	<d.l.	12.34	<d.l.	1.68	0.12	1.81	0.04	0.71	<d.l.	2.87	10.24	0.30	0.00	99.05
2020-KELL-22-B-TS6-Circle G-TUR1A-005	Tur-1	35.97	0.26	35.36	<d.l.	11.28	<d.l.	1.54	0.05	1.49	0.02	0.31	<d.l.	2.98	10.38	0.13	0.00	99.51
2020-KELL-22-B-TS6-Circle G-TUR1A-006	Tur-1	35.21	0.54	33.20	<d.l.	12.95	<d.l.	1.94	0.11	1.93	0.03	0.71	<d.l.	2.90	10.25	0.30	0.00	99.47
2020-KELL-22-B-TS6-Circle G-TUR1A-007	Tur-1	35.12	0.35	34.16	<d.l.	12.12	<d.l.	1.91	0.11	1.75	0.03	0.66	<d.l.	2.88	10.27	0.28	0.00	99.08
2020-KELL-22-B-TS6-Circle G-TUR1A-008	Tur-1	35.53	0.29	34.91	<d.l.	12.08	<d.l.	1.68	0.05	1.76	0.03	0.47	<d.l.	2.99	10.37	0.20	0.00	99.96
2020-KELL-22-B-TS6-Circle H-TUR1A-001	Tur-1	34.67	0.56	34.67	<d.l.	12.67	<d.l.	1.52	0.21	1.96	0.03	0.84	<d.l.	2.87	10.29	0.35	0.00	99.94
2020-KELL-22-B-TS6-Circle H-TUR1A-002	Tur-1	34.52	0.27	35.53	<d.l.	12.27	<d.l.	1.21	0.17	1.69	0.03	0.81	<d.l.	2.80	10.27	0.34	0.00	99.23
2020-KELL-22-B-TS6-Circle H-TUR1A-003	Tur-1	34.79	0.25	35.76	<d.l.	12.24	<d.l.	1.04	0.17	1.78	0.03	0.53	<d.l.	2.97	10.30	0.22	0.00	99.63
2020-KELL-22-B-TS6-Circle H-TUR1A-004	Tur-1	34.34	0.60	34.33	<d.l.	12.68	<d.l.	1.42	0.22	1.96	0.04	0.71	<d.l.	2.91	10.19	0.30	0.00	99.11
2020-KELL-22-B-TS6-Circle H-TUR1A-005	Tur-1	34.78	0.50	34.17	<d.l.	12.91	<d.l.	1.61	0.17	1.90	0.03	0.62	<d.l.	2.95	10.27	0.26	0.00	99.65
2020-KELL-22-B-TS6-Circle J-TUR1A-001	Tur-1	35.15	<d.l.	36.10	<d.l.	12.24	<d.l.	0.74	0.09	1.68	<d.l.	0.63	<d.l.	2.87	10.32	0.27	0.00	99.56
2020-KELL-22-B-TS6-Circle J-TUR1A-002	Tur-1	35.11	<d.l.	36.17	<d.l.	12.25	<d.l.	0.76	0.11	1.59	0.02	0.43	<d.l.	2.95	10.33	0.18	0.00	99.54
2020-KELL-22-B-TS6-Circle J-TUR1A-003	Tur-1	34.86	0.63	33.24	<d.l.	12.72	<d.l.	2.01	0.14	1.88	0.02	0.77	<d.l.	2.85	10.21	0.32	0.00	99.01
2020-KELL-22-B-TS6-Circle J-TUR1A-004	Tur-1	37.47	0.18	37.12	<d.l.	12.32	<d.l.	1.10	0.16	1.95	0.04	0.85	0.03	2.99	10.81	0.36	0.01	104.65
2020-KELL-22-B-TS6-Circle J-TUR1A-005	Tur-1	34.67	0.38	34.68	<d.l.	13.21	<d.l.	1.08	0.18	1.78	0.04	0.80	<d.l.	2.83	10.25	0.34	0.00	99.56
2020-KELL-22-B-TS6-Circle J-TUR1A-006	Tur-1	35.30	0.37	34.40	<d.l.	11.90	<d.l.	1.75	0.12	1.66	0.03	0.40	<d.l.	2.98	10.28	0.17	0.00	99.01
2020-KELL-22-B-TS6-Circle K-TUR1A-001	Tur-1	34.79	0.36	34.32	<d.l.	12.77	<d.l.	1.39	0.16	1.96	0.04	0.86	<d.l.	2.84	10.23	0.36	0.00	99.36

EMPA label	Type	SiO ₂	TiO ₂	Al ₂ O ₃	Cr ₂ O ₃	FeO	MnO	MgO	CaO	Na ₂ O	K ₂ O	F	Cl	H ₂ O*	B ₂ O ₃ *	O=F	O=Cl	Total
2020-KELL-22-B-TS6-Circle K-TUR1A-002	Tur-1	35.26	0.26	35.41	<d.l.	11.77	<d.l.	1.20	0.08	1.71	0.04	0.42	<d.l.	2.98	10.29	0.18	0.00	99.25
2020-KELL-22-B-TS6-Circle K-TUR1A-003	Tur-1	34.46	0.36	34.66	<d.l.	12.70	<d.l.	1.56	0.15	1.90	0.04	0.81	<d.l.	2.85	10.26	0.34	0.00	99.41
2020-KELL-22-B-TS6-Circle K-TUR1A-004	Tur-1	34.38	0.43	33.89	<d.l.	12.48	<d.l.	1.87	0.14	1.90	0.04	0.69	<d.l.	2.89	10.18	0.29	0.00	98.60
2020-KELL-22-B-TS6-Circle K-TUR1A-005	Tur-1	35.05	0.17	35.67	<d.l.	11.72	<d.l.	1.29	0.16	1.69	0.02	0.52	<d.l.	2.94	10.31	0.22	0.00	99.32
2020-KELL-22-B-TS6-Circle K-TUR1A-006	Tur-1	35.04	0.21	35.58	<d.l.	12.07	<d.l.	1.23	0.13	1.63	0.04	0.56	<d.l.	2.91	10.32	0.24	0.00	99.48
2020-KELL-22-B-TS6-Circle L-TUR1A-001	Tur-1	34.68	0.45	33.27	<d.l.	12.43	<d.l.	1.97	0.16	1.88	0.03	0.69	<d.l.	2.88	10.15	0.29	0.00	98.29
2020-KELL-22-B-TS6-Circle L-TUR1A-002	Tur-1	35.04	0.59	33.98	<d.l.	12.76	<d.l.	1.74	0.10	1.85	<d.l.	0.72	<d.l.	2.88	10.29	0.30	0.00	99.64
2020-KELL-22-B-TS6-Circle L-TUR1A-003	Tur-1	35.03	0.59	34.12	<d.l.	12.60	<d.l.	1.58	0.16	1.84	0.03	0.85	<d.l.	2.82	10.26	0.36	0.00	99.53
2020-KELL-22-B-TS6-Circle L-TUR1A-004	Tur-1	34.66	0.42	34.41	<d.l.	12.55	<d.l.	1.48	0.18	1.91	0.04	0.75	<d.l.	2.88	10.22	0.32	0.00	99.19
2020-KELL-22-B-TS6-Circle L-TUR1A-005	Tur-1	34.59	0.52	34.59	<d.l.	12.55	<d.l.	1.71	0.19	1.85	0.05	0.67	<d.l.	2.92	10.29	0.28	0.00	99.65
2020-KELL-22-B-TS6-Circle L-TUR1A-006	Tur-1	34.55	0.56	34.12	<d.l.	13.28	<d.l.	1.23	0.20	1.77	0.03	0.59	<d.l.	2.92	10.21	0.25	0.00	99.21
2020-KELL-23-TS1-Circle A-TUR1A-001	Tur-1	34.42	0.52	34.07	<d.l.	11.88	<d.l.	2.42	0.37	1.78	0.05	0.69	<d.l.	2.91	10.26	0.29	0.00	99.08
2020-KELL-23-TS1-Circle A-TUR1A-002	Tur-1	34.80	0.25	36.62	<d.l.	9.43	<d.l.	2.46	0.50	1.45	0.02	0.48	<d.l.	2.97	10.39	0.20	0.00	99.17
2020-KELL-23-TS1-Circle A-TUR1A-003	Tur-1	34.41	0.34	35.50	<d.l.	9.92	<d.l.	2.74	0.47	1.67	0.04	0.78	<d.l.	2.86	10.30	0.33	0.00	98.70
2020-KELL-23-TS1-Circle A-TUR1A-004	Tur-1	35.80	0.42	34.75	<d.l.	10.77	<d.l.	2.02	0.16	1.55	0.02	0.33	<d.l.	3.00	10.32	0.14	0.00	99.00
2020-KELL-23-TS1-Circle A-TUR1A-005	Tur-1	34.78	0.54	33.83	<d.l.	10.74	<d.l.	3.03	0.51	1.89	0.05	0.75	<d.l.	2.94	10.26	0.32	0.00	99.01
2020-KELL-23-TS1-Circle A-TUR1A-006	Tur-1	34.57	0.40	34.51	<d.l.	10.68	<d.l.	2.92	0.42	1.76	0.04	0.73	<d.l.	2.90	10.29	0.31	0.00	98.92
2020-KELL-23-TS1-Circle A-TUR1A-007	Tur-1	34.13	0.48	35.75	<d.l.	10.62	<d.l.	2.24	0.53	1.59	0.03	0.44	<d.l.	3.01	10.29	0.19	0.00	98.93
2020-KELL-23-TS1-Circle A-TUR1A-008	Tur-1	35.70	0.20	36.62	<d.l.	9.95	<d.l.	2.14	0.27	1.57	0.03	0.31	<d.l.	3.07	10.49	0.13	0.00	100.22
2020-KELL-23-TS1-Circle A-TUR1A-009	Tur-1	35.49	<d.l.	36.33	<d.l.	9.83	<d.l.	1.99	0.27	1.41	0.04	0.53	0.02	2.89	10.37	0.22	0.01	98.94
2020-KELL-23-TS1-Circle A-TUR1A-010	Tur-1	34.39	0.29	36.45	<d.l.	10.01	<d.l.	2.22	0.58	1.64	0.04	0.53	<d.l.	3.00	10.34	0.22	0.00	99.27
2020-KELL-23-TS1-Circle A-TUR1A-011	Tur-1	34.61	0.51	34.79	<d.l.	10.78	<d.l.	2.79	0.66	1.61	0.04	0.74	<d.l.	2.90	10.33	0.31	0.00	99.46
2020-KELL-23-TS1-Circle A-TUR1A-012	Tur-1	34.21	0.53	34.90	<d.l.	10.76	<d.l.	2.58	0.72	1.60	0.05	0.64	<d.l.	2.94	10.26	0.27	0.00	98.93
2020-KELL-23-TS1-Circle B-TUR1A-001	Tur-1	35.47	0.27	36.21	<d.l.	9.83	<d.l.	2.66	0.40	1.56	0.03	0.43	<d.l.	3.03	10.49	0.18	0.00	100.20
2020-KELL-23-TS1-Circle B-TUR1A-002	Tur-1	35.07	0.24	36.50	<d.l.	9.60	<d.l.	2.65	0.39	1.52	0.03	0.56	<d.l.	2.95	10.46	0.24	0.00	99.73
2020-KELL-23-TS1-Circle B-TUR1A-003	Tur-1	35.38	0.64	33.59	<d.l.	10.74	<d.l.	3.20	0.54	1.67	0.04	0.73	<d.l.	2.91	10.34	0.31	0.00	99.47
2020-KELL-23-TS1-Circle B-TUR1A-004	Tur-1	35.22	0.32	35.36	<d.l.	9.91	<d.l.	2.87	0.41	1.49	<d.l.	0.60	<d.l.	2.90	10.39	0.25	0.00	99.23
2020-KELL-23-TS1-Circle B-TUR1A-005	Tur-1	34.44	0.34	35.67	<d.l.	10.64	<d.l.	2.36	0.44	1.73	0.02	0.54	<d.l.	2.99	10.33	0.23	0.00	99.28
2020-KELL-23-TS1-Circle B-TUR1A-006	Tur-1	35.03	0.21	36.64	<d.l.	9.84	<d.l.	2.22	0.31	1.52	<d.l.	0.49	<d.l.	2.96	10.42	0.21	0.00	99.43
2020-KELL-23-TS1-Circle B-TUR1A-007	Tur-1	34.33	0.44	35.58	<d.l.	11.11	<d.l.	2.18	0.47	1.74	0.05	0.65	<d.l.	2.96	10.33	0.27	0.00	99.56
2020-KELL-23-TS1-Circle B-TUR1A-008	Tur-1	34.76	0.66	33.98	<d.l.	11.93	<d.l.	2.39	0.38	1.73	0.04	0.57	<d.l.	2.97	10.29	0.24	0.00	99.46
2020-KELL-23-TS1-Circle B-TUR1A-009	Tur-1	35.06	0.28	36.50	<d.l.	9.53	<d.l.	2.48	0.40	1.64	0.03	0.62	<d.l.	2.95	10.42	0.26	0.00	99.65
2020-KELL-23-TS1-Circle B-TUR1A-010	Tur-1	34.78	0.26	36.40	<d.l.	10.14	<d.l.	1.92	0.36	1.50	0.02	0.59	<d.l.	2.89	10.34	0.25	0.00	98.95
2020-KELL-23-TS1-Circle B-TUR1A-011	Tur-1	34.98	0.44	35.22	<d.l.	10.65	<d.l.	2.56	0.41	1.76	0.03	0.63	0.02	2.96	10.38	0.27	0.01	99.77
2020-KELL-23-TS1-Circle B-TUR1A-012	Tur-1	34.99	0.15	35.79	<d.l.	10.29	<d.l.	2.48	0.29	1.66	0.02	0.57	<d.l.	2.95	10.38	0.24	0.00	99.33
2020-KELL-23-TS1-Circle B-TUR1A-013	Tur-1	35.14	0.49	34.23	<d.l.	11.68	<d.l.	2.49	0.26	1.94	0.03	0.81	<d.l.	2.91	10.35	0.34	0.00	99.99
2020-KELL-23-TS1-Circle B-TUR1A-014	Tur-1	34.95	0.23	35.07	<d.l.	10.33	<d.l.	2.99	0.34	1.59	0.03	0.58	<d.l.	2.93	10.38	0.24	0.00	99.17
2020-KELL-23-TS1-Circle B-TUR1A-015	Tur-1	34.53	0.46	34.32	<d.l.	10.88	<d.l.	3.10	0.42	2.02	0.04	0.78	<d.l.	2.96	10.32	0.33	0.00	99.50
2020-KELL-23-TS1-Circle B-TUR1A-016	Tur-1	34.88	0.38	34.44	<d.l.	10.37	<d.l.	2.99	0.32	1.81	<d.l.	0.70	<d.l.	2.91	10.30	0.30	0.00	98.81

EMPA label	Type	SiO ₂	TiO ₂	Al ₂ O ₃	Cr ₂ O ₃	FeO	MnO	MgO	CaO	Na ₂ O	K ₂ O	F	Cl	H ₂ O*	B ₂ O ₃ *	O=F	O=Cl	Total
2020-KELL-23-TS1-Circle B-TUR1A-017	Tur-1	34.62	0.27	34.31	<d.l.	12.00	<d.l.	1.81	0.27	1.61	0.03	0.72	<d.l.	2.81	10.20	0.30	0.00	98.35
2020-KELL-23-TS1-Circle B-TUR1A-018	Tur-1	34.81	0.56	34.79	<d.l.	10.88	<d.l.	2.88	0.35	1.83	0.03	0.76	<d.l.	2.92	10.39	0.32	0.00	99.88
2020-KELL-23-TS1-Circle B-TUR1A-019	Tur-1	35.13	0.50	34.07	<d.l.	10.99	<d.l.	2.89	0.37	1.79	0.02	0.77	<d.l.	2.89	10.33	0.32	0.00	99.43
2020-KELL-23-TS1-Circle B-TUR1A-020	Tur-1	35.90	0.55	35.04	<d.l.	11.05	<d.l.	2.70	0.44	1.74	0.04	0.67	<d.l.	2.99	10.53	0.28	0.00	101.37
2020-KELL-23-TS1-Circle B-TUR1A-021	Tur-1	35.88	0.16	35.58	<d.l.	11.95	<d.l.	1.02	0.11	1.39	0.03	0.24	<d.l.	3.00	10.36	0.10	0.00	99.62
2020-KELL-23-TS1-Circle B-TUR1A-023	Tur-1	36.21	0.22	35.73	<d.l.	10.46	<d.l.	2.45	0.17	1.62	<d.l.	0.50	<d.l.	2.99	10.53	0.21	0.00	100.67
2020-KELL-23-TS1-Circle B-TUR1A-024	Tur-1	34.39	0.51	34.04	<d.l.	10.53	<d.l.	3.19	0.41	1.92	0.04	0.71	<d.l.	2.95	10.25	0.30	0.00	98.64
2020-KELL-23-TS1-Circle B-TUR1A-025	Tur-1	34.25	<d.l.	35.99	<d.l.	11.63	<d.l.	1.11	0.37	1.53	0.05	0.45	<d.l.	2.94	10.20	0.19	0.00	98.33
2020-KELL-23-TS1-Circle B-TUR1A-026	Tur-1	33.58	0.34	34.42	<d.l.	11.72	<d.l.	1.62	0.39	1.58	0.04	0.51	<d.l.	2.89	10.04	0.22	0.00	96.91
2020-KELL-23-TS1-Circle B-TUR1A-027	Tur-1	35.58	0.33	35.43	<d.l.	10.32	<d.l.	2.41	0.18	1.63	<d.l.	0.30	<d.l.	3.05	10.41	0.13	0.00	99.51
2020-KELL-23-TS1-Circle B-TUR1A-028	Tur-1	35.27	0.26	35.25	<d.l.	10.61	<d.l.	1.99	0.23	1.55	0.02	0.44	0.02	2.94	10.30	0.19	0.01	98.69
2020-KELL-23-TS1-Circle B-TUR1A-029	Tur-1	35.29	0.63	34.24	<d.l.	11.05	<d.l.	2.92	0.40	1.64	0.05	0.68	<d.l.	2.92	10.40	0.29	0.00	99.93
2020-KELL-23-TS1-Circle B-TUR1A-030	Tur-1	34.86	0.52	34.29	<d.l.	11.05	<d.l.	2.80	0.28	1.93	0.05	0.83	<d.l.	2.89	10.32	0.35	0.00	99.48
2020-KELL-23-TS1-Circle B-TUR1A-031	Tur-1	35.15	0.22	34.88	<d.l.	10.55	<d.l.	2.84	0.25	1.63	0.03	0.46	<d.l.	2.98	10.37	0.19	0.00	99.17
2020-KELL-23-TS1-Circle B-TUR1A-032	Tur-1	35.06	0.44	34.06	<d.l.	11.17	<d.l.	3.09	0.41	1.86	0.05	0.86	<d.l.	2.89	10.37	0.36	0.00	99.90
2020-KELL-23-TS1-Circle B-TUR1A-033	Tur-1	33.36	0.59	31.05	<d.l.	12.98	<d.l.	1.74	0.30	1.60	0.04	0.41	<d.l.	2.84	9.72	0.17	0.00	94.45
2020-KELL-24-TS1-Circle A-Tur1a-001	Tur-1	34.14	0.57	31.97	<d.l.	13.24	0.08	2.35	0.16	1.98	0.04	0.88	<d.l.	2.80	10.07	0.37	0.00	97.90
2020-KELL-24-TS1-Circle A-Tur1a-001	Tur-1	34.13	0.57	31.74	<d.l.	13.23	<d.l.	2.39	0.15	2.00	0.03	1.00	<d.l.	2.73	10.03	0.42	0.00	97.59
2020-KELL-24-TS1-Circle A-Tur1a-002	Tur-1	34.11	0.51	31.80	<d.l.	12.98	<d.l.	2.45	0.16	2.00	0.04	0.97	<d.l.	2.75	10.02	0.41	0.00	97.38
2020-KELL-24-TS1-Circle A-Tur1a-003	Tur-1	34.34	0.52	31.88	<d.l.	13.46	<d.l.	2.40	0.16	2.02	0.02	0.75	<d.l.	2.87	10.10	0.32	0.00	98.20
2020-KELL-24-TS1-Circle A-Tur1a-004	Tur-1	34.34	0.52	32.11	<d.l.	13.39	<d.l.	2.25	0.16	2.07	<d.l.	0.95	<d.l.	2.79	10.10	0.40	0.00	98.27
2020-KELL-24-TS1-Circle A-Tur2-core001	Tur-2	34.63	0.19	32.29	<d.l.	16.10	0.15	0.35	0.15	1.31	<d.l.	<d.l.	<d.l.	3.01	10.07	0.00	0.00	98.26
2020-KELL-24-TS1-Circle A-Tur2-core002	Tur-2	34.44	0.22	32.14	<d.l.	16.50	0.16	0.33	0.14	1.32	<d.l.	<d.l.	<d.l.	3.01	10.07	0.00	0.00	98.33
2020-KELL-24-TS1-Circle A-Tur2-core003	Tur-2	34.91	<d.l.	31.81	<d.l.	15.91	0.14	0.43	0.07	1.45	<d.l.	<d.l.	<d.l.	3.03	10.02	0.00	0.00	97.76
2020-KELL-24-TS1-Circle A-Tur2-core004	Tur-2	34.23	0.40	31.35	<d.l.	16.41	<d.l.	0.55	0.15	1.52	0.02	<d.l.	<d.l.	3.05	9.97	0.00	0.00	97.65
2020-KELL-24-TS1-Circle A-Tur2-rim001	Tur-2	34.46	0.18	30.51	<d.l.	15.05	<d.l.	2.21	0.22	1.73	0.03	0.36	<d.l.	2.97	10.02	0.15	0.00	97.58
2020-KELL-24-TS1-Circle A-Tur2-rim002	Tur-2	34.40	0.22	31.31	<d.l.	15.22	<d.l.	1.79	0.23	1.78	0.08	0.29	<d.l.	3.04	10.07	0.12	0.00	98.30
2020-KELL-24-TS1-Circle A-Tur2-001	Tur-2	34.57	<d.l.	29.91	<d.l.	16.25	<d.l.	2.10	0.26	2.18	0.04	0.27	<d.l.	3.15	10.03	0.11	0.00	98.65
2020-KELL-24-TS1-Circle A-Tur2-002	Tur-2	34.71	<d.l.	29.78	<d.l.	15.76	<d.l.	2.44	0.27	2.43	0.05	0.34	<d.l.	3.20	10.04	0.14	0.00	98.87
2020-KELL-24-TS1-Circle A-Tur2-003	Tur-2	34.43	<d.l.	30.14	<d.l.	15.02	<d.l.	2.41	0.29	2.26	0.03	0.26	<d.l.	3.17	9.98	0.11	0.00	97.88
2020-KELL-24-TS1-Circle A-Tur2-004	Tur-2	35.88	<d.l.	34.11	<d.l.	8.30	0.29	4.00	0.21	1.05	<d.l.	0.25	<d.l.	2.90	10.34	0.11	0.00	97.22
2020-KELL-24-TS1-Circle A-Tur2-005	Tur-2	35.14	<d.l.	31.87	<d.l.	12.60	<d.l.	2.66	0.09	1.74	<d.l.	<d.l.	<d.l.	3.14	10.10	0.00	0.00	97.34
2020-KELL-24-TS1-Circle A-Tur2-006	Tur-2	34.55	0.33	30.63	<d.l.	14.73	<d.l.	2.21	0.23	1.97	0.02	0.25	<d.l.	3.09	10.02	0.11	0.00	97.93
2020-KELL-24-TS1-Circle A-Tur2-007	Tur-2	34.54	<d.l.	29.58	<d.l.	15.86	0.09	2.09	0.26	2.06	0.03	0.38	<d.l.	3.04	9.95	0.16	0.00	97.72
2020-KELL-24-TS1-Circle B-Tur1a-001	Tur-1	33.89	0.59	32.90	<d.l.	12.55	<d.l.	2.57	0.21	1.89	0.05	0.65	<d.l.	2.91	10.13	0.27	0.00	98.06
2020-KELL-24-TS1-Circle B-Tur1a-002	Tur-1	34.26	0.65	32.86	<d.l.	12.17	0.10	2.63	0.16	1.84	0.02	0.59	<d.l.	2.91	10.16	0.25	0.00	98.10
2020-KELL-24-TS1-Circle B-Tur2-001	Tur-2	34.74	0.19	30.90	<d.l.	15.23	<d.l.	1.91	0.13	1.74	<d.l.	0.43	<d.l.	2.93	10.07	0.18	0.00	98.09
2020-KELL-24-TS1-Circle B-Tur2-002	Tur-2	35.01	<d.l.	31.99	<d.l.	15.09	<d.l.	1.35	<d.l.	1.19	0.02	0.15	<d.l.	2.90	10.12	0.06	0.00	97.76
2020-KELL-24-TS1-Circle B-Tur2-003	Tur-2	34.75	0.29	30.38	<d.l.	11.66	<d.l.	4.31	0.19	2.18	<d.l.	0.83	<d.l.	2.88	10.08	0.35	0.00	97.19

EMPA label	Type	SiO ₂	TiO ₂	Al ₂ O ₃	Cr ₂ O ₃	FeO	MnO	MgO	CaO	Na ₂ O	K ₂ O	F	Cl	H ₂ O*	B ₂ O ₃ *	O=F	O=Cl	Total
2020-KELL-24-TS1-Circle B-Tur2-004	Tur-2	34.37	0.45	31.32	<d.l.	13.79	<d.l.	2.26	0.08	2.04	0.04	0.80	<d.l.	2.83	10.03	0.34	0.00	97.67
2020-KELL-24-TS1-Circle B-Tur2-005	Tur-2	34.76	0.18	31.71	<d.l.	15.02	<d.l.	1.58	0.19	1.49	<d.l.	0.31	<d.l.	2.93	10.10	0.13	0.00	98.14
2020-KELL-24-TS1-Circle B-Tur2-006	Tur-2	34.45	<d.l.	30.33	<d.l.	14.82	<d.l.	2.31	0.14	1.78	0.03	0.32	<d.l.	2.97	9.97	0.14	0.00	96.99
2020-KELL-24-TS1-Circle B-Tur2-007	Tur-2	34.63	<d.l.	31.38	<d.l.	13.99	<d.l.	2.37	0.20	1.85	<d.l.	0.26	<d.l.	3.05	10.06	0.11	0.00	97.68
2020-KELL-24-TS1-Circle C-Tur2-001	Tur-2	34.06	0.22	29.58	<d.l.	15.71	<d.l.	2.22	0.23	2.29	0.03	0.36	<d.l.	3.10	9.91	0.15	0.00	97.56
2020-KELL-24-TS1-Circle C-Tur2-002	Tur-2	34.54	<d.l.	31.11	<d.l.	13.66	<d.l.	2.40	0.32	2.10	0.03	0.16	<d.l.	3.18	9.99	0.07	0.00	97.42
2020-KELL-24-TS1-Circle C-Tur2-003	Tur-2	33.57	0.41	27.81	<d.l.	18.67	<d.l.	1.65	0.24	2.49	0.06	0.39	<d.l.	3.14	9.82	0.16	0.00	98.08
2020-KELL-24-TS1-Circle C-Tur2-004	Tur-2	34.72	<d.l.	31.06	<d.l.	14.28	<d.l.	2.55	0.24	2.13	0.03	0.16	<d.l.	3.20	10.09	0.07	0.00	98.39
2020-KELL-24-TS1-Circle C-Tur2-005	Tur-2	34.38	0.47	29.12	<d.l.	15.64	<d.l.	2.28	0.22	2.42	0.04	0.43	<d.l.	3.11	9.91	0.18	0.00	97.84
2020-KELL-24-TS1-Circle C-Tur2-006	Tur-2	34.81	0.18	31.67	<d.l.	12.89	<d.l.	2.76	0.19	2.12	0.02	0.26	<d.l.	3.14	10.10	0.11	0.00	98.03
2020-KELL-24-TS1-Circle C-Tur2-007	Tur-2	34.55	<d.l.	30.86	<d.l.	14.59	<d.l.	2.40	0.26	2.13	<d.l.	0.17	<d.l.	3.18	10.05	0.07	0.00	98.11
2020-KELL-24-TS1-Circle C-Tur2-008	Tur-2	34.20	0.22	29.62	<d.l.	16.26	<d.l.	2.01	0.16	2.43	0.05	0.31	<d.l.	3.17	9.95	0.13	0.00	98.25
2020-KELL-24-TS1-Circle D-Tur1a-001	Tur-1	33.80	0.44	30.80	<d.l.	15.25	<d.l.	1.59	0.10	1.93	0.03	0.49	0.02	2.91	9.91	0.21	0.01	97.06
2020-KELL-24-TS1-Circle D-Tur1a-002	Tur-1	33.92	0.59	31.36	<d.l.	15.36	<d.l.	1.49	0.13	1.85	0.03	0.76	<d.l.	2.79	10.01	0.32	0.00	97.97
2020-KELL-24-TS1-Circle D-Tur1a-003	Tur-1	34.38	0.58	31.07	<d.l.	15.10	<d.l.	1.62	0.12	2.00	<d.l.	0.59	<d.l.	2.91	10.02	0.25	0.00	98.15
2020-KELL-24-TS1-Circle E-Tur1a-004	Tur-1	32.69	0.54	33.15	<d.l.	15.00	<d.l.	1.13	0.66	1.53	0.04	0.88	<d.l.	2.73	10.01	0.37	0.00	97.99
2020-KELL-24-TS1-Circle E-Tur1a-005	Tur-1	32.97	0.47	33.02	<d.l.	14.89	<d.l.	1.46	0.69	1.51	0.03	0.82	<d.l.	2.77	10.07	0.35	0.00	98.35
2020-KELL-24-TS1-Circle E-Tur1a-006	Tur-1	32.66	0.56	32.89	<d.l.	15.16	<d.l.	1.17	0.74	1.64	0.06	0.76	<d.l.	2.83	10.00	0.32	0.00	98.15
2020-KELL-24-TS1-Circle E-Tur1a-007	Tur-1	34.54	0.56	32.76	<d.l.	10.43	<d.l.	4.24	0.59	1.55	0.02	0.72	<d.l.	2.87	10.27	0.30	0.00	98.24
2020-KELL-24-TS1-Circle F-Tur1a-001	Tur-1	33.39	0.25	33.09	<d.l.	15.50	<d.l.	0.75	0.40	1.58	0.03	0.75	<d.l.	2.77	10.04	0.32	0.00	98.24
2020-KELL-24-TS1-Circle F-Tur1a-002	Tur-1	33.90	0.50	32.12	<d.l.	11.23	<d.l.	3.59	0.52	1.59	0.04	0.91	<d.l.	2.73	10.07	0.38	0.00	96.81
2020-KELL-24-TS1-Circle F-Tur2-001	Tur-2	34.90	0.24	31.05	<d.l.	14.06	<d.l.	2.64	0.13	1.97	0.04	0.44	<d.l.	3.01	10.12	0.19	0.00	98.42
2020-KELL-24-TS1-Circle F-Tur2-002	Tur-2	34.90	0.19	32.12	<d.l.	14.77	<d.l.	1.36	0.06	1.31	<d.l.	0.21	<d.l.	2.91	10.11	0.09	0.00	97.85
2020-KELL-24-TS1-Circle G-Tur2-001	Tur-2	34.90	0.23	31.05	<d.l.	12.84	0.08	3.18	0.14	2.23	0.04	0.43	<d.l.	3.09	10.11	0.18	0.00	98.13
2020-KELL-24-TS1-Circle G-Tur2-002	Tur-2	34.30	0.46	30.36	<d.l.	15.29	0.11	2.05	0.55	1.79	0.03	0.31	<d.l.	3.06	10.01	0.13	0.00	98.18
2020-KELL-24-TS1-Circle G-Tur2-003	Tur-2	34.31	0.17	32.31	<d.l.	14.74	<d.l.	1.29	0.17	1.20	<d.l.	0.22	<d.l.	2.88	10.05	0.09	0.00	97.25
2020-KELL-24-TS1-Circle H-Tur1a-001	Tur-1	33.61	0.39	32.92	<d.l.	12.65	<d.l.	1.85	0.13	1.92	0.05	0.78	<d.l.	2.80	9.97	0.33	0.00	96.74
2020-KELL-24-TS1-Circle H-Tur2-001	Tur-2	33.92	0.41	29.70	<d.l.	15.63	<d.l.	2.20	0.24	2.08	0.03	0.37	<d.l.	3.04	9.92	0.16	0.00	97.38
2020-KELL-24-TS1-Circle H-Tur2-002	Tur-2	34.55	<d.l.	30.94	<d.l.	14.71	<d.l.	2.25	0.23	2.06	0.05	<d.l.	<d.l.	3.24	10.04	0.00	0.00	98.08
2020-KELL-24-TS1-Circle H-Tur2-003	Tur-2	34.44	<d.l.	31.65	<d.l.	14.18	<d.l.	1.96	0.21	1.69	<d.l.	0.40	<d.l.	2.93	10.03	0.17	0.00	97.32
2020-KELL-24-TS1-Circle I-Tur1a-001	Tur-1	33.14	0.41	33.80	<d.l.	13.09	0.11	1.64	0.14	1.96	0.03	0.61	<d.l.	2.91	10.05	0.26	0.00	97.64
2020-KELL-24-TS1-Circle I-Tur1a-002	Tur-1	35.36	0.19	32.44	<d.l.	14.88	<d.l.	0.96	0.15	1.04	0.14	0.18	<d.l.	2.90	10.15	0.08	0.00	98.31
2020-KELL-24-TS1-Circle I-Tur1a-003	Tur-1	33.29	0.57	33.67	<d.l.	13.19	0.10	1.58	0.17	1.98	0.04	0.61	<d.l.	2.93	10.07	0.26	0.00	97.94
2020-KELL-24-TS1-Circle I-Tur1a-004	Tur-1	34.41	0.22	33.70	<d.l.	12.88	0.11	1.52	0.10	1.77	0.04	0.45	<d.l.	2.95	10.13	0.19	0.00	98.09
2020-KELL-24-TS1-Circle I-Tur2-001	Tur-2	34.30	<d.l.	30.56	<d.l.	13.91	<d.l.	2.35	0.22	2.16	0.02	0.22	<d.l.	3.13	9.90	0.09	0.00	96.67
2020-KELL-24-TS1-Circle I-Tur2-002	Tur-2	35.17	0.22	32.17	<d.l.	14.46	<d.l.	1.54	0.17	1.47	<d.l.	0.24	<d.l.	2.97	10.15	0.10	0.00	98.46
2020-KELL-24-TS1-Circle J-Tur2-001	Tur-2	34.73	<d.l.	31.74	<d.l.	14.99	<d.l.	1.33	0.11	1.33	0.02	0.19	<d.l.	2.92	10.04	0.08	0.00	97.32
2020-KELL-24-TS1-Circle J-Tur2-002	Tur-2	35.47	0.20	31.79	<d.l.	10.03	0.17	4.21	0.24	2.12	0.04	0.31	<d.l.	3.15	10.18	0.13	0.00	97.78
2020-KELL-24-TS1-Circle J-Tur2-003	Tur-2	34.15	<d.l.	31.37	<d.l.	15.51	<d.l.	1.07	0.12	1.44	<d.l.	<d.l.	<d.l.	3.01	9.93	0.00	0.00	96.60

EMPA label	Type	SiO ₂	TiO ₂	Al ₂ O ₃	Cr ₂ O ₃	FeO	MnO	MgO	CaO	Na ₂ O	K ₂ O	F	Cl	H ₂ O*	B ₂ O ₃ *	O=F	O=Cl	Total
2020-KELL-24-TS1-Circle J-Tur2-004	Tur-2	34.29	0.19	30.74	<d.l.	15.03	<d.l.	2.00	0.19	1.61	0.02	0.21	<d.l.	2.99	9.99	0.09	0.00	97.17
2020-KELL-24-TS1-Circle K-Tur2-001	Tur-2	34.50	0.22	31.12	<d.l.	15.25	<d.l.	2.34	0.22	1.87	0.04	0.45	<d.l.	3.01	10.15	0.19	0.00	98.97
2020-KELL-24-TS1-Circle K-Tur2-002	Tur-2	34.56	0.25	30.02	<d.l.	15.56	<d.l.	2.35	0.24	2.20	0.03	0.36	<d.l.	3.11	10.04	0.15	0.00	98.57
2020-KELL-24-TS1-Circle K-Tur2-003	Tur-2	34.73	<d.l.	32.27	<d.l.	14.31	<d.l.	1.87	0.20	1.53	0.04	0.20	<d.l.	3.01	10.14	0.08	0.00	98.22
2020-KELL-24-TS1-Circle K-Tur2-004	Tur-2	34.69	<d.l.	30.44	<d.l.	15.69	<d.l.	1.99	0.18	2.12	<d.l.	0.32	<d.l.	3.09	10.04	0.14	0.00	98.43
2020-KELL-24-TS1-Circle L-Tur2-001	Tur-2	34.73	<d.l.	31.52	<d.l.	14.36	<d.l.	2.32	0.22	2.20	0.03	0.15	<d.l.	3.23	10.12	0.06	0.00	98.82
2020-KELL-24-TS1-Circle L-Tur2-002	Tur-2	35.41	<d.l.	31.39	<d.l.	12.12	<d.l.	3.35	0.16	2.52	0.04	0.32	<d.l.	3.24	10.14	0.14	0.00	98.56
2020-KELL-24-TS1-Circle L-Tur2-003	Tur-2	34.76	0.16	30.10	<d.l.	14.17	<d.l.	2.91	0.19	2.54	0.03	0.35	<d.l.	3.20	10.03	0.15	0.00	98.29
2020-KELL-24-TS1-Circle L-Tur2-004	Tur-2	34.76	0.18	31.13	<d.l.	14.06	<d.l.	2.54	0.20	2.13	<d.l.	0.26	<d.l.	3.14	10.10	0.11	0.00	98.39
2020-KELL-24-TS1-Circle L-Tur2-005	Tur-2	34.75	0.26	31.41	<d.l.	13.83	<d.l.	2.38	0.18	2.30	0.06	0.29	<d.l.	3.18	10.09	0.12	0.00	98.61
2020-KELL-24-TS1-Circle L-Tur2-006	Tur-2	34.53	<d.l.	31.68	<d.l.	14.86	<d.l.	1.62	0.14	1.51	0.02	0.29	<d.l.	2.93	10.05	0.12	0.00	97.50
2020-KELL-24-TS4-Circle A-Tur2-001	Tur-2	34.14	0.16	30.61	<d.l.	14.19	<d.l.	2.51	0.28	1.93	0.03	0.24	<d.l.	3.08	9.96	0.10	0.00	97.02
2020-KELL-24-TS4-Circle A-Tur2-002	Tur-2	34.28	0.37	29.46	<d.l.	15.21	<d.l.	2.54	0.22	2.13	0.02	0.43	<d.l.	3.03	9.94	0.18	0.00	97.45
2020-KELL-24-TS4-Circle A-Tur2-003	Tur-2	32.86	<d.l.	29.02	<d.l.	18.88	<d.l.	1.54	0.33	1.93	0.04	0.35	<d.l.	3.04	9.87	0.15	0.00	97.70
2020-KELL-24-TS4-Circle A-Tur2-004	Tur-2	34.02	<d.l.	30.69	<d.l.	13.52	<d.l.	2.62	0.18	2.01	0.03	0.22	<d.l.	3.08	9.90	0.09	0.00	96.17
2020-KELL-24-TS4-Circle A-Tur2-005	Tur-2	34.07	<d.l.	29.68	<d.l.	16.23	0.09	1.85	0.31	2.11	0.05	0.38	<d.l.	3.06	9.90	0.16	0.00	97.57
2020-KELL-24-TS4-Circle A-Tur2-006	Tur-2	33.93	<d.l.	29.97	<d.l.	15.64	<d.l.	1.92	0.27	2.12	0.05	0.42	<d.l.	3.02	9.87	0.18	0.00	97.04
2020-KELL-24-TS4-Circle A-Tur2-007	Tur-2	33.93	0.27	30.14	<d.l.	14.12	<d.l.	2.69	0.35	1.95	0.04	0.43	<d.l.	2.99	9.90	0.18	0.00	96.63
2020-KELL-24-TS4-Circle A-Tur2-008	Tur-2	34.56	<d.l.	31.02	<d.l.	12.49	0.10	3.53	0.40	1.85	0.06	0.42	<d.l.	3.02	10.07	0.18	0.00	97.34
2020-KELL-24-TS4-Circle A-Tur2-009	Tur-2	34.46	<d.l.	30.78	<d.l.	14.26	<d.l.	2.34	0.31	1.92	0.05	0.33	<d.l.	3.04	9.98	0.14	0.00	97.34
2020-KELL-24-TS4-Circle A-Tur2-010	Tur-2	34.02	<d.l.	30.25	<d.l.	16.47	<d.l.	1.19	0.11	1.51	0.03	0.38	<d.l.	2.85	9.87	0.16	0.00	96.52
2020-KELL-24-TS4-Circle B-Tur2-001	Tur-2	33.98	<d.l.	29.76	<d.l.	16.53	<d.l.	1.36	0.14	2.22	0.02	0.39	<d.l.	3.03	9.84	0.16	0.00	97.11
2020-KELL-24-TS4-Circle B-Tur2-002	Tur-2	33.58	<d.l.	29.79	<d.l.	16.34	<d.l.	1.22	0.23	1.80	0.03	0.29	<d.l.	2.96	9.75	0.12	0.00	95.87
2020-KELL-24-TS4-Circle B-Tur2-003	Tur-2	34.31	<d.l.	29.71	<d.l.	13.91	<d.l.	2.86	0.20	1.97	0.03	0.37	<d.l.	2.99	9.87	0.16	0.00	96.07
2020-KELL-24-TS4-Circle B-Tur2-004	Tur-2	34.29	<d.l.	29.90	<d.l.	16.56	<d.l.	1.39	0.16	2.18	0.03	0.35	<d.l.	3.06	9.90	0.15	0.00	97.68
2020-KELL-24-TS4-Circle B-Tur2-005	Tur-2	34.93	0.17	31.83	<d.l.	12.61	<d.l.	2.52	0.53	1.31	0.06	<d.l.	<d.l.	3.08	10.07	0.00	0.00	97.11
2020-KELL-24-TS4-Circle C-Tur2-001	Tur-2	34.82	0.20	30.61	<d.l.	12.24	<d.l.	3.65	0.20	2.20	0.02	0.53	<d.l.	3.02	10.05	0.22	0.00	97.32
2020-KELL-24-TS4-Circle C-Tur2-002	Tur-2	34.35	0.31	29.35	<d.l.	15.94	0.11	2.13	0.32	2.27	0.04	0.30	<d.l.	3.15	9.94	0.13	0.00	98.08
2020-KELL-24-TS4-Circle C-Tur2-003	Tur-2	34.57	<d.l.	30.57	<d.l.	15.06	<d.l.	1.87	0.28	2.04	0.04	0.43	<d.l.	3.02	9.96	0.18	0.00	97.66
2020-KELL-24-TS4-Circle C-Tur2-004	Tur-2	33.76	0.16	29.46	<d.l.	15.74	<d.l.	2.23	0.34	2.15	0.07	0.43	<d.l.	3.04	9.86	0.18	0.00	97.06
2020-KELL-24-TS4-Circle C-Tur2-005	Tur-2	33.55	0.27	28.23	<d.l.	18.57	<d.l.	1.15	0.22	2.26	0.05	0.40	<d.l.	3.05	9.76	0.17	0.00	97.34
2020-KELL-24-TS4-Circle D-Tur2-001	Tur-2	34.85	<d.l.	29.60	<d.l.	15.07	<d.l.	2.59	0.16	1.97	0.03	0.40	0.02	2.99	9.99	0.17	0.01	97.50
2020-KELL-24-TS4-Circle D-Tur2-002	Tur-2	34.41	0.26	29.93	<d.l.	13.02	<d.l.	3.63	0.39	2.12	0.04	0.43	<d.l.	3.07	9.99	0.18	0.00	97.10
2020-KELL-24-TS4-Circle D-Tur2-003	Tur-2	34.92	0.20	31.19	<d.l.	11.89	<d.l.	3.37	0.19	2.13	0.04	0.50	<d.l.	3.02	10.06	0.21	0.00	97.30
2020-KELL-24-TS4-Circle D-Tur2-004	Tur-2	34.03	<d.l.	30.05	<d.l.	15.31	<d.l.	2.04	0.30	2.03	<d.l.	0.31	<d.l.	3.05	9.88	0.13	0.00	96.87
2020-KELL-24-TS4-Circle D-Tur2-005	Tur-2	34.97	0.18	30.77	<d.l.	11.93	0.13	3.44	0.16	2.23	0.09	0.26	<d.l.	3.16	10.03	0.11	0.00	97.25
2020-KELL-24-TS4-Circle D-Tur2-006	Tur-2	34.64	<d.l.	31.60	<d.l.	13.87	<d.l.	2.49	0.36	1.80	<d.l.	0.31	<d.l.	3.05	10.10	0.13	0.00	98.09
2020-KELL-24-TS4-Circle E-Tur1a-001	Tur-1	33.57	0.37	33.16	<d.l.	12.21	<d.l.	2.14	0.15	1.86	0.03	0.60	<d.l.	2.87	10.00	0.25	0.00	96.72
2020-KELL-24-TS4-Circle E-Tur1a-002	Tur-1	33.16	0.32	32.97	<d.l.	12.50	<d.l.	2.16	0.16	1.97	0.06	0.72	<d.l.	2.85	9.96	0.30	0.00	96.52

EMPA label	Type	SiO ₂	TiO ₂	Al ₂ O ₃	Cr ₂ O ₃	FeO	MnO	MgO	CaO	Na ₂ O	K ₂ O	F	Cl	H ₂ O*	B ₂ O ₃ *	O=F	O=Cl	Total
2020-KELL-24-TS4-Circle E-Tur1a-003	Tur-1	33.76	0.34	33.28	<d.l.	12.14	<d.l.	2.23	0.15	1.82	0.04	0.68	<d.l.	2.84	10.05	0.29	0.00	97.04
2020-KELL-24-TS4-Circle E-Tur1a-004	Tur-1	33.32	0.39	32.80	<d.l.	12.49	<d.l.	2.23	0.16	1.96	0.05	0.73	<d.l.	2.84	9.97	0.31	0.00	96.63
2020-KELL-24-TS4-Circle E-Tur2-001	Tur-2	34.51	<d.l.	30.70	<d.l.	13.39	<d.l.	3.03	0.27	1.97	0.03	0.52	<d.l.	2.97	10.01	0.22	0.00	97.18
2020-KELL-24-TS4-Circle E-Tur2-002	Tur-2	34.41	0.18	30.92	<d.l.	14.54	<d.l.	1.88	0.25	1.49	<d.l.	0.55	<d.l.	2.79	9.96	0.23	0.00	96.74
2020-KELL-24-TS4-Circle E-Tur2-003	Tur-2	34.39	<d.l.	31.77	<d.l.	15.65	<d.l.	0.83	0.10	1.31	0.03	0.18	<d.l.	2.90	9.98	0.08	0.00	97.07
2020-KELL-24-TS4-Circle E-Tur2-004	Tur-2	34.85	<d.l.	31.47	<d.l.	10.96	0.14	3.75	0.31	1.74	0.05	0.27	<d.l.	3.04	10.06	0.11	0.00	96.53
2020-KELL-24-TS4-Circle E-Tur2-005	Tur-2	34.25	<d.l.	31.07	<d.l.	15.13	<d.l.	1.84	0.32	1.72	<d.l.	0.35	<d.l.	2.97	10.00	0.15	0.00	97.50
2020-KELL-24-TS4-Circle E-Tur2-006	Tur-2	34.48	<d.l.	31.16	<d.l.	13.51	<d.l.	2.74	0.31	2.11	0.02	0.38	<d.l.	3.08	10.03	0.16	0.00	97.67
2020-KELL-24-TS4-Circle E-Tur2-007	Tur-2	34.00	0.23	29.14	<d.l.	15.46	<d.l.	2.81	0.29	2.43	0.04	0.45	<d.l.	3.12	9.92	0.19	0.00	97.70
2020-KELL-24-TS4-Circle E-Tur2-008	Tur-2	34.16	<d.l.	29.79	<d.l.	16.94	<d.l.	1.53	0.31	2.05	0.07	0.44	<d.l.	3.02	9.93	0.19	0.00	98.06
2020-KELL-24-TS4-Circle F-Tur2-001	Tur-2	33.29	0.18	27.73	<d.l.	19.16	<d.l.	1.30	0.36	2.41	0.10	0.34	<d.l.	3.15	9.74	0.14	0.00	97.62
2020-KELL-24-TS4-Circle F-Tur2-002	Tur-2	33.91	<d.l.	30.65	<d.l.	14.68	<d.l.	2.31	0.37	1.97	0.04	0.30	<d.l.	3.07	9.94	0.13	0.00	97.11
2020-KELL-24-TS4-Circle F-Tur2-003	Tur-2	34.25	<d.l.	29.54	<d.l.	15.46	<d.l.	2.47	0.27	2.19	0.05	0.29	<d.l.	3.12	9.93	0.12	0.00	97.45
2020-KELL-24-TS4-Circle F-Tur2-004	Tur-2	34.58	0.17	31.80	<d.l.	12.75	<d.l.	2.78	0.33	2.02	0.03	0.28	<d.l.	3.12	10.08	0.12	0.00	97.82
2020-KELL-24-TS4-Circle G-Tur2-001	Tur-2	34.96	<d.l.	32.09	<d.l.	12.22	<d.l.	3.08	0.26	1.97	<d.l.	0.27	<d.l.	3.11	10.15	0.11	0.00	98.00
2020-KELL-24-TS4-Circle G-Tur2-002	Tur-2	34.19	0.27	30.21	<d.l.	14.58	<d.l.	2.80	0.22	2.07	0.03	0.47	<d.l.	3.01	10.01	0.20	0.00	97.66
2020-KELL-24-TS4-Circle G-Tur2-003	Tur-2	35.08	0.18	31.38	<d.l.	11.70	<d.l.	3.21	0.11	2.04	<d.l.	0.27	<d.l.	3.08	10.05	0.11	0.00	96.99
2020-KELL-24-TS4-Circle G-Tur2-004	Tur-2	34.37	<d.l.	31.01	<d.l.	13.93	<d.l.	2.53	0.18	1.96	0.02	0.41	<d.l.	3.00	10.00	0.17	0.00	97.24
2020-KELL-24-TS4-Circle G-Tur1a-001	Tur-1	33.84	0.58	32.53	<d.l.	11.92	<d.l.	2.73	0.23	1.94	<d.l.	0.78	<d.l.	2.83	10.04	0.33	0.00	97.09
2020-KELL-24-TS4-Circle G-Tur1a-002	Tur-1	34.23	0.56	32.30	<d.l.	12.25	<d.l.	2.72	0.21	1.94	0.05	0.60	<d.l.	2.93	10.08	0.25	0.00	97.62
2020-KELL-24-TS4-Circle H-Tur2-001	Tur-2	34.41	0.16	30.55	<d.l.	12.88	<d.l.	3.30	0.33	2.10	<d.l.	0.42	<d.l.	3.05	9.99	0.18	0.00	97.01
2020-KELL-24-TS4-Circle I-Tur1a-001	Tur-1	33.92	0.49	32.31	<d.l.	12.54	<d.l.	2.53	0.13	1.92	0.05	0.67	<d.l.	2.87	10.04	0.28	0.00	97.18
2020-KELL-24-TS4-Circle I-Tur1a-002	Tur-1	34.10	0.47	32.09	<d.l.	12.45	0.09	2.51	0.14	2.01	0.05	0.68	<d.l.	2.89	10.02	0.29	0.00	97.21
2020-KELL-24-TS4-Circle I-Tur1a-003	Tur-1	33.86	0.40	32.93	<d.l.	12.99	0.12	2.21	0.12	1.88	0.04	0.50	<d.l.	2.95	10.11	0.21	0.00	97.90
2020-KELL-24-TS4-Circle J-Tur2-001	Tur-2	34.99	0.35	31.19	<d.l.	15.10	<d.l.	1.68	0.16	1.39	<d.l.	0.55	<d.l.	2.78	10.10	0.23	0.00	98.06
2020-KELL-24-TS4-Circle J-Tur2-002	Tur-2	35.03	<d.l.	32.36	<d.l.	12.14	<d.l.	2.71	0.20	1.79	<d.l.	<d.l.	<d.l.	3.17	10.12	0.00	0.00	97.52
2020-KELL-24-TS4-Circle J-Tur2-003	Tur-2	34.67	<d.l.	31.13	<d.l.	15.22	<d.l.	1.55	0.10	1.27	<d.l.	0.32	<d.l.	2.82	10.01	0.14	0.00	96.96
2020-KELL-24-TS4-Circle K-Tur1a-001	Tur-1	34.08	0.36	29.27	<d.l.	17.66	0.43	1.12	0.17	1.91	0.09	0.48	<d.l.	2.95	9.92	0.20	0.00	98.24
2020-KELL-24-TS4-Circle K-Tur1a-002	Tur-1	34.50	0.46	29.51	<d.l.	17.35	0.23	1.03	0.13	1.61	0.11	0.69	<d.l.	2.76	9.95	0.29	0.00	98.04
2020-KELL-24-TS4-Circle K-Tur1a-003	Tur-1	33.71	0.58	32.80	<d.l.	12.81	<d.l.	2.43	0.17	2.04	0.05	0.97	<d.l.	2.78	10.10	0.41	0.00	98.03
2020-KELL-24-TS4-Circle K-Tur1a-004	Tur-1	34.07	0.52	32.97	<d.l.	12.68	0.11	2.18	0.16	1.93	0.03	0.61	<d.l.	2.92	10.11	0.26	0.00	98.03
2020-KELL-24-TS4-Circle K-Tur1a-005	Tur-1	33.76	0.63	32.75	<d.l.	13.17	<d.l.	2.09	0.16	1.99	0.04	0.57	<d.l.	2.95	10.08	0.24	0.00	97.95
2020-KELL-24-TS4-Circle K-Tur2-001	Tur-2	35.50	<d.l.	33.11	<d.l.	13.91	0.93	0.72	0.09	0.99	0.02	<d.l.	<d.l.	2.95	10.20	0.00	0.00	98.41
2020-KELL-24-TS4-Circle K-Tur2-002	Tur-2	34.19	0.16	31.71	<d.l.	15.02	1.17	0.62	0.15	1.35	0.02	0.47	<d.l.	2.78	9.98	0.20	0.00	97.43
2020-KELL-24-TS4-Circle K-Tur2-003	Tur-2	34.74	<d.l.	33.09	<d.l.	12.66	1.91	0.76	0.16	0.87	0.02	0.17	<d.l.	2.81	10.09	0.07	0.00	97.21
2020-KELL-25-TS3-Circle A-Tur2-001	Tur-2	35.23	<d.l.	31.18	<d.l.	16.29	<d.l.	2.22	0.21	1.97	0.03	0.70	<d.l.	2.96	10.30	0.30	0.00	100.79
2020-KELL-25-TS3-Circle A-Tur2-002	Tur-2	35.37	0.24	30.25	<d.l.	15.86	<d.l.	2.65	0.23	2.39	0.05	0.41	<d.l.	3.20	10.25	0.17	0.00	100.72
2020-KELL-25-TS3-Circle A-Tur2-003	Tur-2	35.13	0.33	31.05	<d.l.	14.53	<d.l.	3.11	0.29	2.27	0.04	0.46	<d.l.	3.16	10.28	0.19	0.00	100.46
2020-KELL-25-TS3-Circle B-Tur2-001	Tur-2	36.07	0.18	32.85	<d.l.	11.39	<d.l.	3.90	0.16	2.33	0.03	0.40	<d.l.	3.23	10.46	0.17	0.00	100.83

EMPA label	Type	SiO ₂	TiO ₂	Al ₂ O ₃	Cr ₂ O ₃	FeO	MnO	MgO	CaO	Na ₂ O	K ₂ O	F	Cl	H ₂ O*	B ₂ O ₃ *	O=F	O=Cl	Total
2020-KELL-25-TS3-Circle B-Tur2-002	Tur-2	35.79	<d.l.	32.57	<d.l.	14.99	<d.l.	2.42	0.30	1.75	0.02	0.36	<d.l.	3.10	10.47	0.15	0.00	101.62
2020-KELL-25-TS3-Circle B-Tur2-003	Tur-2	34.93	0.35	30.02	<d.l.	15.54	<d.l.	2.97	0.26	2.15	0.04	0.69	<d.l.	2.99	10.20	0.29	0.00	99.85
2020-KELL-25-TS3-Circle C-Tur2-001	Tur-2	35.30	0.17	31.74	<d.l.	16.23	<d.l.	1.80	0.10	1.83	0.02	0.31	<d.l.	3.08	10.32	0.13	0.00	100.78
2020-KELL-25-TS3-Circle D-Tur2-001	Tur-2	35.76	0.29	31.63	<d.l.	13.28	<d.l.	3.58	0.35	2.26	0.03	0.28	<d.l.	3.28	10.39	0.12	0.00	101.01
2020-KELL-25-TS3-Circle D-Tur2-002	Tur-2	35.88	0.19	32.19	<d.l.	16.13	<d.l.	0.87	0.23	1.43	0.03	0.20	<d.l.	3.02	10.28	0.08	0.00	100.37
2020-KELL-25-TS3-Circle D-Tur2-003	Tur-2	35.60	0.22	32.92	<d.l.	16.71	<d.l.	0.95	0.16	1.40	0.02	<d.l.	<d.l.	3.14	10.42	0.00	0.00	101.54
2020-KELL-25-TS3-Circle E-Tur2-001	Tur-2	36.15	<d.l.	32.65	<d.l.	13.92	<d.l.	2.20	0.21	1.51	0.03	0.15	<d.l.	3.09	10.38	0.06	0.00	100.23
2020-KELL-25-TS3-Circle E-Tur2-002	Tur-2	34.74	0.16	28.96	<d.l.	18.99	<d.l.	2.08	0.16	2.44	0.07	0.45	<d.l.	3.19	10.19	0.19	0.00	101.25
2020-KELL-25-TS3-Circle F-Tur2-001	Tur-2	35.17	0.55	29.36	<d.l.	16.97	<d.l.	2.76	0.30	2.41	0.04	0.41	<d.l.	3.22	10.25	0.17	0.00	101.27
2020-KELL-25-TS3-Circle F-Tur2-002	Tur-2	35.28	0.32	29.50	<d.l.	17.48	<d.l.	2.20	0.24	2.32	0.05	0.59	<d.l.	3.09	10.22	0.25	0.00	101.04
2020-KELL-25-TS3-Circle F-Tur2-003	Tur-2	35.46	0.16	31.38	<d.l.	15.16	<d.l.	2.63	0.24	1.98	0.04	0.62	<d.l.	3.00	10.33	0.26	0.00	100.74
2020-KELL-25-TS3-Circle H-Tur2-001	Tur-2	35.20	0.15	31.78	<d.l.	14.55	<d.l.	2.80	0.23	1.93	0.04	0.42	<d.l.	3.08	10.33	0.18	0.00	100.33
2020-KELL-25-TS3-Circle H-Tur2-002	Tur-2	35.14	0.16	30.10	<d.l.	16.66	<d.l.	2.55	0.14	2.47	0.07	0.49	<d.l.	3.18	10.25	0.21	0.00	101.01
2020-KELL-25-TS3-Circle H-Tur2-003	Tur-2	35.39	0.16	30.20	<d.l.	17.59	<d.l.	2.27	0.16	2.51	0.06	0.38	<d.l.	3.27	10.34	0.16	0.00	102.17
2020-KELL-25-TS3-Circle J-Tur2-001	Tur-2	36.22	<d.l.	32.51	<d.l.	11.96	<d.l.	3.82	0.15	2.49	0.04	0.63	<d.l.	3.16	10.46	0.27	0.00	101.17
2020-KELL-25-TS3-Circle J-Tur2-002	Tur-2	35.66	0.64	30.51	<d.l.	13.94	<d.l.	3.37	0.15	2.05	0.02	0.74	<d.l.	2.94	10.29	0.31	0.00	99.99
2020-KELL-25-TS3-Circle J-Tur2-003	Tur-2	35.76	0.17	32.59	<d.l.	14.13	<d.l.	2.42	0.20	1.68	<d.l.	0.30	<d.l.	3.07	10.40	0.13	0.00	100.59
KELL-A-TS-Circle A-Tur3-001	Tur-3	35.29	0.36	27.33	<d.l.	15.85	<d.l.	5.13	1.35	1.82	0.02	0.70	0.02	3.09	10.27	0.30	0.01	100.94
KELL-A-TS-Circle A-Tur3-002	Tur-3	34.16	0.66	24.25	<d.l.	22.11	<d.l.	3.38	1.22	2.06	0.04	0.33	<d.l.	3.29	10.05	0.14	0.00	101.41
KELL-A-TS-Circle A-Tur3-003	Tur-3	34.01	0.98	23.55	<d.l.	21.21	<d.l.	3.98	1.71	1.90	0.03	0.61	<d.l.	2.30	9.99	0.26	0.00	100.01
KELL-A-TS-Circle A-Tur3-004	Tur-3	33.99	0.75	23.52	<d.l.	21.29	<d.l.	3.75	1.70	1.74	0.04	0.44	<d.l.	3.18	9.93	0.19	0.00	100.14
KELL-A-TS-Circle B-Tur3-001	Tur-3	35.82	<d.l.	32.14	<d.l.	16.59	<d.l.	1.16	0.14	1.66	0.02	<d.l.	<d.l.	3.19	10.35	0.00	0.00	101.06
KELL-A-TS-Circle B-Tur3-002	Tur-3	35.36	0.39	32.07	<d.l.	15.09	<d.l.	2.52	0.56	1.77	0.02	<d.l.	<d.l.	3.30	10.41	0.00	0.00	101.49
KELL-A-TS-Circle B-Tur3-003	Tur-3	35.56	<d.l.	33.11	<d.l.	15.14	<d.l.	1.55	0.24	1.47	<d.l.	<d.l.	<d.l.	3.15	10.38	0.00	0.00	100.60
KELL-A-TS-Circle B-Tur3-004	Tur-3	35.77	<d.l.	33.22	<d.l.	15.49	<d.l.	1.39	0.22	1.51	<d.l.	<d.l.	<d.l.	3.17	10.42	0.00	0.00	101.19
KELL-A-TS-Circle B-Tur3-005	Tur-3	35.50	0.15	33.15	<d.l.	14.65	<d.l.	2.14	0.49	1.65	<d.l.	<d.l.	<d.l.	3.26	10.44	0.00	0.00	101.43
KELL-A-TS-Circle C-Tur3-001	Tur-3	35.35	0.39	33.02	<d.l.	14.61	<d.l.	2.42	0.59	1.69	<d.l.	<d.l.	<d.l.	3.30	10.47	0.00	0.00	101.84
KELL-A-TS-Circle C-Tur3-002	Tur-3	35.21	0.33	33.14	<d.l.	14.39	<d.l.	2.26	0.54	1.59	0.03	0.19	<d.l.	3.16	10.42	0.08	0.00	101.18
KELL-A-TS-Circle C-Tur3-003	Tur-3	35.16	0.46	32.14	<d.l.	14.82	<d.l.	2.43	0.52	1.79	<d.l.	0.29	<d.l.	3.15	10.36	0.12	0.00	100.99
KELL-A-TS-Circle C-Tur3-004	Tur-3	35.79	0.17	31.51	<d.l.	12.28	<d.l.	4.30	0.81	1.68	<d.l.	0.30	<d.l.	3.17	10.40	0.13	0.00	100.28
KELL-A-TS-Circle C-Tur3-005	Tur-3	35.45	0.50	32.50	<d.l.	15.17	<d.l.	2.08	0.44	1.65	<d.l.	<d.l.	<d.l.	3.25	10.42	0.00	0.00	101.46
KELL-A-TS-Circle C-Tur3-006	Tur-3	35.58	<d.l.	32.86	<d.l.	15.56	<d.l.	1.65	0.28	1.52	<d.l.	<d.l.	<d.l.	3.18	10.40	0.00	0.00	101.03
KELL-A-TS-Circle D-Tur3-001	Tur-3	35.03	0.49	32.49	<d.l.	16.06	<d.l.	1.61	0.51	1.53	<d.l.	0.15	<d.l.	3.14	10.37	0.06	0.00	101.32
KELL-A-TS-Circle D-Tur3-002	Tur-3	35.64	<d.l.	33.03	<d.l.	15.32	<d.l.	1.50	0.22	1.59	<d.l.	<d.l.	<d.l.	3.18	10.38	0.00	0.00	100.87
KELL-A-TS-Circle D-Tur3-003	Tur-3	35.40	0.48	31.52	<d.l.	15.95	<d.l.	2.29	0.55	1.87	0.02	0.19	0.04	3.22	10.39	0.08	0.01	101.83
KELL-A-TS-Circle D-Tur3-004	Tur-3	35.54	0.20	33.19	<d.l.	14.67	<d.l.	2.04	0.45	1.53	<d.l.	<d.l.	<d.l.	3.22	10.44	0.00	0.00	101.28
KELL-A-TS-Circle E-Tur3-001	Tur-3	34.75	1.17	29.74	<d.l.	15.51	<d.l.	3.47	1.08	1.77	<d.l.	0.34	0.02	3.19	10.29	0.14	0.01	101.18
KELL-A-TS-Circle E-Tur3-002	Tur-3	35.10	0.72	30.96	<d.l.	16.14	<d.l.	2.18	0.81	1.75	<d.l.	0.41	<d.l.	3.11	10.30	0.17	0.00	101.31
KELL-A-TS-Circle E-Tur3-003	Tur-3	35.40	<d.l.	32.90	<d.l.	14.67	<d.l.	2.13	0.46	1.60	<d.l.	<d.l.	<d.l.	3.23	10.38	0.00	0.00	100.77

EMPA label	Type	SiO ₂	TiO ₂	Al ₂ O ₃	Cr ₂ O ₃	FeO	MnO	MgO	CaO	Na ₂ O	K ₂ O	F	Cl	H ₂ O*	B ₂ O ₃ *	O=F	O=Cl	Total
KELL-A-TS-Circle E-Tur3-004	Tur-3	35.33	<d.l.	30.15	<d.l.	14.38	<d.l.	3.91	0.44	1.95	<d.l.	0.39	<d.l.	3.12	10.28	0.16	0.00	99.79
KELL-A-TS-Circle E-Tur3-005	Tur-3	35.46	<d.l.	28.16	<d.l.	15.41	<d.l.	5.19	1.14	2.12	<d.l.	0.71	<d.l.	3.16	10.34	0.30	0.00	101.39
KELL-A-TS-Circle E-Tur3-006	Tur-3	35.74	<d.l.	31.31	<d.l.	12.19	<d.l.	4.59	0.78	1.82	<d.l.	0.39	<d.l.	3.16	10.39	0.16	0.00	100.21
KELL-A-TS-Circle E-Tur3-007	Tur-3	35.04	<d.l.	27.05	<d.l.	15.67	<d.l.	5.34	1.02	2.23	0.03	1.00	<d.l.	3.01	10.20	0.42	0.00	100.16
KELL-A-TS-Circle E-Tur3-008	Tur-3	35.35	<d.l.	29.88	<d.l.	15.48	<d.l.	3.82	0.19	2.25	<d.l.	0.21	<d.l.	3.28	10.34	0.09	0.00	100.71
KELL-A-TS-Circle E-Tur3-009	Tur-3	35.22	<d.l.	27.55	<d.l.	16.56	<d.l.	5.10	0.79	2.43	<d.l.	0.82	<d.l.	3.15	10.33	0.35	0.00	101.60
KELL-A-TS-Circle E-Tur3-010	Tur-3	35.65	<d.l.	33.08	<d.l.	14.48	<d.l.	1.93	0.23	1.46	<d.l.	<d.l.	<d.l.	3.15	10.38	0.00	0.00	100.36
KELL-A-TS-Circle F-Tur3-001	Tur-3	35.37	<d.l.	29.61	<d.l.	13.96	<d.l.	5.18	1.00	1.96	<d.l.	0.66	<d.l.	3.12	10.39	0.28	0.00	100.97
KELL-A-TS-Circle F-Tur3-002	Tur-3	34.97	0.84	32.00	<d.l.	14.75	<d.l.	2.75	0.73	1.44	<d.l.	0.33	<d.l.	3.07	10.40	0.14	0.00	101.14
KELL-A-TS-Circle F-Tur3-003	Tur-3	35.89	<d.l.	30.25	<d.l.	13.37	<d.l.	4.83	0.89	1.87	<d.l.	0.55	<d.l.	3.13	10.42	0.23	0.00	100.97
KELL-A-TS-Circle F-Tur3-004	Tur-3	35.43	<d.l.	27.56	<d.l.	16.14	<d.l.	5.44	1.45	1.83	<d.l.	0.58	<d.l.	3.20	10.37	0.24	0.00	101.76
KELL-A-TS-Circle F-Tur3-005	Tur-3	35.19	<d.l.	27.45	<d.l.	16.62	<d.l.	4.89	1.08	2.17	0.02	0.50	<d.l.	3.26	10.28	0.21	0.00	101.25
KELL-A-TS-Circle F-Tur3-006	Tur-3	35.57	<d.l.	28.49	<d.l.	15.29	<d.l.	5.04	0.83	2.37	<d.l.	0.63	<d.l.	3.22	10.36	0.27	0.00	101.54
KELL-A-TS-Circle F-Tur3-007	Tur-3	35.12	<d.l.	27.19	<d.l.	15.98	<d.l.	5.41	1.41	2.09	<d.l.	0.69	<d.l.	3.19	10.27	0.29	0.00	101.05
KELL-A-TS-Circle G-Tur3-001	Tur-3	34.82	<d.l.	27.66	<d.l.	17.30	<d.l.	4.16	1.41	1.86	<d.l.	0.44	<d.l.	3.22	10.21	0.19	0.00	100.89
KELL-A-TS-Circle G-Tur3-002	Tur-3	34.53	<d.l.	25.93	<d.l.	18.19	<d.l.	4.72	1.76	1.82	<d.l.	0.64	<d.l.	3.16	10.12	0.27	0.00	100.60
KELL-A-TS-Circle G-Tur3-003	Tur-3	34.82	<d.l.	25.89	<d.l.	18.01	<d.l.	5.10	1.75	1.85	0.02	0.65	<d.l.	3.18	10.20	0.27	0.00	101.20
KELL-A-TS-Circle G-Tur3-004	Tur-3	35.01	<d.l.	25.59	<d.l.	17.52	<d.l.	5.36	2.23	1.65	<d.l.	0.85	<d.l.	3.09	10.18	0.36	0.00	101.12
KELL-A-TS-Circle G-Tur3-005	Tur-3	34.81	<d.l.	25.79	<d.l.	19.41	<d.l.	4.20	1.29	2.09	0.03	0.59	<d.l.	3.20	10.16	0.25	0.00	101.33
KELL-A-TS-Circle G-Tur3-006	Tur-3	35.19	0.32	32.88	<d.l.	15.16	0.10	2.38	1.12	1.51	<d.l.	0.22	<d.l.	3.23	10.49	0.09	0.00	102.50
KELL-A-TS-Circle G-Tur3-007	Tur-3	35.32	<d.l.	28.25	<d.l.	18.50	<d.l.	2.95	0.61	2.16	0.02	<d.l.	<d.l.	3.40	10.25	0.00	0.00	101.47
KELL-A-TS-Circle G-Tur3-008	Tur-3	35.14	<d.l.	27.38	<d.l.	16.38	<d.l.	4.61	1.13	2.21	0.02	0.46	<d.l.	3.26	10.19	0.19	0.00	100.60
KELL-A-TS-Circle G-Tur3-009	Tur-3	35.43	<d.l.	28.29	<d.l.	14.56	<d.l.	5.46	1.23	2.01	<d.l.	0.50	<d.l.	3.23	10.32	0.21	0.00	100.82
KELL-A-TS-Circle G-Tur3-010	Tur-3	34.88	0.34	32.81	<d.l.	15.29	<d.l.	1.52	0.69	1.32	<d.l.	0.31	<d.l.	3.01	10.30	0.13	0.00	100.34
KELL-A-TS-Circle G-Tur3-011	Tur-3	34.93	<d.l.	28.34	<d.l.	18.40	<d.l.	2.83	0.60	2.20	<d.l.	<d.l.	<d.l.	3.39	10.19	0.00	0.00	100.88
KELL-A-TS-Circle G-Tur3-012	Tur-3	34.35	<d.l.	24.27	<d.l.	20.09	<d.l.	4.58	1.97	1.77	0.03	0.51	<d.l.	2.36	10.03	0.22	0.00	99.75
KELL-A-TS-Circle G-Tur3-013	Tur-3	35.91	<d.l.	34.56	<d.l.	12.96	0.10	1.87	0.43	1.13	<d.l.	<d.l.	<d.l.	3.11	10.47	0.00	0.00	100.54
KELL-A-TS-Circle H-Tur3-001	Tur-3	35.04	0.38	26.82	<d.l.	17.77	<d.l.	4.23	1.32	1.94	<d.l.	0.39	<d.l.	3.25	10.21	0.16	0.00	101.19
KELL-A-TS-Circle H-Tur3-002	Tur-3	34.67	0.29	27.62	<d.l.	16.34	<d.l.	4.42	0.92	2.08	0.02	0.38	<d.l.	3.23	10.16	0.16	0.00	99.97
KELL-A-TS-Circle H-Tur3-003	Tur-3	34.21	0.75	24.68	<d.l.	21.34	<d.l.	3.54	1.33	1.84	0.04	0.41	<d.l.	3.21	10.08	0.17	0.00	101.26
KELL-A-TS-Circle H-Tur3-004	Tur-3	34.38	0.80	24.36	<d.l.	20.38	<d.l.	4.33	1.93	1.74	0.03	0.53	<d.l.	3.22	10.10	0.22	0.00	101.58
KELL-A-TS-Circle H-Tur3-005	Tur-3	34.34	1.14	24.14	<d.l.	20.26	<d.l.	4.12	1.93	1.79	<d.l.	0.34	<d.l.	3.30	10.05	0.14	0.00	101.26
KELL-A-TS-Circle H-Tur3-006	Tur-3	34.16	1.21	23.60	<d.l.	21.66	<d.l.	4.01	1.69	1.82	0.03	0.38	0.02	3.27	10.08	0.16	0.01	101.76
KELL-A-TS-Circle H-Tur3-007	Tur-3	35.32	0.21	29.19	<d.l.	16.85	<d.l.	3.24	0.65	1.84	<d.l.	0.23	<d.l.	3.21	10.29	0.10	0.00	100.93
KELL-A-TS-Circle H-Tur3-008	Tur-3	34.32	0.93	24.16	<d.l.	19.33	<d.l.	4.37	1.82	1.83	0.02	0.47	<d.l.	3.21	9.99	0.20	0.00	100.25
KELL-A-TS-Circle I-Tur3-001	Tur-3	34.00	1.16	23.87	<d.l.	20.77	<d.l.	4.10	1.76	1.88	0.04	0.53	<d.l.	2.35	10.02	0.22	0.00	100.26
KELL-A-TS-Circle I-Tur3-002	Tur-3	34.82	0.28	27.68	<d.l.	16.54	<d.l.	4.49	0.67	2.31	<d.l.	0.63	<d.l.	3.15	10.22	0.27	0.00	100.52
KELL-A-TS-Circle I-Tur3-003	Tur-3	34.83	0.46	26.05	<d.l.	19.53	<d.l.	3.66	1.16	2.15	0.04	0.28	<d.l.	3.34	10.16	0.12	0.00	101.54
KELL-A-TS-Circle I-Tur3-004	Tur-3	34.19	0.65	24.29	<d.l.	21.09	<d.l.	3.68	1.71	1.74	0.03	0.30	<d.l.	3.27	10.01	0.13	0.00	100.84

EMPA label	Type	SiO ₂	TiO ₂	Al ₂ O ₃	Cr ₂ O ₃	FeO	MnO	MgO	CaO	Na ₂ O	K ₂ O	F	Cl	H ₂ O*	B ₂ O ₃ *	O=F	O=Cl	Total
KELL-A-TS-Circle I-Tur3-005	Tur-3	33.86	0.47	22.81	<d.l.	22.69	<d.l.	4.11	1.92	1.68	0.03	0.49	0.02	3.20	9.99	0.21	0.01	101.06
KELL-A-TS-Circle I-Tur3-006	Tur-3	35.57	0.21	28.53	<d.l.	16.14	<d.l.	4.35	0.48	2.48	0.03	0.49	<d.l.	3.27	10.35	0.21	0.00	101.69
KELL-A-TS-Circle I-Tur3-007	Tur-3	34.37	0.99	24.79	<d.l.	19.37	<d.l.	4.42	1.67	1.82	<d.l.	0.53	<d.l.	3.19	10.09	0.22	0.00	101.02
KELL-A-TS-Circle I-Tur3-008	Tur-3	34.66	0.30	27.16	<d.l.	17.69	<d.l.	4.06	1.17	2.16	0.02	0.34	<d.l.	3.31	10.17	0.14	0.00	100.89
KELL-A-TS-Circle I-Tur3-009	Tur-3	34.45	<d.l.	25.09	<d.l.	21.54	<d.l.	3.24	1.42	1.94	0.05	0.21	0.03	3.34	10.07	0.09	0.01	101.28
KELL-A-TS-Circle I-Tur3-010	Tur-3	34.16	1.42	23.62	<d.l.	20.63	<d.l.	4.30	1.74	1.83	0.03	0.50	<d.l.	3.21	10.05	0.21	0.00	101.28
KELL-A-TS-Circle I-Tur3-011	Tur-3	34.30	0.84	23.92	<d.l.	21.68	<d.l.	3.89	1.84	1.72	0.03	0.37	<d.l.	3.27	10.09	0.16	0.00	101.80
KELL-A-TS-Circle I-Tur3-012	Tur-3	34.77	1.13	24.99	<d.l.	19.19	<d.l.	4.50	1.80	1.76	0.05	0.52	<d.l.	3.22	10.18	0.22	0.00	101.89
2020-KELL-1-A-TS1-Circle A-tur3-002	Tur-3	35.91	<d.l.	32.52	<d.l.	11.19	<d.l.	3.48	0.14	1.95	0.02	0.56	<d.l.	2.99	10.29	0.24	0.00	98.81
2020-KELL-1-A-TS1-Circle A-tur3-003	Tur-3	35.44	<d.l.	31.34	<d.l.	11.59	<d.l.	3.36	0.11	2.32	0.03	0.65	<d.l.	3.00	10.09	0.27	0.00	97.66
2020-KELL-1-A-TS1-Circle A-tur3-004	Tur-3	36.42	<d.l.	33.00	<d.l.	9.00	<d.l.	4.88	0.30	1.99	<d.l.	0.64	<d.l.	3.03	10.44	0.27	0.00	99.43
2020-KELL-1-A-TS1-Circle A-tur3-005	Tur-3	36.08	<d.l.	33.65	<d.l.	7.08	<d.l.	5.78	0.49	2.17	0.02	0.35	<d.l.	3.25	10.46	0.15	0.00	99.19
2020-KELL-1-A-TS1-Circle A-tur3-006	Tur-3	35.87	<d.l.	33.78	<d.l.	10.35	<d.l.	3.50	0.37	1.53	<d.l.	0.49	<d.l.	2.96	10.38	0.21	0.00	99.02
2020-KELL-1-A-TS1-Circle A-tur3-007	Tur-3	36.34	0.18	32.31	<d.l.	7.15	<d.l.	6.77	0.85	2.20	<d.l.	0.19	<d.l.	3.40	10.50	0.08	0.00	99.81
2020-KELL-1-A-TS1-Circle A-tur3-008	Tur-3	36.30	<d.l.	32.79	<d.l.	6.41	<d.l.	6.60	0.54	2.28	<d.l.	0.34	<d.l.	3.29	10.45	0.14	0.00	98.85
2020-KELL-1-A-TS1-Circle B-tur3-core-00	Tur-3	36.17	<d.l.	32.54	<d.l.	11.52	<d.l.	3.23	0.26	1.69	<d.l.	<d.l.	<d.l.	3.20	10.31	0.00	0.00	98.92
2020-KELL-1-A-TS1-Circle B-tur3-core-00	Tur-3	36.21	<d.l.	32.86	<d.l.	11.15	<d.l.	3.27	0.28	1.65	<d.l.	<d.l.	<d.l.	3.20	10.33	0.00	0.00	98.95
2020-KELL-1-A-TS1-Circle B-tur3-core-00	Tur-3	36.11	<d.l.	32.31	<d.l.	11.45	<d.l.	3.21	0.33	1.63	<d.l.	<d.l.	<d.l.	3.18	10.26	0.00	0.00	98.48
2020-KELL-1-A-TS1-Circle B-tur3-rim-001	Tur-3	35.19	0.45	31.02	<d.l.	12.03	<d.l.	3.91	1.31	1.59	<d.l.	0.19	<d.l.	3.22	10.19	0.08	0.00	99.02
2020-KELL-1-A-TS1-Circle B-tur3-rim-002	Tur-3	34.76	0.36	30.35	<d.l.	13.80	<d.l.	2.71	1.20	1.51	<d.l.	0.29	<d.l.	3.08	10.01	0.12	0.00	97.95
2020-KELL-1-A-TS1-Circle B-tur3-rim-003	Tur-3	35.93	<d.l.	31.94	<d.l.	10.99	0.08	4.15	0.22	2.43	0.02	0.26	<d.l.	3.29	10.31	0.11	0.00	99.52
2020-KELL-1-A-TS1-Circle B-tur3-rim-004	Tur-3	35.47	0.16	32.31	<d.l.	10.36	<d.l.	3.81	0.47	1.72	0.02	<d.l.	<d.l.	3.22	10.20	0.00	0.00	97.74
2020-KELL-1-A-TS1-Circle C-tur3-001	Tur-3	36.21	0.19	32.78	<d.l.	11.53	0.12	2.72	0.42	1.69	0.03	0.15	<d.l.	3.16	10.29	0.06	0.00	99.22
2020-KELL-1-A-TS1-Circle C-tur3-002	Tur-3	36.43	<d.l.	32.80	<d.l.	9.78	<d.l.	4.42	0.15	2.55	0.03	0.30	<d.l.	3.32	10.41	0.13	0.00	100.07
2020-KELL-1-A-TS1-Circle C-tur3-003	Tur-3	36.40	<d.l.	33.37	<d.l.	10.82	<d.l.	3.28	0.11	2.22	<d.l.	0.19	<d.l.	3.26	10.39	0.08	0.00	99.96
2020-KELL-1-A-TS1-Circle C-tur3-004	Tur-3	35.71	0.24	32.55	<d.l.	10.04	<d.l.	4.38	0.64	1.73	0.03	<d.l.	<d.l.	3.29	10.33	0.00	0.00	98.94
2020-KELL-1-A-TS1-Circle C-tur3-005	Tur-3	35.49	<d.l.	31.70	<d.l.	15.36	<d.l.	1.13	0.10	1.69	0.06	0.52	<d.l.	2.89	10.13	0.22	0.00	98.85
2020-KELL-1-A-TS1-Circle C-tur3-006	Tur-3	34.96	0.24	30.82	<d.l.	13.41	<d.l.	2.78	0.95	1.72	0.03	0.28	<d.l.	3.13	10.06	0.12	0.00	98.26
2020-KELL-1-A-TS1-Circle C-tur3-007	Tur-3	35.99	0.17	33.53	<d.l.	9.60	<d.l.	4.18	0.72	1.56	<d.l.	0.44	<d.l.	3.06	10.42	0.19	0.00	99.48
2020-KELL-1-A-TS1-Circle C-tur3-008	Tur-3	35.23	1.15	29.11	<d.l.	12.85	<d.l.	4.13	1.34	1.58	0.03	0.38	<d.l.	3.12	10.12	0.16	0.00	98.87
2020-KELL-1-A-TS1-Circle C-tur3-core-00	Tur-3	35.68	0.15	33.29	<d.l.	13.60	<d.l.	1.25	0.50	1.33	<d.l.	<d.l.	<d.l.	3.11	10.23	0.00	0.00	99.14
2020-KELL-1-A-TS1-Circle C-tur3-core-00	Tur-3	35.74	<d.l.	33.73	<d.l.	13.70	<d.l.	1.01	0.23	1.06	<d.l.	<d.l.	<d.l.	3.00	10.25	0.00	0.00	98.72
2020-KELL-1-A-TS1-Circle C-tur3-core-00	Tur-3	35.40	0.26	31.69	<d.l.	13.66	<d.l.	2.51	0.78	1.61	0.02	<d.l.	<d.l.	3.24	10.21	0.00	0.00	99.38
2020-KELL-1-A-TS1-Circle C-tur3-rim-001	Tur-3	35.90	<d.l.	32.23	<d.l.	11.45	<d.l.	3.48	0.23	1.87	0.02	0.56	<d.l.	2.98	10.27	0.24	0.00	98.75
2020-KELL-1-A-TS1-Circle C-tur3-rim-002	Tur-3	36.04	0.25	32.26	<d.l.	8.36	<d.l.	5.89	0.91	1.91	<d.l.	0.28	<d.l.	3.27	10.43	0.12	0.00	99.48
2020-KELL-1-A-TS1-Circle D-tur3-core-00	Tur-3	35.05	0.26	28.29	<d.l.	13.80	<d.l.	4.21	0.82	2.17	0.04	0.63	<d.l.	3.06	10.01	0.27	0.00	98.08
2020-KELL-1-A-TS1-Circle D-tur3-core-00	Tur-3	35.19	<d.l.	29.08	<d.l.	13.16	<d.l.	4.33	0.51	2.49	0.03	0.58	<d.l.	3.14	10.07	0.24	0.00	98.34
2020-KELL-1-A-TS1-Circle D-tur3-core-00	Tur-3	35.01	0.21	29.80	<d.l.	13.38	0.11	3.72	0.57	2.30	<d.l.	0.50	<d.l.	3.14	10.09	0.21	0.00	98.62
2020-KELL-1-A-TS1-Circle D-tur3-rim-001	Tur-3	35.10	<d.l.	30.50	<d.l.	15.44	<d.l.	1.33	0.10	1.69	0.06	0.55	<d.l.	2.84	9.96	0.23	0.00	97.33

EMPA label	Type	SiO ₂	TiO ₂	Al ₂ O ₃	Cr ₂ O ₃	FeO	MnO	MgO	CaO	Na ₂ O	K ₂ O	F	Cl	H ₂ O*	B ₂ O ₃ *	O=F	O=Cl	Total
2020-KELL-1-A-TS1-Circle D-tur3-rim-002	Tur-3	34.71	0.60	29.98	<d.l.	14.91	<d.l.	2.47	0.77	1.85	0.02	0.25	<d.l.	3.15	10.04	0.11	0.00	98.64
2020-KELL-1-A-TS1-Circle D-tur3-rim-003	Tur-3	35.22	<d.l.	30.99	<d.l.	15.09	<d.l.	1.47	0.24	1.66	0.05	0.43	<d.l.	2.92	10.03	0.18	0.00	97.92
2020-KELL-1-A-TS1-Circle D-tur3-001	Tur-3	36.29	<d.l.	32.88	<d.l.	10.23	<d.l.	3.65	0.21	2.09	0.03	0.22	<d.l.	3.21	10.32	0.09	0.00	99.04
2020-KELL-1-A-TS1-Circle D-tur3-002	Tur-3	35.61	0.22	32.20	<d.l.	13.95	<d.l.	1.45	0.11	1.27	0.03	0.43	<d.l.	2.81	10.15	0.18	0.00	98.05
2020-KELL-1-A-TS1-Circle D-tur3-003	Tur-3	35.84	0.26	31.41	<d.l.	8.75	<d.l.	6.26	0.84	2.25	<d.l.	0.34	<d.l.	3.32	10.39	0.14	0.00	99.52
2020-KELL-1-A-TS1-Circle D-tur3-004	Tur-3	36.19	<d.l.	31.62	<d.l.	11.92	<d.l.	3.48	0.05	2.52	0.04	0.64	<d.l.	3.10	10.27	0.27	0.00	99.56
2020-KELL-1-A-TS1-Circle D-tur3-005	Tur-3	36.74	0.29	32.43	<d.l.	6.72	<d.l.	6.38	0.65	2.38	0.03	0.29	<d.l.	3.37	10.46	0.12	0.00	99.62
2020-KELL-1-A-TS1-Circle D-tur3-006	Tur-3	38.91	0.36	32.81	<d.l.	10.69	<d.l.	5.07	0.09	3.03	<d.l.	0.69	<d.l.	3.40	10.93	0.29	0.00	105.69
2020-KELL-1-A-TS1-Circle D-tur3-007	Tur-3	35.64	0.17	31.96	<d.l.	11.17	<d.l.	3.68	0.09	2.44	0.04	0.64	<d.l.	3.07	10.23	0.27	0.00	98.86
2020-KELL-1-A-TS1-Circle D-tur3-008	Tur-3	35.76	0.24	31.19	<d.l.	12.84	<d.l.	3.56	0.53	1.92	0.02	0.53	<d.l.	3.06	10.28	0.22	0.00	99.71
2020-KELL-1-A-TS1-Circle D-tur3-009	Tur-3	35.40	0.19	29.19	<d.l.	13.77	<d.l.	3.85	0.35	2.37	<d.l.	0.49	<d.l.	3.13	10.10	0.21	0.00	98.64
2020-KELL-1-A-TS1-Circle D-tur3-010	Tur-3	36.44	<d.l.	33.05	<d.l.	9.65	<d.l.	4.29	0.17	2.35	<d.l.	0.22	<d.l.	3.30	10.41	0.09	0.00	99.79
2020-KELL-1-A-TS1-Circle D-tur3-011	Tur-3	35.93	0.35	31.81	<d.l.	9.85	<d.l.	5.09	0.25	2.32	0.03	0.52	<d.l.	3.16	10.37	0.22	0.00	99.46
2020-KELL-1-A-TS1-Circle E-tur3-001	Tur-3	35.23	0.81	30.45	<d.l.	11.83	<d.l.	4.04	0.79	1.89	<d.l.	0.47	<d.l.	3.08	10.16	0.20	0.00	98.55
2020-KELL-1-A-TS1-Circle F-tur3-002	Tur-3	35.69	0.53	29.49	<d.l.	10.38	<d.l.	5.34	1.32	1.65	<d.l.	0.37	<d.l.	3.14	10.14	0.16	0.00	97.89
2020-KELL-1-A-TS1-Circle E-tur3-002	Tur-3	35.58	0.22	32.86	<d.l.	11.94	<d.l.	2.77	0.35	2.00	<d.l.	0.38	<d.l.	3.11	10.26	0.16	0.00	99.32
2020-KELL-1-A-TS1-Circle E-tur3-rim-002	Tur-3	35.20	0.24	30.58	<d.l.	14.14	<d.l.	2.69	0.82	1.80	0.03	0.19	<d.l.	3.19	10.11	0.08	0.00	98.91
2020-KELL-1-A-TS1-Circle E-tur3-001	Tur-3	36.48	<d.l.	32.94	<d.l.	9.87	<d.l.	4.14	0.08	2.75	0.03	0.40	<d.l.	3.32	10.40	0.17	0.00	100.24
2020-KELL-1-A-TS1-Circle E-tur3-002	Tur-3	35.64	0.24	28.81	<d.l.	13.63	<d.l.	4.07	0.49	2.29	0.02	0.56	<d.l.	3.10	10.11	0.24	0.00	98.72
2020-KELL-1-A-TS1-Circle E-tur3-003	Tur-3	35.44	0.25	28.83	<d.l.	13.57	<d.l.	4.25	0.57	2.32	<d.l.	0.59	<d.l.	3.10	10.11	0.25	0.00	98.79
2020-KELL-1-A-TS1-Circle E-tur3-core2-0	Tur-3	35.41	0.24	28.53	<d.l.	13.45	<d.l.	4.31	0.60	2.30	0.02	0.55	<d.l.	3.11	10.07	0.23	0.00	98.36
2020-KELL-1-A-TS1-Circle E-tur3-rim2-00	Tur-3	35.26	0.19	30.45	<d.l.	15.44	<d.l.	1.68	0.33	1.84	0.06	0.62	<d.l.	2.91	10.05	0.26	0.00	98.56
2020-KELL-1-A-TS1-Circle E-tur3-rim2-00	Tur-3	35.59	<d.l.	31.82	<d.l.	15.21	<d.l.	1.25	0.10	1.66	0.07	0.35	<d.l.	2.98	10.16	0.15	0.00	99.04
2020-KELL-1-A-TS1-Circle E-tur3-rim2-00	Tur-3	35.27	<d.l.	31.02	<d.l.	15.40	<d.l.	1.27	0.09	1.80	0.06	0.75	<d.l.	2.79	10.03	0.32	0.00	98.17
2020-KELL-1-A-TS1-Circle F-tur3-core-00	Tur-3	35.37	<d.l.	30.22	<d.l.	12.76	0.09	3.56	0.58	1.98	<d.l.	0.28	<d.l.	3.15	10.09	0.12	0.00	97.95
2020-KELL-1-A-TS1-Circle F-tur3-core-00	Tur-3	35.24	<d.l.	29.54	<d.l.	13.03	<d.l.	4.30	0.53	2.35	0.02	0.58	<d.l.	3.12	10.12	0.24	0.00	98.59
2020-KELL-1-A-TS1-Circle F-tur3-core-00	Tur-3	35.79	0.17	29.69	<d.l.	12.99	<d.l.	3.95	0.53	2.31	0.02	0.45	<d.l.	3.18	10.16	0.19	0.00	99.04
2020-KELL-1-A-TS1-Circle F-tur3-rim-004	Tur-3	35.06	<d.l.	31.38	<d.l.	15.25	<d.l.	1.17	0.08	1.66	0.06	0.63	<d.l.	2.80	10.03	0.27	0.00	97.86
2020-KELL-1-A-TS1-Circle F-tur3-rim-005	Tur-3	35.78	<d.l.	32.03	<d.l.	15.17	<d.l.	1.21	0.12	1.48	0.04	0.41	<d.l.	2.90	10.20	0.17	0.00	99.17
2020-KELL-1-A-TS1-Circle F-tur3-rim-006	Tur-3	35.32	<d.l.	31.03	<d.l.	15.31	<d.l.	1.16	0.12	1.62	0.06	0.49	<d.l.	2.86	10.01	0.21	0.00	97.78
2020-KELL-1-A-TS1-Circle F-tur3-007	Tur-3	36.42	0.25	32.29	<d.l.	6.88	<d.l.	6.92	0.77	2.26	<d.l.	0.23	<d.l.	3.39	10.51	0.10	0.00	99.83
2020-KELL-1-A-TS1-Circle H-tur3-core-00	Tur-3	36.04	<d.l.	32.59	<d.l.	9.38	<d.l.	4.72	0.54	1.71	<d.l.	<d.l.	<d.l.	3.26	10.35	0.00	0.00	98.59
2020-KELL-1-A-TS1-Circle H-tur3-core-00	Tur-3	36.04	0.17	33.14	<d.l.	10.04	<d.l.	4.20	0.52	1.74	<d.l.	<d.l.	<d.l.	3.28	10.42	0.00	0.00	99.55
2020-KELL-1-A-TS1-Circle H-tur3-core-00	Tur-3	36.17	<d.l.	32.44	<d.l.	9.75	<d.l.	4.53	0.44	1.62	<d.l.	<d.l.	<d.l.	3.22	10.35	0.00	0.00	98.52
2020-KELL-1-A-TS1-Circle H-tur3-core-00	Tur-3	36.16	<d.l.	33.51	<d.l.	10.05	<d.l.	3.45	0.14	2.09	<d.l.	0.18	<d.l.	3.22	10.34	0.08	0.00	99.06
2020-KELL-1-A-TS1-Circle H-tur3-core-00	Tur-3	35.96	0.25	32.51	<d.l.	10.01	<d.l.	4.22	0.67	1.75	<d.l.	<d.l.	<d.l.	3.29	10.33	0.00	0.00	98.99
2020-KELL-1-A-TS1-Circle H-tur3-core-00	Tur-3	36.54	<d.l.	32.35	<d.l.	9.48	<d.l.	4.54	0.46	1.60	<d.l.	0.19	<d.l.	3.13	10.35	0.08	0.00	98.56
2020-KELL-1-A-TS1-Circle H-tur3-rim-007	Tur-3	35.51	<d.l.	31.43	<d.l.	14.51	<d.l.	2.07	0.40	1.65	0.03	0.47	<d.l.	2.96	10.17	0.20	0.00	99.00
2020-KELL-1-A-TS1-Circle H-tur3-rim-008	Tur-3	35.26	0.23	31.61	<d.l.	13.22	0.09	2.37	0.51	1.81	0.03	0.43	<d.l.	3.03	10.12	0.18	0.00	98.53

EMPA label	Type	SiO ₂	TiO ₂	Al ₂ O ₃	Cr ₂ O ₃	FeO	MnO	MgO	CaO	Na ₂ O	K ₂ O	F	Cl	H ₂ O*	B ₂ O ₃ *	O=F	O=Cl	Total
2020-KELL-1-A-TS1-Circle H-tur3-rim-009	Tur-3	35.56	0.21	30.85	<d.l.	10.08	<d.l.	5.78	1.28	1.76	<d.l.	0.26	<d.l.	3.27	10.33	0.11	0.00	99.26
2020-KELL-1-A-TS1-Circle H-tur3-rim-010	Tur-3	34.82	0.21	31.57	<d.l.	12.07	<d.l.	3.33	1.03	1.70	0.03	0.35	<d.l.	3.12	10.11	0.15	0.00	98.19
2020-KELL-1-A-TS1-Circle H-tur3-rim-011	Tur-3	35.45	<d.l.	30.39	<d.l.	15.12	<d.l.	2.36	0.47	1.98	0.03	0.57	<d.l.	3.01	10.13	0.24	0.00	99.27
2020-KELL-1-A-TS1-Circle H-tur3-rim-012	Tur-3	35.50	<d.l.	31.36	<d.l.	15.90	<d.l.	1.40	0.23	1.92	0.04	0.39	<d.l.	3.05	10.18	0.16	0.00	99.81
2020-KELL-1-A-TS1-Circle H-tur3-013	Tur-3	36.30	<d.l.	33.18	<d.l.	10.05	<d.l.	3.74	0.21	1.95	0.03	0.49	<d.l.	3.05	10.36	0.21	0.00	99.16
2020-KELL-1-A-TS3-Circle A-tur3-001	Tur-3	36.19	<d.l.	33.19	<d.l.	9.57	0.09	4.16	0.27	1.96	<d.l.	0.47	<d.l.	3.08	10.38	0.20	0.00	99.16
2020-KELL-1-A-TS3-Circle A-tur3-002	Tur-3	36.31	<d.l.	33.28	<d.l.	9.82	<d.l.	3.71	0.13	2.08	0.03	0.23	<d.l.	3.20	10.34	0.10	0.00	99.04
2020-KELL-1-A-TS3-Circle A-tur3-003	Tur-3	35.81	<d.l.	32.68	<d.l.	9.82	<d.l.	4.09	0.36	1.90	0.02	0.49	<d.l.	3.04	10.27	0.21	0.00	98.27
2020-KELL-1-A-TS3-Circle B-tur3-001	Tur-3	36.10	<d.l.	32.50	<d.l.	11.16	<d.l.	3.50	0.08	2.43	<d.l.	0.31	<d.l.	3.24	10.31	0.13	0.00	99.50
2020-KELL-1-A-TS3-Circle B-tur3-002	Tur-3	36.17	<d.l.	32.00	<d.l.	10.55	<d.l.	3.87	0.40	1.70	<d.l.	<d.l.	<d.l.	3.21	10.25	0.00	0.00	98.15
2020-KELL-1-A-TS3-Circle B-tur3-003	Tur-3	35.57	0.21	31.90	<d.l.	12.92	0.14	2.36	0.12	1.74	0.03	<d.l.	<d.l.	3.16	10.17	0.00	0.00	98.32
2020-KELL-1-A-TS3-Circle B-tur3-004	Tur-3	35.46	<d.l.	33.11	<d.l.	13.29	<d.l.	1.36	0.20	1.21	<d.l.	<d.l.	<d.l.	3.01	10.15	0.00	0.00	97.79
2020-KELL-1-A-TS3-Circle B-tur3-005	Tur-3	35.30	0.19	31.33	<d.l.	14.03	<d.l.	2.19	0.70	1.61	<d.l.	<d.l.	<d.l.	3.20	10.12	0.00	0.00	98.67
2020-KELL-1-A-TS3-Circle C-tur3-core-00	Tur-3	35.92	<d.l.	32.23	<d.l.	11.40	<d.l.	3.31	0.10	2.26	<d.l.	0.24	<d.l.	3.21	10.24	0.10	0.00	98.81
2020-KELL-1-A-TS3-Circle C-tur3-core-00	Tur-3	35.91	<d.l.	32.62	<d.l.	12.00	<d.l.	2.73	0.27	1.62	<d.l.	<d.l.	<d.l.	3.17	10.25	0.00	0.00	98.57
2020-KELL-1-A-TS3-Circle C-tur3-core-00	Tur-3	35.82	<d.l.	32.28	<d.l.	12.05	<d.l.	2.75	0.27	1.64	<d.l.	<d.l.	<d.l.	3.16	10.20	0.00	0.00	98.17
2020-KELL-1-A-TS3-Circle C-tur3-rim-004	Tur-3	35.26	<d.l.	31.18	<d.l.	15.84	<d.l.	0.98	0.10	1.55	0.04	0.75	<d.l.	2.72	10.05	0.32	0.00	98.15
2020-KELL-1-A-TS3-Circle C-tur3-rim-005	Tur-3	35.69	<d.l.	31.22	<d.l.	14.53	<d.l.	1.59	0.14	1.70	0.05	0.52	<d.l.	2.89	10.08	0.22	0.00	98.19
2020-KELL-1-A-TS3-Circle C-tur3-rim-006	Tur-3	34.76	0.17	31.03	<d.l.	14.80	<d.l.	1.52	0.35	1.68	0.04	0.27	<d.l.	3.01	9.98	0.11	0.00	97.49
2020-KELL-1-A-TS3-Circle D-tur3-001	Tur-3	35.39	0.18	28.84	<d.l.	13.81	<d.l.	3.96	0.55	2.34	<d.l.	0.50	<d.l.	3.14	10.08	0.21	0.00	98.58
2020-KELL-1-A-TS3-Circle D-tur3-002	Tur-3	36.12	<d.l.	31.69	<d.l.	12.22	<d.l.	3.35	0.47	1.71	<d.l.	<d.l.	<d.l.	3.23	10.28	0.00	0.00	99.07
2020-KELL-1-A-TS3-Circle D-tur3-003	Tur-3	37.38	0.16	33.48	<d.l.	6.57	0.14	5.38	0.49	1.42	0.03	0.14	0.02	3.14	10.50	0.06	0.01	98.79
2020-KELL-1-A-TS3-Circle D-tur3-004	Tur-3	36.21	<d.l.	32.79	<d.l.	9.75	<d.l.	3.87	0.06	2.62	<d.l.	0.45	<d.l.	3.22	10.29	0.19	0.00	99.07
2020-KELL-1-A-TS3-Circle D-tur3-005	Tur-3	36.08	0.23	31.97	<d.l.	7.14	<d.l.	6.87	0.72	2.29	<d.l.	0.32	<d.l.	3.33	10.45	0.14	0.00	99.26
2020-KELL-1-A-TS3-Circle E-tur3-core-00	Tur-3	36.26	<d.l.	32.61	<d.l.	10.98	<d.l.	3.47	0.16	2.25	<d.l.	0.17	<d.l.	3.27	10.32	0.07	0.00	99.42
2020-KELL-1-A-TS3-Circle E-tur3-core-00	Tur-3	36.36	<d.l.	32.11	<d.l.	10.78	<d.l.	3.99	0.35	1.85	0.02	<d.l.	<d.l.	3.27	10.33	0.00	0.00	99.06
2020-KELL-1-A-TS3-Circle E-tur3-rim-003	Tur-3	35.45	<d.l.	31.22	<d.l.	15.78	<d.l.	1.16	0.06	1.62	0.05	0.56	<d.l.	2.84	10.10	0.24	0.00	98.60
2020-KELL-1-A-TS3-Circle E-tur3-rim-004	Tur-3	35.40	0.31	30.37	<d.l.	11.46	<d.l.	4.47	1.06	1.94	0.02	0.28	<d.l.	3.23	10.16	0.12	0.00	98.59
2020-KELL-1-A-TS3-Circle E-tur3-rim-005	Tur-3	34.74	0.49	30.60	<d.l.	13.87	<d.l.	2.56	1.13	1.54	<d.l.	0.23	<d.l.	3.12	10.03	0.10	0.00	98.21
2020-KELL-1-A-TS3-Circle E-tur3-rim-006	Tur-3	34.86	0.32	30.23	<d.l.	12.75	<d.l.	3.80	1.28	1.58	<d.l.	0.25	<d.l.	3.16	10.09	0.11	0.00	98.21
2020-KELL-1-A-TS3-Circle E-tur3-core-00	Tur-3	35.68	0.15	31.86	<d.l.	11.12	<d.l.	3.83	0.54	1.65	<d.l.	0.19	<d.l.	3.13	10.24	0.08	0.00	98.30
2020-KELL-1-A-TS3-Circle F-tur3-core-00	Tur-3	35.73	<d.l.	32.06	<d.l.	11.40	<d.l.	3.55	0.46	1.93	<d.l.	0.44	<d.l.	3.08	10.24	0.19	0.00	98.70
2020-KELL-1-A-TS3-Circle F-tur3-core-00	Tur-3	35.32	0.28	29.08	<d.l.	13.57	<d.l.	3.97	0.47	2.38	0.03	0.44	<d.l.	3.18	10.09	0.19	0.00	98.62
2020-KELL-1-A-TS3-Circle F-tur3-core-00	Tur-3	36.76	<d.l.	33.65	<d.l.	9.43	<d.l.	3.92	0.11	2.44	0.03	0.24	<d.l.	3.32	10.45	0.10	0.00	100.25
2020-KELL-1-A-TS3-Circle F-tur3-rim-004	Tur-3	35.76	0.25	30.49	<d.l.	11.06	0.09	4.84	1.59	1.63	<d.l.	0.19	<d.l.	3.29	10.25	0.08	0.00	99.36
2020-KELL-1-A-TS3-Circle F-tur3-rim-005	Tur-3	35.39	<d.l.	31.07	<d.l.	15.10	<d.l.	1.64	0.13	1.76	0.06	0.78	<d.l.	2.79	10.09	0.33	0.00	98.48
2020-KELL-1-A-TS3-Circle F-tur3-rim-006	Tur-3	34.86	<d.l.	31.43	<d.l.	15.76	<d.l.	0.82	0.12	1.45	0.05	0.53	<d.l.	2.79	10.00	0.22	0.00	97.58
2020-KELL-1-A-TS3-Circle F-tur3-rim-007	Tur-3	34.78	<d.l.	31.56	<d.l.	15.15	<d.l.	1.20	0.11	1.45	0.04	0.63	<d.l.	2.74	10.02	0.27	0.00	97.41
2020-KELL-1-A-TS3-Circle F-tur3-rim-008	Tur-3	35.34	0.17	31.29	<d.l.	14.45	<d.l.	2.05	0.42	1.84	0.05	0.29	<d.l.	3.10	10.14	0.12	0.00	99.01

EMPA label	Type	SiO ₂	TiO ₂	Al ₂ O ₃	Cr ₂ O ₃	FeO	MnO	MgO	CaO	Na ₂ O	K ₂ O	F	Cl	H ₂ O*	B ₂ O ₃ *	O=F	O=Cl	Total
2020-KELL-1-A-TS3-Circle F-tur3-rim-009	Tur-3	35.60	<d.l.	31.76	<d.l.	14.88	<d.l.	1.26	0.09	1.60	0.06	0.56	<d.l.	2.85	10.12	0.24	0.00	98.54
2020-KELL-1-A-TS3-Circle F-tur3-core-01	Tur-3	35.72	0.21	32.19	<d.l.	11.79	<d.l.	3.38	0.30	2.08	0.03	0.34	<d.l.	3.16	10.28	0.14	0.00	99.33
2020-KELL-1-A-TS3-Circle F-tur3-core-01	Tur-3	35.57	0.17	32.31	<d.l.	11.38	<d.l.	3.35	0.32	1.94	0.03	0.17	<d.l.	3.19	10.23	0.07	0.00	98.59
2020-KELL-1-A-TS3-Circle F-tur3-core-01	Tur-3	35.45	0.20	32.13	<d.l.	12.09	<d.l.	2.94	0.12	2.20	0.04	0.41	<d.l.	3.11	10.19	0.17	0.00	98.71
2020-KELL-1-A-TS3-Circle F-tur3-core-01	Tur-3	36.04	<d.l.	32.36	<d.l.	11.64	<d.l.	3.40	0.10	2.26	0.04	0.27	<d.l.	3.22	10.31	0.11	0.00	99.53
2020-KELL-1-A-TS3-Circle F-tur3-core-01	Tur-3	35.54	0.43	30.42	<d.l.	9.66	<d.l.	5.71	1.35	1.74	<d.l.	0.36	<d.l.	3.20	10.23	0.15	0.00	98.49
2020-KELL-1-A-TS3-Circle F-tur3-core-01	Tur-3	35.82	<d.l.	32.13	<d.l.	11.26	<d.l.	3.72	0.45	1.67	<d.l.	<d.l.	<d.l.	3.22	10.27	0.00	0.00	98.54
2020-KELL-1-A-TS3-Circle G-tur3-core-00	Tur-3	35.88	0.24	31.65	<d.l.	10.49	<d.l.	4.25	0.18	2.34	0.02	0.50	<d.l.	3.13	10.25	0.21	0.00	98.72
2020-KELL-1-A-TS3-Circle G-tur3-rim-002	Tur-3	35.38	<d.l.	31.55	<d.l.	15.00	<d.l.	1.06	0.08	1.61	0.04	0.53	<d.l.	2.84	10.04	0.22	0.00	97.91
2020-KELL-1-A-TS3-Circle G-tur3-core-00	Tur-3	35.61	<d.l.	32.29	<d.l.	11.53	0.08	3.11	0.28	1.69	<d.l.	<d.l.	<d.l.	3.18	10.20	0.00	0.00	97.96
2020-KELL-1-A-TS3-Circle G-tur3-core-00	Tur-3	35.62	<d.l.	32.23	<d.l.	11.58	<d.l.	3.15	0.29	1.67	0.03	<d.l.	<d.l.	3.18	10.20	0.00	0.00	97.94
2020-KELL-1-A-TS3-Circle G-tur3-core-00	Tur-3	35.80	<d.l.	32.30	<d.l.	11.21	<d.l.	3.31	0.34	1.58	<d.l.	<d.l.	<d.l.	3.16	10.22	0.00	0.00	97.92
2020-KELL-1-A-TS3-Circle G-tur3-core-00	Tur-3	36.12	<d.l.	32.30	<d.l.	10.93	<d.l.	3.39	0.46	1.65	0.03	<d.l.	<d.l.	3.21	10.24	0.00	0.00	98.33
2020-KELL-1-A-TS3-Circle G-tur3-core-00	Tur-3	36.06	<d.l.	33.54	<d.l.	9.46	<d.l.	3.80	0.25	2.15	0.02	0.15	<d.l.	3.27	10.33	0.06	0.00	98.97
2020-KELL-17-C-TS2-Circle A-tur3-001	Tur-3	35.07	0.25	31.93	<d.l.	13.03	<d.l.	2.57	0.75	1.55	<d.l.	0.24	<d.l.	3.08	10.15	0.10	0.00	98.53
2020-KELL-17-C-TS2-Circle A-tur3-002	Tur-3	35.58	<d.l.	33.61	<d.l.	12.28	<d.l.	2.23	0.47	1.40	0.02	<d.l.	<d.l.	3.15	10.29	0.00	0.00	99.03
2020-KELL-17-C-TS2-Circle A-tur3-003	Tur-3	34.76	0.22	32.73	<d.l.	12.82	<d.l.	2.34	0.59	1.56	<d.l.	<d.l.	<d.l.	3.18	10.16	0.00	0.00	98.36
2020-KELL-17-C-TS2-Circle A-tur3-004	Tur-3	35.26	0.16	33.15	<d.l.	13.34	<d.l.	2.13	0.59	1.50	<d.l.	0.21	<d.l.	3.09	10.29	0.09	0.00	99.63
2020-KELL-17-C-TS2-Circle A-tur3-005	Tur-3	35.53	<d.l.	32.74	<d.l.	13.50	<d.l.	1.78	0.34	1.70	<d.l.	<d.l.	<d.l.	3.19	10.20	0.00	0.00	98.98
2020-KELL-17-C-TS2-Circle A-tur3-006	Tur-3	35.33	<d.l.	33.11	<d.l.	12.87	<d.l.	2.02	0.47	1.46	<d.l.	0.17	<d.l.	3.06	10.21	0.07	0.00	98.63
2020-KELL-17-C-TS2-Circle A-tur3-007	Tur-3	35.30	0.17	32.41	<d.l.	13.27	<d.l.	1.89	0.39	1.72	<d.l.	<d.l.	<d.l.	3.19	10.14	0.00	0.00	98.48
2020-KELL-17-C-TS2-Circle A-tur3-008	Tur-3	35.77	<d.l.	32.89	<d.l.	13.57	<d.l.	1.51	0.31	1.55	<d.l.	<d.l.	<d.l.	3.14	10.21	0.00	0.00	98.96
2020-KELL-17-C-TS2-Circle A-tur3-009	Tur-3	34.85	0.34	32.15	<d.l.	13.99	<d.l.	2.06	0.74	1.57	<d.l.	0.18	<d.l.	3.12	10.17	0.08	0.00	99.10
2020-KELL-17-C-TS2-Circle B-tur3-001	Tur-3	35.57	0.43	31.67	<d.l.	13.56	<d.l.	2.26	0.55	1.53	<d.l.	0.31	<d.l.	3.02	10.19	0.13	0.00	98.96
2020-KELL-17-C-TS2-Circle B-tur3-002	Tur-3	35.03	0.58	31.04	<d.l.	13.87	<d.l.	2.77	0.67	1.68	<d.l.	0.17	<d.l.	3.15	10.17	0.07	0.00	99.06
2020-KELL-17-C-TS2-Circle B-tur3-003	Tur-3	36.11	0.22	34.74	<d.l.	10.85	0.12	2.16	0.32	1.08	<d.l.	<d.l.	<d.l.	3.05	10.38	0.00	0.00	99.04
2020-KELL-17-C-TS2-Circle C-tur3-001	Tur-3	35.41	0.24	33.31	<d.l.	12.90	<d.l.	2.29	0.56	1.36	<d.l.	0.18	<d.l.	3.07	10.32	0.08	0.00	99.56
2020-KELL-17-C-TS2-Circle C-tur3-002	Tur-3	35.18	<d.l.	32.45	<d.l.	13.00	0.10	2.04	0.62	1.55	<d.l.	0.18	<d.l.	3.09	10.13	0.08	0.00	98.26
2020-KELL-17-C-TS2-Circle C-tur3-003	Tur-3	34.92	0.32	31.69	<d.l.	13.49	<d.l.	2.50	0.64	1.86	<d.l.	<d.l.	<d.l.	3.27	10.14	0.00	0.00	98.83
2020-KELL-17-C-TS2-Circle C-tur3-004	Tur-3	34.92	0.36	31.53	<d.l.	14.68	<d.l.	1.80	0.80	1.53	<d.l.	0.28	<d.l.	3.06	10.12	0.12	0.00	98.96
2020-KELL-17-C-TS2-Circle C-tur3-005	Tur-3	35.68	0.44	33.40	<d.l.	12.53	<d.l.	2.44	0.69	1.61	<d.l.	0.21	<d.l.	3.16	10.37	0.09	0.00	100.44
2020-KELL-17-C-TS2-Circle D-tur3-001	Tur-3	35.01	0.27	31.77	<d.l.	13.62	<d.l.	2.35	0.86	1.54	<d.l.	0.26	<d.l.	3.09	10.14	0.11	0.00	98.80
2020-KELL-17-C-TS2-Circle D-tur3-002	Tur-3	34.77	0.42	32.03	<d.l.	13.47	<d.l.	2.28	0.86	1.55	0.03	0.27	<d.l.	3.09	10.14	0.11	0.00	98.80
2020-KELL-17-C-TS2-Circle D-tur3-003	Tur-3	35.41	<d.l.	31.76	<d.l.	14.56	<d.l.	1.69	0.36	1.67	<d.l.	<d.l.	<d.l.	3.17	10.14	0.00	0.00	98.76
2020-KELL-17-C-TS2-Circle D-tur3-004	Tur-3	34.44	0.77	30.04	<d.l.	16.76	<d.l.	1.05	0.64	1.78	0.03	0.55	<d.l.	2.94	9.97	0.23	0.00	98.74
2020-KELL-17-C-TS2-Circle E-tur3-001	Tur-3	35.48	0.30	30.65	<d.l.	13.41	<d.l.	3.16	0.72	1.99	0.04	0.28	<d.l.	3.20	10.17	0.12	0.00	99.28
2020-KELL-17-C-TS2-Circle E-tur3-002	Tur-3	35.41	0.98	30.77	<d.l.	13.51	<d.l.	2.58	0.56	1.58	<d.l.	0.22	<d.l.	3.07	10.15	0.09	0.00	98.73
2020-KELL-17-C-TS2-Circle E-tur3-003	Tur-3	35.59	<d.l.	33.24	<d.l.	12.34	<d.l.	2.55	0.49	1.57	0.02	0.16	<d.l.	3.13	10.30	0.07	0.00	99.32
2020-KELL-17-C-TS2-Circle E-tur3-004	Tur-3	34.54	0.92	25.28	<d.l.	16.94	<d.l.	4.13	2.20	1.42	0.03	0.45	<d.l.	3.12	9.89	0.19	0.00	98.73

EMPA label	Type	SiO ₂	TiO ₂	Al ₂ O ₃	Cr ₂ O ₃	FeO	MnO	MgO	CaO	Na ₂ O	K ₂ O	F	Cl	H ₂ O*	B ₂ O ₃ *	O=F	O=Cl	Total
2020-KELL-17-C-TS2-Circle F-tur3-001	Tur-3	35.09	0.37	28.09	<d.l.	16.14	<d.l.	3.43	1.22	1.78	0.02	0.35	<d.l.	3.16	10.09	0.15	0.00	99.60
2020-KELL-17-C-TS2-Circle F-tur3-002	Tur-3	34.96	0.36	27.62	<d.l.	16.05	<d.l.	3.57	1.55	1.58	0.02	0.50	<d.l.	3.07	10.03	0.21	0.00	99.10
2020-KELL-17-C-TS2-Circle F-tur3-003	Tur-3	35.31	0.19	33.80	<d.l.	11.10	<d.l.	3.00	0.82	1.52	<d.l.	0.18	<d.l.	3.16	10.32	0.08	0.00	99.32
2020-KELL-17-C-TS2-Circle F-tur3-004	Tur-3	35.28	0.32	32.34	<d.l.	12.76	<d.l.	3.03	1.06	1.38	0.02	0.41	<d.l.	3.04	10.29	0.17	0.00	99.76
2020-KELL-17-C-TS2-Circle F-tur3-005	Tur-3	35.73	0.37	29.38	<d.l.	15.64	<d.l.	2.73	0.78	1.66	<d.l.	0.29	<d.l.	3.10	10.17	0.12	0.00	99.73
2020-KELL-17-C-TS2-Circle F-tur3-006	Tur-3	35.43	0.46	26.58	<d.l.	16.08	<d.l.	4.14	1.78	1.68	0.03	0.55	<d.l.	3.12	10.05	0.23	0.00	99.67
2020-KELL-17-C-TS2-Circle G-tur3-001	Tur-3	35.72	<d.l.	33.59	<d.l.	13.08	<d.l.	1.62	0.38	1.61	<d.l.	<d.l.	<d.l.	3.19	10.27	0.00	0.00	99.46
2020-KELL-17-C-TS2-Circle G-tur3-002	Tur-3	35.44	0.41	32.17	<d.l.	13.82	<d.l.	1.96	0.41	1.54	0.02	0.21	<d.l.	3.06	10.21	0.09	0.00	99.17
2020-KELL-17-C-TS2-Circle G-tur3-003	Tur-3	35.20	<d.l.	33.25	<d.l.	13.38	<d.l.	1.68	0.42	1.27	<d.l.	<d.l.	<d.l.	3.08	10.21	0.00	0.00	98.48
2020-KELL-17-C-TS2-Circle G-tur3-004	Tur-3	35.30	0.54	31.79	<d.l.	13.44	<d.l.	2.72	0.63	1.67	0.03	0.31	<d.l.	3.10	10.25	0.13	0.00	99.65
2020-KELL-17-C-TS2-Circle H-tur3-001	Tur-3	35.26	0.33	32.02	<d.l.	13.66	<d.l.	2.07	0.53	1.78	0.03	<d.l.	<d.l.	3.24	10.17	0.00	0.00	99.09
2020-KELL-17-C-TS2-Circle H-tur3-002	Tur-3	35.72	0.16	32.13	<d.l.	14.57	<d.l.	1.16	0.23	1.62	<d.l.	<d.l.	<d.l.	3.14	10.15	0.00	0.00	98.88
2020-KELL-17-C-TS2-Circle H-tur3-003	Tur-3	35.47	0.23	31.52	<d.l.	13.58	<d.l.	2.74	0.58	1.80	<d.l.	0.22	<d.l.	3.16	10.22	0.09	0.00	99.43
2020-KELL-17-C-TS2-Circle H-tur3-004	Tur-3	34.96	0.24	33.50	<d.l.	12.75	<d.l.	2.02	0.52	1.37	0.03	0.17	<d.l.	3.05	10.23	0.07	0.00	98.77
2020-KELL-17-C-TS2-Circle H-tur3-005	Tur-3	36.07	<d.l.	33.01	<d.l.	13.47	<d.l.	1.60	0.20	1.39	<d.l.	<d.l.	<d.l.	3.09	10.27	0.00	0.00	99.10
2020-KELL-48-TS1-Circle A-tur3-001	Tur-3	35.28	<d.l.	29.50	<d.l.	16.15	<d.l.	2.34	0.24	2.20	0.15	0.48	<d.l.	3.09	10.09	0.20	0.00	99.31
2020-KELL-48-TS1-Circle A-tur3-002	Tur-3	35.00	<d.l.	30.57	<d.l.	16.87	0.10	1.25	0.42	1.57	0.21	0.26	<d.l.	3.05	10.09	0.11	0.00	99.28
2020-KELL-48-TS1-Circle B-tur3-001	Tur-3	33.67	<d.l.	26.44	<d.l.	20.35	<d.l.	1.64	0.80	1.09	0.74	0.36	<d.l.	2.97	9.77	0.15	0.00	97.68
2020-KELL-48-TS1-Circle B-tur3-002	Tur-3	34.99	0.44	29.86	<d.l.	15.34	<d.l.	2.22	0.33	1.36	0.29	0.50	<d.l.	2.87	10.04	0.21	0.00	98.02
2020-KELL-48-TS1-Circle B-tur3-003	Tur-3	35.06	0.18	30.99	<d.l.	13.04	0.08	3.11	0.05	2.54	0.06	0.78	<d.l.	3.01	10.12	0.33	0.00	98.69
2020-KELL-48-TS1-Circle B-tur3-004	Tur-3	33.44	<d.l.	26.73	<d.l.	20.51	0.10	1.40	0.73	0.97	0.73	0.25	<d.l.	2.98	9.76	0.11	0.00	97.50
2020-KELL-48-TS1-Circle B-tur3-005	Tur-3	35.11	0.37	30.35	<d.l.	14.29	<d.l.	2.76	0.54	1.72	0.15	0.69	<d.l.	2.90	10.11	0.29	0.00	98.70
2020-KELL-48-TS1-Circle B-tur3-006	Tur-3	33.37	<d.l.	25.77	<d.l.	21.06	0.12	1.59	0.92	0.93	0.87	0.33	0.02	2.97	9.71	0.14	0.01	97.52
2020-KELL-48-TS1-Circle C-tur3-001	Tur-3	35.62	0.16	31.08	<d.l.	12.34	<d.l.	3.70	0.08	2.57	0.06	0.26	<d.l.	3.29	10.22	0.11	0.00	99.27
2020-KELL-48-TS1-Circle C-tur3-002	Tur-3	35.02	0.30	30.04	<d.l.	15.20	<d.l.	2.47	0.14	2.40	0.07	0.37	<d.l.	3.17	10.09	0.16	0.00	99.11
2020-KELL-48-TS1-Circle C-tur3-003	Tur-3	34.30	<d.l.	30.17	<d.l.	16.41	0.20	1.51	0.41	1.70	0.06	0.15	<d.l.	3.08	9.97	0.06	0.00	97.90
2020-KELL-48-TS1-Circle D-tur3-001	Tur-3	35.45	0.42	29.29	<d.l.	14.74	0.16	3.00	0.36	2.35	0.05	0.59	<d.l.	3.09	10.11	0.25	0.00	99.35
2020-KELL-48-TS1-Circle D-tur3-002	Tur-3	35.44	0.33	30.82	<d.l.	13.45	0.10	2.43	0.29	1.91	0.03	0.23	<d.l.	3.11	10.08	0.10	0.00	98.12
2020-KELL-48-TS1-Circle D-tur3-003	Tur-3	34.03	0.29	27.73	<d.l.	18.49	0.11	1.75	0.19	2.00	0.10	0.42	<d.l.	3.00	9.86	0.18	0.00	97.79
2020-KELL-48-TS1-Circle D-tur3-004	Tur-3	34.90	0.67	28.57	<d.l.	16.34	<d.l.	2.48	0.62	1.36	0.27	0.39	<d.l.	2.95	10.02	0.16	0.00	98.40
2020-KELL-48-TS1-Circle E-tur3-001	Tur-3	34.96	0.62	29.23	<d.l.	15.04	<d.l.	2.51	0.22	1.96	0.14	0.54	<d.l.	2.96	9.99	0.23	0.00	97.94
2020-KELL-48-TS1-Circle E-tur3-002	Tur-3	35.08	0.35	29.72	<d.l.	13.46	<d.l.	3.59	0.11	2.50	0.09	0.61	<d.l.	3.08	10.08	0.26	0.00	98.41
2020-KELL-48-TS1-Circle E-tur3-003	Tur-3	35.40	0.40	30.03	<d.l.	14.71	<d.l.	2.51	0.44	1.60	0.19	0.51	<d.l.	2.94	10.10	0.22	0.00	98.62
2020-KELL-48-TS1-Circle F-tur3-004	Tur-3	35.86	<d.l.	32.40	<d.l.	13.39	0.12	2.06	<d.l.	1.88	0.04	0.45	<d.l.	2.99	10.25	0.19	0.00	99.25
2020-KELL-48-TS1-Circle F-tur3-005	Tur-3	35.60	<d.l.	31.75	<d.l.	12.25	0.10	2.92	<d.l.	2.55	0.03	0.83	<d.l.	2.98	10.16	0.35	0.00	98.83
2020-KELL-48-TS1-Circle G-tur3-001	Tur-3	35.65	<d.l.	31.76	<d.l.	14.65	<d.l.	1.53	0.14	1.49	0.07	0.16	<d.l.	3.02	10.15	0.07	0.00	98.55
2020-KELL-48-TS1-Circle G-tur3-002	Tur-3	35.18	<d.l.	30.71	<d.l.	14.95	<d.l.	1.69	0.16	1.56	0.04	0.17	<d.l.	3.00	10.01	0.07	0.00	97.40
2020-KELL-48-TS1-Circle G-tur3-003	Tur-3	35.89	<d.l.	31.90	<d.l.	14.41	<d.l.	1.77	0.08	1.55	<d.l.	0.18	<d.l.	3.02	10.22	0.08	0.00	98.94
2020-KELL-48-TS1-Circle G-tur3-004	Tur-3	35.92	<d.l.	33.65	<d.l.	12.32	<d.l.	2.18	<d.l.	1.32	<d.l.	0.16	<d.l.	2.98	10.33	0.07	0.00	98.79

EMPA label	Type	SiO ₂	TiO ₂	Al ₂ O ₃	Cr ₂ O ₃	FeO	MnO	MgO	CaO	Na ₂ O	K ₂ O	F	Cl	H ₂ O*	B ₂ O ₃ *	O=F	O=Cl	Total
2020-KELL-48-TS1-Circle H-tur3-001	Tur-3	35.33	<d.l.	30.03	<d.l.	16.07	<d.l.	1.92	0.34	1.62	0.29	0.46	<d.l.	2.97	10.08	0.19	0.00	98.92
2020-KELL-48-TS1-Circle H-tur3-002	Tur-3	35.28	<d.l.	29.66	<d.l.	16.87	0.09	1.78	0.46	1.40	0.27	0.53	<d.l.	2.89	10.09	0.22	0.00	99.10
2020-KELL-48-TS1-Circle I-tur3-001	Tur-3	34.10	<d.l.	30.23	<d.l.	17.14	0.11	1.05	0.42	0.73	0.21	<d.l.	<d.l.	2.91	9.93	0.00	0.00	96.83
2020-KELL-48-TS1-Circle I-tur3-002	Tur-3	33.88	<d.l.	30.45	<d.l.	17.25	0.13	1.02	0.45	0.61	0.24	<d.l.	<d.l.	2.89	9.94	0.00	0.00	96.86
2020-KELL-48-TS1-Circle I-tur3-003	Tur-3	35.04	<d.l.	29.17	<d.l.	18.09	0.16	0.87	0.19	1.01	0.66	0.21	<d.l.	2.93	9.96	0.09	0.00	98.20
2020-KELL-48-TS1-Circle I-tur3-004	Tur-3	34.13	<d.l.	30.75	<d.l.	17.21	0.12	0.97	0.45	0.65	0.21	<d.l.	<d.l.	2.91	10.00	0.00	0.00	97.40
2020-KELL-48-TS1-Circle I-tur3-005	Tur-3	33.17	<d.l.	27.74	<d.l.	16.38	0.14	0.88	0.19	0.94	0.61	0.21	<d.l.	2.75	9.38	0.09	0.00	92.31

